Reports of the Finnish Geodetic Institute

2013:1

Proceedings of the 21st Meeting of the European VLBI Group for Geodesy and Astronomy

Ed. by N. Zubko and M. Poutanen

Kirkkonummi 2013

ISBN: 978-951-711-296-3 (printed)
ISBN: 978-951-711-297-0 (pdf)
ISSN: 0355-1962

Contents

Software developments

Geodetic VLBI analysis and modeling

ICRF, source structure

Observational programs, strategies, scheduling

Local ties, reference point determination

Report on 2012 Digital Backend Intercomparison Testing

A. Whitney

Abstract As VLBI expands the scope of digital signal-processing in VLBI systems, it is important that each sub-system be validated for proper function and interoperability. While every VLBI developer strives to ensure that these criteria are met, it is often only by comparison that problems can be uncovered. One area of particular interest is digital-backend (DBE) systems, where some issues are difficult to evaluate in either local tests or actual VLBI experiments. The 2nd DBE intercomparison workshop at Haystack Observatory on 25-26 October 2012 provided a forum to explicitly address validation and interoperability issues among independent global developers of DBE equipment, and builds on the work of the first such workshop held at Haystack Observatory in May 2009. The 2012 workshop took advantage of the completion of a new Instrumentation Lab at Haystack Observatory that provided the space and signal connections needed to efficiently support the comparison exercise.

Keywords DBE, VLBI

1 The DBE Systems

Five systems were assembled at Haystack for testing:

- The European 'DBBC' system, configured as a polyphase filter bank (PFB) converter .
- The Chinese VLBI Data Acquisition System (CDAS) configured as 16 tunable DDCs.
- The CDAS with polyphase filter-bank signal processing.
- The Japanese 'ADS3000+' system configured with 16 tunable DDC processors.

A. Whitney
MIT Haystack Observatory, Route 40, Westford, MA 01886, U.S.A.

Fig. 1 Gino Tuccari with the DBBC system

- The Haystack 'RDBE-H' PFB system.

2 Test Objectives

The test objective was to ensure, as much as possible, that all DBE units were operating properly, including both functional and interoperability criteria. This was done by providing all units with a common frequency reference, 1pps timing signal, and a common broadband noise source spanning approximately 100MHz to 2GHz. For some testing, embedded test tones at frequencies (575 MHz and 961 MHz), were added to the broadband noise source. The testing was divided into three specific phases:

1. Verification of compatibility with laboratory interfaces, command and control functionality, and digital-output format compatibility.

Fig. 4 Chet Ruszczyk controlling the recording while Arthur Niell (nominal test director) looks on. In the background Kazuhiro Takefuji explains the ADS3000+ system.

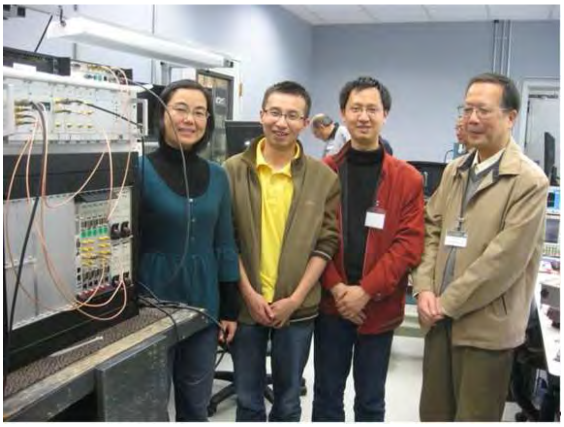

Fig. 2 Lan Chen, Yajun Wu, Renjie Zhu and Xiuzhong Zhang with the CDAS system

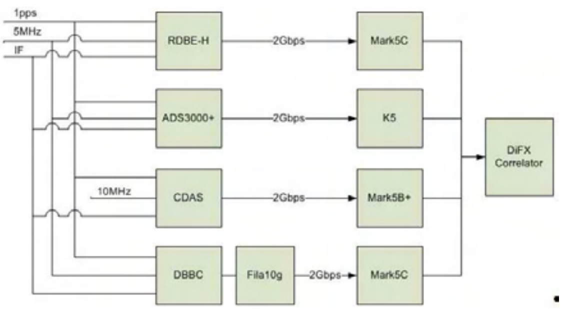

Fig. 3 Setup for the zero-baseline inter-comparison test

2. Single baseline cross-correlation test of each unit paired with RDBE-H unit; all station auto-correlations.
3. Simultaneous 4-station zero-baseline cross-correlation of all six possible station pairs; all station auto-correlations.

2.1 4-station zero-baseline cross-correlation

The most stringent test of intercompatibility was a 4-station zero-baseline cross-correlation test that captured simultaneous data using the common broadband IF noise source to all systems under test. The setup is shown in Figure 3, where the broadband noise input is labeled 'IF' and Nyquist zone 2 filters are assumed internal to the individual DBE units.

Data were recorded from all four units simultaneously and the six cross-correlation pairs were processed on the DiFX correlator. Detailed examination of the correlation results from all baselines allowed the identification of problems with specific units.

3 Summary

Only one unit was found to have apparent significant problems, and another with more minor issues. A complete report on the intercomparison testing is available at `http://www.haystack.mit.edu/workshop/ivtw/2012.12.17_DBE_testing_memo_final.pdf`. A detailed comparison of the digital backends tested has been compiled by Bill Petrachenko and is available at `http://www.haystack.edu/tech/vlbi/digital/dbe_memos/2013.01.21_dbe_comparison-Petrachenko.pdf`

We thank everyone who participated. We hope that this exercise was useful for all of the participants, and we at Haystack were happy to be able to help support this effort.

DBBC3 - Full digital EVN and VLBI2010 Backend, Project Progress

G. Tuccari, W. Alef, M. Wunderlich, S. Buttaccio, D. Graham, G. Comoretto, A. Bertarini, S. Casey, A. Roy, J. Wagner, M. Lindqvist

Abstract DBBC3 is a project to develop the third generation of a digital backend system for VLBI and other scientific applications. The development started about ten years ago and evolved in the course of time by improving all its components, hardware, firmware and software, passing from DBBC1 to DBBC2. Now the latest and third generation will allow to fully implement digitally all the functionality required of a complete VLBI backend for the EVN and VGOS (formerly named VLBI2010), with a maximum output data rate in the range from 32 Gbps to up to 128 Gbps. The architecture and adopted methods are described.

Keywords Digital Backends, VGOS

1 Introduction

The development of the DBBC started in the first years of the new millennium (Tuccari (2004a) & Tuccari (2004b)). In the first few years ad hoc laboratory experiments and experiments with real sky signals had indeed demonstrated that it could be possible to emulate the entire functionality of the MK4 VLBI analogue terminal with a fully digital backend. In the digital process the analogue signal available as IF from the receiver is, after potential equalization and gain adjustments, immediately converted to a digital representation before any mixing or filtering stage as is required for VLBI to produce recordable sub-bands. Before this time the digital mixing/filtering stage could not be fully implemented digitally at a reasonable cost, and moreover it was a technical challenge due to the wide band and the high frequencies involved. With progressive improvements the DBBC project evolved to allow an input bandwidth of up to 4×1 GHz.

The first DBBC version (DBBC1) was a backwards compatible replacement of the existing VLBI terminal, while with the DBBC2 additional observing modes became available, which did not exist in the analogue backend. The enhanced version of the DBBC2 for VLBI2010 (Niell et al. (2005)) the DBBC2010 (2009 to date) is compatible with the proposed VGOS observing mode.

One way to increase the sensitivity of a VLBI network is to increase the observing bandwidth. With new wide-band receivers the demand for backends which can handle bandwidths of several GHz has arisen. Also the EVN has been increasing its maximum data rate from a maximum of 1 Gbps with the MK4 analogue backend to a maximum of 4 Gbps with the present DBBC2 — a data rate which is being tested in the EVN now.

In preparation for receivers and IF systems which will deliver up to 4 GHz (and later more) bandwidth to the backends, it was felt necessary to develop a system which can process an instantaneous bandwidth of 4 GHz per polarization as a minimum. The resulting output data rate for a dual polarisation receiver should be at least 32 Gbps, with the option of 64 Gbps for a system with four IFs. Such a backend is the intermediate goal of the DBBC3 project.

The specifications of VLBI2010 define a set of requirements of the receiving/backend system to achieve the goal of greatly improved geodetic measurement precision. The telescopes will operate in a single broad band ranging from 2 to 14 GHz observing in dual linear polarization. Inside this frequency range a subset

Gino Tuccari, Salvo Buttaccio
INAF – Istituto di Radioastronomia, Ctr.da Renna, Noto, Italy
Walter Alef, Michael Wunderlich, David A. Graham, Alessandra Bertarini, Alan Roy, Jan Wagner
Max-Planck-Institut für Radioastronomie, Auf dem Hügel 69, Bonn, Germany
Gianni Comoretto
Osservatorio Astrofisico di Arcetri, Largo E. Fermi 5, Firenze, Italy
Simon Casey and Michael Lindqvist
Onsala Space Observatory, SE-439 92 Onsala, Sweden

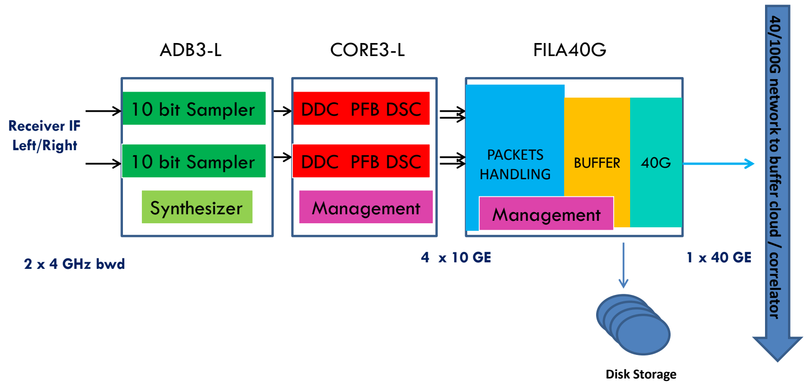

Fig. 1 DBBC3-L block diagram with sampler ADB3-L, processor CORE3-L, and FILA40G packetizer.

of four 1024 MHz wide pieces will be selected, in both polarizations, so that a total of eight portions of 1 GHz will have to be processed. This will allow bandwidth synthesis (phase slopes fitted over a wide frequency range) for a much wider portion of the spectrum than is possible with the present system.

Such a wide input band could also be of great interest for astronomy because of the significant increase in sensitivity it will offer. Being able to process an entire 14 GHz wide piece of band could be a quantum leap in the digital radio astronomy data acquisition. This goal is very ambitious and its implementation in a radio astronomy backend would be a novelty. To digitally sample and process the whole 14 GHz wide band or a number of sub-bands thereof is the final goal for the DBBC3 project.

2 DBBC3 Structure

For the DBBC3 system there are some obligatory requirements: it has to be backwards compatible with the existing backends of the previous generations and has to be able to offer the new functionality for a very wide band. In particular it should incorporate all the required functionality, for the planned goals of the EVN (min 2×4 GHz bandwidth) and VLBI2010 (2×14 GHz bandwidth). As many stations observe for both networks a single system is mandatory. Flexibility is a requirement due to the different radio telescopes and their dissimilar receivers and IF systems in terms of number and type of IFs.

To be compatible with the existing systems, the new hardware needs to be mechanically and electrically level-compatible. This aspect is useful because existing DBBC2 and DBBC2010 backends in the field could be upgraded to meet the new performance requirements by replacing some of the old components with DBBC3 hardware.

The much increased capability of the new backends requires new hardware parts, together with new firmware. A clear development path has been laid-out to minimise the risk in the project. In a first step a DBBC3-L will be developed which can be seen as a fully qualified 4 GHz DBBC, but at the same time the final goal to achieve a 14 GHz DBBC3-H is pursued.

The main features of the DBBC3-L system are:

- Maximum number of wide input IFs: 4 (typ. 2)
- Instantaneous bandwidth in each IF : 4 GHz
- Sampling representation: 10 bit
- Processing capability $N \times 5$ TMACS (multiplication-accumulations per second), with N number of processing nodes
- Output data rate: max 64 Gbps
- Compatibility with the existing DBBC environment.

The main features of the DBBC3-H system are:

- Max number of wide input IFs: 4 (typ. 2)
- Instantaneous bandwidth in each IF: 14 GHz
- Sampling representation: 8 bit
- Processing capability $N \times 5$ TMACS (multiplication-accumulations per second), with N number of processing nodes
- Output data rate: max. 896 Gbps
- Compatibility with the existing DBBC environment.

In figures 1 and 2 the schematic views of the DBBC3-L and DBBC3-H are shown.

The structure of the system is straightforward. Due to the very broad band to be sampled a dedicated receiver named DBBR (Digital Broad Band Receiver) is developed including the entire digital section. After initial amplification of the signal collected by the feed

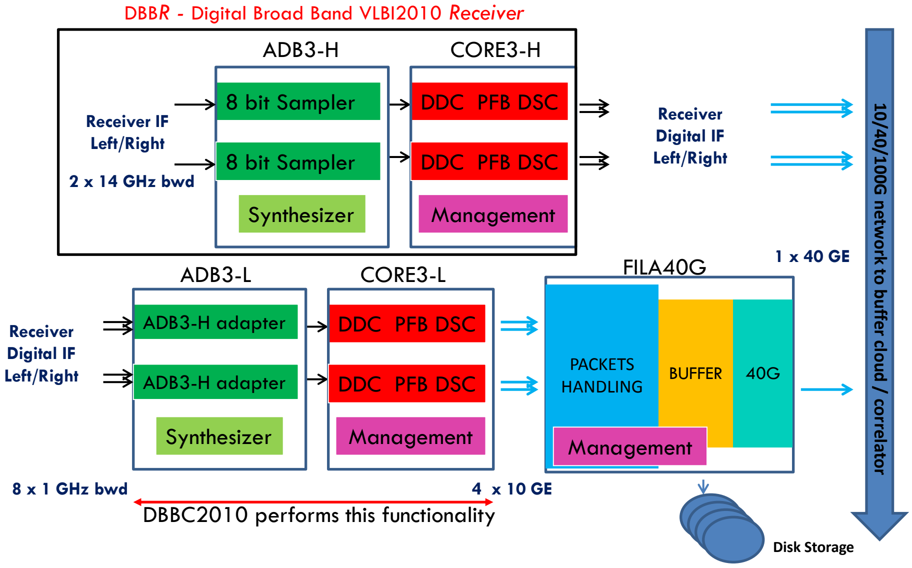

Fig. 2 Complete DBBC3 block diagram. Top: DBBC3-H as Digital Broad Band Receiver. Bottom: DBBC3-L.

in both polarizations, two IFs 14 GHz wide are sampled with 8-bit representation. Next this data is transferred to a dedicated processing node. The processor extracts from the digital data eight streams, portions of the band, in DDC (tunable digital down converter) and PFB (fixed polyphase filterbank) modes, from the entire input range. These tuned/filtered 'digital IFs' are transferred and processed in the DBBC3-L section to further extract and select portion of bands to produce VLBI-compatible output VDIF packets.

The last element of the chain is the FILA40G subunit whose function is to condense the data onto single optical fibres at a data rate of 40 Gbps and to handle the data at network packet level. A dedicated version, the FILA40G-ST, will in addition have storing capabilities.

3 ADB3-L/H components

The massive sampling is performed by a state of the art sampler chips. A single ADB3-L has four complete samplers on-board, with the possibility to arrange them for a variety of functionalities, single and multiple, real or complex sampling. For example in real mode the four samplers can be fed with a single input signal 4 GHz wide, or they can be fed with two signals of 2 GHz instantaneous bandwidth each, or finally with four signals 1 GHz bandwidth.

The ADB3-H single board sampler similarly has the capability to digitise up to four independent 14 GHz bands. Sampled data have to be transferred to the processing stage. Due to the high data rate a parallel bus cannot be implemented, because the very large number of differential lines required and the high operational frequency. Pre-processing is used to pipe this large data rate to a manageable number of serial connections for linking the Sampler with the Processing unit.

Data coming from the sampler board ADB3-L/H are routed to the processing node CORE3-L/H using the lanes of the high speed input bus. The CORE3-L/H board is capable of processing data in different ways: with DSC (Direct Sampling Conversion) resulting in one single sampled sub-band, DDC (Digital Down Converter) and PFB (Polyphase Filter Bank) personalities. Additional capabilities will allow spectroscopic and polarimetric observations.

From the pool of channels a subset is selected according to the desired output data rate defined by the observer or allowed by the recording media or the network capacity. The data is output via the high speed output bus. Additional input and output connectors are available to maintain the compatibility with the DBBC2 stack of boards.

The large DSP resources available in the FPGA chosen for the CORE3-L allows digital filters in the class of 100 dB in/out band rejection. This feature is required for the expected presence of large RFI signals in the very wide input band. This very strong discrimination together with the tuning ability should be sufficient to obtain useful and clean pieces of the down-converted observed band.

As an alternative input the CORE3-L board will be able to receive data packets from a block of ADB3-

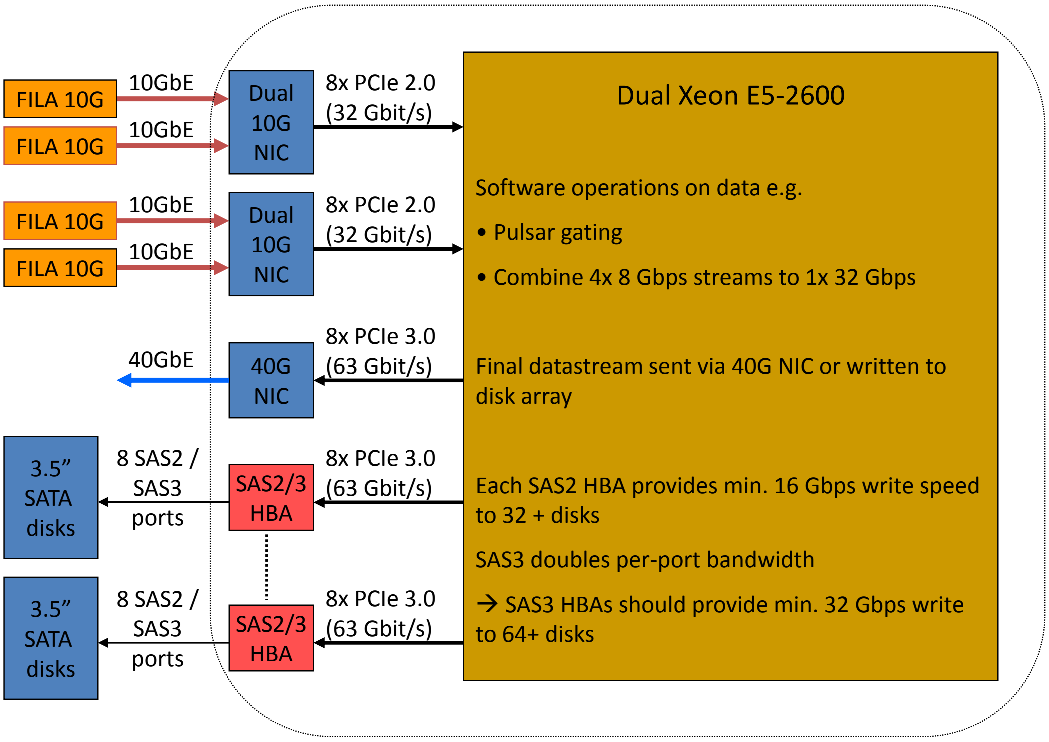

Fig. 3 Block diagram of the FILA40G unit. Input 4×1 Gb. Output: 1×40 Gb to fibre or alternatively to disks.

H/CORE3-H units to be routed to the rest of of the system for additional data processing.

Data from the converted bands are finally transferred to the network controller FILA40G as multiple 10 GE connections. The number of connections is then accumulated into a 40 GE data stream to be transferred to the final destination points. Such final points could be recorders, nodes of VLBI correlators or a buffer cloud. In addition to the 40 GE network capability the FILA40G unit will be able to manipulate the data packets in order to perform functions like corner-turning, pulsar-gating, packet filtering and routing, burst mode accumulation, and others that could be required at the packet level as soon as the VLBI methods evolve. In addition a dedicated version will be provided which can include storage elements for data buffering and recording. The FILA40G block schematic view is shown in figure 3.

Most of the data communications in the system will be implemented making use of a collection of serial point to point connections to represent the aggregate block information. In order to maintain the data block structure representing in a complete form the single band information the quantity sbit (serial bit) is defined. So the number of sbit is the number of serial links, running at the indicated data rate, necessary to fully represent the information belonging to a single information quanta like in our case is a complete sampled input band. The wide bandwidth involved in the process, and so the very high data rate necessary to represent it, is greatly simplified by this compressed definition, that we adopt and use for all the project description. The schematic block in figure 4, shows in such terms the complete system data flow.

4 Preliminary Results

The DBBC3 project is progressing as planned and the first prototypes are under development and construction. These will produce the proper information and know-how to proceed to the final version. The evaluation performed in the laboratory until now shows that the project will reach the planned goals in the scheduled time without big risks or problems, despite of the very challenging performance to be obtained.

Tests and experiments performed with the ADB3-H and ADB3-L first prototypes are available and in particular showed that direct data conversion to the digital domain for the full 14 GHz band is possible, without the need for an initial analogue down conversion.

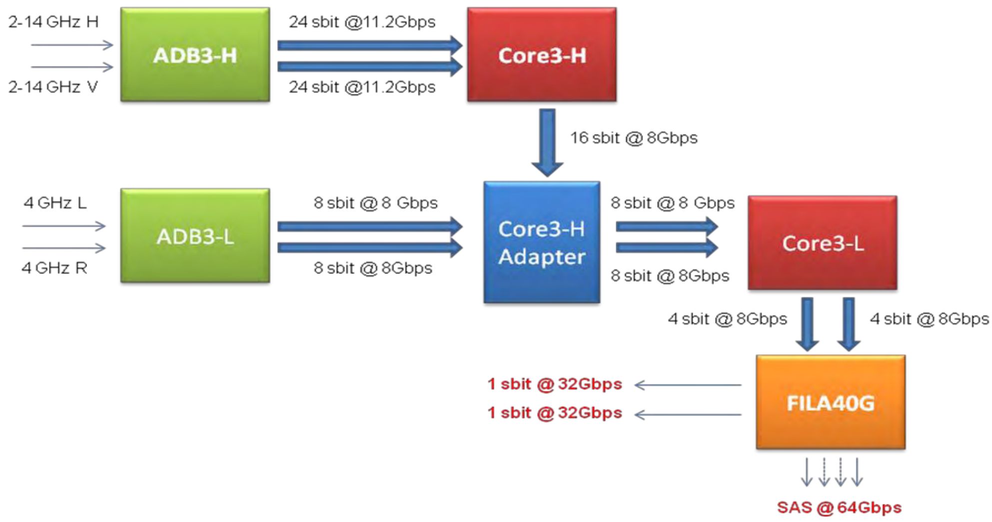

Fig. 4 DBBC3 Data flow. Data sampled and preprocessed with the H-version is fed into the data path of the L-version via an adapter.

This represents a huge challenging and intriguing step ahead in the simplification and in the improvement of the VGOS electronics which should significantly reduce the system cost.

The very challenging firmware development, for the huge data rate and very fast clocks involved, is underway on hardware platforms with the FPGA device to be used for both Core3-L and Core3-H.

References

G. Tuccari, *Development of a Digital Base Band Converter (DBBC): Basic Elements and Preliminary Results* New Technologies in VLBI, Astronomical Society of the Pacific Conference Series, ISSN 1050-3390, Vol. 306, 177–252, 2004.

G. Tuccari, *DBBC - a Wide Band Digital Base Band Converter*, in: International VLBI Service for Geodesy and Astrometry 2004 General Meeting Proceedings. Ottawa, Canada, NASA/CP-2004-212255,

A.E. Niell, A. Whitney, B. Petrachenko, W. Schlter, N. Vandenberg, H. Hase, Y. Koyama, C. Ma, H. Schuh, and G. Tuccari, *VLBI2010: Current and Future Requirements for Geodetic VLBI Systems* 2005 IVS Annual Report, pp. 1340, 2006.

Mark6: Design and Status

R. Cappallo, C. Ruszczyk, A. Whitney

Abstract The Mark 6 system is a disk-based data capture and record system, optimized for VLBI. As a follow-on to the successful Mark 5 family, it increases the maximum record rate to 16 Gb/s, using high-performance COTS (Commercial Off-the-Shelf) hardware and open-source software. This paper presents the Mark 6 design, with special emphasis on the software, and its current and future capabilities.

Keywords Mark 6, Data Recording, VLBI

1 Introduction

The Mark 6 data capture and recording system has been developed in response to ever-increasing need for greater sensitivity in VLBI systems. In geodesy, for example, the VGOS (formerly called VLBI2010) system (Niell et al. 2007) is designed around relatively small (12 m), agile antennas, whose decreased gain is compensated for by increased bandwidths (4 GHz). Similarly, in astronomical instruments such as the Event Horizon Telescope (Doeleman 2010), which operates in the (sub) mm wavelength range, amplitudes are affected by extreme atmospheric coherence issues, and wide bandwidths are needed to get sufficient sensitivity over short timescales.

The Mark 6 system (Whitney and Lapsley, 2012) follows closely upon the design of the Mark 5 recording system (Whitney, et al. 2010), with two key improvements: the datarate (and thus recordable bandwidth) is increased by a factor of at least x8, and the design has been changed to be Commercial Off-The-Shelf (COTS) hardware, and entirely open-source software.

Roger Cappallo, Chet Ruszczyk, and Alan Whitney
MIT Haystack Observatory, Off Route 40, Westford, MA, USA

2 General Considerations

The goals for the Mark6 can be conveniently placed into two categories, one for essential goals that must be met, and the other of secondary goals, which are desirable, and should be met only if the effort to do so is not too great. All of the essential goals have been achieved, and all of the secondary goals are also expected to be feasible.

Principal goals

- 16 Gb/s sustained record capability
- support all common VLBI formats
- COTS hardware
- 100% open-source software
- relatively inexpensive
- upgradeable to follow Moores Law progress
- smooth user transition from Mark 5
- preserve Mark 5 hardware investments, where possible

Secondary goals

- 32 Gb/s (or more) burst-mode capability
- generalized ethernet packet recorder
- e-VLBI support
- single-step playback as standard Linux files

3 Software Design

The Mark 6 software has been designed using a layered model (see Fig. 1). The interface to the user (or more likely to the user's software) is accomplished by a program called *cplane* (for control plane). The interface to the network and disk hardware is handled by another program, called *dplane* (for data plane). The two programs/planes communicate via UDP messages.

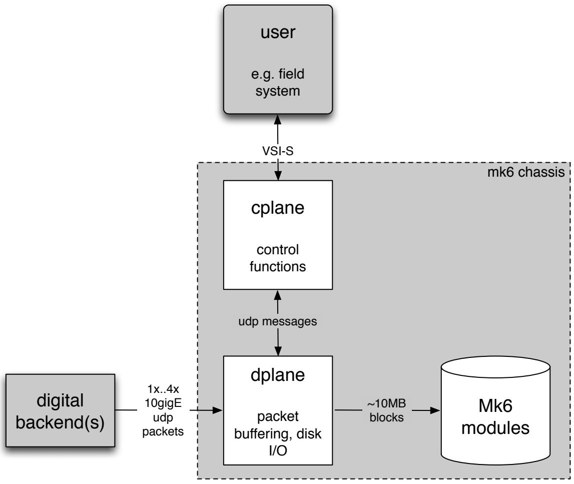

Fig. 1 Top-level block diagram of the Mark 6 software modules, showing the relationship of the two principal software modules, *cplane* and *dplane*.

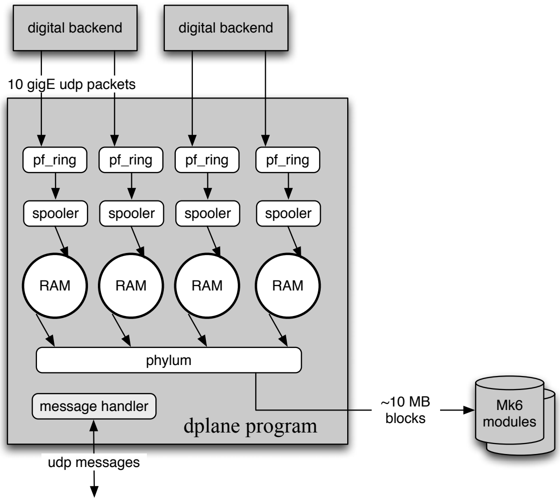

Fig. 2 Block diagram of the *dplane* software module. Each of the 4 parallel datastreams is processed by a separate thread, in a dedicated core for speed.

3.1 Control Plane

The control-plane module *cplane* provides an interface to the user, and it implements a number of different high-level monitor and control functions. Due to its relaxed performance demands, *cplane* has been written in Python. The user interface is the standard VSI-S protocol (VSI-S 2003) with command set enhancements specific to the Mark 6 system. The *cplane* program is also responsible for managing the disk modules: it mounts, dismounts, and binds the individual disks as groups comprised of up to 32 disks. Performing and reporting error-checks as well as statuses is another *cplane* responsibility.

During the test and integration phase of the software, *cplane* has been controlled via an XML-based control script called RM6_CC. This script allows simple time-sequencing of scan-based observations. It is expected that a transition will eventually be made to control via standard experiment control software, such as the ”Field System” software from Goddard Space Flight Center (Himwich and Gipson 2011).

3.2 Data Plane

The data-plane module *dplane* handles all tasks specific to the high-speed flow of data. It reads in data from the 10 Gb/s network interface cards, buffers the data in large RAM buffers, and writes it out (if desired) into disk files on multiple disks. The start and end of the data is controlled precisely, by way of inspection of the time stamps within the data packets. Since the performance demands upon *dplane* are very high, the code is written in *C*, and is highly optimized.

The relevant hardware resources of the Mark 6 data pathway include:

- Intel core i7 3930K hex-core hyper-threaded processor
- ASRock Fatal1ty X79 Champion motherboard with 64 GB RAM
- 2 dual-channel 10 Gb/s NIC's
- 1 to 32 SATA hard drives

3.2.1 Architecture

The program is written with multiple threads, dedicating a processor core to each of the 4 input streams (see Fig. 2). The *pf_ring* I/O library (Deri 2004) is used for high-performance buffering of the incoming data packets. SMP affinity is used to spread the interrupt-handling load across different cores. The packets are then spooled into large circular FIFO buffers in RAM. These large ring buffers are given nearly all (e.g. 56 of 64 GB) of the physical memory space, and are locked in, saving only a modest amount of RAM for the OS to use for file caching, etc. The available space is used for 1–4 datastreams, and can be allocated on a dynamic basis if the user so desires. A single disk-writing thread empties these buffers, writing out data blocks to multiple disks.

3.2.2 Scattered File System

In order to be resilient to individual disk failures, and write-speed variations (which can be nearly a factor of 2 between the outer-edge starting tracks on the disks, and the inner-edge ending tracks), we have developed a scattered file system. This system writes blocks (≈ 10 MB in length) to drives based upon which of the drives are ready to accept more data. For this application a RAID data-striping approach would not work so well, as the speed of the ensemble of disks would be limited by the slowest disk in the set.

In order to facilitate reassembly of the data into a continuous stream, a small amount of identifying meta-data is prepended to each block. Three methods of data-reassembly may ultimately be used. Currently we use a progam, called *gather*, that efficiently reassembles the scattered data into a single disk file, in the correct time sequence. If data are missing then a fill-pattern is inserted in its place. The disadvantage of using *gather* is obvious – there is an extra copy step in the data pipeline, which is perhaps not an issue if the data need to be copied anyway onto a local storage device at the correlator.

A native-mode reader for the difx correlation software (Deller et al. 2012) is also planned for development, which would allow reassembly on the fly at correlation time. Finally, another flexible approach would be to write a FUSE (File-system in User Space) interface to allow the scattered files to appear as a single, standard Linux file.

There is a option of the program in which only a single file is written out, with no additional metadata inserted. In such a case it is not necessary to perform the extra reassembly step. This mode may be particularly attractive for modules comprised of solid state disks (SSD's), since they could be placed in a high-performance RAID configuration without much jeopardy from a slow disk.

3.2.3 Data Formats

The current software version supports the VDIF format (Whitney, et al. 2009) as well as the Mark5B format, which is converted to VDIF format. In the case of Mark5B input streams, the data are converted to VDIF encoding and a proper VDIF header is generated and prepended to each packet. Words 5 through 8 of the VDIF header then contain the original 4 word Mark5B header. For multiple input streams, each Mark5B stream is assigned to a separate VDIF thread.

3.3 Additonal Features

In order to facilate eventual use of the system as an eVLBI node, the capture of data to ring buffers is managed separately from file writing. The use of a single large FIFO per stream design decouples writing from capturing. This allows the system to keep writing to disks during the antenna slew time, so that the dataflow limitation is that the mean acquisition rate must not exceed the mean disk writing rate. However, an additional constraint is imposed by the finite size of the FIFO buffers. At an input datarate of 16 Gb/s ($\bar{2}$ GB/s) The large RAM is only about 30 seconds deep. This headroom is increased by the continual drain of data to disks; e.g. if 8 Gb/s were being written out, the buffer headroom would increase to 1 minute.

Mark 6 hardware is non-proprietary and the specifications and parts list are openly published. For convenience, but not by necessity, a Conduant chassis and Conduant modules may be used, as they are known to be both reliable and convenient. An upgrade kit, available from Conduant, is offered to facilitate reuse of Mark 5 modules in the Mark 6 system. A dedicated eVLBI site, though, may find it convenient to use non-Conduant hardware with Mark 6 software, as then there would be no module-interoperability concern.

4 Demonstration Experiment

In June of 2012 we performed a proof-of-concept experiment, which was used to demonstrate that the Mark6 works as intended, and that its combination with the digital backend signal processing performs as expected (see Whitney et al. 2013). A prototype version of the Mark 6 software was used, which captured 16 Gb/s onto 4 x 8 disk modules in RAID mode 0. An aggregate of 4 GHz on the sky was used to observe 3C84 on a Westford, MA – Goddard Space Flight Center baseline (see Fig. 3). The increase in signal-to-noise ratio due to the increased bandwidth was as expected, and no unusual anomalies were detected.

5 Future Plans

The Mark 6 system is expected to be used in an operational setting beginning in the summer of 2013, principally for wideband observations. Work is continuing

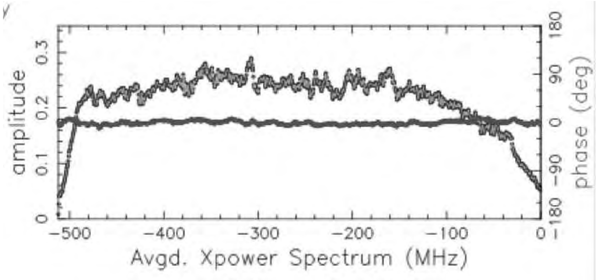

Fig. 3 Cross-power spectrum amplitude and phase, averaged over all four 512 MHz bands.

on the software, with the following list of desired capabilities, placed in very rough priority order:

- performance enhancements and increased diagnostic tools
- native Mark 6 reader for the difx correlation software
- FUSE / Mark 6 file interface
- full support for generalized (i.e. non-VLBI) packet capture
- support for eVLBI via retransmission of the captured ring buffer

References

VSI-S Committee VLBI Standard Software Interface Specification. Web document `http://www.vlbi.org/vsi/docs/2003_02_13_vsi-s_final_rev_1.pdf`, 2003.

Deri, L. Improving passive packet capture: Beyond device polling. Proc. of SANE. Vol. 9. 2004.

A. Niell, A. Whitney, W. Petrachenko, W. Schlter, N. Vandenberg, H. Hase, Y. Koyama, C. Ma, H. Schuh, and G. Tuccari VLBI2010: A Vision for Future Geodetic VLBI in Dynamic Planet, International Association of Geodesy Symposia Volume **130**, 2007, pages 757–759.

Whitney, A., Kettenis, M., Phillips, C., and Sekido, M. VLBI Data Interchange Format (VDIF). Proceedings of the 8th International e-VLBI Workshop, PoS (EXPReS09), **42**, 2009.

Doeleman, S. Building an event horizon telescope: (sub)mm VLBI in the ALMA era. "Proceedings of the 10th European VLBI Network Symposium and EVN Users Meeting: VLBI and the new generation of radio arrays. September 20-24, 2010.

A. Whitney, C. Ruszczyk, J. Romney, and K. Owens The Mark 5C VLBI Data System. *International VLBI Service for Geodesy and Astrometry: 2010 General Meeting Proceedings*

Himwich, Ed, and John Gipson. GSFC Technology Development Center Report. *International VLBI Service for Geodesy and Astrometry: Annual Report 2011*

A. Whitney and D. Lapsley. Mark6 Next-Generation VLBI Data System. *International VLBI Service for Geodesy and Astrometry: 2012 General Meeting Proceedings*

Whitney, A.R., Beaudoin, C.J., Cappallo, R.J., Corey, B.E., Crew, G.B., Doeleman, S.S., Lapsley, D.E., Hinton, A.A., McWhirter, S.R., Niell, A.E. Rogers, A.E.E., Ruszczyk, C.A., Smythe, D.L., SooHoo, J., Titus, M., (2013) Demonstration of a 16 Gbps per Station Broadband-RF VLBI System. PASP, **125**, pages 196–203.

Receiver Upgrade for the GGAO 12m VLBI system

C. Beaudoin, P. Bolis, J. Byford, S. Cappallo, T. Clark, B. Corey, I. Diegel, M. Derome, C. Eckert, C. Ma, A. Niell, B. Petrachenko, A. Whitney

Abstract The MIT Haystack Observatory, with support from Honeywell Technology Solutions Inc. and funding from NASA Space Geodesy Project (SGP), has developed a receiver upgrade for the 12m VLBI radio telescope installed at the Goddard Geophysical Astronomical Observatory (GGAO) in Greenbelt, MD. The first stages of the upgrade to the receiver frontend incorporate the quadruple-ridge flared horn (QRFH) and CRYO1-12 LNA, both designed at the California Institute of Technology. The frontend upgrade also incorporates a custom diplexer that decomposes the receiver into low and high-band sections in consideration of dynamic range limitations. The upgrade to the radio telescope also incorporates a modern, mechanized positioning system that will facilitate routine maintenance and operation of the radio telescope.

Keywords GGAO, Upgrade, Dynamic Range, SEFD, Receiver

1 Introduction

In response to recommendations of the IVS Working Group 3 on VLBI2010(Petrachenko et al., 2009), the MIT Haystack Observatory engaged in the development of a prototype broadband receiver which was installed on the Westford 18m and GGAO 5m antennas in late 2007. These two stations formed a broadband VLBI baseline which was utilized to conduct proof-of-concept (POC) studies and demonstrate the feasibility of VLBI2010 observing strategies. In October 2010, the Patriot/Cobham 12m antenna was installed at GGAO in support of the antenna requirements outlined in (Petrachenko et al., 2009) and was subsequently custom fit with a POC receiver as well. Through POC operations, two functional limitations specific to the GGAO installation were identified.

The S-band RFI environment at GGAO was sufficiently strong that the dynamic range (DR) in the fiber optic downlink was compromised and limited the receivers available bandwidth. The fiber downlink component is the broadband DR limiting component since it possesses approximately 100 dB of dynamic range. The California Institute of Technology CRYO1-12A 2-12 GHz LNA incorporated in the POC receiver possesses approximately 120 dB of DR based on intermodulation distortion laboratory measurements conducted at Haystack. The fiber optic link also possesses a strongly frequency dependent noise figure which requires more receiver gain at 12 GHz than at 2 GHz. Since the POC receiver did not incorporate any custom tailoring of the receiver gain performance, it was not possible to achieve uniform receiver sensitivity over the entire frequency range.

Another underlying issue identified in the POC operations was the ability of the station operators to service and maintain the cryogenic receiver. The volume available to install the cryogenic POC receiver frontend on the Patriot/Cobham 12m antenna is limited. The limited space within the antenna for such hardware introduced logistical problems when servicing the frontend and required significantly more time than has traditionally been necessary.

C. Beaudoin, P. Bolis, J. Byford, S. Cappallo, B. Corey, M. Derome, C. Eckert, A. Niell, A. Whitney
MIT Haystack Observatory, Westford, MA 01886, U.S.A.
T. Clark
NVI, Inc., Greenbelt, MD 20770, U.S.A.
C. Ma NASA/GSFC, Greenbelt MD, 20771, U.S.A.
I. Diegel
Honeywell Technology Solutions Inc., Columbia, MD 21046, U.S.A.
B. Petrachenko
Natural Resources Canada, Dominion Radio Observatory, Penticton, British Columbia, Canada.

2 Dynamic Range Upgrade

A block diagram of the receiver frontend to downlink sections is shown in Figure 1. Because of its superior dynamic range performance, a coaxial cable downlink was incorporated at GGAO to alleviate this deficiency as discovered in the POC receiver. However, a fundamental upper frequency limitation exists in coaxial cables; the lower the loss of the cable per unit length, the lower available frequency range of the cable due to the multimode effects. This multimode characteristic of caoxial cables places an upper limit on the design frequency of coaxial downlink. From POC studies, the majority of strong RFI sources detected at GGAO were below 4 GHz while the physical distance required to downlink the received signals from the frontend to the control room is 76 meters. Given these conditions, a coaxial cable downlink implemented with LMR-400 cable can be incorporated for frequencies up to 5 GHz without significant influence on the receivers overall system temperature. Hence, the broadband downlink was split into frequency-overlapped low and high-band sections covering 2.2-5 GHz and 4-14 GHz where the high-band section incorporates a fiber optic downlink. The overlapped nature of the downlink avoids the introduction of a constraint in sky frequency coverage by the dual-band design and maintains the flexibility to set the local oscillator frequencies to support overlapped low/high band observations in 1 GHz IF bands.

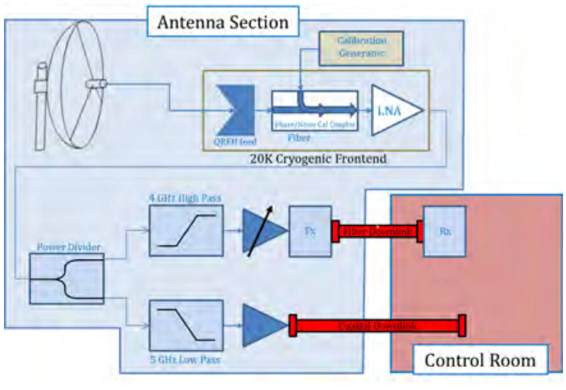

Fig. 1 Block diagram of the GGAO 12m receiver dynamic range upgrade.

Since the high-band fiber optic downlink possesses less dynamic range than the amplifier stages preceding the link, it is not possible to preserve both the low noise characteristic of the LNA/frontend as well as the saturation limit of the LNA in the overall performance of the receiver. For this reason, the gain of the preamp stages driving the fiber optic link was designed to be variable. In this way, the low noise performance of the LNA can be realized when the receiver is not exposed to strong RFI signals by driving the link with maximum preamp gain. The performance of the receiver configured in this mode is shown in figure 2.

In the situations when the receiver is exposed to RFI that is driving the link into modest saturation, the gain of the preamp stages can be reduced to accommodate the power limitation of the link. This reduction of preamp gain will also incur a modest increase in receiver noise temperature dependent on the reduction in gain.

3 Mechanical Upgrade

In order to realize an operational receiver frontend that can be easily serviced and maintained, Haystack Observatory initiated a receiver upgrade project that was focused on providing the following features in the mechanical design:

- Electronic Control of Feed Position
  – Feed Positioning Uncertainty < 1mm
- Remote Servicing of Cryogenics
  – Control Vacuum Pumps and Valve
- Monitor
  – Cryogenic refrigerator temperature
  – Supply/return helium pressure
  – Air pressure in vacuum vessel
  – Crosshead motor electrical drive power
- Ease of Receiver Removal for Servicing outside Antenna
- In-situ Access to the following Components:
  – LNA power supply and cryo temp sensor connectors
  – Bias box adjustments/test points
  – SMA connectors accessible to 5/16" wrench
  – Coupler outputs for RF sampling
  – Fiber optic connectors

As shown in Figures 2 and 3, the mechanical upgrade to the receiver installation consists of two major components; the payload and the payload positioner. The cryogenic receiver frontend and all associated electronics are integrated into the payload section. The payload translates within the feed support tower on a linear bearing and is coupled to the positioning system timing belt which provides a means of conveyance.

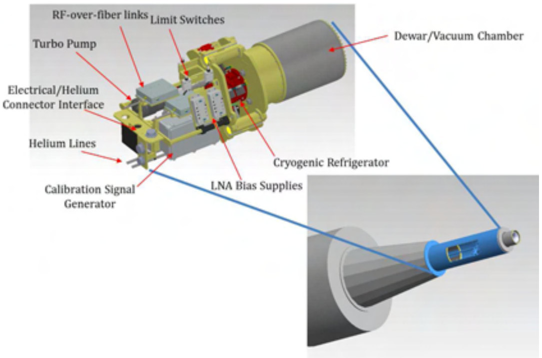

Fig. 2 3D model rendering of the payload upgrade for the GGAO 12m receiver.

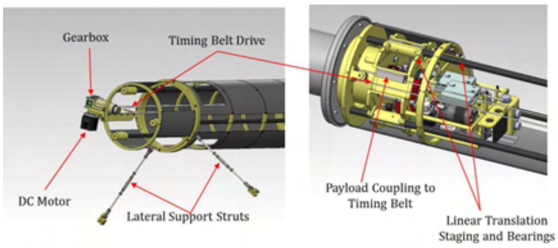

Fig. 3 3D model rendering of the positioner staging that provides conveyance of the payload section.

The payload position is controlled by a DC electric motor also coupled to the timing belt through a small gearbox at the base of the positioner staging or by a field-replaceable handwheel. The payload can be extended into the focal position for normal telescope operations or retracted into the base of the feed support tower for servicing or complete removal from the antenna.

4 Current Status and Outlook

The receiver upgrades described in sections 2 and 3 were installed on the GGAO 12m antenna in November 2012. Shortly thereafter, the antenna optics were realigned and the sensitivity of the radio telescope system was assessed. Figure 4 presents the resultant system equivalent flux density (SEFD) of the radio telescope as a function of sky frequency within the operating frequency range of the LNA. The off-scale sensitivities between 2 and 3 GHz and at approximately 4.2 GHz are due to RFI sources which bias the SEFD estimates; there is also evidence of bias from the GGAO SLR aircraft radar between 9.2 and 9.4 GHz. Based on figure 4, the receiver sensitivity meets the VLBI2010 specification for SEFD of 2500 Jy over most of the frequency range.

Two factors contribute to the steady increase of the SEFD from 10-12 GHz in figure 4. The first factor is the result of the installation of diode limiters in the LNA which increases the system temperature by approximately 10 Kelvin between 10 and 12 GHz. This protection was incorporated to prevent sudden failures of an LNA due to RFI. The second factor is due to the fact that the QRFH feed installed on the 12m antenna is a first prototype and was designed for the 2 to 12 GHz range. As a result, the aperture effciency degrades from approximately 70% at 10 GHz to 60% at 12 GHz. Future designs will be scaled to optimize the aperture efficiency in the 2.2-14 GHz frequency range which will improve the high frequency SEFD performance. It is also possible to improve this performance by removing the protector diodes from the LNAs, however, this will need to be considered carefully in light of the possibility of amplifier failures.

An important requirement of the VLBI2010 specifications is the capability to co-observe with legacy S/X band stations. Because a significant portion of the S-band spectrum is corrupted by RFI as indicated in Figure 4, the SEFD of the radio telescope within the frequency channels observed in the IVS R1 schedules is plotted in Figure 5. Given the S and X-band SEFDs of the 12m radio telescope shown in figures 4 and 5, the GGAO 12m radio telescope is expected to be capable of participating in IVS scheduled observations.

5 Acknowledgements

We thank the ITT/Excelis staff members Jay Redmond and Kathryn Pazamickas for their support of the upgrade activities at GGAO.

References

B. Petrachenko et. al. Ďesign Aspects of the VLBI2010 System¨ Progress Report of the IVS VLBI2010 Committee volume NASA/TM-2009-214180 Hanover, MD: NASA Center for AeroSpace Information June 2009.

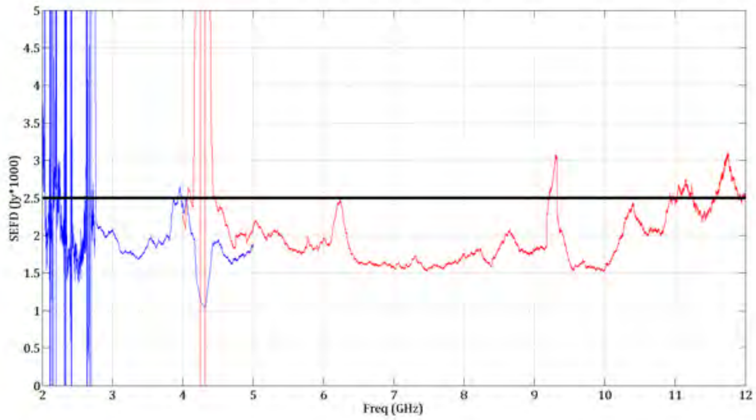

Fig. 4 Low (2.2-5 GHz) and high (4-14 GHz) band SEFD performance of the GGAO 12m radio telescope following the installation of the receiver dynamic range upgrade. The bold trace at 2500Jy reflects the VLBI2010 SEFD specification for 12m antennas.

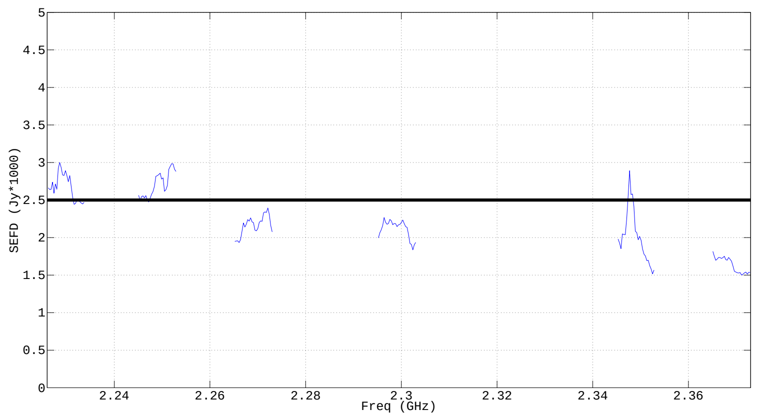

Fig. 5 SEFD performance of the GGAO 12m radio telescope shown in Figure 4 but plotted within the IVS R1 S-band frequency channels. The bold trace at 2500Jy reflects the VLBI2010 SEFD specification for 12m antennas.

When “IVS Live” meets “e-RemoteCtrl” real-time data...

A. Collioud, A. Neidhardt

Abstract “IVS Live” is a tool that can be used to follow the observing sessions, organized by the International VLBI Service for Geodesy and Astrometry (IVS), navigate through past or coming sessions, or search and display specific information about sessions, sources (like VLBI images) and stations. In parallel, “e-RemoteCtrl” is a software, which enables the control of VLBI telescopes from remote over the World Wide Web, using a server as extension to the NASA Field System. As the software has direct access to the status information about the current observation (schedule, scan, source,etc.) and the telescope (current state, temperature, pressure, etc.) in real-time, these useful information can also be offered as input to a central VLBI network status monitoring. This is the point where IVS Live meets e-RemoteCtrl, so that such information are now, for part of it, included into the IVS Live Web interface, providing a convenient global network vision of any IVS session.

Keywords IVS activities, dynamic Web site, remote control, real-time data

1 Introduction

The International VLBI Service for Geodesy and Astrometry (IVS) supports geodetic, geophysical and astrometric research and operational activities for the Very Long Baseline Interferometry (VLBI) technique, as for example, organizing and coordinating all the VLBI observing sessions. Even if most of these sessions are currently controlled and attended locally at the radio telescopes, a new observing method, generically called “remote control”, is being developed and tested in the past few years. This method allows to conduct and control sessions remotely, shared between different world-wide telescopes or completely unattended. These new control methods are now routinely possible, using a dedicated software extension to the existing NASA Field System. This software with the name “e-RemoteCtrl”[1] is developed and maintained at the Geodetic Observatory Wettzell (Germany) (Neidhardt (2011)).

In parallel, the “IVS Live” dynamic web site[2], developed at the Laboratoire d’Astrophysique de Bordeaux (France), may be used to follow the progression of any IVS session based on its predetermined schedule. It also provides a convenient way to navigate through past or coming sessions, or search and display specific information about sessions, sources (like VLBI images) and stations. As the “e-RemoteCtrl” software has a real-time access to the status information about the current observation and the telescope, these useful information can also be offered as input to a central VLBI network status monitoring. This is the point where IVS Live meets e-RemoteCtrl, so that such information complete the schedule-based information of the IVS Live Web site, providing a convenient global network vision of any IVS session.

The first section presents a brief summary of the major IVS Live capabilities. The inclusion of real-time data provided by e-RemoteCtrl into the IVS Live Web page is described in the second section. Finally, the last section presents e-QuickStatus, the data stream which allows the sharing of radio telescopes real-time information from e-RemoteCtrl to IVS Live.

Arnaud Collioud
Laboratoire d’Astrophysique de Bordeaux, Université de Bordeaux – CNRS, 2 rue de l’observatoire, F-33271 Floirac Cedex, France
Alexander Neidhardt
Forschungseinrichtung Satellitengeodäsie, Technische Universität München, Geodätisches Observatorium Wettzell, Sackenrieder Straße 25, D-93444 Bad Kötzting, Germany

[1] e-RemoteCtrl is available at http://www.econtrol-software.de/
[2] IVS Live may be accessed at http://ivslive.obs.u-bordeaux1.fr/

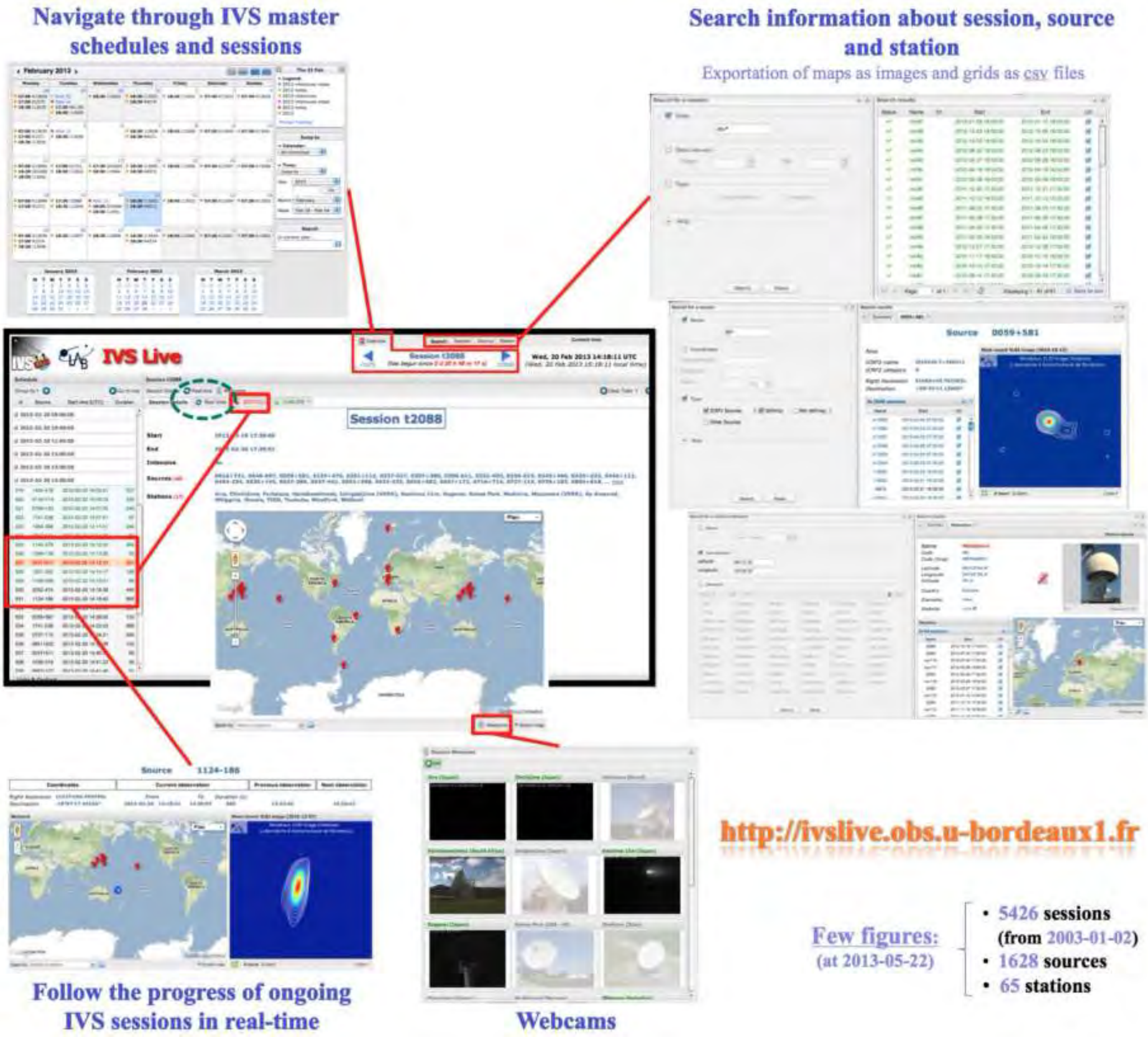

Fig. 1 The IVS Live functionalities displayed as a single montage. The main interface is located in the center (inside the black box). All around it are displayed screenshots of the main features of IVS Live along with the way to access them indicated as red/gray rectangles and lines. The dashed-green/gray circle corresponds to the new “real-time data” functionality (see Section 3).

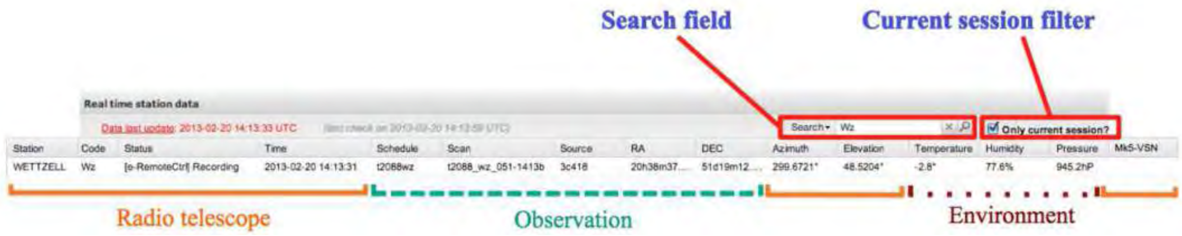

Fig. 2 Example of IVS Live real-time data captured during the IVS session t2088 (2013-02-19) at 14:13:59 UTC for the radio telescope Wettzell (Germany). Only the line which contain the string "Wz" for the currently loaded session is displayed.

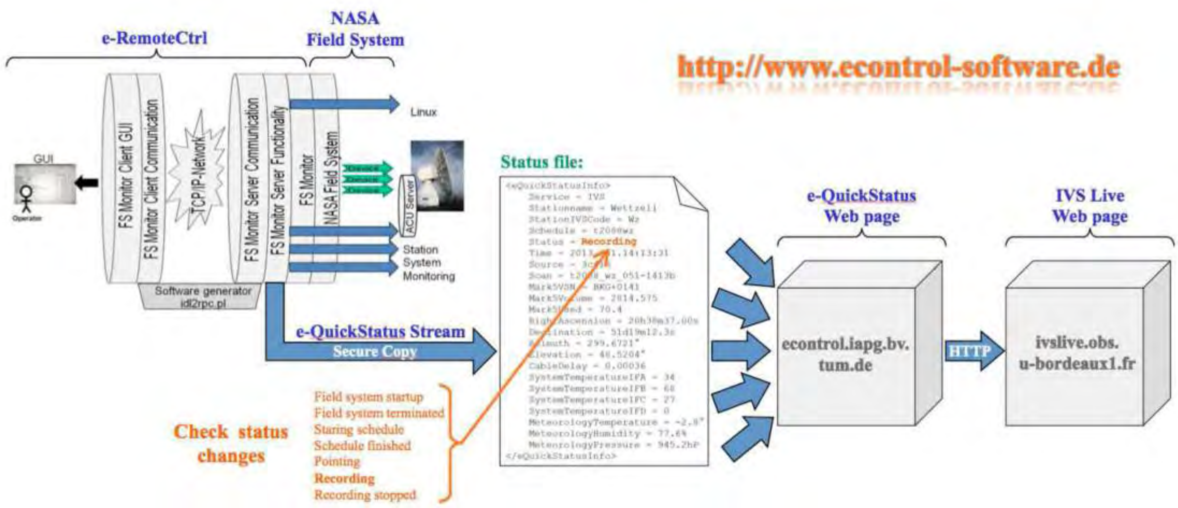

Fig. 3 Providing real-time data from radio telescopes to IVS Live. e-RemoteCtrl provides a status stream, named e-QuickStatus. Every second, and when the status changed, the status file is updated and copied to a dedicated server, then displayed on the e-QuickStatus Web page. From here, the data is fetched by IVS Live which centralizes the display of the real-time data and the monitoring of the session.

2 IVS Live description and capabilities

The IVS Live main reason of existence is the monitoring of IVS sessions. It is a fully dynamic Web site developed in javascript and PHP, with a MySQL database as back-end, which contains 5426 sessions (starting from 2 January 2003), 1628 sources and 65 stations at present. IVS Live is organized as a single user interface divided into several sub-panels (schedule of the session, main panel with an overview of the session, etc.). By default, the ongoing IVS session (if any) or the next coming session is displayed. While the session is running, the main interface is automatically updated thanks to a synchronization procedure with the displayed master clock. For example, a new tab is created in the main panel for each source once a new observation begins. An interesting feature is to have a look at the "Webcams" page during the session progress.

In addition to be a monitoring tool for IVS sessions, you may also use IVS Live to look for a given session thanks to the "Calendar" tool, which provides a convenient way to navigate through all IVS master schedules (from 1979 to 2013 thus far). If you want to retrieve information about a specific session, source, or station, you may query the IVS Live database using the corresponding search forms. Each such query leads to a list of results, which may be exported as a csv (comma-separated values) file. For example, on the one hand a session search results in the list of the matching sessions. On the other hand source and station queries result in a list of matching sources or stations with links to additional details (e.g., position, images, map location, webcam link, and list of sessions which include the selected source or station, also exportable as a csv file).

The major IVS Live functionalities are summarized in Figure 1. For more details, a full description of the IVS capabilities is available in Collioud (2011).

3 IVS Live and real-time data

All information displayed in IVS Live (with the exception of the webcam streams/images) come from the session schedules, which are frozen before the session start. On the opposite, the "e-RemoteCtrl" software gives access to real-time information about the current observation (schedule, scan, source, etc.) and the telescope (current state, temperature, pressure, etc.), which may be stored on a global monitoring server (see Section 4 for more details).

The real-time information provided by the e-RemoteCtrl software are now available in the IVS Live main interface as a separate tab with the name "Real time" (indicated as a dashed-green/gray circle in Figure 1). This tab contains a table, which displays information related to all radio telescopes using the e-RemoteCtrl software. These information is updated every second. As explained above, some of these information are related to the observation (schedule name, scan name, source name, source coordinates) and the others to the current status of the radio telescope (station name and code, current state, pointing azimuth and elevation, recording Mk5 VSN number) or its environment (temperature, pressure and humidity). An example of real-time values is displayed in Figure 2.

The data table may be filtered by any specific values or strings, which have to be entered into the search field, located above the table (see Figure 2). In addition, the right-hand side check-box allows to only display the real-time data of the the session, which is currently loaded into the IVS Live interface. By default, some data are hidden. But they may be easily displayed thanks to a dedicated drop-down menu.

4 Provinding real-time data: e-QuickStatus

e-RemoteCtrl is a software extension to the NASA Field System to operate and control radio telescopes from remote. Additionally, it broadcasts a stream named "e-QuickStatus" coded in form of status files which contains the status information after each schedule or radio telescope status change, such as the start/end of the schedule, the pointing to the source, the recording of the data, etc. (see Figure 3). After a status change, this file is created and copied with Secure Copy (SCP) to the data collecting Web server, which is located at the Technische Universität München (Technical University Munich, TUM), Germany. To enable the secure copy, a key for the Secure Shell (SSH) is required. It can be requested by any station from the distributor of the e-RemoteCtrl software. While all telescopes, using e-RemoteCtrl, directly have this new ability available, also legacy systems can join. If they implement the file transfer of the status file to the TUM Web server themselves, they can also participate. The TUM server scans the directory for incoming files each second. Each scan updates the local e-QuickStatus Web page. From there, IVS Live fetches the data regularly to present them interactively as described in Section 3.

5 Conclusion

Thanks to the "IVS Live" Web page, which may be used to monitor the IVS observing sessions, and the "e-RemoteCtrl" software (through the e-QuickStatus stream), which broadcasts in real-time the status information about the current observation (schedule, scan, source, etc.) and some radio telescopes (current state, temperature, pressure, etc.), useful information can be accessible to the IVS users, providing a convenient global network view on the VLBI network and on any IVS session.

References

A. Collioud: IVS Live: All IVS on your desktop. In: Alef, W.; Bernhart, S.; Nothnagel, A. (eds.): *Proceedings of the 20th Meeting of the European VLBI Group for Geodesy and Astronomy (EVGA)*, Schriftenreihe des Instituts fr Geodäsie und Geoinformation, Heft 22, pp 14–18, Universität Bonn, ISSN 1864-1113, 2011.

Neidhardt, A.; Ettl, M.; Rottmann, H.; Plötz, C.; Mühlbauer, M.; Hase, H.; Alef, W.; Sobarzo, S.; Herrera, C.; Beaudoin, C.; Himwich, E.: New technical observation strategies with e-control (new name: e-RemoteCtrl). In: Alef, W.; Bernhart, S.; Nothnagel, A. (eds.): *Proceedings of the 20th Meeting of the European VLBI Group for Geodesy and Astronomy (EVGA)*, Schriftenreihe des Instituts fr Geodäsie und Geoinformation, Heft 22, pp 26–30, Universität Bonn, ISSN 1864-1113, 2011.

Status and future plans for the Bonn Software Correlator

W. Alef, A. Nothnagel, S. Bernhart, A. Bertarini, L. La Porta, A. Müskens, H. Rottmann

Abstract We present the present status of the Bonn Correlator Center with emphasis on the geodetic correlation. The correlator center has been operated jointly by the Max Planck Institute for Radio Astronomy in Bonn (MPIfR), the Federal Agency for Cartography and Geodesy (BKG) in Frankfurt with support from the Institute of Geodesy and Geoinformation (IGG) in Bonn. We also discuss the severe requirements of the future VGOS (VLBI2010 Global Observing System) observations on the computing and playback resources and options for dealing with the tremendous increases in bandwidth, data-rate and number of observations.

Keywords correlator, software correlator, VLBI, geodetic VLBI, VLBI2010, VGOS techniques: interferometric, instrumentation: interferometers

1 Introduction

The MPIfR has been operating four generations of hardware VLBI correlators since 1978 — Mark II, Mark III, Mark IIIA, Mark IV (Whitney et al. (2004)). MPIfR and BKG have been jointly operating the Mark IV correlator from January 2000 to December 2012 on a 50:50 basis.

The fifth generation, DiFX (Distributed FX) software correlator, was used at MPIfR in test mode from about 2007 to 2009 (Deller et al. (2007)). Since 2009 all astronomical observations have been processed with the DiFX software correlator. Up to December 2010, geodetic observations were still correlated with the Mark IV hardware correlator, but in December 2010 the Mark IV broke beyond repair. After this event geodesy correlation had to be performed with DiFX too. Since the path into geodetic analysis does not use FITS files, as DiFX produces, some ancilliary programs like `difx2mark4` had to be written and some others like `fourfit` required modification like. These features became available with the DiFX version 2.0.

Walter Alef, Alessandra Bertarini, Helge Rottmann
Max Planck Institute for Radio Astronomy, Auf dem Hügel 69, D-53121 Bonn, Germany
Axel Nothnagel, Simone Bernhart, Alessandra Bertarini, Laura La Porta, Arno Müskens
Rheinische Friedrich-Wilhelms Universität Bonn, IGG, Nussallee 17, D-53115 Bonn, Germany

2 Correlator status

Currently we use DiFX version 2.1 for production. DiFX runs on a High Performance Cluster (HPC see Fig. 1). All the nodes and the Mark 5 units are interconnected through 40 Gbps InfiniBand, but the playback speed remains limited to about 1.5 Gbps due to the maximum playback speed of the Mark 5 units. Local data storage, used mostly for e-VLBI transfers, consists of 11 RAIDs with a total capacity of 230 TB.

Recently both DiFX and the Mark 5 units became more reliable so, for example, a typical 24-hour-long IVS Euro experiment, with 10 stations, data rate of 128 Mb/s, one polarization and one-bit sampling, can be correlated without human intervention within 5 hours.

We wrote a new database for handling experiments and disk modules. This new database `comedia` does not allow one to release a module before all experiments on that module have been correlated and archived. The database can be accessed via a GUI or command line, and interfaces to the MPIfR archive server.

To use the computational capacity of the cluster more efficiently, we installed a batch system. When the cluster resources are idle, the system allows other applications to be executed in batch mode.

Fig. 1 Schematic view of the MPIfR correlator cluster. From right to left: rack with 40 nodes; rack with 20 nodes, 3 control computers, Infiniband switch; rack with fxmanager, 5 RAIDs; rack with 8 RAIDs

Unfortunately some important changes required in some of the DiFX routines could not yet be implemented due to lack of manpower.

3 Correlator usage 2011/2012

A total of 151 R1s, EUROs, T2s and OHIGs were correlated since the last meeting two years ago, as well as 83 of the three-station INT3 e-VLBI observations of one hour duration each. Thirty-six astronomical user experiments comprised of up to 15 stations were correlated.

The correlation time was roughly balanced between astronomical and geodetic processing as foreseen in current agreements between MPIfR and BKG, with a slight excess of geodetic correlation.

4 e-VLBI status

An increasing number of stations prefer to transfer the data via Internet (e-VLBI transfers). Currently, about 60 % of the geodetic data are transferred to Bonn via e-VLBI. The volume of data transferred range between 6 TB to 8 TB weekly.

Five of the storage RAIDs (125 TB total) are connected to the outside world with a 1 Gbps line via DFN / GÉANT. For security reasons, restrictions in the router have been implemented for e-transfer servers since late 2011.

To organize the transfers in an orderly fashion the geodesy VLBI group has set up a web page which shows the active transfers. All available RAIDs at Bonn, Haystack and USNO are listed with their capacity, and free space. Colours green, yellow, red are used to quickly visualize the disk status. Stations can sign up for a transfer and data-rate on this webpage under a first come, first serve policy.

It is expected that in the near future a faster line for e-VLBI might become affordable.

5 Correlation and VLBI2010

The next 5 years will be characterized by the transition from the established dual-band (2.3 GHz/ 8.4 GHz) observations performed with the legacy antennas to VGOS (Petrachenko et al. (2009)). The latter is mainly characterized by small and agile radio telescopes and a wide bandwidth. The VGOS specifications require at least 6°/s slew rates in both antenna axes.

An estimate of the data volume for a typical VGOS session can be calculated as follow. Let us consider about 1500 scans/session observed in 24 hours using four separated frequency bands each 1 GHz wide, each recorded at 4 Gbps, for each polarization. The total recording rate is then about 32 Gbps, which requires two Mark 6 recorders be used in parallel at each station. Considering a slewing time equal to 33 % of the total time, then there will be 57600 s in a day of data collected per station. The total volume of data per station per day will be then about 230 TB. Considering 10 antennas observing the same session, there will be about 2.3 PB per session to be transported and correlated.

Assuming a doubling of disk capacity every 18 months, Mark 6 modules (with 8 disks each) will have at least 32 TB capacity in 2016 requiring 8 modules per station per session. The data shipment both in form of disk module shipment or via e-VLBI will become significantly more expensive.

Currently a geodetic experiment, like an IVS-R1, with 10 antennas, and data rate of 256 Mbps, creates a data volume of about 18 TB per day. This means that VGOS will have an increase in data volume by a factor of 120 leading to a correlation time of four weeks for one day of VGOS observations for the present correlator system. This is definitely an unacceptable situation for the time of full VGOS observing towards the end of this decade.

However, there is some relaxation on the horizon. Currently the maximum Mark 5 playback rate of 1.5 Gbps limits the usage of the cluster to about 20% of its capability. The use of Mark 6 (maximum playback rate about 16 Gbps) will permit a cluster usage of about 100%, which will reduce the correlation time by a factor 5. This means that the processing factor will reduce from 120 to about 25.

Under the assumption of a 32 Gbps recording data-rate for wide-band observations, Tab. 1 shows an overview of the transition period to wide-band sessions and the projected correlator usage based on today's throughput. The second column represents the number of wide-band sessions projected per year (WB sess.). A maximum of 146 sessions represents a share of 40% of the total IVS correlation which is the contribution of the Bonn MPIfR/BKG correlator today.

It takes 25 times as long to correlate a wide-band experiment compared to a legacy observation at 256 Mbps which is about 12 hours wall clock time at the moment. The factor of 25 multiplied with 12 hours, thus, results in a 12.5 (full) day processing time (CPU time) for a single VGOS session. So, the third column shows the expected number of correlator days needed for the correlation (in addition to the legacy sessions) if the number of nodes in the cluster and its capabilities remain constant.

Year	WB sessions	correlation days	corr. days with new clusters *
2013	1	13	13
2014	6	75	75
2015	12	150	19*
2016	24	300	38
2017	48	600	75
2018	96	1200	150
2019	121	1513	189
2020	146	1825	40*

Table 1 Summary of the expected evolution of CPU time to meet the VGOS requirements (correlation days of 24 hours each) with the computing cluster being replaced completely in the years 2014 and 2019.

Assuming only a few wide-band sessions in 2013 and 2014, the correlation requirements will outdate the existing correlation capacity within the geodesist's share of 50% of the correlator usage already in 2015. This does not even take into account that the narrow band sessions with legacy antennas will continue to contribute a significant share of the overall correlation for some time to come. From 2016 onwards, the correlation volume would go beyond the cluster's capacity even if the geodesists would fully occupy the installation.

The correlation demand of VGOS can only be satisfied if the cluster is modernized in regular intervals. For a projection of future capabilities, Moore's Law predicts a factor of 2 increase in computing power every 2 years. Since the current cluster has gone operational in 2008, this year has to be taken as the basis (= 1). The last column lists the correlation time under the assumption that complete replacements of the cluster will take place in the years 2014 and 2019. This will lead to a considerable reduction in processing time from the following years onwards. However, a replacement of the cluster in 2014 will only bring relieve until about 2017. When the number of VGOS sessions will be increased by a factor of two again in 2018, a cluster modernization has to be preponed or alternative solutions have to be found.

6 Extending the Bonn correlation cluster

The gloomy predictions expressed in Table 1 can only be improved if the HPC in Bonn will be modernized. Since the cluster was bought in 2007 and enlarged in 2008, it has already reached the end of the standard lifetime for a cluster, which is about five years.

Later in 2013 MPIfR will prepare a proposal to the Max Planck Society for renewal of the VLBI cluster in 2014. This time probably other groups in the institute will join in, so that acquiring a bigger cluster makes a lot of sense. The maximum size is defined by the space available (four racks) and the cooling capacity of about 60 kW. A possible configuration could have up to as many as 2000 compute cores along with about 50 Gbps InfiniBand interconnections and new Mark 6 or similar playback units and at least 10 Gbps Internet connectivity.

The chances of approval will increase considerably if BKG will contribute a similar share in the investment as was the case in previous years. This is particularly important because the Twin Telescopes of BKG in Wettzell will be the first and most important contributors to the emerging VGOS network and will, thus, deliver most of the data to be correlated.

7 Conclusions

While the correlation of the present narrow-band VLBI observations can easily be handled by the existing VLBI cluster in Bonn, a massive increase in correlation power will be required for VGOS wide-band observations. The VGOS data volume could be handled at the correlator only with new equipment, requiring a large investment and higher ongoing operating cost in the form of additional man power and electricity.

The scale of the required upgrade exceeds the capacity of the MPIfR alone, and the continued involvement of BKG in VLBI correlation at Bonn is essential to realize the challenging goals of VGOS within the next decades.

References

A.T. Deller, S. J. Tingay, M. Bailes & C. West. DiFX: A Software Correlator for Very Long Baseline Interferometry Using Multiprocessor Computing Environments PASP, 2007, 119, 318-336

A.R. Whitney, R. Cappallo, W. Aldrich, B. Anderson, A. Bos, J. Casse, J. Goodman, S. Parsley, S. Pogrebenko, R. Schilizzi & D. Smythe. Mark 4 VLBI correlator: Architecture and algorithms Radio Science, 2004, 39, 1007

B. Petrachenko, A. Niell, D. Behrend, B. Corey, J. Böhm, P. Charlot, A. Collioud, J. Gipson, R. Haas, T. Hobiger, Y. Koyama, D. MacMillan, T. Nilsson, A. Pany, G. Tuccari, A. Whitney, J. Wresnik. Design Aspects of the VLBI2010 System. Progress Report of the VLBI2010 Committee. NASA Technical Memorandum, NASA/TM-2009-214180, 58 pp., June 2009

Safe and secure remote control for the Twin Radio Telescope Wettzell

A. Neidhardt, M. Ettl, M. Mühlbauer, G. Kronschnabl, W. Alef, E. Himwich, C. Beaudoin, C. Plötz, J. Lovell

Abstract More VLBI stations, more experiments, more data and a faster analysis for a real-time monitoring of earth parameters and reference frames are the goals of the future VLBI2010 network. One key technology is e-VLBI. But also the control might follow to adapt and to manage these new challenges. Therefore the Technische Universität München (TUM), Germany realizes concepts for continuous quality monitoring and station remote control in cooperation with the Max Planck Institute for Radio Astronomy, Germany. The development is funded by the European Seventh Framework program in the three year project Novel EXploration Pushing Robust e-VLBI Services (NEXPReS) of the European VLBI Network (EVN). Within this project, the TUM focuses on developments for a safe, secure and reliable remote control (e-RemoteCtrl) of the NASA Field System with authentication, authorization and user roles to operate and automate radio telescopes, like the new Twin Radio Telescope Wettzell (TTW) at the Geodetic Observatory Wettzell, Germany. One of these telescopes will become operative this year, so that this is a first real-life test for the new control software and realizations.

Alexander Neidhardt, Martin Ettl
Forschungseinrichtung Satellitengeodäsie, Technische Universität München, Geodätisches Observatorium Wettzell, Sackenrieder Straße 25, D-93444 Bad Kötzting, Germany
Matthias Mühlbauer, Gerhard Kronschnabl, Christian Plötz
Bundesamt für Kartographie und Geodäsie, Geodätisches Observatorium Wettzell, Sackenrieder Straße 25, D-93444 Bad Kötzting, Germany
Walter Alef
Max-Planck-Institut fr Radioastronomie, Auf dem Hügel 69, D-53121 Bonn, Germany
Ed Himwich
NASA(GSFC/NVI, Mail Code 698.2, Greenbelt, MD 20771, USA
Chris Beaudoin
MIT Haystack Observatory, Off Route 40, Westford, MA 01886-1299, USA
Jim Lovell
University of Tasmania, Sandy Bay Campus, Maths-Physics Building, Private Bag 86, HOBART TAS 7001, Tasmania

Keywords TWIN telescope, remote control, operational safety, operational security

1 Introduction

On the basis of the future requirements for geodetic radio telescopes as recommended by the International VLBI Service (IVS) [Niell (2005)], the BKG has launched the TWIN project at Wettzell in 2008. Two rapidly moving radio telescopes were built and equipped with a broadband receiving system including the two geodetically used frequency bands S and X. Both telescopes are designed for continuous operation.

To manage the amount of the future observation load, the telescopes can be controlled from remote or should run completely unattended. Therefore it is quite important to guarantee operational stability, access control and security. This is realized within an own software project at the Geodetic Observatory Wettzell.

2 The Twin Radio Telescope Wettzell (TTW)

The antennas of the newly build Twin Radio Telescope Wettzell (TTW) (see fig. 1) are designed and constructed by Vertex Antennentechnik GmbH Duisburg, Germany. They use a radial symmetric reflector concept, which combines the advantages of a dual offset antenna, as low noise temperature, with the advantages of a Cassegrain or Gregory antenna regarding the mechanical stability, the control possibility, and the weight. The advantage of the ring focus antenna is a better illumination of the feed horn. This design is properly suited for broadband feed horns, which need a wider opening angle. As a consequence the feed must be positioned close to the sub-reflector.

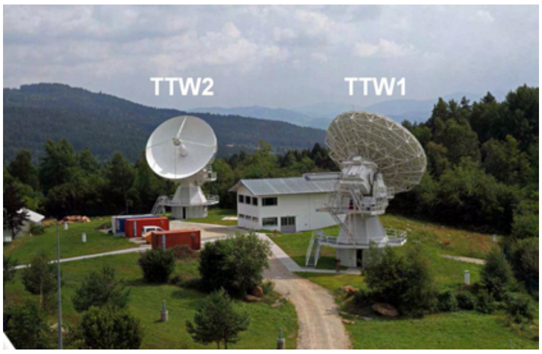

Fig. 1 The two antennas of the Twin Radio Telescope Wettzell.

The further technical data of the antennas are:
- Diameter Main reflector: 13.2 m
- Diameter sub-reflector: 1.48 m
- Ring Focus Design with f/D = 0.29
- Surface quality of the reflectors: < 0.2 mm RMS
- Way length error : < 0.3 mm
- Surface quality of the panel: < 0.065 mm RMS
- ALMA mounting with angular velocities
- Angular velocities of $12°/s$ in azimuth and $6°/s$ in elevation
- Acceleration: Az/El = $3°/s^2$
- Ranges of rotation: Azimuth $540°/s$, Elevation $0-115°/s$
- Balanced outrigger
- Excellent bearing
- 27 bit encoder: $0.0003°/s$ resolution
- Sub-reflector adjustable via a hexapod

The VLBI2010 concept [Niell (2005)] also suggests a broadband receiving bandwidth of 2 - 14 GHz, with the option to integrate the Ka-band (28 - 36 GHz). Realizing these ideas, new receiving systems had to be developed. Such a system must ensure homogeneous illumination of the main reflector, must have a stable phase center, and a system-noise temperature below 50 K. BKG has commissioned a tri-band feed horn (see fig. 2) that is able to work in the two geodetic frequency bands (S/X-Band), and also in the Ka-band. With this feed the participation in all standard VLBI and deep space network observations is possible to make a substantial contribution to the improvement of the celestial reference frame in the Ka-band. The Eleven feed of Prof. Kildal (Chalmers University, Sweden) presently offers the best preconditions for the reception of a continuous frequency range of 2 to 14 GHz. Extensive simulations showed good performance of the feed up to 10 GHz. From 10 to 14 GHz the performance is also suitable. Problems with the ohmic attenuation of the copper lines and the differential outputs are solved by cryogenic cooling and the use of special low-noise-amplifiers.

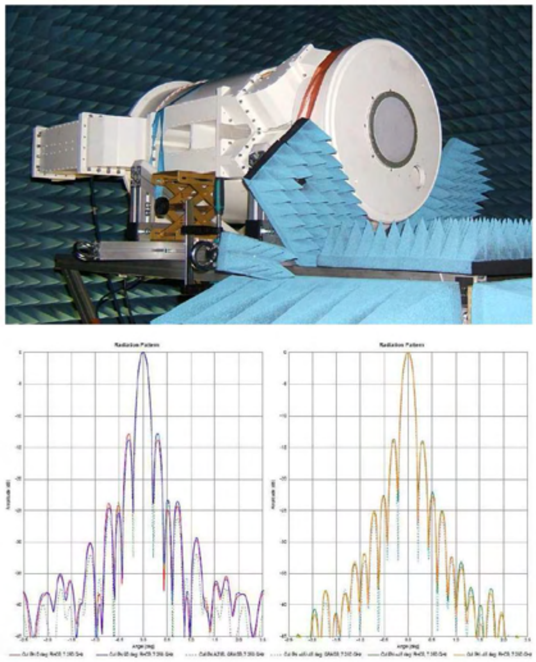

Fig. 2 The tri-band coaxial feed in anechoic chamber and its far field beam patterns, it it is installed on one of the Twin antennas.

The performance of the tri-band feed in numbers:
Frequency bands:
- S-band: 2.2 - 2.7 GHz
- X-Band: 7.0 - 9.5 GHz
- Ka-band: 28 - 33 GHz

Insertion loss:
- S-band : < 0.12 dB
- X-Band: < 0.08 dB
- Ka-Band: < 0.5 dB

Return loss:
- S-band : > 25 dB
- X-Band: > 20 dB
- Ka-Band: > 35 dB

The performance of the used dewar in numbers:
Cold head: T1 = 9 K and T2 = 25 K
LNA noise temperature:
- S-band : < 20 K
- X-Band: < 12 K
- Ka-Band: < 35 K

LNA-gain:

- S-band : > 40 dB
- X-Band: > 30 dB
- Ka-Band: > 25 dB

The TWIN radio telescopes are especially developed for geodetic applications. All components are designed for high availability and precise tracking of 1000 sources per day on 360 days per year. All telescope components are also designed for extreme load cases (wind, gravity effects, temperature) to guarantee the specified stability. The sub-reflector can be adjusted by a hexapod for gravity corrections.

3 The control of the Twin Radio Telescope Wettzell (TTW)

Even if most of the observation sessions are currently controlled and attended locally at the radio telescopes, new observing methods are being developed and tested in the past few years (see fig. 3). These methods allow to conduct and control sessions remotely, shared between different world-wide telescopes or run completely unattended. These new control methods are now routinely possible and will be used for the control of the Twin telescopes. The background is the usage of a dedicated software extension to the existing NASA Field System, which is used on each site to run the operations. This remote control software with the name ”e-RemoteCtrl”[1] is developed and maintained at the Geodetic Observatory Wettzell, Germany [Neidhardt (2011)].

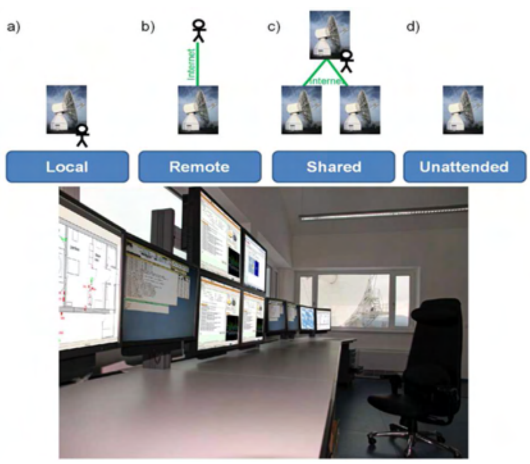

Fig. 3 The new control strategies, which are enabled in the new operators room of the TTW.

[1] e-RemoteCtrl is available at http://www.econtrol-software.de/

While the software is already used now for several years to run the local weekend sessions [Neidhardt (2010)], new extensions allow a higher security and safety. The current version of the software generator ”idl2rpc.pl” information [Neidhardt (2009)]), which is used for generating the communication layer of the remote control, was extended to support authentication and authorization techniques. The authentication is based on the Linux user authentication mechanism. Therefore a system user with a valid user name and password can be authenticated to connect to a telescope. In order to prevent potential security issues while transferring data over the Internet, the connection between the remote operator (client) and the telescope (server) is encrypted, using a save connection based on the Secure Shell (SSH) network protocol. Therefore the control computers of the Twin telescope can also be protected behind a firewall, which then can be tunneled with SSH. A tool for an automatic connection control (*sshbroker*) was developed to (re-)establish the connection automatically after a potential breakdown of the connection to the telescope. In order to increase security at the client side the required password to tunnel through firewalls and for authentication can be stored, using the AES-256 encryption standard [Ettl (2012)].

In order to give the telescope-staff the possibility to control the access rights on their system, a role management is important. Each client, which is allowed to access a telescope, is associated to a dedicated role. A set of available roles is shown in fig.4. These roles are categorized into dynamic and static roles. A static role is a fixed role with no changes at all. A dynamic role is used for remote operators, temporarily taking over the control as operator. In between they simply monitor the system passively. The changing of the active control is realized by a three-way-handshake strategy, to ask and inform all responsible operators about the handover of the control [Ettl (2012)].

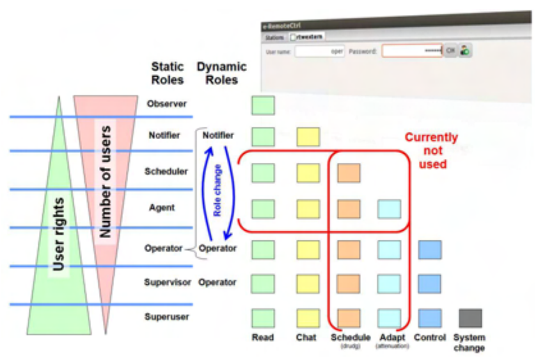

Fig. 4 The available user roles for operators of the TTW.

The local safety of the system is realized with an additional equipment of a System Monitoring. It uses different sensors (temperature, power, current, inertial position), which data are then registered, evaluated and stored. It can produce alarm levels to stop the control. The development of such a system is currently under progress.

4 Conclusion

The operation of the Twin Telecope Wettzell with its predicted load of observations is not possible without technologies, which enable unattended and remote observations. These technologies not only reduce the burdens of shifts for the three telescopes at Wettzell but additionally enable, that local engineers can do their maintenance, research and development work, even under the heavy load of coming observations. The remote control is a proofed technique now, as it was used for several years at Wettzell. The new mechanisms offer the operational control of the new telescopes together with the existing.

References

Ettl M.; Neidhardt A.; Schönberger M.; Alef W.; Himwich E.; Beaudoin C.; Plötz C.; Lovell J.; Hase H. e-RemoteCtrl: Concepts for VLBI Station Control as Part of NEXPReS. In: Behrend, D.; Baver, K.D. (eds.) Launching the Next-Generation IVS Network, IVS 2012 General Meeting Proceedings, NASA/CP-2012-217504, pp 128–132, National Aeronautics and Space Administration, 2012 http://ivscc.gsfc.nasa.gov/publications/gm2012/ettl2.pdf, Download 2013-05-28.

Neidhardt, A. Manual for the remote procedure call generator idl2rpc.pl. Geodetic Observatory Wettzell, 2009.

Neidhardt, A.; Ettl, M.; Plötz, C.; Mühlbauer, M.; Hase, H.; Sobarzo Guzmán, S.; Herrera Ruztort, C.; Alef, W.; Rottmann, H.; Himwich, E.: Interacting with radio telescopes in real-time during VLBI sessions using e-control. In: Proceedings of Science (PoS) - 10th European VLBI Network Symposium and EVN Users Meeting: VLBI and the new generation of radio arrays, EID PoS(10th EVN Symposium)025, Scuola Internazionale Superiore di Studi Avanzati (SISSA), 2010.

Neidhardt, A.; Ettl, M.; Rottmann, H.; Plötz, C.; Mühlbauer, M.; Hase, H.; Alef, W.; Sobarzo, S.; Herrera, C.; Beaudoin, C.; Himwich, E.: New technical observation strategies with e-control (new name: e-RemoteCtrl). In: Alef, W.; Bernhart, S.; Nothnagel, A. (eds.): *Proceedings of the 20th Meeting of the European VLBI Group for Geodesy and Astronomy (EVGA)*, Schriftenreihe des Instituts fr Geodäsie und Geoinformation, Heft 22, pp 26–30, Universität Bonn, ISSN 1864-1113, 2011.

Niell, Arthur; Whitney, Alan; Petrachenko, Bill; Schlüter, Wolfgang; Vandenberg, Nancy; Hase, Hayo; Koyama, Yasuhiro; Ma, Chopo; Schuh, Harald; Tuccari, Gino: VLBI2010: Current and Future Requirements for Geodetic VLBI Systems. Report of Working Group 3 to the IVS Directing Board. GSFC/NASA 2005. http://ivscc.gsfc.nasa.gov/about/wg/wg3/IVS_WG3_report_050916.pdf, Download 2013-01-19.

First results with the GGAO12M VGOS System

A. Niell, C. Beaudoin, R. Cappallo, B. Corey, M. Titus

Abstract The first geodetic sessions with the new VLBI2010 broadband system were carried out in 2012 October using the new 12m antenna at GGAO and the 18m antenna at Westford. For the two six-hour sessions approximately 33 scans per hour were observed. In one session sources within a 40° cone of sky to the south centered on the collocated SLR system were excluded in order to avoid possible damage to the frontend by the SLR aircraft avoidance radar. The horizontal (H) and vertical (V) polarizations for each antenna were correlated and analyzed separately. The standard deviations of the four estimates (2 days, 2 parallel polarizations) for the Up component of GGAO relative to Westford, and the baseline length, are 0.7 mm and 1.3 mm, respectively. The standard deviations of the GGAO East and North components are 2.5 mm and 1.3 mm.

Keywords GGAO, Upgrade, Dynamic Range, SEFD, Receiver

1 Introduction

The broadband instrumentation for the next generation geodetic VLBI system, previously called VLBI2010 but now referred to as VGOS (for VLBI2010 Geodetic Observing System), has been implemented on a new 12m antenna at Goddard Space Flight Center near Washington, D.C., and on the Westford 18m antenna at Haystack Observatory near Boston, Massachusetts, USA. In 2012 October the first two geodetic observing sessions, each of six hours duration, were conducted using the broadband system, and in 2013 May the first 24-hour session was conducted.

The new features for the VGOS system are:

- four bands of 512 MHz each, rather than the two (S and X) for the Mark4 systems
- dual linear polarization in all bands
- 2 GHz aggregate bandwidth vs. 128 MHz aggregate bandwidth for the Mark4
- more than 30 scans per hour due to the short scans and relatively high slew rates of the smaller antennas proposed for VGOS systems
- multitone phase cal delay for every channel in both polarizations
- group delay estimation from the full spanned bandwidth (~2.2 GHz to potentially 14 GHz)
- estimation of the ionosphere TEC difference between sites simultaneously with the group delay, using the phases across all four bands

Implementation of the features indicated in the last three bullets has required changes in analysis of the geodetic delays, and these changes have been implemented in the post-correlation fringe-fitting software *fourfit*.

2 The observations

For the first two sessions the frequency range spanned by the four bands was limited by the hardware capability at the time of the observations. The low-edge frequencies for the lowest and highest bands were chosen to be 3200 MHz and 9344 MHz. A simulation by Bill Petrachenko found that the best frequencies for the other two bands were 5248 MHz and 6272 MHz.

While the goal for the VLBI2010 systems is to reduce the scan length to the minimum in order to obtain the greatest temporal density of sources, the minimum scan length for these sessions was chosen to be 30 seconds to ensure high SNR. A conservative bound was used due to uncertainty in the measured sensitivity of the antennas and in the scaling factors used for the SEFDs in *sked*.

MIT Haystack Observatory, Westford, MA 01886, U.S.A.

These considerations resulted in an observation rate of approximately 33 scans per hour for the first two sessions and 48 scans per hour for the 24-hour session. (The reduced number in the first two sessions resulted from an inadvertent error in the specification of the cable wrap for GGAO12M.) These scan rates are about double and triple the rates for the usual IVS R1 schedule.

A problem that was not anticipated until observations were first made with an earlier proof-of-concept system at GGAO is the strong impact of the SLR aircraft avoidance radar on the VLBI system. The radar signal, at about 9.3 GHz, is strong enough to saturate, or even to damage, the VLBI front end. It is now recognized that the VLBI antenna must avoid pointing too close to the radar when the SLR system is tracking. This means that a cone of the sky with an opening angle of about 40 degrees must be excluded.

Six-hour sessions were scheduled for adjacent days in 2012 Oct. On the first day the SLR systems at GGAO did not observe, so the radar was off and a mask on the sky available to the VLBI observations was not required. On the second day the SLR system was observing, the radar was on, and the VLBI schedule avoided the danger zone. The same number of observations was obtained on the two days, but there is a decrease in geometric strength on the second day along the direction to the SLR system (azimuth 195°) due to the loss of scheduled observations in that direction.

Each of the four bands was sampled and formatted in an RDBE-H digital backend running FPGA code version 1.4 which produced eight 32 MHz channels in each polarization. The output from each RDBE was recorded on a Mark5C.

Phase calibration pulses were injected between the feed and the low noise amplifier to produce tones every 5 MHz in the spectrum.

3 Correlation and observable extraction

The data from the October sessions were correlated on the DiFX software correlator at Haystack Observatory. A separate correlation pass was required for each band, but both the polarization parallel-hands and cross-hands of a scan were correlated in that pass. For each scan *fourfit* was used to obtain a coherent fit to all phase and amplitude observables for all 1-second accumulation periods in the scan.

The instrumental delay from the pulse cal injection point to the digitization point was calculated within *fourfit* for each channel using all of the phase cal phases in that channel.

The estimation of the coherent amplitude, delay, and TEC difference was achieved using recent improvements in the program *fourfit*, and the new capabilities of the VGOS systems require additional steps.

The steps are:

- *fourfit* the four polarization correlation products separately for each band to obtain amplitude, delay, phase, and delay rate (16 values of each)
- merge the data from the four bands and polarization products into one file
- input an *a priori* station delay from the point of phase cal pulse insertion on the antenna to the digitization point in the control room based on the length of the cable
- input an *a priori* difference in TECs between the sites
- *fourfit* the merged data for each of the four polarization products for one or more strong sources to verify (or adjust) the station delays and to determine the phase and delay offsets among the bands
- *fourfit* the merged data for all bands of each of the polarizations to find the amplitude, delay, phase, and delay rate for the individual polarizations
- *fourfit* the merged data combining all bands and polarizations to form the Stokes I visibility and its associated amplitude, delay, phase, delay rate, and ΔTEC

The extracted observables were exported to GSFC where databases for the parallel hands and for I were generated by David Gordon; this required modification of the *dbedit* software in order to bring in the delay with ionosphere (charged particle dispersion) already estimated.

4 Analysis

The geodetic analysis was done using *nuSolve*, a new GUI-based program for editing and parameter estimation that is being developed by Sergei Bolotin of GSFC. *nuSolve* was used because of the potential to model the clocks and atmospheres as stochastic processes. However, for the period covered by this report the temporal modeling of these parameters was piecewise linear (PWL). The estimated parameters for the results reported below are the position of GGAO12M, and atmosphere zenith delays and gradients and clock values for both sites. Various time intervals from 2 hours down to 10 minutes were tested for all of the atmosphere and clock parameters. This process was applied to the parallel-hands (H and V) and to I for both days. However, the H and V delay analysis did not include estimation of the ionosphere since the baseline is so short. On the other hand, the results for I are not presented in this report due to uncertainty in the correlation of phase errors and the ΔTEC estimate.

A series of trials with varying intervals for atmospheres, atmosphere gradients, and clocks indicated that consistent results and minimum RMS delay scatter could be obtained using 20-minute intervals for the atmosphere zenith delays and clocks and 40 minutes for the atmosphere gradients. The default constraints included in the *nuSolve* setup were not adjusted. Outliers were excluded in an iterative process of estimation, outlier rejection, and re-estimation, leaving approximately 140 of the original 178 points in the solution. These observations should be examined carefully to determine if the cause for being an outlier can be ascertained.

The delay uncertainties for all observations, not scaled for scatter in the phases, have a median value of less than one picosecond. Taking the scatter into account results in delay uncertainties of about 4 psec. After arriving at a set of estimated parameters and retained observations, the additional quadratically-added delay required to obtain chi-square per degree of freedom of 1.0 was calculated within *nuSolve* (a process known as re-weighting). The additive delay value for both days is about 12 psec. This is not unexpected due at least in part to the PWL parameterization of the atmosphere and clock values.

5 Results

The H and V polarization observables are statistically independent as far as system noise is concerned, and thus they provide two separate solutions. However, other sources of noise, such as the atmosphere delay, source structure and positions, and clock variations, are almost completely correlated. Therefore the agreement of the estimated parameters for H and V should be much better than the formal uncertainties.

The topocentric offsets from the mean position for GGAO12M, and the estimates of baseline length relative to the mean are shown in Figure 1. The agreement among the components and length for H and V is reasonable. The standard deviations of the four estimates (2 days, 2 polarizations) for the baseline length and for the Up component of GGAO relative to Westford are 1.3 mm and 0.7 mm, respectively. The standard deviations of the GGAO East and North components are 2.5 mm and 1.3 mm.

Delays obtained from the phasecal signals indicate that there is a large (~30 psec) dependence of the delays on the direction the antenna is pointing for both Westford and GGAO12M. If the variations were in the signal path from the receiver to the digital back end, the multitone delays would correct them. However, there is evidence that the variation occurs in the 5 MHz uplink cable, in which case the delays are not corrected. Most of the variation is in azimuth for Westford. Since azimuth-dependent delay errors primarily affect the horizontal position, this variation in delay with azimuth, coupled with a slightly different schedule on the two days, may be at least partly responsible for the larger scatter in the East component between the two days. Detection of this effect in the VGOS systems emphasizes the need for a cable delay calibration system.

6 24-hour session

On 2013 May 12 the first 24-hour session took place using GGAO12M and Westford. The session was run under Field System control with a setup identical to the sessions described above. Sources stronger than 0.2 Jy were observed with a minimum scan length set to 30 seconds. For some of the weaker sources the scans were as long as 48 seconds. This was the result of requiring a minimum SNR of 15 in each polarization for each band. Approximately 48 scans were observed per hour. In the completed correlation, out of the approximately 1136 total scans, only six were not detected. The first analysis effort will be to calibrate the fringe amplitudes to obtain correlated flux densities for comparison with expected values. A geodetic analysis will follow using *nuSolve*.

7 Plans

Regular observations using the 12m and Westford are scheduled to begin mid-2013, including participation in R1, RDV, and two-station VGOS sessions of the type described here. The correlation and data analysis chains (DiFX correlator/*fourfit*/*solve*) for the standalone Broadband observations (VGOS) and for the mixed Broadband-Mark4 observations (R1 and R4) need to be further developed and made operational.

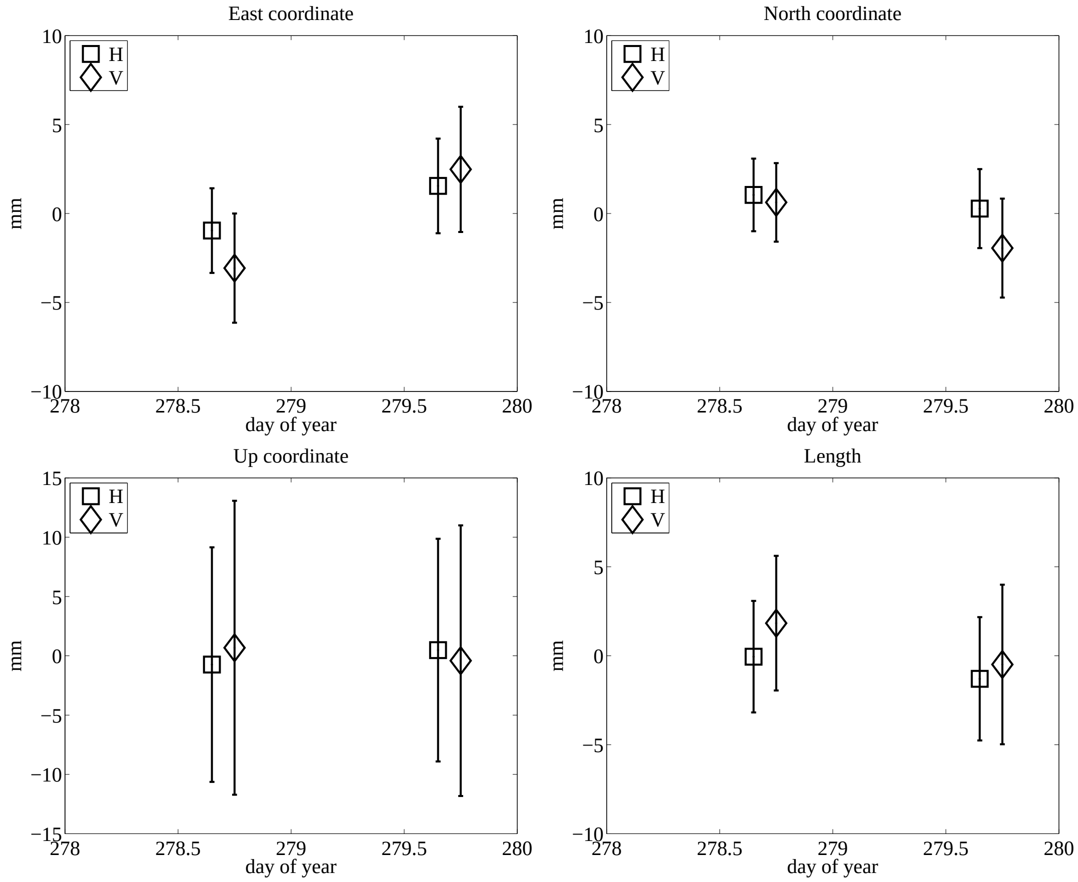

Fig. 1 Adjustments to the topocentric position of the GGAO12M position and to the length of the baseline for H and V polarizations.

8 Acknowledgments

We thank the other members of the Broadband Development Group for their efforts in constructing, implementing, and operating the systems at GGAO and at Westford and for assisting in the testing and observations; John Gipson for guidance in getting *sked* to work; David Gordon for getting the broadband output into databases; and Sergei Bolotin for developing *nuSolve* and for help getting it to work with the new broadband observable.

The Broadband Development Group includes:

- MIT Haystack Observatory
  C. Beaudoin, J. Byford, R. Cappallo, B. Corey, M. Derome, A. Hinton, R. McWhirter, A. Niell, M. Poirier, C. Ruszczyk, A. Rogers, D. Smythe, J. SooHoo, M. Titus, A. Whitney, B. Whittier
- NASA GSFC
  C. Ma
- GSFC/NVI
  T. Clark, E. Himwich
- HTSI
  P. Christopolous, I. Diegel, M. Evangelista, S. Gordon
- ITT
  R. Allshouse,W. Avelar, R. Figueroa, C. Kodak, K. Pazamickas, J. Redmond

VGOS RFI Survey

B. Petrachenko, B. Corey, C. Beaudoin

Abstract Radio Frequency Interference (RFI) is one of the major risk factors for successful operation of the new VGOS broadband system. Strong RFI within the 2–14 GHz VGOS band could drive the receiver electronics into nonlinear operation and thereby degrade the system sensitivity at all frequencies. RFI survey data taken at 22 locations around the world have been analyzed to ascertain the likelihood this would occur. Much of the data is limited in angular and temporal coverage. To the extent the data represent faithfully the RFI environment, we find that, except at a few sites, RFI-driven nonlinear effects should not limit VGOS sensitivity, provided antenna pointing masks of order 10° in radius are placed around a few RFI sources.

Keywords RFI, VLBI2010, VGOS

1 Background

VGOS-compatible receiving systems incorporate various approaches to reduce the detrimental effects of RFI over the 2–14 GHz input frequency range. These include flexible tuning of the downconverters, to avoid spectral regions of strong RFI, and high isolation between frequency channels, to reduce RFI spillover into adjoining channels. But if the RFI is sufficiently intense, it can saturate the frontend electronics and degrade the sensitivity over the full 2–14 GHz range.

The risk to successful VGOS operations from saturation by RFI was clearly recognized at the IVS VLBI2010 Workshop on Technical Specifications at Bad Kötzting, Germany, in March 2012. In response, the VLBI2010 Project Executive Group (V2PEG) initiated an investigation into the broadband RFI environment at potential VGOS sites. In the initial phase, sites were asked to submit any existing RFI-related data, without regard to the data format or how much of the 2–14 GHz range was covered. The intent was to get an impression of the severity of the RFI problem, especially with regard to the likelihood that a broadband frontend might saturate. Here we report the methodology and preliminary results of this initial phase.

B. Petrachenko
Natural Resources Canada, 580 Booth Street, Ottawa, Ontario, Canada
B. Corey, C. Beaudoin
MIT Haystack Observatory, Westford, MA 01886, U.S.A.

Organization	*# Locations*	*Country*	*Freqs. (GHz)*
IAR/BKG	1	Argentina	2–14
GSI	2	Japan	2.0–2.7 & 9.72–9.90
IAA	3	Russia	1–14
Metsähovi	1	Finland	0.4–2.4
NICT	4	Japan	3–14
RAEGE	10	Portugal & Spain	0.5–26.5
Sejong	1	Korea	1.87–2.87
VLBA	10	U.S.A.	7 bands from 0.3 to 16.1

Table 1 Summary of RFI information received

2 RFI survey data

In the 12 months following the Bad Kötzting workshop, RFI information was received from the eight organizations listed in Table 1. Most organizations provided data for multiple locations, as shown in the table.

The data formats, frequency coverage, and data-acquisition methods were highly heterogeneous. RFI levels were reported in many different units, e.g., spectral power flux density (W m^{-2} Hz^{-1}), antenna temperature (K), electric field strength (μV m^{-1}), and power (dBm). Sejong and the VLBA measured RFI levels with their VLBI antennas; all other surveys were done with special-purpose hardware, which consisted essen-

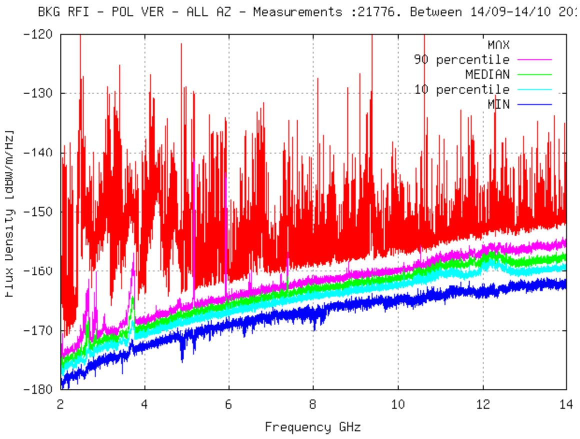

Fig. 1 RFI spectral power flux density statistics for spectra acquired at La Plata, Argentina, over one month. Shown, top to bottom, are maximum, 90th-percentile, median, 10th-percentile, and minimum values. Figure from Hase, Gancio, et al., 2013.

tially of a horn antenna or small dish, an RF amplifier, and a spectrum analyzer. Three of the surveys covered at least 2–14 GHz, NICT spanned 3–14 GHz,[1] and most of the others were restricted to portions of 0.4–2.7 GHz, where the strongest RFI is expected – see table 1. Most surveys were done along the horizon, with the antenna either scanned around 360° in azimuth or pointed in one, four, eight, or twelve discrete azimuth directions; the exception was the VLBA, where the antennas were pointed near the north celestial pole.

Individual spectra were acquired over seconds to a few minutes, typically with the spectrum analyzer set to record the maximum power observed at each frequency. For most surveys only a single spectrum per direction was provided. Given the time-variable nature of RFI, a more complete picture of the RFI environment can be obtained from repeated "snapshot" spectra accumulated over long time spans. Figure 1 presents an example of the statistical information that repeated measurements afford. It also illustrates that a system designed to withstand RFI at its maximum level must be far more robust than one designed for the 90th-percentile level, say.

In this paper we focus on the likelihood that the observed RFI is strong enough to saturate a broadband frontend. Evaluating this risk entails two tasks:

- Calculating, from the RFI survey data, what the RFI level would be at the input to a VGOS frontend, and
- Identifying at what power level the frontend saturates.

We address these matters in the next two sections.

[1] A highpass filter with 3.5-GHz cutoff was installed ahead of the amplifier in the NICT equipment to attenuate S-band RFI that might otherwise have saturated the amplifier.

3 RFI power estimation

The RFI power at the frontend input (or, nearly equivalently, at the output terminals of the VLBI antenna feed) can be expressed as the product of two factors:

1. RFI spectral power flux density integrated over the frequency span of the RFI, and
2. effective collecting area of VLBI antenna.

The first factor is calculated from the RFI survey data. (Data reported in units other than spectral power flux density were converted to this unit with the aid of ancillary information.) The second factor we get from an empirical model, as described in this section.

If a VLBI antenna points directly at a source, the collecting area is typically 0.3–0.7 times the antenna geometrical area. But when an antenna is not pointed right at an RFI source, as is generally the case, the collecting area in the direction of the source is much smaller and is also nearly independent of the physical size of the antenna.

In the absence of maps of the sidelobe and backlobe patterns for VGOS antennas, we resort to empirical models. Figure 2 shows the ITU-R SA.509-2 model (ITU, 1998) for the far-field pattern of large, symmetrical, paraboloid antennas in directions $\theta > 1°$ away from the main beam. This model, which has been validated by pattern simulations and measurements, is commonly employed in RFI studies for telecommunications and radio astronomy. It is a conservative model in the sense that 90% of the sidelobe peaks of a typical antenna should lie below the line in figure 2. Measured sidelobe levels generally agree with the model to within ~10 dB (ITU, 1998; Dhawan, 2002). For $\theta > 1°$ the pattern of most antennas is dominated by scattering off feed support struts or a subreflector and by direct radiation into the feed (spillover). As a result the sidelobe pattern at distances less than the antenna far-field distance (2–14 km for a 12m antenna at 2–14 GHz) is similar to the far-field pattern.

We assume the validity of this model in our analysis. Collecting area is related to gain by

$$\text{area} = \text{gain} \times (\text{wavelength})^2/4\pi.$$

In our analysis the collecting area therefore depends only on direction relative to the main beam and on observing wavelength.

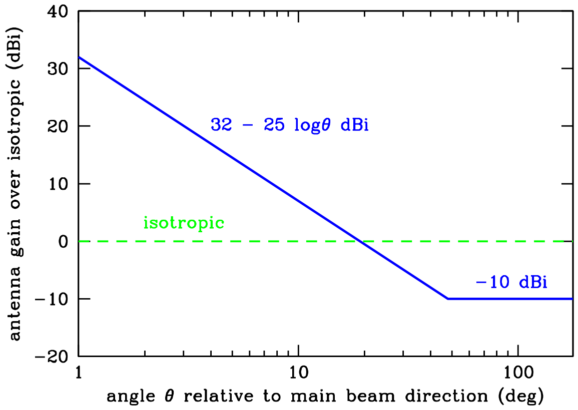

Fig. 2 ITU-R SA.509-2 empirical model for far-field sidelobe antenna gain of large (diameter > 100 wavelengths), symmetrical reflector antennas operating at 1–30 GHz. An isotropic antenna has gain 0 dBi.

4 Frontend saturation

Ideally, analog devices operate in the linear regime, where the output voltage varies linearly with input. In this regime, an input RFI signal at frequency f_0 appears in the output only at f_0. In the presence of strong RFI, however, the device response becomes nonlinear. In such circumstances the RFI appears in the output at harmonic frequencies Nf_0; furthermore, intermodulation products may be generated between multiple RFI signals or between RFI and RFI-free spectral regions. Both effects raise the effective system temperature, and hence decrease the sensitivity, in spectral regions that might otherwise be free of RFI. At still higher RFI levels, the output may saturate ("clip"), and the sensitivity drop to zero.

Simulations (Beaudoin, Corey, and Petrachenko, 2010) of the effects of RFI on VGOS hardware demonstrate that nonlinear effects in a broadband low-noise amplifier (LNA) degrade the SNR by more than a few percent at all frequencies when the input power exceeds IP1dB – 10 dB, where IP1dB is the LNA input 1-dB compression point. For the CITCRYO1-12A LNA used in the GGAO and Westford broadband receivers, IP1dB is nominally –70 dBW; other LNAs have similar values. We therefore identify –80 dBW as the input threshold that should not be crossed.[2] Henceforth we refer colloquially to –80 dBW as the level at which the LNA "saturates".[3]

[2] Devices following the LNA may saturate at RFI levels that do not saturate the LNA itself. We assume here that such signals are removed by post-LNA filters, so that we need worry only about the LNA.

5 Results

In order to summarize all the data in a single plot, we initially ignore the direction dependence of the antenna gain and calculate, by the method outlined in section 3, the RFI power P_{iso} received by a hypothetical antenna with isotropic gain. We did this calculation for the 2–4 strongest RFI signals at each site, excluding the VLBA.[4] For La Plata, P_{iso} was calculated for both the strongest maximum and 90th-percentile levels.

Results are shown in figure 3 for 1–15 GHz. Figure 4 shows the lower-frequency portion where the RFI is concentrated.

The assumption of 0 dBi antenna gain made in calculating P_{iso} is valid only at $\theta = 19°$, according to the ITU sidelobe model (see figure 2). By section 4, we require the received power be < -80 dBW. Therefore, for an antenna pointing $> 19°$ away from an RFI source with $P_{iso} = -80$ dBW, the LNA will not saturate. This threshold is shown as a dashed horizontal line labeled 19° in figures 3 and 4.

For pointing directions other than 19°, the sidelobe model in figure 2 and the LNA input limit of –80 dBW can be combined to produce figure 5. Shown in addition to the –80 dBW threshold for $\theta = 19°$ is the –95 dBW threshold for $\theta = 5°$. The latter threshold is also displayed in figures 3 and 4.

6 Discussion

Two points in figures 3 and 4 are above –80 dBW. The upper one labeled 'J' is so strong that, according to figure 5, a VGOS LNA could saturate when the antenna is pointed anywhere on the sky. The site where this RFI was observed has since been ruled out as a candidate VGOS site by the funding agency. The lower point labeled 'O' is caused by a nearby DORIS transmitter. Avoiding saturation from this signal would entail severely restricting the sky coverage of VGOS observations. Better alternatives include moving the transmit-

[3] True saturation occurs at power levels more than 10 dB higher. –80 dBW is the level at which nonlinearity causes significant SNR degradation.

[4] For this analysis we grouped the ten RAEGE locations into four "sites": Yebes, Santa Marìa and Flores islands in the Açores, and Tenerife in the Canary Islands.

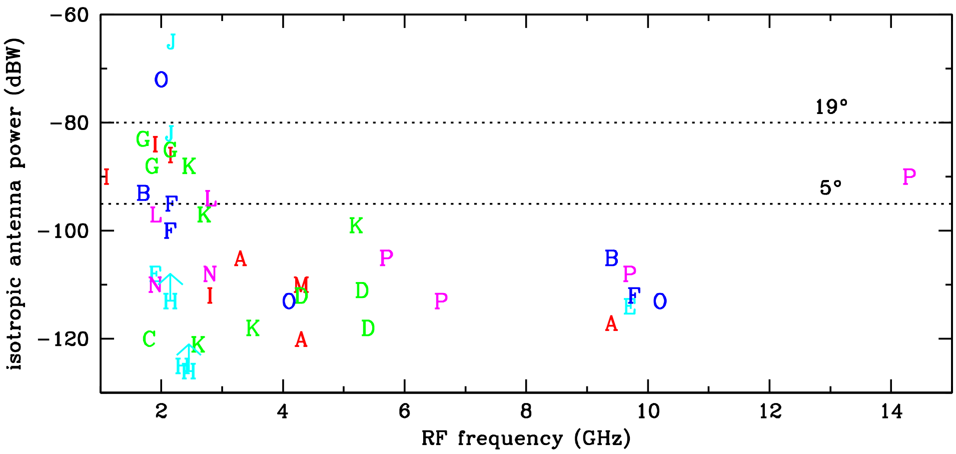

Fig. 3 Power received by a hypothetical isotropic antenna from the strongest RFI signals measured at 16 globally distributed sites, each represented by a different letter. Dashed horizontal lines indicate maximum RFI power level for which LNA does not saturate if antenna is pointed further away from the RFI source than the indicated angle. See section 3 for additional explanation.

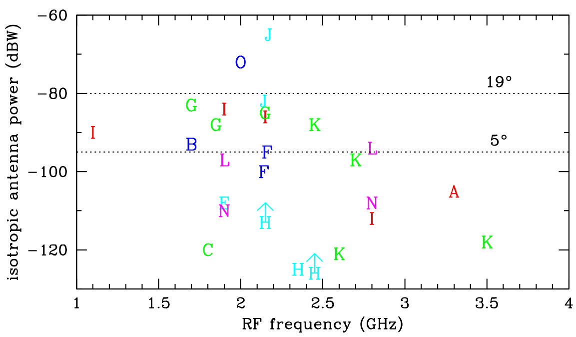

Fig. 4 Same as figure 3 except that frequency range is 1–4 GHz.

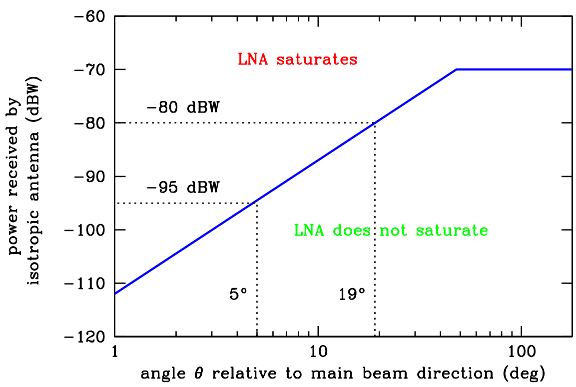

Fig. 5 LNA saturation threshold as a function of RFI level and direction toward RFI source relative to main beam. LNA is expected to saturate in regions above the solid line and not saturate below the line.

ter out of the direct line of sight to the antenna or erecting a barrier between them. Another option is low-loss filtering ahead of the LNA, as with a high-temperature superconducting notch filter.

Two points in the figures are shown as lower limits because an S-band bandpass filter of unknown attenuation at the RFI frequencies was present ahead of the LNA, and the 3.5-GHz highpass filter in the NICT equipment suppressed RFI below 3 GHz by an unknown amount. The RFI at these two sites may therefore be much worse than is portrayed in the figures.

The power level of the other RFI signals in the figures is low enough that saturation can be avoided ~90% of the time by staying 1° – 15° away from each source, depending on the level. However, this conclusion and the P_{iso} levels on which they are based depend critically on several factors including

1. survey power measurement accuracy,
2. accuracy of conversion to power flux density,
3. RFI bandwidth estimation accuracy,
4. antenna sidelobe gain pattern accuracy,
5. degree of completeness of survey sky coverage, and
6. degree of temporal variability of RFI.

Cumulative errors from the first three factors should be <5–10 dB, and averaged over sites they should not bias the estimated power levels one way or the other. An error in the assumed sidelobe pattern will bias the levels for all sites in the same direction, but the bias should be <10 dB. Incomplete angular or temporal coverage can cause underestimation of the worst-case RFI. Surveys along the horizon will miss airborne or satellite RFI.

There are two other potential threats besides saturation that RFI can pose to VGOS. The first is damage to the LNA if the input power level is too high. The LNA damage threshold is typically of order –20 dBW, or 60 dB higher than the saturation threshold defined here. The strongest RFI seen in the surveys (‘J’ in figure 4) would yield –33 dBW at the LNA input if the antenna were pointed 1° from the source. Pointing closer to the source than 1° should be avoided to prevent damage.

The other threat is the more customary one of RFI in the observing band raising the system temperature, even when the system operates perfectly linearly. The sensitivity of these survey data is too low to detect RFI that would double the temperature, say, unless the RFI is extremely narrowband.

7 Conclusions and future work

With a few exceptions, RFI was found to be weak enough that, at worst, a pointing mask of radius < 15° applied toward the stronger offenders should prevent LNA saturation at most sites.

Given the limited temporal and angular coverage of most of the surveys, definitive conclusions about individual sites are not possible. Our results are encouraging, however, and indicate that saturation from 2–14 GHz RFI is not a serious threat to broadband VGOS observations at most sites.

The strongest RFI is below 3 GHz. One scenario for observations during the transition from S/X to VGOS is to have the VGOS antennas at the low-RFI sites observe with legacy S/X systems at S/X and, in separate sessions, with high-RFI VGOS antennas above 3 GHz. Eventually, once the tie between VGOS and S/X networks is well established, all VGOS observing would move to above 3 GHz.

Survey data have been submitted from additional sites since March 2013, and further submissions are encouraged, including from sites where the initial data were limited. As broadband VGOS antennas come on line, data taken with them will also be of great interest. We will update the analysis as new data arrive.

8 Acknowledgments

We thank the staffs at the participating observatories for submitting their RFI data, and we thank Hayo Hase, Guillermo Gancio, and their colleagues for permission to include figure 1.

References

C. Beaudoin, B. Corey, and B. Petrachenko. Radio frequency compatibility of VLBI, SLR, and DORIS at GGOS stations. American Geophysical Union fall 2010 meeting. Online at http://ivscc.gsfc.nasa.gov/technology/vlbi2010-docs/AGUPoster2010.pdf.

V. Dhawan. Far sidelobes of VLA & VLBA 25m antennas at λ 18cm. VLA/VLBA Interference Memo No. 25, NRAO, 2002. Online at http://www.vla.nrao.edu/memos/rfi/25/25.ps.

H. Hase, G. Gancio, et al. Radio frequency interference observations at IAR La Plata. Proceedings of 2013 EVGA meeting, 2013.

International Telecommunication Union. Recommendation ITU-R SA.509-2, 1998. Online at http://www.itu.int/rec/R-REC-SA.509/en.

New VLBI2010 scheduling options and implications on terrestrial and celestial reference frames

J. Böhm, C. Tierno Ros, J. Sun, S. Böhm, H. Krásná, T. Nilsson

Abstract We apply the newly developed source-based scheduling approach in the Vienna VLBI Software (VieVS) to run a series of tests with Monte-Carlo simulations. We find that increasing the number of stations from 16 to 24 and 32 in a VLBI2010 network improves the Earth orientation parameters estimated from 24-hour sessions by roughly 10% and 20%, respectively. On the other hand, we do not find an improvement of the 3D position rms of the individual stations with larger networks. As expected due to the larger number of observations, the formal uncertainties of terrestrial and celestial reference frame coordinates are improved by about 20% with 24 compared to 16 stations in the network, but we also find non-zero mean reference frame coordinates which are probably due to the small number of 25 simulated sessions. Finally, the investigations show that baseline length repeatabilities are improved if we raise the cutoff elevation angle from 5 to 10 and 15 degrees in a 16-station network.

Keywords VieVS, VLBI2010, Scheduling, Terrestrial and Celestial Reference Frames

1 Introduction

The Vienna VLBI Software (VieVS) has been developed at the Department of Geodesy and Geoinformation (GEO) at the Vienna University of Technology since 2008. It is written in Matlab, and it has been equipped recently with scheduling and simulation tools as well as with the ability of running global solutions (Böhm et al., 2012).

In terms of scheduling, the so-called *source-based approach* has been added to the classical *station-based approach* which is also implemented in SKED, the scheduling software maintained at Goddard Space Flight Center. Source-based scheduling in VieVS has been initiated following an idea by Bill Petrachenko and Anthony Searle (both Natural Resources Canada) and it implies that always a certain number of equally distributed sources on the sky is selected for observation. In case of source-based scheduling with two sources, the sources are on opposite parts of the celestial sphere, and in case of source-based scheduling with four sources, they are at the corners of a regular tetrahedron (Sun, 2013).

Compared to the classical station-based approach, source-based scheduling has some advantages and disadvantages. It is faster because there are not so many options to be tested, and it automatically results in a good global distribution of sources on the celestial sphere. On the other hand, source-based scheduling does not optimize the sky distribution above the individual sites; however, a good coverage of the celestial sphere typically implies a good sky distribution above the stations. With more and similar (VLBI2010-) stations in the future source-based scheduling will become more important. The more telescopes participate in a session, the more sources should be observed at a time (i.e., four instead of two).

In this study, we apply the source-based scheduling approach with four sources to answer the following questions: what is the impact of increasing the network size from 16 to 24 or 32 stations on the terrestrial and celestial reference frames and on the Earth orientation parameters (Section 2)? How does the repeatability of baseline lengths and station coordinates change if we raise the cutoff elevation angle from 5 to 10, 15, or 30 degrees (Section 3)?

J. Böhm, C. Tierno Ros, S. Böhm, and H. Krásná
Technische Universität Wien, GEO, Gußhausstraße 27-29, A-1040 Wien, Austria
J. Sun
Shanghai Astronomical Observatory, China
T. Nilsson
GeoForschungsZentrum Potsdam, Germany

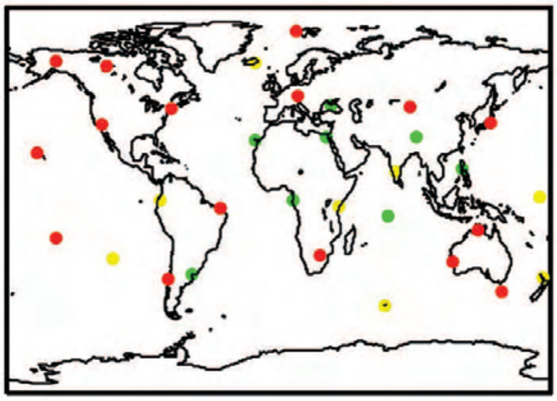

Fig. 1 Observing station network: we start with a network of 16 stations (red circles) and then add two times 8 stations to get a network with 24 (yellow circles) and 32 stations (green circles).

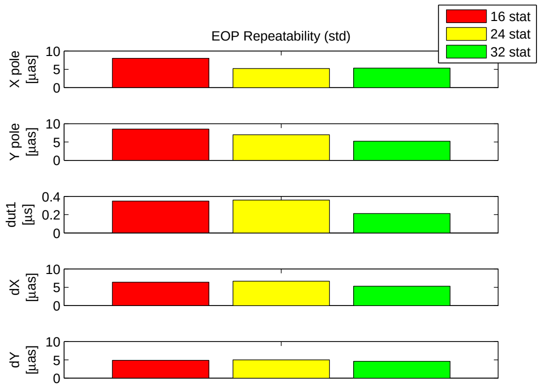

Fig. 2 Standard deviation of Earth orientation parameters estimated with networks of 16, 24, and 32 stations. From top to bottom we show polar motion, UT1-UTC, and nutation.

2 Increasing the network size

We start with a network of 16 fast VLBI2010 antennas (slew rates of $12^o/s$ and $6^o/s$ in azimuth and elevation, respectively, slew acceleration of $12^o/s^2$ in both axes) and then add more stations of the same type to realize a 24- and a 32-station network (see Figure 4 for the distribution of the sites). The global distribution of stations is quite uniform in all three cases.

For scheduling, we use a list of 211 radio sources with a positional accuracy of better than $200\mu as$, with an X-band structure index lower than 3, and which are stronger than $0.25Jy$ at both X- and S-band. The same System Equivalent Flux Density (SEFD) of 2500 is used for all antennas, and the data rate is 8 Gbps (assuming a bandwidth of 128 MHz, a sample rate of 256 MHz, 16 channels, and 2 bits quantification). A minimum SNR of 20 and 15 is required in the schedules for X- and S-band, respectively, and 5/20 seconds are set as minimum/maximum for the scan lengths.

We apply source-based scheduling with four sources observed at a time and a cutoff elevation angle of 5 degrees to create schedules for all three networks. Then we run the VieVS simulator (Pany et al., 2011) to create 25 24-hour simulated observation files for each network. We simulate the reduced observation vectors ($observed - computed$) as sum of slant tropospheric delays, clock random walk series, and white noise per baseline observation. For the description of the tropospheric delay, we apply the turbulence model as proposed by Nilsson et al. (2007) with station-dependent Cn values (Nilsson and Haas, 2010) and constant scale heights of 2 km at all stations. For the simulation of the clocks, we assumed a random walk process with an Allan Standard Deviation (ASD) of $1 \cdot 10^{-14}$@ 50 minutes, and the values of white noise added per baseline observation have a standard deviation of 8 ps.

In the least-squares estimation, we estimate zenith wet delays every 15 minutes, and gradients and clocks every 60 minutes as piecewise linear offsets. A full set of Earth orientation parameters (EOP) is estimated once per 24-hour session. In a first solution, station coordinates are estimated once per 24-hour session with no-net-rotation and no-net-translation (NNR/NNT) conditions on all stations in the network and with the source coordinates fixed. In a second solution we estimated terrestrial and celestial reference frames globally from all 25 sessions of the 16- and 24-station network with NNR/NNT on the same 16 stations and NNR on all sources with more than 100 observations.

As expected, the repeatability (standard deviation) of the Earth orientation parameters (polar motion, UT1-UTC, and nutation) estimated per 24-hour session improves considerably when using larger networks (see Figure 2). Compared to the 16 station network, we find a mean improvement of 8 % for the 24-station network, and a 26 % improvement for the 32-station network.

Next, we use the session-wise estimates of station coordinates to calculate their 3D position root-mean-square (rms) values. Figure 3 shows these values for those 16 stations which are participating in all three networks together with the corresponding numbers of observations. It is interesting to note that - although there are more observations with more stations in the larger networks - the median 3D position rms value over the same 16 stations does not significantly change. It is 1.2 mm, 1.3 mm, and 1.2 mm for the networks with 16, 24, and 32 stations, respectively.

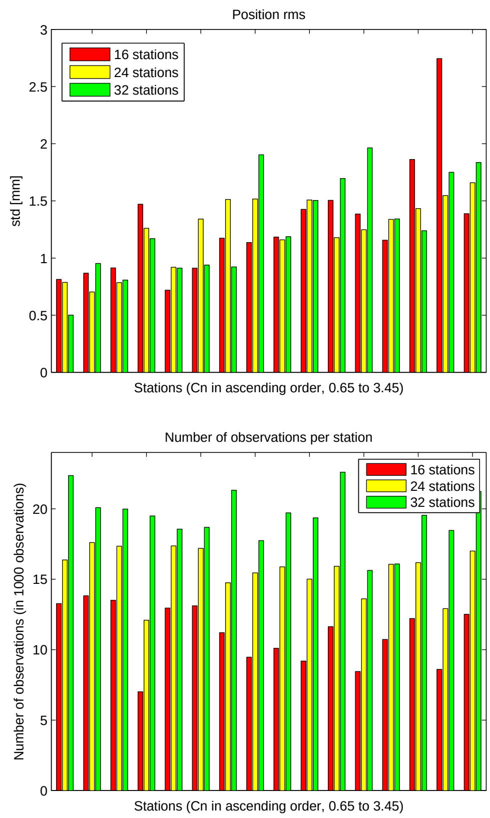

Fig. 3 3D position rms values of station coordinates (upper plot) and the corresponding numbers of observations (lower plot). The stations are sorted by their Cn values which describe the tropospheric turbulence. Only those stations are plotted which are part of all three networks.

As already mentioned above, we ran a global solution to estimate terrestrial and celestial reference frames for the 16- and 24-station networks. Due to the significantly larger number of observations with the 24-station networks, the formal uncertainties for the coordinates in the terrestrial and celestial reference frames are reduced by about 20% in the 24-station network. We also determined the mean coordinate differences with respect to the a priori coordinates for the stations and sources. Surprisingly, we find a systematic behavior in the north components of the stations (Figure 4) which is also reflected in the declinations of the sources (Figure 5). This is not expected because we did not simulate any systematic effects like gradients. We assume that the Monte-Carlo simulations should be based on more realizations of the same session, i.e., we should use at least 100 instead of 25 realizations.

3 Raising the cutoff elevation angle

The source-based scheduling approach is well suited to raise the cutoff elevation angle, because with four sources equally distributed on the celestial sphere, at least one source should be observable at a relatively high elevation angle. We take the 16-station network and create schedules for 10, 15, and 30 degrees elevation cutoff angles in addition to 5 degrees. Running Monte-Carlo simulations with 25 realizations, we find the best 3D position rms values for cutoff angles of 10 and 15 degrees. The median 3D rms values are 1.0, 0.9, 0.9, and 2.0 for cutoff angles of 5, 10, 15, and 30 degrees, respectively. Figure 6 shows a significant improvement in baseline length repeatabilities with a cutoff angle of 10 degrees compared to a cutoff angle of 5 degrees. This underlines, that very low observations (below 10 degrees) are difficult to model due to effects of turbulence. And with more stations available, it is possible to do better without those observations because there are enough common visibilities.

4 Conclusions

Applying the Vienna VLBI Software (VieVS), we created schedules following the newly developed source-based scheduling approach with four sources observed at a time and ran Monte-Carlo simulations. We find that increasing the number of stations in the network (from 16 to 24 and 32 stations) improves the Earth orientation parameters estimated in 24-hour sessions, but it does not improve the 3D position rms of the individual stations. Moreover, we showed that increasing the cutoff elevation angle from 5 to 10 and 15 degrees elevation improves baseline length repeatabilities in a 16-station VLBI2010 network.

5 Acknowledgements

The authors would like to thank the Austrian Science Fund (FWF) for supporting this work within projects Integrated VLBI (P23143), GGOS Atmosphere (P20902), and SCHED2010 (P21049).

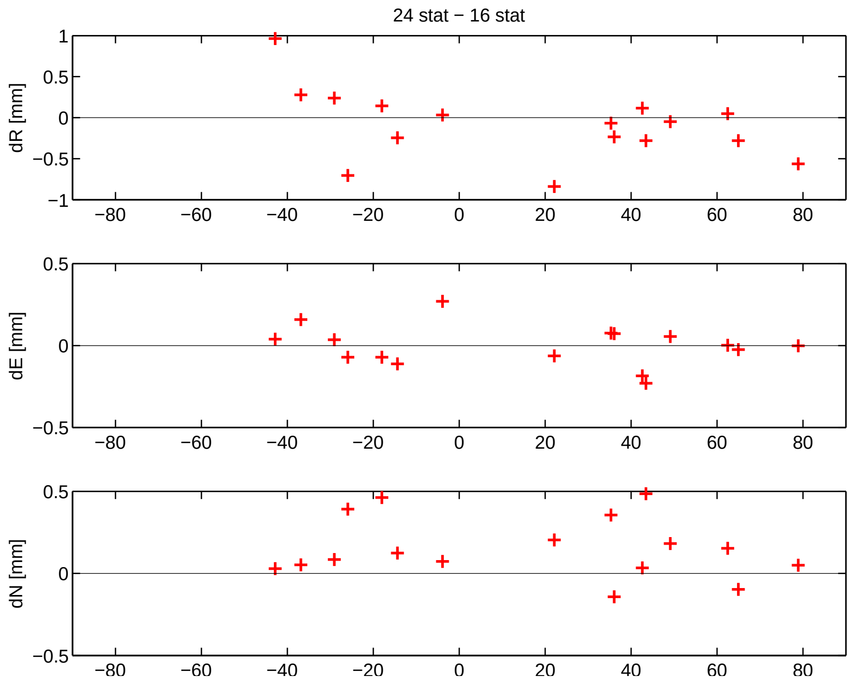

Fig. 4 Difference in the terrestrial reference frame coordinates with the 24-station network compared to the 16-station network. Radial, east, and north components are shown with respect to latitude. It is interesting to note that all north components are positive in the southern hemisphere.

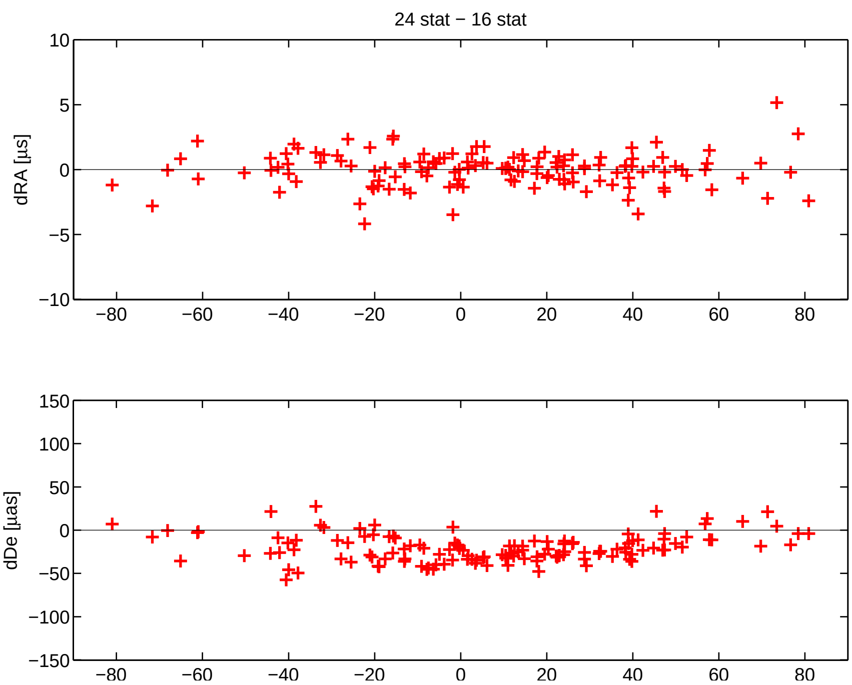

Fig. 5 Difference in the celestial reference frame coordinates with the 24-station network compared to the 16-station network. Right ascension and declination are shown with respect to declination of the source.

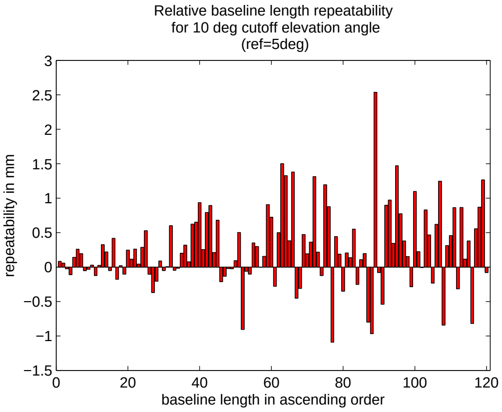

Fig. 6 Improvement in baseline length repeatability with a cutoff angle of 10 degrees compared to 5 degrees. The baselines are ordered by length.

References

J. Böhm, S. Böhm, T. Nilsson, A. Pany, L. Plank, H. Spicakova, K. Teke, and H. Schuh. The New Vienna VLBI Software. In S. Kenyon, M. Pacino, U. Marti, editors, *Proceedings of the 2009 IAG Symposium, Buenos Aires, Argentina, 31 August 2009 - 4 September 2009, Series: International Association of Geodesy Symposia, Vol. 136*, pages 1007-1012, 2012. 2007.

T. Nilsson and R. Haas. Impact of atmospheric turbulence on geodetic very long baseline interferometry. *Journal of Geophysical Research (Solid Earth)*, 115, B03407, 2010. doi: 10.1029/2009JB006579.

T. Nilsson, R. Haas, and G. Elgered. Simulations of atmospheric path delays using turbulence models. In J. Böhm, A. Pany, and H. Schuh, editors, *Proceedings of the 18th Workshop Meeting on European VLBI for Geodesy and Astrometry*, Volume 79 of *Geowissenschaftliche Mitteilungen, Schriftenreihe Vermessung und Geoinformation der TU Wien*, pages 175-180. TU Wien, 2007.

A. Pany, J. Böhm, D. MacMillan, H. Schuh, T. Nilsson, and J. Wresnik. Monte Carlo simulations of the impact of troposphere, clock and measurement errors on the repeatability of VLBI positions. *Journal of Geodesy*, 85(1), pp. 39-50, 2011.

J. Sun. VLBI scheduling strategies with respect to VLBI2010. PhD thesis at the Vienna University of Technology. 2013.

An Overview of Geodetic and Astrometric VLBI at the Hartebeesthoek Radio Astronomy Observatory

A. de Witt, M. Gaylard, J. Quick, L. Combrinck

Abstract For astronomical Very Long Baseline Interferometry (VLBI), the Hartebeesthoek Radio Astronomy Observatory (HartRAO), in South Africa operates as part of a number of networks including the European and Australian VLBI networks, global arrays and also space VLBI. HartRAO is the only African representative in the international geodetic VLBI network and participates in regular astrometric and geodetic VLBI programmes. HartRAO will play a major role in the realization of the next generation full-sky celestial reference frame, especially the improvement of the celestial reference frame in the South. The observatory also provides a base for developing the African VLBI Network (AVN), a project to convert redundant satellite Earth-station antennas across Africa to use for radio astronomy. The AVN would greatly facilitate VLBI observations of southern objects. We present an overview of the current capabilities as well as future opportunities for astrometric and geodetic VLBI at HartRAO.

Keywords VLBI, Astrometric, Geodetic

1 Introduction

What is now the Hartebeesthoek Radio Astronomy Observatory was originally built in 1961 by NASA (National Aeronautics and Space Administration) as a tracking station for its probes that were being sent to explore space beyond Earth orbit. The facility was operated by the South African Council for Scientific and Industrial Research (CSIR) on behalf of NASA, and was known as the Deep Space Instrumentation Facility 51, later Deep Space Station 51 (DSS51). After the closure of DSS51 in 1974 it became a radio astronomy observatory, operating under first the CSIR, then the Foundation for Research Development (FRD), which became the National Research Foundation (NRF) in 1999.

The HartRAO 26-m telescope has always been the only operational radio telescope in Africa that has geodetic VLBI capability and operates as part of the international geodetic VLBI network. HartRAO is also a crucial station in ground-based VLBI networks achieving sub-milliarcsecond astrometric accuracy and regularly operates as part of VLBI and e-VLBI observations. Recent years has seen the implementation of a new telescope system at HartRAO and we are expanding our efforts toward further developments that would benefit astrometric and geodetic VLBI work. We present an overview of the current VLBI instrumentation, capabilities, observing programmes and research at HartRAO, as well as possible future opportunities and contributions.

Aletha de Witt, Michael Gaylard, Jonathan Quick and Ludwig Combrinck
Hartebeesthoek Radio Astronomy Observatory, PO Box 443 Krugerdorp, 1740, South Africa

2 Current HartRAO Radio Telescopes available for VLBI

2.1 The HartRAO 26-m Telescope

The HartRAO 26-m telescope is an equatorially mounted 85-foot (26-m) Cassegrain design built by Blaw Knox in 1961 and provides a multi-frequency VLBI capability unique in Africa. Being an equatorially mounted telescope, it is constrained by mechanical limits in the south and north, and the local topography in the north-east and south-west. The absolute northern declination limit is +45 degrees. The antenna has a slew rate of 0.5 deg/s on each axis and receivers operating at 1.3, 2.5, 3.5, 4.5, 6, 13 and 18 cm. A 2-cm receiver is in development. For dual-frequency

(2.3 / 8.4 GHz) geodetic VLBI a dichroic reflector is manually installed above the 2.3-GHz and 8.4-GHz receivers to permit simultaneous observation at the two frequencies.

The HartRAO 26-m telescope was upgraded and resurfaced by NASA in 1965-7 to raise the operating frequency from 0.96 to 2.3 GHz, and was again resurfaced with solid panels ten years ago in 1998-2005 to provide an rms surface error of 0.5 mm at zenith. An uncooled single-feed 22-GHz wavelength receiver was installed on the 26-m telescope in 2007 to test the performance of the antenna at this very short wavelength. The current uncooled 22–24-GHz test and evaluation receiver is VLBI capable although it has a high noise temperature (200 K). Operational K-band at 22 GHz for VLBI purposes is potentially achievable on the 26-m telescope, but an improved pointing model and a cryogenic K-band receiver is desirable to improve sensitivity. Further evaluation of performance at 22 GHz awaits the completion of a higher accuracy readout system for the subreflector tilt in order to determine the variation of gain with subreflector position. Active refocusing of the subreflector as a function of antenna position may help to reduce gain variation with position. The backing structure of the telescope also remains more flexible than required, so at 22 GHz the performance falls off substantially away from zenith, and the antenna deformation away from zenith needs to be measured more accurately.

2.2 The HartRAO 15-m Telescope

The 15-m alt-azimuth mount telescope at HartRAO is a conversion of the eXperimental Development Model (XDM) telescope built in 2007 as a prototype for the Karoo Array Telescope (KAT). It has been converted for operational use with concentric 2.3- and 8.4-GHz feeds and cryogenic receivers. Several full duration (24 hour) geodetic VLBI experiments have been carried out successfully operating in parallel with the HartRAO 26-m telescope. It has also successfully participated in an astronomical VLBI and spacecraft VLBI on the Venus Express in orbit around Venus. The HartRAO 15-m telescope is now regarded as commissional for VLBI and will take over most of the standard geodetic VLBI at HartRAO, with only S/X observations requiring high sensitivity being done on the 26-m telescope. For geodetic purposes the HartRAO 15-m telescope has the following advantages:

1. Its ability to observe down to the horizon in all directions enhances the geodetic capability compared to the equatorial-mount 26-m telescope at HartRAO, which has a large blind segment below the South Celestial Pole (SCP). The 15-m telescope can do complete circumpolar tracks on sources within about 23 degrees of the SCP.
2. The HartRAO 15-m telescope has a SEFD of about 1050 Jy at S-band (2.3 GHz) and 1400 Jy at X-band (8.4 GHz). The reduced sensitivity at X-band is because the antenna was originally designed only for L-band operation up to 1.7 GHz. For comparison the SEFDs of the HartRAO 26-m telescope is 1200 Jy at S-band and 850 Jy at X-band (the sensitivity is degraded by the current dichroic reflector). By comparison the SEFD of the Auscope 12-m antennas is 3500 Jy in both bands (McCallum et al., 2012).
3. The 15-m telescope does not have the current commitments to astronomical VLBI and single-dish research of the 26-m telescope and will thus be available almost exclusively for geodetic and astrometric VLBI.
4. The HartRAO 15-m telescope has a slew rate of 2 deg/s in azimuth and 1 deg/s in elevation compared to the 0.5 deg/s on each axis of the HartRAO 26-m telescope. Observing schedules on the HartRAO 15-m telescope can be much better optimized than those including the 26-m telescope.

2.3 Near Real-Time VLBI for Geodesy

The networking capability at HartRAO is such that we are already involved in near real-time measurements of Earth Orientation Parameters (EOP). The HartRAO 26-m telescope participates in a test VLBI programme designed to provide an ultra-rapid measure of EOP, where data are streamed to a correlator at Tsukuba immediately after each observation completes and while the telescope is slewing to the next source. This test VLBI programme previously used just three telescopes, namely the 32-m Tsukuba telescope (Japan), the 20-m Onsala telescope (Sweden) and the 12-m Auscope telescope at Hobart (Tasmania). The inclusion of HartRAO in these observations produces long east-west baselines in the Southern hemisphere, which provide the differential Earth rotation rate, as well as more long north-south baselines, which provide the Earth's axis orientation parameters. In December 2012 the HartRAO 15-m telescope successfully participated in a 35 hour duration ultra-rapid VLBI and even longer ones in January 2013.

3 Future Considerations for VLBI Capable Radio Telescopes

3.1 The African VLBI Network

The AVN is a project to build an African VLBI network by converting redundant satellite Earth-station antennas across Africa to use for radio astronomy. The AVN would greatly facilitate VLBI observations of southern objects. HartRAO provides a base for developing the AVN, both for hardware development and technical and scientific human capacity development. We are also currently developing the specification for potential new build AVN antennas.

3.2 Telkom 32-m Antennas

The Telkom Satellite Earth Station 3 km south of HartRAO has three 32-m antennas, designed for 4- to 6-GHz (C-band) operation, that are no longer commercially viable, most traffic having moved to fibre optic links. If one (or more) of these could be made available and converted for astronomical use, it could operate as a single dish or as a part of a two or three element interferometer with the HartRAO telescopes and as part of larger VLBI networks. A Telkom 32-m antenna equipped for C-band would make an excellent testbed for the conversion process for the similar antennas being acquired for the AVN. In addition we would also like to test the 32-m dishes for potential K-band operation and possibly Ka band. Astrometric programs to extend the International Celestial Reference Frame (ICRF) to radio frequencies higher than S- and X-band is underway and NASA is also migrating its space communications and navigation capabilities to the Ka-band region of the radio spectrum (e.g. Lanyi et al., 2010). Calculations from the antenna specifications of the Telkom 32-m antennas suggest that in ideal conditions the aperture efficiency would be 0.48 at 22 GHz and 0.30 at 32 GHz.

3.3 VGOS Antennas

Implementation of radio telescopes compliant with the VLBI2010 Global Observing System (VGOS) at HartRAO will be necessary to remain competitive in the geodetic VLBI field in the longer term. HartRAO is the only African representative in the international geodetic VLBI network and the network will be weakened considerably should we not be able to meet VGOS requirements. HartRAO has begun initiatives to obtain funding locally and internationally. We are carrying out a geological site survey and a radio frequency interference (RFI) survey to identify a suitable location at HartRAO.

4 VLBI Instrumentation and HartRAO

All the installed receivers on the HartRAO 26-m telescope are VLBI-capable, as is the cryogenic S/X-band receiver on the 15-m telescope. The local oscillator systems are phase-locked to a hydrogen maser frequency standard. The two telescopes can run VLBIs in parallel. At the moment HartRAO has three recording terminals. The original, analogue Mark5 terminal is capable of recording at 1024 Mbps to a Mark5B recorder. We also have two new, digital DBBC terminals capable of 2048 Mbps to Mark5B+ recorders. We are currently using the analogue terminal but are in the process of switching to the digital terminals now that support for them in the Field System has been released. Data are recorded on disk packs in a Mark 5B and a Mark 5B+ recorder. A third Mark 5B+ is used for diskpack conditioning and e-shipment of VLBI data. There is a 10 Gb/s international network connection for real-time eVLBI and for e-shipment of VLBI data.

5 HartRAO Research Programmes Involving Astrometric and Geodetic VLBI

The National Research Foundation (NRF) in South Africa signed an agreement to join the Joint institute for VLBI in Europe (JIVE), which correlates the data from the European VLBI Network (EVN) and provides support for EVN science. The partnership in JIVE provide exciting opportunities for future research, as well as making more available a considerable pool of expertise in VLBI which will likely prove invaluable in the development of the AVN.

HartRAO joined the International Astronomical Union (IAU) working group on the next generation ICRF, which is the ICRF-3. HartRAO is involved in various astrometric projects of reference sources toward the improvement of the ICRF in the south. Efforts are also underway to increase the number of known calibrator sources in the south, in particular the LBA calibrator survey (LCS). This survey has already produced a significant improvement at an observing frequency of 8.4 GHz (Petrov et al., 2011). HartRAO has taken part in numerous observations for the LCS, and is also involved in the imaging of the sources from the LCS experiments (de Witt and Bietenholz, 2012).

HartRAO is part of the TANAMI (Tracking Active Galactic Nuclei with Austral Milliarcsecond Interferometry) collaboration including follow-up observations from the Large Area Telescope on the Fermi Gamma Ray Space Telescope (FERMI-LAT), and has previously collaborated on radio follow-ups of discoveries of the High Energy Stereoscopic System (H.E.S.S.) in Namibia. HarRAO is also involved in early science groups of the RadioAstron Space-VLBI satellite on AGN as well as masers and pulsars.

6 Technical Developments at HartRAO to Support the Science

We are expanding our efforts to determine and monitor the terrestrial positions for the HartRAO telescopes relative to the other geodetic equipment and monumentation. We are adding permanent targets to HartRAO's 15-m and 26-m radio telescopes to allow frequent and regular monitoring of positions of the telescopes at the sub-mm level. We have constructed extra calibration target pillars for the satellite lunar ranger (SLR) on the bedrock east of the SLR. We are investigating an electronic distance measuring (EDM) system to permit continuous monitoring of the three-dimensional positions of the telescopes, the co-located geodetic instruments and the calibration target pillars to comply with the Global Geodetic Observing System (GGOS) accuracy target.

Currently, in order obtain dual-frequency S/X observations, a dichroic reflector must be manually installed on the HartRAO 26-m telescope. The current dichroic system somewhat degrades 8.4-GHz performance (to 70% of normal) and greatly degrades 2.3-GHz performance (to 30% of normal). An improved dichroic reflector system would let us regain much of the lost sensitivity, and automating the dichroic positioning would reduce lost time and remove a regular safety hazard. Designing and building an improved dichroic system has long been considered at HartRAO.

Previously mentioned developments that would benefit geodetic and astrometric VLBI work include a cryogenic 22-GHz receiver for the HartRAO 26-m telescope, the use of K- or Ka-band receivers on one of the Telkom 32-m antennas near HartRAO, the implementation of a VGOS compliant system at HartRAO and AVN antennas that can potentially participate in astrometric observations.

References

A. de Witt and M. Bietenholz. Analysis of Potential VLBI Southern Hemisphere Radio Calibrators. *11th European VLBI Network Symposium & Users Meeting.* 2012, Proceedings not yet available.

G. E. Lanyi, D. A. Boboltz, P.-Charlot, A. L. Fey, E.-B. Fomalont, B. J. Geldzahler, D. Gordon, C. S. Jacobs, C. Ma, C. J. Naudet, J. D. Romney, O. J. Sovers, and L. D. Zhang. The Celestial Reference Frame at 24 and 43 GHz. I. Astrometry *ApJ*, 139, 1695–1712, 2010.

J. McCallum, J. Lovell, S. Shabala, J. Dickey, C. Watson and O. Titov. Remote Operation and Performance of the AuScope VLBI Array. In J. Behrend and K. D. Baver, editors, *IVS 2012 General Meeting Proceedings*, *Launching the Next-Generation IVS Network*, pages 191–193. NASA/CP-2012-217504, 2012.

L. Petrov, C. Phillips, A. Bertarini, T. Murphy and E. M. Sadler. The LBA Calibrator Survey of southern compact extragalactic radio sources - LCS1. *MNRAS*, 414, 2528, 2011.

Radio Frequency Interference Observations at IAR La Plata

H. Hase, G. Gancio, D. Perilli, J. J. Larrarte, L. Guarrera, L. García, G. Kronschnabl, C. Plötz

Abstract The Wettzell RFI-Monitoring system was developed to monitor radio frequency interference at existing and potential VLBI sites. It was used at the Instituto Argentino de Radioastronomía (IAR) in La Plata, Argentina, to evaluate a future site for the Transportable Integrated Geodetic Observatory (TIGO). A 24h/7d survey was conducted during September and October 2012. This huge data set required the development of a specific analysis strategy and data representation. The results of this survey revealed, that IAR is a suitable site for geodetic VLBI observations: most of the present RFI signals occure sporadically and may take away less than 5% of the observation time; moreover VLBI receivers will not be saturated.

Keywords RFI monitoring, VLBI sites, TIGO

1 Motivation

The existing global VLBI network infrastructure is lacking radio telescope installations especially in the Southern hemisphere. The German Transportable Integrated Geodetic Observatory (TIGO) of the Bundesamt für Kartographie und Geodäsie (BKG) is one initiative to improve the global distribution of geodetic observatories. Since 2002, TIGO has been operating in Concepción, Chile, within the context of technical and scientific cooperation. After Chilean partner universities have withdrawn from the TIGO project, BKG needs to find a new project partner. A proposed site for the future operation of TIGO is the Instituto Argentino de Radioastronomía near the city of La Plata. Prior to the decision about the proposal the suitability of this site for VLBI and SLR observations has to be evaluated. As far as VLBI is concerned it is essential to know the use of the electromagnetic spectrum in the vicinity of the urban region of La Plata and Buenos Aires. Therefore BKG and IAR conducted a measuring campaign with their radio frequency interference (RFI)-monitoring equipments during the period June to October 2012.

Hayo Hase, Gerhard Kronschnabl, Christian Plötz
Bundesamt für Kartographie und Geodäsie, Sackenrieder Str. 25, D-93444 Bad Kötzting, Germany
Guillermo Gancio, Daniel Perilli, Juan José Larrarte, Leonardo Guarrera, Leandro García
Instituto Argentino de Radioastronomía, Camino Gral. Belgrano Km 40 - Berazategui - Prov. de Buenos Aires - Argentina

2 Equipments

Radio frequency interference monitoring requires a radiometer capable to measure the amplitudes and frequencies of signals above noise floor within a given spectral range. The ideal equipment to realize this monitoring would be radio telescopes with cryogenic cooled receivers, but previous to the costly installation of a radio telescope, mobile RFI monitoring systems are used for a site evaluation, although their technical performance is minor compared to a fully equipped VLBI-radio telescope. The RFI monitoring system permits quantitative measurements about the presence or absence of man made noise. A qualitative analysis can be done, if the measuring system includes a noise calibration system. With a careful selection of low noise components, such as amplifiers, cables and spectrum analyzer, the thermal noise of the measuring system must be minimized. Two systems were available for the evaluation: (a.) BKG Wettzell RFI Measurement System, (b.) IAR La Plata RFI Measurement System.

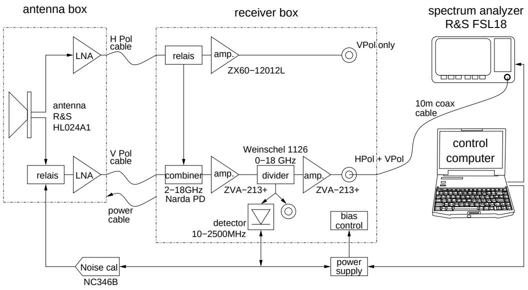

Fig. 1 Block diagram of the Wettzell RFI monitoring system.

2.1 BKG Wettzell RFI Measurement System

This system was developed for VLBI2010 site investigations and is described in (Kronschnabl (2012)). Fig. 1 shows a block diagram of the components. It uses a Rohde& Schwarz HL024A1 antenna covering the frequency range from 1-18 GHz in a beam of approximately 40 degree, hosting two low noise amplifiers supplying two output signals of horizontal and vertical polarisation. The antenna box contains also an input signal for the noise calibration diode NC346B. The receiver box contains a relais with a combiner in order to produce a mixed output of both vertical and horizontal polarisation as an alternative to the individual polarizations. Later on the signals are finally registered and displayed with a spectrum analyzer Rohde& Schwarz FSL18. A control computer is used to setup the spectrum analyzer, to record its images and to switch on/off the noise diode. Once the antenna is pointed manually to one direction at the horizon, the data acquisition runs automatically.

2.2 IAR La Plata RFI Measurement System

This system was developed for SKA site investigations in Argentina (IAR-Report-110 (2012)). Therefore its frequency range is limited to 2-8 GHz. (With the exchange of two low noise amplifiers and cables it covers an extended range to higher frequencies up to 18 GHz.) The antenna is a dual ridge horn type, Emco 3115, supporting the range of 1-18 GHz. It delivers one linear polarization. Rotating the antenna by 90 degree enables the measurement of horizontal and vertical polarization. The antenna is mounted on a pedestal with two perpendicular axes: one rotates along the antenna axis (polarisation) and the other rotates the antenna azimuthal by computer controlled motor drives. The pedestal is a fixed installation at La Plata. The noise calibrator is realized by a 50 Ohm reference load. The signals are registered with a spectrum analyzer HP9583E. The system is fully automated and secured by an uninterruptable power supply.

3 Measurements

3.1 Flux density

Among many ways of expressing energy received by a receiving system, we chose the flux density with the unit $dBWm^{-2}Hz^{-1}$. This unit can be easily related to the radio source flux density of VLBI observations which is expressed in Jansky $1Jy = 10^{-26}Wm^{-2}Hz^{-1} = 260dBWm^{-2}Hz^{-1} = 230dBmm^{-2}Hz^{-1}$. The flux density of the electromagnetic spectrum can be written after (Millenaar (2006)) as

$$
\begin{aligned}
S_{dB} &= P_{SA_{dBm}} - 10\log(B_S) - G_{R_{dB}} + k_{A_{dB}} - 35.77 \\
&\text{with} \\
S_{dB} &\text{ in } \left[\frac{dBW}{m^2 Hz}\right] \qquad (1) \\
P_{SA_{dBm}} &= \text{power in dBm read at spectrum analyzer} \\
B_S &= \text{resolution bandwidth} = setto30kHz \\
G_{R_{dB}} &= \text{receiver system gain} \\
&= \text{median from calibration measurement} \\
k_{A_{dB}} &= 20log(f_{MHz}) - G_{dBi} - 29.79 \qquad (2) \\
&\text{with} \\
f_{MHz} &= \text{ant. frequency} = 2000\ldots14000MHz \\
G_{dBi} &= \sim 7dBi \qquad \text{(data sheet)}
\end{aligned}
$$

From equation 1 follows, that for the determination of the flux density only two measures have to be taken: the amplitude per frequency from the spectrum analyzer of the targeted direction $P_{SA_{dBm}}$ and the calibrated gain of the system $G_{R_{dB}}$. The other parameters are settings or conversion factors.

The RFI measurement systems used in the evaluation have uncooled wide beamwidth antennas. Pointing to the horizon at least half of the beam pattern intersects with the ground and raises the system temperature to higher levels than those that are typical for the VLBI radio telescope. Moreover without a reflector the antenna gain is low and the RFI signals may not stand out far enough above the noise floor (which is composed by ground pickup and amplifier noise). However, with the collected data it is possible to conclude, whether the detected signals above noise floor will saturate the LNA used in VLBI radio telescopes or not.

3.2 Setup and yield of RFI measurements

Once the Wettzell RFI measurement system had arrived at IAR in La Plata a comparison between both systems was carried out. It was confirmed that both systems detected the same signals in the overlapping frequency range. The advantage of the Argentinean system was its computer controlled pedestal which enabled 24h/7d measurements, while the German system had the advantage of covering the full spectral range of interest from 2-14 GHz. Therefore, it was decided to temporarily mount the Wettzell equipment on the La Plata pedestal in order to carry out an almost continuous measurement for one month (s. fig. 2). The spectrum analyzer was set to 30 kHz resolution bandwidth in order to pick up any possible narrow band signal. The spectrum 2-14 GHz was subdivided into 1 GHz wide bands. Each subband required 2.5 seconds sweepttime; hence 12 subbands needed 30 seconds. The antenna beamsize of about 40 degree suggested to used eight pointing directions (N, NE, E, SE, S, SW, W, NW). Together with the calibration an entire azimuth scan registring the spectrum 2-14 GHz needed 15 minutes. The yield was 96 azimuth scans per day respectively 768 spectrum analyzer images each with 9600 amplitude data points (spaced by 1.25 MHz). Thus, within 30 days of measurements (September 14 to October 14, 2012), a total of 21776 images of the spectrum analyzer respectively 209 million data points had been registered.

4 Analysis and results

The analysis of the huge amount of collected data took several steps. Firstly the calibration data was applied to the spectrum analyzer readings according to equation 1. Secondly, a statistical method was applied to all the monitoring data regardless of the antenna pointing direction. The measured signal amplitude data was superimposed and five parameters were identified: maximum, 90-percentile, median, 10-percentile and minimum. (The maximum and minimum are equivalent to the max hold and min hold button at the spectrum analyzer throughout the measured period.) This quantitative approach revealed, that radio interference is

Fig. 2 Foto of pedestal mounted on the roof of the operation house with the broadband antenna from the Wettzell RFI monitoring system. This configuration was used almost continuously from September 14 until October 14, 2012.

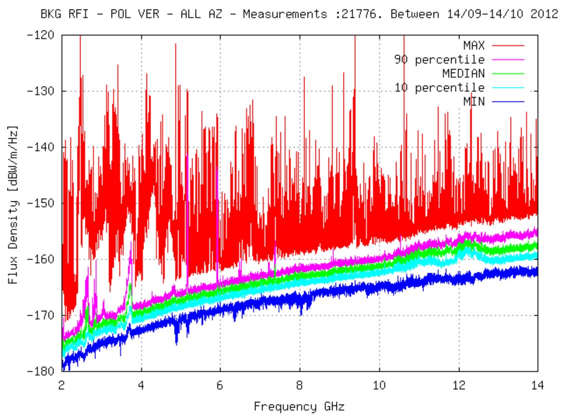

Fig. 3 Flux density vs. frequency from 21776 measurements at IAR La Plata during September 14 - October 14, 2012.

present almost throughout the entire spectrum during the period of 30 days. The maximum level was up to 50dB significantly above the minimum noise level. However, the 90-percentile line shows where 90% of the amplitude measurements are equal or less. Thus, it is an indicator for the temporary or continuous nature of a signal. The median value shows the value which is in the middle of measured samples. It means that half of measured signals are found above that line and half below.

Fig. 3 shows fluctuation of the noise floor with some signals peaking out of it. A filter of $+6dB > median$ was applied as a criteria to discriminate noise from an interference signal . The result of this process applied to all measurements is shown in fig. 4. Fig. 4 shows strong peaks at 5.16 and 5.8 GHz which are related to a local internet link from IAR to the National University of La Plata. Below that frequency the other interfering signals are related to wireless lan above 2.4

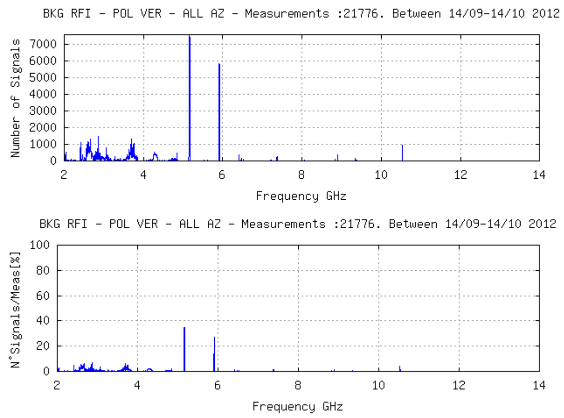

Fig. 4 RFI detections based on a filter $+6dB > median$. The upper plot shows the absolute number of detected RFI events during one month, the lower plot shows the percentage of the overall measurements in all directions.

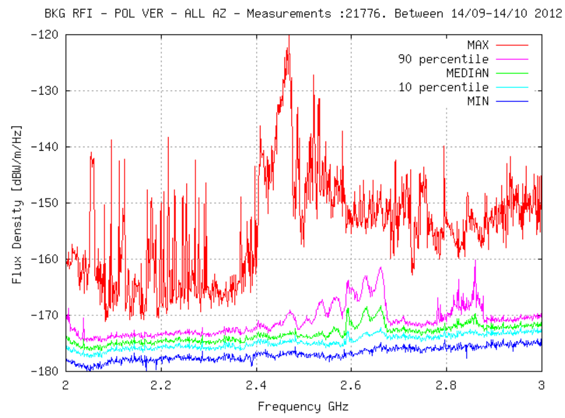

Fig. 6 S-band 2.0-3.0 GHz. Some intereference is present at 2.4-2.7 GHz and 2.8-2.9 GHz. The VLBI band 2.2-2.35 GHz does not contain any continuous interference signal.

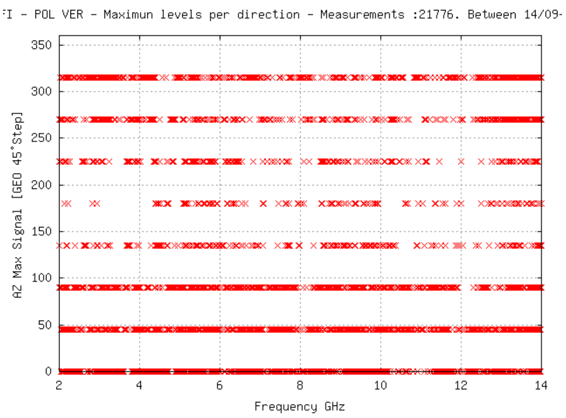

Fig. 5 Azimuth direction vs. observed spectrum. The amount of detected events is correlated with the directions in which urbanized areas are located. The Southern direction points to a rural area and less events have shown up.

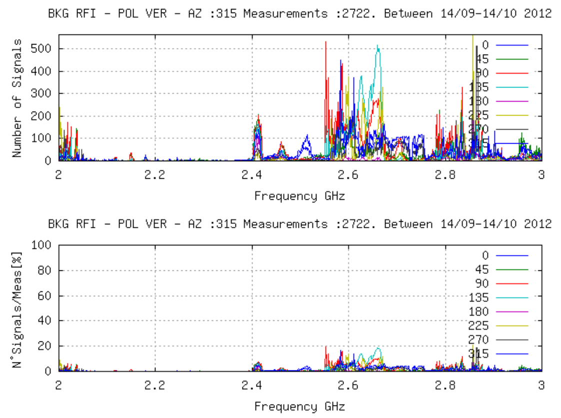

Fig. 7 S-band 2.0-3.0 GHz. The colour coded antenna directions show, that most of the interfering signals are directional. The wifi signal at 2.4 GHz is omnidirectional and locally generated. The VLBI-frequencies at 2.2-2.35 GHz are not disturbed.

GHz, Wimax above 2.5 GHz, mobile telephone frequencies (LTE) above 2.6 GHz and air radar systems between 2.7 and 2.9 GHz. Interference signals are also visible at 3.7-3.9 GHz, 8.80-8.85 GHz.

How is the relation between the eight observed directions and the detected radiation? To answer this question the azimuth direction was plotted versus the observed spectrum. Fig. 5 shows the observed directions. The city of Buenos Aires is located in the North-West of the monitoring site at IAR, the city of La Plata lays in the East and in the South direction we find rural areas. As indicated in fig. 5 the presence of detected signals is correlated with urbanized areas. This result can be considered typical for sites near urban regions.

Fig. 6 and fig. 8 give a closer look to the S-band and X-band. The colour-coded directions in fig. 7 and fig. 9 show, that those signals are directional and may possibly limit the applied elevation mask in VLBI-observations. However, the observed S-band spectrum and observed X-band spectrum tend to be free of interference signals in the corresponding spectrum.

5 Conclusions

A RFI-monitoring system for 1-18 GHz was developed at the Geodetic Observatory Wettzell and was used in an automated measuring campaign at IAR La Plata for 30 days. In the frequency range of 2-14 GHz 21776 radiation images were taken and processed. The most important findings are: The largest interference signal was caused by a local internet radio link at the IAR site. This is not a problem because this signal will be switched off as soon as a cable connection will have

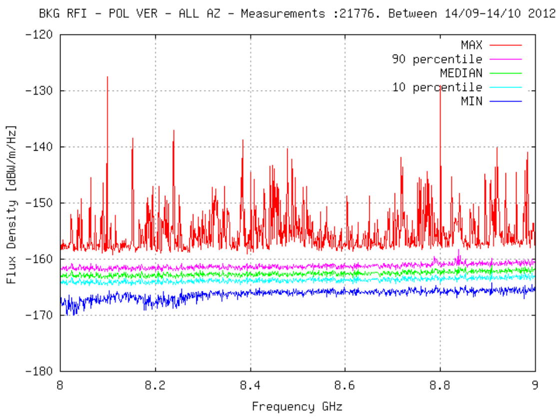

Fig. 8 X-band 8.0-9.0 GHz. Some intereference is present in the VLBI band 8.1-8.9 GHz at 8.80-8.85 GHz.

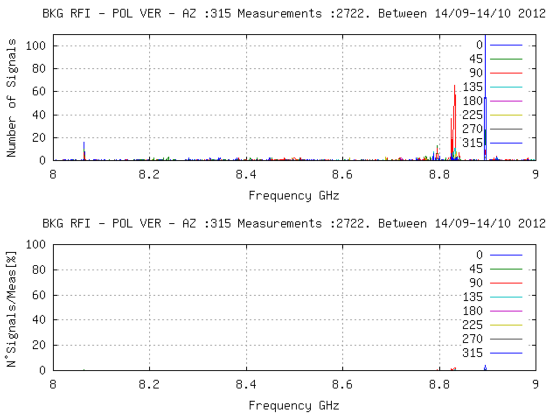

Fig. 9 X-band 8.0-9.0 GHz. The colour coded antenna directions indicate, that the signal at 8.82 and 8.85 GHz are directional and can be filtered out by an adjustment of the elevation mask in those directions if necessary.

been intalled. Interference signals exist in the range of 2.4-2.9 GHz and around 8.81 GHz. As for the rest of the signals most of them appear sporadically. Directional continuous interference signals will determine the elevation mask for future VLBI-observations. RFI monitoring should be a permanent task. The presented results have been further analyzed by the IVS RFI-group and confirmed that the present RFI noise levels will not saturate the LNA of a VLBI radio telescope (Petrachenko et al. (2013)). This analysis confirms, that the IAR La Plata is a suitable site for geodetic VLBI measurements using S-band and X-band.

References

G. Kronschnabl. Projekt RFI-Meßsystem, Beschreibung: Empfangssystem zur Überprüfung des jeweiligen Standortes auf hochfrequente Störsignale im Bezug auf die Empfangseigenschaften von VLBI Radioteleskopen *(internal document)*, 18.08.2012

G. Gancio. Equipamiento para monitoreo RFI disponible en IAR, Descripción general OBS-RFI-00110-DG, Instituto Argentino de Radioastronomía, *(internal report)* 04.04.2012

G. Gancio,D. Perilli,H. Hase,J.J. Larrarte. BKG RFI Month Report. OBS-RFI-00126-RP, Instituto Argentino de Radioastronoma, *(internal report)*, 22.10.2012

R.P. Millenaar. SSSM System Design Considerations. ASTRON-RP-013 Document, *10.1.1.103.3528.pdf*, 21.02.2006

B. Petrachenko, B. Corey, C. Beaudoin. VGOS RFI Survey Proceedings of the EVGA-Meeting 2013, Espoo, Finland

Improved focal length results of the Effelsberg 100 m radio telescope

A. Nothnagel, M. Eichborn, C. Holst

Abstract The main reflector surfaces of radio telescopes are generally deformed by varying gravitational loads at different elevation angles. For the construction of a VLBI delay correction model, it is necessary to know the variations in the focal length caused by these deformations. The Effelsberg 100 m radio telescope was scanned with a terrestrial laser scanner and focal length variations had been deduced from these measurements. New in this publication are revised focal length estimates which result from a different preprocessing of the raw laser scanner data.

Keywords Radio Telescope Deformation, Focal Length, Terrestrial Laser Scanning

1 Introduction

Deformations of radio telescopes cause errors in geodetic and astrometric VLBI observations which cannot be neglected within today's accuracy requirements (Sarti et al. , 2009b). Several authors have described terrestrial laser scanner measurements of radio telescopes to investigate the deformations which occur when the main reflector is tilted in various elevation angles between horizon and zenith (e.g., Sarti et al. (2009a), Dutescu et al. (2009)).

In 2011, members of the Institute of Geodesy and Geoinformation of the University of Bonn carried out terrestrial laser scanning on the main reflector of the 100 m radio telescope of the Max Planck Institute for Radio Astronomy at Effelsberg, Germany. The paraboloid was scanned from a position in the center of the sub-reflector and the telescope was positioned in elevation angle at 7.5°, 15°, 30°, 45°, 60°, 75° and 90° to figure out the effects of different gravitational loads (Holst et al. , 2012). Compared to previous studies of, e.g., Sarti et al. (2009a), the advantage of the concept used here was that the whole paraboloid could be scanned from one scanner position. So, no further uncertainty was introduced by the matching process of two or more sub-surfaces which are required when the paraboloid has to be scanned from two or more instrument positions to cover it completely.

The paraboloid of the Effelsberg telescope had been constructed as a homologeous surface. This means that at all elevation angles, the surface always forms a paraboloid, though with variation in the focal length. So, from each point cloud a different focal length had been estimated. In the course of the analysis, it turned out that the distribution of the point cloud sampling the paraboloid has a severe impact on the estimated parameters.

2 Scanner data preprocessing

A terrestrial laser scanner is a device which samples an object with a fast laser distance measurement beam. Similar to a radio telescope, the scanner has a vertical (azimuth) and a horizontal (elevation) axis. The optics of the scanner rotates very fast around the horizontal axis measuring the distances in equal fractions of seconds and recording the respective vertical angle readings. At the same time the head turns around slowly forming individual meridians to cover the full horizontal range. The limits of the scanning process depend on whether the rotation around the horizontal axis goes only from the lowest (elevation) limit to zenith or through zenith to the opposite side, i.e., to elevations larger than 90°. In the latter case, the horizontal rotation needs to be only 180°. Here, the scanner automatically generates two overlap areas of a few degrees in

Axel Nothnagel, Malwin Eichborn and Christoph Holst
Rheinische Friedrich-Wilhelms Universität Bonn, IGG, Nußallee 17, D-53115 Bonn, Germany

azimuth when the scanner covers a full horizontal circle.

The general way of operation of laser scanners produces a sampling which is most dense at zenith because the meridiens converge at zenith (see Fig. 1). In our case where the scanner is mounted head-down in the radio telecope, the zenith point is near or at the vertex of the paraboloid. Thus, there is a natural gradient in point density towards the vertex ($\propto$ cos (zenith distance)).

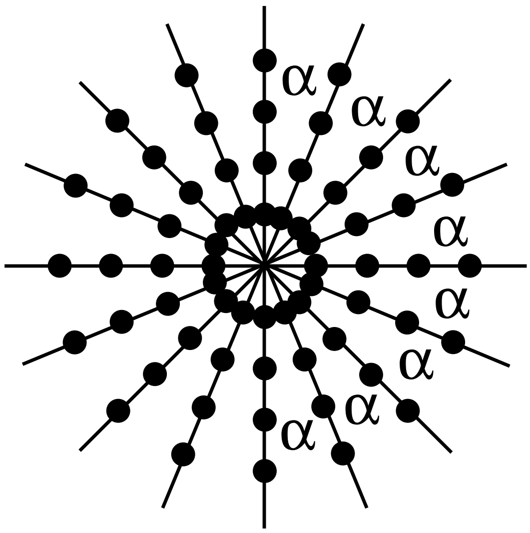

Fig. 1 Central section of the paraboloid as seen by the instrument. The scan paths along the meridians produce a monotoneous increase in point density towards the center (zenith of the laser scanner).

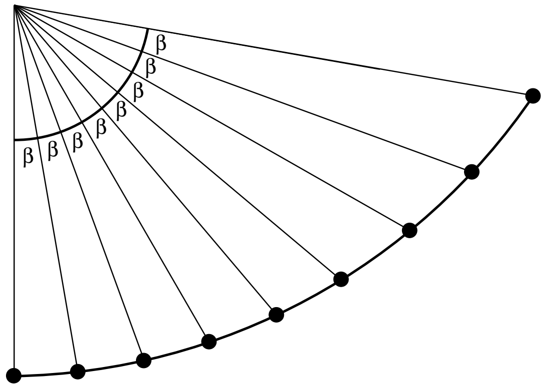

Fig. 2 Vertical cross section of paraboloid with focus and meridian. Scan rays with identical angular increments produce a monotoneous decrease in point density towards the edge.

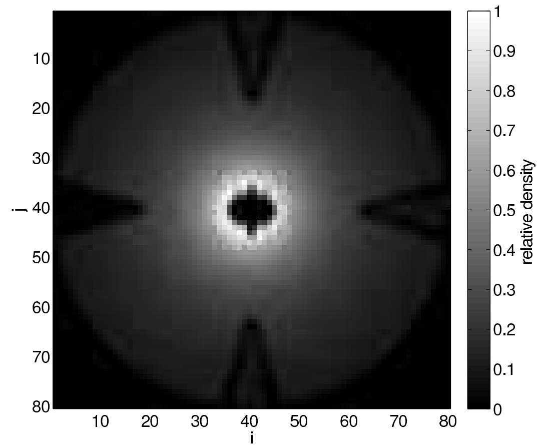

Fig. 3 Point density distribution resulting from the specific position and orientation of the laser scanner w.r.t. the paraboloid. The central part of the plot is the vertex of the paraboloid with the secondary focus feed horn housing.

The second effect which amplifies the uneven point distribution even more is caused by the fact that the scanner is mounted near the focal point of a paraboloid. Since the scanner samples at identical increments in the vertical angle and the distance to the surface increases with increasing zenith distance, the lateral separations of the scanner's foot prints increase towards the edge of the telescope (Fig. 2) as well.

These two simple monotoneous geometric effects produce a prominent concentration of the sampling near the vertex of the paraboloid due to their multiplicative effect (Fig. 3). It is immediately obvious that the least squares adjustment of the observations with the focal length as one of the main parameters is dominated by the central area of the paraboloid. In a separate paper, it will be shown in more detail that local deformations in the such over-sampled areas have an adverse effect on the estimation of the form and location parameters.

In order to produce a suitable distribution, the raw data points are, therefore, reduced by a dedicated data reduction program. The aim of this program is to create a point cloud with a homogeneous distribution of the sampling points on the paraboloid. The method is based on volume elements rather than on plain surfaces. The resulting point distribution is displayed in Fig. 4.

From the figure, one could get the impression that there still is a discernable gradient towards the vertex. However, the reason for this appearance is that the graph is constructed in the X/Y plane rather than on the paraboloid surface projected into the plane. In the latter case, the graph would consist of a single color all over the surface.

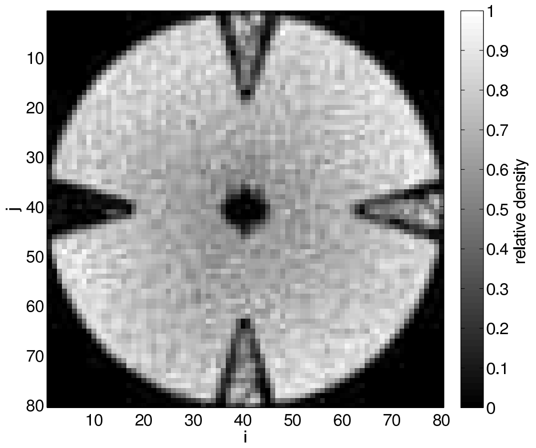

Fig. 4 Point density distribution after reduction.

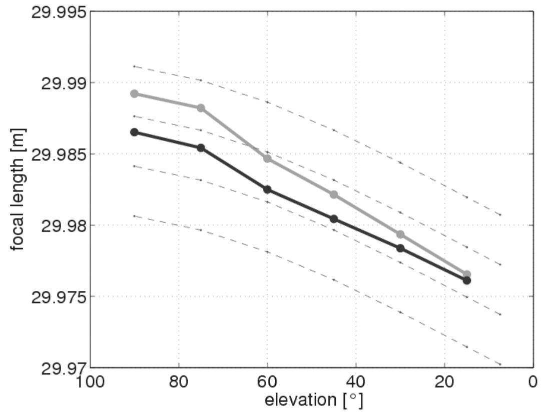

Fig. 5 Focal length estimates. The top solid line depicts the estimates with the reduced point density. The bottom solid line shows the estimates with full point density. The dashed lines represent the empirical focal point displacement function which does not have an absolute reference.

3 Focal length results

With the reduced point clouds, new estimates for the focal lengths at the six different elevation angles were carried out according to the formulations published in (Holst et al. , 2012). The seventh elevation at 7.5° was excluded due to the fact that the scanner measurements turned out to be severely hampered by the sun shining into the paraboloid producing rather noisy measurements with strong systematic elements and an unreliable estimate of the parameters.

The standard deviations of $\widehat{\sigma}_f = 0.05\,mm$ and $\widehat{\sigma}_{\Delta f} = 0.07\,mm$ should not be considered seriously since they are too optimistic due to the large number of observations and due to the neglect of correlations in the stochastic model.

Elevation	Point distribution original $\widehat{f}$ [m]	reduced $\widehat{f}$ [m]	$\widehat{\Delta f}$ [m]
90°	29.9865	29.9892	0.0027
75°	29.9854	29.9880	0.0026
60°	29.9825	29.9847	0.0022
45°	29.9804	29.9822	0.0018
30°	29.9784	29.9794	0.0010
15°	29.9761	29.9766	0.0005
7.5°	*	*	*

Table 1 Focal length estimates $\widehat{f}$ and the corresponding differences $\widehat{\Delta f}$ (new - old) for the raw and the reduced laser scanner observations. * The results of the 7.5° elevation have been omitted due to obvious deficits in the data.

Table 1 shows a monotoneous decrease in focal length in both estimates, i.e., in the one with the full set of observations and in the second one with the reduced set. The differences between the two data sets in the sense of new minus old show that the effect of the re-computation is biggest at 90° elevation. This is also depicted in Fig. 5 where the two sets of results are displayed together.

In this figure, also four dashed lines are depicted. A single line represents the shift which is applied to the sub-reflector in the line-of-sight direction for optimal gain of the antenna at X band. This was determined empirically by observing multiple calibrator sources at various elevation angles (Bach et al. , 2007). Since the shift is relative to some arbitrary origin, it was introduced at four different equally spaced separations to allow visual comparison with the two geodetic sets of results. Although it is clear that the results from the reduced observation set will be used for further work, the results of the full raw data set are included for comparison purposes as well. Here, both sets have a similar level of agreement to the empirical model at the level of 1 - 2 mm. There is no obvious evidence that the values estimated from the raw data set are much worse than those of the homogeneous data set.

The fact that the shapes of the empirical model and of the geodetic results do not quite match is not unexpected. The reason is that the empirical model covers the complete signal path which also contains the deformation of the quadrupod holding the sub-reflector. Nevertheless, an RMS agreement of less than 1.5 mm is an extremely good agreement of a telescope with a 7800 m^2 main reflector.

4 Movements of the sub-reflector

The least squares adjustment of the terrestrial laser scanner data contains not only the focal length as a target parameter but also the position and the orientation of the instrument in a paraboloid-fixed system with the origin at the vertex of the paraboloid. In a vertex centered coordinate system, ΔX is the shift parallel to the elevation axis, ΔZ is the displacement pointing in the direction of the telescope's optical axis while ΔY stands perpendicular on both of these axes. The numbers (Tab. 2), most of them monotoneously decreasing with increasing tilt towards the horizon, can be easily interpreted. The decreasing ΔZ means that the focus cabin in fact approaches the vertex by about 5 mm. The large decrease in ΔY is caused by the focus cabin pulling downwards when the telescopes looks close to zenith. The displacement in X direction is a bit abnormal because the force vectors should be symmetrical to the tilt direction. However, the two beams with their roots at the elevation axis are not symmetrical in construction, stability, and load. The left support consists of four longitudinal beams forming a square profile with diagonal support pipes at the outer surfaces (Fig. 6). The support on the right hand side is of identical base structure as the one on the left hand side but contains a walkway with additional longitudinal beams as well as steps. These differences in construction lead to the fact that the sub-reflector is shifted to the left (-X) by up to 6.1 mm when the telescope is tilted to the horizon.

Elevation	ΔX $[mm]$	ΔY $[mm]$	ΔZ $[mm]$
90°	0.00	0.00	0.00
75°	-4.48	-40.53	-0.07
60°	-5.23	-72.75	-0.65
45°	-4.35	-104.30	-1.79
30°	-6.27	-125.04	-3.15
15°	-6.06	-137.00	-4.75

Table 2 Displacements of the scanner instrument in a vertex centered reference frame depending on the elevation angle.

While the displacements of the instruments and consequently the subreflector in X and Y direction do not have any effect on the VLBI delay, the shift in Z direction would enter the delay directly with a certain scaling factor. However, since the subreflector is shifted by the empirical model mentioned above, the situation is more complicated and is under investigation at the moment to come up with a full delay correction model which includes all these effects.

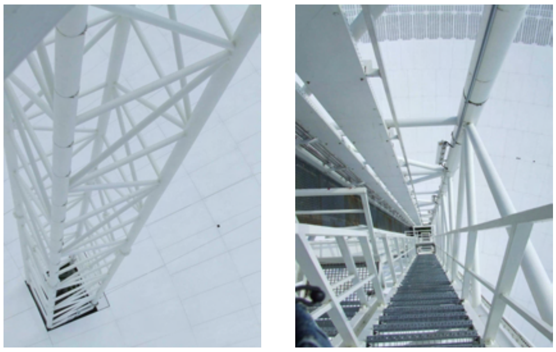

Fig. 6 Support structures holding the sub-reflector. Left the "left hand" one and on the right, the "right hand" one with the walkway

5 Conclusions

Corrected estimates of the focal length at 6 different elevation angles were computed for the main reflector of the Effelsberg 100 m radio telescope. The recomputation became necessary because the terrestrial laser scanner data was overly dense at the area close to the vertex of the paraboloid. This fact over-emphazised the central paraboloid area in the parameter estimation process which may have adverse effects when local deformations are present. The new data distribution is much more homogeneous being a much better basis for a reliable estimation of the focal lengths and the scanner's location parameters.

The new values differ from the original estimates by up to 2.7 mm at zenith. This sounds to be small but when tackling the 1 mm accuracy threshold, it is definitely necessary to use the new focal length series in a VLBI delay correction model.

In general, it has to be said that the elevation dependent focal length variations of the Effelsberg 100 m radio telescope are much smaller than originally expected. From 90° elevation down to 15°, the focal length reduces by only 12.6 mm. (Abbondanza and Sarti , 2010) reported 23.8 mm and 17.8 mm focal length differences between 90° and 15° for the Medicina and Noto telescopes, respectively. However, these telescopes have a 32 m diameter and the reflecting area is, thus, smaller by a factor of almost 10. For this reason, it is not quite appropriate to extrapolate the Medicina and Noto results to the global VLBI telescope network. This rather emphasizes the necessity for further investigations in this subject and further terrestrial laser scanner monitoring at other radio telescopes as well.

References

Abbondanza, C. and Sarti, P. (2010). "Effects of illumination functions on the computation of gravity-dependent signal path variation models in primary focus and Cassegrainian VLBI telescopes." *J Geodesy*, 84 (8), 515-525, DOI: 10.1007/s00190-010-0389-z

Bach U, Kraus A, Fürst E, Polatidis A (2007) First report about the commissioning of the new Effelsberg sub-reflector. Effelsberg Memo Series. http://www3.mpifr-bonn.mpg.de/div/effelsberg/EffMemo/12092007_memo.pdf.

Dutescu E, Heunecke O, Krack K (2009). "Formbestimmung bei Radioteleskopen mittels Terrestrischem Laserscanning." *Allgem Verm Nachr*, 6, 239-245

Holst C, Zeimetz P, Nothnagel A, Schauerte W, Kuhlmann H (2012) Estimation of Focal Length Variations of a 100 m Radio Telescope's Main Reflector by Laser Scanner Measurements. *J Surv Eng*, 138 (3), 126-135, DOI: 10.1061/(ASCE)SU.1943-5428.0000082

Sarti P, Vittuari L, Abbondanza C (2009a) Laser scanner and terrestrial surveying applied to gravitational deformation monitoring of large VLBI telescopes' primary reflector. *J Surv Eng*, 135 (4), 136-148, DOI: 10.1061/(ASCE)SU.1943-5428.0000008

Sarti, P., Abbondanza, C. and Vittuari, L. (2009b) Gravity-dependent signal path variation in a large VLBI telescope modelled with a combination of surveying methods. *J Geodesy*, 83 (11), 1115-1126, DOI: 10.1007/s00190-009-0331-4

The Onsala Twin Telescope Project

R. Haas

Abstract This paper described the Onsala Twin Telescope project. The project aims at the construction of two new radio telescopes at the Onsala Space Observatory, following the VLBI2010 concept. The project starts in 2013 and is expected to be finalized in 2017.

Keywords Onsala Space Observatory, VLBI2010, Twin Telescope

1 Introduction

In September 2011 a project team consisting of Hans Olofsson, the director of the Onsala Space Observatory, Gunnar Elgered, the head of the Department for Earth and Space Sciences at Chalmers University of Technology, Rüdiger Haas, the research group leader of the Space Geodesy and Geodynamics research group at Chalmers, Mikael Lilje, the head of the Geodesy Division of Lantmäteriet, the Swedish Mapping, Cadastral and Land Registration Authorty, and Jan Johansson, the deputy head of the Department for Measurement Technology at SP Technical Research Institute of Sweden, submitted a proposal to the National Infrastructure programme of the Knut and Alice Wallenberg (KAW) Foundation. This proposal concerned a twin-telescope system for geodetic Very Long Baseline Interferometry (VLBI) at the Onsala Space Observatory, following the VLBI2010 recommendations (Petrachenko et al., 2009). The proposal was accepted in April 2012 by KAW, and a total amount of 29.7 MSEK was granted for the project.

Rüdiger Haas
Chalmers University of Technology, Onsala Space Observatory, SE-439 92 Onsala, Sweden

2 The Onsala Space Observatory

The Onsala Space Observatory (OSO) is the National Facility for Radio Astronomy in Sweden and has the official mission to support research within radio astronomy and geosciences. The observatory was established in 1949 and is located at Råö on the Onsala-pensinsula at the Swedish West coast, about 40 km south of Gothenburg. Onsala belongs to the municipality of Kungsbacka. An aerial photo of the observatory is presented in Figure 1.

Since 1949 the observatory has been equipped with several radio telescopes of various sizes. The three existing ones today are the 25 m diameter radio telescope built in 1963, the 20 m radio telescope built in 1976, and the LOFAR station built in 2011. However, remaining parts of older telescopes, e.g. concrete foundations, are still there.

The observatory has a long and very successful record in Very Long Baseline Interferometry (VLBI) going back to 1968 (Scherneck et al., 1998). Onsala was the first European observatory to contribute to

Fig. 1 An aerial photo of Råö with the Onsala Space Observatory (Credit: Onsala Space Observtory/Västkustflyg, 2011). The white spot approximately in the center of the photo is the 30 m diameter radome that is enclosing the 20 m radio telescope.

VLBI observations (Whitney, 1974). Today OSO is contributing to observations in the European VLBI Network for Astronomy (EVN) and the International VLBI Service for Geodesy and Astrometry (IVS).

The geoscientific observations are performed using the 20 m radio telescope for geodetic VLBI, several receiving stations for Global Navigation Satellite Systems (GNSS), a superconducting gravimeter, a seismometer, a GNSS-based tide gauge, and several ground-based microwave radiometers for observations of the atmosphere (Haas et al., 2012).

3 The planned location of the Onsala Twin Telescope

The geological situation at Råö is very suitable for the construction radio telescopes since the area is dominated by bed rock of type Gneiss. A first geotechnical inspection indicated that new radio telescopes could be constructed anyywhere on the observatory premises. However, there are additional constraints. The new telescopes should be located not too far away from each other, so that they share the same atmospheric conditions, but not too close to each other either in order to avoid sky blockage. Their elevation axes should be approximately at the same height in order to guarantee equally good visibility. Furthermore, the majority of the horizon shall be free down to an elevation angle of 5°, and the existing equipment at the observatory should not be disturbed by the new telescopes. Other considerations concern the closeness to the sea, wind influence and closeness to a natural reserve in the northern part of the observatory.

Based on these considerations we located two suitable sites for the telescopes. They are in about 140 m and 210 m distance to the existing 25 m telescope and form a short east-west oriented baseline of approximately 76 m distance. Actually, the chosen places were occupied in the 1950'ies and 1960'ies by two so-called Würzburg antennas with 9 m diameter and the concrete foundations for these antennas are still there. The Würzburg antenna at the Eastern location was rebuild into a 12 m telescope in the 1960'ies. A photograph of these two antennas, taken in the 1960'ies, is presented in Figure 2. In late 1969 the 12 m telescope was unfortunately destroyed in a storm (Rydbeck, 1991).

Simulations were performed to investigate the horizon masks for the Onsala Twin Telescope. Also the impact on the horizon mask of the existing 25 m and 20 m radio telescopes was inspected. Figure 3 depicts a digital elevation model of the area, showing the location of the 25 m telescope and the planned twins, OTT1 and OTT2. The local topography is indicated by contour lines with 2 m resolution. The three telescopes are on a small peninsula that is surrounded on three sides by the sea and wetland, respectively. In about 200 to the north, there is a rocky hill with a height of more than

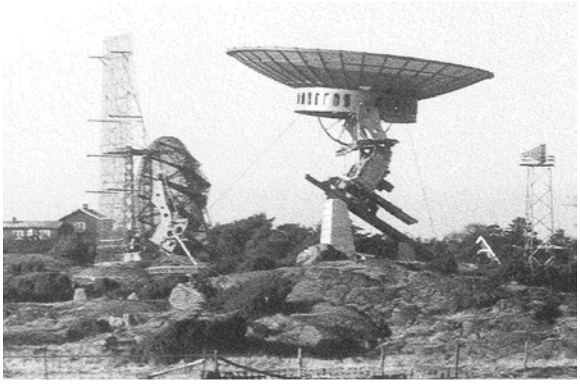

Fig. 2 Two of the parabolic antennas at Onsala in the 1960'ies. Right: The 12 m diameter telescope ("nr. 1") that was destroyed in a storm in 1969. Left: A 9 m diameter Würzburg antenna ("nr. 2"). The antennas formed a west-east baseline ("nr. 2" to "nr. 1"). The photo is taken from Rydbeck (1991).

Table 1 Distances (m) between the existing and the planned telescopes at OSO.

	25 m	OTT1	OTT2
20 m	601.1	397.3	465.3
25 m	–	209.0	136.1
OTT1	–	–	75.7

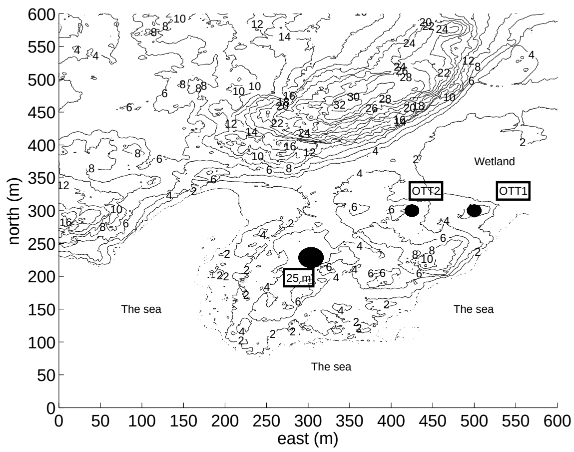

Fig. 3 Digital elevation model of a selected area of OSO, showing the location of the 25 m telescope, and the planned Onsala Twin Telescope antennas, OTT1 and OTT2. These three telescopes are on a small peninsula that is surrounded by the sea from south-west to south-east and wetland in the east. In the north, there is a rocky hill of more than 32 m height.

32 m. The foundations of the OTT twins are planned to be at a height of 5.5 m. Table 1 lists the distances between the existing and planned telescopes.

The planned OTT telescopes do not significantly impact the horizon masks of the existing 20 m and 25 m telescopes. Since the twin telescopes are not located in the same direction towards the 25 m telescope, they will not see the 25 m telescope in the same azimuth direction. This reduces the area of the horizon that is blocked for both telescopes together. Figure 4 depicts the horizon masks of the twin telescopes individually (dashed and dashed-dotted lines), and the combined horizon mask of both telescopes (solid line). The calculations were performed as seen from the lower edge of the prime reflectors, i.e. this is a kind of worst case scenario. The combined horizon of OTT is completely free above 7° elevation and blocked by less than 11 % above 5° elevation. The largest obstacle is the rocky hill towards the north of the twin telescope.

4 The environmental conditions at Onsala

The OSO site is located directly at the Swedish west coast, see Figure 1, and surrounded by the salty sea waters of the Kattegatt. It is thus experiencing a rather harsh marine climate with a high percentage of salt in the air, often westerly winds with a salty sea breeze, and salty spray in the direct vicinity of the shore. Metal constructions that are located in this environment need a very good corrosion protection to survive this harsh marine climate.

Figure 5 depicts the meteorological records of air pressure, air temperature, and relative humidity recorded at OSO during 2010–2012. The pressure variation show the frequently passing weather fronts. The annual temperature variation extends over about 40 °C, and the median relative humidity is 75 %. The extreme values that were recorded during this period are listed in Table 2.

Table 2 Information on pressure (P), temperature (T), relative humidity (RH), mean wind (MW) and gust wind (GW) recorded at the OSO during 2012–2012.

	P (hPa)	T (°C)	RH (%)	MW (m/s)	GW (m/s)
maximum	1047.1	+27.1	98.6	31.5	38.0
median	1010.8	+8.2	79.3	6.4	7.6
mean	1010.6	+7.7	77.8	5.7	8.4
minimum	962.5	−15.6	22.0	0.0	0.0

Table 3 Statistics on mean wind (MW) and gust wind (GW) for OSO during 2010–2012.

percentage of time %	MW (m/s)	GW (m/s)
99.00	≤ 16.3	≤ 20.5
99.50	≤ 17.5	≤ 22.3
99.75	≤ 19.0	≤ 24.2
100.00	≤ 31.5	≤ 38.0

Cumulative distribution functions of mean wind and gust wind recorded during 2010–2012 are pre-

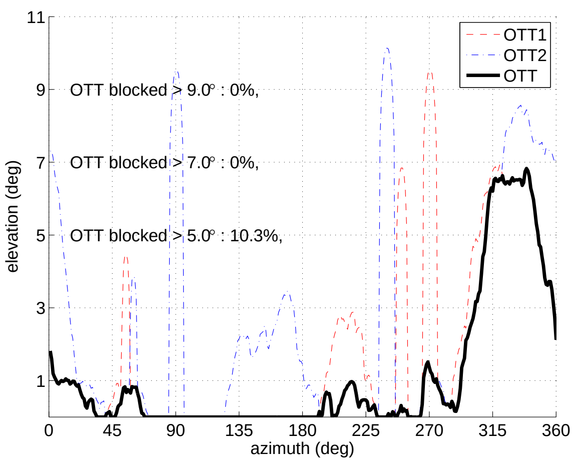

Fig. 4 Horizon masks for the individual twin telescopes, OTT1 (dashed line, red) and OTT2 (dashed-dotted line, blue), and for both OTT antennas together (solid line, black), as seen from the lower edge of the prime reflectors. The rocky hill in the north is the largest obstacle. However, the OTT horizon is completely free above 7° elevation, and less than 11 % of the horizon is blocked above 5° elevation.

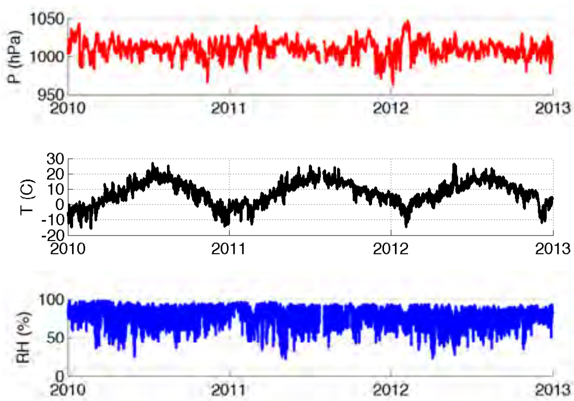

Fig. 5 Observations of air pressure (top, red), air temperature (middle, black) and relative humidity (bottom, blue) at OSO for 2010–2012.

sented in Figure 6. The standard definitions of mean wind and gust wind following the World Meteorological Organisation (WMO) are used, i.e. mean wind is the average wind speed in a 10 minute time interval, and gust wind is the maximum 3 s average wind speed during in a 10 minute time interval (Harper et al., 2010).

The corresponding wind statistics are given in Table 3. For 1 % of the time, i.e. less than 4 days per year, the mean and the gust winds exceed 16.3 m/s and 20.5 m/s, respectively. For 0.5 % of the time, i.e. less than 2 days per year, the mean and the gust winds exceed 17.5 m/s and 22.3 m/s, respectively. For 0.25 % of the time, i.e. less than 1 day per year, the mean and the gust winds exceed 19.0 m/s and 24.2 m/s, respectively.

A rose diagram of mean wind directions and mean wind speeds that were recorded during 2010–2012 is presented in Figure 7. The predominant wind direction at OSO is west-south-west where also the stronger wind speeds are observed. Wind from north-east is very seldomly exceeding 10 m/s wind speed.

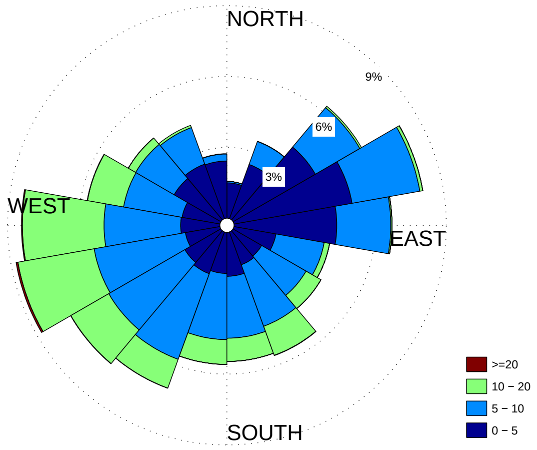

Fig. 7 Rose diagram of the mean wind direction and speed recorded at OSO during 2010–2012. Mean wind speed is represented in four colour coded groups: 0–5 m/s (dark blue), 5–10 m/s (light blue), 10–20 m/s (green), and > 20 m/s (red).

5 Status and Outlook

The request for the OTT building permit has been submitted to Kungsbacka municipality in December 2012, together with the request for an exemption from the law for shoreline protection (i.e. permit of constructions within 300 m from the shoreline). In early April 2013 both request were approved by Kungsbacka municipality. However, the authorities of the county of Halland, to which Kungsbacka and Onsala belong, decided to appeal the decision of Kungsbacka municipality to grant exemption from the law for shoreline protection.

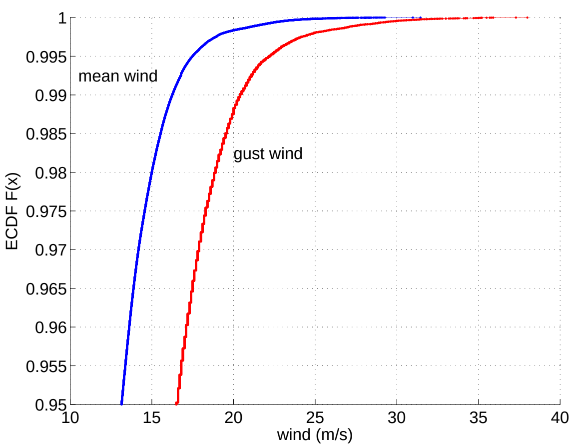

Fig. 6 Cumulative distribution functions of mean wind (blue) and gust wind (red) observed at OSO during 2010–2012.

The county's environmental department inspected the planned construction sites and concluded that the eastern location (OTT1) is close to wetlands where waders were seen, in particular the Northern Lapwing (*vanellus vanellus*). According to the county's environmental department could OTT1 disturb the breeding of waders in the area. Furthermore, there are plans by the county to include the wetlands in a natural reserve. Thus, in June 2013 the county of Halland withdraw the exemption from the law for shoreline protection for OTT1.

The Onsala Space Observatory will appeal against the county's decision and thus filed an official complaint. A first meeting with lawyers will take place in late summer. Currently it is hard to foresee by how long the Onsala Twin Telescope project will be delayed, but we expect at least 6 months of delay.

Meanwhile, we are preparing the procurement papers for the antennas, so that the documents can be sent out as soon as the legal case with the county of Halland is solved. The procurement papers will basically follow the VLBI2010 recommendations (Petrachenko et al., 2009). The main features that will be required can be shortly summarized as:

- the sensitivity of each system must be better than 2000 Jy for broadband observations over 2–14 GHz
- the antennas must be fast moving and of at least 12 m diameter
- the antennas must be mechanically stiff with a good control on thermal and gravitational deformations
- the antennas have to be well suited for the harsh environmental conditions at Onsala and have to allow 24/7 operations.

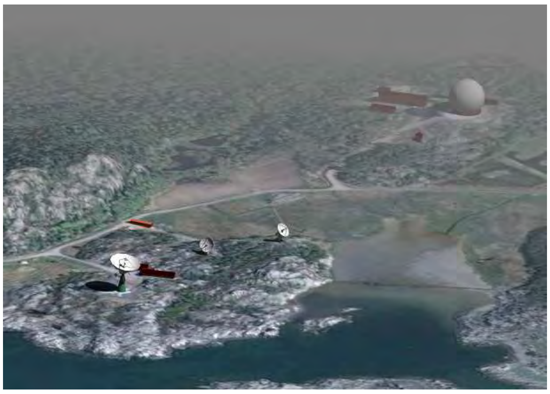

Fig. 8 An artist's view of the future Onsala Twin Telescope, together with the 25 m telescope (foreground, left) and the radome enclosed 20 m telescope (background, right).

Table 4 Expected time line of the OTT project.

2013	Approvement of building permit and exemption from the law for shoreline protection.
	Procurement process and contract for the antennas.
2014	Construction of foundation and infrastructure.
	Procurement process and contract for the signal chain.
2015	Delivery and installation of the antennas.
	Establishment of a local survey network.
2016	Delivery and installation of signal chain and electronics.
	First system tests, and local survey work.
2017	Inauguration of the Onsala Twin Telescope.
	System tests and test observations.
	Transition to regular operations.

Once the procurement for the antennas has been completed and contracts have been signed, we will continue with the procurement process of the signal chain. We also will start the preparations for the actual installation of the antennas. The expected time line of the OTT project is given in Table 4. An artist's view of the future Onsala Twin Telescope is given in Figure 8.

References

O. Rydbeck. Femtio år som rymdforskare och ingenjörsutbildare, Del 2, 1951 – 1989. Chalmers Tekniska Högskola, Göteborg, ISBN 91-7032-621-5, 407–823, 1991.

B. Petrachenko, A. Niell, D. Behrend, B. Corey, J. Böhm, P. Charlot, A. Collioud, J. Gipson, R. Haas, Th. Hobiger, Y. Koyama, D. MacMillan, Z. Malkin, T. Nilsson, A. Pany, G. Tuccari, A. Whitney, and J. Wresnik. Design Aspects of the VLBI2010 System. NASA/TM-2009-214180, 58 pp., 2009.

R. Haas, G. Elgered, J. Löfgren, T. Ning, and H.-G. Scherneck. Onsala Space Observatory - IVS Network Station. In K. D. Baver and D. Behrend, editors, *International VLBI Service for Geodesy and Astrometry 2011 Annual Report* NASA/TP-2012-217505, 88–91, 2012.

H.-G. Scherneck, G. Elgered, J. M. Johansson, and B. O. Rönnäng. Space Geodetic Activities at the Onsala Space Observatory: 25 years in the Service of Plate Tectonics. *Phys. Chem. Earth*, Vol. 23, No. 7-8, 811–823, 1998.

A. R. Whitney. Precision Geodesy and Astrometry via Very Long Baseline Interferometry. Ph.D. thesis, Dept. of Electrical engineering, MIT Cambridge, MA., 1974.

B. A. Harper, J. D. Kepert, and J. D. Ginger. Guidelines for converting between various wind averaging periods in tropical cyclone conditions. WMO/TD-No. 1555, 64 pp., 2010. (available at `http://www.wmo.int/pages/prog/www/tcp/documents/WMO_TD_1555_en.pdf`)

Renewal of Metsähovi Observatory

M. Poutanen, U. Kallio, H. Koivula, J. Näränen, A. Raja-Halli, N. Zubko

Abstract The Metsähovi Geodetic Observatory was established in 1975 and it has through the years become an essential part of the activities of the Finnish Geodetic Institute. The instrumentation covers the satellite laser ranging (SLR), geodetic VLBI, GPS and GLONASS receivers, DORIS beacon, super-conducting gravimeter and a seismometer. It is an IAG GGOS Core station. As a co-operation with the Metsähovi Radio Observatory of the Aalto University, geodetic VLBI observations were started in 2005. Metsähovi participates in 6–8 geo-VLBI campaigns annually, as a part of the IVS (International VLBI Service) network (IVS-T2) and the European geodynamics project (EUROPE campaigns). In 2012 Ministry of Agriculture and Forestry allocated a special 5-year funding for renewal of Metsähovi instrumentation. This includes a new SLR, and dedicated radio telescope for geodetic VLBI. We describe the renewal plans of Metsähovi and plans for the new VLBI2010 compatible system.

Keywords Fundamental stations, Metsähovi, renewal, geodetic VLBI

1 Introduction

Finnish Geodetic Institute (FGI) is a governmental research institute (established 1918) carrying out, among other things, geodetic measurements and research to establish and maintain national geodetic frames of Finland, including the coordinate system, precise levelling network and the national gravity network. FGI is also responsible to attach these to the corresponding measurements of the neighbouring countries and international networks. This implies participation on global and regional observing networks.

Metsähovi geodetic observatory was established in 1975 at the same site where the University of Helsinki had an optical telescope and the Helsinki University of Technology (nowadays Aalto University) built a radio telescope. The site was suitable for such observatories because of its remote location and a minimal environmental interference (light, traffic disturbance, radio interference).

Satellite Laser Ranging (SLR) observations begun in 1978, followed by a mobile VLBI point in 1988 (for the first EUREF campaign to establish a European reference frame ETRS89), the French DORIS beacon and a permanent GPS station in 1991/1992, and a superconducting gravimeter in 1994. Metsähovi has through the years become an essential part of the activities of the FGI and now it is a key infrastructure of the FGI both internationally and on the national level (Fig. 1).

Metsähovi is a part of the core station network of GGOS (Global Geodetic Observing System of the International Association of Geodesy, IAG). The global network of multi-technique geodetic stations are used in maintaining terrestrial and celestial reference frames, for computation of satellite orbits, and for geophysical studies. Metsähovi is one of the northernmost geodetic stations in this network, thus being of an ultimate importance for maintenance of global reference frames and satellite orbits. Its long existence is important for maintenance of stability of the global reference frames and it contributes to the GGOS via the respective IAG/GGOS services.

Metsähovi is the core station also for the national Euref-FIN reference system, new Finnish height system N2000 and the Finnish gravity network. It is the fundamental point of the National permanent GNSS network FinnRef, the highest order network for the Euref-FIN. Euref-FIN, created by the FGI, is the national realization of the European reference system

Markku Poutanen, Ulla Kallio, Hannu Koivula, Jyri Näränen, Arttu Raja-Halli and Nataliya Zubko
Finnish Geodetic Institute, Geodeetinrinne 2, 02430 Masala, Finland

Fig. 1 Metsähovi observatory

ETRS89, fulfilling the requirements of the EU directive INSPIRE. The fundamental benchmark defining the national height system N2000 is at Metsähovi which is connected to the precise levelling network of Finland by a traditional spirit levelling. In Metsähovi there is also the Finnish gravity network basic point and facilities for comparison of absolute gravimeters.

A list of facilities are shown in Table 1. Today, most of the major large instruments are either under renovation (SLR), do not fulfil the current specifications of the GGOS services (VLBI, GNSS) or are so old that no service or spare parts are available (SG, GPS). Therefore it was mandatory to upgrade instruments and facilities to maintain operations at Metsähovi as a part of the GGOS Core Station network.

Based on the special funding from the Ministry of Agriculture and Forestry, the major instruments will be renewed in 2012–2016. The renewal plan includes GNSS network, a new SLR telescope with relevant hardware, software, a new dome, and other facilities to operate the SLR. To initiate a 24/7 geodetic VLBI observations there will be also a new radio telescope dedicated for the geodetic VLBI observations and fulfilling the specifications of the VLBI2010 plan. The absolute gravimeter will be upgraded and there will be a new superconducting gravimeter replacing the old one dated back to 1994. Moreover, general infrastructure will be improved and quite extensive work on establishing and improving local ties between instruments has already been initiated.

2 Importance of combining VLBI and other space geodetic techniques at Fundamental Stations

Creation and maintenance of two fundamental reference systems and their realizations, namely the celestial and the terrestrial reference systems and frames, are the ultimate tasks in geodesy. The International Celestial Reference System (ICRS) is realized through the International Celestial Reference Frame (ICRF), which is a set of coordinate positions of extragalactic radio sources, quasars, distributed over the celestial sphere.

The International Terrestrial Reference System (ITRS) is realized through the International Terrestrial Reference Frame (ITRF), a network of globally distributed geodetic observing stations. The coordinate positions and velocities of these points are derived from space-geodetic observations, mainly by C-GNSS (continuous GNSS, primarily GPS, but in the future also by GLONASS, Galileo and BeiDou satellite positioning systems).

The link between ITRF and ICRF is provided by the set of the Earth Orientation Parameters (EOP) which are obtained by using the observations of the space-geodetic techniques, primarily VLBI. These parameters include precession, nutation, polar motion, and the rotation of the Earth (UT1). The information on the orientation of the Earth in space is needed for operation of the navigation satellites, and without

Table 1 Current instruments and facilities at Metsähovi and the planned renewal schedule

Facility (IAG/GGOS Service)	Renewal
Satellite laser ranging, SLR, since 1978. (ILRS)	2013-2015
Geodetic VLBI, since 2004. (IVS)	2013-2016
Geodetic permanent GPS receiver, since 1992. (IGS, EPN)	2013
Geodetic GLONASS receiver, since 1998. (IGS)	2013
Superconducting gravimeter, since 1994. (GGP)	2012-2013
Absolute gravimeter and fundamental gravity point of Finland, since1988.	2013
Site for absolute gravimeter inter-comparison, since 1994	N/A
Doris beacon owned by CNES, France, since 1991 (IDS)	2012
Photogrammetric test field	2013-2014
GPS receiver owned by NASA/JPL, in a real-time NASA tracking network	N/A
Seismometer owned by the Institute of Seismology, University of Helsinki	N/A
Fundamental point of the new Finnish height system N2000	N/A
Precise levelling test field	N/A
Pillar network for local ties and EDM (electronic distance measurement) tests	2013
Soil-moisture tracking network	2012-2013
Weather stations	2013
ILRS = International Laser Ranging Service; IVS = International VLBI and Astrometry Service; IGS = International GNSS Service; EPN = Euref Permanent GNSS Network; GGP = Global Geodynamics Project; IDS = International DORIS Service.	

continuous monitoring of the EOP, precise use of the GNSS satellites would not be possible.

During last two decades satellite observations and global geodetic networks have revolutionized our possibilities to observe the Earth‘s surface and gravity, their temporal variations, and consequences of the global change. The increased accuracy, however, reveals inconsistencies between different observation techniques, requiring more precise reference frames, and especially requesting co-location of techniques and observing networks (Altamimi *et al.* (2011)). There is also a need to connect geometrical (GNSS based) and gravity field related heights, e.g. for studies of the sea level changes or glacier mass changes (e.g. Poutanen *et al.* (2013)).

The most important elements for the determination and maintenance of the EOP and ITRF are the geodetic stations which have at least three independent co-located space-geodetic techniques (in addition to ground based absolute and relative gravity observations, seismometers and tide gauges, where possible). However, globally, there are currently only about a dozen of stations with more than three techniques, Metsähovi being one of these. Each technique has its own strength or it contributes to different parameters as shown in Table 2.

Essential part at the multi-technique sites are the local ties, ground vectors between the instruments. The current GGOS recommendation for the local tie accuracies between techniques is 1 mm (Pearlman and Plag (2009)). However, it is not possible today to fulfil the requirement, and further development must be done in the future to reach the goal (see e.g. Krügel and Angermann (2008); Kallio and Poutanen (2012)). The origin of discrepancies are uncertainties in local tie measurements, biases between space geodetic solutions or site specific effects.

New promising technique to directly tie GNSS and VLBI during the geo-VLI sessions has been developed at Metsähovi (Kallio and Poutanen (2012), Kallio and Poutanen (2013)). This will improve the real-time tracking of local ties, especially at sites with a radome around the radio telescope.

Table 2 Contribution of different geodetic techniques. According to Rothacher *et al.* (2009)

Item	VLBI	GNSS	DORIS	SLR	AG—SG
Celestial Reference frame	+				
Nutation	+	(+)		(+)	
Polar variation	+	+	+	+	+
Earth rotation (UT1)	+				
Length of Day (LOD)	(+)	+	+	+	
Global reference frames	+	+	+	+	+
Local reference frames, navigation		+			
Earth Center of Mass		+	+	+	+
Earth Gravity Field		+	+	+	+
Geoid					+
GNSS satellite orbits		+	+	+	
Orbits of environmental satellites		+	+	+	
Ionosphere and troposphere	+	+	+		
National reference frames		+			
Time/frequency	+	+		(+)	

3 Metsähovi renewal

The Ministry of Agriculture and Forestry allocated a total of 8 M Euros for renewal of Metsähovi instrumentation. This includes a new SLR, a radio telescope dedicated for geodetic VLBI, a superconducting gravimeter, renewal of the Finnish permanent GNSS network, FinnRef, and a number of minor upgrading of instruments or facilities. The ear-marked funds are available in 2012–2016 which will set strict limits on the schedule and also on the budget.

The GNSS network FinnRef was established in mid-1990's and it consists of 13 stations. After completing the renewal the total number of stations will be increased to 19 to better cover the territory of Finland. New GNSS receivers, capable to track all GNSS satellites, were purchased in 2012 and the renewal of the network will be ready in 2013. Old receivers will observe parallel with the new ones as long as they are able to maintain operational, preferably one to two years. This will ensure seamless continuation of GNSS time series for geodynamics studies.

Starting from 2014, the network data of the renewed FinnRef network will be freely available in real time, and a free public navigation service capable of reaching an accuracy of about 0.5 m will be released. Metsähovi is one of the FinnRef stations and a new receiver will be installed also there. Metshovi GNSS is a part of EPN (EUREF Permanent Network) and IGS (International GNSS Service).

A tender for a new SLR telescope was open in the first half of 2013. Selection of the vendor and signing the contract will be made before the end of the year. The aim is a 0.5–1 m telescope fulfilling the ILRS (International Laser Ranging Service) recommendations for the speed and accuracy. A 2 kHz pulse laser already exists at the FGI and the software development for the controlling system has been started. The new system is expected to be operational in 2016.

A new observatory building and a dome will be constructed for the SLR. It will contain a temperature-stabilized instrument room, a control room for the operator, and other facilities which can be used also for operating and monitoring the new VLBI telescope. A new hydrogen maser is also planned to be placed in the same building.

A superconducting gravimeter (SG) has been ordered in 2012, and the installation is expected in the latter half of 2013. The old SG will remain one year more in parallel with the new one to allow simultaneous observations of both instruments, and more importantly, to study possible differences between the observations, and to see any temporal variation in the horizontal gradient of gravity. The absolute gravimeter FG5-221 has already been upgraded in early 2013 for model FG5-X.

The biggest instrument will be a new radio telescope dedicated for the geodetic VLBI only. The telescope will be VLBI2010 compatible, with a 12–14 m dish and the slew rate fast enough to fulfil the specifications. The plans and requirements will be finalized in 2013, and the tender is planned to be opened also before the end of the year 2013. Several practical issues, like to have a radome or not a radome around the telescope has to be solved before this.

There will be a close co-operation with the Onsala radio observatory of the Chalmers University of Technology in Sweden because they have similar plans and schedule for a new telescope or a pair of identical telescopes (R. Haas, private communication, 2013). Also there will be a lot of practical work on technical and local issues with the Aalto University Metsähovi Radio Observatory.

A co-operation is planned also with the Finnish centre for metrology and accreditation (MIKES). A plan for time and frequency transfer and use of results from the development of a primary frequency standard, an optical ion clock at MIKES, will allow the use of a new ultra stable clock in VLBI observations, and possibly even a common clock experiment with another VLBI facility at Onsala. Such a connection has not been established before due to the technical challenges of the link.

In addition to the major instruments, many smaller improvements and enhancements are planned. These include renovation of the observatory buildings, and improvement of local tie and GNSS antenna calibration facilities. The latter one relates to a EMRP (European Metrology Research Programme) project where the metrological traceability is implemented in geodetic measurements, especially in precise length measurements over hundreds of meters (SIB60 (2013)). Two central parts in the EMRP project are the traceability in local ties at fundamental geodetic stations, and a test field for GNSS antenna calibrations, both facilities already existing at Metsähovi.

4 Summary

The on-going renovation and upgrading of Metsähovi facilities and instrumentation is a great opportunity to recover and improve some activities and keep the station up-to-date in the global geodetic network. This would not be possible without special funding from the

Ministry. If renovation is realized as planned, all new instruments will be operational in Metsähovi within next few years, the last one being the new radio telescope in 2016–2017. As the national authority to maintain the national reference system, FGI is committed to develop Metsähovi as the key infrastructure also in the future.

References

Z. Altamimi, X. Collilieux and L. Métivier (2011), ITRF2008: an improved solution of the international terrestrial reference frame. *Journal of Geodesy*, Vol. **85**, N:o 8, pp. 457-473, Springer Verlag. doi: 10.1007/s00190-011-0444-4.

U. Kallio and M. Poutanen (2012), Can we really promise a mm-accuracy for the local ties on a geo-VLBI antenna. In: S. Kenyon, M. Pacino, U. Marti (Eds.) *Geodesy for Planet Earth*. IAG Symposia, Vol. **136** pp. 35–42, Springer Verlag. doi: 10.1007/978-3-642-20338-1_5.

U. Kallio and M. Poutanen (2013), Local Ties at Fundamental Stations. In Z. Altamimi and X. Collilieux (eds.), *Reference Frames for Applications in Geosciences*, IAG Symposia **138**, Springer Verlag doi: 10.1007/978-3-642-32998-2_23 (in print)

M. Krügel and D. Angermann (2008), Frontiers in the combination of space geodetic techniques. In P. Tregoning and C. Rizos (Eds.) *Dynamic Planet*. IAG Symposia, Vol. **130**, 158–165, Springer Verlag, doi: 10.1007/978-3-540-49350-1_25

M. Pearlman and H.-P. Plag (Eds.) (2009), *Global Geodetic Observing System: Meeting the Requirements of a Global Society on a Changing Planet in 2020*. Springer Verlag. doi: 10.1007/978-3-642-02687-4.

M. Poutanen, J. Ihde, C. Bruyninx, O. Francis, U. Kallio, A. Kenyeres, G. Liebsch, J. Mäkinen, S. Shipman, J. Simek, S. Williams, H. Wilmes (2013), Future and development of the European Combined Geodetic Network ECGN In: Chris Rizos, Pascal Willis (Eds.) *Earth on the Edge: Science for a Sustainable Planet.* IAG Symp. **139**. Springer Verlag. doi: 10.1007/978-3-642-37222-3. (In print)

M. Rothacher, G. Beutler, W. Bosch, A. Donnellan, R. Gross, J. Hinderer, C. Ma, M. Pearlman, H.-P. Plag, B. Richter, J. Ries, H. Schuh, F. Seitz, C. K. Shum, D. Smith, M. Thomas, E. Velacognia, J. Wahr, P. Willis, P. Woodworth (2009), The future Global Geodetic Observing System (GGOS). In: Pearlman, M., H.-P. Plag (eds.). *Geodetic Observing System: Meeting the Requirements of a Global Society on a Changing Planet in 2020.* Springer Verlag. doi: 10.1007/978-3-642-02687-4.

SIB60 (2013), Publishable JRP Summary Report for JRP SIB60 Surveying. Metrology for Long Distance Surveying. http://www.euramet.org/fileadmin/docs/EMRP/JRP/JRP_Summaries_2012/SI_Broader_Scope_JRPs/SIB60_Publishable_JRP_Summary.pdf

Vienna VLBI Software – Current release and plans for the future

M. Madzak, J. Böhm, S. Böhm, H. Krásná, T. Nilsson, L. Plank, C. Tierno Ros, H. Schuh, B. Soja, J. Sun, K. Teke

Abstract The Vienna VLBI Software (VieVS) is a geodetic Very Long Baseline Interferometry (VLBI) data analysis software which has been developed at the Vienna University of Technology since 2008. This paper gives an overview about its capabilities, including scheduling and simulation of VLBI observations. The latest release, version 2.1 includes a a graphical user interface. A few results and planned future developments are presented as well.

Keywords VLBI, data analysis, Scheduling, Simulation

1 Introduction

To meet the requirements of future geodetic VLBI experiments, e.g. VLBI2010, the VLBI group at Vienna University of Technology has been developing and maintaining a VLBI data analysis software called VieVS (Vienna VLBI Software, Böhm et al., 2012). Several institutions worldwide use the software to perform various investigations. The code can be read and changed easily since it is written in Matlab. Therefore VieVS runs on all operating systems which are able to run Matlab.

M. Madzak, J. Böhm, S. Böhm, H. Krásná, L. Plank, C. Tierno Ros
Vienna University of Technology, Department of Geodesy and Geoinformation, Gußhausstraße 27-29, A-1040 Vienna, Austria
T. Nilsson, H. Schuh, B. Soja
GFZ German Research Centre for Geosciences, Telegrafenberg, D-14473 Potsdam, Germany
J. Sun
Chinese Academy of Sciences, 319 Yueyang Road, Shanghai 200031, China
K. Teke
Hacettepe University, Department of Geomatics Engineering, Beytepe 06800, Ankara, Turkey

In the latest release versions (2.0 and 2.1) we have focused on a new Graphical User Interface (GUI) which makes the use of the program even easier, for experienced users as well as for students. This GUI provides a consistent treatment of all capabilities of the software, i.e. single session analysis, scheduling, simulation and global parameter estimation. Furthermore the new version includes a plotting tool to visualize several useful information as well as the estimated parameters.

2 VieVS overview

The idea behind VieVS was to develop a new state-of-the-art VLBI data analysis software to perform single-session analysis. VieVS now is able to read NGS-files as well as openDB files in NetCDF format (Gipson, 2010) and includes the most recent IERS Conventions (Petit and Luzum, 2010). The parameter estimation is done in a least squares adjustment; clock parameters, zenith wet delays, tropospheric gradients, Earth Orientation Parameters (EOP), station and source coordinates can be estimated as piece-wise linear offsets at fractions of integer hours.

The structure and different modules are shown in Fig. 1.

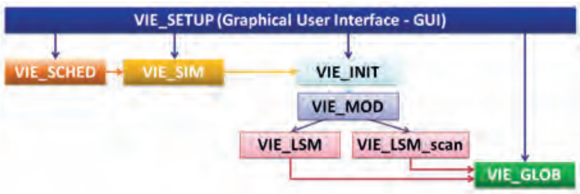

Fig. 1 VieVS structure and different modules of the software.

3 Graphical User Interface

All processing options and output settings can be modified in VIE_SETUP, the graphical user interface of VieVS (Fig. 2). It is built in Matlab as well and therefore allows easy manipulation.

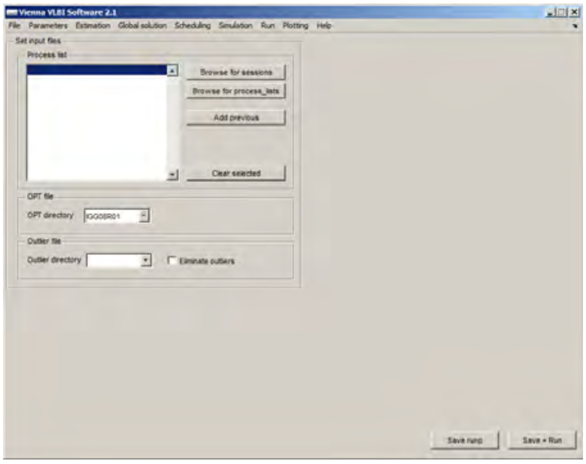

Fig. 2 Graphical user interface of VieVS.

The interface includes a plotting tool where estimated parameters, post-fit residuals and session information can be visualized. Observations can be marked as outliers, clock break information added, and solutions can be compared with each other (Fig. 3). Analysts can furthermore see the station network and the correlation matrix between estimated parameters, as well as plot the baseline length repeatabilities of up to four solutions.

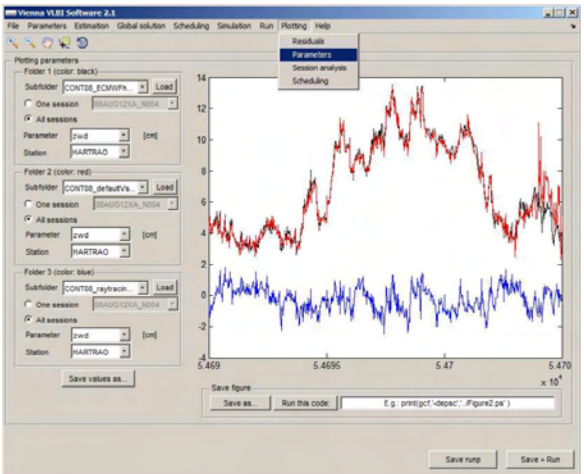

Fig. 3 Comparison of VLBI solutions using the VieVS plotting tool.

4 Additional features

Besides single session analysis, VieVS has several other modules for geodetic VLBI applications.

- Scheduling
  Towards VLBI2010 (Petrachenko et al., 2009) new scheduling strategies have to be developed due to changing equipment at VLBI sites, for example fast-slewing antennas and Twin telescopes. Therefore we have developed VIE_SCHED (Sun, 2013), a scheduling program as part of the VieVS software package. It creates observation schedules and has been used to schedule seven R&D sessions in 2012 to study the Sun corona. As an alternative to the classical 'station-based' algorithm, we can also use the 'source-based' strategy which is simpler and yields similar results as the classical approach. The idea behind the new strategy is to have a simple scheduling algorithm that still achieves a good sky-coverage for an accurate troposphere estimation (Sun, 2013). Using VIE_SCHED we will schedule the AUSTRAL sessions in the second half of 2013.
- Global solution
  The global solution module, VIE_GLOB (Krásná, 2013a), combines normal equations of several single sessions to estimate global parameters, such as Terrestrial Reference Frame (TRF) or Celestial Reference Frame (CRF) solutions. Fig. 4 shows horizontal position differences at epoch 2000.0 between our VieTRF10a (Krásná et al., 2013b) and VTRF2008 (Böckmann et al., 2010). Red arrows denote the datum stations and blue ones the remaining stations.

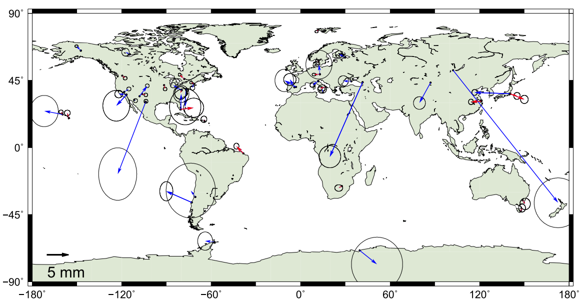

Fig. 4 Horizontal position differences between VieTRF10a and VTRF2008.

- Simulation
  This tool simulates artificial VLBI observations based on theoretical (model) delays plus simulated errors for the main error sources: wet troposphere

(Nilsson and Haas, 2010), clock errors as random walk plus integrated random walk process and white observation noise. Those delays can be written into NGS files and then analyzed like a standard VLBI session.

- Spacecraft tracking
  VieVS, with slight modifications, has successfully been used to process differential VLBI observations of the Japanese lunar spacecraft SELENE (Plank et al., 2013).
- External delays
  In order to make the program more flexible and the structure more similar to the one proposed by the Working Group 4 (Gipson, 2010), we use ASCII files containing tropospheric or ionospheric delays from external sources, such as ray-tracing, GNSS, or TEC-maps.
- Main station/source file
  Since version 2.0 we store all static station- or source-dependent information in a file which makes it easier for the different modules to use those information consistently. The station-file contains different TRF and antenna and equipment information as well as tidal loading coefficients. The source-file is more or less a translation table and includes different CRF.
- Parallel computing
  To decrease the processing time VieVS can run in parallel mode on a CPU with more than one core.
- Documentation
  Since version 2.1 there exists a user manual for the software. It includes a fundamentals chapter about VLBI analysis and exercises for beginners. The document can be downloaded from our webpage: `http://vievs.geo.tuwien.ac.at`.

5 Automatic processing and results

We have set up an automatic processing batch job which automatically downloads and processes all new VLBI sessions. A processing report including information about the session (e.g. date and participating stations), statistics as well as a residuals plot is sent to the analyst who decides if more action has to be taken to derive useful results. This procedure makes an operational analysis of VLBI sessions feasible.

We also estimate UT1–UTC from VLBI Intensive sessions on an operational basis. The estimated values are shown in Fig. 5.

Several geodynamic and astronomical parameters have been estimated using the global solution module VIE_GLOB. Fig. 6 shows the real and imaginary parts of Love numbers for twelve diurnal tidal waves (Krásná et al., 2013c). The two solutions differ in the a priori ocean loading model, where the 'FES2004 solution' is plotted in red and the 'AG06a solution' in light blue. The black line denotes the theoretical values from the IERS Conventions 2010 (Petit and Luzum, 2010).

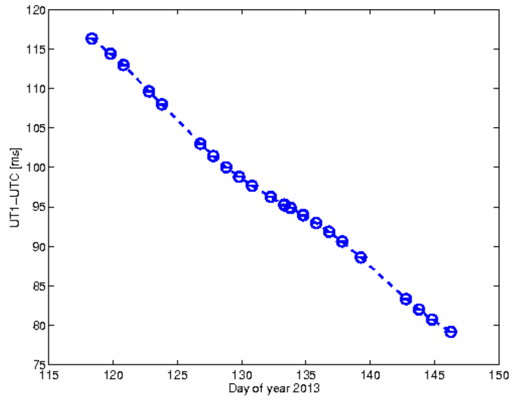

Fig. 5 UT1–UTC from VLBI Intensive sessions estimated with VieVS from April 28th to May 26th 2013.

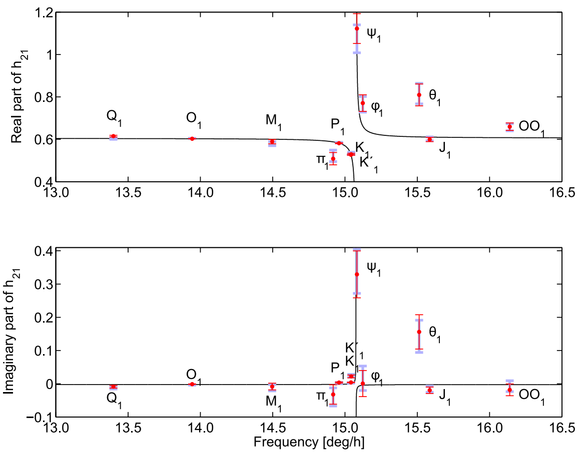

Fig. 6 Real and imaginary parts of Love numbers for twelve diurnal tidal waves estimated with VIE_GLOB.

6 Future plans

- Kalman filter
  As an additional estimation algorithm we will use a Kalman filter which allows to model the stochastic behaviour of e.g. clocks more accurately. Furthermore it may be used for real-time applications.

- Spacecraft observations
  At the moment, VieVS is extended for the possibility to process and simulate VLBI observations to near-Earth targets, e.g. satellites (Plank et al., this issue).
- Group delay ambiguity resolution
  We want to add the possibility to resolve group delay ambiguities, and calculating the ionospheric delay. Then we could use the correlator output to perform analyses earlier.
- Source-structure
  In a cooperation with the University of Tasmania we will include source-structure corrections in the Vienna VLBI Software. As a first step we will perform simulations to study the error due to the structure of sources.

7 Concluding remarks

VieVS is freely available for registered users. Registration and more information can be found at the VieVS webpage: `http://vievs.geo.tuwien.ac.at`.

References

S. Böckmann, T. Artz, A. Nothnagel VLBI terrestrial reference frame contributions to ITRF2008. *J Geod* 84:201–219, 2010. doi: 10.1007/s00190-009-0357-7.

J. Böhm, S. Böhm, T. Nilsson, A. Pany, L. Plank, H. Krásná, K. Teke, H. Schuh. The new Vienna VLBI Software VieVS. In: *Proceedings of IAG Scientific Assembly 2009, International Association of Geodesy Symposia Series Vol. 136*, ed. by S. Kenyon, M. C. Pacino, and U. Marti, pp. 1007-1011, 2012. doi: 10.1007/978-3-642-20338-1_126.

J. Gipson. IVS working group 4: VLBI data structures. In: *Proceedings of IVS General Meeting: VLBI2010: From Vision to Reality*, ed. by D. Behrend and K. D. Baver, NASA/CP-2010-215864, pp. 187-191, 2010.

H. Krásná. Estimation of solid earth tidal parameters and FCN with VLBI. Dissertation, Vienna University of Technology, 2013.

H. Krásná, J. Böhm, L. Plank, T. Nilsson, H. Schuh. Atmospheric Effects on VLBI-derived Terrestrial and Celestial Reference Frames. In: *IAG Symposium 2011, 139*, ed. by C. Rizos and P. Willis, In press, 2013a.

H. Krásná, J. Böhm, H. Schuh. Tidal Love and Shida numbers estimated by geodetic VLBI. *J Geodyn*, In press, 2013b.

T. Nilsson, J. Böhm, S. Böhm, M. Madzak, V. Nafisi, L. Plank, H. Spicakova, C. Tierno Ros, H. Schuh. Status and future plans for the Vienna VLBI Software VieVS. In: *Proceedings of the 20th EVGA meeting 2011*, ed. by W. Alef, S. Bernhart and A. Nothnagel, pp. 93–96, 2011.

T. Nilsson, R. Haas. Impact of atmospheric turbulence on geodetic very long baseline interferometry. *J. Geophys. Res., 115*, B03,407, 2010. doi: 10.1029/2009JB006579.

G. Petit and B. Luzum (eds.). IERS Conventions (2010). *IERS Technical Note; 36*, Frankfurt am Main: Verlag des Bundesamts für Kartographie und Geodäsie, 2010. 179 pp., ISBN 3-89888-989-6

B. Petrachenko, A. Niell, D. Behrend, B. Corey, J. Böhm, P. Charlot, A. Collioud, J. Gipson, R. Haas, T. Hobiger, Y. Koyama, D. MacMillan, Z. Malkin, T. Nilsson, A. Pany, G. Tuccari, A. Whitney, J. Wresnik. Design Aspects of the VLBI2010 System: Progress Report of the IVS VLBI2010 Committee. In: *International VLBI Service for Geodesy and Astrometry 2008 Annual Report*, ed. by D. Behrend and K. D. Baver, NASA/TP-2009-214183, pp. 13–67, 2009.

L. Plank, J. Böhm, M. Madzak, C. Tierno Ros, H. Schuh. Processing SELENE Differential VLBI Data In: *International VLBI Service for Geodesy and Astrometry 2012 General Meeting Proceedings*, ed. by D. Behrend and K. D. Baver, NASA/CP-2012-217504, pp. 291–295, 2013.

L. Plank, J. Böhm, H. Krásná, H. Schuh. VLBI satellite tracking for precise coordinate determination – a simulation study. *this issue*.

J. Sun. VLBI scheduling strategies with respect to VLBI2010. Dissertation, Vienna University of Technology, 2013.

Current status of νSolve

S. Bolotin, K. Baver, J. Gipson, D. Gordon, D. MacMillan

Abstract The software νSolve is a part of the CALC/SOLVE VLBI data analysis system. The primary purpose of νSolve is for preliminary data analysis of new VLBI sessions. In this paper we present the capabilities of the software, its current status and our plans for future development.

Keywords VLBI data analysis software, CALC/SOLVE

1 Introduction

Realization of the VLBI Geodetic Observing System (VGOS) technology and the increasing number of observing VLBI stations lead to new requirements for data analysis software. The necessary flexibility and capacity of the software require new approaches in the software development process.

Having a long experience with the development of the CALC/SOLVE VLBI data analysis software, the VLBI group at the NASA Goddard Space Flight Center initiated creation of the new generation software.

The first step in developing new data analysis software was made in 2007. Active work on software development began in 2010, and in 2012 the first release, called νSolve, was available (Bolotin et al., 2012).

Currently νSolve is used for routine data analysis of the IVS-R4 and IVS-INT sessions at the NASA GSFC VLBI Analysis Center. It is also a good platform for various tests and analysis experiments.

Sergei Bolotin, Karen Baver, John M. Gipson, David Gordon and Daniel S. MacMillan
NVI, Inc., NASA GSFC Code 698.2, 8800 Greenbelt Road, Greenbelt, Maryland 20771 USA

2 Data flow of geodetic VLBI observations

Data produced at a correlator are subject to various changes before it becomes available to an end user. Historically, results of correlation of a VLBI session are stored in a special self-descriptive file called a *database*. Each modification or introduction of new information leads to a new version of the database. Figure 1 shows the data flow of the geodetic VLBI observations. Traditionally, the numbers of versions correspond to the following Mk3 DBH (database handler) modifications:

Ver 1: data from correlator output are extracted and organized in the database format;
Ver 2: the software `calc` reads the observations and adds into the database precalculated theoretical values and partials;
Ver 3: meteorological data and cable calibration readings are extracted from station log files and added into the database;
Ver 4: all necessary editing (ambiguity resolution, outlier determination, clock breaks, etc.) is performed for the session. Ionospheric corrections are evaluated (using a corresponding database file for the S band) and stored in the database.

It is assumed that databases of version 4 and higher are suitable for batch data processing. Databases of version 1 and version 4, as a rule, are available on the IVS public ftp sites.

IVS WG4 developed a new representation of VLBI data called openDB, which removes unnecessary redundancy. The new format keeps data in netCDF binary files (NetCDF, network Common Data Form, is an open source input/output library). Access to the netCDF files are organized by using *wrapper files*. Use of different wrapper files makes it possible to represent information corresponding to different database

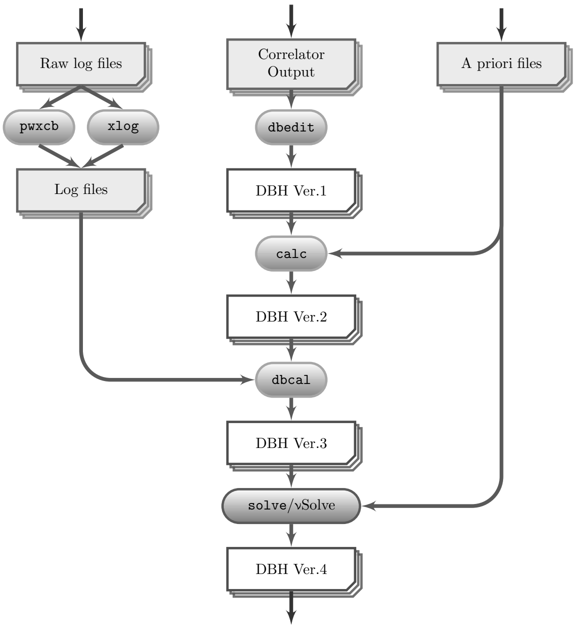

Fig. 1 Traditional data flow of the geodetic VLBI observations

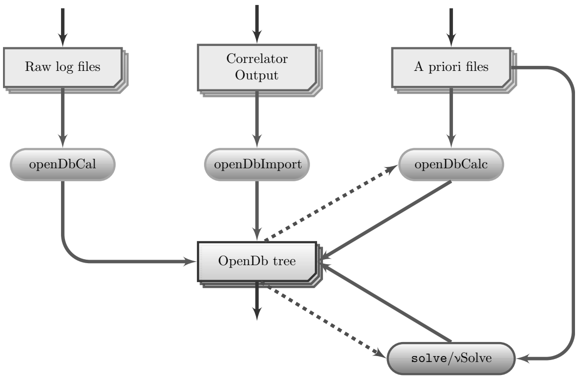

Fig. 2 The forthcoming CALC/SOLVE release data flow

versions in one data set. For more details on openDB format see (Gipson, 2012).

While all previous releases of CALC/SOLVE software implemented thetraditional data flow, the release of the software in 2013 will introduce the use of openDB format. The interaction between various executables and data is shown on the Figure 2. The software *ν*Solve is able to work with both Mk3 DBH and openDB data formats.

3 New VLBI data analysis software

The architecture of *ν*Solve was discussed in detail in (Bolotin et al., 2010) and (Bolotin et al., 2012). Here we just outline the main features of the architecture.

The software is written in the *C++* programming language. It is being developed with the Linux/GNU operating system but its use is not limited only to Linux. We tried to use a minimal set of external libraries for its functionality. In addition, to the system libraries, *libc* and *libm*, the *Qt* library is used for the graphical user interface, data containers and auxiliary tools. To have access to data stored in netCDF files we use the *netCDF* library.

The software consists of two parts:

1. Space Geodesy Library, a library where data structures and algorithms are implemented (about 90% of the total source code);
2. an executable `nuSolve` – a driver that calls the library functions and organizes work with an end-user (about 10% of total source code).

Such organization of the software allows us to reuse the source code in other applications. In the first public releases, while we have only one executable, `nuSolve`, the distributive and the whole software is called *ν*Solve. Later, the library and drivers will be distributed in separate packages.

The modular structure of the software makes it flexible and stable. By a *module* one means a logical block of the source code that is loosely tied with other parts of the software. A detailed description of modules is given in (Bolotin et al., 2010).

4 Functionality of the software

The software *ν*Solve is designed to be a replacement for interactive SOLVE. It is capable of analyzing a single VLBI session: it performs necessary calibrations and data editing and stores results in an appropriate format. Later *ν*Solve will evolve into a powerful session editor that will allow us to fix all known anomalies of the VLBI observation, e.g., subambiguities.

We should note that *ν*Solve does not make global solutions. A separate executable (driver) will be developed later to perform data analysis of multiple sessions of VLBI observations.

The general features of the software are the following. It is able to read and write data in the Mk3 DBH format as well as in the new openDB format. There are no limitations on the numbers of stations and sources that participate in one session or the number of observations. The software can work either through the CALC/SOLVE catalog subsystem or in a standalone mode. The process of data analysis can be automated to some extent.

The module *Estimator* of νSolve allows one to estimate the following types of parameters: (1) *local* parameter, an unbiased parameter that is determined for whole session, (2) *arc* parameter, an unbiased parameter estimated for specified by user interval (e.g., 1 hour), (3) *piecewise linear function*, coefficients of continuous linear function are estimated from data, where the interval between nodes is specified by the user, and (4) *stochastic* parameters, an alternative to a piecewise linear function. The realization of least square estimation is made with a square root information filter (SRIF) (Biermann, 1977). Using SRIF and its derivations makes it possible to implement a model where arc and piecewise linear functions can have different lengths of segment intervals or have overlapping segments.

The software can estimate the following parameters:

- Coefficients of polynomial model for station clocks
- Tropospheric zenith delays and horizontal gradients
- Station positions
- Antenna axis offsets
- Source coordinates
- Polar motion offsets and rates
- Earth rotation, $d(UT1-UTC)$ and its rate
- Angles of nutation
- Baseline clock offsets
- Baseline vectors.

The user can assign any of the parameter types to each of these parameters. The user can select a list of stations to estimate their positions or sources to estimate their coordinates. If all available stations or sources are selected, the user can specify what station or source *a priori* coordinates will be used in the equations of No-Net-Rotation and/or No-Net-Translation constraint.

4.1 Data processing operations

Essential operations that are necessary to perform to make a VLBI session usable in a batch solution are the following: clock break detection, ambiguity resolution, evaluation of ionospheric correction, corrections of weights of observations, and outlier processing. We now discuss these operations.

A clock break is a discontinuity in the time marks of the observations due to hardware problems at the station. There are also other effects (e.g., manually applied phase calibration which consists of several segments) that are manifested as clock breaks. SOLVE software estimates parameters of a clock break as additional parameters to the whole model. In contrast, νSolve estimates clock break parameters in a separate solution and then applies them in further data analysis. Such an approach allows processing of rare cases of multiple clock breaks. Clock breaks can be detected and corrected in automatic, semi-automatic and manual mode.

Ambiguity resolution of group delays is done using the same ideas implemented in interactive SOLVE. The algorithms implemented in νSolve are less restrictive. The software can process VLBI sessions that have different ambiguity spacing of group delays on different baselines or even on one baseline. In addition, νSolve allows the user to adjust the number of ambiguities manually.

The ionosphere corrections for group delays, phase rates and phase delays are evaluated using dual band VLBI observations. Since the group delays are determined up to an arbitrary number of ambiguity spacings, the evaluated ionospheric correction is not unique. It is a good practice to process clock breaks and resolve group ambiguities before evaluating the ionospheric corrections.

We perform adjustment of observation weights to make normalized χ^2 equal to unity. Additional standard deviations can be computed in two modes: a session wide (one weight correction is for the whole set of observations); and a baseline dependent mode. Weighting corrections change the solution and distribution of residuals, making the process of weight correction an iterative process. Weight corrections can be imported from an external file. Reweighting is performed in conjunction with the next operation, outlier elimination.

An outlier is an observation with an absolute value of a normalized residual greater than a user specified threshold. Typically, this threshold is 3 or 5. The normalized residuals can be evaluated either for the whole set of processed observations or on a baseline basis. This process is iterative. After excluding an outlier from a solution, the new solution and normalized residuals have to be recalculated. Excluded observations can be restored action. Reweighting is performed in conjunction with the reweighting.

4.2 Use of alternative models and external a priori information

Interactive SOLVE takes into account models of geophysical effects applying corrections to the theoretical values caused by the effect. Such corrections are called *contributions*. The same mechanism is realized in νSolve.

As it was mentioned above, `calc` software evaluates and stores in corresponding Mk3 DBH file or openDB files theoretical values and partials. In addition, it stores the contributions that were applied to the theoretical values. Therefore, to apply an alternative model one should subtract from the theoretical value the corresponding contribution and add then a corrections to the theoretical value evaluated according to the alternative model.

Historically, not all models that are described in IERS Conventions (McCarthy and Petit, 2004) are included in theoretical values. For example, ocean loading effects and diurnal/semidiurnal variations in Earth rotation parameters (ERP) are not added by default. Some alternative models, like tropospheric delay, mapping functions or high frequency variations in ERP, are already implemented in νSolve; others will be added later.

Sometimes it is useful to use in the analysis initial values of geophysical parameters that differ from those used in evaluation of theoretical values. One good examples of this is the earthquake in Chile in 2010. As a result of this event, coordinates of the VLBI station in Concepcion, TIGOCONC, shifted more than three meters. On the other hand, CALC software evaluates theoretical values and partials using standard station positions (e.g, VTRF). Under these circumstances, one will get large residuals for observations at TIGOCONC and values of these residuals are big enough to make it hard to resolve group delay ambiguities.

SOLVE as well as νSolve adjusts theoretical values for external *a priori* values in the following way:

$$\delta\tau = \frac{\partial\tau}{\partial\mathbf{x}}(\mathbf{x_0}^{new} - \mathbf{x_0}),$$

where $\delta\tau$ is a correction to theoretical value, $\mathbf{x_0}$ is the *a priori* value that was used in calculations of the theoretical value, $\mathbf{x_0}^{new}$ is new *a priori*, and $\frac{\partial\tau}{\partial\mathbf{x}}$ is the matrix of corresponding partial derivatives. The following types of external *a priori* data can be altered in νSolve:

1. Station positions and velocities;
2. Sources coordinates;
3. Axis offsets of antenna;
4. Mean site tropospheric gradients;
5. Earth rotation parameters.

For compatibility reasons, νSolve uses the same formats for external *a priori* files as interactive SOLVE does.

5 Conclusions

As the software νSolve is a part of the CALC/SOLVE system, it will be publicly available in the next release of CALC/SOLVE. After release, we welcome users to provide comments and suggestions, that will improve the software.

In the next releases we will focus on the following issues: 1) optimizing of data processing time; 2) improvement of the plotting system; 3) extending the functionality; and 4) introducing elements of automatic data processing.

References

G.J., Biermann, *Factorization Methods for Discrete Sequential Estimation. V128, Mathematics in Science and Engineering Series*, Academic Press, 1977.

S. Bolotin, J.M. Gipson and D. MacMillan. *Development of a New VLBI Data Analysis Software*. In D. Behrend, and K.D. Baver, editors, *IVS 2010 General Meeting Proceedings*, NASA CP 2010-215864, NASA GSFC, Maryland, pages 197–201, 2010.

S. Bolotin, J.M. Gipson, D. Gordon and D. MacMillan, *Current Status of Development of New VLBI Data Analysis Software* In W. Alef, S. Bernhart and A. Nothnagel, editors, *Proc. of the 20th Meeting of the EVGA*, Bonn, Germany, pages 86–88, 2011.

S. Bolotin, K. Baver, J. Gipson, D. Gordon and D. MacMillan *The First Release of νSolve.* In D. Behrend, and K.D. Baver, editors, *IVS 2012 General Meeting Proceedings*, NASA CP 2012-217504, NASA GSFC, Maryland, pages 222–226, 2012.

J.M. Gipson *The Report of IVS-WG4.* In D. Behrend, and K.D. Baver, editors, *IVS 2012 General Meeting Proceedings*, NASA CP 2012-217504, NASA GSFC, Maryland, pages 212–221, 2012.

D. D. McCarthy and G. Petit. *IERS Conventions (2003).* IERS Conventions (2003). Dennis D. McCarthy and Gérard Petit (eds.), International Earth Rotation and Reference Systems Service (IERS). IERS Technical Note, No. 32, Frankfurt am Main, Germany: Verlag des Bundesamtes für Kartographie und Geodäsie, ISBN 3-89888-884-3, 2004, 127 pp., 2004.

Continuous integration and quality control for scientific software

A. Neidhardt, M. Ettl, W. Brisken, R. Dassing

Abstract Modern software has to be stable, portable, fast and reliable. This is going to be also more and more important for scientific software. But this requires a sophisticated way to inspect, check and evaluate the quality of source code with a suitable, automated infrastructure. A centralized server with a software repository and a version control system is one essential part, to manage the code basis and to control the different development versions. While each project can be compiled separately, the whole code basis can also be compiled with one central Makefile. This is used to create automated, nightly builds. Additionally all sources are inspected automatically with static code analysis and inspection tools, which check well-none error situations, memory and resource leaks, performance issues, or style issues. In combination with an automatic documentation generator it is possible to create the developer documentation directly from the code and the inline comments. All reports and generated information are presented as HTML page on a Web server. Because this environment increased the stability and quality of the software of the Geodetic Observatory Wettzell tremendously, it is now also available for scientific communities. One regular customer is already the developer group of the DiFX software correlator project.

Keywords software quality, continuous integration, static code analysis, code inspections

Alexander Neidhardt
Forschungseinrichtung Satellitengeodäsie, Technische Universität München, Geodätisches Observatorium Wettzell, Sackenrieder Straße 25, D-93444 Bad Kötzting, Germany
Martin Ettl
Forschungseinrichtung Satellitengeodäsie, Technische Universität München, Geodätisches Observatorium Wettzell, Sackenrieder Straße 25, D-93444 Bad Kötzting, Germany
Walter Brisken
National Radio Astronomy Observatory, Array Operations Center, P.O. Box O, 1003 Lopezville Road, Socorro, New Mexico 87801-0387, USA
Reiner Dassing
Bundesamt für Kartographie und Geodäsie, Geodätisches Observatorium Wettzell, Sackenrieder Straße 25, D-93444 Bad Kötzting, Germany

1 Continuous integration at a glance

Evaluating the state of a software project or rating the quality of a current software release is quite ambitious. On the one hand it is necessary to define a suitable quality metrics while on the other hand regular checks, inspections and evaluations of these metric parameters must be performed. Continuous integration can give here beneficial support. It is a software development practice by what software, developed parallel by different developers, is frequently (at least once per day) and continually integrated in a centralized environment to reduce integration problems. Each integration is automatically compiled, verified and validated with automated builds, tests and inspections to develop cohesive software more rapidly [Duvall (2011)].

The heart of such a system is a central code repository in a version control system. Each developer regularly commits his code changes, updates and add-ons to this code stock. The system manages the different versions, forces the merging of different contents and logs all changes, so that it a revert to one of the previous versions is possible at any time. It is also possible to checkout the latest version for a continuous self-testing and inspection automatically. It includes code beautifier preparations, nightly builds, documentation generation, unit tests, static code analyses and statistics generations (see fig. 1). The results are presented online on Web pages (see fig. 2).

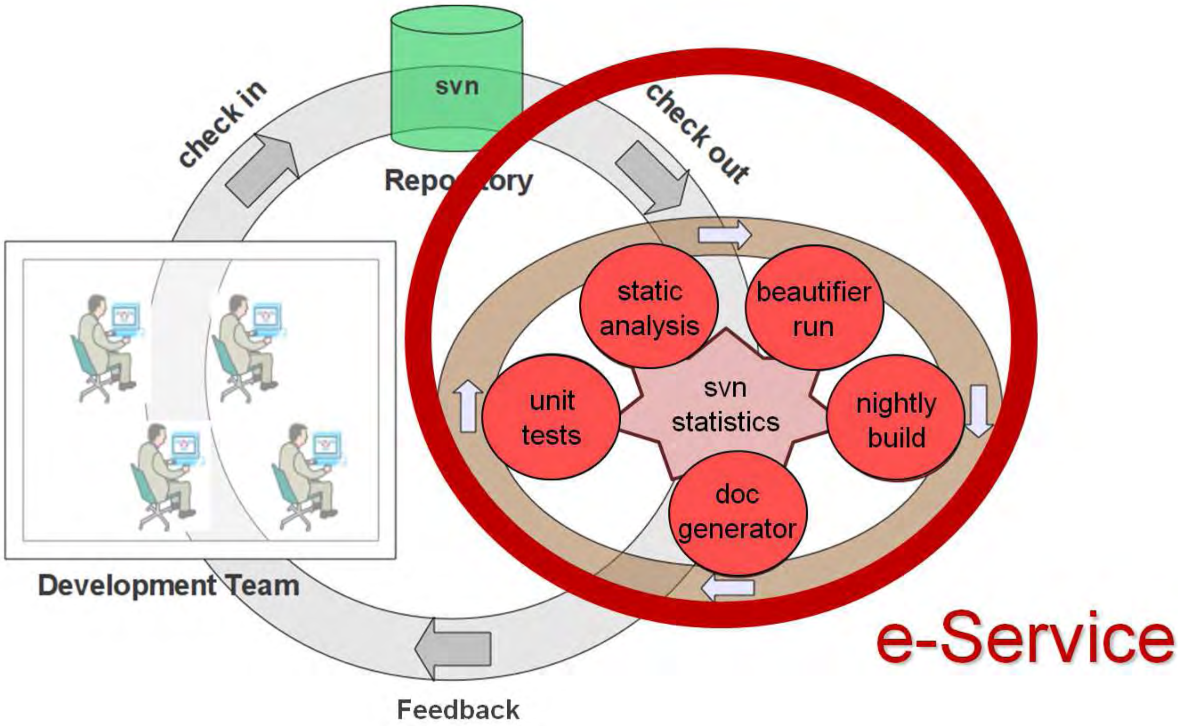

Fig. 1 The concept of continuous integration: developers participate to a common code base from which automatic code checking and inspection tools check out local copies to run different quality analysis.

2 Different methods of code inspection

The continuous integration environment at the Geodetic Observatory Wettzell uses several different automatic inspections each night [Ettl (2012)], which are briefly introduced in the following sections.

2.1 Code beautifier

Due to the limited spell checking capabilities of programming editors, an automated spell checking tool can help to reduce the number of misspelled words in source code and ASCII files. Finally, this improves the readability of the code and reduces errors in the automatically generated documentation.

Additionally, an automatic formatting tool is used in regular intervals to format the source code according to specific design rules. This ensures the use of the same indentations and programming style in the whole software project. It improves the readability and maintainability.

2.2 Static code analysis

Static code analysis inspects the code, to find potential programming flaws. The programs are not executed or compiled for these tests. Currently, a collection of open source static analyzing tools are used available. These tools are aimed to find bugs, which usually a compiler does not detect in C/C++-source code, as e.g. memory leaks, null pointer dereferencing, unused variables, not initialized variables, mismatching allocations/deallocations, buffer overruns, or memory accesses out of bound and many others.

2.3 Nightly builds

An automated build system compiles and links the whole sources each night. It is based on standard GNU-Makefiles for each project. Projects with several sub-projects have a top level Makefile, which starts the building processes of the sub-projects. This is done automatically on a Linux server every night, using several GNU-compiler versions. The output is converted into

HTML, so that the developers can easily check each day if their committed source code is compilable in the project.

2.4 Unit tests

Unit tests are small test programs to check the plausibility of the behavior and results of functions. At Wettzell a unit test environment was adapted to collect all the functional testing programs for different test cases (*simple_testsuite*). This suite validates all the basic software components and the generated code if the developer has written dedicated tests. The suite runs on different architectures (32-/64-bit) with different compilers and in combination with different Linux operating systems to reveal portability issues. Furthermore, the test coverage is captured using the GNU-compiler functionality. Based on this information, it is possible to measure the quality of the tested source code in a dedicated code metric.

2.5 Documentation generator

The developer documentation is created automatically with an open source documentation generator. This tool reads the source code and especially the comments inside, to extract the needed information for a HTML documentation. It includes call graphs, function headers, links between functions, and so on. This automated generation of developer documents supports a quick sharing of information. For newbies, it offers an quick overview of the object oriented software structure and the relationship of software components belonging to the projects.

3 Useful tools

Therefore the developer teams at the Geodetic Observatory Wettzell use several separate tools, which are combined to an own, proprietary Continuous Integration system, consisting of a set of hierarchically arranged Perl scripts for the Continuous Integration build. Currently it is a sequential processing triggered once a day as a cron job. It presents the results via generated Web pages, using an Apache Web server. This Continuous Integration system is also offered to a dedicated group of external developers in the Geodetic community on an external Web server, so that they can build and check their own code assets with the selective tools[1]. It is almost automated and can also deal with archive files. The used open source tools are[2]:

- **Version control statistics:**
  - StatSVN: Create a statistic about the version control system status
    http://statsvn.org/
- **Coding style:**
  - Artistic Style 2.02: Beautify the code according to the coding style
    http://astyle.sourceforge.net/astyle.html
- **Code build:**
  - GNU make: Automatic code builds with different compilers
    http://www.gnu.org/software/make/
- **Static code inspection:**
  - Cppcheck: Static code analysis
    http://sourceforge.net/projects/cppcheck
  - codespell: Spell check of program and text files
    http://git.profusion.mobi/cgit.cgi/lucas/codespell
  - nsiqcppstyle: Find non-reentrant functions in code
    http://code.google.com/p/nsiqcppstyle/
  - Flawfinder: Find security problems
    http://www.dwheeler.com/flawfinder/
  - PScan: Detect common printf/scanf format errors
    http://deployingradius.com/pscan/
  - Simian: Detect duplicated code
    http://www.harukizaemon.com/simian/
  - Own, proprietary shell development: Detect redundant files in the repository
  - Own, proprietary Perl development: Detect project style flaws
- **Documentation generation:**
  - Doxygen: Generate developer documentation
    http://www.stack.nl/~dimitri/doxygen/index.html

---

[1] Currently the service exists as a free ”e-Service” of the ”e-Control Software” environment on the Web page http://www.econtrol-software.de. Each project has own user rights and credentials.

[2] All Web pages were checked for correctness on July 26th, 2012.

Projekt	SVN Statistics (statsvn)	Developer Docu (doxygen)	Static analysis (cppcheck)	Redundant files	Duplicated code (simian)	Project checker	Beautify files (artistic style)	xsamba.wtz Debian 32bit Autobuild	xsamba.wtz Debian 32bit Unit tests
Run time	(Daily 04:00)	(So. 12:00)	(Daily 22:00)	(Daily 23:00)	(Daily 03:30)	(Daily 04:00)	(Sa. 00:00)	(Daily 02:00)	(Daily 00:00)
slr	statistics	n.a.	report Sun Mar 4 07:42:20 2012	report Sun Mar 4 02:02:00 2012	report Sun Mar 4 04:13:56 2012	n.a.	report Sat Mar 3 00:34:05 2012	report Sun Mar 4 05:05:41 2012	n.a.
tools vendor	statistics	n.a. ---	report Sun Mar 4 05:04:34 2012 report Sun Mar 4 03:55:43 2012	report Sun Mar 4 02:33:16 2012 n.a.	report Sun Mar 4 03:48:40 2012 n.a.	report ---	report Sat Mar 3 00:26:42 2012 ---	report Sun Mar 4 03:48:32 2012 ---	report/ coverage Sun Mar 4 02:32:35 2012 ---
vlbi	statistics	n.a.	report Sun Mar 4 07:57:06 2012	report Sun Mar 4 02:15:17 2012	report Sun Mar 4 04:02:05 2012	n.a.	report Sat Mar 3 00:45:02 2012	gcc-4.1 gcc-4.2 gcc-4.3 Sat Mar 3 23:53:28 2012	n.a.
sysmon	statistics	n.a.	report Sat Mar 3 22:15:25 2012	report Sun Mar 4 02:03:51 2012	report Sun Mar 4 04:22:19 2012	n.a.	report Sat Mar 3 00:48:49 2012	gcc-4.1 gcc-4.2 gcc-4.3 Sat Mar 3 23:28:11 2012	n.a.
wxgui	statistics	n.a.	report Sun Mar 4 05:40:08 2012	report Sun Mar 4 02:33:51 2012	report Sun Mar 4 04:31:53 2012	n.a.	report Sat Mar 3 00:47:04 2012	gcc-4.1 gcc-4.2 gcc-4.3 Wed Dec 7 12:34:22 2011	n.a.

Fig. 2 A HTML Web page offers a quick look on the quality states of the different projects.

4 Conclusion

This continuous integration work-flow reduces the amount of severe security and safety issues during the whole software development process at the Geodetic Observatory Wettzell. Currently, all software developments at the observatory are checked internally. But parts of it are also offered as a service to the community (see http://www.econtrol-software.de). Also the DiFX community uses this service frequently to check its software correlator code[3].

References

Duvall, Paul M.; Matyas, Steve; Glover, Andrew: Continuous Integration. Improving software quality and reducing risk. Sixth printing. Rearson Education, Inc. 2011.

Ettl, M.; Neidhardt, A.: Continuous integration and quality control during software development Proceedings of the 17th International Workshop on Laser Ranging, Nr. 48, pp 416-418, Verlag des Bundesamtes fr Kartographie und Geodsie, 2012.

[3] The authors wish to thank especially the DiFX developer group for using the continuous integration web environment.

Rapid UT1 Estimation Derived from Tsukuba VLBI Measurements after 2011 Earthquake

G. Engelhardt, V. Thorandt, D. Ullrich

Abstract The Tsukuba station is an essential station in two IVS Intensive series for rapid UT1 estimation. The use of this station in rapid UT1 estimation requires a set of best predetermined station coordinates but the Earthquake in Japan in March 2011 moved the station Tsukuba and the motion is still continuing. The VLBI group at BKG developed a procedure to get most probable station positions of Tsukuba for the epochs of the Intensive sessions. The procedure is explained and the results show that the analysis of the post-quake Intensive sessions with station Tsukuba can be used for operational UT1 estimation.

Keywords UT1 Estimation, VLBI Measurements, Data Analysis, TSUKUBA Earthquake

1 Situation before and after the 2011 Earthquake

After a big earthquake in the region of the VLBI station TSUKUBA (IVS name TSUKUB32) in Japan on March 11th, 2011 station displacements up to 67 centimeters occurred. The time series of the station coordinates about 1.5 years before and after the earthquake can be seen in Figures 1, 2, and 3. You can see a big offset in east component but also different rates in all components after the Earthquake.

Gerald Engelhardt, Volkmar Thorandt, Dieter Ullrich
Bundesamt für Kartographie und Geodäsie (BKG), Karl-Rothe-Str. 10-14, D-04105 Leipzig, Germany

2 Procedure of Intensive Session Processing (Int2/3)

a) TSUKUB32 coordinate series from BKG global solution bkg00013

The BKG global solution bkg00013 for generating terrestrial reference frame (TRF) and celestial reference frame (CRF) realizations, tropospheric parameters, and EOP series based on a solution mode with common estimation of all parameter types from 24-hours sessions since 1984. The station coordinates of TSUKUB32 are one part of the arc-parameters in sessions with station TSUKUB32. The station position time series of TSUKUB32 in X, Y, Z coordinate components and their standard deviations are extracted in a first step.

b) TSUKUB32 smoothed pseudo-coordinate series

The locally determined station coordinates of TSUKUB32 and their standard deviations are used for the estimation of a weighted mean between two sequent station positions in mid-epoch of both single solutions. Thus a smoothed pseudo-coordinate series of station TSUKUB32 can be generated for all coordinate components (X, Y, Z). Figure 4 shows an example for the X coordinate component.

c) Linear interpolation

The smoothed pseudo-coordinate series of TSUKUB32 is used for linear interpolation between the epochs of two sequent data points to get most probable station positions for the epochs of Int2/3 sessions. An example for the first Int2 session after the earthquake in X component can be seen in Figure 5. If epochs of Int2/3 sessions are after the last estimated TSUKUB32 position, coordinates

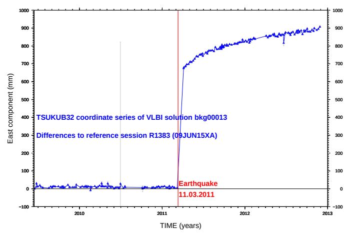

Fig. 1 Station position time series of TSUKUB32 (Japan) in east component

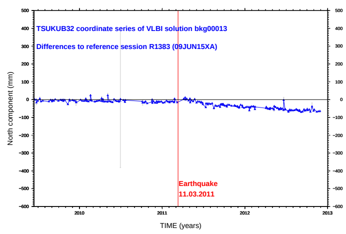

Fig. 2 Station position time series of TSUKUB32 (Japan) in north component

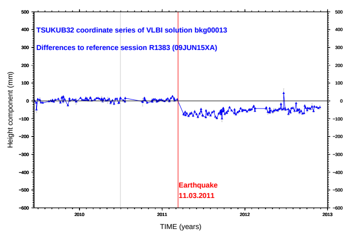

Fig. 3 Station position time series of TSUKUB32 (Japan) in height component

of the last 24-hours session of TSUKUB32 are used.

d) UT1 estimation

After determination of most probable station positions of TSUKUB32 for the epochs of Int2/3 sessions regular analysis can be executed. The estimated parameter types are UT1-TAI, station clock, and zenith troposphere together with fixed station coordinates (VTRF2008a) and radio source positions (ICRF2).

3 Comparison with IERS C04 Series

The estimated UT1-UTC values of Int2/3 sessions were compared with the official EOP (IERS) 08 C04

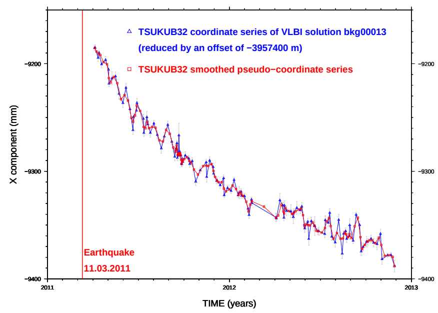

Fig. 4 Really determined coordinate series and smoothed pseudo-coordinate series of TSUKUB32 after the March 2011 earthquake for X component

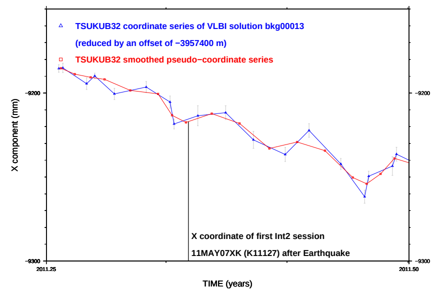

Fig. 5 More detailed graphic of really determined coordinate series and smoothed pseudo-coordinate series of TSUKUB32 for the epoch of the first Int2 session after the March 2011 earthquake in X component

daily series (IERS C04, 2013). Data about 1.5 years before and after the March 2011 earthquake were regarded. For each period of time a weighted root mean square (WRMS) was computed on the basis of differences to IERS C04. The WRMS derived from data before (28 microseconds) and after the earthquake (27 microseconds) is nearly the same and no significant differences can be seen in the diagram of all single differences UT1 Int2/3 minus UT1 C04 (Figure 6).

4 Integration in Technological Process

The above described single steps for handling the Int2/3 sessions with station TSUKUB32 were joined to a semi-automatic process. The newly determined a priori station coordinates for each TSUKUB32 Intensive session are used as input for the session by session TSUKUB32 Intensive cycle run. Finally an IVS formatted EOP list is created and mixed with the non-TSUKUB32 IVS EOP list. These algorithms

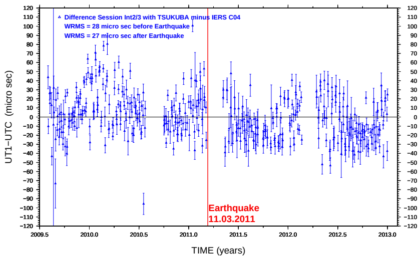

Fig. 6 Differences of UT1-UTC from Int2/3 sessions with TSUKUB32 and official IERS C04 values before and after the March 2011 earthquake

were included in the BKG post-interactive parts for establishing the IVS EOP solutions.

5 Conclusions

On the basis of an interpolation procedure of the station position time series of TSUKUB32 derived from a global solution with all 24-hours sessions most probable station positions of TSUKUB32 for the epochs of the Intensive sessions can be estimated. Based on a comparison with IERS C04 series no differences in accuracy of the UT1 estimation from Int2/3 sessions with epochs before and after the March 2011 earthquake near the TSUKUB32 VLBI station are visible.

References

IERS C04 series (2013): UT1-UTC values from EOP (IERS) 08 C04 daily series, (Web reference: http://hpiers.obspm.fr/eoppc/eop/eopc04/eopc04.62-now).

On the Impact of the Seasonal Station Motions on the Intensive UT1 Results

Z. Malkin

Abstract UT1 estimates obtained from the VLBI Intensives data depend on the station displacement model used during processing. In particular, because of seasonal variations, the instantaneous station position during the specific Intensive session differs from the position predicted by the linear model generally used. This can cause systematic errors in UT1 Intensives results. In this paper, we first investigated the seasonal signal in the station displacements for the 5 VLBI antennas participating in UT1 Intensives observing programs, along with the 8 collocated GPS stations. It was found that a significant annual term is present in the time series for most stations, and its amplitude can reach 8 mm in the height component, and 2 mm in horizontal components. However, the annual signals found in the displacements of the collocated VLBI and GPS stations at some sites differ substantially in amplitude and phase. The semiannual harmonics are relatively small and unstable, and for most stations no prevailing signal was found in the corresponding frequency band. Then two UT1 Intensives series were computed with and without including the seasonal term found in the previous step in the station movement model. Comparison of these series has shown that neglecting the seasonal station position variations can cause a systematic error in UT1 estimates, which can exceed 1 microarcsecond, depending on the observing program.

Keywords VLBI, IVS, Earth orientation parameters, UT1 Intensives

Zinovy Malkin
Pulkovo Observatory, St. Petersburg State University, Pulkovskoe Sh. 65, St. Petersburg 196140, Russia; e-mail: malkin@gao.spb.ru

1 Introduction

To get more frequent and timely VLBI UT1 estimates, several special IVS observing programs called Intensives are conducted daily on one or two baselines, have 1-hour duration, mostly employ electronic data transfer (e-VLBI), and hence provide rapid turnaround time from several hours to 2 days. Due to the short session duration (usually 1 hour) and poor network geometry, only a limited number of parameters can be effectively estimated from these observations. Generally, this includes only UT1, station clocks offsets, and zenith troposphere delays. Thus UT1 estimates derived from the Intensives sessions decisively depend on many a priori parameters used during data processing, in particular, on the station displacement model. Generally, station displacements are modelled using linear model. However, because of seasonal variations, the instantaneous station position during the specific session differs from the position predicted by such a model. This can cause systematic errors in UT1 Intensives results as was suggested by Malkin et al. (2012b).

In this paper, we first studied the seasonal signal in the station displacements for the five VLBI antennas participating in the main Intensives observing programs. The displacement of the collocated GPS stations were also considered to estimate a site-specific seasonal signal in the movements of the stations belonging to the site. If this effect prevails over the station-specific phenomena, the GPS data can be used to adjust the parameters of the VLBI station seasonal displacement model. Then the impact of the seasonal VLBI station position variations on UT1 Intensives estimates is investigated.

2 Seasonal station movements

In accordance with the goal of this study, the 5 VLBI stations most actively participating in the current IVS UT1 Intensives observing programs were considered. We also used GPS data from 8 collocated GPS stations having good observational history to investigate if it could be useful to improve the seasonal displacement model of the VLBI stations.

Finally, we used 13 stations located at five sites: Kokee Park (Hawaii, USA), Ny-Ålesund (Spitsbergen, Norway), Svetloe (Russia), Tsukuba (Japan), and Wettzell (Germany). All 13 stations are included in the ITRF2008 (Altamimi et al., 2011).

The data time interval was taken as 2004.0 to 2009.6. The latter date coincides with the end of the ITRF2008 data. The beginning of the interval is defined by the beginning of active observations by the Svetloe VLBI station.

For our analysis, we used the time series of the VLBI and GPS residuals computed from the ITRF2008 solution[1]. Using the ITRF2008 residuals has a large advantage over other series because it directly corresponds to the seasonal discrepancy in station position one introduces by using the ITRF2008 model in space geodesy applications.

Amplitude and phase analysis of the results presented in Table 1 can help us to decide what part of the seasonal signal is related to the site, and what part is station- or technique-specific. Detailed analysis of this problem is beyond the scope of this study. It is mostly important for us to make a decision on whether the parameters of the seasonal signal found in the GPS station displacement time series can help to improve the model of seasonal variations in the VLBI station positions.

One can see that the semiannual signal in the horizontal components of the station displacements is small, mostly well below 1 mm, and unstable. Analysis of the phases of the semiannual signal (see Table 1) shows that they are mostly different for the VLBI and GPS stations belonging to the same site. As to VLBI stations, Ts shows the greatest semiannual dN component with the amplitude of 0.6 mm. As to the height variations, the semiannual signal is more substantial at several stations: Ny, Sv, Ts, KOKB, NYAL, NYA1, and SVTL.

So, in this paper we concentrate on the investigation of the annual signal in station displacements. A statistically significant annual signal is present in most series. The largest dH amplitude is observed at Tsukuba stations Ts and TSKB—a well known fact from previous

[1] http://itrf.ensg.ign.fr/ITRF_solutions/2008/ITRF2008_ts.php

Table 1 Seasonal harmonics in the stations motion: A_1, P_1 are the amplitude and phase of the annual term, A_2, P_2 are the amplitude and phase of the semiannual term. Units: mm, deg.

Station	A/P	dE	dN	dH
		Kokee Park		
Kk	A_1	0.9 ± 0.2	0.8 ± 0.2	2.2 ± 0.5
	P_1	326 ± 15	96 ± 19	288 ± 15
	A_2	0.0 ± 0.2	0.3 ± 0.3	0.4 ± 0.5
	P_2	294 ± 269	67 ± 55	346 ± 81
KOKB	A_1	0.2 ± 0.1	0.9 ± 0.1	1.5 ± 0.3
	P_1	140 ± 30	354 ± 5	275 ± 10
	A_2	0.3 ± 0.1	0.3 ± 0.1	1.7 ± 0.3
	P_2	343 ± 24	91 ± 14	325 ± 9
		Ny-Ålesund		
Ny	A_1	0.6 ± 0.1	0.9 ± 0.1	2.7 ± 0.5
	P_1	186 ± 12	107 ± 10	56 ± 10
	A_2	0.2 ± 0.1	0.1 ± 0.1	1.8 ± 0.5
	P_2	4 ± 39	210 ± 72	119 ± 15
NYAL	A_1	0.2 ± 0.1	1.0 ± 0.1	1.7 ± 0.3
	P_1	70 ± 20	121 ± 5	78 ± 11
	A_2	0.2 ± 0.1	0.7 ± 0.1	2.4 ± 0.3
	P_2	90 ± 14	230 ± 7	206 ± 8
NYA1	A_1	0.5 ± 0.1	0.6 ± 0.1	3.5 ± 0.3
	P_1	48 ± 7	106 ± 5	26 ± 4
	A_2	0.3 ± 0.1	0.5 ± 0.1	2.5 ± 0.3
	P_2	115 ± 10	255 ± 7	219 ± 6
		Svetloe		
Sv	A_1	0.1 ± 0.3	1.0 ± 0.3	1.3 ± 0.9
	P_1	219 ± 105	200 ± 13	44 ± 37
	A_2	0.4 ± 0.3	0.1 ± 0.3	1.4 ± 0.9
	P_2	125 ± 37	338 ± 150	204 ± 38
SVTL	A_1	0.8 ± 0.1	0.2 ± 0.1	1.6 ± 0.4
	P_1	194 ± 5	243 ± 30	149 ± 12
	A_2	0.3 ± 0.1	0.2 ± 0.1	1.7 ± 0.4
	P_2	185 ± 14	78 ± 27	291 ± 12
		Tsukuba		
Ts	A_1	0.8 ± 0.3	1.4 ± 0.3	5.1 ± 0.5
	P_1	155 ± 19	336 ± 11	318 ± 5
	A_2	0.1 ± 0.2	0.6 ± 0.3	3.3 ± 0.4
	P_2	5 ± 134	316 ± 27	348 ± 7
TSKB	A_1	1.1 ± 0.2	1.6 ± 0.1	7.4 ± 0.2
	P_1	255 ± 10	352 ± 3	328 ± 2
	A_2	0.5 ± 0.2	0.4 ± 0.1	1.7 ± 0.2
	P_2	336 ± 22	24 ± 15	108 ± 7
		Wettzell		
Wz	A_1	0.1 ± 0.1	0.2 ± 0.1	1.8 ± 0.3
	P_1	221 ± 53	223 ± 37	240 ± 11
	A_2	0.1 ± 0.1	0.1 ± 0.1	0.7 ± 0.3
	P_2	53 ± 78	145 ± 82	18 ± 31
WTZA	A_1	0.7 ± 0.1	0.1 ± 0.1	1.6 ± 0.3
	P_1	38 ± 5	62 ± 31	185 ± 8
	A_2	0.0 ± 0.1	0.1 ± 0.1	0.9 ± 0.2
	P_2	32 ± 74	96 ± 27	325 ± 15
WTZR	A_1	0.6 ± 0.1	0.1 ± 0.1	2.3 ± 0.3
	P_1	42 ± 5	37 ± 51	154 ± 6
	A_2	0.1 ± 0.1	0.1 ± 0.1	0.5 ± 0.3
	P_2	194 ± 31	27 ± 31	332 ± 26
WTZZ	A_1	0.8 ± 0.1	0.3 ± 0.1	2.2 ± 0.2
	P_1	14 ± 4	265 ± 12	166 ± 6
	A_2	0.1 ± 0.1	0.1 ± 0.1	0.8 ± 0.2
	P_2	336 ± 38	208 ± 40	354 ± 16

studies, see, e.g., Munekane et al. (2004). One can see that at all the sites, the annual signals for the stations belonging to the site differ substantially in amplitude and/or phase in at least one component. Table 1 gives detailed information about the differences between the parameters of the annual signals found for collocated GPS and VLBI stations. This results agree well with Tesmer et al. (2009) and Ding et al. (2005). However, the phase of the annual term in the height variations for Kk and Ny (the only common stations between this study and Ding et al. (2005)) found in our analysis agree much better than found in Ding et al. (2005).

Finally, we can make two main conclusions from the results of this section:

- Using the seasonal signal parameters found in the GPS stations position time series for refinement of the model of seasonal variations of VLBI station positions generally cannot be justified without additional investigation of the structure and nature of seasonal displacements.
- An annual harmonic model is a simple, but still sufficiently good approach for our study.

3 VLBI data analysis

Assessment of the impact of seasonal station position variations on UT1 Intensives results was made by processing VLBI data collected from the main Intensives programs for a 6-year interval from the beginning of March 2005 till the end of February 2011. The end of the interval is defined by the strong earthquake in Japan on March 11, 2011, which resulted, in particular, in a large displacement of the TSUKUB32, one of the key stations for the Int2 and Int3 IVS Intensives observing programs. This event was not accounted for in the ITRF2008 because it happened after its completion. Any current extension of the ITRF TSUKUB32 displacement model might be inconsistent with ITRF2008, and thus is inappropriate for our study. The 10 days in March 2011 immediately preceding the March 11 earthquake were not included in the processing to avoid the possible impact of pre-quake earth surface deformations.

The observing programs used in this work are: Int1 (KkWz, Int1a (KkSvWz), Int2 (TsWz), and Int3 (NyTsWz). The observations were processed in two solution modes: modeling station motion according to the ITRF2008 linear model and with addition of only the annual variations in the station displacement with the amplitude and phase found in the previous section for the VLBI stations.

Consequently, four pairs of time series were obtained for four IVS UT1 observing programs described above. The results of these computations and comparison of UT1 estimates are shown in Fig. 1. The gap in the series in 2010 is caused by the Wettzell antenna repairs in the period from the beginning of September to the end of November.

The results of this test presented in Fig 1 show that the strong annual signal is present in all the UT1 series, but with different amplitude: just over 1 μs for Int1 and Int1a series and 2–3 times smaller for Int2 and Int3 ones. The uncertainty of the amplitude estimates is much smaller than the amplitude itself. The annual spectral peak for Int3 is shifted slightly with respect to the nominal period of 1 yr, but there are too few observations for this observing program to allow us to get a reliable spectrum. The amplitude of the semiannual term is below 0.15 μs for all the series.

The Int2 and Int3 differences also show signal at the periods of 90 and 60 days, which can be a result of the periodicity in schedules (Hefty and Gontier, 1997; Titov, 2000). The amplitude of the 90-day term in the Int2 and Int3 differences are 0.28 and 0.36 μs, respectively. The amplitude of the 60-day term in the Int2 and Int3 differences are 0.31 and 0.33 μs, respectively.

One can see that the annual signal in the Int1a (KkSvWz baselines) UT1 series is similar to the annual signal in the Int1 series (KkWz baseline). This is also the case for Int3 (NyTsWz baselines) and Int2 (TsWz baseline). This means that the addition of a third station to the Int1 and Int2 networks does not significantly change the impact of the annual signal in the station displacement on UT1 estimates. A similar conclusion was made in Malkin (2011) with respect to the impact of celestial pole modeling on Intensives UT1 results. Unfortunately, the small number of Int1a and Int3 sessions does not allow us to make a more detailed reliable analysis.

4 Conclusions

In this paper, we investigated the impact of the seasonal station position variations on UT1 estimates obtained from the processing of VLBI Intensives observations.

At the first stage, we detected and investigated the seasonal signal in the 5 VLBI station displacement time series, along with position time series of 8 collocated GPS stations. The time series of the ITRF2008 residuals computed in the framework of computation of the ITRF2008 solution were used for this analysis. The differences were fitted to the model consisting of

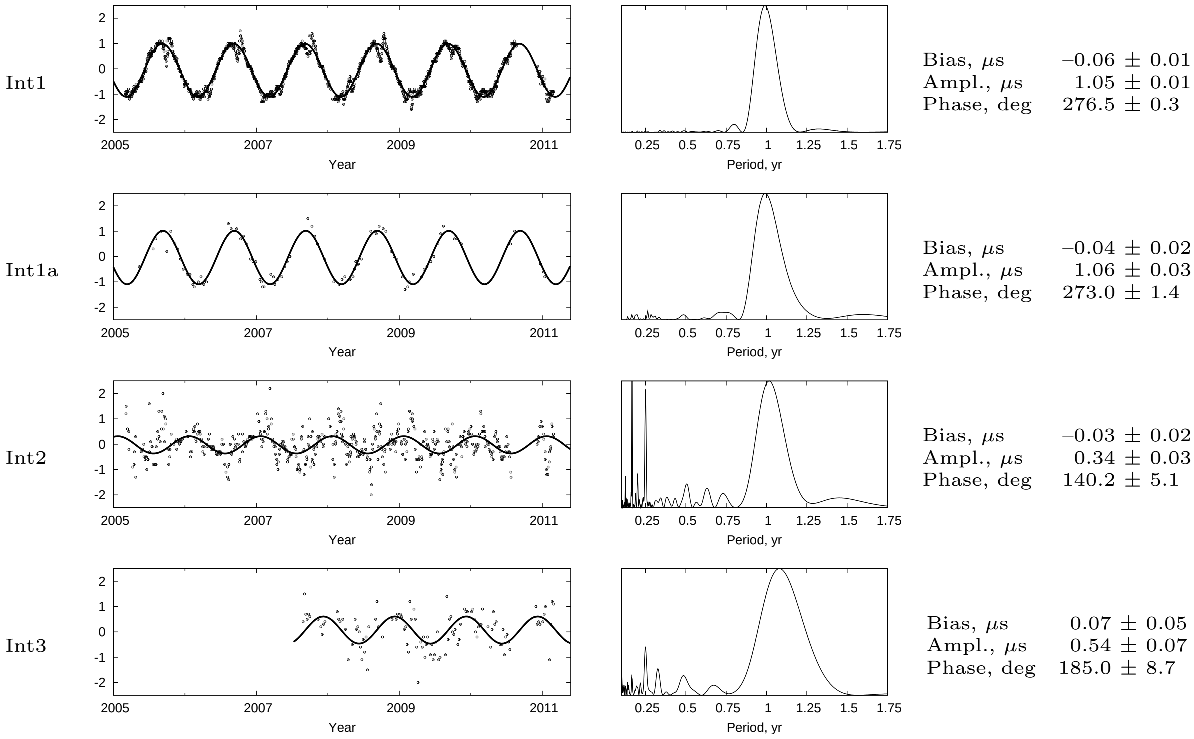

Fig. 1 Differences between two series of UT1 estimates computed with and without including the annual term in station position modeling. Data for four observing programs are shown from top to bottom: Int1 (baseline KkWz), Int1a (baselines KkSvWz), Int2 (baseline TsWz), Int3 (baselines NyTsWz). The red line corresponds to the model (bias and annual harmonics) fitted to the data. The middle column contains power spectra of the differences in arbitrary units. The best-fit model parameters (bias, amplitude and phase of the harmonics) are given in the right column. Unit: μs.

the linear trend and annual and semiannual harmonics. It was found that the amplitude of the seasonal term can reach 8 mm in the height component and 2 mm in the horizontal components. The semiannual harmonics is relatively small and unstable, and for most stations no prevailing semiannual signal was found in the corresponding frequency band. So, only the annual term was used for further detailed analysis. Comparison of annual signals found in the displacements of the collocated VLBI and GPS stations has shown that for some sites they differ substantially in amplitude and phase.

Further, it has been shown that the seasonal variations in the station movements cause systematic errors in UT1 results obtained from the processing of the VLBI Intensives observations. This error depends on the observing program design and schedule and exceeds 1 μs for the longest currently active IVS Intensives program Int1 (baseline KOKEE–WETTZELL). This value may seem insignificant, for it is below the current precision and accuracy of UT1 Intensives results. However, taking into account its systematic (seasonal) behavior, it should be considered substantial when using Intensives results for densification of UT1 series obtained from the multibaseline 24-hour VLBI UT1 series with the accuracy at the level of a few microseconds (Gambis and Luzum, 2011). Also, it becomes more substantial with coming improvements in the VLBI technique in the framework of the IVS VLBI2010 project (Petrachenko et al., 2009).

In our opinion, the results of this study give more weight to including a seasonal term(s) (as well as the post-quake exponential relaxation not considered in this paper) in the ITRF station position model as suggested, e.g., by Hugentobler et al. (2010); Malkin (2010); Malkin et al. (2012b); Altamimi et al. (2012), as is routine in some analysis centers for GPS station position modeling (Nikolaidis, 2002). In this connection, it is very important to understand how it should be done. Generally speaking, two main options can be considered: define a non-linear motion model for the whole site (analogously to velocities) or use a specific models for each stations. It seems, that obtained results have clearly shown that the second option should be used to achieve a mm-level accuracy of the stations motion modeling.

It should be emphasized that such an extension of the standard linear trend ITRF model is important not only for the current and future operational processing of the UT1 Intensives observations. The many-year UT1 Intensives series is important for densification of the UT1 series obtained from the 24-hour VLBI sessions. Reprocessing all the historical data collected, in the first place, on the intercontinental baselines, indeed after investigation of the seasonal variations of the stations involved, may be of importance for investigation of the Earth's rotation.

Finally, the method of analysis used in this work can be useful for the refinement of a scheduling strategy with respect to mitigation of the impact of the station non-linear motions on UT1 Intensives results, as well as on other parameters determined from the VLBI observations.

More details of this work can be found in Malkin (2013), which should be used as the primary reference to this study.

References

Z. Altamimi, X. Collilieux, and L. Métivier. ITRF2008: an improved solution of the international terrestrial reference frame. *J. of Geodesy*, 85:457–473, 2011. doi: 10.1007/s00190-011-0444-4.

Z. Altamimi, X. Collilieux, L. Metivier, and P. Rebischung. Strengths and weaknesses of the IGS contribution to the ITRF. *IGS Workshop, Olsztyn, Poland, July 2012*.

X. L. Ding, D. W. Zheng, D. N. Dong, C. Ma, Y. Q. Chen, and G. L. Wang. Seasonal and secular positional variations at eight co-located GPS and VLBI stations. *J. of Geodesy*, 79:71–81, 2005. doi: 10.1007/s00190-005-0444-3.

D. Gambis and B. Luzum. Earth rotation monitoring, UT1 determination and prediction. *Metrologia*, 48:S165–S170, 2011. doi: 10.1088/0026-1394/48/4/S06

J. Hefty and A. M. Gontier. Sensitivity of UT1 determined by single-baseline VLBI to atmospheric delay model, terrestrial and celestial reference frames. *J. of Geodesy*, 71:253–261, 1997. doi: 10.1007/s001900050093

U. Hugentobler, D. Angermann, H. Drewes, M. Gerstl, M. Seitz, and P. Steigenberger. Standards and conventions relevant for the ITRF. *IAG Commission 1 Symposium REFAG2010, Marne la Vallée, France, 4–8 October 2010*. http://iag.ign.fr/abstract/pdf/Hugentobler_REFAG2010.pdf.

Z. Malkin. Terrestrial and celestial reference frames: synergy and mutual impact. *IAG Commission 1 Symposium REFAG2010, Marne la Vallée, France, 4–8 October 2010*. http://iag.ign.fr/abstract/pdf/Malkin_REFAG2010.pdf

Z. Malkin. The impact of celestial pole offset modelling on VLBI UT1 intensive results. *J. of Geodesy*, 85:617–622, 2011. doi: 10.1007/s00190-011-0468-9.

Z. Malkin, H. Schuh, C. Ma, and S. Lambert. Interaction between celestial and terrestrial reference frames and some considerations for the next VLBI-based ICRF. H. Schuh, S. Böhm, T. Nilsson, and N. Capitaine (eds), *Proc. Journés Systèmes de Référence Spatio-temporels, Vienna, Austria, 19-21 Sep 2011*, p. 66–69, 2012.

Z. Malkin. Impact of seasonal station motions on VLBI UT1 intensives results. *J. of Geodesy*, 2013. doi: 10.1007/s00190-013-0624-5.

H. Munekane, M. Tobita, and K. Takashima. Groundwater-induced vertical movements observed in Tsukuba, Japan. *Geophys. Res. Lett.*, 31:L12608, 2004. doi: 10.1029/2004GL020158.

R. Nikolaidis. *Observation of geodetic and seismic deformation with the Global Positioning System*. PhD thesis, University of California, San Diego, 2002.

B. Petrachenko, A. Niell, D. Behrend, B. Corey, J. Boehm, P. Charlot, A. Collioud, J. Gipson, R. Haas, T. Hobiger, Y. Koyama, D. MacMillan, Z. Malkin, T. Nilsson, A. Pany, G. Tuccari, A. Whitney, and J. Wresnik. *Design Aspects of the VLBI2010 System. Progress Report of the IVS VLBI2010 Committee, June 2009*. NASA/TM-2009-214180, 2009.

V. Tesmer, P. Steigenberger, M. Rothacher, J. Böhm, and B. Meisel. Annual deformation signals from homogeneously reprocessed VLBI and GPS height time series. *J. of Geodesy*, 83:973–988, 2009. doi: 10.1007/s00190-009-0316-3.

O. Titov. Influence of Adopted Nutation Model on VLBI NEOS-Intensives Data Analysis. K. J. Johnston, D. D. McCarthy, B. J. Luzum, and G. H. Kaplan (eds), *IAU Colloq. 180: Towards Models and Constants for Sub-Microarcsecond Astrometry, 27-30 March 2000, U.S. Naval Observatory, Washington, DC, USA*, p. 259–262, 2000.

VLBI-Art: VLBI analysis in real-time

M. Karbon, T. Nilsson, C. Tierno Ros, R. Heinkelmann, H. Schuh

Abstract Geodetic Very Long Baseline Interferometry (VLBI) is one of the primary space geodetic techniques providing the full set of Earth Orientation Parameters (EOP) and it is unique for observing long term Universal Time (UT1). Accurate and continuous EOP obtained in near real-time are essential for satellite-based navigation and positioning, enable the precise tracking of interplanetary spacecraft and thus are the aim of the VGOS (VLBI2010 Global Observing System). With this next generation VLBI system and network, the International VLBI Service for Geodesy and Astrometry (IVS) increased its efforts to reduce the time span between the collection of VLBI observations and the availability of the final results. Project VLBI-Art contributes to these objectives by considerably accelerating the VLBI analysis procedure by implementing an elaborate Kalman filter, which represents a perfect tool for analyzing VLBI data in quasi real-time. The Kalman filter will be embedded in the Vienna VLBI Software (VieVS) as a completely automated tool, i.e. with no need of human interaction.

Keywords VLBI2010, Kalman filter

1 Introduction

Geodetic Very Long Baseline Interferometry (VLBI) ist the only space geodetic technique that allows the estimation of the full set of Earth Orientation Parameters (EOP), especially Universal Time (UT1) and celestial pole offsets. Furthermore, it is the only technique for the ralization of the International Celestial Reference Frame (ICRF). Additionally estimates of the tropospheric delay and other geodynamical and astronomical parameters can be provided (Sovers et al., 1998; Krásná et al., 2013).The International VLBI Service for Geodesy and Astrometry (IVS) currently conducts two to four 24-hourly VLBI sessions every week; the results are usually available within two weeks (Schuh and Behrend, 2012). The so-called intensive sessions are about one hour long and are observed by two to four stations with a particular focus on the UT1 determination. They are carried out almost every day and the results usually have a delay of one to two days. However, for (near) real-time navigation and positioning on the Earth and in space, real-time continuous EOP are necessary. For example, for the precise orbit determination of GNSS (Global Navigation Satellite Systems) satellites, accurate EOP are needed. Also for the tracking of interplanetary spacecrafts the exact orientation of the Earth in space is required (Ichikawa et al., 2004).To reach these goals, the VLBI2010 Global Observing System (VGOS; Petrachenko et al. (2009)) was proposed, where a dense network of very fast moving 'VLBI2010' antennas (slewing speed >6°/s) is foreseen, which are able to provide a high number of observations per time and are continuously operating. The aim is to reach an accuracy of 1 mm (position), 1 mm/year (velocity), respectively, from a global solution of 24-hour sessions, and near real-time operation with the help of electronic transfer of the data to the correlators. In order to retrieve the analysis results in near real-time, a solution algorithm is also required applying completely automated processes.

Maria Karbon, Tobias Nilsson, Robert Heinkelmann and Harald Schuh
Deutsches GeoForschungsZentrum Potsdam, 1.1 GPS/Galileo Earth Observation, Telegrafenberg, 14473 Potsdam, Germany
Claudia Tierno Ros
Technische Universität Wien, GEO, Gusshaussstraße 27-29, 1040 Wien, Austria

2 Concept

The aim of the project VLBI-Art is to considerably shorten the time between the availability of VLBI observations and the availability of their respective results. The Kalman filter is a convenient method for real-time applications and it already proofed its suitability for VLBI analysis some time ago (Herring et al., 1990; Titov et al., 2004). However, the algorithms in the existing software packages implement the Kalman filter in the form of a post-processing tool, as the applied Kalman filters are not designed for true real-time applications. Within project VLBI-Art a Kalman filter will be realized that is in particular designated for analyzing VLBI data in (near) real-time. Since 2008, a VLBI analysis software has been developed at the Department of Geodesy and Geoinformation at Vienna University of Technology, called Vienna VLBI Software (VieVS) (Böhm et al., 2011; Nilsson et al., 2011). The Kalman filter developments of this project will be inserted into VieVS enabling the software package to automatically analyze VLBI data in real-time. The VieVS software consists of several parts. A schematic diagram is shown in Fig. 1, which includes how the near real-time VLBI data flow is intended to be realized. VIE_INIT reads the observed group delays currently from the so-called NGS-files. In VIE_MOD the theoretical VLBI delays and the partial derivatives of the observations w.r.t. the unknown parameters are calculated according to the most recent IERS Conventions (2010) and IVS standards (`http://vlbi.geod.uni-bonn.de/IVS-AC/`). The planned extensions of the existing program code, labeled as VIE_KALMAN, will include the new code, where the unknown parameters are estimated through the Kalman filter instead of the least-squares method, which is usually applied in VLBI analysis. To optimize the performance of the algorithm and to tweak the real-time capabilities of the Kalman filter, various investigations are foreseen in project VLBI-Art with real as well as simulated data. The results will be compared to other VLBI analysis packages and to corresponding parameter series from other techniques such as the Global Navigation Satellite Systems (GNSS). As VieVS contains a scheduling (VIE_SCHED) as well as a simulation tool, we will be able to simulate artificial observations for the complete future VLBI2010 network and assess the real-time accuracy which can be achieved. Moreover we will investigate the promising possibility of feeding data provided by other sensors into the Kalman filter, like atmospheric angular momentum calculated from numerical weather models or tropospheric delays from GNSS or water vapor radiometer.

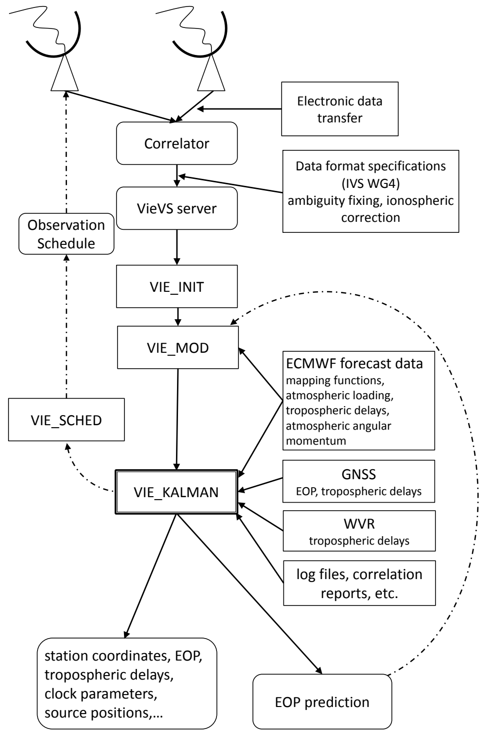

Fig. 1 Flowchart of automated real-time VLBI data processing with VieVS

3 Method

The Kalman filter is widely applied in various fields of research and developement including the analysis of space geodetic data (c.f. Morabito et al. (1988); Herring et al. (1990); Nilsson et al. (2011)). The advantage of such a filter over ordinary least-squares is that the estimation is made sequentially, epoch by epoch, by combining the observations at each epoch with the estimation of the previous epochs, making it ideal for real-time applications (Kalman, 1960). If $\mathbf{x_k}$ is the state vector containing all unknown parameters to be estimated at epoch k, it can be related to the estimates at a previous epoch $\mathbf{x_{k-1}}$ through

$$\mathbf{x_k} = \mathbf{F_k}\mathbf{x_{k-1}} + \mathbf{w_k}\ , \tag{1}$$

where $\mathbf{F_k}\mathbf{x_{k-1}}$ is the prediction of $\mathbf{x_k}$ based on $\mathbf{x_{k-1}}$ and $\mathbf{w_k}$ is the error in the prediction. The covariance matrix of the total error $\mathbf{P}_k^-$ can be calculated by

$$\mathbf{P}_k^- = \mathbf{F_k P_{k-1} F_k^T + Q_k} \,, \tag{2}$$

with $\mathbf{P_{k-1}}$ denoting the variance-covariance matrix of $\mathbf{x_{k-1}}$ and $\mathbf{Q}_k$ the variance-covariance matrix of the prediction error $\mathbf{w}_k$. The observations $\mathbf{z}_k$ at epoch t_k are introduced through

$$\mathbf{z_k = H_k x_k + v_k} \,. \tag{3}$$

$\mathbf{H_k}$ is the observation matrix and v_k is the observation noise. To get the optimal estimation for $\mathbf{x_k}$ and its covariance matrix $\mathbf{P_k}$ the prediction $\mathbf{x_k^-}$ and the observation $\mathbf{z_k}$ can be combined

$$\mathbf{x_k = x_k^- + K_k(z_k - Hx_k^-)} \,, \mathbf{P_k = (I - K_k H_k) P_k^-} \,, \tag{4}$$

with the Kalman gain $\mathbf{K_k}$

$$\mathbf{K_k = P_k^- H_k^T (H_k P_k^- H_k^T + R_k)}^{-1} \,, \tag{5}$$

where $\mathbf{R_k}$ is the variance-covariance matrix of the observation noise $\mathbf{v_k}$.

4 Conclusions

Within project VLBI-Art we will develop a software module for near real-time analysis of VLBI data extending the existing analysis software VieVS. This step will enable the software to process VLBI data in near real-time and to predict various parameters, like EOP, necessary for example for space craft navigation or tropospheric parameters, which are of interest for meteorology. We will compare our Kalman filter solution with the results from other software packages and from other data series and test the effects of feeding additional data like atmospheric angular momentum functions or information about the local water vapor content into the filter. With this software we aim to be prepared for the VLBI2010 analysis requirements with its huge data amount and its ambitious goals to continuous observations and derive results in near real-time. Since VieVS is a freely available software for registered users, also this module will be freely available after the Kalman filter is correctly implemented and thoroughly tested.

Acknowledgements We are grateful to the International VLBI Service for Geodesy and Astrometry (IVS) for providing the VLBI data. This work was supported by the Austrian Science Fund (FWF), project P24187-N21.

References

J. Böhm, S. Böhm, T. Nilsson, A. Pany, L. Plank, H. Spicakova, K. Teke, and H. Schuh. The new Vienna VLBI software. In S. Kenyon, M. C. Pacino, and U. Marti (eds.), *IAG Scientific Assembly 2009*, 136, 2012.

T. A. Herring, J. L. Davis, and I. I. Shapiro. Geodesy by radio interferometry: The application of Kalman filtering to the analysis of Very Long Baseline Interferometry data. *J. Geophys. Res.* , 95(B8): 12, 561-581, 1990.

R. Ichikawa, M. Ryuichi, H. Osaki, Y. Koyama, T. Kondo, T. Ohnishi, M. Yoshikawa, W. Cannon, A. Novikov, M. Bérubé and NOZOMI VLBI group, An Evaluation of VLBI Observations for the Deep Space Tracking of the Interplanetary Spacecrafts. *International VLBI Service for Geodesy and Astrometry*, 253-257, 2004.

R. E. Kalman. A new approach to linear filtering and prediction problems. *J. Basic Eng.*, 82D: 35-45, 1960.

H. Krásná, J. Bhm, and H. Schuh (2013). Tidal Love and Shida numbers estimated by geodetic VLBI. In press. *Journal of Geodynamics*, in press, 2013.

D. D. Morabito, T. M. Eubanks, and J. A. Steppe Kalman filtering of earth orientation changes. In A. Babecock and G. A. Wilkins (eds.), *The Earths rotation and reference frames for geodesy and geodynamics*, 257-267, Dordrecht, Holland, 1988.

T. Nilsson and L. Gradinarsky. Water vapor tomography using GPS phase observations: Simulaton results. *IEEE Trans. Geosci. Remote Sensing*, 44(10): 2927-2941, 2006. doi:10.1109/TGRS.2006.877755.

T. Nilsson, J. Böhm, S. Böhm, M. Madzak, V. Nafisi, L. Plank, H. Spicakova, J. Sun, C. Tierno Ros, and H. Schuh. Status and future plans for the Vienna VLBI software VieVS. In W. Alef, S. Bernhart, and A. Nothnagel (eds.), *Proceedings 20th European VLBI for Geodesy and Astrometry (EVGA) Working Meeting*, Bonn, Germany, 2011.

A. Nothnagel. Conventions on thermal expansion modelling of radio telescopes for geodetic and astrometric VLBI. *J. Geodesy*, 83: 787-792, 2009. doi:10.1007/s00190-008-0284-z.

B. Petrachenko, A. Niell, D. Behrend, B. Corey, J. Böhm, P. Charlot, A. Collioud, J. Gipson, R. Haas, T. Hobiger, Y. Koyama, D. MacMillan, Z. Malkin, T. Nilsson, A. Pany, G. Tuccari, A. Whitney, and J. Wresnik. Design aspects of the VLBI2010 system. In D. Behrend and K. Baver (eds.), *International VLBI Service for Gerodesy and Astrometry 2008 Annual Report*, NASA Technical Publications, NASA/TP-2009-214183, 2009.

H. Schuh and D. Behrend. VLBI: A fascinating technique for geodesy and astrometry. *J Geodyn*, 61: 68-80, 2012. doi:10.1016/j.jog.2012.07.007.

O. J. Sovers and J.L. Fanselow. Astrometry and geodesy with radio interferometry: experiments, models, results. *Rewievs of Modern Physics*, 70(4), 1998.

O. Titov, V. Tesmer, and J. Böhm. OCCAM v. 6.0 software for VLBI data analysis. In N. R. Vandenberg and K. D. Baver (eds.), *International VLBI Service for Geodesy and Astrometry 2004 General Meeting Proceedings*, 267-271, NASA Technical publications,NASA/CP-2004-212255, 2004.

Automated analysis of dUT1 with VieVS using new post-earthquake coordinates for Tsukuba

N. Kareinen, M. Uunila

Abstract The automated analysis of dUT1 from intensive sessions performed in Aalto University Metsähovi Radio Observatory include IVS-INT2 and IVS-INT3 sessions. These sessions are sensitive to a priori positions of the stations due to the small number of baselines. We analyze IVS-R1 sessions to estimate the new a priori coordinates for Tsukuba affected by the March 2011 Tohoku Earthquake in order to include IVS-INT2 and to improve the accuracy of IVS-INT3 sessions in the analysis. The procedure for utilising new a priori coordinates is automated and included in the dUT1 analysis. It can be utilised in case of another event distrupting the stations in the observation network.

Keywords UT1, Tsukuba, earthquake

1 Introduction

In the analysis conducted at Aalto University Metsähovi Radio Observatory the Earth rotation parameter dUT1 is automatically derived from the hour-long daily International VLBI Service for Astrometry and Geodesy (IVS) intensive sessions, which consists of three types: IVS-INT1, IVS-INT2, and IVS-INT3. The sessions are analysed with VieVS 1d in batch mode using three different analysis strategies (S-1, S-2, S-3) (Uunila et al., 2012).

Due to the network geometry in the IVS intensive sessions it is necessary to have an accurate knowledge of the a priori positions of the participating stations. The Tsukuba VLBI station (TSUKUB32), which participates weekly in IVS-INT2 and IVS-INT3 sessions, was affected by the March 11th 2011 Tohoku Earthquake causing it to shift over 60 cm due East(Kareinen and Uunila, 2012). The ongoing postseismic relaxation continues to affect the coordinates of TSUKUB32. The error in the station position propagates to UT1 and thus a post-earthquake correction must be applied to the a priori position of TSUKUB32.

We applied post-earthquake correction to the a priori position of TSUKUB32 by using the GPS based Tsukuba Position Service [1] (MacMillan et al., 2012) as well as coordinates derived from IVS-R1 sessions. Results from the automated analysis were reprocessed with new a priori positions and the results of two approaches were compared both with one another and to the old uncorrected results.

2 Automated analysis with new TSUKUB32 coordinates

The automated analysis of dUT1 from intensive sessions is currently done using VieVS 1d in batch mode. Common modelling options for all three automated analysis strategies include TRF, CRF, precession and nutation, ocean loading and ephemerides. The models used respectively are VTRF2008 (modified for TSUKUB32), ICRF2, IAU 2000A, FES 2004, and JPL421. Different modelling options are used for dUT1, mapping function and atmospheric loading. (Uunila et al., 2012) The modelling options incorporated for these parameters are listed in Table 1.

Strategy	EOP	Mapping function	Atm. loading
S-1	USNO finals2000A	GMF	No
S-2	USNO finals2000A	VM1	Yes
S-3	IERS C04 08	VM1	Yes

Table 1 Modelling options varying with strategy used with IVS-INT2/3 sessions in automated VieVS analysis.

Niko Kareinen and Minttu Uunila
Aalto University Metsähovi Radio Observatory, Metsähovintie 114, 02540 Kylmälä, Finland

[1] ftp://gemini.gsfc.nasa.gov/pub/misc/dsm/tsukuba/TSUKUB32_XYZ

To study the effect of new a priori coordinates of TSUKUB32 to the dUT1 estimate a total of 243 IVS-INT2 and 80 IVS-INT3 sessions from January 1st 2010 to February 25th 2013 were reprocessed. All modelling options and parameters used in the analysis were kept identical except for a priori TSUKUB32 position.

Two different methods were used to provide new a priori coordinates for TSUKUB32. First, by analyzing IVS-R1 sessions covering the reprocessing period. Second, by using the postseismic correction data derived from JPL GPS series.

For the first approach a total of 95 24-hour IVS-R1 sessions were analyzed with VieVS. The modelling options and estimated parameters are listed in Tables 2 and 3. In general the analysis was carried out with loose constraints. The position of TSUKUB32 was excluded from the VTRF2008 and the position was estimated w.r.t. to the a priori value in the NGS cards.

Model	VieVS modelling option
TRF	VTRF2008
CRF	ICRF2
Ephemerides	JPL421
A priori EOP	IERS C04 08
Precession/Nutation	IAU 2006/2000
Tidal ocean loading	FES2004
Pole tide	Cubic (IERS2010)
Tropospheric mapping function	VM1
Interpolation method	Lagrange

Table 2 Modelling options used with 24-hour IVS-R1 sessions in VieVS analysis.

Parameter	Interval	VieVS modelling option
Clock parameters	60 min	Relative 0.5 ps^2/s
ZWD	30 min	Relative 0.7 ps^2/s
NGR/EGR	360 min	Relative 2 mm/day
TRF coordinates	One offset/session	NNT/NNR
EOPs	1440 min	Relative 10^{-4} mas/ms/day

Table 3 Estimated parameters and constraints used with 24-hour IVS-R1 sessions in VieVS analysis.

To implement the new coordinates for TSUKUB32 in the automated analysis matlab scripts were written to generate mat-files with the estimated and GPS coordinates and corresponding MJD values as well as a script and to create a modified VTRF2008.mat file for VieVS. The shell script used in the original automated analysis (Uunila et al., 2012) was modified to call the VTRF-generating script to create a VTRF2008-file with an epoch corresponding with the date of the analysed IVS intensive session.

Since IVS-R1 sessions are carried out on Mondays with an interval of one week the a priori TSUKUB32 coordinates for IVS-INT2 and IVS-INT3 have to be estimated for epochs between IVS-R1 sessions. The corresponding a priori value for an intensive session is linearily interpolated from the R1 results in the VTRF-generating script. With a priori values from the GPS data no interpolation is needed since coordinate values are provided daily and can be assigned to corresponding intensive session epochs.

3 Results

The effect of corrected a priori TSUKUB32 coordinates to the dUT1 estimate is presented in Tables 4 and 5 for both the R1 and GPS approaches, respectively. The results are divided by analysis strategy (S-1, S-2, S-3) and session type (IVS-INT2, IVS-INT3). Included in the tables are WRMS values and mean formal errors for dUT1 w.r.t. to the a priori value. Mean bias is removed prior to WRMS computation. Also included is the number of accepted sessions and the ratio of accepted sessions to the total number of sessions. The outlier limits for the dUT1 estimate and formal error were 200 μs and 100 μs, respectively. Each session with estimates below these threshold values were included in the computation and counted as an accepted session.

When compared to the results without the corrected a priori TSUKUB32 coordinates the number of accepted sessions increased considerably for both approaches. With a priori coordinates derived from IVS-R1 sessions the accepted IVS-INT2 sessions for the strategies S-1, S-2, and S-3 increased 41, 25, and 20 percentage units, respectively. Similarly for the IVS-INT3 sessions the increase in accepted sessions was 18, 10, and 20 percentage units. With the GPS a priori coordinates the number of accepted sessions for S-1, S-2 and S-3 increased by 43, 27 and 20 percentage units for the IVS-INT2 sessions and by 16, 9 and 19 percentage units for IVS-INT3 sessions. Mean formal errors reduced with both the R1 and GPS a priori values for all strategies. The dUT1 estimates with R1 and GPS a priori coordinates are relatively similar. The most notable differences between the R1 and GPS a priori approaches are in the WRMS values. For IVS-INT2 sessions the largest difference is with R1 a prioris resulting in approximately 10 μs smaller WRMS values compared to the GPS for the strategies S-1 and S-2. For IVS-INT3 sessions the largest difference is approximately 5 μs for the S-3 strategy.

The dUT1 estimates and formal errors with R1 and GPS a priori values for each strategy are illustrated in Figures 1-2.

Session/strategy	**INT2/S-1**	**INT2/S-2**	**INT2/S-3**
Bias$_{dUT1_estimate}$(μs)	-6.43	-6.60	-3.63
WRMS$_{dUT1_estimate}$(μs)	80.69	80.43	24.62
Mean err. (μs)	12.52	12.55	12.07
N$_{sessions}$/Acc.%	243/86	243/86	239/99
Session/strategy	**INT3/S-1**	**INT3/S-2**	**INT3/S-3**
Bias$_{dUT1_estimate}$(μs)	-5.54	-3.36	2.67
WRMS$_{dUT1_estimate}$(μs)	87.93	87.22	23.38
Mean err. (μs)	17.80	17.22	16.69
N$_{sessions}$/Acc.%	77/78	77/77	72/97

Table 4 WRMS, bias, and mean errors for dUT1 corrections, total number of sessions, and number of accepted sessions for three strategies (S-1, S-2, S-3) for IVS-INT2 and IVS-INT3 sessions with a priori TSUKUB32 position computed from IVS-R1 sessions.

Session/strategy	**INT2/S-1**	**INT2/S-2**	**INT2/S-3**
Bias$_{dUT1_estimate}$(μs)	0.23	-0.85	11.71
WRMS$_{dUT1_estimate}$(μs)	91.02	91.29	26.74
Mean err. (μs)	12.40	12.43	12.48
N$_{sessions}$/Acc.%	239/88	239/88	227/99
Session/strategy	**INT3/S-1**	**INT3/S-2**	**INT3/S-3**
Bias$_{dUT1_estimate}$(μs)	7.26	6.06	15.64
WRMS$_{dUT1_estimate}$(μs)	85.76	87.02	28.22
Mean err. (μs)	17.13	17.41	16.39
N$_{sessions}$/Acc.%	80/76	80/76	71/96

Table 5 WRMS, bias, and mean errors for dUT1 corrections, total number of sessions, and number of accepted sessions for three strategies (S-1, S-2, S-3) for IVS-INT2 and IVS-INT3 sessions with a priori TSUKUB32 position computed from GPS data.

4 Conclusions

By using corrected a priori coordinates for TSUKUB32 we were able to increase the number of analyzed sessions significantly. The improvement was most notable in the single baseline IVS-INT2 sessions with a 30-50 percentage unit increase in the accepted sessions. This increase will improve the overall quality of the estimates. In terms of the WRMS the a priori values derived from IVS-R1 sessions produced slightly better results compared to the GPS. However, from the viewpoint of the VieVS automatization there are still challenges in implementing the R1 a priori coordinates to the analysis procedure. The analysis of 24-hour sessions usually requires the detection of clock breaks and the turnaround for IVS-R1 sessions dictates that the forward prediction necessary to provide a priori coordinates for the intensive sessions would be based on relatively sparse data set. The turnaround time is not so much of an issue with the S-3 strategy, since it is at the moment limited by the 30-day latency of the IERS C0408 data. For the S-1 and S-2 strategies the GPS based post-earthquake correction service offers a good source of a priori coordinates. The results of the automated analysis with a post-earthquake corrected a priori coordinates are updated to Metsähovi Radio Observatory web page [2].

References

D. MacMillan, D. Behrend, S. Kurihara. Effects of the 2011 Tohoku Earthquake on VLBI Geodetic Measurements. In D. Behrend and K.D. Baver, editors, *International VLBI Service for Geodesy and Astrometry 2012 General Meeting Proceedings*, 440-444, 2012.

M. Uunila, R. Haas, N. Kareinen, and T. Lindfors. Automated Analysis of dUT1 from IVS Intensive Sessions with VieVS. In D. Behrend and K.D. Baver, editors, *International VLBI Service for Geodesy and Astrometry 2012 General Meeting Proceedings*, 281-285, 2012.

N. Kareinen and M. Uunila. Determination of Tsukuba VLBI Station post-Tohoku Earthquake Coordinates using VieVS. In D. Behrend and K.D. Baver, editors, *International VLBI Service for Geodesy and Astrometry 2012 General Meeting Proceedings*, 445-449, 2012.

[2] http://www.metsahovi.fi/vlbi/vievs/autom/

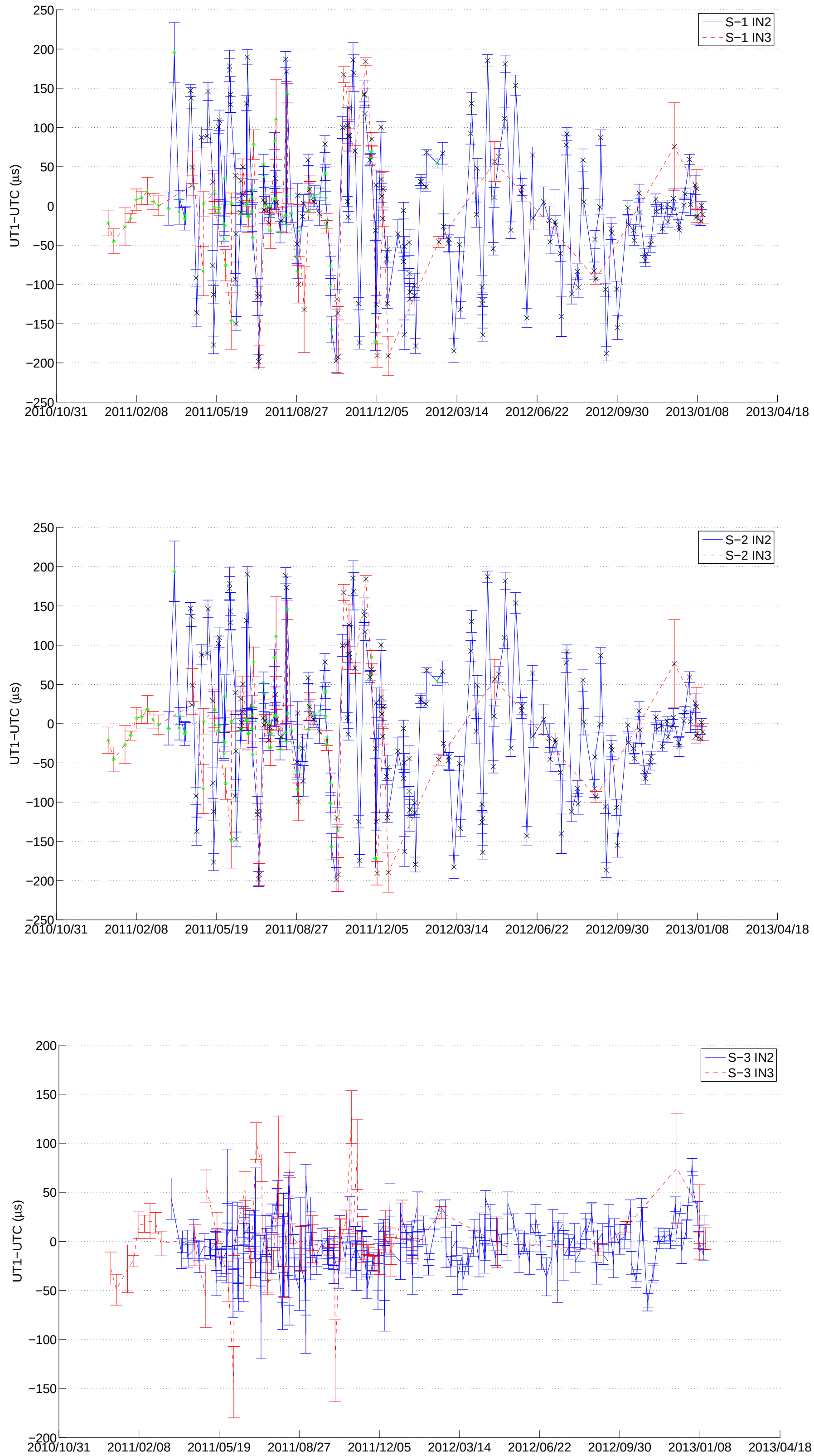

Fig. 1 dUT1 adjustment from IVS-INT2 and IVS-INT3 for strategies S-1, S-2, and S-3 using a priori TSUKUB32 coordinates computed from R1 sessions.

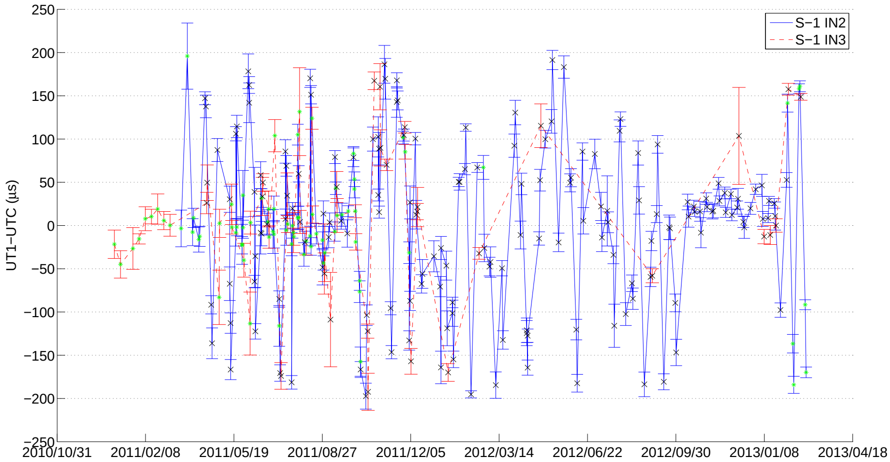

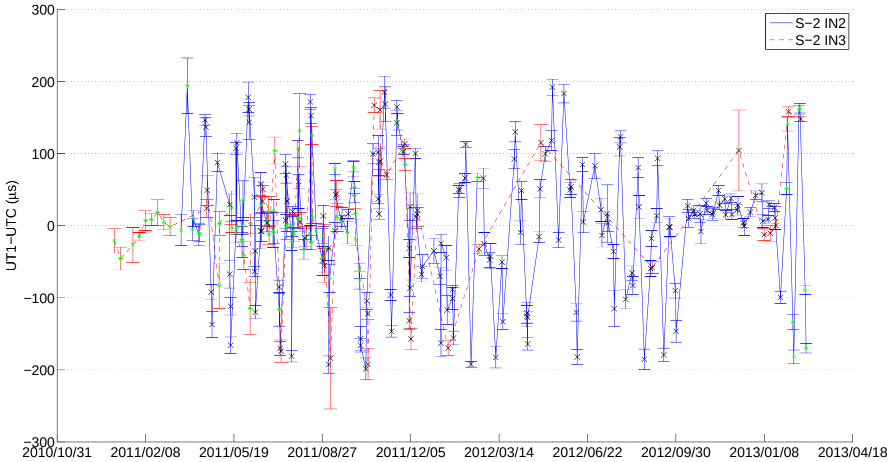

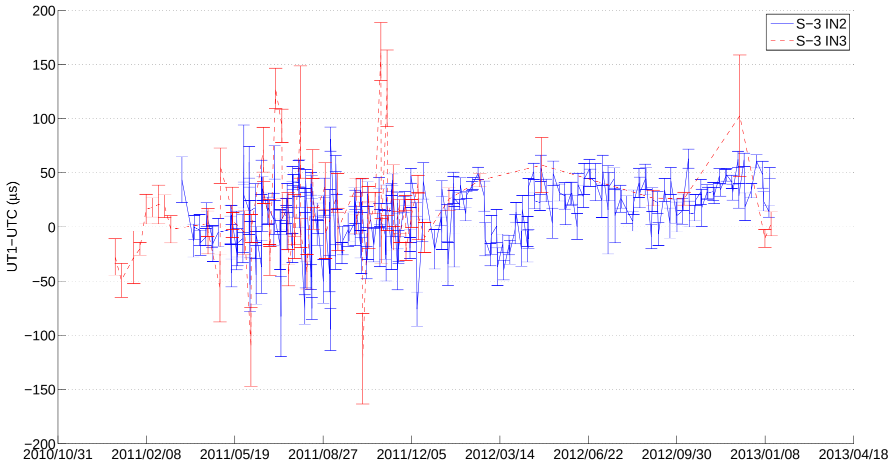

Fig. 2 dUT1 adjustment from IVS-INT2 and IVS-INT3 for strategies S-1, S-2, and S-3 using a priori TSUKUB32 coordinates computed from GPS data.

VLBI satellite tracking for precise coordinate determination - a simulation study

L. Plank, J. Böhm, H. Krásná, H. Schuh

Abstract VLBI observations to satellites offer interesting new applications. The use of existing satellites like those from Global Navigation Satellite Systems (GNSS) or a dedicated new mission like the proposed Geodetic Reference Antenna in Space (GRASP) mission for co-location in space are possible concepts. In this contribution, key parameters of such observations are investigated, as for example the station network, the observation interval, or the accuracy of derived coordinates, as determined in a global solution for one week of observations. We use simulated VLBI observations which account for noise, clock errors, and tropospheric disturbances and focus on the position errors in the estimated station coordinates. Both regional and global networks are investigated, considering the potential height of the observed satellite and the attendant restrictions on common visibility. Facing the troposphere as the main error source, changing the observation interval and the possibility of additional observations to quasars in order to increase the sky coverage for each station are found to be proper means to reach the expected accuracies of a few millimeters 3D station root mean square (rms).

Keywords VLBI satellite tracking, co-location in space, GRASP

1 Introduction

Soon after the first VLBI experiments, the potential of this technique for satellite tracking and orbit determination was recognized (e.g. Preston et al., 1972; Rosenbaum, 1972; Counselman and Gourevitch, 1981). While the advance of alternative tracking methods dominated developments in the past, recently the option of VLBI observing satellites came back into the geodesists' focus (e.g. Dickey, 2010). Whether it is an experiment on observations to GNSS satellites (e.g. Tornatore et al., 2011) or the proposal of a particular satellite mission like GRASP (Geodetic Reference Antenna in Space; Nerem and Draper, 2011), several scenarios are investigated at the moment. The driving force behind these activities is an aspired improvement of inter-technique frame ties, the backbone of the International Terrestrial Reference Frame (ITRF) as a combined product of four techniques, namely VLBI, GNSS, SLR and DORIS. At co-location sites, the antenna positions of different geodetic techniques are usually tied together by local measurements. However, the measured local tie vectors often do not fit the ones derived from the TRF solution at the expected accuracies and future ITRF improvement resides in improving the consistency between them (Altamimi et al., 2011). The idea followed in this contribution is illustrated in Fig. 1. A satellite which can be tracked by several space geodetic techniques (e.g. VLBI, GNSS, SLR) shall serve as a space-tie, directly connecting the frames determined by the different techniques.

Lucia Plank, Johannes Böhm, Hana Krásná and Harald Schuh
Vienna University of Technology, GEO, Gußhausstraße 27-29, 1040 Vienna, Austria
Harald Schuh
GeoForschungsZentrum Potsdam GFZ, Telegrafenberg, A17, 14473 Potsdam, Germany

2 Procedure

Goal of this simulation study is to investigate expected accuracies of derived antenna positions in dependence of different observing strategies. Therefore we use simulated observations that are based on the common stochastic error sources of geodetic VLBI today. The actual technical realization of VLBI observations to satellites with sufficient precision is disregarded in our study. The simulations were done using the Vienna

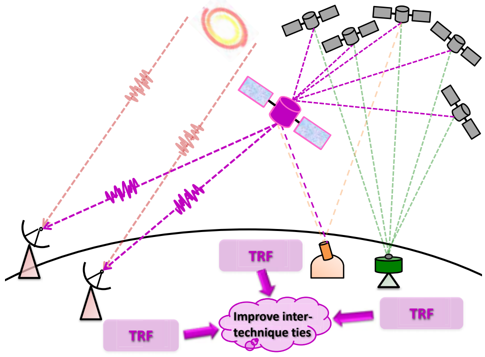

Fig. 1 Concept of co-location in space. A satellite that can be tracked by several space geodetic techniques (e.g. VLBI, SLR, GNSS) realizes a space-tie, directly connecting the frames determined by the different techniques.

	height h	inclination i	eccentricity e
GRASP	2000 km	104.89°	0.0001
GPS	20200 km	~ 55°	nearly circular

Table 1 Orbital elements of the simulated satellites.

VLBI Software VieVS (Böhm et al., 2012), including a number of adaptations for this special processing. Main steps of the processing are the scheduling of observations, the simulation of them and the estimation of station coordinates with a corresponding statistical interpretation.

2.1 Scheduling

The scheduling is simply based on common visibility between two antennas. With a given satellite orbit, a selected antenna network and a fixed observation interval, observations were scheduled for seven consecutive days, split into 24 hour sessions. The cutoff elevation angle was set to 5°. For our investigations we selected (a) one of the initially proposed orbits for the GRASP satellite mission idea (Nerem and Draper, 2011) and (b) a GPS satellite. The corresponding orbital parameters are given in Table 1.

VLBI satellite observations were simulated for a dense, regional network consisting of seven existing European stations (Fig. 2) and for a global artificial VLBI2010 network with 32 stations (Fig. 3).

2.2 Simulation

For the simulations, the VieVS simulator was used, following the procedure described by Pany et al. (2010).

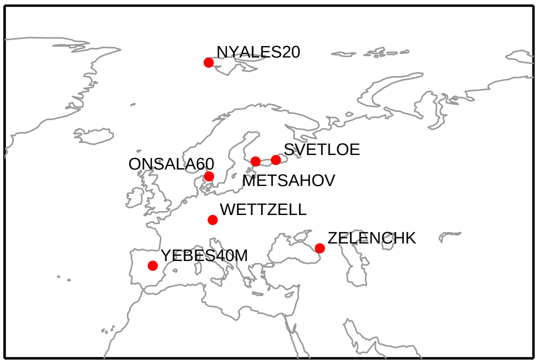

Fig. 2 European network.

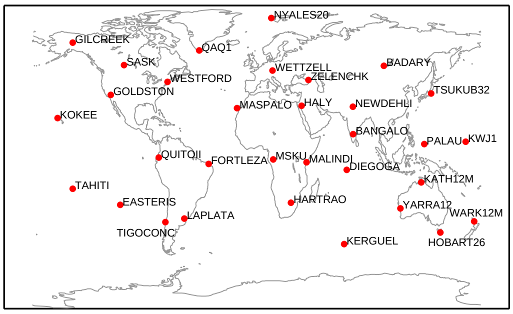

Fig. 3 Global 32 station network.

Based on Monte-Carlo simulations, the observed minus computed values are set up as the sum of the stochastical error sources due to the wet troposphere, the clock and the delay precision. We assume a turbulent troposphere with the characteristic structure constant $Cn = 2.5 \cdot 10^{-7} \mathrm{m}^{-1/3}$ and the effective height of the wet troposphere $H = 2$ km. For the clocks, an Allan standard deviation of $1 \cdot 10^{-14}$ @ 50 minutes is chosen and the delay precision is simulated as white noise of 30 picoseconds. The simulations are repeated 30 times.

2.3 Station position estimation

The simulated 24-h sessions are first processed separately with the analysis settings according to Table 2.

In a subsequent global solution, seven consecutive days are combined and one set of antenna coordinates is estimated for each station, 30 times. The rms of these estimates gives a measure of the expected accuracy in a weekly solution. This is expressed either in repeatability, respectively rms for the north-, east-, and up-components, or in terms of a 3D station rms.

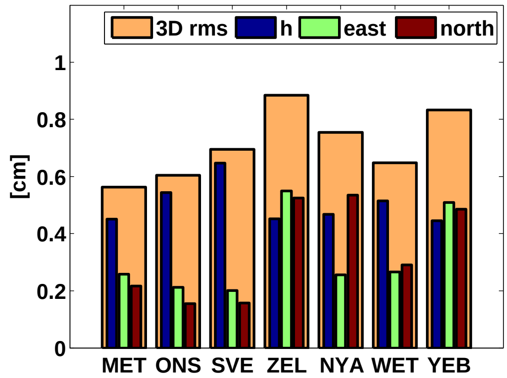

Fig. 4 Expected accuracies of station position repeatabilities if the GRASP satellite was observed in a 7-station European network in 5-min intervals.

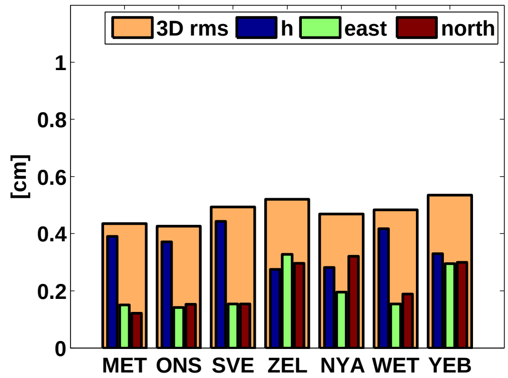

Fig. 5 Expected accuracies of station position repeatabilities if the GRASP satellite was observed in a 7-station European network in 1-min intervals.

EOP	fixed
Troposphere *zwd*	30 min pwl offsets
	0.7 ps^2/s constraints, no gradients
Clock	quadratic polynomial + 60 min pwl
	0.5 ps^2/s constraints
Station coordinates	NNT, NNR applied

Table 2 Analysis settings for the parameter estimation.

3 Observations to GRASP

In Fig. 4 the results are shown if the GRASP satellite was observed every 5 minutes. According to our simulations, the station positions can be determined in the satellite system with an accuracy of a few mm, with the height component being significantly worse than the horizontal position. This is not true for the stations Ny Ålesund (NYA), Zelenchukskaya (ZEL) and Yebes (YEB), which are located at the edges of the network. They only form baselines with the other stations more or less in one direction, causing their east- and north-components being not as well determined as for the other stations in the center of the network.

Improvement of the results is found when the observation interval is shortened from 5 to 1 min (Fig. 5). However, this improvement is not as big as probably expected and a further reduction of the interval gives no additional impact. Since the spatial and temporal correlation is included in the model applied in the simulator, additional observations into similar directions and at approximately the same time do not provide new information about the tropospheric conditions.

When going from a regional network to a global one, the results are slightly worse. In Fig. 6 the expected station position repeatabilities for the global 32-station network observing GRASP in 30 sec intervals is shown. A major reason for the worsening is the small number of possible observations, as indicated by the red line in the figure. This is a result of the longer baselines and the low satellite height reducing common visibility.

4 GPS observations

Next, we investigate VLBI observations to a single GPS satellite. Using the same approach as for GRASP in the previous section, station position repeatabilities of several cm are achieved. The reason for this is the poor sky coverage over each station, what results in an insufficient modeling of the troposphere. In Fig. 7 the sky coverage for station Wettzell is shown for one day observing the GRASP satellite in 1-min intervals (left plot) and 5-min intervals (right plot). With its low height GRASP passes the station several times per day resulting in observations well distributed on the sky. Unlike GRASP, the GPS satellite flies much higher and passes the station only twice per day, as can be seen in Fig. 8, left plot.

As a consequence, we propose to include VLBI observations to a single GPS satellite in a conventional geodetic VLBI session. As illustrated in Fig. 9, in a first step the troposphere then can be estimated using all observations and subsequently the antenna positions are determined using the GPS observations only. With this 2-step procedure the stations are determined in the satellite system, which further on can be directly compared to the station positions determined from VLBI observations to radio sources. Deviations between both determined station positions represent the difference between the satellite and the VLBI system and can help

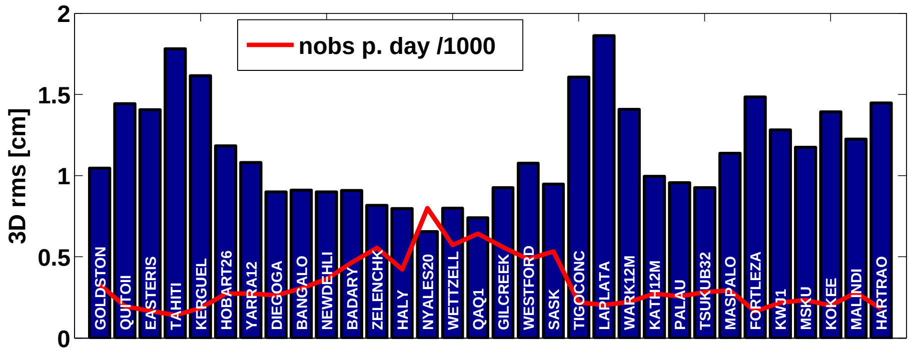

Fig. 6 Expected accuracies of station position repeatabilities if the GRASP satellite was observed in an artificial 32-station global network in 30 sec intervals. The red line indicates the mean number of observations per day.

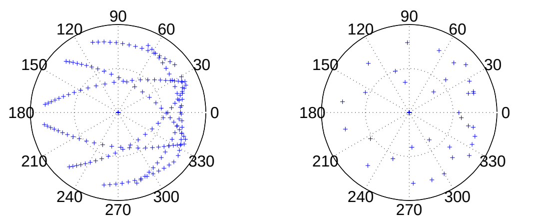

Fig. 7 1-day skyplot for station Wettzell observing GRASP in 1 min intervals (left) and 5 min intervals (right).

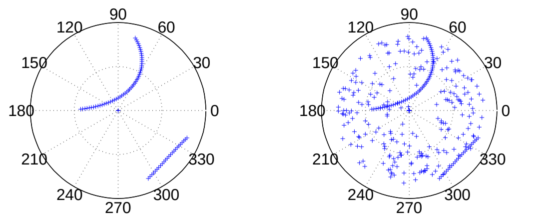

Fig. 8 1-day skyplot for station Wettzell observing one GPS satellite in 5 min intervals (left). On the right the corresponding skyplot is shown for the combined approach, including observations to radio sources.

to identify and remove possible inadequacies of the two frames.

Applying this combined approach (with the corresponding sky plot shown in Fig. 8, right plot), station rms of a few mm are achieved, as shown in Fig. 10. This is an improvement by a factor of 10 compared to the GPS-only solution. With a good estimation of the troposphere, the determined station errors are dominated by the geometrical conditions due to the stations' positions in the network and the satellite orbit, resulting in a significantly better determined height component than the horizontal components.

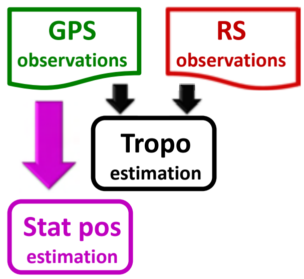

Fig. 9 Concept of combined GPS and radio source (RS) observations.

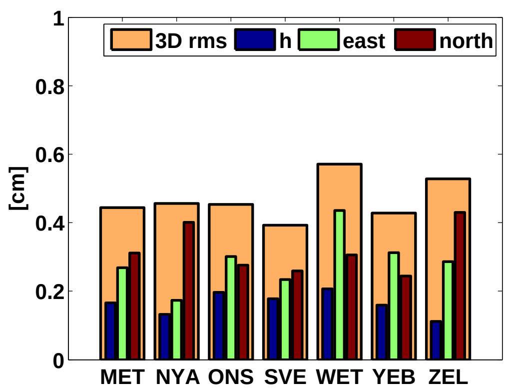

Fig. 10 Station position repeatabilities using the GPS combined approach. The results shown are from a weekly global solution where a GPS satellite was observed in 5 min intervals, flanked by VLBI observations to radio sources.

5 Conclusions

With the goal to improve inter-technique ties, we investigate VLBI observations to satellites. Based on simulated observations, strategies are found to precisely determine antenna positions on ground in the satellite system with accuracies of 5 – 10 mm 3D rms. This is possible for either very low (h = 2000 km) or GPS satellites, in a dense, regional antenna network. For a global network the results are worse by a factor of about 2 due to the longer baselines and limited common visibility. The optimal observation interval varies for satellites at different heights as no additional information is gained through consecutive observations in similar directions. For higher satellites like those from the GPS we propose to include the observations into standard geodetic VLBI sessions in order to successfully resolve the troposphere.

Acknowledgements: The presented research was done within the project D-VLBI as part of the DFG Research Unit *Space-Time Reference Systems for Monitoring Global Change and for Precise Navigation in Space* funded by the German Research Foundation (FOR 1503). Hana Krásná thanks the Austrian Science Fund (FWF), project P23143-N21.

References

Z. Altamimi, X. Collilieux, and L. Métivier. ITRF2008: an improved solution of the international terrestrial reference frame. *Journal of Geodesy*, Springer Berlin/Heidelberg, 85:8, pp. 457–473, 2011. doi: 10.1007/s00190-011-0444-4.

J. Böhm, S. Böhm, T. Nilsson, A. Pany, L. Plank, H. Spicakova, K. Teke, and H. Schuh. The new Vienna VLBI Software VieVS. *Proceedings of the 2009 IAG Symposium*, Buenos Aires, Argentina, S. Kenyon, M. C. Pacino, and U. Marti (eds.), International Association of Geodesy Symposia, vol. 136, pp. 1007–1011, 2012.

C. Counselman and S. A. Gourevitch. Miniature Interferometer Terminals for Earth Surveying: Ambiguity and Multipath with Global Positioning System. *IEEE Transactions on Geoscience and Remote Sensing*, GE-19, No. 4, pp. 244–252, 1981.

J. M. Dickey. How and Why Do VLBI on GPS. In *IVS 2010 General Meeting Proceedings*, D. Behrend and K. D. Baver (eds.), NASA/CP 2010-215864, pp. 65-69, 2010.

R. S. Nerem and R. W. Draper. Geodetic Reference Antenna in SPace. GRASP proposal submitted in response to NNH11ZDA0120, prepared for National Aeronautics and Space Administration Science Mission Directorate, September 29, 2011.

A. Pany, J. Böhm, D. S. MacMillan, H. Schuh, T. Nilsson, and J. Wresnik. Monte Carlo simulations of the impact of troposphere, clock and measurement errors on the repeatability of VLBI positions. *Journal of Geodesy*, 85:1, pp.39–50, 2010. doi: 10.1007/s00190-010-0415-1.

R. A. Preston, R. Ergas, H. F. Hinteregger, C. A. Knight, D. S. Robertson, I. I. Shapiro, A. R. Whitney, A. E. E. Rogers, and T. A. Clark. Interferometric Observations of an Artificial Satellite. *Science*, 178-4059, pp. 407–409, 1972.

B. Rosenbaum. The VLBI Time Delay Function for Synchronous Orbits. *NASA/TM-X-66122*, GSFC, 1972.

V. Tornatore, R. Haas, D. Duev, S. Pogrebenko, S. Casey, G. Molera Calvés, and A. Keimpema. Single baseline GLONASS observations with VLBI: data processing and first results. In *Proceedings of the* 20th *Meeting of the European VLBI Group for Geodesy and Astrometry*, W. Alef, S. Bernhart and A. Nothnagel (eds.), Institut für Geodäsie und Geoinformation der Universität Bonn, 22, pp. 162–165, 2011.

Influence of source distribution on UT1 derived from IVS INT1 sessions

M. Uunila, A. Nothnagel, J. Leek, N. Kareinen

Abstract The influence of the spatial distribution of the observations on the quality of UT1 results derived from IVS Schlüter and Behrend (2007) INT1 sessions is explored. The Kokee - Wettzell baseline midpoint was chosen as a reference point for the analysis. The results of the research will be compared to those of the GSFC group's results Baver et al. (2012), Gipson et al. (2011) and Baver and Gipson (2010). In their research, the reference point was Kokee Park North direction, and not the midpoint of the baseline, which makes this investigation, and its results novel.

Keywords UT1, intensive sessions, INT1

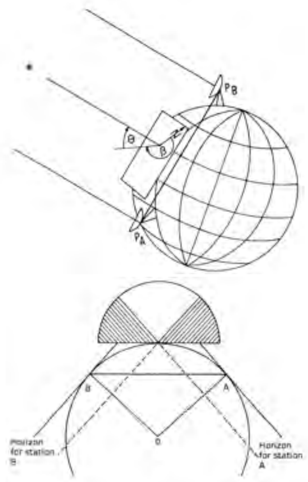

Fig. 1 An example of the midpoint based reference system. Geometry of baseline reference system and horizon mask are shown (modified from Nothnagel and Campbell (1991)). The two stations are located at the points A and B.

1 Introduction

The effect of the source constellations on the quality of the dUT1 results is examined.

IVS intensive sessions INT1 with the baseline Kokee - Wettzell were chosen for the analysis because these sessions are measured five times per week, and therefore there are enough data to obtain reasonable results.

A fictitious baseline reference point is defined as the projection of the baseline midpoint onto the ellipsoid and serves as the origin of a topocentric system with the tangential plane being the equatorial plane of this system.

The baseline system can be interpreted as a hemisphere put on top of the ellipsoid at the baseline reference point (Figure 1).

Minttu Uunila and Niko Kareinen
Aalto University Metsähovi Radio Observatory, Metsähovintie 114, 02540 Kylmälä, Finland Axel Nothnagel and Judith Leek
Rheinische Friedrich-Wilhelms Universität Bonn, IGG,Nußallee 17, D-53115 Bonn, Germany

There are various reasons to include low elevation sources in the schedules of the intensive sessions. For example, it is necessary to include observations with different elevation angles, to distinguish between the elevation dependent tropospheric delay and the clock parameters, which are independent of elevation. Observations with low elevation angles are essential for the estimation of the tropospheric path delay.

Several tests with intensive session observing schedules showed that the inclusion of 20 to 30% low elevation sources (≤ 25 degrees) is associated with an improvement of the theoretical UT1 sigmas of about 45% in average Schnell (2006).

The precision of the ZWD estimates for characteristic times of order 20 minutes improves as data are included from lower elevation angles. However, systematic errors on the timescale of a day, due to errors in the mapping functions, for example, will increase significantly when observations at elevation angles below 10 degrees are added to the solutions MacMillan and Ma (1994) Niell et al. (2001).

2 Analysis strategy

Both the horizon limits of the two stations and the observations are best displayed in a stereographic projection, which is created with the SkyPlot program Uunila et al. (2012).

The stereographic projection from the SkyPlot program was divided into six sections as shown in Figure 2. Quality codes AA-D are assigned when 1 or more sources in two sections on opposite parts of the sky are seen from the midpoint of the baseline.

The azimuth and elevation limits are calculated based on the azimuth - elevation files from the Skyplot. Due to plotting reasons, the files have the values in the format of:

- azimuth = -azimuth + $\pi/2$
- elevation = $\pi/2$ - elevation,

- The azimuth limits for sections 1, 3 and 5 are: $\pi/2 > azimuth \geq -\pi/2$ and for sections 2, 4 and 6, $-\pi/2 > azimuth \geq -3\pi/2$.

- The elevation limits are in sections 1 and 2, $\pi/2 > elevation \geq \pi/3$, in sections 3 and 4, $\pi/3 > elevation \geq \pi/6$ and in sections 5 and 6, $\pi/6 > elevation \geq 0$.

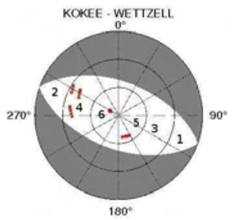

Fig. 2 Stereographical projection with the division to different sky sections. Division to sections 1-6 was done with azimuth and elevation values obtained from the SkyPlot program.

- AA is assigned if there are two sources in one of the sections 1 and 2, and two or more sources in the other. Quality code A is assigned, if there is one source in one of the two sections, and one or more in the other.
- BBB is assigned if there are three or more sources either in sections 1 and 4, or 2 and 3. BB is assigned if there are two sources in one of the sections (1 and 4, or 2 and 3), and two or more in the other. B is assigned if there is one source in one of the sections, and one or more in the other.
- Quality code C is assigned, if there are three or more sources in sections 3 and 4.
- If any of the quality codes from AA to C cannot be assigned (if there are not enough sources in any of the section pairs to enable the session to get a code AA-C), quality code D is assigned.

3 Results

Standard VLBI data analysis was performed following the IERS Conventions 2010 Petit and Luzum (2010) with the Vienna VLBI Software (VieVS Böhm et al. (2012)).

A Matlab program was written to divide the data into different sections, to assign quality codes and to calculate session counts and mean scan counts for each quality code. All INT1 sessions from January, 2010 to October, 2011 were analyzed.

It is striking that categories AA-BB have no outliers (3 σ was used for outlier elimination).

The RMS difference for dUT1 from the intensive analysis with respect to the combined solution from IVS EOP-S are listed in the fourth column of Table 1. The category AA gives the best result. Also listed are the mean differences between EOP-S. When the outliers are removed, categories AA and BBB still give the best results. Codes C and D have the largest mean values of formal errors of the dUT1 estimates with respect to *a priori* IVS EOP-S. The mean values of formal errors are the smallest with quality codes AA and BBB.

When the outlier limit was set to 3 σ for both dUT1 difference with respect to *a priori*, and its formal error, all categories except AA-BB had outliers. For the only one session with quality code AA, the dUT1 estimate with the respect to EOP-S is 34.5 μs and has a formal error is 10.4 μs, (Table 1). After the outlier elimination the RMS values of the dUT1 with respect to EOP-S, for example with category D, decreased from 51.7 μs to 34.0 μs, after the elimination of the outliers. Figure 10 shows the formal errors and dUT1 estimates with the respect to the IVS EOP-S. The values for categories AA and BBB are remarkably low.

When the six sessions in category A with formal errors larger than 30 μs were investigated, it was noticed that three of the sessions had 2-4 bad scans, two sessions had high atmospheric adjustments and one had a poorer sky coverage.

Table 1 Mean formal error of the dUT1 difference, RMS difference to IVS EOP-S, mean difference to EOP-S, all results with the values before outlier elimination in parentheses for each code, AA-D in μs.

Code	Mean FE	RMS EOP-S	Mean EOP-S
AA	10.4	-	34.5
A	19.7	32.3	-9.2
BBB	17.8	32.4	-9.6
BB	19.3	34.6	-4.6
B	20.8 (24.6)	30.6 (41.5)	-3.1 (-5.5)
C	21.4 (23.0)	28.9 (34.8)	-0.5 (-2.9)
D	25.4 (25.7)	34.0 (51.7)	-7.7 (-3.2)

4 SkyPlots

Figures 3-9 show the sky plots generated with the SkyPlot program for the categories AA-D. The sky plots for the sessions producing the smallest (in the left) and largest (in the right) formal errors in all categories are displayed in the figures. The sessions with the largest formal errors appear to produce sky plots with the sources clustered in sub-groups.

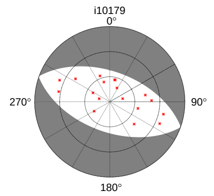

Fig. 3 Sky plot for AA. Formal error is 10.4 μs and scan count is 18.

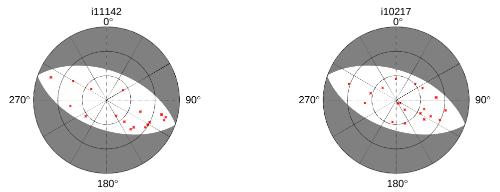

Fig. 4 Sky plots for A: sessions resulting in the smallest (8.9 μs) and largest (55.5 μs) formal errors. Scan counts are 17 and 19.

According to the Skyplots, it is evident that the sessions with a uniform source distribution produce the smallest formal errors in all categories. In this aspect the results are in good agreement with those of the GSFC group's results Baver et al. (2012), Gipson et al. (2011) and Baver and Gipson (2010).

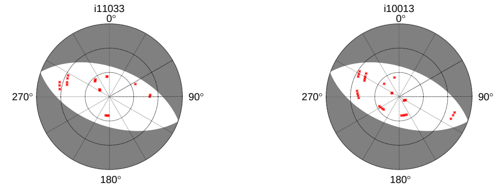

Fig. 5 Sky plots for BBB: sessions resulting in the smallest (8.4 μs) and largest (28.6 μs) formal errors. Scan counts are 21 and 29.

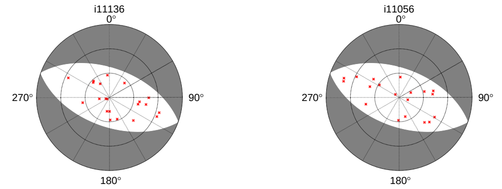

Fig. 6 Sky plots for BB: sessions resulting in the smallest (7.3 μs) and largest (40.7 μs) formal errors. Scan counts are 21 and 19.

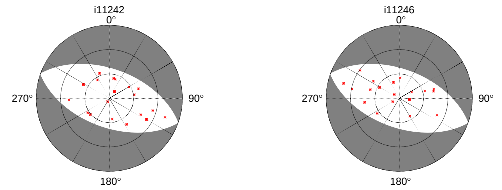

Fig. 7 Sky plots for B: sessions resulting in the smallest (7.7 μs) and largest (53.2 μs) formal errors. Scan counts is 19 for both sessions.

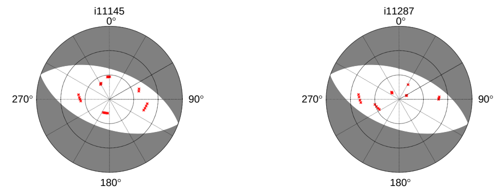

Fig. 8 Sky plots for C: sessions resulting in the smallest (7.2 μs) and largest (53.1 μs) formal errors. Scan counts are 21 and 17.

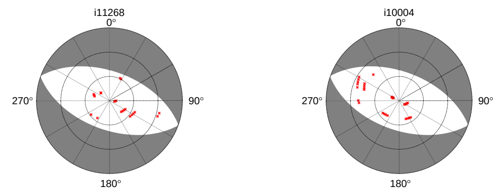

Fig. 9 Sky plots for D: sessions resulting in the smallest (6.8 μs) and largest (61.7 μs) formal errors. Scan counts are 22 and 30.

5 Conclusions

All INT1 observing sessions from January, 2010 - October, 2011 were categorized with respect to their geometric distribution of observations in a baseline-fixed reference system. Categories AA and BBB with observations far down in the baseline sky plot cusps appeared to be the best categories, but there was only one session in AA category. While categories from B to D with hardly any observations in the cusps, or almost all observations close to the zenith of the baseline, are the worst. The formal errors appeared to be convincingly low in categories AA and BBB with no values larger than 30 μs. This could be expected because of the good geometry of the sessions. The categories AA-BB have no outliers. The six sessions which had formal errors larger than 30 μs in A category were investigated individually. Three of the sessions had 2-4 bad scans, two sessions had high atmospheric adjustments and one had a poorer sky coverage.

Better sky coverage is known to be linked with improved accuracy of the UT1 estimates Baver and Gipson (2010). From the sky plots it is evident that the more uniform the source distribution is, the smaller the formal errors are. On the basis of the sky plots and number of scans per session, it is concluded that a uniform source distribution with sources in the far down cusps improves the accuracy of the dUT1 more than a large number of scans.

Our research strongly implies that scheduling sources to the far down cusps is essential in improving the accuracy of dUT1.

References

Schlüter, W. and D. Behrend. The International VLBI Service for Geodesy and Astrometry (IVS): current capabilities and future prospects. *Journal of Geodesy*, Vol. 81, Nos. 6-8, pp. 379-387, June 2007.

J. Gipson, K. Baver, K. Kingham and M. S. Carter. Better Scheduling of the IVS-Intensives for Improved UT1 estimates. Presented at EGU, Vienna, Austria, 2011.

K. Baver, J. Gipson, K. Kingham and M. S. Carter. Assessment of the First Use of the Uniform Sky Strategy in Scheduling the Operational IVS-INT01 Sessions. Presented at IVS General Meeting, Madrid, Spain, 2012.

K. Baver and J. Gipson. Strategies for Improving the IVS-INT01 UT1 Estimates. *IVS 2010 General Meeting Proceedings*, p.256-260, 2010.

A. Nothnagel and J. Campbell. Polar Motion Observed by Daily VLBI Measurements. *Proceedings of the AGU Chapman Conference on Geodetic VLBI: Monitoring Global Change, NOAA Technical Report NOS 137 NGS 49*, 345-354, Washington D.C., 1991.

D. Schnell. Quality Aspects of Short Duration VLBI Observations for UT1 Determinations. Doctoral dissertation, Rheinischen Friedrich-Wilhelms-Universitt Bonn, http://hss.ulb.uni-bonn.de/2006/0918/0918.pdf, 2006.

D. MacMillan and C. Ma. Evaluation of Very Long Baseline Interferometry Atmospheric Modeling Improvements. *Journal of Geophysical Research*, 99 (B1), 637-651, 1994.

A. E. Niell, A. J. Coster, F. S. Solheim, V. B. Mendes, P. C. Toor, R. B. Langley and C. A. Upham. Comparison of Measurements of Atmospheric Wet Delay by Radiosonde, Water Vapor Radiometer, GPS, and VLBI. *J. Atmos. Oceanic Technol.*, 18, 830-850, 2001.

M. Uunila, A. Nothnagel and J. Leek. Influence of source constellations on UT1 derived from IVS INT1 sessions. *2012 IVS General Meeting proceedings* (in print).

G. Petit and B. Luzum (eds.). IERS Conventions (2010). *IERS Technical Note; 36*, Frankfurt am Main: Verlag des Bundesamts für Kartographie und Geodäsie, 2010.

J. Böhm, S. Böhm, T. Nilsson, A. Pany, L. Plank, H. Spicakova, K. Teke and H. Schuh. The New Vienna VLBI Software VieVS. *Proceedings of IAG Scientific Assembly 2009*, In: International Association of Geodesy Symposia Series Vol. 136, edited by S. Kenyon, M. C. Pacino, and U. Marti, 1007-1011, doi: $10.1007/978-3-642-20338-1\_126$, 2012.

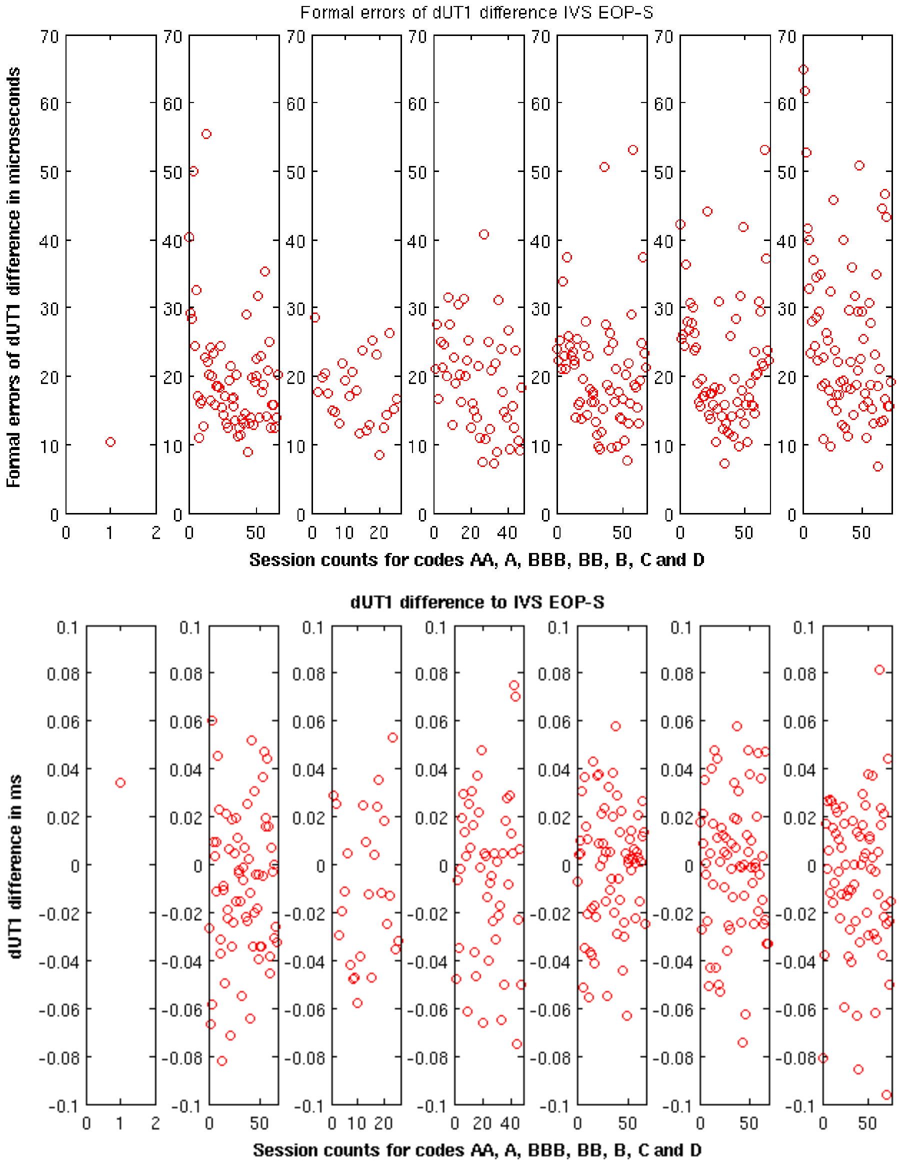

Fig. 10 Formal errors and dUT1 estimates compared to IVS EOP-S *a priori* and quality code counts for categories AA, A, BBB, BB, B, C, and D, in that order. On X-axis is the session count, and on the Y-axis the formal errrors and dUT1 difference to EOP-S in μs. Category AA has only one session. AA and BBB appear to be the best categories with no formal error values larger than 30 μs and the smallest scatter of dUT1 estimates.

A Kalman filter for combining high frequency Earth rotation parameters from VLBI and GNSS

T. Nilsson, M. Karbon, H. Schuh

Abstract We present a Kalman filter for combination of sub-diurnal Earth Rotation Parameters (ERP) estimated from different techniques. We test this filter by combining ERP estimated from VLBI and GPS for the CONT08 campaign. We find that the Kalman filter works and give reasonable results. The combined solution is dominated by the GPS data since the ERP from this technique have much lower formal errors. However VLBI is important for providing the absolute value of dUT1 since GPS is only sensitive to the time derivative of dUT1, i.e. the length of day.

Keywords VLBI, GPS, Kalman Filter, High Frequency Earth Rotation

1 Introduction

The rotation of the Earth varies on a multitude of time scales, from decades and longer down to sub-diurnal frequencies. For all types of precise navigation on the Earth and in space, accurate knowledge about these variations is essential. Commonly the Earth Rotation Parameters (ERP, i.e. polar motion and UT1) are measured by space geodetic techniques such as Very Long Baseline Interferometry (VLBI) and Global Navigation Satellite Systems (GNSS). Each technique has its own advantages and weaknesses. For example, with GNSS, e.g. the Global Positioning System (GPS), you can easily have many observations from global ground networks consisting of several hundred stations, hence the formal errors of the estimated ERP will be small. However, GNSS are not able to estimate long-term variations in UT1 nor precession/nutation. VLBI, on the other hand, can estimate the full set of Earth orientation parameters (polar motion, UT1, and precession/nutation). However, the network of a typical VLBI session is relatively small (< 10 stations), which limits the precision. Furthermore, due to operational reasons and budget constraints, the networks of the various VLBI sessions contain different stations what degrades the accuracy of the ERP time series obtained within the IVS (International VLBI Service for Geodesy and Astrometry).

Hence, in order to obtain the highest accuracy the results from different techniques should be combined. This is done on a regular basis, e.g. by constructing the IERS 08 C04 series (Bizouard and Gambis, 2009). Kalman filtering has turned out to be a good procedure for combining ERP from different techniques (Morabito et al, 1988). This method is for example used in the ERP combination run by JPL (Gross et al, 1998).

In the above mentioned combinations the ERP are provided with daily resolution. It is however of interest to obtain ERP series with higher temporal resolution. In this work we present a Kalman filter able to combine high frequency ERP (e.g. hourly) from different techniques. This Kalman filter is presented in Section 2. In Section 3 we test the filter by combining ERP estimated from GPS and VLBI for the CONT08 period. The conclusions are presented in Section 4.

2 Theory

A Kalman filter is a recursive filter which makes the estimation epoch by epoch (Brown and Hwang, 1997). At each epoch the predictions from the previous epoch are combined with the observations in an optimum way. The prediction of the unknown variables $\mathbf{x}_k$ at epoch t_k, $\mathbf{x}_k^-$, is given by:

$$\mathbf{x}_k^- = F_k \, \mathbf{x}_{k-1} \quad (1)$$

Tobias Nilsson, Maria Karbon, and Harald Schuh
Department 1: Geodesy and Remote Sensing, GFZ German Research Centre for Geosciences, Telegrafenberg A17, D-14473 Potsdam, Germany

where $\mathbf{x}_{k-1}$ are the estimates at epoch t_{k-1} and F_k the state transition matrix. The variance-covariance matrix of $\mathbf{x}_k^-$ will then be:

$$P_k^- = F_k P_{k-1} F_k^T + Q_k \tag{2}$$

where P_{k-1} and Q_k are the variance-covariance matrices of $\mathbf{x}_{k-1}$ and the prediction error, respectively.

At epoch t_k we have the observations $\mathbf{z}_k$. These are related to $\mathbf{x}_k$ by:

$$\mathbf{z}_k = H_k \mathbf{x}_k \tag{3}$$

We can combine $\mathbf{z}_k$ and $\mathbf{x}_k^-$ to obtain the optimum estimates of $\mathbf{x}_k$ and it variance-covariance matrix P_k:

$$\mathbf{x}_k = \mathbf{x}_k^- + K_k \left(\mathbf{z}_k - H_k \mathbf{x}_k^-\right) \tag{4}$$

$$P_k = (I - K_k H_k) P_k^- \tag{5}$$

The Kalman filter gain K_k is given by:

$$K_k = P_k^- H_k^T \left(H_k P_k^- H_k^T + R_k\right)^{-1} \tag{6}$$

For the Kalman filter implementation we need a model for making the predictions of the ERP forward in time. In this work we model the polar motion, $p = x_{pole} - i y_{pole}$, and dUT1, U, by the following equations:

$$p = \bar{p} + \sum_{k=1}^{n} \left[A_k e^{ik\Omega t} + B_k e^{-ik\Omega t}\right] \tag{7}$$

$$U = \bar{U} + \sum_{k=1}^{n} \left[C_k \cos k\Omega t + D_k \sin k\Omega t\right] \tag{8}$$

A_k, B_k, C_k, and D_k are amplitudes of the (sub-)diurnal variations, and Ω is the rotation frequency of the Earth. In this work $n = 2$, i.e. only diurnal and semi-diurnal variations are considered. The low frequency ERP variations (periods > 1 day) are described by the terms $\bar{p}$ and $\bar{U}$. Their temporal variations can be expressed by the Euler-Liouville equations (Morabito et al, 1988):

$$\frac{\partial \bar{p}}{\partial t} = i\sigma_{ch}(\bar{p} - \bar{\chi}) \tag{9}$$

$$\frac{\partial \bar{U}}{\partial t} = -\frac{\delta \bar{L}}{L_0} \tag{10}$$

where $\bar{\chi} = \bar{\chi}_x + i\bar{\chi}_y$ is the polar motion excitation function, σ_{ch} is the frequency of the Chandler wobble (0.0145 rad/day), $\delta\bar{L}$ describes the low frequency length of day variations, and L_0 is the nominal length of day (86400 s).

In our Kalman filter implementation the unknown quantities are $\bar{p}$, $\bar{U}$, $\bar{\chi}$, $\delta\bar{L}$, A_k, B_k, C_k, and D_k. Furthermore, in this work a constant polar motion offset between the polar motion estimates from GPS and VLBI are estimated in order to account for a possible misalignment of the GPS and VLBI terrestrial reference frames. The temporal evolution of $\bar{p}$ and $\bar{U}$ are described by equations (9) and (10), respectively, while the other parameters are described as random walk processes. For example, the temporal variation of A_k is:

$$\frac{\partial A_k}{\partial t} = w_{A_k} \tag{11}$$

where w_{A_k} is a white noise process with power spectral density q_{A_k}. The values of the power spectral densities related to the different random walk processes are given in Table 1.

Table 1 Power spectral densities of the different parameters.

Parameter	Value	Unit
q_{A_1}, q_{B_1}	900	μas^2/day
q_{A_2}, q_{B_2}	900	μas^2/day
q_{C_1}, q_{D_1}	9	μs^2/day
q_{C_2}, q_{D_2}	9	μs^2/day
q_{χ}	246.6	mas^2/day
$q_{\delta\bar{L}}$	0.0036	ms^2/day^3

In addition to the normal forward Kalman filter loop (Eq. (4)), we also run a backward smoothing loop (Rauch-Tung-Striebel smoothing, Brown and Hwang (1997)) in order to improve the earlier estimates using the later estimates.

3 Results

The Kalman filter was tested by combining ERP from VLBI and GPS for the CONT08 campaign (12-16 August, 2008). The VLBI ERP were obtained from a VLBI solution made with the Vienna VLBI Software (VieVS, Böhm et al (2012)), providing polar motion and UT1 with 1 hour resolution. The GPS ERP were obtained from a global GPS solution providing polar motion and length of day with hourly resolution (Steigenberger et al, 2006).

Figure 1 shows the ERP determined by the Kalman filter combination. We can note that the combined series are smoother than the original time series. Overall, GPS has the strongest impact on the combined series, which is not surprising given that the formal errors of the GPS solution are much smaller than those of the VLBI solution (mean polar motion formal error is 20 μas for GPS, compared to 100 μas for VLBI). However, VLBI is important for the long period dUT1 variations since GPS is not sensitive to dUT1 (only to its time derivative, i.e. length of day).

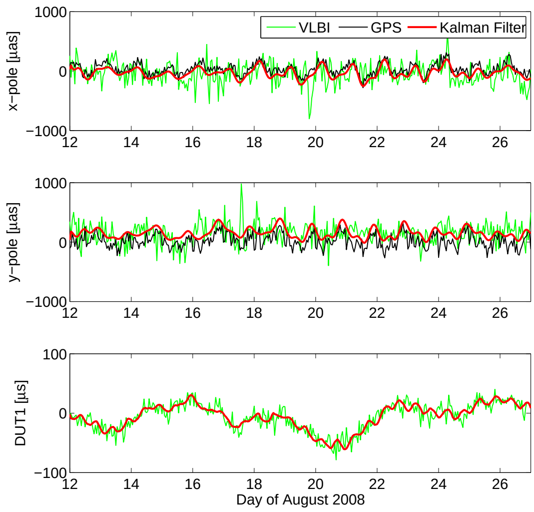

Fig. 1 Polar motion and dUT1 estimated for the CONT08 period from the Kalman filter and from the original VLBI and GPS time series. From all time series the IERS 08 C04 values and the IERS high frequency ERP model (Petit and Luzum, 2010) have been subtracted.

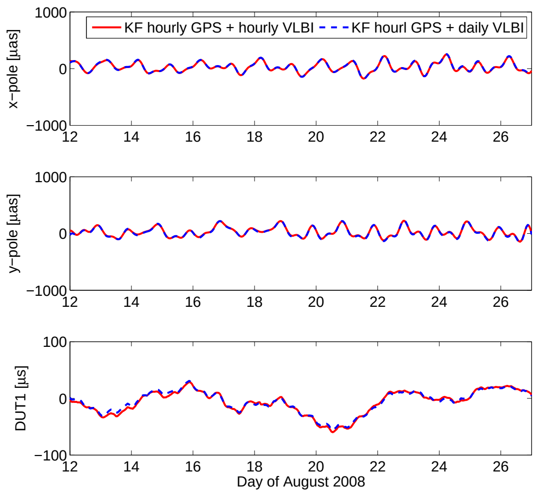

Fig. 2 Polar motion and dUT1 estimated for the CONT08 period when combining daily VLBI estimates with hourly GPS estimates, compared to the estimates obtained when using hourly data from both techniques.

One advantage of our Kalman filter implementation is that it allows for combination of daily ERP estimated with one technique with hourly ERP from another technique. This is accomplished by assuming that the daily ERP are observation only of the low frequency polar motion and dUT1, $\bar{p}$ and $\bar{U}$. We tested this by combining ERP estimated with daily resolution from VLBI with the hourly GPS results. The results can be seen in

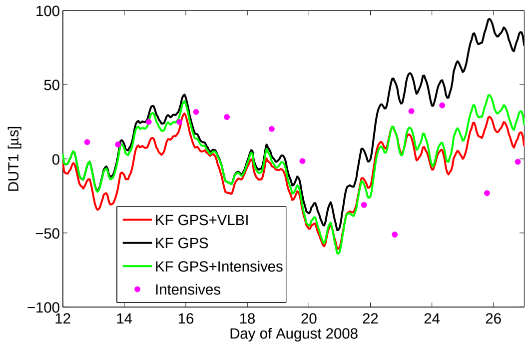

Fig. 3 UT1 estimated for the CONT08 period from a combination of the VLBI Intensives and GPS data, compared to the results when using only GPS as well as when combining hourly GPS and VLBI data.

Fig. 2. There are no significant differences to the case when combining hourly ERP from both techniques, further showing that the VLBI is mainly important for the low frequency ERP variations.

We also investigated the possibility to combine UT1 estimated from the VLBI 1-hour Intensives with GPS data. In total 14 Intensive sessions were successfully observed during CONT08. The dUT1 time series obtained when combing the results from these with the hourly GPS data can be seen in Fig. 3. For comparison, the dUT1 estimated from the GPS only (initialised by VLBI data at the first epoch) and the full GPS + VLBI combination are shown. We can see that the dUT1 estimated from GPS only drifts away from the GPS + VLBI solution after about a week, which is expected since GPS does not provide any absolute information about UT1. The GPS + Intensives combination, however, remain close to the GPS + VLBI solution.

4 Conclusions

The Kalman filter presented in this work has been successfully applied for combining high frequency ERP estimated from VLBI and GPS. The Kalman filter is flexible in that it offers the possibility to combine ERP time series with different temporal resolution, e.g. daily and hourly. The results from the combination are dominated by the original GPS time series due to their significantly lower formal errors. However the formal errors may not completely represent the actual accuracy of the ERP estimated from the respective techniques. In the future we will investigate applying technique specific weights in the filter, i.e.

down-weighting techniques with too optimistic formal errors. Furthermore, we will consider modelling of possible technique-specific systematic errors, like GPS length of day biases (Senior et al, 2010).

The filter can easily be extended to include data from other sensors. It is straight-forward to include ERP estimated from other space geodetic techniques, such as satellite laser ranging. It is also possible to include measurements from ring laser gyroscopes. A combination of ring laser and VLBI data has been successfully performed at the normal equation level (Nilsson et al, 2012), thus it should also be possible to do such a combination with a Kalman filter. However, the findings of Nilsson et al (2012) show that the ring laser data will mostly contribute to the very high frequency ERP variations, e.g. over one hour. Thus, presently it probably only makes sense to include ring laser data in the filter when considering higher frequencies in Eqs. (7) and (8), not only diurnal and semi-diurnal variations as was done in this work.

Acknowledgement We are grateful to Peter Steigenberger, TU Munich, for providing the GPS time series, and the IVS for providing the VLBI data. This work was supported by the German Science Foundation (DFG), project SCHU-1103/3-2, and the Austrian Science Fund (FWF), project P24187-N21.

References

Bizouard C, Gambis D The combined solution C04 for Earth orientation parameters consistent with international terrestial reference frame 2005. In: Geodetic Reference Frames, Springer, Munich, Germany, IAG Symposium, vol 134, pp 265–270, 2009. doi: 10.1007/978-3-642-00860-3_41.

Böhm J, Böhm S, Nilsson T, Pany A, Plank L, Spicakova H, Teke K, Schuh H The new Vienna VLBI software. In: Kenyon S, Pacino MC, Marti U (eds) IAG Scientific Assembly 2009, Springer, Buenos Aires, Argentina, no. 136 in International Association of Geodesy Symposia, pp 1007–1011, 2012 doi: 10.1007/978-3-642-20338-1_126

Brown RG, Hwang PYC Introduction to Random Signals and Applied Kalman Filtering, 3rd edn. John Wiley & Sons, 1997

Gross RS, Eubanks TM, Steppe JA, Freedman AP, Dickey JO, Runge TF A Kalman-filter-based approach to combining independent Earth-orientation series 72(4):215–235, 1998

Morabito DD, Eubanks TM, JA JAS Kalman filtering of earth orientation changes. In: Babecock A, Wilkins GA (eds) The Earths rotation and reference frames for geodesy and geodynamics, Reidel, Dordrecht, Holland, pp 257–267, 1988

Nilsson T, Böhm J, Schuh H, Schreiber U, Gebauer A, Klügel T Combining VLBI and ring laser observations for determination of high frequency Earth rotation variation. J Geodyn 62:69–73,2012 doi: 10.1016/j.jog.2012.02.002

Petit G, Luzum B (eds) IERS Conventions (2010). IERS Technical Note 36, Verlag des Bundesamts für Kartographie und Geodäsie, Frankfurt am Main, Germany, 2010

Senior K, Kouba J, Ray J Status and prospects for combined gps lod and vlbi ut1 measurements. Artificial Satellites 45(2):57–73, 2010 doi: 10.2478/v10018-010-0006-7

Steigenberger P, Rothacher M, Dietrich R, Fritsche M, Rülke A, Vey S Reprocessing of a global GPS network. J Geophys Res 111:B05,402, 2006 doi: 10.1029/2005JB003747

Zonal Love and Shida numbers estimated by VLBI

H. Krásná, J. Böhm, R. Haas, H. Schuh

Abstract The deformation of the anelastic Earth as a response to external forces from the Moon and Sun is characterized with proportionality parameters, the so-called Love and Shida numbers. The increasing precision and quality of the VLBI (Very Long Baseline Interferometry) measurements allow determining those parameters. In particular, the long history of the VLBI data enables the estimation of Love and Shida numbers at the low frequencies with the longest period of a tidal wave at 18.6 years. In this study we analyze 27 years of VLBI measurements (1984.0 - 2011.0) following the recent IERS Conventions 2010. In several global solutions, we estimate the complex Love and Shida numbers of the solid Earth tides for the main long-period tidal waves. Furthermore, we determine the Love and Shida numbers of the rotational deformation due to polar motion, the so-called pole tide.

Keywords Love and Shida numbers, solid Earth tides, pole tide

1 Introduction

Deformation of the Earth due to solid Earth tides is caused by tidal forces arising from the gravitation attraction of celestial bodies surrounding the Earth. The displacement of the Earth is proportional to the tidal potential by factors which reflect the amount by which the surface of the Earth responds to the tidal forces. The proportionality numbers which link the tidal potential to the surface displacement are so-called Love (h) and Shida (l) numbers. For a basic Earth model where the Earth is considered to be spherical, non-rotating, elastic and isotropic the Love and Shida numbers are dependent on the degree n of the tidal potential V_n^t. The displacement vector Δd^t induced by the tidal potential in the local coordinate system (radial ($\hat{r}$), east($\hat{e}$), north ($\hat{n}$)) is then written as:

$$\begin{aligned}\Delta d^t =& \frac{1}{g}\sum_{n=2}^{\infty} h_n \cdot V_n^t\, \hat{r} \\ &+ \frac{1}{g\cos\Phi}\sum_{n=2}^{\infty} l_n \cdot \frac{\partial V_n^t}{\partial \Lambda}\, \hat{e} \\ &+ \frac{1}{g}\sum_{n=2}^{\infty} l_n \cdot \frac{\partial V_n^t}{\partial \Phi}\, \hat{n},\end{aligned} \tag{1}$$

where Φ and Λ are geocentric coordinates of the station and g is gravitational acceleration. The recent theory of solid Earth tidal displacements is based upon the model of Wahr (1981) who considered the effects of rotation and ellipticity of the Earth. The deformation of the Earth's surface caused by lunisolar tides is based on the sum of the tidal potential with spherical harmonic degrees n and orders m, where the effective values of Love and Shida numbers additionally depend on the frequency of the tidal wave. In the long-period band the frequency dependence is mainly due to mantle anelasticity. The anelasticity model adopted in Petit and Luzum (2010) is the one from Widmer et al. (1991). The variation of the Love and Shida number across the zonal tidal band (h_{20} and l_{20}) is described by equations (2) and (3) (formula (7.4) in Petit and Luzum (2010)). Love and Shida numbers from these equations are also tabulated in the IERS Conventions 2010 and we used them as a priori values for their estimation in

Hana Krásná and Johannes Böhm
Vienna University of Technology, Department of Geodesy and Geoinformation, Gußhausstraße 27-29, A-1040 Wien, Austria

Rüdiger Haas
Chalmers University of Technology, Department of Earth and Space Sciences, Gothenburg, Sweden

Harald Schuh
Helmholtz-Zentrum Potsdam, DeutschesGeoForschungsZentrum GFZ, Department Geodesy and Remote Sensing, Potsdam, Germany

the global adjustment.

$$h_{20} = 0.5998 - 9.96 \times 10^{-4} \cdot X, \tag{2}$$

$$l_{20} = 0.0831 - 3.01 \times 10^{-4} \cdot X, \tag{3}$$

where

$$X = \left\{ \cot \frac{\alpha\pi}{2} \left[1 - \left(\frac{f_m}{f} \right)^{\alpha} \right] + i \left(\frac{f_m}{f} \right)^{\alpha} \right\}. \tag{4}$$

f is the frequency of the zonal tidal constituent, f_m is a reference frequency equivalent to a period of 200 s, and the power law index α = 15. To ensure 1 mm accuracy by the computed displacement of the crust five tidal waves have to be taken into account (Petit and Luzum, 2010). In addition for purpose of this work, the annual tidal wave S_a was added to this group. The tidal waves are described in Table 1. The frequency-dependent correction of the displacement caused by the long-period tides follows from Mathews et al. (1997, equation (2)):

$$\delta d_f = \sqrt{\frac{5}{4\pi}} H_f \left\{ \left(\tfrac{3}{2} \sin^2 \Phi - \tfrac{1}{2} \right) (\delta h_f \cos\theta_f)\, \hat{r} \right.$$
$$\left. + \quad \tfrac{3}{2} \sin 2\Phi (\delta l_f \cos\theta_f)\, \hat{n} \right\}. \tag{5}$$

H_f is the amplitude of a tidal term of frequency f defined by the convention of Cartwright and Tayler (1971), θ_f is the argument for the tidal constituent with the frequency f, and δh_f and δl_f are the corrections to the Love and Shida numbers of degree two.

Similar to the deformation of the solid Earth due to the tidal potential, there is deformation of the crust Δd^c caused by variations in centrifugal potential V^c. This change of centrifugal potential arises from variations in orientation of the rotation axis, i.e. from variations in the pole position. The direct response of the crust is called the pole tide and its maximum in radial direction can reach 25 mm, with a maximum horizontal displacement of about 7 mm (Petit and Luzum, 2010). The perturbation in the centrifugal potential caused by the changes in position of the rotation axis can be written as (Wahr, 1985; Petit and Luzum, 2010):

$$V^c(\Theta, \Lambda) = -\frac{\Omega^2 r_{\oplus}^2}{2} \sin 2\Theta (m_1 \cos\Lambda + m_2 \sin\Lambda), \tag{6}$$

where $r_{\oplus}$ is the geocentric distance to the station (6378000 m), Θ and Λ geocentric co-latitude and longitude of the station. Ω is the mean angular velocity of the Earth rotation (7.292115e-5 rad/s) and m_1 with m_2 describe the time-dependent offset of the instantaneous rotation pole from the mean rotation pole.

By using the basic relation between the displacement vector and the perturbing potential (equation (1)) the final expression for the pole tide at a particular station follows as:

$$\begin{aligned} \Delta d^c = & dR^c \sin 2\Theta (m_1 \cos\Lambda + m_2 \sin\Lambda)\, \hat{r} \\ & - dT^c \cos\Theta (m_1 \sin\Lambda - m_2 \cos\Lambda)\, \hat{e} \\ & - dT^c \cos 2\Theta (m_1 \cos\Lambda + m_2 \sin\Lambda)\, \hat{n}, \end{aligned} \tag{7}$$

where dR^c and dT^c are given in [m/as] as:

$$\begin{aligned} dR^c &= h_{20} \frac{-\Omega^2 r_{\oplus}^2}{2g} \cdot \pi/180/3600, \\ dT^c &= l_{20} \frac{-\Omega^2 r_{\oplus}^2}{g} \cdot \pi/180/3600. \end{aligned} \tag{8}$$

The nominal values for the Love and Shida numbers are computed following equations (2) and (3) for the frequency appropriate to the pole tide, where we used the frequency of the Chandler wobble. The theoretical pole tide Love number is then 0.6206 and the Shida number 0.0894.

2 VLBI analysis

We used the Vienna VLBI Software VieVS (Böhm et al., 2012) to analyze 4.6 million observations from 1984.0 to 2011.0 included in 3360 24-hour sessions of the International VLBI Service for Geodesy and Astrometry (IVS; (Schuh and Behrend, 2012)). For the modeling of the theoretical time delays the IERS Conventions 2010 (Petit and Luzum, 2010) were followed, with the exception of applying a priori corrections on station coordinates due to non-tidal atmospheric loading (Petrov and Boy, 2004) which is a common procedure in the VLBI analysis. For each session the normal equation (NEQ) system was formulated including the station coordinates and velocities, source coordinates,

Table 1 Period and amplitude H_f of six zonal tidal waves for which the Love and Shida numbers were estimated.

Name	Period [solar days]	Cartwright-Tayler amplitude [mm]
Ω_1	6797.38 (= 18.6 yr)	27.9
S_a	365.25	−4.9
S_{sa}	182.62	−30.9
M_m	27.55	−35.2
M_f	13.66	−66.7
M'_f	13.63	−27.6

Earth orientation parameters, zenith wet delays, tropospheric gradients, clock parameters, and the Love and Shida numbers. In the module Vie_GLOB (Krásná et al., 2013a) of VieVS a common adjustment of all sessions was carried out after local parameters (connected only to a single session) were reduced from the normal equations per session in a first step. The NEQ system of the global solution contains only the station coordinates, station velocities, source coordinates, and the Love and Shida parameters.

3 Love and Shida numbers for the long-period tides

To ensure an accuracy of 0.05 mm for the computed radial displacements of the crust in the long-period band, five tidal waves (M'_f, M_f, M_m, S_{sa}, and Ω_1) have to be taken into account (Petit and Luzum, 2010). Three solutions for the estimation of the zonal Love and Shida numbers were performed. In the first solution S1 the default parametrization was applied and Love and Shida numbers for the five main zonal tidal waves were estimated. In the second solution S2 hydrology loading corrections (provided by the NASA GSFC VLBI group (Eriksson and MacMillan; http://lacerta.gsfc.nasa.gov/hydlo)) were additionally applied a priori to the station coordinates. These corrections mainly contain annual and semi-annual signals. Solution S3 is identical to solution S2, but the Love and Shida numbers for the annual tidal wave S_a were also estimated. The real parts of the estimated complex Love and Shida numbers are listed in Tables 2 and 3. The second column of both tables contains the theoretical real part of the complex Love and Shida numbers (Mathews et al. (1997) and Petit and Luzum (2010)). Columns three, four and five list the real parts of the estimated Love and Shida numbers from solution S1, S2, and S3. In the last columns the differences between the a priori and the estimated Love and Shida numbers from solution S3, expressed as differences in amplitudes of the tidal term in millimeters are given:

$$\delta R^t_f = \sqrt{\frac{5}{4\pi}} H_f \delta h^R_f, \tag{9}$$

$$\delta T^t_f = \frac{3}{2}\sqrt{\frac{5}{4\pi}} H_f \delta l^R_f. \tag{10}$$

The real parts of the Love numbers from solution S1 show a relatively large difference of about 0.073 ± 0.019 and −0.078 ± 0.009 with respect to their theoretical values for the tidal waves Ω_1 and S_{sa}. The application of hydrology loading corrections on station coordinates (solution S2) leads to a decrease of the difference between the theoretical and estimated values of the Love number for the Ω_1 wave (0.003 ± 0.020), whereas the expected improvement of the estimated Love number of the semi-annual tide S_{sa} is small (the difference to the theoretical value is now −0.065 ± 0.009). In the third solution S3 the additional estimation of the Love number for the annual tide S_a causes another slight decrease of the difference between estimated and theoretical Love number for the semi-annual term S_{sa} (−0.055 ± 0.010). The larger formal error of the estimated Love number for the annual tide S_a is related to its small amplitude. The estimated Love number of the semi-annual tide S_{sa}, which corresponds to a 1.07 ± 0.19 mm difference in the radial amplitude of the crustal displacement with respect to the theoretical value, may reflect deficiencies in the a priori station displacement modeling of long-period origin. The larger formal error of the displacement amplitude for the Ω_1 tide is likely due to the not sufficiently long history of observations. A more detailed description of the analysis including our estimates of the imaginary parts of the Love and Shida numbers is given in Krásná et al. (2013b).

4 Love and Shida number for the pole tide

Several solutions were computed where the Love and Shida numbers for the polar motion were estimated. In these solutions the influence of a priori modeling of the mean pole and the application of hydrology loading corrections on station coordinates were investigated. The analysis of VLBI data was done according to the default parametrization with the following differences between the solutions:

- P1 - default parametrization (cubic function for mean pole (IERS Conventions 2010)),
- P2 - amplitudes of annual and semi-annual station position variations were estimated as additional parameters in the global solution and a cubic function for the mean pole was applied,
- P3 - as P2 but the mean pole was modeled by a linear approximation,
- P4 - as P2 but the mean pole was set to zero,
- P5 - as P1 but hydrology loading corrections were applied a priori on the station coordinates, ampli-

Table 2 Real parts of the complex Love numbers h_f^R for the long-period tidal waves estimated within three different solutions. $\Delta\delta R_f^t$ shows the difference in displacements when using solution S3 and values given in IERS Conventions 2010.

Name	h_f^R from (2)	h_f^R this work S1	h_f^R this work S2	h_f^R this work S3	$\Delta\delta R_f^t$ from S3 [mm]
Ω_1	0.6344	0.7071 ± 0.0188	0.6372 ± 0.0199	0.6372 ± 0.0199	0.05 ± 0.35
S_a	0.6207	-	-	0.5708 ± 0.0612	0.15 ± 0.19
S_{sa}	0.6182	0.5405 ± 0.0090	0.5531 ± 0.0094	0.5635 ± 0.0095	1.07 ± 0.19
M_m	0.6126	0.5965 ± 0.0076	0.5887 ± 0.0079	0.5905 ± 0.0079	0.49 ± 0.18
M_f	0.6109	0.6036 ± 0.0042	0.6052 ± 0.0043	0.6049 ± 0.0043	0.25 ± 0.18
M'_f	0.6109	0.6024 ± 0.0100	0.5878 ± 0.0105	0.5893 ± 0.0105	0.38 ± 0.18

Table 3 Real parts of the complex Shida numbers l_f^R for the long-period tidal waves estimated within three different solutions. $\Delta\delta T_f^t$ shows the difference in displacements when using solution S3 and values given in IERS Conventions 2010.

Name	l_f^R from (3)	l_f^R this work S1	l_f^R this work S2	l_f^R this work S3	$\Delta\delta T_f^t$ from S3 [mm]
Ω_1	0.0936	0.1147 ± 0.0044	0.1079 ± 0.0047	0.1078 ± 0.0047	0.37 ± 0.12
S_a	0.0894	-	-	0.1079 ± 0.0146	−0.09 ± 0.07
S_{sa}	0.0886	0.0955 ± 0.0021	0.0954 ± 0.0022	0.0984 ± 0.0023	−0.28 ± 0.07
M_m	0.0870	0.0851 ± 0.0018	0.0819 ± 0.0019	0.0825 ± 0.0019	0.15 ± 0.06
M_f	0.0864	0.0855 ± 0.0010	0.0865 ± 0.0010	0.0864 ± 0.0010	0.01 ± 0.06
M'_f	0.0864	0.0842 ± 0.0024	0.0771 ± 0.0025	0.0772 ± 0.0025	0.24 ± 0.07

tudes of annual station position variations were estimated as additional parameters in the global solution together with the complex Love and Shida numbers for the five main zonal tidal waves.

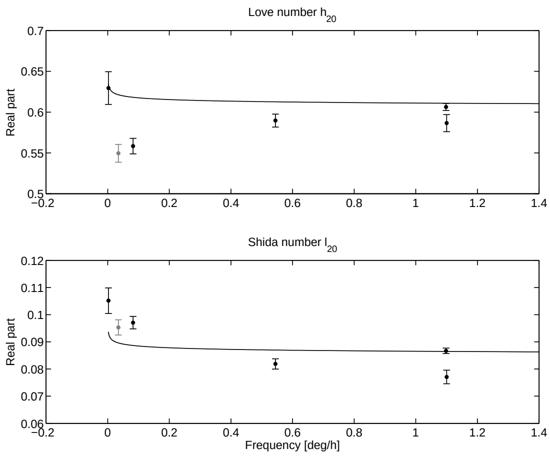

Fig. 1 Real parts of the five zonal Love and Shida numbers (black color) estimated together with the Love and Shida numbers for the pole tide (grey color) in solution P5. The solid black lines represent the theoretical values given by equations (2) and (3).

Table 4 Pole tide Love and Shida numbers.

solutions	h_2 - pole tide	l_2 - pole tide
theoretical value	0.6206	0.0894
P1	0.4638 ± 0.0092	0.1038 ± 0.0023
P2	0.5354 ± 0.0118	0.0943 ± 0.0029
P3	0.5353 ± 0.0118	0.0946 ± 0.0029
P4	0.5353 ± 0.0118	0.0956 ± 0.0029
P5	0.5495 ± 0.0109	0.0953 ± 0.0028
(Petrov, 1998)	0.65 ± 0.20	0.11 ± 0.05
(Gipson and Ma, 1998)	0.636 ± 0.025	0.087 ± 0.007

In Table 4 results of the estimated Love and Shida numbers from the five solutions are summarized. The largest difference to the theoretical value appears in solution P1. In solution P2 the determination of the remaining annual and semi-annual signals in the station coordinates (especially height) within the global adjustment brings the estimated Love number closer to its theoretical value. The Love numbers obtained from solutions P2, P3 and P4 are almost identical. This shows that the modeling of the mean pole (cubic, linear, or a total omission) does not have any influence on the Love and Shida number estimates. In solution P5 the hydrology loading corrections were applied a priori on the station coordinates and in the global adjustment the complex Love and Shida for the five zonal tidal waves (Ω_1, S_{sa}, M_m, M_f, M'_f) together with the remaining annual signal in the station coordinates were estimated. The corresponding Love and Shida numbers are plotted in Figure 1. The good agreement between the estimated Love number of the semi-annual tide S_{sa} (0.558 ± 0.010) and of the pole tide (0.550 ± 0.011) is clearly visible. The vertical amplitude of the estimated harmonic annual signal at most of the stations reaches several millimeters (not shown here). This approach in solution P5 gives the best agreement between the estimated and theoretical pole tide Love number from all five solutions which were carried out. In the last two rows of Table 4 results obtained by Petrov (1998) and Gipson and Ma (1998) are shown. Petrov

(1998) used only early VLBI data covering time span of 4 years (from 1984 to 1987) for his computation. Even though his Love number estimate (0.65) lies close to the theoretical value (0.62) its large formal error of 0.20 reflects the high uncertainty of the result. Gipson and Ma (1998) included VLBI sessions from 1979 to 1996 and their estimates agree with the theoretical values within the formal errors.

5 Conclusions

Our estimate of the Love number for the semi-annual tide is 9.7% lower than the theoretical value. Similarly, the Love number of the pole tide is lower by about 11.4% than in theory. Both the a priori application of a hydrology loading model (mainly annual and semi-annual frequency content) in the analysis and the estimation of annual station positions slightly bring the estimates of zonal Love numbers closer to their theoretical values but still a significant difference remains. The empirical Shida numbers for the periods of half year and longer are always bigger than the theoretical values. A next step could be a revision of the theoretical model of solid Earth tides by re-estimating the included Earth parameters.

References

Böhm J., S. Böhm, T. Nilsson, A. Pany, L. Plank, H. Spicakova, K. Teke and H. Schuh. The new Vienna VLBI Software VieVS. *IAG Symposium 2009*, 136. Ed. Kenyon S., M.C. Pacino and U. Marti. pp. 1007-1012, 2012.

Cartwright D. E. and R. J. Tayler. New computations of the tide-generating potential. *Geophys J Roy Astr S* 23/1. pp. 45-74, 1971.

Gipson J. and C. Ma. Site displacement due to variation in Earth rotation. *J Geophys Res* 103/B4. pp. 7337-7350, 1998.

Krásná H., J. Böhm, L. Plank, T. Nilsson and H. Schuh. Atmospheric Effects on VLBI-derived Terrestrial and Celestial Reference Frames. *IAG Symposium 2011*, 139. Ed. Rizos C. and P. Willis. In press, 2013a.

Krásná H., J. Böhm and H. Schuh. Tidal Love and Shida numbers estimated by geodetic VLBI. *J Geodyn*. In press, 2013b.

Mathews P. M., V. Dehant and J. M. Gipson. Tidal station displacement. *J Geophys Res* 102/B9. pp. 20,469-20,477, 1997.

Munk W. H. and G. J. F. MacDonald. The rotation of the Earth. *Cambridge Univ. Press. New York* pp. 24-25, 1960.

Petit G. and B. Luzum. IERS Conventions 2010. IERS Technical Note No. 36. p. 179, 2010.

Petrov L. VLBI Measurements of the Crustal Deformation Induced by Polar Motion. *Physics of the Solid Earth* 34. pp. 228-230, 1998.

Petrov L., J. Hinderer and J.-P. Boy. Combined analysis of VLBI and superconducting gravimeter data. *Viewgraphs at 15th Earth tide Symposium in Ottawa on 02-AUG-2004*, 2004.

Petrov L. and J.-P. Boy. Study of the atmospheric pressure loading signal in very long baseline interferometry observations. *J Geophys Res* 109. p. 14, 2004.

Schuh H. and D. Behrend. VLBI: A fascinating technique for geodesy and astrometry. *J Geodyn* 61. pp. 68-80, 2012.

Wahr J. M. Body tides on an elliptical, rotating, elastic, and oceanless Earth. *Geophys J Roy Astr S* 64/3. pp. 677-703, 1981.

Wahr J. M. Deformation induced by polar motion. *J Geophys Res* 90/B11. pp. 9363-9368, 1985.

Widmer R., G. Masters and F. Gilbert. Spherically symmetric attenuation within the Earth from normal mode data. *Geophys J Int* 104. pp. 541-553, 1991.

New time series of the EOP and the source coordinates

V. Zharov

Abstract Time series of the coordinates of the ICRF radio sources were analyzed. We show that part of radio sources, including “defining” sources, reveals the significant apparent motion. The stability of the celestial reference frame is provided by the no-net-rotation condition applied to the defining sources. In our case this condition leads to rotation of the frame axes with time. Effect of this rotation on the Earth orientation parameters (EOP) was calculated. It was shown that this rotation is transformed to secular variations of EOP that is decreased or removed if motion of sources is took into account.

Keywords ICRF, Earth orientation parameters

1 Introduction

Rotation of the Earth is described as motion of the Earth’s axis of figure relative to the International Celestial Reference Frame (ICRF) that is defined by the precise coordinates of extragalactic radio sources. The rotational stability of the frame is based on the assumption that the sources have no proper motion and it means that there is no global rotation of the universe.

Very Long Baseline Interferometry (VLBI) technique is used by the International Earth Rotation Service and Reference System Service (IERS) for production of the Earth orientation parameters (EOP). They are required to study Earth orientation variations and to transform between the ICRF and the International Terrestrial Reference Frame (ITRF). VLBI is currently the only method available for measuring of the Universal Time (UT).

Vladimir Zharov
Lomonosov Moscow State University, Sternberg Astronomical Institute, Universitetskij pr.,13, 119234 Moscow, Russia

But analysis of time series of coordinates of the ICRF radio sources shows that many of them including the defining sources have significant apparent motion (Zharov et al. , 2009). It is explained by motion of an emission region that is called by the ICRF source inside the jet of a quasar.

Software ARIADNA (Zharov , 2013) was used for estimation of the Earth orientation parameters (EOP) for period 1984–2012. In our previous work (Zharov et al. , 2009) solution (EOP and the sources positions and velocities) was obtained for the first catalog of the ICRF sources (Ma et al., 1990).

The first realization of the International Celestial Reference Frame (ICRF) was based on the positions of selected 608 compact extragalactic radio sources (quasars, active galactic nuclei, and blazars) (Ma et al., 1990). Stability of the system axes is guaranteed by precise positions of the ”defining” radio sources. One assumes that coordinates of them are known as precise as possible. These sources are unresolved with VLBI baselines comparable to the Earth diameter, and it was assumed that variations of their coordinates are negligible.

The new realization of the International Celestial Reference Frame (ICRF-2) was established in 2009. The ICRF-2 contains approximately 3000 radio sources, the noise floor is of the order of 40 μas which leads to axis stability of approximately 10 μas (Ma et.al. , 2009).

New solution (EOP and the sources positions and velocities) was obtained for catalog ICRF-2 (Ma et.al. , 2009).

We show that

- many of new defining sources show significant apparent motion;
- small rotation of ICRF is transformed into long-term variations of the EOP.

To obtain the time series of the EOP and the ICRF sources coordinates the ARIADNA software was used. Solution ”sai2012a.eops” was based on accepted positions of the sources ICRF2, precession-nutation model IAU2000. The terrestrial reference frame was fixed by the VTRF2008 coordinates and velocities of stations. Solution "sai2012b.eops" differs from previous one by adding the velocities of sources.

Secular variations of the EOP can be calculated by subtracting of two solutions "a" and "b".

2 Solution Description

All of these solutions have in common the same model for calculation of the VLBI delay and parametrization of clocks and troposphere wet zenith delay. Station clocks are estimated w.r.t. combined clock by a 2^{nd} order polynomial according equation:

$$\sum_j [C_0^j + C_1^j t + C_2^j t^2] = 0.$$

The zenith wet delay is parameterized by polynomial function too but order of it can be chosen as 3 or more in 2 h intervals.

For all of these solutions a priori EOP are taken from IERS final products. Displacement of reference points, tidal variations in the Earth's rotation, transformation between the ITRF and ICRF are calculated according the IERS Conventions (2010) (Petit and Luzum, 2010). Atmospheric pressure loading have been applied according model developed in paper (Zharov , 2004).

The solutions presented here are all run in a two step procedure. First, the data is processed by the VLBI analysis software ARIADNA and the normal equation system (NEQ) is prepared, stored in SINEX file and solved. The NEQ are build up for each single session. The SINEX files will be used later for global solution.

The NEQ can contain corrections of the source positions and velocities. In this case the no-net-rotation (NNR) condition is applied only for the defining sources.

Second step procedure is used for analysis of the source motion. To calculate them we used the approximation of time series of coordinates by a polynomial model. Linear model with respect to regression polynomial coefficients β_i $(i = 0, 1, 2)$ is

$$y(t) = \beta_0 + \beta_1 t + \beta_2 t^2 + \varepsilon(t), \tag{1}$$

where t is time, $y(t)$ are corrections $(\Delta\alpha\cos\delta, \Delta\delta)$ to the ICRF coordinates (right ascension or declination) of a source, and $\varepsilon(t)$ are residuals. The coefficients of polynomials were found out by regression analysis. The order of polynomial was determined by R^2 statistic, where

$$R^2 = \frac{\sum(\hat{y}_j - \bar{y})^2}{\sum(y_j - \bar{y})^2} = 1 - \frac{\sum(y_j - \hat{y}_j)^2}{\sum(y_j - \bar{y})^2}. \tag{2}$$

Here y_j is correction of right ascension or declination at the moment $t = t_j$, $j = 1, 2, \ldots, N$, and $\hat{y}_j$ is estimation of polynomial function at t_j and $\bar{y}$ is average value of series over whole span interval. The value R depends on the correlation between y and $\hat{y}$ (Draper , 1998). Obviously, if the polynomial model is correct, that is values $\hat{y}_j$ are equal to y_j, the coefficient $R = 1$. Actually, $\hat{y}_j \neq y_j$ and $R < 1$, but the maximal value of R corresponds to the best fitting model.

Below we show several examples of our data analyzes. These figures represent variation of celestial coordinates as polynomial function of time. One can see that all of these sources have significant apparent motion.

Motion of the source 0106+013 that was "other" source in the ICRF is shown on of Fig.1. The total number of observations is more than 1500. Motion is modeled by linear function 40.5 ± 0.3 for α and 8.6 ± 0.4 for δ (in μas/year).

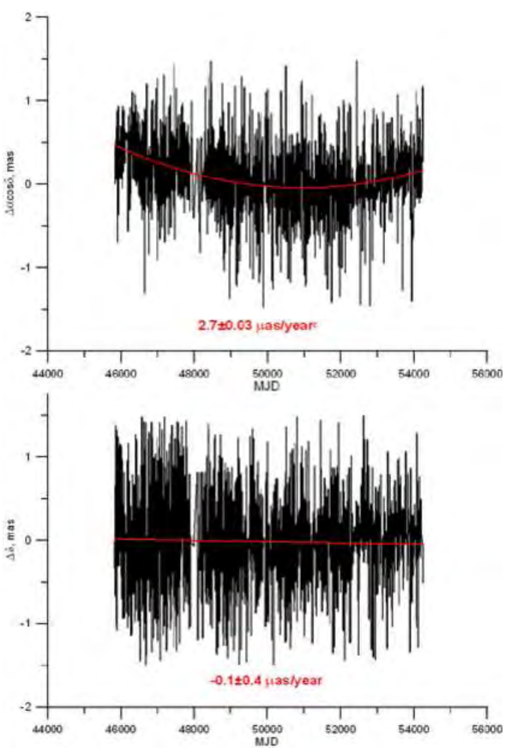

Fig. 1 Right ascension (up) and declination (down) variations of the defining sources 0106+013 as function of time.

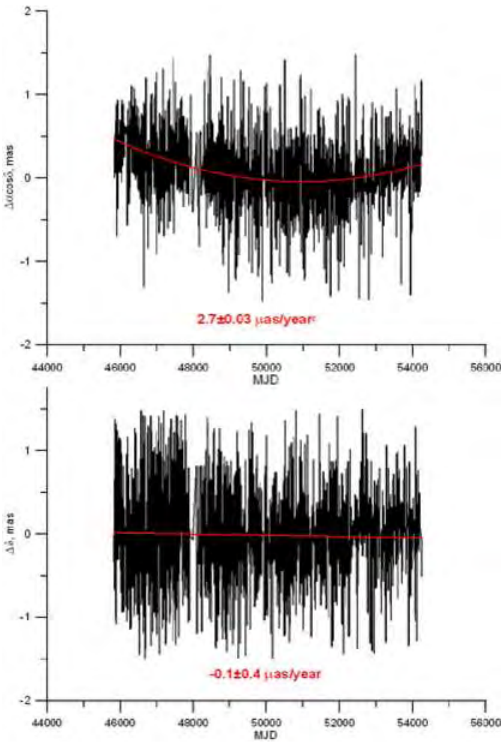

Fig. 2 Right ascension (up) and declination (down) variations of the defining sources 0229+131 as function of time.

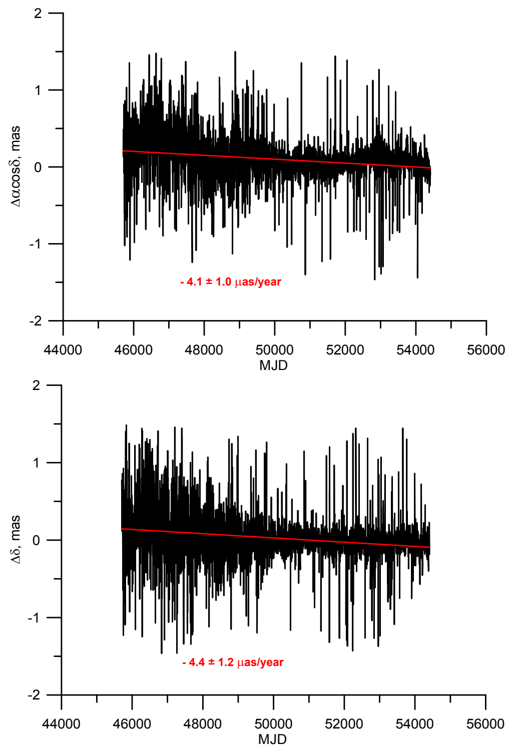

Fig. 3 Right ascension (up) and declination (down) variations of the defining sources 0552+398 as function of time.

The total number of observation of former "candidate" source 0229+131 was more than 2500. It is the defining source in the ICRF2 catalog. The motion is quadratic along right ascension 2.70 ± 0.03 μas/year^2 and linear 0.1 ± 0.4 μas/year along declination (Fig.2).

The motion of the most observable source 0552+398 which is the defining source is modeled by linear function -4.1 ± 1.0 for α and -4.4 ± 1.2 for δ (in μas/year)(Fig.3) but short period variations are existed.

As we can see the values of velocities of defining sources can reach a few microarcseconds per year. The variation of the ICRF source coordinates leads to small rotation of reference frame. To estimate the stability of the frame three small angles θ_1, θ_2, θ_3, which describe small rotation were calculated:

$$\mathbf{s}(t) = \begin{pmatrix} 1 & -\theta_3 & \theta_2 \\ \theta_3 & 1 & -\theta_1 \\ -\theta_2 & \theta_1 & 1 \end{pmatrix} \mathbf{s}(t_0)$$

where $\mathbf{s}(t)$, $\mathbf{s}(t_0)$ are unit vectors of a source at moments t and $t_0 = J2000.0$. Obviously, that variations of angles θ_1, θ_2, θ_3 are connected with motion of the defining sources and NNR condition. Stability of the ICRF (or constancy of θ_1, θ_2, θ_3) can be improved by correct choice of the defining source or extension of their number.

Rotation of the ICRF is due to the motions of sources. Variations of angles θ_1, θ_2, θ_3 are connected with the EOP or the effect of the source apparent motion has an impact on the determination of the EOP.

To calculate this effect two solutions "sai2012a.eops" and "sai2012b.eops" were obtained. From difference of solutions linear trend in x-coordinate of pole equal to $-2.77 \pm 0.22\mu$as/year was found. Variations of y-coordinate of pole, nutation in longitude and obliquity are $1.60 \pm 0.15\mu$as/year, $0.47 \pm 0.46\mu$as/year, $-0.54 \pm 0.15\mu$as/year respectively, and UT is $0.144 \pm 0.007\mu$s/year.

Motion of extragalatic radio source can be decomposed on systematic and stochastic parts. The first of them can be explained by secular aberration drift of the extragalatic radio source motions caused by the rotation of the Solar System barycenter around the Galactic center (Titov , 2007). The dipole component of the velocity field is defined by the velocity of the Solar System barycenter and galactic coordinates of the radio source and can be estimated. Other regular part of the extragalatic radio source motions can be caused by the errors of the precession constants. It is planned to estimate this effect from our solutions.

3 Conclusions

New time series of the EOP and the ICRF sources coordinates the ARIADNA software was used. Solutions were based on accepted positions of the sources ICRF2, precession-nutation model IAU2000. It was shown that rotation of the ICRF is due to the motions of sources. The effect of the source apparent motion has an impact on the determination of the EOP.

This work was supported by the RFBR grant 11-02-01009.

References

V.E. Zharov, M.V. Sazhin, V.N. Sementsov, K.V. Kuimov, O.S. Sazhina. Physical origins for variations in the apparent positions of quasars. *Astr. Rep.*, 53, 579–589, 2009.

V.E. Zharov. ARIADNA — software for analysis of VLBI observations. *Astr. Rep.*, submitted.

C. Ma, E.F. Arias, T.M. Eubanks, et al. The International Celestial Reference Frame as Realized by Very Long Baseline Interferometry. *AJ*, 116:516–546, 1998.

C. Ma, E.F. Arias, G. Bianco, et al. The Second Realization of the International Celestial Reference Frame by Very Long Baseline Interferometry. In Alan Fey, David Gordon, and Christopher S. Jacobs editors, *IERS Technical Note No. 35, Frankfurt am Main: Verlag des Bundesamts fur Kartographie und Geodasie*, 2009.

G. Petit and B. Luzum. *IERS Conventions (2010).* IERS Conventions (2010). Gérard Petit and Brian Luzum (eds.), International Earth Rotation and Reference Systems Service (IERS). IERS Technical Note, No. 36, Frankfurt am Main, Germany: Verlag des Bundesamtes für Kartographie und Geodäsie, 179 pp., 2010.

V.E. Zharov. New models for reduction of the VLBI data. In A. Finkelstein and N. Capitaine, (eds.), *Proceedings of the "Journees 2003 Systemes de Reference Spatio-Temporels",, Institute of Applied Astronomy, St.Petersburg*, pages 231–235, 2004.

N.R. Draper, H. Smith. Applied Regression Analysis. 3-rd edition. John Wiley & Sons, Inc. 1998.

O. Titov, S.B. Lambert, A.-M. Gontier. VLBI measurement of the secular aberration drift *Astron. & Astroph.*, 2011. doi: 10.1051/0004-6361/201015718.

Sub-daily Antenna Position Estimates from the CONT11 Campaign

K. Teke, J. Böhm, T. Nilsson, H. Krásná

Abstract The CONT11 campaign was observed by the International VLBI Service for Geodesy and Astrometry (IVS) during 15 days from 15 to 29 September 2011. In this study, we divided the observation files of the 24 hour sessions of the CONT11 campaign into 2 h sessions. These sub-daily sessions were analyzed with the Vienna VLBI Software (VieVS) to obtain coordinate time series with 2 h resolution for each station. We found that the coordinate repeatability from the 2 h sessions is clearly reflected in a change of the tropospheric parameters like zenith delays and gradients, an effect being boosted by the non-uniform sky distribution at the stations over 2 h segments.

Keywords VLBI, CONT11, TRF, sub-daily antenna coordinates, zenith wet delays

1 Introduction

The continuous VLBI campaign, CONT11, was carried out by the International VLBI Service for Geodesy and Astrometry (IVS, Schuh and Behrend (2012)) over two weeks, from 15 to 29 September 2011, to demonstrate the highest accuracy of the VLBI system. In this study, we investigated the possibility to estimate reliable antenna coordinates every 2 hours (2 h).

Kamil Teke
Hacettepe University, Department of Geomatics Engineering, Ankara, Turkey
Johannes Böhm and Hana Krásná
Vienna University of Technology, Department of Geodesy and Geoinformation, Vienna, Austria
Tobias Nilsson
Geoforschungszentrum Potsdam, Germany

2 Data Analysis

We divided the observation files of the 24 hour sessions of the CONT11 campaign into 2 h sessions. These were then analyzed using the Vienna VLBI Software (VieVS, Böhm et al. (2012)), which is developed at the Department of Geodesy and Geoinformation at the Vienna University of Technology. The a priori terrestrial reference frame (TRF) catalogue, nutation offsets, and Earth rotation parameters (ERP) were obtained as follows:

1. First, we estimated a CONT11 specific TRF catalogue from a global TRF solution with the observations of CONT11 (named in this paper as TRF11). In this global TRF solution we applied No-Net-Rotation (NNR) and No-Net-Translation (NNT) conditions w.r.t. VTRF2008 (Böckmann et al. (2010)) and we fixed velocities to those of VTRF2008. Those datum conditions were not imposed on the antennas TSUKUB32, HOBART12, YEBES40M, and TIGOCONC since VTRF2008 coordinates of these antennas are not available for the CONT11 period.
2. We then estimated nutation offsets for CONT11 at 1 day intervals in a global solution (named in this paper as NUT11) of which a priori values were taken from the IERS 08 C04 corrections (Bizouard and Gambis (2009)) in addition to the IAU2006 precession-nutation model.
3. The ERP for CONT11 (named in this paper as ERP11) were estimated at 2 h intervals, i.e. at 1, 3, 5, ..., 21, 23 UT, in a global solution where a priori nutation offsets were fixed to daily NUT11 and a priori ERP were taken from IERS 08 C04 plus high frequency corrections. The high frequency ERP variations were modeled as recommended by the IERS Conventions 2010 (Petit and Luzum (2010)).

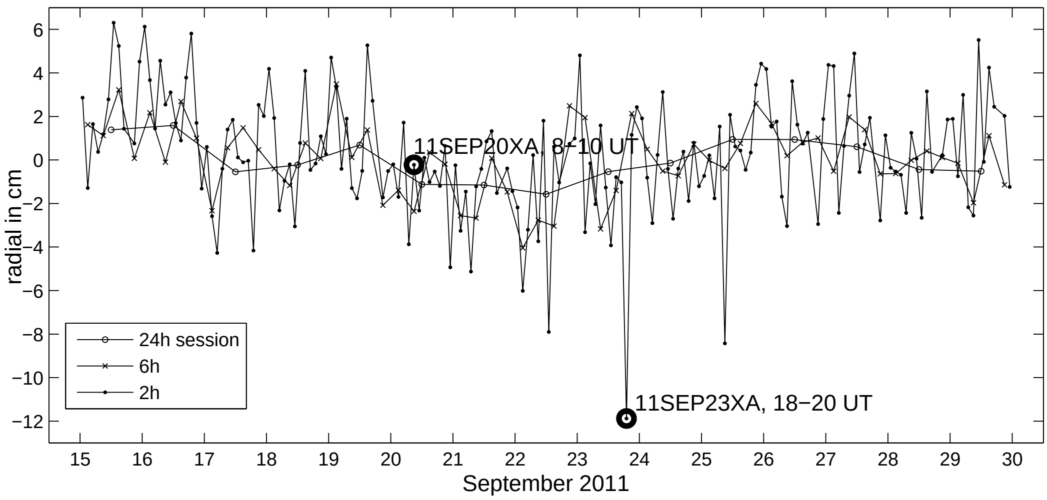

Fig. 1 KOKEE antenna TRF position time series in radial direction from the analyses of 24 h, 6 h, and 2 h sessions during CONT11 campaign. 11SEP20XA, 8-10 UT and 11SEP23XA, 18-20 UT are the examples of 2 h sessions with good (right plot of Fig. 3) and bad (left plot of Fig. 3) sky coverage of observations.

In the data analysis of the 2 h sessions we did not remove observations below a certain elevation angle, nor did we down-weight observations at low elevation angles. Source coordinates were fixed to IRCF2 (International Celestial Reference Frame 2, Fey et al. (2009)) except for sources not in the ICRF2 catalogue which were estimated. We did not estimate Earth orientation parameters (EOP) when analysing 2 h sessions. Tidal and non-tidal atmospheric loading (Petrov and Boy (2004)) as well as tidal ocean loading corrections based on the ocean model FES2004 (Lyard et al. (2006)) were introduced for each observation prior to the adjustment. Troposphere zenith hydrostatic delays (ZHD) were computed using surface pressure values recorded at the sites (Saastamoinen (1972); Davis et al. (1985)) and mapped down with the hydrostatic Vienna Mapping Functions 1 (VMF1, Böhm et al. (2006)). Antenna 2 h TRF coordinates were estimated at the epochs 1, 3, 5, ..., 21, 23 UT (see e.g. Fig. 1) using NNR and NNT conditions w.r.t. TRF11 (see the first item of this section) coordinates of the participating antennas. In the 2 h session analyses, zenith wet delays (ZWD) were estimated as piece-wise linear offsets at 1 h intervals with loose relative constraints as 1.5 cm after 1 h. Troposphere east and north horizontal total gradients were estimated as piece-wise linear offsets at 2 h intervals with absolute constraints as 1 mm in addition to tight relative constraints as 0.01 mm after 2 h. We used the wet VMF1 and the gradient mapping function as introduced by Chen and Herring (1997).

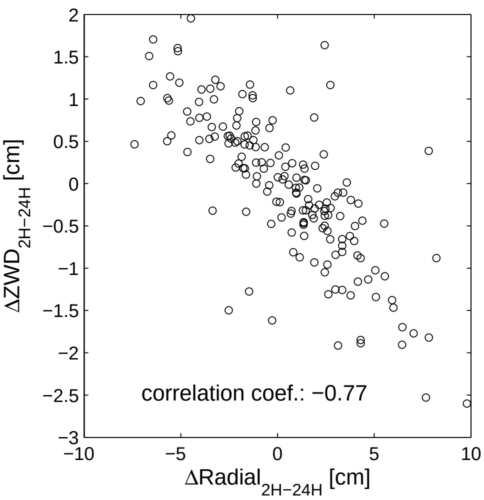

Fig. 2 The circles show the correlations between ZWD and radial position differences estimated once for each 2 h session at TIGOCONC for common epochs, i.e. 1, 3, 5,..., 23 UT.

3 Correlations between estimated coordinates and ZWD

We subtracted the 24 h radial coordinates from those estimated from the 2 h sessions (radial(2 h)-radial(24 h)) and did the same for zenith wet delays, ZWD(2 h)-ZWD(24 h). The differences of antenna TRF radial coordinates vary in $[-2\ +2]$ cm to $[-8\ +8]$ cm and the differences of ZWD in $[-1\ +1]$ cm to $[-4\ +4]$ cm for all VLBI sites for CONT11 (see e.g. Fig. 4 for TIGOCONC). Troposphere delay estimates and antenna TRF positions are highly correlated when

Antenna	Standard deviation		Correlation
	ΔZWD (cm)	Δradial (cm)	coefficient
NYALES20	0.4	1.5	-0.54
ONSALA60	0.7	1.8	-0.52
BADARY	0.7	2.3	-0.71
WETTZELL	0.5	1.5	-0.51
WESTFORD	0.7	2.2	-0.61
YEBES40M	0.6	1.7	-0.50
TSUKUB32	0.8	2.4	-0.35
KOKEE	0.7	2.5	-0.38
FORTLEZA	1.5	4.3	-0.77
HARTRAO	0.8	2.6	-0.68
TIGOCONC	0.9	3.4	-0.77
HOBART12	1.1	4.0	-0.70

Table 1 Correlations between ΔZWD and Δradial at the VLBI sites contributing to CONT11 campaign

inhomogeneous sky distribution of the observations are in 2 h sessions (see e.g. Fig. 5 for TIGOCONC). Due to small number of observations (less than 30) and inhomogeneous sky distribution (see e.g. left plot of Fig. 3) the least squares adjustment cannot de-correlate the parameters of troposphere delays and antenna TRF positions completely. Thus, troposphere delays propagate into antenna TRF positions. A ZWD offset of 1 to 2 cm propagates to antenna radial coordinates in opposite direction from 2 to 8 cm for a 2 h session depending mainly on the sky distribution of the observations. From Table 1 one can infer that the number and the sky distribution of the observations of KOKEE and TSUKUB32 are better than that of FORTLEZA and TIGOCONC during CONT11 2 h sessions.

4 Conclusions

From our analyses of the CONT11 sub-daily (2 h) sessions, the following results were drawn:

- All negative correlations between the ΔZWD, [ZWD(2 h)-ZWD(24 h)] and Δradial, [radial(2 h)-radial(24 h)] at the VLBI sites are statistically significant (p values < 0.05).
- 1 cm ΔZWD variation corresponds to approximately 2 to 4 cm Δradial when 2 h sessions are analyzed.
- Due to the large correlations between the troposphere delay estimates and the antenna TRF positions for CONT11 2 h sessions (see Table 1), troposphere delays propagate into antenna positions in parameter estimation. Correlations between the two parameters can be mitigated if homogeneously distributed adequate number of observations are carried out at each antenna at each sub-daily session e.g. 2 h.
- We are planning for the future to reduce troposphere delays estimated from 24 h sessions from the observations of 2 h sessions before the parameter estimation. Thus other effects than troposphere on the antenna coordinates will be unveiled, e.g. residual displacements to the a priori geodynamic effects on the antenna positions at sub-daily tidal frequencies.

Acknowledgements

The authors would like to thank the Austrian Science Fund (FWF) for supporting this work within projects Integrated VLBI (P23143) and GGOS Atmosphere (P20902). One of the authors, Kamil Teke, acknowledges Scientific and Technological Research Council of Turkey (Tübitak) for the financial support of the postdoctoral research programme, 2219.

References

C. Bizouard and D. Gambis. The combined solution C04 for Earth orientation parameters consistent with International Terrestrial Reference Frame. In: *Geodetic reference frames, IAG Symp, vol.134*, ed. by H. Drewes, pp. 265–270, 2009, doi:10.1007/978-3-642-00860-3-41.

S. Böckmann, T. Artz, A. Nothnagel. VLBI terrestrial reference frame contributions to ITRF2008. *J. Geod.*, 84:201–219, 2010, doi:10.1007/s00190-009-0357-7.

J. Böhm, S. Böhm, T. Nilsson, A. Pany, L. Plank, H. Krásná, K. Teke, H. Schuh. The new Vienna VLBI Software VieVS. In: *Proceedings of IAG Scientific Assembly 2009, Vol. 136*, ed. by S. Kenyon, M.C. Pacino, and U. Marti, 1007-1011, 2012, doi:10.1007/978-3-642-20338-1126.

J. Böhm, B. Werl, H. Schuh. Troposphere mapping functions for GPS and very long baseline interferometry from European Center for Medium-Range Weather Forecasts operational analysis data. *J. Geophys. Res.*, 111:B02406, 2006, doi:10.129/2005JB003629.

G. Chen and T.A. Herring. Effects of atmospheric azimuthal asymmetry on the analysis from space geodetic data. *J. Geophys. Res.*, 102(B9):20489–20502, 1997, doi:10.1029/97JB01739.

J.L. Davis, T.A. Herring, I.I. Shapiro, A.E.E. Rogers, G. Elgered. Geodesy by radio interferometry: Effects of atmospheric modeling errors on estimates of baseline length. *Radio Sci.*, 20(6):1593–1607, 1985, doi:10.1029/RS020i006p01593.

A. Fey, D. Gordon, C.S. Jacobs. The Second Realization of the International Celestial Reference Frame by Very Long Baseline Interferometry. IERS Technical Note; 35, Frankfurt am Main: Verlag des Bundesamts für Kartographie und Geodäsie, 204 p., 2009, ISBN 3-89888-918-6.

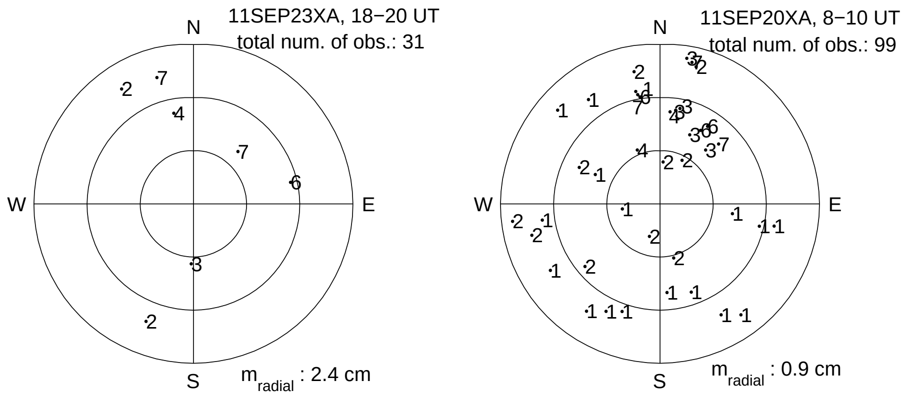

Fig. 3 Sky plots at KOKEE for the 2 h sessions observed during 11SEP23XA, 18 - 20 UT (left plot) and 11SEP20XA, 8 - 10 UT (right plot) illustrate bad and good sky coverage of observations in 2 h segments which results in inaccurate and better antenna position estimates. The number of observations per scan with the total number of the observations of the sessions and the formal errors of the estimated antenna coordinates in radial direction are written on the sky plots.

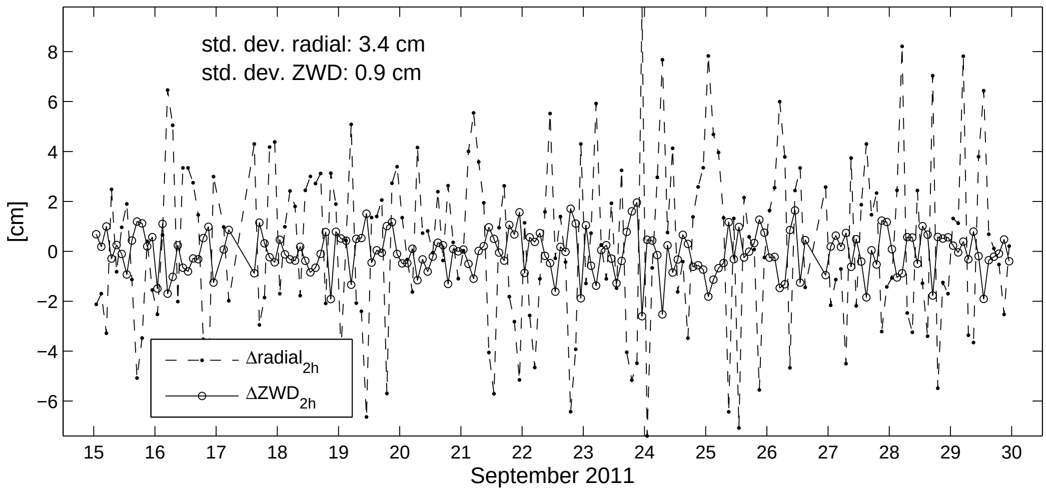

Fig. 4 The circles on solid lines and dots on dashed lines show ZWD and antenna radial coordinate differences between those estimated from 2 h and 24 h sessions of CONT11 campaign at TIGOCONC for the common epochs, i.e. 1, 3, 5,..., 23 UT.

F. Lyard, F. Lefevre, T. Lettelier, O. Francis. Modelling the global ocean tides, Modern insights from FES2004. *Ocean Dyn.*, 56(6):394–415, 2006, doi:10.1007/s10236-006-0086-x.

G. Petit and B. Luzum. IERS Conventions 2010. IERS Technical Note ; 36, Frankfurt am Main: Verlag des Bundesamts für Kartographie und Geodäsie, 179 p., 2010, ISBN 3-89888-989-6.

L. Petrov and J.P. Boy. Study of the atmospheric pressure loading signal in Very Long Baseline Interferometry observations. *J. Geophys. Res.*, 109(B3):B03405, 2004, doi:10.1029/2003JB002500.

J. Saastamoinen. Atmospheric correction for the troposphere and stratosphere in radio ranging of satellites. In: *The use of artificial satellites for geodesy, Geophys. Monogr. Ser. 15, AGU*, 251–274, 1972, doi:10.1007/978-3-642-00860-3-41.

H. Schuh and D. Behrend. VLBI: A fascinating technique for geodesy and astrometry. *J. Geodyn.*, 61:68–80, 2012, doi:10.1016/j.jog.2012.07.007.

Nontidal Ocean Loading Observed by VLBI Measurements

D. S. MacMillan and D. Eriksson

Abstract Both vertical and horizontal deformations due to nontidal ocean loading are large enough to be seen in VLBI geodetic parameter estimates. Typical peak-to-peak vertical variations are as much as 4-6 mm at VLBI sites, while horizontal variations are at the mm-level. We have calculated the mass loading by convolving a loading Green's function with the gridded ocean bottom pressures derived from the JPL ECCO model. Applying the resulting loading series in VLBI analysis reduces baseline length and station position scatter as well as annual vertical amplitudes.

Keywords Nontidal Ocean Loading

1 Introduction

Vertical deformation due to nontidal ocean loading is large enough to be seen in VLBI geodetic parameter estimates. Typical peak-to-peak vertical variations are 4-6 mm at VLBI sites. At VLBI sites, the loading signal has an annual character, but as with atmospheric and hydrological loading, we also observe interannual variations. Variations in the loading are caused by temporal variations of the geographic distribution of ocean surface mass. Here, we report on our calculation of the mass loading derived from JPL (Jet Propulsion Laboratory) ECCO (Estimating the Circulation and Climate of the Ocean) model ocean bottom pressure estimates from 1993 to 2009. To perform the calculation, we evaluated the convolution of a loading Greens function similar to that of Farrell (1972) with the ocean loading mass field, given by a global grid of ECCO model bottom pressures. We investigated the reduction in baseline length, site position scatter, and site vertical annual amplitudes when nontidal ocean loading is applied in VLBI analysis.

Daniel MacMillan and David Eriksson
NVI, Inc. NASA Goddard Space Flight Center, Greenbelt Road, Maryland, USA

2 Nontidal Ocean Loading Data

Vertical and horizontal nontidal ocean loading is computed using the ECCO ocean model maintained JPL. Fukumori (2002) describes the model. The ECCO model is available on a latitude/longitude grid with 224 latitudes and 360 longitudes where the latitude range is -80 to +80 degrees with a 12-hour time resolution. Data is available since 1993 and has a latency of about 3 weeks. The model conserves oceanic volume but is not mass conserving.

It can be seen in Fig. 1 that the RMS variation of bottom pressure is largest along coasts. The variations are much smaller than those observed for atmospheric pressure loading, which are typically 20-40 hPa peak-to-peak. Therefore, we expect smaller ocean loading displacements of a several millimeters. Coastal sites will experience much stronger loading signals than inland sites.

3 Green's Function Approach

According to Farrell (1972), the vertical displacement at a point with coordinates (longitude and geocentric latitude) (λ,φ) at time t due to a mass loading distribution, Δm, is given by

$$u_V(\lambda,\varphi,t) = \int\int \Delta m(\lambda',\varphi',t) G_R(\psi)\cos(\varphi')d\lambda' d\varphi'. \tag{1}$$

Here, Δm is the change in mass at (λ',φ') and ψ is the angle between the radial vectors to the points (λ',φ') and (λ,φ). There are similar expressions for the horizontal displacement (e.g, Eriksson and MacMillan

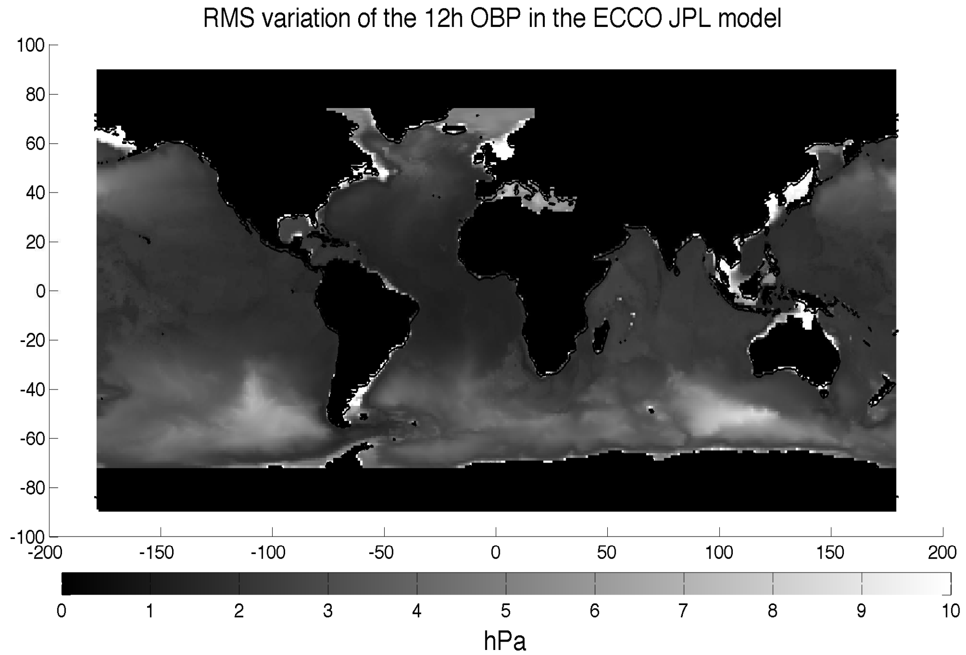

Fig. 1 RMS variation of the 12 hour ocean bottom pressure from the ECCO model (1993-2008)

(2012)). The loading Greens function is the response at the station due to a mass load at an angular distance ψ from the station. The closer the mass is to the station, the larger the response. By integrating over the surface of the earth, we will get the total adjustment of the station position caused by the surface mass distribution. The loading contribution is dominated by loading near the station as well as any large coherent regional loads far from the station.

4 Nontidal Ocean Loading Displacement Series

Fig. 2 below shows some typical vertical loading series from the ECCO data period (1993-2009). The loading series shown are for the four sites Matera (Italy), Onsala (Sweden), Tsukuba (Japan), and Wettzell (Germany). The first three are coastal sites in areas with large variations in the ECCO bottom pressure data, while Wettzell is an inland site. We therefore expect the loading series for Wettzell to have a much smaller variance than the coastal sites. The signals for Tsukuba and Matera are clearly seasonal. It is also clear that the 3-dimensional loading displacements are predominantly in the vertical direction. Generally peak-to-peak loading displacements at VLBI coastal sites are 4-6 mm in the vertical and less than 1 mm in the horizontal.

5 Annual Variation of Vertical Loading

We ran two terrestrial reference frame solutions with the Calc/Solve VLBI analysis program, described by Ma et al. (1990), where station positions, velocities, and annual site position amplitudes were estimated globally. In the first solution, we applied hydrology loading series generated using GLDAS data, which is described by Rodell et al. (2004). In the second solution, nontidal ocean loading was also applied. As shown in Fig. 3, there was a reduction in the vertical annual amplitude for most of the coastal VLBI sites.

6 Reduction of Variance in VLBI Analysis

We applied our loading series in standard Calc/Solve VLBI analysis to determine whether our solution site postion estimates were improved. We ran two solutions to estimate daily site positions for the sites in our weekly operational R1 and R4 networks from 2003-2009: 1) hydrology loading was applied and 2) ECCO ocean loading series was applied in addition to hydrology loading.

Comparing these solutions, we find that after applying the ECCO loading corrections, 57% of the baselines show a strictly positive reduction in variance. We

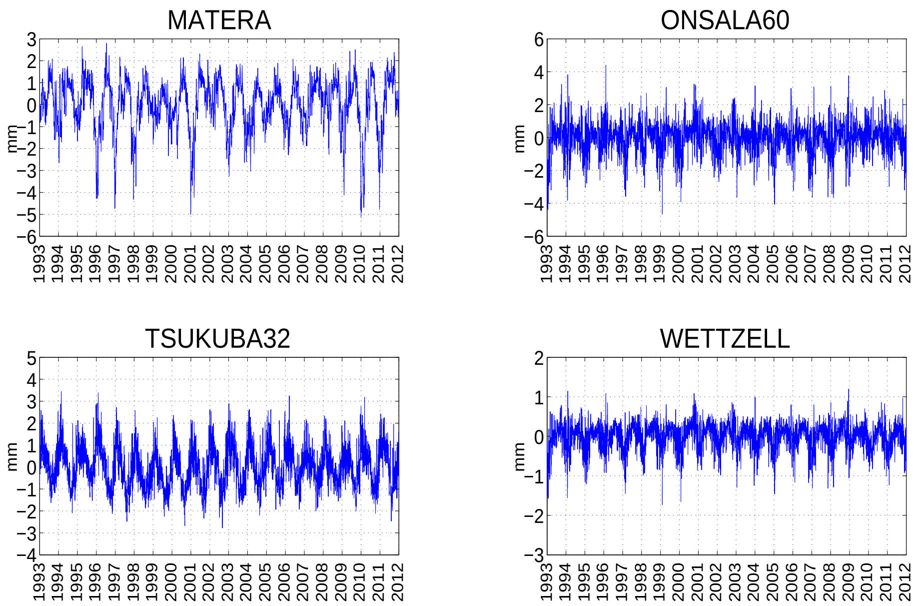

Fig. 2 Vertical loading series and corresponding vertical RMS for 3 coastal VLBI sites: Matera (1.26 mm), Tsukuba (1.18 mm), and Onsala (1.03 mm) and one inland site, Wettzell (0.54 mm)

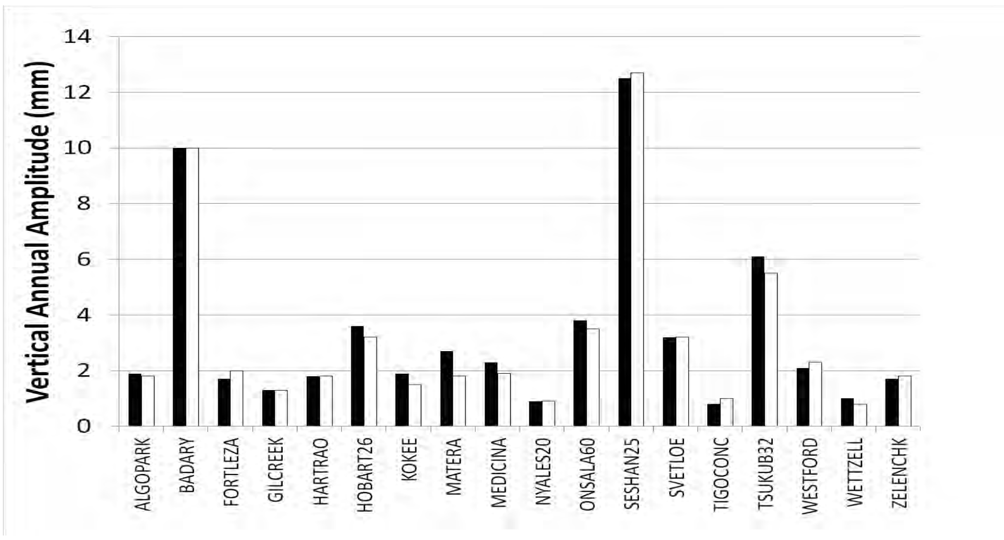

Fig. 3 Vertical annual amplitude reduction after applying nontidal ocean loading in analyis of R1 and R4 sessions from 2002-2009. Amplitudes are shown for hydrology loading only case (black bars) and with ocean loading also applied (white bars).

included all baselines even those with non-coastal sites at one end of the baseline, where the nontidal loading signal is small. The variance of vertical position estimates is reduced for most sites. The position estimates are improved most for coastal stations where the nontidal ocean loading signal is strongest, although Forteleza (Brazil) shows no improvement.

7 Conclusions

We have seen that ocean bottom pressures have the largest variations near coastlines, which implies that ocean loading displacements will be greatest for coastal sites. Applying the ECCO ocean loading displacement series reduces the vertical RMS scatter

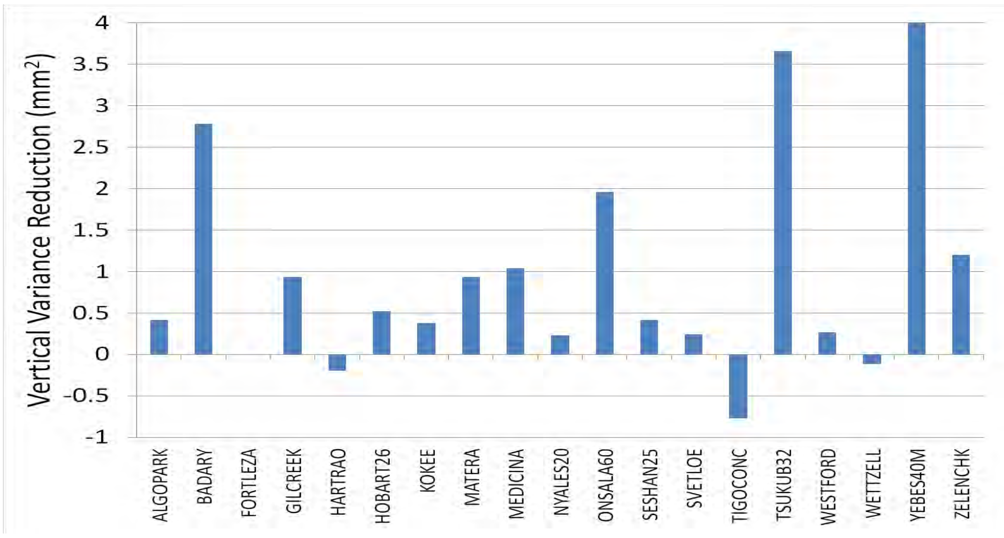

Fig. 4 Vertical site position reduction in variance due to applying nontidal ocean loading.

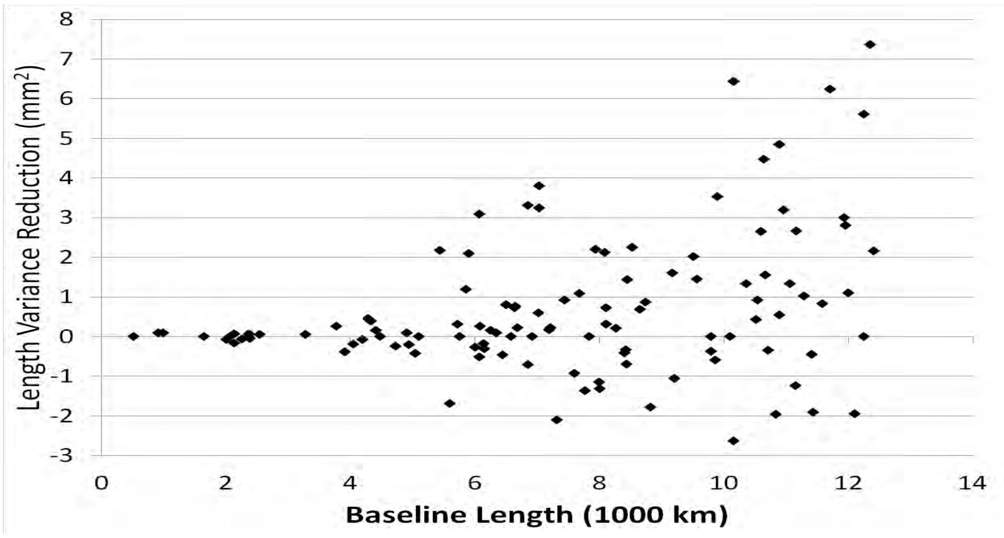

Fig. 5 Baseline length reduction in variance due to applying nontidal ocean loading.

for most sites, particularly those near coasts. Baseline length scatter is reduced for 57% of VLBI baselines including those without coastal sites. Nontidal ocean loading modeling also reduces annual vertical amplitudes for most coastal sites. We have developed a service at http://lacerta.gsfc.nasa.gov/oclo to provide our 12-hour nontidal ocean loading series for all VLBI sites from 1993 to the present. In the future, we plan to extend this by providing a globally gridded product from which one can interpolate to a site location of interest.

References

D. Eriksson and D. MacMillan. Continental hydrology loading observed by VLBI measurements. *IVS 2012 General Meeting Proceedings*, 415-419, 2012.

W. E. Farrell. Deformation of the earth by surface loads. *Rev. Geophys. and Spac. Phys.*, 10(3), 761-797, 1972.

I. Fukumori. A partitioned Kalman filter and smoother. *Mon. Weather Rev.*, 130, 1370-1383, 2002.

Ma, C., J. M. Sauber, L. J. Bell, T. A. Clark, D. Gordon, W. E. Himwich, and J. W. Ryan, Measurement of horizontal motions in Alaska using very long baseline interferometry, *J. Geophys. Res.*, 95(B13), 21991–22011, 1990.

M. Rodell, P. R. Houser, U. Jambor, J. Gottschalck, K. Mitchell, C. -J. Meng, K. Arsenault, B. Cosgrove, J. Radakovich, M. Bosilovich, J. K. Entin, J. P. Walker, D. Lohmann, and D. Toll. The global land data assimilation system. *Bull. Amer. Meteor. Soc.*, 85(3), 381-394, 2004.

The comparison between the UT1 results determined by the IVS Intensive observations

M. H. Xu, G. L. Wang

Abstract In this paper the history and status of the International VLBI Service for Astrometry and Geodesy (IVS) Intensive observations are briefly reviewed. The analysis of the IVS Intensive observation data from February 1984 to August 2011 with different observation networks is carried out. By comparing the results from different networks, a difference of some dozens of microseconds (μs) between these results is found. The results of the IVS Intensive observations that Sheshan station has participated in are analyzed as well, it shows that the Sheshan station performance as well as other stations. Finally, from the comparison and analysis of different UT1 series, it is concluded that there is an uncertainty at the level of about 10 μs between the results of UT1 obtained from the IVS Intensive observations with respect to those of the IERS (International Earth Rotation Service) C04.

Keywords Intensive Observation, UT1

1 Introduction

The precise earth orientation parameters (EOP) are very important to various kinds of ground-based observations and space navigations. Among the earth orientation parameters, the earth rotation angle (UT1) varies most quickly, and so it is most difficult to be precisely predicted. The earth orientation parameters of high precision, therefore, are obtained with space techniques. Very Long Baselibe Interferometry (VLBI) is the fundamental one to measure UT1, which becomes gradually a routine measurement since the 1980s.

Since its foundation at the end of last century, IVS (Schlüter and Behrend, 2007) measures EOP three times every week with 5 ~ 8 globally distributed VLBI stations, from which the accuracy of the obtained UT1-UTC ($\Delta UT1$) is estimated to be about 7 μs (Schuh et al., 2009). The results can only be obtained about 2 weeks after the measurements. According to the study by Luzum and Nothnagel (2010) , if the real time UT1 values can be obtained, the accuracy of $\Delta UT1$ provided by the IERS Rapid/Prediction Service Center (RS/PC) can be raised by 50%, and for that of its predicted value it is 21%. The nearly-real-time UT1 values, therefore, are very important to the EOP prediction.

In order to monitor the UT1 with shorter time latency, a new kind of VLBI experiments, called Intensive observations, began to carry out in 1984 (Robertson et al., 1985) with a single west-east baseline, and every observation lasted for 1 hour. This baseline has been changed for 3 times. From 1984 to February 1994, the Wettzell (Bavaria, Germany)-Westford (Massachusetts, USA) baseline was used. From March 1994 to June 2000 it was replaced by Wettzell-Green Bank (West Virginia, USA) (Eubanks M et al., 1994), since 2000 which wasWettzell- Kokee Park (Hawaii, USA). All these routine observations are called as INT1, in general, these observations are carried out from Monday to Friday every week, and every session lasts for 1 hour from 18h30mUT. Because the hard disc that records the data from Kokee Park need be transported to Navy Observatory with ship, so 2 ~ 3 days are needed in average.

Because of the importance of the UT1 monitoring, the IVS has added another baseline to the Intensive observations, called INT2 (Nothnagel and Schnell , 2008). This single baseline is made up of Wettzell-Tsukuba (Japan), the observation also lasts for 1 hour from 7h 30m UT every Saturday and Sunday. It is a very nice supplement to INT1. The data of INT2 are transmitted through network to the correlation center at Tsukuba, but the data handling would be made just

Minghui Xu, Guangli Wang
Shanghai Astronomical Observatory, CAS, Nandan Road 80, Shanghai, China

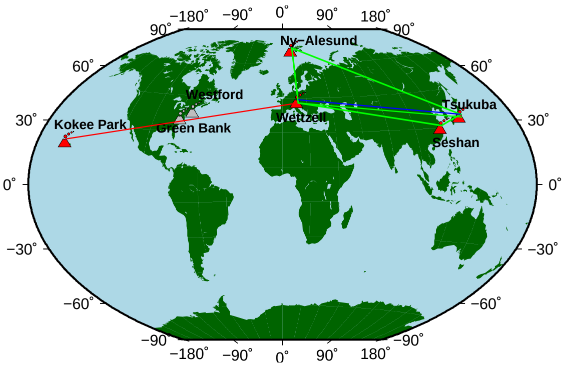

Fig. 1 The baseline networks of the Intensive sessions

in Monday morning (Japanese time) next week, and so the time delay is at least 1 day.

In order to fill the observation blank from 8h30m UT Sunday to 18h30m UT Monday, INT3 observation was proposed (Luzum and Nothnagel, 2010). Since February 2008, INT3 carries on its sessions, each of which lasts for 1 hour from 7h00m UT every Monday. Three stations Ny-Ålesund (Spitsbergen, Norway), Tsukuba and Wettzell participate in the sessions. The data of INT3 are transmitted through the internet to the correlation center of Bonn, the correlation are finished at about 15h00m UT every Monday, and after 1 hour the result of $\Delta UT1$ can be obtained. With the joinment of INT3, the longest interval of VLBI Intensive observations does not go beyond 24 hours. Since Tsukuba station shows a strong non-linear movement after the big earthquake in Japan in March 2011, Sheshan Station in Shanghai joins as well the INT3 observations.

It is obviours that the accuracy of the predicted UT1 depends upon two aspects, the precision and the latency of $\Delta UT1$ obtained from observations. At present, studies are developing towards these two aspects. In order to improve the observing accuracy of $\Delta UT1$, Baver et al. (2004); Baver and Gipson (2010) compared the results from INT1 and INT2 observations, and discussed the effect of the distributions of radio sources on UT1. They concluded that it is necessary to extend the spatial distribution of radio sources as wide as possible in the schedule. Nothnagel and Schnell (2008) considered errors in polar motion and nutation should be one of error sources of the UT1 Intensive observations and have given a mathematical model to correct the effect. Hobiger et al. (2009) analyzed the clock errors of reference stations, and concluded that it should cause an error of about 0.2 μs in the $\Delta UT1$ from INT2 observations. Böhm et al. (2010a,b) thought that the main error source was the azimuthal asymmetry of atmosphere in the troposphere. Japanese researchers have done a lot of work on the decrease of the latency by means of the ultra-rapid measurement of UT1 with e-VLBI (Matsuzaka et al., 2008; Sekido et al., 2008). The $\Delta UT1$ can be abtained as soon as 30 mininuts after the observation finished (Matsuzaka et al., 2008). Meanwhile, Hobiger et al. (2010) realized the full-automation of the UT1 rapid determination using the VLBI analysis software C5++, the $\Delta UT1$ can be obtained several minutes after an observation. It is a pity that the results of the Japanese ultra-rapid UT1 measurements do not be provided to IERS, consequently, there is no any contribution to the UT1 predicting routine for these observations (Luzum and Nothnagel, 2010).

In this paper, all the data of the IVS Intensive observations that currently exist are utilized to obtain the $\Delta UT1$ time-series and the differences between them are compared. In Section 2, the data and VLBI data analysis will be described. The calculated results of all the historical data and their analysis present in Section 3. The calculations and analysis of different types of current Intensive observations and the analyzed results of the Intensive observations with Sheshan station participated in will be described in Section 4. The conclusion will be given in Section 5.

2 Data and their processing

The data we used are the IVS Intensive observations from February 1984 to August 2011, including 6552 sessions of INT1, INT2 and INT3. 353 sessions of the Intensive observations having been rejected since the observable number of these observations is less than 8. An overview of the current Intensive observations is shown in Table 1, in which the INT1 information indicates the INT1 observations after 2000.

Figure 1 illustrates the positions of the stations that carried out the Intensive observations. In this figure the red line indicates the single baseline of INT1 observations after 2000; the blue line, that of INT2 observations; the green lines, the INT3 network; and the grey mark, the stations of early INT1 observations.

The software used for the data analysis is Calc10.0/SOLVE. The ITRF2008 and ICRF2 are adopted for the coordinates of stations and those of radio sources, respectively. The EOP series given in IERS C04 (C04) are adopted for the precession and nutation. Thus, in each observation it is only needed to estimate the following parameters: zenith time-delay correction, the clock offset and clock rate parameters and the UT1 correction. For the sake of its comparison with C04, the calculated $\Delta UT1$ has been corrected for

	INT1	INT2	INT3
Stations	Wettzell Kokee Park	Wettzell Tsukuba	Wettzell Ny-Ålesund Tsukuba Seshan
Longest baseline of the network(km)	10357	8445	8445
East-West-dimension(km)	10072	8378	8378
North-South-dimension(km)	2414	1064	2962
Observing days	Mon. to Fri.	Sat. and Sun.	Mon.
Starting epoch	18:30	7:30	7:00
Correlator	NASA (USA)	GSI (Japan)	Bonn (Germany)
Delay(day)	2 - 3	1 - 2	0.4

Table 1 Overview of the current *Intensive* observing routines

high-frequency variations, hence the $\varDelta UT1$ series in this paper does not contain high-frequency variation. Meanwhile, before the comparison with C04, the third-order spline interpolation of 15 points has been used for C04 to give the values with respect to the moments of observations.

3 INT1 observations in 1984 ~ 2011

According to the participated stations, the INT1 observations are divided into 3 phases: sessions with the baseline Wettzell-Westford in 1984 ~ 1994, sessions with the baseline Wettzell-Green Bank (NRAO 80m and NRAO 20m) in 1994 ~ 2000, sessions with the baseline Wettzell-Kokee Park in 2000 ~ 2011. The esults and the statistical information are listed in Table 2. The 4th line shows the number of sessions in each of 3 phases; the 5th and 6th lines indicate the length of baseline and its projection in the west-east direction, respectively; the 7th line is the averaged number of scans per session; the 8th line demonstrates the averaged normal error of $\varDelta UT1$. It is obvious in Table 2 that there is a significant improvement in the INT1 sessions. The average number of scans has increased by two times. Due to the increasing average number of scans, the improving accuracy of observation, and the increasing length of baseline, the accuracies of $\varDelta UT1$ at different phases are evidently improving. The difference between the time series of $\varDelta UT1$ and that of C04 is illustrated in Figure 2. From Figure 2 and Table 2, it is demonstrated that the solution of $\varDelta UT1$ of the Intensive observations since 2000 is in better accordance with C04, but there exist systematic differences among the $\varDelta UT1$ values which were measured in different phases (with different baselines). Among them, the difference between the first phase and the second one is nearly 30 μs, and that between the second and the third is nearly 4 μs. In general, there is a deviation

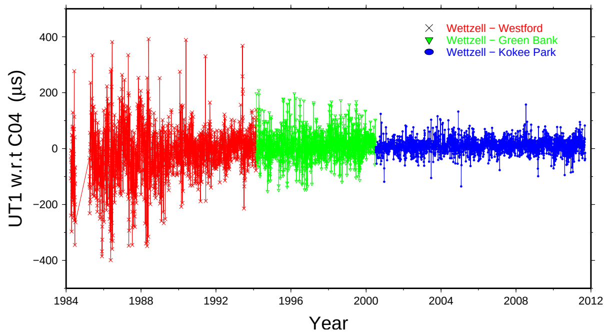

Fig. 2 ΔUT1 time series with respect to C04 obtained from INT1 observations.

with a level of 10 μs between the $\varDelta UT1$ series of INT1 and that of C04.

Year	1984-1994	1994-2000	2000-2011
Stations	Wettzell Westford	Wettzell Green Bank	Wettzell Kokee Park
Number of session	1854	1359	2374
Length of baseline(km)	5998	6724	10357
East-West-dimension(km)	5977	6669	10072
Avg. number of scans per session	9.6	17.2	20.9
Avg. normal error of ΔUT1(μs)	124.6	26.2	11.7
Avg. offset w.r.t. C04/precision(μs)	-14.1 / 2.4	14.0 / 1.7	10.4 / 0.5
Standard derivation w.r.t. C04(μs)	101.8	61.8	25.6

Table 2 Statistical information of the results from the different INT1 types

4 Comparisons of current different types of Intensive observations

We used the INT1, INT2 and INT3 after 2000. The data consist of 2374 sessions of INT1, 632 sessions

	Avg. number of scans per session	Avg. normal error (μs)	Avg. offset / precision w.r.t. C04(μs)	Standard derivation w.r.t. C04(μs)
INT1	20.9	11.7	10.4 / 0.5	25.6
INT2	29.7	10.3	10.3 / 0.9	21.4
INT3	70.2	8.6	31.0 / 2.8	28.3

Table 3 Comparison of the results from the different Intensive types

Session name	Number of scans	Normal error (μs)	Offset w. r. t. C04 (μs)
11APR18XK	37	11.5	12.0
11MAY02XK	43	24.1	-15.0
11MAY16XK	39	22.7	22.2
11JUN20XK	14	18.4	26.2
11JUL04XK	33	38.3	186.0
11JUL11XK	41	7.8	-11.7

Table 4 The UT1 and its precision from 6 Seshan involved INT3 observations

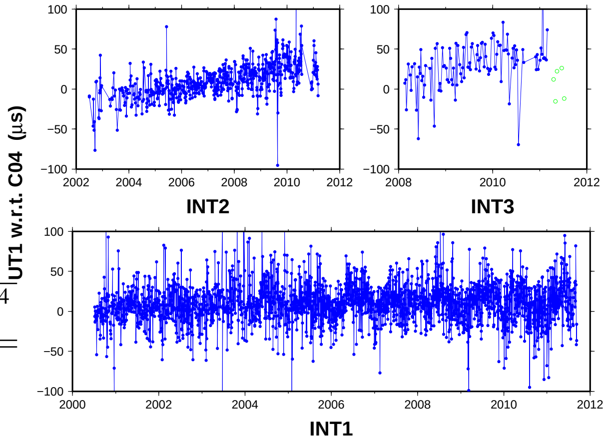

Fig. 3 ΔUT1 time series with respect to C04 obtained from three types of Intensive observations.

of INT2 and 112 sessions of INT3. Basically, there are 3 stations to participate in the INT3 sessions. For the convenience of comparisons, the sessions besides those of 3 stations were deleted. Because of the non-linear movement of Tsukuba station after the big earthquake in Japan, the sessions of INT2 and INT3 of this station after the earthquake were not included in the analysis. No mutually overlapping sessions exist in daily observation schedule. The calculated time series of $\Delta UT1$ with respect to C04 are illustrated in Figure 3. By interpolations, as mentioned before, the C04 are deduced to the epochs of UT1 observations, and the statistical information of the results is listed in Table 3. It is found from Figure 3 that there exist evident trends between INT2, INT3 and C04, the trend term obtained with weighted fitting is about 5 μs per year, while INT1 varies rather stably with respect to C04. In spite of the single baseline observations in both INT1 and INT2, the average number of scans of INT2 is obviously greater than that of INT1, and so the normal error and mean square error of INT2 are less than those of INT1. Although the number of scans of the 3 stations of INT3 is apparently increased, the estimated average deviation of $\Delta UT1$ with respect to C04 attains 31 μs, it is possible that the north-south directed baseline Wettzell-Ny-Ålesund in INT3 has enforced the effect of error in polar motion on the $\Delta UT1$.

There are six observations totally with a 3-station network composing of Wettzell, Ny-Ålesund and Sheshan (Tsukuba Station was taken out), the results of these 6 sessions are listed in Table 4. Among them, the deviation of $\Delta UT1$ obtained from the Session 11JUL04XK with respect to C04 is abnormal, up to 186 μs. The other 5 results are shown in Figure 3 with little hollow circles. Because of the absence of Ny-Ålesund Station, there were only 11 scans in the Session 11JUL04XK, and in fact it was a single baseline observation. The numbers of scans for all the 6 sessions are obviously less than the averaged number 70 of the routine INT3 observations, and their normal errors are also somewhat worse. But the accordance of the estimated $\Delta UT1$ with the C04 series is still good. Excluding the abnormal values of 11JUL04XK, the average deviation of $\Delta UT1$ is 11 μs, the dispersion is 16 μs. This accuracy can match with that of routine Intensive observations.

5 Conclusions

At present, the IVS Intensive observation has carried out every day, and this plays a nice role in monitoring UT1 variations. In the EOP prediction and the synthetic series (Bulletin A [1], Bulletin B [2] and C04 [3]) published by IERS, all of $\Delta UT1$ determined by IVS Intensive observations are important data sources. In the course of the Intensive observations, the baselines and the accuracy of the Intensive observations have greatly increased after 2000, and their normal accuracies are on the level of 10 μs, and the accuracy of $\Delta UT1$ obtained currently by the Intensive observations in comparison with C04 is on the level of 20 μs. Compared the analyzed results of different types of the Intensive observations, it is found that the observed values of

[1] http://hpiers.obspm.fr/eoppc/bul/bulb/explanatory.html
[2] http://hpiers.obspm.fr/iers/bul/bulb/explanatory.html
[3] ftp://hpiers.obspm.fr/iers/eop/eopc04/C04.guide.pdf

$\Delta UT1$ depend on baselines. The results of observations with an identical baseline (such as INT2 and INT3) are relatively consistent, while the differences between the measurements with different baselines are considerable, such as the observations of INT1 in different periods and the difference between INT1 and INT2 after 2000. With regard to the series of estimated $\Delta UT1$, INT1 possesses the most data and the longest observation time, as well as the best accordance with C04, while there exist some drifts in INT2 and INT3. But the accuracy of INT2 is better than those of the two others.

Because of the irregular movement of Tsukuba Station, the twice observations per week of INT2 is now changed into a single baseline of INT1, and INT3 in which Tsukuba is engaged is also affected. Hence Sheshan Station in Shanghai dedicates into the INT3 observation. In spite of the fresh observation with the less scan numbers than that of routine INT3 observation, the accuracy of $\Delta UT1$ estimated from the sessions with Sheshan Station participated in is in accordance with that of the routine Intensive observations.

It can be concluded from the analysis of the Intensive observations that there may exist systematic deviations between $\Delta UT1$ measurements of INT1 with different baselines; the $\Delta UT1$ measurement of INT1 is in better accordance with C04; the UT1 results of the Intensive observations with Sheshan Station engaged in are on the same level; in general, there is an uncertainty at the level of 10 μs between the present UT1 from the IVS Intensive observations and C04.

References

Schlüter W, Behrend D., The International VLBI Service for Geodesy and Astrometry (IVS): Current capabilities and future prospects, *J Geodesy*, 2007, 81: 379

Schuh H et al., Determination of UT1 by VLBI *In proceedings of XXVIIth IAU General Assembly*, 2009

Luzum B, Nothnagel A., Improved UT1 predictions through low-latency VLBI observations, *Journal of Geodesy*, 2010, 6, 399-402

Robertson, D. S., Carter, W. E., Campbell, J., Schuh, H., Daily earth rotation determinations from IRIS very long baseline interferometry, *Nature*, 1985, 316, 424

Eubanks M et al., IERS Technical Note; 17, 1994

Nothnagel A, Schnell D., The impact of errors in polar motion and nutation on UT1 determinations from VLBI Intensive observations, *Journal of Geodesy*, 2008, 82: 863

Baver K, MacMillan D, Petrov L, Gordon D., Analysis of the VLBI Intensive Sessions, *In proceedings of IVS 2004 General Meeting*, 2004, 394

Baver K, Gipson J., Strategies for Improving the IVS-INT01 UT1 Estimates, *In proceedings of IVS 2010 General Meeting*, 2010, 256

Luzum B, Nothnagel A., The effect of neglecting VLBI reference station clock offsets on UT1 estimates, *Advances in Space Research*, 2009, 43: 910

Böhm J, Nillson T, Schuh H., Prospects for UT1 Measurements from VLBI Intensive Sessions, *In proceedings of IVS 2010 General Meeting*, 2010, 251

Böhm J. et al., Improved UT1 predictions through low-latency VLBI observations, *Journal of Geodesy*, 2010, 84: 319

Matsuzaka S et al., Ultra Rapid UT1 Experiment with e-VLBI, *In proceedings of IVS 2008 General Meeting*, 2008, 68

Luzum B, Nothnagel A., Ultra-rapid UT1 measurement by e-VLBI, *Earth Planets Space*, 2008, 60: 865

Hobiger T et al., Fully automated VLBI analysis with c5++ for ultra-rapid determination of UT1, *Earth Planets Space*, 2010, 62: 933

Comparison of Russian and IVS intensive series

S.L. Kurdubov

Abstract The article presents results of first comparison the Russian National UT1-UTC estimation program Ru-U and IVS-intensive international campaign. It is shown that the Ru-U sessions are performing with good accuracy and results can be included into international VLBI data processing scheme. Comparison of different distributions shows that the problem of correlation lack between single delay formal errors and UT1 estimations are presented both in Ru-U and IVS-intensive series.

Keywords VLBI, UT1

1 Introduction

Russian National VLBI Network "Quasar" starts to operate in 2006. In 2009 it was adopted what Quasar Network will provide the fundamental time-positioning service of the GLONASS space system (Finkelstein et al (2008), Finkelstein et al (2012)). Quasar network performs regular daily VLBI sessions in standart VLBI S/X band for EOP estimations every week and every day hourly sessions for the UT1-UTC estimations. Hourly sessions are carried out on the baseline Zelenchukskaya — Badary. Observation are delivered to the IAA hardware correlator by the e-VLBI data transfer (Finkelstein et al (2011)). Quasar network works in every day mode since 01.07.2012, before than UT1-UTC estimations was also once a week. Between observation starts and UT1-UTC obtained lasts from 2 up to 6 hours. Observations available for analysis in NGS card format at the IAA website.

Sergey L. Kurdubov
Institute of Applied Astronomy RAS, nab. Kutuzova 10, Saint-Petersburg, Russia

2 Data processing with QUASAR software

We process data from 01.07.2012 to 20.11.2012 with the QUASAR VLBI data processing software (Kurdubov, Gubanov (2011)):

- 141 Ru-U sessions
- 152 IVS-Int sessions

All reduction calculations was implemented according to the IERS Conventions 2003 (McCarthy and Petit (2004)). Parametric model includes 5 constant parameters and 2 stochastic: linear + stochastic clock, constant + stochastic troposphere for each station, UT1-UTC.

3 Ru-U vs IVS-Int UT1-UTC estimation statistic

There are several different formal errors and WRMS considered in the article:

- mean formal error of UT1 estimations (averaged over all processed sessions);
- mean formal error of single delay measurement (mean per session);
- WRMS of UT1-UTC series vs IERS finals;
- observations RMS after solution (for single session).

Mean formal errors and WRMS for Ru-U and IVS-int presented at the Table 1. Relation between Ru-U and IVS-int estimations are in good agreement with the baseline lenght relation (see Table 2). Our results for IVS-int sessions also consistent with the results of over VLBI data analysis centers (see Table 3).

Session UT1-UTC estimation formal error vs number of observations chart presented at the fig 1. One can see that Ru-U sessions shows faster error decreasing with number of obsevations. It can be explained by

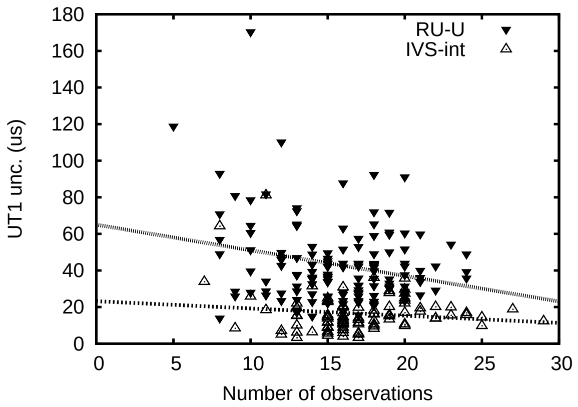

Fig. 1 UT1-UTC formal errors vs number of observations in session (solid line — Ru-U trend, dashed line — IVS-int trend).

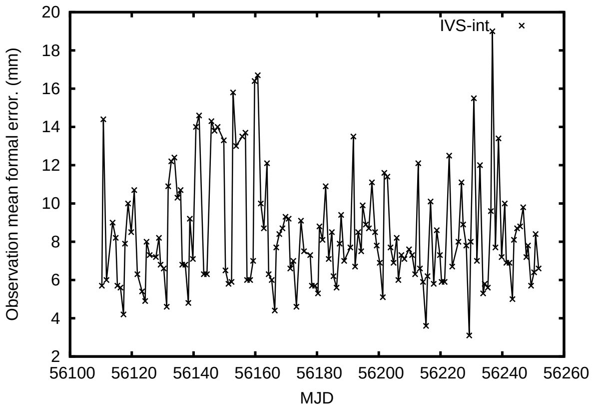

Fig. 2 Mean formal uncertainty of single delay (IVS-intensive).

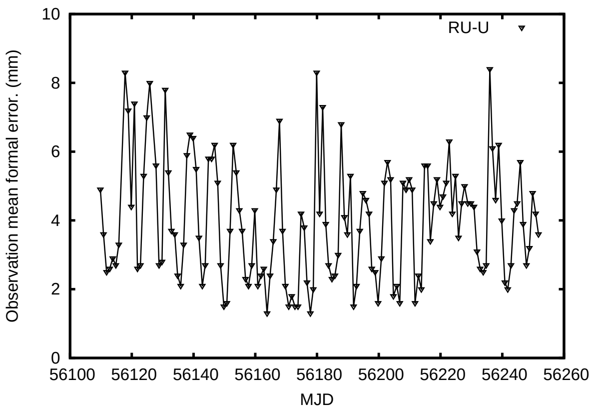

Fig. 3 Mean formal uncertainty of single delay (Ru-U).

differences in the scheduling procedure (sky coverege optimization for IVS-int and parameters optimization for Ru-U).

Mean formal error of single delay presented at the fig 2 for the IVS-int sessions and 3 for the Ru-U. As one can see from fig 2 and 3 the accurcy of observations differs up to 4-5 times from one session to another (it is not secondary processing result, it is mean correlator formal errors). The differences can be explained by the some sessions was performed with cool recivers and some without criogenic.

Notice that the RMS after solution have no correlation with the formal errors of single delay as seen from fig. 4. The problem looks similar both for Ru-U and IVS-int sessions. RMS after solution is crucial parameter and direct affects accuracy of the UT1-UTC estimation: fig. 5.

	Ru-U	IVS-int
mean unc.	43	18
WRMS	50	22

Table 1 Ru-U vs IVS-Int UT1-UTC estimation statistic in μas (WRMS vs IERS finals series)

Badary — Zelenchukskaya	4404
Wettzell — Tsukuba	8445
Wettzell — Kokee	10357

Table 2 Ru-U vs IVS-Int baseline lenghts in meters

AC		Dec	Nov	Oct	Sep	Aug	Jul
BKG	mean unc.	13	11	14	14	15	13
	WRMS	18	12	18	20	19	15
GSFC	mean unc.	20	15	17	22	18	15
	WRMS	73	20	26	24	27	15
IAA	mean unc.	15	15	21	16	18	15
	WRMS	13	9	19	20	22	13
PUL	mean unc.	16	18	21	20	29	18
	WRMS	18	14	21	19	22	14
USNO	mean unc.	16	16	0	0	21	30
	WRMS	20	21	0	0	24	19

Table 3 IVS-intensive statistic in μas (IERS Bulletin B 293-298 data)

4 Conclusions

The main result of this article: IAA Ru-U UT1-UTC estimations have comparable accuracy with the IVS-intensive results and can be used by IERS and IVS as contribution to the IERS UT1-UTC series. Raw observation data and results of UT1-UTC estimations can be obtained at the IAA ftp:

ftp://quasar.ipa.nw.ru/pub/EOS/IAA/ngs/

ftp://quasar.ipa.nw.ru/pub/EOS/IAA/veopi-ru.dat

Moreover it should be noticed:

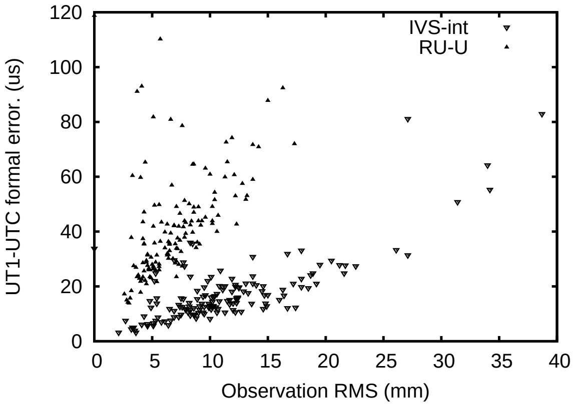

Fig. 5 RMS after solution vs UT1-UTC formal errors.

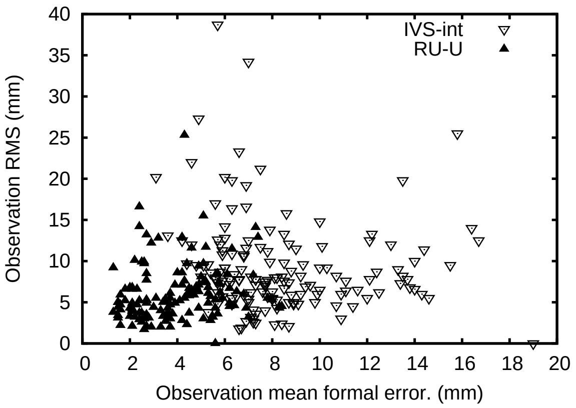

Fig. 4 Mean formal error of single delay vs RMS after solution.

- Ru-U sessions have better single delay formal errors (see fig. 4)
- Ru-U sessions shows faster error decreasing with number of obsevations.
- There is no correlation between delay formal error and RMS both for Ru-U and IVS-int

References

Finkelstein, A. M.; Skurikhina, E. A.; Surkis, I. F.; Ipatov, A. V.; Rakhimov, I. A.; Smolentsev, S. G. Using the quasar VLBI network for the fundamental time-positioning service of the GLONASS space system. *Astronomy Letters*, Volume 34, Issue 1, pp.59-68, 2008 doi: 10.1134/S1063773708010076.

Finkelstein, A. M.; Ipatov, A. V.; Skurikhina, E. A.; Surkis, I. F.; Smolentsev, S. G.; Fedotov, L. V. Geodynamic observations on the quasar VLBI network in 2009-2011. *Astronomy Letters*, Volume 38, Issue 6, pp.394-398, 2012 doi: 10.1134/S1063773712060023.

Finkelstein, A. M.; Kaidanovskii, M. N.; Sal'Nikov, A. I.; Mikhailov, A. G.; Bezrukov, I. A.; Skurikhina, E. A.; Surkis, I. F. Prompt determination of universal time corrections in e-VLBI mode. *Astronomy Letters*, Volume 37, Issue 6, pp.431-439, 2011 doi: 10.1134/S1063773711060028.

Kurdubov, S. L.; Gubanov, V. S. Main results of the global adjustment of VLBI observations. *Astronomy Letters*, Volume 37, Issue 4, pp.267-275, 2011 doi: 10.1134/S1063773711010063.

D. D. McCarthy and G. Petit. *IERS Conventions (2003)*. IERS Conventions (2003). Dennis D. McCarthy and Gérard Petit (eds.), International Earth Rotation and Reference Systems Service (IERS). IERS Technical Note, No. 32, Frankfurt am Main, Germany: Verlag des Bundesamtes für Kartographie und Geodäsie, ISBN 3-89888-884-3, 2004, 127 pp., 2004.

Comparison of wet troposphere variations estimated from VLBI and WVR

O. Titov, L. Stanford

Abstract Wet troposphere instability serves as one of the major contributors to the total error budget of the VLBI group delay. The least squares collocation method (LSCM) is suited to estimate the wet troposphere delay for each observational epoch with sufficient precision. The LSCM is incorporated into the OCCAM software for routine reduction of the geodetic VLBI data. This paper presents a comparison of the wet troposphere delay estimates obtained with OCCAM and the Water Vapour Radiometer (WVR) data from the VLBI station Onsala during the CONT'11 campaign.

Keywords CONT'11, WVR, VLBI, Wet troposphere delays

1 Introduction

Geodetic VLBI data are adjusted by variations of the least squares method developed by Gauss and Legendre 200 years ago. One approach is to split a typical 24-hour session into sets of 1-hour or 2-hour segments and model the stochastic parameters (clock offset, wet troposphere delay) by piece-wise linear functions. Then 24 or 12 points per session for the troposphere variations are obtained.

In contrast to this approach the LSCM implement the priori covariance functions of the stochastic parameters (Moritz, 1980). This approach makes it possible to obtain the time series of the stochastic parameters with a time resolution corresponding to the scheduled rate of observations. The LSCM was adopted for reduction of geodetic VLBI data (Titov and Schuh, 2000). The time series of so-called stochastic parameters (wet troposphere delays, clock offset variations) could be estimated with a high temporal resolution (e.g. one point for 2-4 minutes) (Titov, 2004).

Oleg Titov and Laura Stanford
Geoscience Australia, PO Box 378, Canberra, 2601, ACT, Australia

2 Analysis of observational data from the CONT'11

CONT'11 was a campaign of continuous VLBI sessions, scheduled to be observed in the second half of September 2011 (15-Sep-2011 00:00 UT through 29-Sep-2011 24:00 UT). Thirteen VLBI radio telescopes participated in this campaign. The New Zealand radio telescope Warkworth joined this network on one day, 26-Sep-2011. One of the goals of CONT'11 was to estimate the troposphere zentih delays and gradients and compare them with WVR and GPS results.

We have calculated the wet troposphere delays with OCCAM software by the LSCM. Fig 1 shows the zenith delays measured with WVR at Onsala geodetic site (kindly provided by Dr Rudiger Haas) and those obtained with the data from Onsala60 radio telescope. It is obvious that the variations of the wet troposphere delays are similar to the WVR data.

The statistical comparison, though, is not a straightforward procedure. The WVR available data are unevenly spaced due to technical reasons, whereas the VLBI-originated time series are unevenly spaced due to scheduling irregularities. The interpolation scheme was developed to obtain the WVR data for the same epochs as VLBI for statistical comparison. Given the larger number of time series data points for the WVR data, they were rebinned and averaged about each VLBI data point to give a corresponding value. The width of each bin was determined by the half distance to the next and previous VLBI data points. We gained 5235 single wet troposphere zenith delays in total for the comparison.

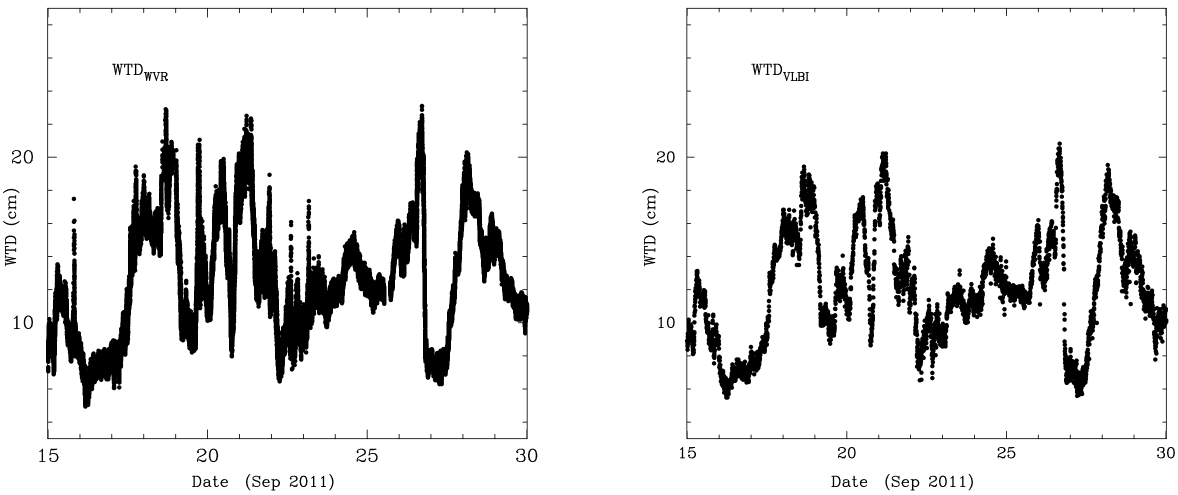

Fig. 1 WVR (left) and VLBI(right) wet troposphere variations for Onsala60 during CONT'11

At the first step the times series were fitted by linear function across the whole two-week time span. The corresponding differences VLBI-WVR are shown on Fig 2. The mean root-mean-square (rms) parameter was found to be around 0.77 cm. The times series highlight some trends on a short-time scale. Therefore, the presented rms is likely to be affected by improper fitting.

Consequently, we fitted the time series by linear function for each day separately. Fitting of the variations by the linear trend is shown at Fig 3. Fig 4 shows differences VLBI-WVR after removal of the linear trends for each 24-hour session. The mean rms of the resulted numbers is 0.67 cm. Daily rms parameters on Fig 5 mostly lie within the range 0.5 – 0.8 cm in a good agreement with the mean rms over the two-week set of data. The only rms value exceeding 1 cm (19 September 2011) is likely to be induced by large outliers at the WVR time series.

The new differences VLBI-WVR do not display obvious short-time scale trends, and we could say that there is a reasonable agreement between the time series from two independent techniques.

It is worth of mention that this statistic may be exagerrated by insufficient calibration of the WVR data, presence of outliers, adopted interpolation scheme and and, finally, formal errors of the observables.

To check out the effect of outliers to the statistics, we removed those post-fit residuals which exceed 2 cm on Fig 4. New plot shows the residuals without the outliers in on Fig 6. New daily rms shown on Fig 7 lie within the range 0.3 – 0.6 cm, i.e. the they are about 30% better than the residuals presented on Fig 4 and 5.

The WVR data may be affected by heavy rain. Fig 8 and Fig 9 shows comparison of WVR and VLBI data from CONT'05 campaign for two consequtive days. Once on the left plot the curves of troposphere zenith delays from the both techniques match each other, on the right plot the WVR data show a strong level of noise caused by rain at that day.

3 Conclusions

We have considered the wet troposphere delays obtained with WVR technique and estimated from VLBI using the LSCM. The wet troposphere delays measured with WVR may be affected by rain weather or improper calibration of the equipment. The estimates obtained with VLBI may be affected by inadequate apriori assumption, e.g. the independency of the delays for two radio telescope at the same site. It is shown that weighted rms between the time series varies between 3 and 6 mm after removing of the outliers (individual differences exceeding 2 cm).

Overall, we believe that the wet troposphere delays obtained with the LSCM are more accurate. The high time resolution estimates (1 point for 2-4 minutes) of the stochastic parameters could be obtained in a frame of a normal VLBI schedule with a standard number of scans per hour (5-15 scans per hour for a single station). It is not necessary to design a highly intensive session included up to 100 scans per hour for a single station. Moreover, it is also not necessary to purchase expensive WVR facilities for monitoring the water vapour variations.

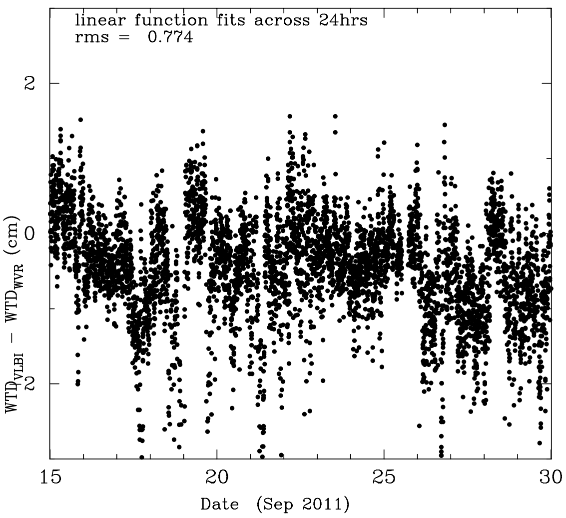

Fig. 2 Differences VLBI-WVR after fitting by linear function across two week period

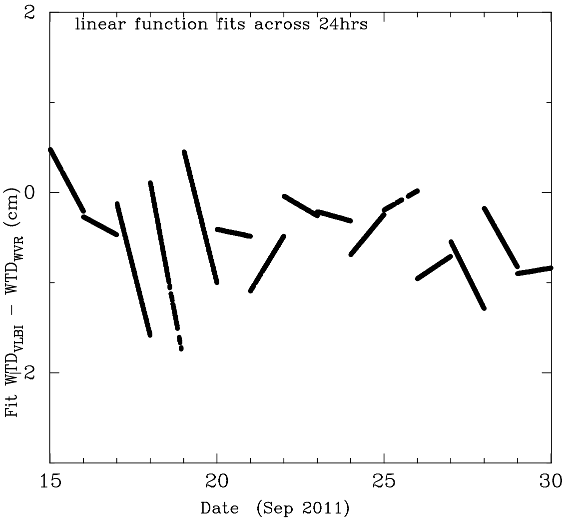

Fig. 3 Fitting of the differences VLBI-WVR by piece-wise linear function

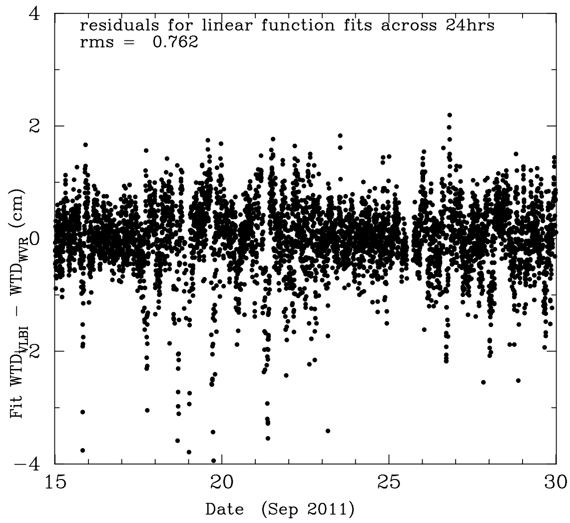

Fig. 4 Differences VLBI-WVR after fitting by piece-wise linear function

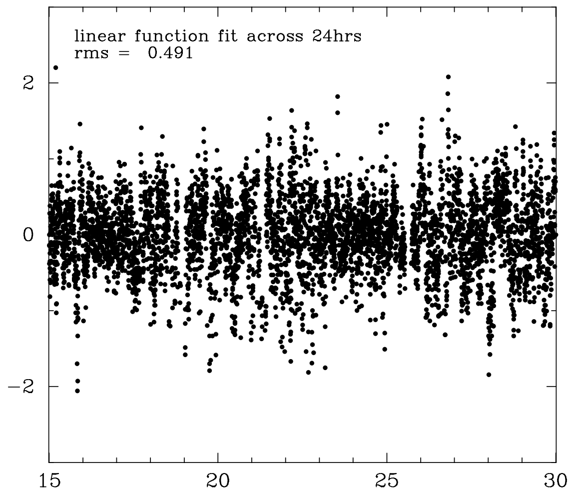

Fig. 5 Daily rms values for all 15 sessions

4 Acknowledgement

We are thankful to the staff from Wettzell and Onsala observatories for the WVR data from the CONT'05 and CONT'11 campaings. This paper is published with the permission of the CEO, Geoscience Australia.

References

H. Moritz. Advanced Physical Geodesy. Wichman, 1980, 500 p.

O. Titov and H. Schuh. Short-periods in Earth Rotation seen in VLBI Data analysed by the least squares collocation technique. *IERS Technical Notes 28* (2000). B. Kolaczek, H. Schuh and D. Gambis (eds.), International Earth Rotation and Reference Systems Service (IERS). Paris Observatory, Paris, pp. 11-14, 2000.

O. Titov. Construction of a Celestial Coordinate Reference Frame from VLBI Data. *Astr.Rep.*, 48, 941, 2004.

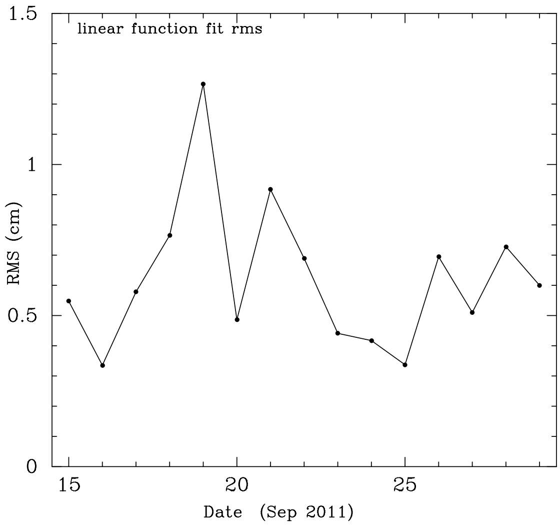

Fig. 6 Differences VLBI-WVR after fitting by piece-wise linear function after removing of outliers

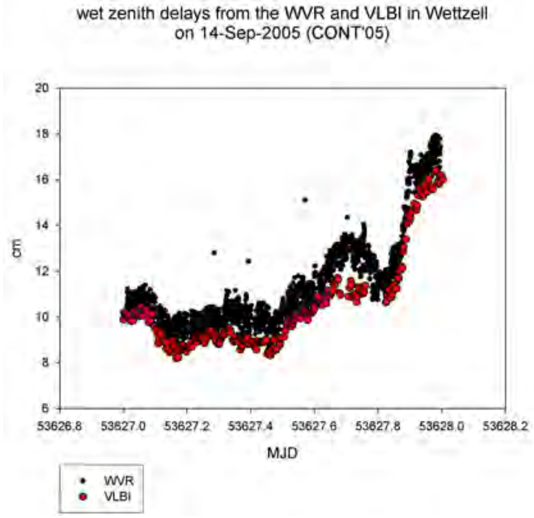

Fig. 8 Wet troposphere zenith delays for Wettzell on 14-Sep-2005 (CONT'05)

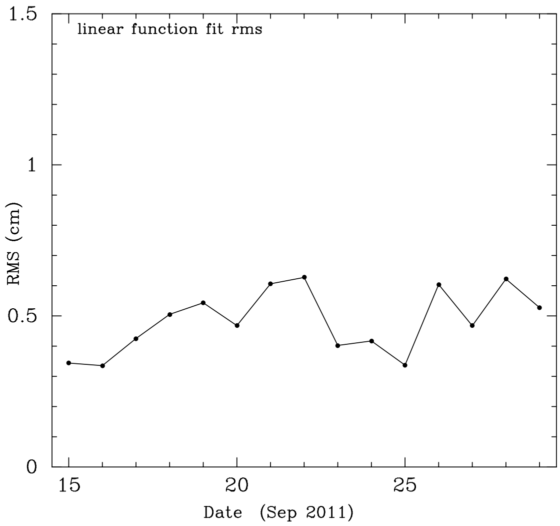

Fig. 7 Daily rms values for all 15 sessions after removing of outliers

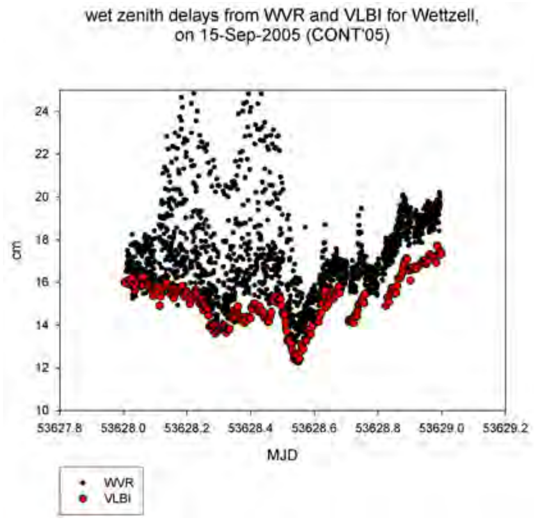

Fig. 9 Wet troposphere zenith delays for Wettzell on 15-Sep-2005 (CONT'05)

The state-of-the-art of Russian VLBI network

A. Ipatov, S. Smolentsev, A. Salnikov,I. Surkis, I. Gayazov, S. Kurdubov, I. Rahimov, A. Diakov, V. Shpilevsky, A. Melnikov, V. Zimovsky, L. Fedotov, E. Skurikhina

Abstract The state-of-the-art of the of Russian VLBI network "Quasar" is presented. The observations are carried out within the scope of two domestic programs: Ru-U for the operational determination of Universal Time in near real-time and Ru-E for the determination of EOP from 24-hour sessions. Correlation of the data is performed at the IAA correlator ARC. The IAA analysis center performs data processing with the QUASAR and OCCAM/GROSS software packages. Since July 2012 we start everyday Ru-U observations. The results and analysis of this data is presented.

Keywords EOP, VLBI observations, "Quasar" network

1 Introduction

Observations at the Russian Domestic "Quasar" network with the aim of Earth Orientation Parameters (EOP) and Universal Time determination is one of the main directions of the IAA activity (Finkelstein et al., 2008). The observations are carried out in the framework of two national programs:

(1) Ru-E: 24-hour sessions for the determination of the five EOP parameters.

(2) Ru-U: 1-hour sessions for the determination of Universal time.

The purpose of the Ru-E program is to provide EOP results on regular basis from 24-hours sessions on three-station network: "Svetloe" – "Zelenchukskaya" – "Badary".

A. Ipatov, S. Smolentsev, A. Salnikov,I. Surkis, I. Gayazov, S. Kurdubov, I. Rahimov, A. Diakov, V. Shpilevsky, A. Melnikov, V. Zimovsky, L. Fedotov, E. Skurikhina
Institute of Applied Astronomy of RAS, 10, Kutuzova emb., 191187 Saint Petersburg, Russia

The purpose of the Ru-U program is to provide UT1-UTC results on regular basis from Intensive sessions on one base "Badary" – "Zelenchukskaya" ("Badary" – "Svetloe").

Statistics of "Quasar" domestic observational programs is shown in Tab. 1. Planned numbers of sessions in 2013 are indicated in brackets of the table. Number of session for 2013 year is presented for the time span till the end of May.

Year	Ru-U			Ru-E		
	Sv	Zc	Bd	Sv	Zc	Bd
2006		6	6	9	9	9
2007	10	12	17	9	9	9
2008	18	15	18	14	14	14
2009	13	26	30	23	23	23
2010	3	50	50	20	20	20
2011	9	65	69	41	41	41
2012	31	172	187	47	47	47
2013	4	137(350)	139(350)	20(50)	20(50)	20(50)

Table 1 "Quasar" network observations

2 "Quasar" complex equipment

"Quasar" complex consist from the "Quasar" network, connected by digital communication channels with the Operating and Data Processing Center (Surkis et al., 2011) and the Analysis Center. In 2011 significant modernization of the "Quasar" complex was finished. As a result all observatories of the "Quasar" network are equipped uniformly: 32-m radio telescope with low noise receivers, frequency and time keeping systems with H-masers (VCH-1003M), control computers, recording terminals Mark5B+, DAS R1002M (Fedotov et al., 2010). New digital DAS R1002M has been designed and created at the IAA RAS. In 2011 correlator control software was improved to obtain almost fully automatical data transfer and processing in e-vlbi mode.

All observatories collocated with GPS and SLR, and Badary has DORIS receiver(Finkelstein, 2012-1).

Since 2010 all domestic observations are correlated using 6-station correlator IAA ”ARC” (Surkis et al., 2010). The data of observations in NGS format are available at IAA ftp-area: `ftp://quasar.ipa.nw.ru/pub/EOS/IAA/ngs`.

3 Russian Domestic Programs of VLBI Observations

All operations within the framework of the ”Quasar” network are are performed as alike as in IVS. Sessions are scheduled by the Technical Consulate once for a year and are approved every month. Observations are carried out at S and X band. Operating Center prepares the file with schedule of observations session. For planning sessions we use NASA/SCED software adopted for LINEX in IAA (Melnikov, 2005) with optimization for EOP, clock parameters and tropospheric parameters. For typical Ru-EOP session stations observe about 50 sources with flux 0.50-10.83 J from the list of 63 sources, about 300 scans. Typical Ru-U contains about 20 scans for about 20 sources with flux 0.25–10.83J from the list of 159 geodetic sources. Ru-U sessions performs with 1-bit sampling and bandwith 8 MHz, data rate is 256 Mbit/s. Ru-E sessions performs with 1-bit data sampling and bandwith 8 MHz, data rate is 512 Mbit/s. Turnaround time for Ru-U sessions is about 2 hours, for Ru-E sessions from 2 till 4 days. The brife summary of the Ru-U and Ru-E session description is presented at the Table 2.

Observational data from 1-hour Ru-U sessions are transmitted to the correlator using e-vlbi data transfer (Finkelstein et al., 2010-1). Calculation of UT1 time series is performed automatically. The results is UT1-UTC time series available at ftp://quasar.ipa.nw.ru/pub/EOS/IAA/eopi-ru.dat. Data of 24-hour sessions are shipped to the IAA correlator on disk modules only from ”Svetloe” observatory. Since April 2013 we use e-vlbi data transfer for the data of 24-hours observations from ”Badary” and ”Zelenchukskaya”. The EOP time series available at ftp://quasar.ipa.nw.ru/pub/EOS/IAA/eops-ru.dat.

Table 2 Specifications of Ru-U and Ru-E sessions

Program	Ru-U	Ru-E
Stations	BdZc(Sv)	SvZcBd
Duration, hours	1	24
Aim	dUT1	EOP
Turn-around time	2 hours	2-4 days
Schedule	daily (20:00UT)	weekly(22:00UT)
Range	X/S	X/S
Scan duration, min	1	1
Sources set	159 (>0.25 Jn)	63 (>0.5 Jn)
Number of sources per session	20	50
Sampling	1-bit	1-bit
Bandwidth, MHz	8(cold), 16 (warm)	8
Data Rate, Mbit/s	256	512
Number of scans	20	300-350
Number of observations	20	1000

4 The results of EOP Determination

For secondary data treatment of Domestic ”Quasar” sessions we use QUASAR (Kurdubov and Gubanov, 2011) and OCCAM/GROSS (Malkin, 2005) software. All reductions correspond IERS Conventions (2003) (McCarthy and Petit, 2004). Celestial coordinate system is fixed by catalog of radio sources ICRF2, Earth coordinate system is fixed by catalog of station positions and velocities obtaining from QUASAR global solution iaa2009a.trf. (Kurdubov and Gubanov, 2011)

We don’t estimate tropospheric gradients in routine ”Quasar” data treatment. The time span from observation till secondary data processing is from 6 hour for Ru-U sessions till 10 days for Ru-E sessions. Sometimes VMF1 (Boehm et al., 2006) and 3-D Atmospheric loading data (Petrov and Boy, 2004) is unavailable to this time, we use this data when they available for recalculation our EOP time series. As this case we use numeric models – Niell mapping function (Niell, 1996) for atmospheric delay and regression model for atmospheric loading account.

Since September 2009 Ru-U sessions are hold with e-data transfer. When ngs-file after correlation data treatment appears at server secondary data processing performs automatically using QUASAR software and special command files.

The accuracy of EOP estimations (rms differences with IERS EOP 08 C04 time series) for Ru-E sessions

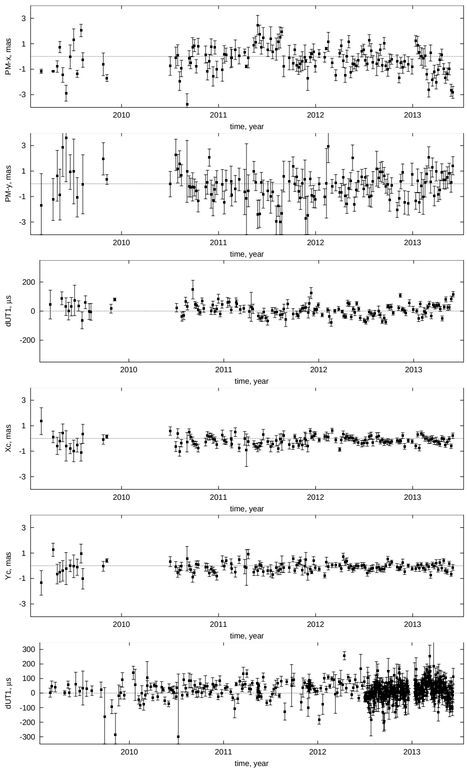

Fig. 1 2009 - 2013: Differences of the individual session estimates IAA minus IERS EOP 08 C04

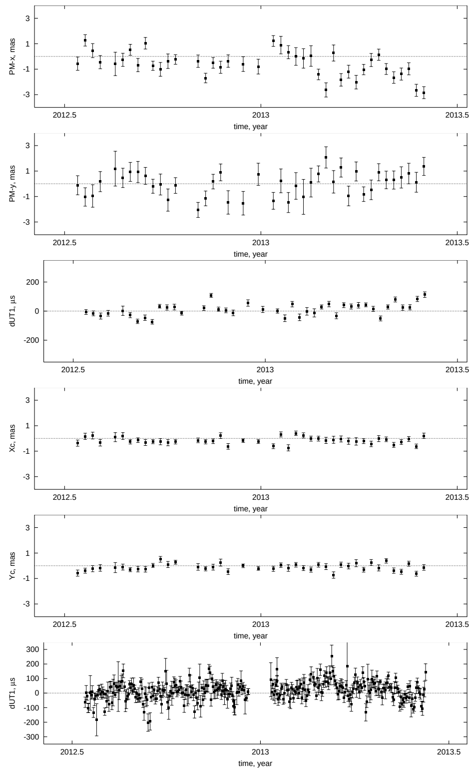

Fig. 2 2012.5 - 2013: Differences of the individual session estimates IAA minus IERS EOP 08 C04

and Ru-U sessions are presented at the Table 3 for all period since August 2006, the Table 4 for observations with Mark5B recorder and the Table 5 contain the results for the period since July 2012 (when we start to observe Ru-U sessions in every day mode) till the end of May 2013.

Differences of between IAA estimations of EOP with time series IERS EOP 08 C04 time series for data with Mark5B registrator (since February 2009) are presented in Fig. 1 and the differences of between IAA estimations of EOP with time series IERS EOP 08 C04 time series for the period since July 2012 are presented in Fig. 2.

EOP	N_{sess}	Bias	RMS
X_p, mas	163	-0.29	1.4
Y_p, mas	163	-0.23	1.6
UT1-UTC,μs	163	13	56
X_c,mas	163	-0.19	0.63
Y_c, mas	163	-0.12	0.61
UT1-UTC Int., μs	505	14	76

Table 3 Statistics of differences with EOP IERS EOP 08 C04 (2006.6 - 2013.4)

EOP	N_{sess}	Bias	RMS
X_p, mas	131	-0.26	1.1
Y_p, mas	131	-0.18	1.2
UT1-UTC,μs	131	10	43
X_c,mas	131	-0.17	0.39
Y_c, mas	131	-0.11	0.38
UT1-UTC Int., μs	479	18	65

Table 4 Statistics of differences with EOP IERS EOP 08 C04 (2009.6 - 2013.4)

EOP	N_{sess}	Bias	RMS
X_p, mas	41	-0.60	0.98
Y_p, mas	41	0.01	0.95
UT1-UTC,μs	41	-0.6	43
X_c,mas	41	0.11	0.27
Y_c, mas	41	-0.16	0.28
UT1-UTC Int., μs	315	16	63

Table 5 RMS differences IAA and EOP IERS EOP 08 C04 series (2012.5 - 2013.4)

Brief history of "Quasar" complex development was presented at (Finkelstein, 2011, 2012-2). In February 2013 we have performed first test of e-vlbi data transfer of 24-hour Ru-E session with from "Badary". Since April 2013 we use e-vlbi for data transfer of 24-hours sessions from "Badary" and "Zelenchukskaya" on regular bases.

5 Future plans

Further development of the ”Quasar” network is connected with VLBI2010 technology. We are planning to install VLBI2010 antennas (RT-13) at ”Badary” and ”Zelenchukskaya” observatories in 2014. VLBI2010 software correlaror snd DAS is under development.

References

A. Finkelstein, E. Skurikhina, I. Surkis, A. Ipatov, I. Rakhimov, S. Smolentsev. Using the quasar VLBI network for the fundamental time-positioning service of the GLONASS space system. In *Astronomy Letters* , Volume 34, Issue 1, pages 59–68, 2008 doi: 10.1134/S1063773708010076.

A. Finkelstein, A. Ipatov, S. Smolentsev, V. Mardyshkin, L. Fedotov, I. Surkis, D. Ivanov, I. Gayazov. The New Generation Russian VLBI Network. In D. Behrend, K. D. Baver, editors, *6th IVS General Meeting Proc.*, pages 161–165. NASA/CP-2004-212255, 2010.

A. Finkelstein, M. Kaidanovskii, A. Salnikov, A. Mikhailov, I. Bezrukov, E. Skurikhina, I. Surkis. Prompt determination of universal time corrections in e-VLBI mode. In *Astronomy Letters*, Volume 37, Issue 6, pages 431–439, 2011 doi: 10.1134/S1063773711060028.

I. Surkis, A. Melnikov, V. Shantyr, V. Zimovsky. The IAA RAS Correlator First Results. In D. Behrend, K. D. Baver, editors, *6th IVS General Meeting Proc.*, pages 167-170. NASA/CP-2004-212255, 2010.

I. Surkis, V. Ken, A. Melnikov, V. Mishin, N. Sokolova, V. Shantyr, V. Zimovsky IAA Correlator Center. In D. Behrend, K. D. Baver, editors, *International VLBI Service for Geodesy and Astrometry 2011 Annual Report*, pages 159–160. NASA/TP-2012-217505, 2012.

L. Fedotov, E. Nosov, S. Grenkov, D. Marshalov. The Digital Data Acquisition System for the Russian VLBI Network of New Generation. In D. Behrend, K. D. Baver, editors, *6th IVS General Meeting Proc.*, pages 400404. NASA/CP-2004-212255, 2010.

A. Melnikov, J. Gipson. Running SKED under Linux. In *Proceedings of the 17th Working Meeting on European VLBI for Geodesy and Astrometry*. INAF, Noto, Italy, pages 131–132, 2005.

Z. Malkin, E. Skurikhina. OCCAM/GROSS software for VLBI data processing for IAA EOP Service. *Communications of IAA, Num. 93*, 1996 (in Russian).

S. Kurdubov, V. Gubanov. Main results of the global adjustment of VLBI observations. *Astronomy Letters, Volume 37, Issue 4, pages 267-275, 2011* doi: 10.1134/S1063773711010063.

A. Finkelstein, A. Salnikov, A. Ipatov, S. Smolentsev, I. Surkis, I. Gayazov, I. Rahimov, A. Dyakov, R. Sergeev, E. Skurikhina, S. Kurdubov. EOP determinations from observations of Russian VLBI-network ”Quasar”. *Procceedings of the 20th EVGA Meeting. 2011, Bonn, pages 8285*

A. Finkelstein, A. Ipatov, I. Gayazov, V. Shargorodsky, S. Smolentsev, V. Mitryaev, A. Diyakov, V. Olifirov, I. Rahimov Co-location of Space Geodetic Instruments at the ”Quasar” VLBI Network Observatories, In D. Behrend, K. D. Baver, editors, *IVS 2012 General Meeting Proc.*, pages 157–160. NASA/CP-2012-217504, 2012.

A. Finkelstein, A. Ipatov, S. Smolentsev, A. Salnikov, I. Surkis, I. Gayazov, E. Skurikhina, S. Kurdubov, I. Rahimov, A. Diakov, R. Sergeev, V. Shpilevsky, A. Melnikov, V. Zimovsky, L. Fedotov, D. Ivanov, V. Mardishkin EOP Determination from Domestic Observations of the Russian VLBI Network ”Quasar”. In D. Behrend, K. D. Baver, editors, *IVS 2012 General Meeting Proc.*, pages 181–185. NASA/CP-2012-217504, 2012.

D. D.McCarthy and G. Petit. *IERS Conventions (2003)*. IERS Conventions (2003). Dennis D. McCarthy and Gérard Petit (eds.), International Earth Rotation and Reference Systems Service (IERS). IERS Technical Note, No. 32, Frankfurt am Main, Germany: Verlag des Bundesamtes für Kartographie und Geodäsie, ISBN 3-89888-884-3, 2004, 127 pp., 2004.

L. Petrov and J.-P. Boy. Study of the atmospheric pressure loading signal in very long baseline interferometry observations. *Journal of Geophysical Research (Solid Earth)*, 109:3405–+, Mar. 2004. doi: 10.1029/2003JB002500.

A. Niell. Global mapping functions for the atmosphere delay at radio wavelengths. emphJournal of Geophysical Research, Vol. 111, Num. B2, pages 3227-3246, 1996.

J. Boehm, B. Werl, H. Schuh. Troposphere mapping functions for GPS and very long baseline interferometry from European Centre for Medium-Range Weather Forecasts operational analysis data. In D. Behrend, K. D. Baver, editors, *Journal of Geophysical Research, Vol. 111*, 2006. doi: 10.1029/2005JB003629.

Sun Corona Electron Densities Derived from VLBI Sessions in 2011/2012

B. Soja, J. Sun, R. Heinkelmann, H. Schuh, J. Böhm

Abstract Twelve IVS R&D sessions in 2011/2012 primarily aimed to increase the sensitivity of VLBI to relativistic phenomena by including observations closer than 15 degrees to the heliocenter. These observations are also affected by the plasma of the Sun corona, a dispersive medium which is the target of our research presented here. Starting with the ionospheric delay corrections derived from two-frequency VLBI measurements, Sun corona electron densities were estimated together with other dispersive effects like instrumental biases and the Earth ionosphere. The results for the R&D sessions were analysed and compared with external information like Sunspot numbers and solar flux indices. The estimated electron densities show good agreement with previous models of the Sun corona obtained by various spacecraft missions.

Keywords Sun corona, Ionosphere, VLBI

1 Introduction

The Sun corona is part of the atmosphere of the Sun, located between the chromosphere and interplanetary medium. It consists of fully ionized gas (i.e. plasma) and is primarily affected by the magnetic field of the Sun. The magnetic field is responsible for temperatures over 1 million K (the exact mechanism being the topic of current research) and the existence of diverse and timely-variable regions. The climatology of the corona follows the 11-year solar cycle (Aschwanden, 2004).

Benedikt Soja, Robert Heinkelmann and Harald Schuh
GFZ German Research Centre for Geosciences. Telegrafenberg, D-14473 Potsdam, Germany
Jing Sun and Johannes Böhm
Vienna University of Technology, Gusshausstraße 27-29, A-1040 Vienna, Austria

One of the most important characteristics of the corona is its electron density N_e. In the undisturbed case, it can be described as decreasing with distance from the Sun, following a power law:

$$N_e(r) = N_0 \cdot r^{-\beta} \tag{1}$$

with r as the distance from the heliocentre in solar radii, N_0 as the (theoretical) electron density at the surface of the Sun and the radial fall-off parameter β.

Depending on the distance from the Sun the model of electron density can also include terms of higher order (Tyler et al., 1977).

Electron density models following (1) have been successfully estimated from measurements of space missions during superior solar conjunctions in the past 45 years (Bird et al., 2012). Here we show the first determination of such a model from VLBI data.

2 Methods

The Sun corona is a dispersive medium for electromagnetic waves. For VLBI observations close to the Sun the effects of the corona need to be taken into account (Shapiro et al., 1977). Other dispersive phenomena affecting VLBI observations are the delays due to the Earth ionosphere and receiver hardware (Kondo, 1991). For the total dispersive contribution to group delay observations in X-band (usually called "ionospheric delay" τ'_{igx}) the following observation equation is applied:

$$\tau'_{igx} = \frac{40.3}{c f_x^2} (\Delta STEC_{corona} + \Delta STEC_{iono}) + \Delta\tau_{inst} \ . \tag{2}$$

Most of all, the delay is dependent on the slant total electron content (STEC) of the Earth ionosphere and the Sun corona. The effective frequency f_x of the X-band and the dispersive instrumental delays τ_{inst} are

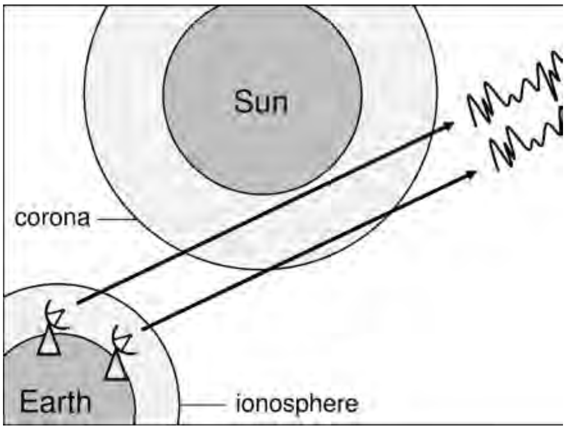

Fig. 1 The ray paths of the two radio telescopes pass through different regions of the Earth ionosphere and the Sun corona.

assumed to stay constant over each 24 hour VLBI experiment. The constant c is the vacuum speed of light and Δ indicates that for the respective quantities the difference between the two radio telescopes is taken. The basic observation configuration is shown in Fig. 1.

For equation (2) the influences of the interplanetary, interstellar and intergalactic media are neglected. This is admissible since in these regions the gradients in electron density are usually negligible in scales of typical baseline lengths (Hobiger et al., 2006). For observations in S- and X-band the higher order terms of the dispersive delay can be neglected (Hawarey et al., 2006).

The STEC can be determined by numerical integration of an electron density model along the ray path:

$$STEC = \int_S N_e ds \approx \sum_S N_e \Delta s \ . \tag{3}$$

In the case of the Sun corona, a power law (Eq. 1) is applied for modelling N_e. For the ionosphere it is assumed that all the free electrons are concentrated in a thin-layer at about the height of the F2 layer. This allows the conversion of the STEC into the vertical total electron content (VTEC) at the ionospheric pierce point (IPP) using a mapping function (Ros et al., 2011):

$$STEC = mf \cdot VTEC' \ . \tag{4}$$

The VTEC at the IPP (geographic coordinates λ', ϕ') can be related to the $VTEC$ above the station by (Hobiger, 2006):

$$VTEC'(\lambda', \phi', t') = (1 + G_{ns}\Delta\phi) \cdot VTEC(\lambda, \phi, t) \ . \tag{5}$$

The difference in latitude is considered by estimating one or two north-south gradients. For our studies we apply two gradients as recommended by Dettmering et al. (2011). Assuming that the ionospheric VTEC distribution co-rotates with the apparent movement of the Sun (360° per day) and that it is invariable during the parameter time interval of about 45 min., differences in longitude can be related to differences in time (Hobiger et al., 2006):

$$t - t' = (\lambda - \lambda')/15 \tag{6}$$

with t in hours and λ in degrees. Referring the observations to time t instead of t' the VTEC above the station can be estimated. In order to achieve redundancy, $VTEC(t)$ is parametrized by piece-wise linear functions. The intervals are chosen in a way that a certain number of observations (n_{obs}) falls in each interval. For our studies a value of n_{obs} = 15 is applied yielding a temporal resolution of VTEC of roughly 45 min.

Another possibility would be to use ionosphere VTEC data in terms of global ionospheric maps from GNSS. At the moment, the precision (2–8 TECU) and temporal resolution of two hours (Ros et al., 2011) are inferior to those of estimating station VTECs with VLBI (about 1 TECU, minimal temporal resolution 30 min., according to Hobiger (2006)).

The left hand side of (2) is the result of a linear combination of the observed group delays in X- and S-band, while the right hand side describes the theoretical delay depending on the unknown parameters. The latter are solved for by minimizing the difference "observed minus computed" in a least-squares sense. The stochastic model is obtained by weighting the observations based on their formal errors, which are provided in NGS files of the International VLBI Service for Geodesy & Astrometry (Schuh and Behrend, 2012).

3 Data

To study the Sun corona with VLBI, observations close to the Sun are necessary. Such observations are sparse before 2002 and non-existing afterwards due to a change of the elongation cut-off angle to 15 degrees introduced within the IVS (cf. Heinkelmann and Schuh, 2009). However, close observations to the Sun are valuable, e.g. for relativistic studies, so the IVS decided to dedicate twelve R&D-sessions in 2011 and 2012 to particularly observing close to the Sun.

The 24 hour sessions were observed by global networks of up to eight telescopes. The scheduling was done similar to the standard R1/R4 sessions, but with the addition of observations closer than 15° elongation. The last seven of these R&D sessions were scheduled

Table 1 The IVS R&D sessions in 2011 and 2012 which include observations close to the Sun. For each session, the minimum Sun elongation, the number of successful observations closer than 15 degrees and the estimated electron densities (1σ) are shown.

Session	Date	Min. Elongation	Obs. < 15°	N_0 $[10^{12}\ \mathrm{m}^{-3}]$
RD1106	Nov 29	3.9°	33	0.5 ± 0.4
RD1107	Dez 06	4.0°	59	1.1 ± 0.4
RD1201	Jan 24	4.8°	21	2.9 ± 1.0
RD1202	Apr 03	5.8°	39	1.3 ± 0.4
RD1203	May 30	10.5°	52	6.1 ± 1.5
RD1204	Jun 19	4.4°	32	1.3 ± 0.7
RD1205	Jul 10	6.1°	186	0.7 ± 0.3
RD1206	Aug 28	3.9° (1.8°)	193	0.5 ± 0.1
RD1207	Sep 25	6.1°	120	0.2 ± 0.7
RD1208	Oct 02	3.9°	103	0.5 ± 0.3
RD1209	Nov 27	4.2°	57	0.1 ± 0.3
RD1210	Dez 11	4.7°	80	2.2 ± 0.5
Weighted mean over all R&D sessions				0.63 ± 0.17

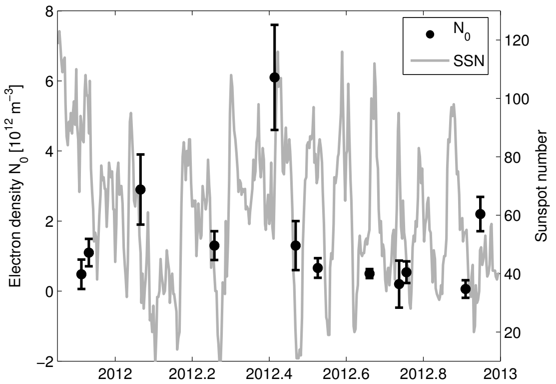

Fig. 2 Electron densities from VLBI compared to daily Sunspot numbers.

using the Vienna VLBI Software (Sun et al., 2011). For the other sessions the scheduling software SKED was used. Table 1 shows the characteristics of each of the sessions, including the elongation of the closest observation and the number of observations which are closer than 15° elongation.

In session RD1206 a radio source with 1.8° elongation was scheduled for observation. Unfortunately, for all scans to this particular source the correlation in S-band failed, making it impossible to derive dispersive corrections. Nevertheless, in the session many observations to another source at 3.9° were successful.

4 Results

For the distances from the heliocentre at which successful VLBI observations to radio sources are available (i.e. ≥ 3.9°elongation), the parameters N_0 and β are highly correlated, making it impossible to estimate both at the same time. Previous models found a value for β between 1.9 and 2.5. For our purposes the parameter was fixed to $\beta = 2$, what equals the theoretical value for constant solar wind velocity (Bird et al., 1994). An outlier test based on the residuals v was applied: all observations with $v/\sigma_v > 5$ were excluded to get more reliable results. Table 1 shows the estimated electron densities N_0 together with their 1σ standard deviations. The largest uncertainty is found for session RD1203. During this session no sources closer than 10 degrees were observed.

During times of high solar activity, higher Sun corona temperature, turbulence and electron density are expected (Bird et al., 1994). The estimated electron densities are therefore compared to indicators for the solar activity. Fig. 2 shows daily relative Sunspot numbers (SSN) together with the electron densities estimated from the twelve R&D sessions. Some sessions show a good temporal agreement, while others diverge. Similar results are obtained when comparing the electron densities to solar flux indices, e.g. the F10.7 index (not shown here).

The differences might be explained by deviations of the Sun corona from a simplified axial model. Sessions with unexpected high or low electron density are analysed in greater detail using images of the Sun, provided e.g. by the X-ray telescope (XRT) on the Hinode spacecraft[1]. For instance, in the case of session RD1106, three sources closer than 15° were observed, one at 4° (1622-253) and the others farther away (11°, 13°). The source 1622-253 was most sensitive for the effects of the Sun corona and the estimated electron density mostly depended on the observations to this source. In Fig. 3 the positions of the sources together with the variable and quiet regions of the Sun are plotted. 1622-253 is located above a region of low solar activity and most likely lower electron density compared to the active regions. This might explain the low value of the estimated electron density in contrast to the high Sunspot number or solar flux.

Effects due to different observation geometries or deficiencies in the model are assumed to have a random impact and are reduced by computing the weighted mean over all available VLBI sessions. The resulting value for N_0 is $(0.63 \pm 0.17)\ 10^{12}\ \mathrm{m}^{-3}$ coming from data obtained during the 14 months in 2011 and 2012. The average solar activity during this time was medium.

This electron density model, representative for the VLBI observations, is compared to previous models derived by measurements to spacecraft during superior

[1] http://www.isas.jaxa.jp/e/enterp/missions/hinode/

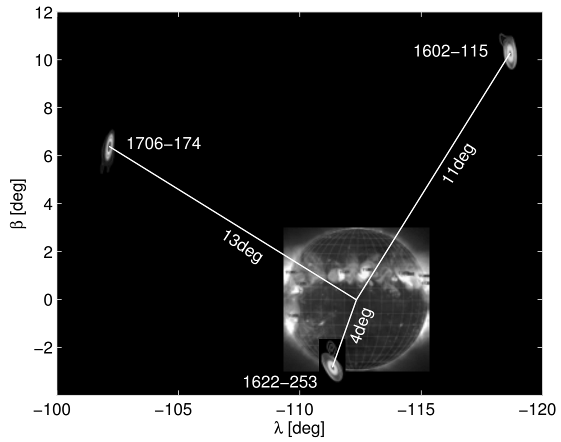

Fig. 3 Source geometry of session RD1106 w.r.t. an out of scale XRT image of the Sun.

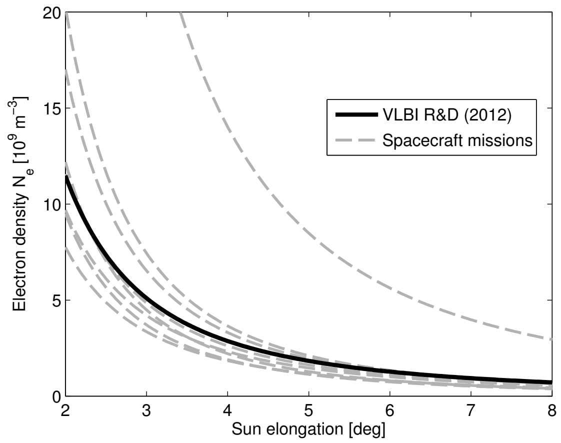

Fig. 4 Comparison between the electron density models from VLBI and various spacecraft missions.

solar conjunctions. Fig. 4 shows the VLBI model along with the models derived from various space probes, such as Mariner 6/7, Viking 1/2, Voyager 2, Ulysses, Mars Express and Rosetta with data collected between 1970 and 2008. The various spacecraft models are from periods of different solar activity. For example the Ulysses conjunctions in 1991 happened during a solar maximum, while the one with Mars Express in 2008 was during very low activity (Bird et al., 2012). The electron density models were accordingly higher and lower, respectively. The VLBI model agrees well with the previous models, especially with those when the data were obtained during medium solar activity.

5 Conclusions and Outlook

For the first time, the electron density of the plasma of the solar corona has been estimated utilising VLBI observations. Good agreement is found when comparing the VLBI model with previous models derived from measurements to spacecraft. The latter have the advantage that they include observations much closer to the Sun (up to 0.8 degrees elongation) and are therefore able to estimate both parameters N_0 and β. The strength of VLBI compared to spacecraft missions is that radio sources are more often in the vicinity of the Sun.

At 11 out of 12 R&D sessions, observations between 4 and 6 degrees elongation were possible. This shows that VLBI could monitor the Sun corona on a daily basis. It should be mentioned that no problems at all (technical problems, extensive loss of signals) occured for observations as close as 4 degrees to the Sun.

In the future, when improved global ionospheric maps will be available, it is planned to test different approaches of separating the effects of the Earth ionosphere and the Sun corona to get more reliable corona electron densities. VLBI2010 will bring interesting new options, such as observations of phase scintillations, which could be used to investigate the turbulence in the Sun corona. The precision and reliability of the dispersive delays determined with VLBI2010 are expected to be significantly higher due to the foreseen broadband delay approach. Thus, we expect a positive impact on the quality of the derived parameters of the Earth ionosphere and Sun corona once VLBI2010 will be in place.

References

M.J. Aschwanden. Physics ff the Solar Corona. Chichester: Springer, 2004.

M.K. Bird, M. Pätzold, B. Häusler, S.W. Asmar, S. Tellmann, M. Hahn, A.I. Efimov, and I.V. Chashei. Coronal radio sounding experiments with the ESA spacecraft MEX, VEX, and Rosetta. *511th WE-Heraeus-Seminar*, Bad Honnef, Germany, 31 Jan - 3 Feb 2012.

M.K. Bird, H. Volland, M. Paetzold, P. Edenhofer, S.W. Asmar, and J.P. Brenkle The coronal electron density distribution determined from dual-frequency ranging measurements during the 1991 solar conjunction of the ULYSSES spacecraft. *Astrophysical Journal*, 426:373–381, 1994.

D. Dettmering, R. Heinkelmann, and M. Schmidt. Systematic differences between VTEC obtained by different space-geodetic techniques during CONT08. *J. Geod.*, 85:443–451, 2011.

M. Hawarey, T. Hobiger, and H. Schuh. Effects of the 2nd order ionospheric terms on VLBI measurements. *Geophys. Res. Lett.*, 32:11, 2005.

R. Heinkelmann and H. Schuh. Very Long Baseline Interferometry: Accuracy limits and relativistic tests. In S. Klioner, P.K. Seidelmann and M. Soffel, eds., *Proceedings IAU Symposium No. 261: Relativity in Fundamental Astronomy: Dynamics, Reference Frames and Data Analysis*, 286–290, 2009.

T. Hobiger, T. Kondo, and H. Schuh. Very long baseline interferometry as a tool to probe the ionosphere. *Radio Sci.*, 41(1):RS1006, 2006.

T. Hobiger. VLBI as a tool to probe the ionosphere. PhD thesis, Vienna University of Technology, published under: *Schriftenreihe der Studienrichtung Vermessung und Geoinformation, Technische Universität Wien*, ISSN 1811-8380, 2006.

T. Kondo. Application of VLBI data to measurements of ionospheric total electron content. *Journal of the Communications Research Laboratory*, 38:613–622, 1991.

C.T. Ros, J. Böhm, and H. Schuh. Use of GNSS-derived TEC maps for VLBI observations. In W. Alef, S. Bernhart and A. Nothnagel, eds., *Proceedings of the 20th Meeting of the European VLBI Group for Geodesy and Astrometry*, 114–117, 2011.

H. Schuh and D. Behrend. VLBI: A fascinating technique for geodesy and astrometry. *J. Geodyn.*, 61:68–80, 2012.

I.I. Shapiro, R.D. Reasenberg, P.E. Macneil, R.B. Goldstein, J.P. Brenkle, D.L. Cain, T. Komarek, A.I. Zygielbaum, W.F. Cuddihy, and W.H. Michael jr. The Viking Relativity Experiment. *J. Geophys. Res.*, 82(28):4329–4334, 1977.

J. Sun, A. Pany, T. Nilsson, J. Böhm, and H. Schuh Status and future plans for the VieVS scheduling package. In W. Alef, S. Bernhart, and A. Nothnagel, eds., *Proceedings of the 20th Meeting of the European VLBI Group for Geodesy and Astrometry*, 44–48, 2011.

G.L. Tyler, J.P. Brenkle, T.A. Komarek, and A.I. Zygielbaum. The Viking Solar Corona Experiment. *J. Geophys. Res.*, 82(28):4335–4340, 1977.

Optimal time lags to use in modeling the thermal deformation of VLBI Antennas

K. Le Bail, J. M. Gipson, J. Juhl, D. S. MacMillan

Abstract One of the most significant effects on VLBI antennas is thermal expansion which can change the height of the VLBI reference point by as much as 20mm. In this paper, we investigate how using a thermal expansion model in VLBI processing improves the solution, as well as the optimal time delay for the variations in temperature to introduce for the steel telescope structure and for a concrete structure. We use the software *Solve* and the conventional model of Nothnagel (2009) implemented in *Solve*. We compare different solutions processed using the R1 and R4 sessions from January 2002 to March 2011: 1) not using the thermal expansion model, 2) using it with no time delay and then 3) different time delays. We show that using the thermal deformation model improves the baseline length repeatability of the solutions by more than 1mm and for more than 75% of the baselines, as well as reduces the WRMS per station.

Keywords Thermal Deformation modeling, Time lags

1 Introduction

Thermal expansion of VLBI antennas has been shown to be a significant effect. Nothnagel (2009) defined a conventional model in his paper "Conventions on thermal expansion modeling of radio telescopes for geodetic and astrometric VLBI". This model assumes a time delay for the variations in measured air temperature to affect the antenna, which depends on the telescope structure and its component, and suggests the time lag of 2 hours for the steel telescope structure and 6 hours for the concrete foundation. The 2-hour time lag was determined by Nothnagel et al. (1995) in studying the VLBI station at Hartebeesthoek. The 6-hour time lag for the foundation was found by Elgered and Carlsson (1995) in studying the VLBI station at Onsala (20-m antenna).

In this study, we investigate what time lags are optimal. We modify the thermal expansion model in *Solve* to use arbitrary time lags for the antenna and the foundation. We compared different solutions and look at the WRMS of the solution per baseline, as well as the average per station to identify systematic effects.

2 Studied VLBI solutions

The set of data used consists of 932 R1 and R4 sessions available from January 2002 to March 2011. During this period the R1's and R4's used nineteen stations.

We ran solutions with *Solve* using different options. The first solution, called $NoTD$, is processed using no thermal deformation model. The second solution, called T_{avg}, is processed using the thermal deformation model with session-based average temperatures from the databases (recorded onsite when available or constant default value otherwise). We then ran a series of solutions where we independently varied the antenna and foundation time lags. These solutions used G-ECM temperatures (homogeneous set of temperature time series derived from the ECMWF ERA-Interim reanalysis model, see Juhl et al. (2012) for details) and different time lags for the antenna (Δt_a) and the foundation (Δt_f) ranging from 0 to 9 hour. Each of the 100 solutions corresponds to a pair (Δt_a, Δt_f). These solutions are called $GECMXY$, where X is Δt_a and Y is Δt_f.

Karine Le Bail, John M. Gipson and Daniel S. MacMillan
NVI, Inc., Code 698.2, Goddard Space Flight Center, Greenbelt, MD 20771, United States
Johanna Juhl
Chalmers University of Technology, Gothenburg, Sweden

	$NoTD$ - T_{avg}	$NoTD$ - $GECM00$	$NoTD$ - $GECM26$
> 0	74.3%	74.3%	75.0%
= 0	24.3%	22.2%	22.9%
< 0	1.4%	3.5%	2.1%
Max. value	1.23mm	1.26mm	1.27mm

Table 1 Percentage of baselines with improvement and maximum value.

3 Using the Thermal Deformation Modeling

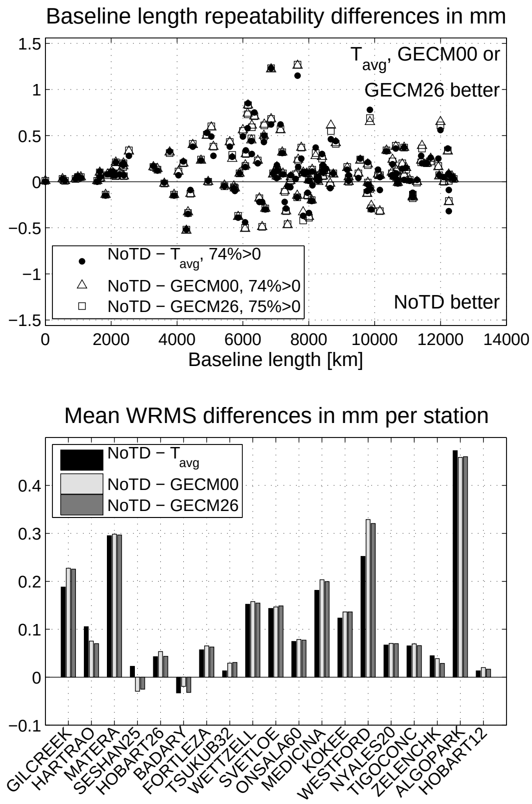

Fig. 1 Differences in baseline length repeatability (top) and mean WRMS differences over all baselines for each station (bottom) between using no thermal deformation model in *Solve* ($NoTD$) and using the thermal deformation model with the Average *Solve* option T_{avg} (points), or using the thermal deformation model with G-ECM temperature and no time lags $GECM00$ (triangles), or using the thermal deformation model with G-ECM temperature and (2,6) time lags $GECM26$ (squares).

We compare the solutions T_{avg}, $GECM00$ and $GECM26$ with the solution $NoTD$. The $GECM26$ corresponds to the conventions in Nothnagel (2009). Figure 1 and Table 1 show that using the thermal deformation with session-based average temperatures from the databases T_{avg}, or G-ECM temperatures with (0,0) or (2,6) as time lags ($GECM00$ and $GECM26$) improves the VLBI solution. The baseline length repeatability of the solutions shows an improvement of up to 1.27mm and for up to 75% of the baselines. The average WRMS (length repeatability) of all stations, except Seshan25 and Badary, are reduced by up to 0.47mm (Algopark), except for Seshan25 and Badary.

4 Optimal time lags for Δt_a and Δt_f

In this section, we look at the $GECMXY$ solutions in detail to determine the optimal time lags for the antenna (Δt_a) and the foundation (Δt_f).

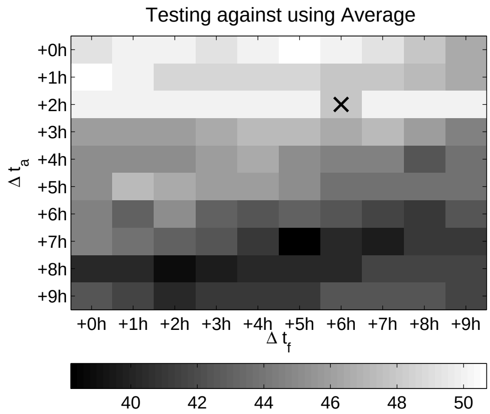

Fig. 2 Percentage of baselines with strictly positive WRMS reduction when using G-ECM temperature with different time lags, versus using the Average option in *Solve* (T_{avg}). Each box correspond to one solution. Example: the box (0,0) corresponds to $GECM00$. The cross indicates the value (2,6) which is the conventions value from Nothnagel (2009).

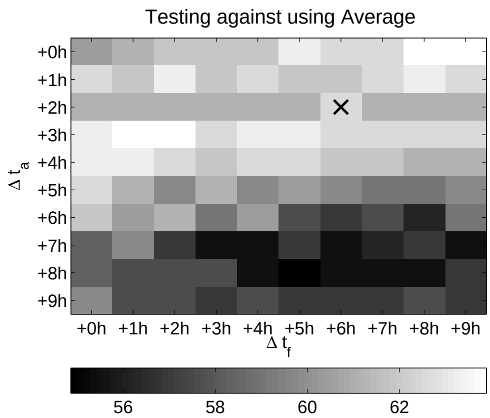

Fig. 3 Percentage of baselines with positive or equal to 0 WRMS reduction when using G-ECM temperature with different time lags, versus using the Average option in *Solve* (T_{avg}).

In Figures 2 and 3, we compare the percentage of baselines with WRMS reduction when using G-ECM temperature with or without time lags, against using the Average option in *Solve* (T_{avg}). The conventional values from Nothnagel (2009) are not the optimal values, but the difference in percentage is relatively small: when considering only the strictly improved baselines, the percentage of improvement for the value (2,6) is 47.9% while the percentage for the optimal time lags values is 50.7%; and when considering the improved or unchanged baselines, the percentage for the value (2,6) is 62.5% while the optimal gives 63.9%.

In Figure 4, we look at the impact of varying one time lag when the other is fixed. In Figures 2, 3 and 4, we see that the time lag for the antenna should preferably be 2 hours or less. When considering a fixed time lag for the antenna (see Figure 4), varying the time lag for the foundation does not significantly modify the percentages.

We expect larger antennas to be more affected by thermal deformation than smaller ones. To see if this is so, we looked at different parameters that describe an antenna (antenna diameter, foundation height and depth, etc.) and plotted them versus the reduction in WRMS. We found significant correlation between reduction of WRMS and two of these parameters (see Figure 5).

The correlation with the height of foundation reaches 0.56, when the correlation with the distance from the movable axis to the antenna vertex reaches 0.59.

We determined the optimal time lag for the antenna for each of the nineteen stations. The correlation between the optimal time lag for the antenna and the antenna diameter is 0.51, suggesting that the bigger the antenna is, the slower it expands (see Figure 6).

5 Conclusions and discussion

Using the thermal deformation modeling significantly improves the VLBI solutions. 1) The time lag for the antenna is optimal when it is equal to 0, 1 or 2 hours; 2) When studying the time lag for the foundation, the results are insensitive to the time lag used. We believe the reason for this is that the foundation structure is much smaller than the steel part. Preliminary results show significant correlations between 1) the maximum WRMS improvement and the height of the foundation, 2) the maximum WRMS improvement and the distance from movable axis to antenna vertex, and 3) the optimal time lag for the antenna and the antenna diameter. To confirm these conclusions in further research, we will run a series of solutions where we vary the time lags for a single antenna at a time, keeping the others fixed.

References

G. Elgered and T. R. Carlsson. Temperature Stability of the Onsala 20-m Antenna and Its Impact on Geodetic VLBI. In Proceedings of the 10th working meeting on European VLBI for geodesy and astrometry, pages 69–78, 1995.

J. Juhl, K. Le Bail, J. Gipson, and D. MacMillan. Improving VLBI processing by using homogeneous data for pressure and temperature. In Proceedings of the 7th IVS General Meeting, 2012.

A. Nothnagel, M. Pilhatsch, and R. Haas. Investigations of Thermal Height Changes of Geodetic VLBI Radio Telescopes. In Proceedings of the 10th working meeting on European VLBI for geodesy and astrometry, pages 121-133, 1995.

A. Nothnagel. Conventions on thermal expansion modelling of radio telescopes for geodetic and astrometric VLBI. *J. Geodesy*, 83(8):787–792, 2009.

J. Wresnik, R. Haas, J. Boehm, and H. Schuh. Modeling thermal deformation of VLBI antennas with a new temperature model. *J. Geodesy*, 81:423–431, 2007. doi: 10.1007/s00190-006-0129-2.

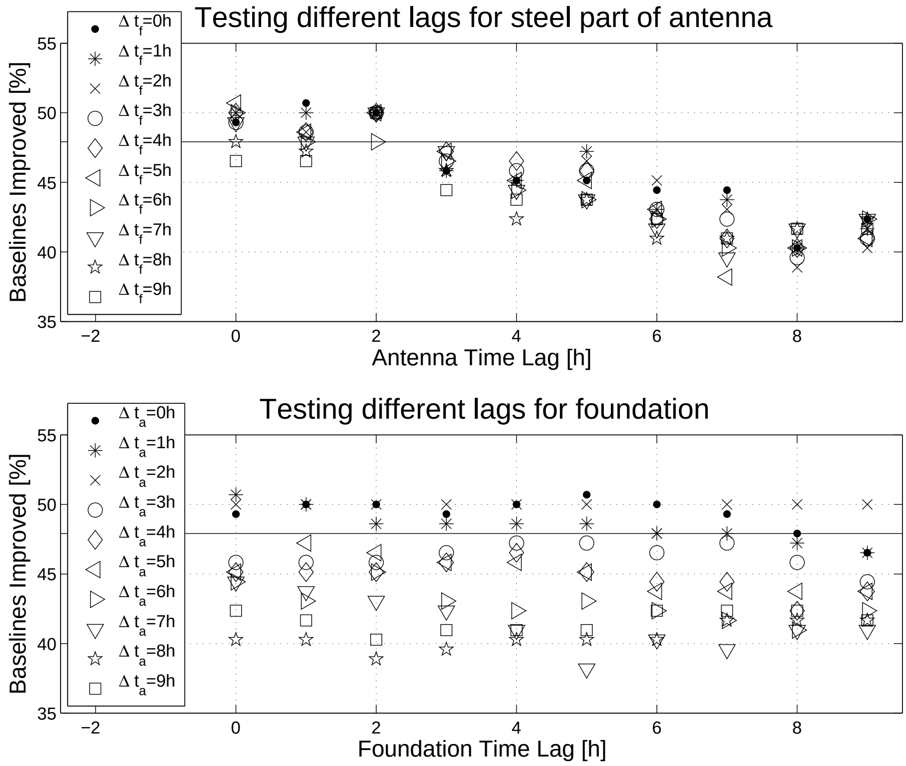

Fig. 4 Percentage of baselines with improved WRMS when using the thermal deformation modeling with different time lags compared to using the thermal deformation modeling with a session-based Average temperature from the databases (T_{avg}). Top: Δt_f is fixed, Δt_a is varying. Bottom: Δt_a is fixed, Δt_f is varying.

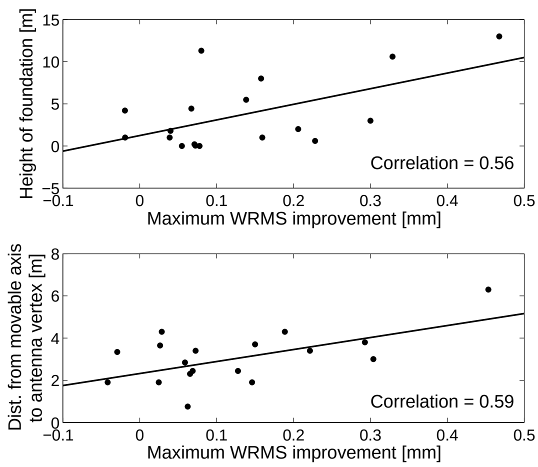

Fig. 5 Correlation between the maximum WRMS improvement per station for all time lags and the height of the foundation (top), or the distance from the movable axis to the antenna vertex (bottom).

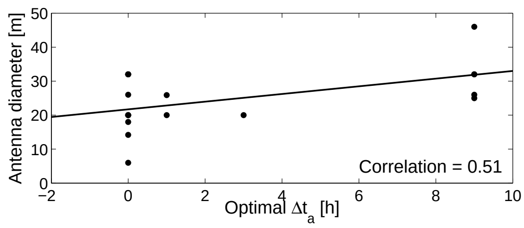

Fig. 6 Correlation between the optimal time lag for the antenna and the antenna diameter.

Activities and Products at IVS combination center at BKG

S. Bachmann, M. Lösler

Abstract The IVS combination center is primarily responsible to provide rapid EOP products based on observation campaigns twice a week and a long-term EOP series which is updated four times a year. Besides EOP products, methods and analysis of combined station coordinates and source positions are evolving and new products are developed in order to expand the range of combined VLBI products. Within the last year the combination center continuously worked on several improvements and refinements of the combination procedure: outlier test have been improved, the detection of unsuitable sessions in order to improve the stability of the results, the modeling of station coordinates of the reference frame generation and the data presentation on the combination centers website. Besides the routine combination of 24h VLBI sessions, several other projects have been developed, e.g. the preparation of the latest VLBI reference frame (VTRF) including the calculation of station height variations and baseline lengths generation derived by the combination of station coordinates. The combination center is furthermore intensely working on the combination of source coordinates and on providing user friendly online analysis tools on the combination centers website in order to meet the user requirements.

Keywords Combination, Station Coordinates, VLBI, VTRF

Sabine Bachmann, Michael Lösler
BKG, Federal Agency for Cartography and Geodesy, Richard-Strauss-Allee 11, D-60598 Frankfurt am Main, Germany

1 Activities and Products

1.1 Rapid solution

The rapid solution is a session-wise combined product of VLBI observations. Actually six IVS Analysis Centers (AC) submit Sinex files containing station coordinates, EOP and (for most of the ACs) source positions in terms of normal equations of 24h VLBI observations. The Sinex files can be found at `ftp://ivs.bkg.bund.de/pub/vlbi/ivsproducts/daily\_sinex`. A pre-analysis process transforms the normal equations to equal apriori values and equal epochs, before the normal equations are stacked and inverted to generate a combined solution. A detailed description of the combination process can be found in Böckmann et al. (2010). The combined solution is submitted in the IVS data center and the results are presented at the IVS combination center homepage at `http://ccivs.bkg.bund.de/rapid`. For a detailed analysis of the combined solutions, a web tool has been implemented which allows comparisons between the individual solutions and the combined solution as well as external comparisons to C04 series and IGS EOP series. The analysis tool offers to select interactively a time span and one or more ACs and - optionally - an error bar plot. A table with statistic values and a residual plot is generated as shown in Figure 1.

1.2 Quarterly solution

The IVS regularly provides a combined quarterly solution which includes all available 24h sessions at the IVS data center[1]. A ”reprocessing” of the IVS sessions

[1] `ftp://ivs.bkg.bund.de/pub/vlbi/ivsproducts/daily\_sinex`

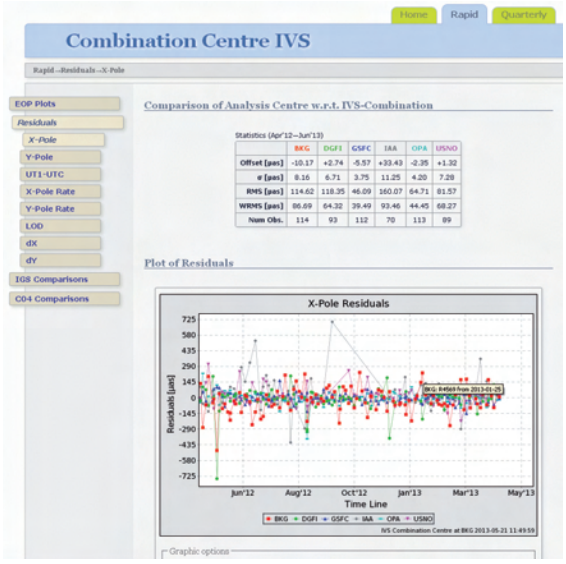

Fig. 1 Screenshot of X-Pole residuals for rapid solutions.

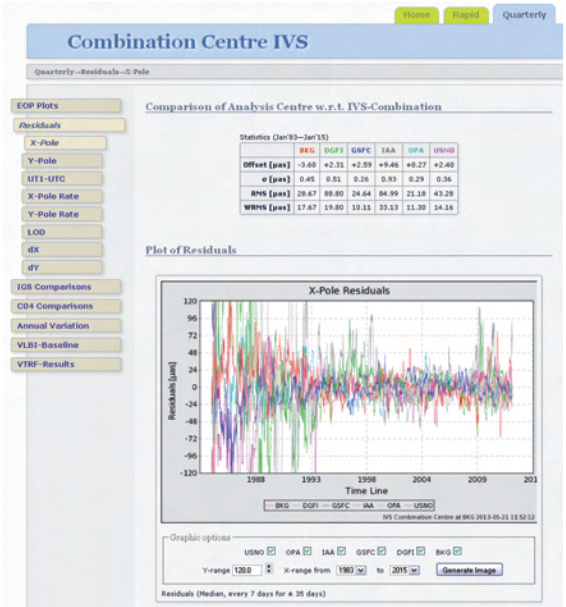

Fig. 2 Screenshot of X-Pole residuals for quarterly solutions.

back to the 1980s until now aims to generate a consistent long term EOP series regarding apriori values, outlier test etc. The combination procedure is in general similar to the rapid solution. Products of the quarterly solutions are EOP series[2], a terrestrial reference frame based on VLBI observations (VTRF) and station coordinates products like baseline lengths and annual height variations. Figure 2 shows a screenshot of the web tool for EOP residuals of the quarterly solution.

1.3 VTRF

The regular generation of a TRF based on VLBI observations contains station coordinates and velocities of VLBI stations and is used as common apriori value for the individual Analysis Center (AC) solution. The quality of the apriori values for station coordinates directly influences the quality of the network and thus the quality of the resulting EOPs. This is especially important for new VLBI stations and stations which underwent major displacements (e.g. earthquakes). A regular generation of a VTRF allows to react appropriate and with a short delay to these kinds of network changes and to provide new coordinates as soon as enough observations are available for the concerned station. This is one of the advantages of a VTRF compared to the ITRF with an update interval of several years. In the latest VTRF (IVS_TRF2012d.SSC.txt[3]) several new stations have been included, e.g. YARRA12M, HOBART12 and KATH12M, as well as new coordinates for earthquake affected stations: TIGOCONC and TSUKUB32. Figures 3 shows plots of the Y-component time series of KATH12M with observation data until 12/2011 (left) and with data until 12/2012 (right).

Station positions are used for further investigations of the combination solution, like significance tests or the visualization of the annual height variations of the station (see section 1.4).

If new antennas are built on existing sites - this kind of set-up will increase with the upcoming realization of the VLBI2010 initiative - a F-Test (also called significance test) can be applied. This test can be used to decide whether a station velocity has been determined accurate enough, or if the time series is still too short and more observations are needed for this specific station. Equation 1 gives the basic formulas for the significance test. The H_0-Hypothesis is, that the new telescope undergoes the same velocity as the already existing telescope.

$$T = \frac{\mathbf{d}^T \mathbf{Q}_{dd}^{-1} \mathbf{d}}{n} \sim F_{n,\infty,1-0.001} \quad | \quad H_0 \qquad (1)$$

Where $\mathbf{d} = \mathbf{v}_2 - \mathbf{v}_1$, $\mathbf{Q}_{dd} = \mathbf{Q}_{\mathbf{v}_1\mathbf{v}_1} + \mathbf{Q}_{\mathbf{v}_2\mathbf{v}_2}$, v_1, v_2 = station velocities for station 1 and 2 respectively and n = numbers of test relevant components.

[2] `ftp://ivs.bkg.bund.de/pub/vlbi/ivsproducts/eops`

[3] `http://ccivs.bkg.bund.de/quarterly/vtrf`

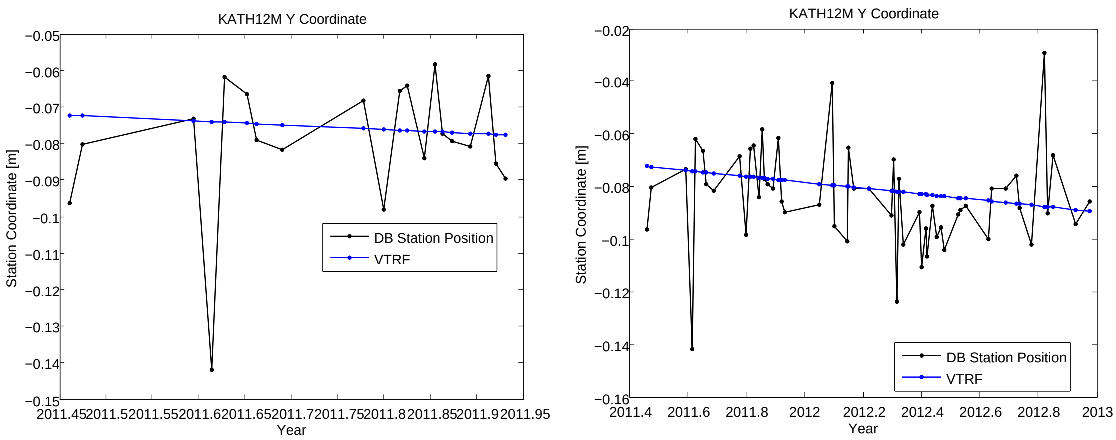

Fig. 3 KATH12M Y-component comparison: observations until 12/2011 (left) and 12/2012(right).

Table 1 shows exemplary the station velocities for Hobart12 and Hobart26 in North, East and Height component. The test statistics of the significance test (T) and the quantile of the F-distribution (F) for a level of significance of 0.1% are given in Table 2. The F-test is applied for horizontal components (North and East), for vertical component (Height) and for all three components. In this example the F-test rejects the H_0-Hypothesis for all components. The number of observations of station Hobart12 is assumed to be too short to estimate appropriate station velocities.

Table 1 Velocities for station Hobart12 and Hobart26.

Component	Hobart12	Hobart26
v_N [m/y]	0.024	0.020
v_E [m/y]	0.061	0.055
v_H [m/y]	-0.002	-0.001

Table 2 Test statistics (T) and quantile of F-distribution (F)for station velocities for Hobart.

Components	T	F
horizontal	69.94	6.91
vertical	29.9	10.83
all	48.39	5.42

1.4 Annual Variation

The station time series which have been generated within a quarterly solution are used to study systematic effects of the station height component.

In order to identify outlier sessions, the robust session-wise outlier test has been extended to a global outlier test which comprises every combined session.

Figure 4 shows a screenshot of the annual variation of the height component. The station plot uses coordinate data calculated on the basis of the latest VTRF and stored in a database.

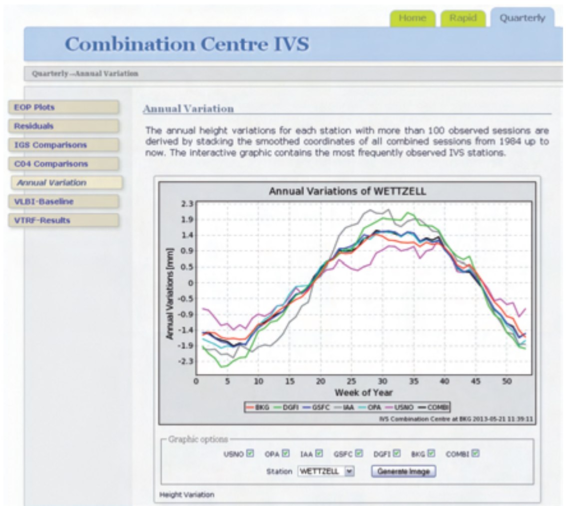

Fig. 4 Screenshot of annual variations web analysis tool.

1.5 Baseline Lengths

Another product which is derived by the station coordinates are baseline lengths. The baselines are generated by a web service which uses the station coordinates stored in a database. The user can interactively

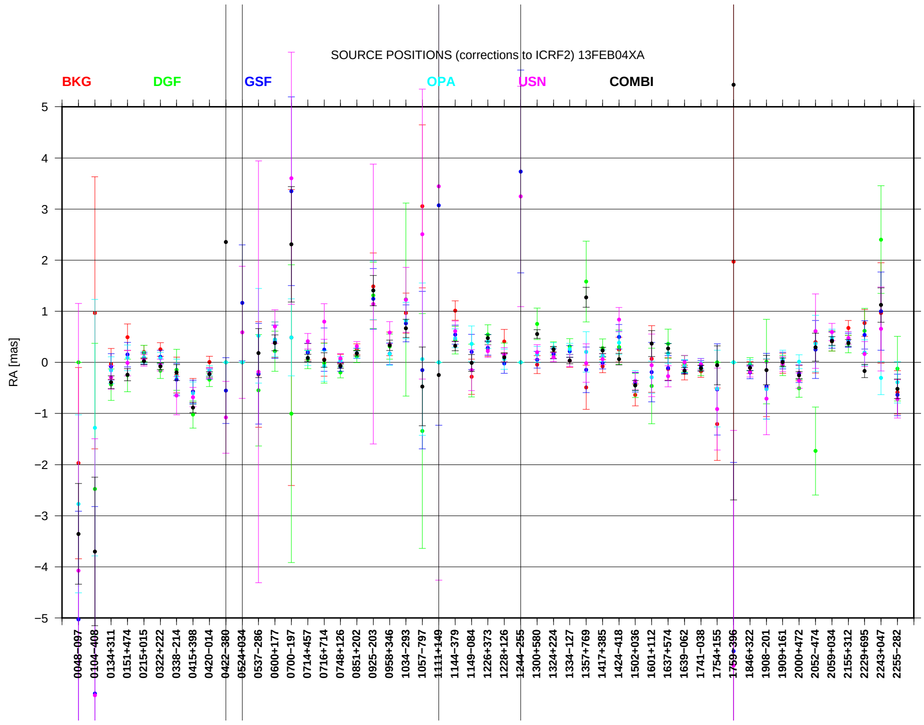

Fig. 5 Residuals of combined sources of Session 13FEB04XA (R1571) w.r.t. to ICRF 2.

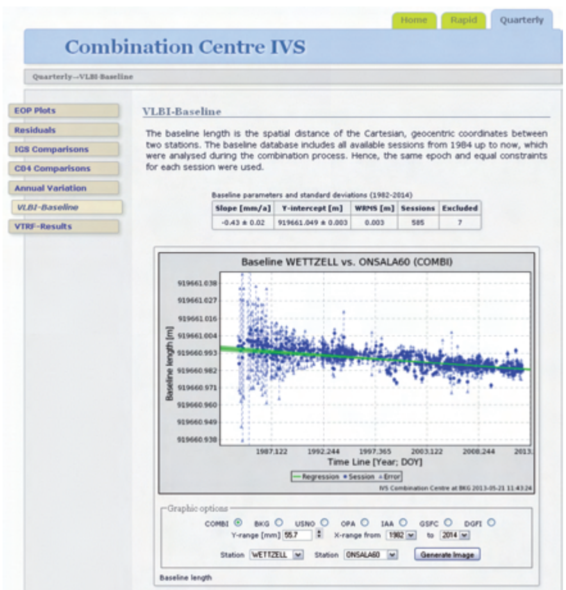

Fig. 6 Screenshot of baseline lengths web analysis tool.

choose the station and the type of solution (individual or combined), as well as the time span and a scale for a zooming function. The results are statistical values like slope $[mm/a]$, Y-intercept $[m]$, WRMS $[m]$ and the number of excluded sessions based on a median outlier test (ref. Bachmann and Lösler (2012)) and a plot of the baseline lengths.

A screen shot of the baseline lengths site is shown in Figure 6 and the web tool can be found at `http://ccivs.bkg.bund.de/quarterly/baseline`.

1.6 Source positions

First steps have been taken to generate a combined solution of source positions. Currently, 5 ACs out of 6 are providing source positions in the Sinex files. These additional information has not been used for the combination of the rapid sessions so far. The combination procedure has been extended for two source parameters (right ascension and declination); format problems have been solved and first source position have been combined successfully. Results will be published on the Combination Centers website.

Figure 5 shows an example of the residuals of the combined solution and the individual solution in comparison to ICRF 2 for right ascension (RA). The plot shows a good agreement between the individual solutions and the combined solution within a few μas for most of the sources.As the number and choice of sources for the analysis differs between the ACs, not all observed sources of one sessions have been analyzed.

This leads to significant larger uncertainties for sources which have not been analyzed by all ACs.

2 Further Plans

Upcoming activities will be the combination of source positions including the definition of a product and the adequate presentation of the results on the website.

References

S. Bachmann and M. Lösler. IVS combination center at BKG - Robust outlier detection and weighting strategies. In D. Behrend and K.D. Baver, editors, *IVS 2012 General Meeting Proceedings*of *NASA/CP-2012-217504*, pages 266–270, Madrid, 2012.

S. Böckmann, T. Artz, A. Nothnagel and V. Tesmer. International VLBI Service for Geodesy and Astrometry: Earth orientation parameter combination methodology and quality of the combined products. In *Journal of Geophysical Research*, Volume 115, 2010.

On Application of the 3-Cornered Hat Technique to Radio Source Position Catalogs

Z. Malkin

Abstract Assessment of the stochastic errors of the radio source position catalogs derived from VLBI observations is important for such tasks as estimating the quality of the catalogs, their weighting during combination, etc. One of the widely used methods for estimation of the catalog stochastic errors is the 3-cornered hat technique. A critical point of this method is the proper accounting for the correlations between the compared catalogs. In this paper, we discuss a new approach to solve this problem based on pair comparison of several catalogs. To compute the correlation between two given catalogs, first the differences between these catalogs and a third arbitrary catalog are computed. Then the correlation between these two sets of differences is considered as an estimate of the correlation between catalogs under investigation. Using several arbitrary catalogs several such estimates can be obtained. The average value of these estimates is taken as a final estimate of the desired correlation between two first catalogs.

Keywords VLBI, IVS, Radio source position catalogs, position random errors, catalog comparison

1 Introduction

So called "3-cornered hat" method (3CH) was originally developed for estimation of the stability of frequency standards (Gray and Allan, 1974). It was then applied for investigation of the noise level of various data, in particular, astronomical and geodetic time series and radio source position catalogs. However, despite this method is widely used, its application is not straightforward because it requires a reliable estimate of the correlations between series under investigation. Neglecting correlations often produces unacceptable results, like negative variances. In this work, we investigate a new possibility to estimate correlations between radio source position catalogs (RSC) obtained from VLBI observations.

Zinovy Malkin
Pulkovo Observatory, St. Petersburg State University, Pulkovskoe Sh. 65, St. Petersburg 196140, Russia; e-mail: malkin@gao.spb.ru

2 3-cornered hat method

In original formulation, the 3CH method is applied to three series of measurements, which allows us to write the following system of three equations for the pair differences between the series supposing they are uncorrelated: Given a set of three pairs of measurements for three independent frequency sources a, b and c whose variances add:

$$\begin{aligned} \sigma_{12}^2 &= \sigma_1^2 + \sigma_2^2 , \\ \sigma_{13}^2 &= \sigma_1^2 + \sigma_3^2 , \\ \sigma_{23}^2 &= \sigma_2^2 + \sigma_3^2 . \end{aligned} \tag{1}$$

with solution

$$\begin{aligned} \sigma_1^2 &= (\sigma_{12}^2 + \sigma_{13}^2 - \sigma_{23}^2)/2 , \\ \sigma_2^2 &= (\sigma_{12}^2 + \sigma_{23}^2 - \sigma_{13}^2)/2 , \\ \sigma_3^2 &= (\sigma_{13}^2 + \sigma_{23}^2 - \sigma_{12}^2)/2 . \end{aligned} \tag{2}$$

For an arbitrary number of series M, one can use the following solution derived by Barnes (1992).

$$\begin{aligned} \sigma_i^2 &= \frac{1}{M-2}\left(\sum_{j=1}^{M} \sigma_{ij}^2 - B\right) , \\ B &= \frac{1}{2(M-1)} \sum_{k=1}^{M} \sum_{j=1}^{M} \sigma_{kj}^2 , \\ \sigma_{ii} &= 0,\ \sigma_{ij} = \sigma_{ji} . \end{aligned} \tag{3}$$

Although useful for determining the individual stabilities of units having similar performance, the method may fail by producing negative variances for units that have widely differing stabilities, if the units are correlated, or for which there is insufficient data. With correlations, the system to be solved consists of the equations:

$$\sigma_{ij}^2 = \sigma_i^2 + \sigma_j^2 - 2\rho_{ij}\sigma_i\sigma_j\,, \qquad (4)$$

The key point is to obtain a reliable estimates of ρ_{ij}.

3 Application to RSC

Several developments in using the 3CH for RSC made since the 1990s in the Main Astronomical Observatory (MAO) of the National Academy of Sciences, Ukraine (Molotaj et al., 1998; Bolotin and Lytvyn, 2010). In these papers, several 3CH modifications were tested, all based on analysis of differences between the pairs of input RSCs and combined one. To compute correlations between three catalogs Molotaj et al. (1998) first compute an averaged catalog. Then the differences between input and average catalogs are calculated. For the coefficient of correlation ρ_{ij} between i-th and j-th catalogs, the correlation between the differences of these catalogs and the average one is accepted. As noted by Bolotin and Lytvyn (2010), this approach has some shortcomings connected with very different errors of source positions and position outliers. They developed a modified method based on combined processing of the differences between the input and average catalogs. In case of three compared catalogs, such an approach allows to obtain the correlations between them. However, in both cases, the computed correlation coefficients may have a bias depending on the method of computation of the average catalog and some other factors. Besides, both MAO approaches are intended for comparison of three catalogs only.

In this study, we tested another method for computation correlation between catalogs for arbitrary number of catalogs greater than 3, and without using of an arbitrary averaged catalog. The computational procedure is the following. Let we have n catalogs, and we want to compute correlation between each pair of catalogs. First we select common sources in all the catalogs, which will be used for further analysis. It may be all common sources or common ICRF defining sources, or other selection depending on the goal of the study.

Now let us consider i-th and j-th catalogs. At the first step we compute the differences between each of these two catalogs with all k-th catalogs, $k = 1,...,n, k \neq i, k \neq j$. After that for each k we compute correlation $Corr(\Delta_{ik},\Delta_{jk})$ between catalog differences $\Delta_{ik} = Cat_i - Cat_k$ and $\Delta_{jk} = Cat_j - Cat_k$, where Cat_i, Cat_j, Cat_k are the common source positions in i-th, j-th anh k-th catalogs respectively. Computations are made separately for right ascension (RA) and declination (DE). RA differences are normally multiplied by $\cos(DE)$. Here $Cat_i, Cat_j, Cat_k, \Delta_{ik}, \Delta_{jk}$ are vectors of dimension equal to the number of common sources selected as noted above. Averaged Δ_{jk} value over all k is considered as an approximation to correlation ρ_{ij} between i-th and k-th catalogs.

The results of this computation are presented in Table 1. One can see some features of the correlations:

- correlation in RA and DE are very similar, which confirms results of other authors;
- discrepancies between the columns show discrepancies between corresponding catalogs confirmed by the WRMS;
- there is no clear dependence on the software used.

4 Conclusions

Proposed method of computation of the correlations between RSCs can provide a reasonable estimates of correlations between radio source position catalogs in a case of sufficiently large number of compared catalogs. It is expected that the more catalogs are used, the more accurate estimates of the correlations between them can be obtained. However, more supplement investigations are needed, in particular, of the impact of the large-scale systematic differences between RSCs.

References

J. A. Barnes. *The Analysis of Frequency and Time Data*. Austron, Inc., 1992.

S. L. Bolotin and S. O. Lytvyn. Comparison of the Combined Catalogues RSC(GAOUA)05 C 03 and RSC(PUL)06 C 02 with the Current Realization of the International Celestial Reference Frame (ICRF). *Kinematika i Fizika Nebesnykh Tel*, 26:41–42, 2010.

J. E. Gray and D. Allan. A Method for Estimating the Frequency Stability of an Individual Oscillator. *28th Annual Symposium on Frequency Control*, p. 243–246, 1974. doi: 10.1109/FREQ.1974.200027.

O.A. Molotaj, V. V. Tel'nyuk-Adamchuk, and Y. S. Yatskiv. Celestial reference frame RSC (GAOUA) 98 C 01. *Kinematics and Physics of Celestial Bodies*, 14:393–399, 1998.

Table 1 Correlations between RSC differences $Corr(\Delta_{ik},\Delta_{jk})$ approaching correlation between i-th and j-th catalogs shown in the first column; the next 7 columns corresponds to k-th catalog. For each pair of catalogs, the first line is related to right ascension and the second line is related to declination.

Catalogs	Catalog k							Mean
i j	AUS	BKG	GSF	IAA	MAO	OPA	USN	
AUS BKG			0.0259	0.1870	0.1199	0.0057	0.0159	0.0709
			−.0807	0.1533	0.0604	−.1081	0.1137	0.0277
AUS GSF		−.1868		0.2932	0.1493	−.0173	0.0302	0.0537
		−.2932		0.3056	0.1381	−.1742	0.1392	0.0231
AUS IAA		−.1723	−.0909		0.1013	0.0414	0.0533	−.0134
		−.1807	0.0087		0.0346	−.0723	0.1498	−.0120
AUS MAO		−.1934	−.1408	−.3258		0.0470	0.0709	−.1084
		−.2939	−.1606	−.3361		0.0500	0.2325	−.1016
AUS OPA		−.2004	−.1317	−.3114	−.1720		0.0565	−.1518
		−.3461	−.3034	−.3820	−.2157		0.2801	−.1934
AUS USN		−.2059	−.1595	−.3318	−.1929	−.0722		−.1925
		−.2208	−.0670	−.2261	−.1303	0.0389		−.1211
BKG GSF	0.8861			0.6182	0.7319	0.2891	0.5264	0.6103
	0.9473			0.6901	0.7355	0.4078	0.6137	0.6789
BKG IAA	0.6918		−.2146		0.5439	0.2419	0.3826	0.3291
	0.8501		−.2247		0.5640	0.3013	0.6202	0.4222
BKG MAO	0.9338		−.0243	−.4356		0.0391	0.3737	0.1773
	0.9182		−.0233	−.3848		0.1063	0.5263	0.2285
BKG OPA	0.9553		−.0305	−.5838	−.7074		0.5047	0.0277
	0.9503		0.0832	−.6311	−.6825		0.6572	0.0754
BKG USN	0.9546		−.2769	−.5805	−.7059	−.3158		−.1849
	0.9278		0.0039	−.4490	−.5252	−.0821		−.0249
GSF IAA	0.8597	0.5391			0.5383	0.1396	0.4398	0.5033
	0.9131	0.5375			0.5779	0.2329	0.5475	0.5618
GSF MAO	0.8623	0.6230		−.7176		0.0242	0.6252	0.2834
	0.9239	0.6336		−.6057		0.1718	0.5734	0.3394
GSF OPA	0.8373	0.9463		−.9694	−.9470		0.9209	0.1576
	0.9452	0.9414		−.9484	−.9336		0.7672	0.1544
GSF USN	0.8316	0.6626		−.8019	−.8209	−.2426		−.0742
	0.9255	0.6911		−.6795	−.7137	−.1620		0.0123
IAA MAO	0.6505	0.4284	0.1595			0.1563	0.4145	0.3618
	0.8170	0.5258	0.2652			0.2925	0.6425	0.5086
IAA OPA	0.5894	0.5490	0.1041		−.5286		0.4546	0.2337
	0.7985	0.5379	0.0826		−.5622		0.6848	0.3083
IAA USN	0.5863	0.4369	0.1708		−.5239	−.1777		0.0985
	0.7879	0.4039	0.0351		−.4554	−.0732		0.1396
MAO OPA	0.9584	0.6547	0.2196	0.7408			0.6601	0.6467
	0.9535	0.6377	0.1491	0.6094			0.7115	0.6122
MAO USN	0.9499	0.3558	−.0876	0.5303		0.1123		0.3721
	0.9236	0.4239	−.0393	0.3668		0.0297		0.3409
OPA USN	0.9904	0.6570	0.1234	0.7943	0.8014			0.6733
	0.9679	0.6950	0.2910	0.6641	0.7044			0.6645

Time Series Analysis and Stability of ICRF2 sources

V. Raposo-Pulido, H. Krásná, T. Nilsson, R. Heinkelmann, H. Schuh

Abstract We have studied the precision and stability of the positions of the radio sources observed in 3450 VLBI sessions from 1984 to 2011 using VieVS (Vienna VLBI Software). We first estimated time-series of the radio source coordinates. Each time series was then analyzed according to stability and apparent proper motion of the source. The results were compared with the requirements for defining sources as specified by the IERS (Fey et al. 2009). Thus, with this study we aim to produce an updated list of radio sources useful for geodetic and astrometric VLBI as well as to assess the precision of them. Furthermore, we intend to provide an input to the realization of the next ICRF3.

Keywords radio sources, time series, global solution, software VieVS

1 Introduction

VLBI is the only available technique for the determination of the International Celestial Reference Frame (ICRF), which is materialized by the positions of radio sources, whose coordinates are estimated with a mean precision of 40 μas. ICRF is the practical realization of the current conventional space-fixed reference system, the International Celestial Reference System (ICRS, Arias et al. 1995). The last realization, the ICRF2, consists of 3414 sources. 295 of them were selected as defining sources (Fey et al. 2009). All of them have position errors smaller than 0.1 mas and 97 of them had been defining sources of the previous realization ICRF1 (Ma et al. 1998). 2197 out of 3414 sources were observed only in VLBA Calibrator Survey (VCS)sessions, that are astrometric survey campaigns, which are specifically designed to observe a large number of new radio sources. Our research focusses on the 1217 multi-session sources, which are regularly observed by the standard IVS (International VLBI Service for Geodesy and Astrometry) networks (Schuh and Behrend). In this study we show preliminary results of our potential contribution to ICRF3 by checking the stability of the defining sources and looking for new candidates. Where indicated, we explain the variability of the estimated coordinates and other findings determined in our VLBI solution obtained by VieVS, a geodetic VLBI analysis software (Böhm et al. 2012).

Virginia Raposo-Pulido[1,3], Hana Krásná[2], Tobias Nilsson[3], Robert Heinkelmann[3] and Harald Schuh[3]
IGN, National Geographic Institute Madrid, Spain[1]
TU Vienna, Vienna University of Technology, Austria[2]
Helmholtz Centre Potsdam, German Research Centre for Geosciences (GFZ), Germany[3]

2 Selection of Defining Sources

Following the criteria of the IERS (Fey et al. 2009), based on the VLBI data analysis of the IERS/IVS Working Group on the Second Realization of the International Celestial Reference Frame: ICRF2, a source is rejected as defining source if one of the following conditions apply:

1. Formal error > 1 mas
2. Excessive structure[1]
3. < 20 observations (group delays)[2]
4. < 2-year span of data[2]
5. > 500 μas discrepancy between catalogs[2,3]
6. Position not adjusted for each session[4]

[1] Structure index (SI) at X band, when available, is 3 or 4 the source must be rejected

[2] Assessed with global VLBI solution

[3] Offsets or coordinate differences with respect to ICRF2

[4] The source must have shown enough positional stability so as to not qualify as 'arc' source. Assessed with time series of radio sources

7. Large, significant apparent proper motions[5]

In this study we check the last five criteria with our GFZ VieVS VLBI solution using three different analysis methods. The structure index (SI) from The Bordeaux VLBI Image Database (http://vlbi.obs.u-bordeaux1.fr/) is taken into account to serve as a reference to identify significant proper motions caused by radio source structure.

3 Input Data

3450 sessions (6266771 group delays) are analyzed between the beginning of 1984 and the end of 2011 with

$$\chi^2 = \frac{v^T P^{-1} v}{n-m} < 2 \tag{1}$$

where v denotes the post-fit residuals vector, n the number of observation and constraint equations, m the number of unknown parameters and P the diagonal matrix of formal errors which are the sum of formal errors from the correlator plus an error floor of 1 cm ^{2} ($\sigma_i^2 = \sigma_{i,corr}^2 + 1\ cm^2$).

4 A priori models and parameterization

All models were chosen according to the second realization of the ICRF by VLBI: ICRF2. For every single session piecewise linear offsets were estimated for the clocks (60 min + 0.5 ps^2/s), for zenith wet delays (30 min + 0.7 ps^2/s) and for troposphere gradients (360 min + 2 mm/day + constraints 1 mm). One offset was estimated for each EOP, for station coordinates, and for radio source coordinates. For the global solution the clock parameters, zenith wet delays, troposphere gradients and EOP were reduced. The antenna positions and velocities, and the source positions were estimated as one offset each.

5 Data Analysis

The data were analyzed with the Vienna VLBI Software, VieVS. In VieVS the least squares adjustment method is used, based on a sequence of estimated constant values defined at integer hours and/or integer fractions of hour of UTC, which are linearly connected by the so-called piecewise linear offsets function. Analysis options for every session were individualized to correct the clock breaks and to remove the large outlying observations. In that way, times of clock breaks were manually specified. Particular baselines, or individual stations or sources were excluded to reach a χ^2 <2. With these options, we run VieVS twice: the first run is to get the outliers and the second run to remove them. We consider an observation as outlier, if the absolute value of the residual is larger than five times the root mean square of all residuals. The cut-off elevation angle was set to 0°, however, only a very few observations were below 5°.

[5] Assessed with yearly-binned global solutions. The analysis used in our study is the Allan standard deviation (Allan, 1966)

5.1 Global solution

At first we processed the global VLBI solution by accumulating normal equations from the set of single sessions. The datum definition of the TRF was realized by applying no-net-translation and no-net-rotation conditions (NNT+NNR) for the most stable stations. The stations, that observed in a few sessions (velocities fixed to a priori values) were reduced, keeping the velocities of the stations with breaks due to antenna repairs, Earthquakes etc, constant and applying velocity ties between stations that are close to each other. Two different datums were applied to the source coordinates (see Tab. 1). In both cases radio sources with less than three observations were fixed and sources with less than eleven observations were reduced. Fixing a radio source means, that the coordinates are not estimated and the a priori values are used for the analysis, while reducing a radio source denotes that still estimated by equation but the parameters are not explicitly given. Special handling sources, i.e. radio sources with large structure and time dependency, were also reduced. For the datum, defining sources from ICRF2 were used but the global solution 2 only considers defining sources with more than ten observations. In our solution, characteristics of the sources and the repeatability of the observations are taken into account. However, the geometrical distribution is not considered. 16 defining sources had less than eleven observations, which were not included in the datum of the global solution 2 and they were reduced or fixed according to the number of observations (see Tab. 1). Eight additional defining sources were not found in any session: 0522-611, 1143-696, 1420-679, 1633-810, 1725-795, 1925-610, 2250+190, 2344-514, most of them with declinations smaller than -50 °. The small number of observations is due to the lack of antennas in the southern hemisphere. Comparing the differences between global solution 1 and 2, we find that the formal errors of the sources with less than ten sessions decrease in global solution 2 by about 120 μas. All of them have negative declinations. Sources with more than 49 sessions reach an improvement of 3 μas independently of the declination. The results although better, are far below the error floor of ICRF2.

Two different kinds of sources were analyzed separately: defining sources and candidate sources. Offsets from a priori values of defining sources were compared with the number of sessions and the declination. About 65% of both offsets (dαcosδ and dδ) are smaller than 100 μas. We notice that very few sources are frequently observed (see Tab. 2), and most of them have positive declinations. Most of these sources have good visibility, however, very few sources have high-flux density. Only for negative declinations the offsets show larger scatter. The reason is that these defining sources are selected for geometrical reasons to configure the ICRF2 datum. That is not the case for candidates sources. In Table 2, a mean value for each of the six groups is estimated. Nine sources have at least one of the offsets larger than 0.5 mas: five with less than twenty observations or/and an observing period less than two years and four with less than twenty sessions or/and SI close to 3. We did the same comparison for candidate sources (see Tab. 2). 67 sources with less than 500 sessions have offsets larger than 500 μas: 49 with less than twenty observations or/and an observing period less than two years and the rest with a high SI (larger than 3 valid for 55% of these sources). In total 182 radio sources have problems with the number of observations, year span of data or discrepancy between catalogs, about 97% of them were observed in less than twenty sessions. On the other hand, eleven ICRF2 radio sources observed in less than three sessions have offsets smaller than 100 μas with declinations bigger than 15°: 0741+214, 119+183, 1420+326, 0119+247, 0602+405, 1317+520, 1335+552, 1526+670, 1756+237, 2159+505, 2340+233. These sources have an insufficient number of observations for reliable designation as defining sources. As a consequence they have formal errors between 100 to 400 μas. However, future observations could reveal a stationary character. The radio source 1420+326 has a SI of 1 for X-band and S-band, but for most of the other sources, i.e. eight out of eleven, SI were not found.

Table 1 Configuration of the two global VLBI solutions

	global solution 1	global solution 2
Number of sessions	3450	3450
Time interval	1984-2011	1984-2011
Sources analyzed	827	811
	759 from ICRF2	743 from ICRF2
Datum sources	287	271
Fixed sources	38	42
Reduced sources	135	147

Table 2 Mean absolute values of the offsets for defining (first value) and candidate sources (second value)

Sessions	Offsets [mas]	Number of sources
< 500	0.11 / 0.22	213 / 458
500 - 999	0.03 / 0.048	25 / 9
1000 - 1499	0.02 / 0.033	16 / 4
1500 - 1999	0.017 / 0.013	9 / 1
2000 - 2499	0.032 / -	4 / -
> 2499	0.02 / -	4 / -

5.2 Time Series

For this approach 24h single session solutions were computed. A total of 822 radio sources were included. The datum definition was realized by applying NNT+NNR w.r.t. VTRF2008 (Böckmann et al. 2010) and NNR w.r.t. ICRF2 for defining sources, fixing sources with less than six observations. The time series are provided with the offset estimates in right ascension and declination for every source and every session. However, some sources have a limited number of offsets, what makes it impossible to analyze their time series. With the plots we studied the stability and repeatability of the most observed radio sources (> 1000 sessions), by checking the variation of the coordinates with time. An additional criterium was introduced to remove the outliers which were not manually discarded. Radio sources with a long time series are included in sessions which are not optimally solved for them. As a preliminary approach, sessions, where at least two radio sources with more than 1000 sessions have significant offsets, were removed (116 sessions). A total of 32 sources were observed in more than 1000 sessions: 21 defining sources, three candidate sources and eight so called special handling sources. These three kinds of sources were separately analyzed, estimating the number of sessions, where each of them have offsets smaller than 1 mas and 0.5 mas to check the stability and variations of their positions (see Tab. 3). The unexpected result is that

Table 3 Sessions with offsets smaller than 0.5 mas and 1 mas for defining, candidate, and special handling sources

Sources	Sessions with offsets < 0.5 mas	Sessions with offsets < 1 mas
Defining	~ 64%	~ 81%
Candidate	~ 55%	~ 80%
Special handling	~ 46%	~ 82%

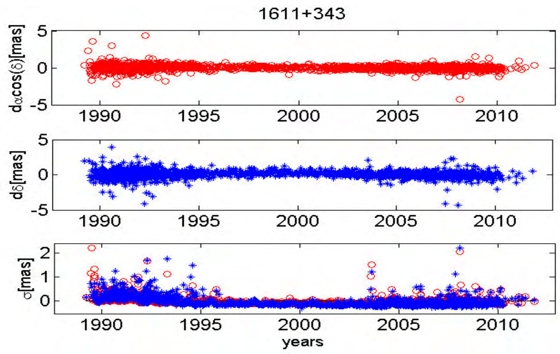

Fig. 1 Time series and difference between standard deviation estimates (with respect to the mean value) for the special handling source 1611+343

Table 4 Structure indices (SI) (first value) and total VLBI fluxes [Jy] (second value) for defining, candidate, and special handling sources. Values taken from The Bordeaux VLBI Image Database

Sources	X-band	S-band
Defining	[1,3] / ~ 2.14	[1,2] / ~ 1.54
Candidate	[2,3] / ~ 1.50	[1,3] / ~ 1.82
Special handling	[2,4] / ~ 2.66	[1,2] / ~ 2.39

special handling sources have the largest percentage of sessions with offsets smaller than 1 mas. Special handling sources exhibit significant non-linear positional variations due to the extended structure. For different epochs we can see the source either as point-like or with extended structure. At the epochs, when the source appears point-like, the offsets can be as small as those for defining sources. The source 1611+343 (Fig. 5.2) is an example, where for eight years (1996-2003) the source structure is very good. The bottom plot of Figure 1 shows the differences of the formal errors from the mean formal error (about 0.2 mas for $d\alpha\cos\delta$ and about 0.3 mas for $d\delta$). The SI for these three kind of sources is between 1 and 4 and no bias is found (see Tab. 4). However, for all the sources the flux is in the order of several Jy. Hence, these sources were observed often because of their high-flux density and good visibility.

5.3 Yearly Global Solutions

For the yearly global solutions we divided the whole time period (1984-2011) into one year long segments. For every segment we used the same configuration as for the global solution 2 (the datum with the smallest formal errors) but including the special handling sources. We estimated the yearly global solutions, by computing the time series of the CRF. 484 sources were included in this analysis, all of them with more than one year of observation. Allan standard deviation analysis (Allan, 1966) was applied to assess the apparent proper motion of the most observed radio sources (> 1000 sessions): $\sigma_A(\tau) = \sqrt{\frac{1}{2N}\sum_{i=1}^{N-1}(x_{i+1}-x_i)^2}$ where x_i are the offsets, N is the number of yearly bins between 1 and 28 and τ is the sampling time. The criterium adapted is the partial stability criterium (Feissel-Vernier, 2003) such as the values range from 1 (AlSd $\leq$ 0.1 mas), 2 (0.1 mas $\leq$ AlSd $\leq$ 0.2 mas), 3 (0.2 mas $\leq$ AlSd $\leq$ 0.3 mas), with a rejection value of 10 for AlSd $\geq$ 0.3 mas. These partial indices clarify whether the source is stable, unstable or drifting. When we have a time series of yearly global solutions, apparent proper motions can be studied. The Allan standard deviation for sampling times is a statistical measure that takes into account the statistical scatter of coordinates. For a given length of the available time series, one could consider Allan standard deviation for sampling times longer than one year, but this estimation is expected to be more robust than for longer time spans. This is described by Feissel-Vernier (2003). In comparison to the criteria of Table 3, this analysis was made for 28 years of observations and it was applied for three different kinds of sources. The special handling sources got a partial index of 2, candidates a rejection value of 10 and defining sources between 1 and 2. 30 out of 32 radio sources were observed before 1993, when they show differences of the offsets up to 500 μas. When we consider these years in our study, the defining sources have an index of 2 or 1. It is due to the deficiency of the VLBI networks and small quantity of sources with good visibility in that years (see Tab. 5). Special handling sources show an index of 2 and candidates minimally of 3. The candidate 0119+041 (see Fig. 5.3) shows an anomalous behavior in the year 2010 (offsets ~ 4 mas) although the source was observed 91 times in this year. More observations should be scheduled in order to clarify if this source has to be considered as a special handling source for ICRF3.

Table 5 Allan standard deviations for defining, candidate, and special handling sources. The first value considers the period 1984-2011 and the second 1993-2011

Sources	AlSd [mas] ($d\alpha\cos\delta$)	AlSd [mas] ($d\delta$)	Years
Defining	0.09 / 0.07	0.11 / 0.08	> 18
Candidate	0.46 / 0.47	0.33 / 0.23	> 22
Special handling	0.11 / 0.09	0.12 / 0.11	> 22

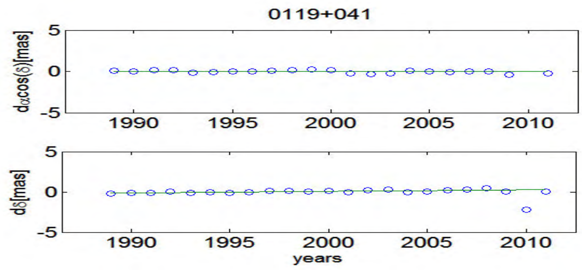

Fig. 2 Yearly global solutions for the source 0119+041

6 Conclusions

The ICRF2 defining sources are not necessarily a better configuration than a different individual datum. In our solution, where some defining sources have very few observations, we conclude that the quality of the datum is more dependent on the number of observations than the geometry. Most of the radio sources that do not satisfy the IERS criteria have a small number of observations. We could not find a clear reason for the negative results (offsets larger than 0.5 mas in global solution 2) of the defining source 1504+377. The time series show that this source was not observed during nine years (1995-2003), which worsens the results due to the lack of continuous observation. Including this source in future sessions or studying deeply the source structure would help to clarify it. In total ten non-defining sources have offsets smaller than 100 μas in less than three sessions. SI is only reported for two of them, so it would be very helpful to complete the source SI data base and to schedule more sessions including these sources in order to enable the analysis of their stabilities.

References

M. Feissel-Vernier (2003). Selecting stable extragalactic compact radio sources from the permanent astrogeodetic VLBI program. *A&A*, 403,105-110(2003). doi: 10.1051/0004-6361:20030348.

A. L. Fey, D. Gordon, and C. S. Jacobs (eds.) (2009). The Second Realization of the International Celestial Reference Frame by Very Long Baseline Interferometry. *Presented on behalf of the IERS / IVS Working Group (IERS Technical Note No. 35).*

D. W. Allan (1966). Proc. IEEE, 54, 221.

C. Ma, E. F. Arias, T. M. Eubanks, A. L. Fey, A.-M. Gontier, C. S. Jacobs, O. J. Sovers, B. A. Archinal, and P. Charlot (1998). The International Celestial Reference Frame as realized by Very Long Baseline Interferometry. *The Astronomical Journal, 116:516-546, 1998 July.*

J. Böhm, S. Böhm, T. Nilsson, A. Pany, L. Plank, H. Spicakova, K. Teke, and H. Schuh (2012). The New Vienna VLBI Software VieVS. *S. Kenyon et al. (eds.), Geodesy for Planet Earth, International Association of Geodesy Symposia 136.* doi: 10.1007/978-3-642-20338-1_126, Springer-Verlag Berlin Heidelberg 2012.

H. Krásná, J. Böhm, L. Plank, T. Nilsson, and H. Schuh (2013). Atmospheric Effects on VLBI-derived Terrestrial and Celestial Reference Frames. *International Association of Geodesy Symposia. Editors Chris Rizos, Pascal Willis.* ISSN: 0939-9585.

S. Böckmann, T. Artz, A. Nothnagel (2010). VLBI terrestrial reference frame contributions to ITRF2008. *Journal of Geodesy, 84.* doi: 10.1007/s00190-009-0357-7 pp. 201-219.

Correlation between source structure evolution and VLBI position instabilities

R. Bouffet, P. Charlot, S. Lambert

Abstract Astrometric positions of extragalactic radio sources derived from VLBI data are used to build highly-accurate reference frames such as the International Celestial Reference Frame. Despite their distant locations, instabilities in the position of these sources are often seen on time scales of months to years, which is generally thought to be caused by source structure evolution. In this paper, we compare position instabilities and structural evolution for a sample of 68 sources observed over a 10-year period (1994–2003). Our results indicate that the two phenomena are linked at some level although the correlation is not perfect.

Keywords Reference systems, astrometry, active galactic nuclei, quasars, VLBI

1 Introduction

The current IAU fundamental celestial reference frame, namely the ICRF2 (second realization of the International Celestial Reference Frame), which has been in use since January 1, 2010, includes positions for a total of 3414 extragalactic radio sources distributed over the entire sky. Such positions were determined from VLBI data acquired at 8.4 and 2.3 GHz over 30 years (1979–2009). The ICRF2 has a floor of 40 microarcseconds (μas) in the individual source coordinate accuracies and an axis stability of 10 μas (IERS, 2009). Joint observational efforts of the VLBI community aiming at a denser and even more accurate celestial frame continue in order to further improve the quality of the frame.

Romuald Bouffet[1,2] and Patrick Charlot[1,2]
[1]Univ. Bordeaux, LAB, UMR 5804, F-33270, Floirac, France
[2]CNRS, LAB, UMR 5804, F-33270, Floirac, France
Sébastien Lambert
Observatoire de Paris - SYRTE, CNRS/UMR 8630 & Université Pierre et Marie Curie,75005 Paris, France

One limitation in improving the accuracy of the individual VLBI source positions originates in actual astrometric instabilities which are found in these positions. Due to their location at cosmological distances, no proper motion are expected for these sources and their astrometric positions should thus be stable with time. While this is indeed the case on the long term, it is not true for shorter time scales (months to years) where instabilities at the level of several hundreds of microarcseconds are commonly detected (IERS, 2009). Such instabilities are usually attributed to varying source structure which is often spatially-extended at the level of the VLBI resolution (Fey et al. , 2009). Structural variations are generally due to ejection of material from the central VLBI core in a recurrent although unpredictable manner causing shifts in the brightness centroid of the radio emission and hence potential VLBI astrometric instabilities.

In this paper we compare source position instabilities and structural variations based on astrometric and imaging VLBI data covering a period of 10 years (1994–2003). The datasets are presented in Sect. 2 while Sect. 3 describes the analysis scheme. Section 3 reports our findings and discusses the correlation level between the two phenomena. In the last section, we draw prospects for further work in this area.

2 Observations

The data used to derive astrometric positions were acquired during numerous VLBI sessions conducted by the International VLBI Service for geodesy and astrometry (IVS) over the past 30 years (Behrend, 2013). A large number of observations is available for many sources which permits monitoring of their astrometric positions on time scales of days to weeks. Analysis was carried out in a similar way as that described in Gontier et al. (2006). For our study we averaged the individual

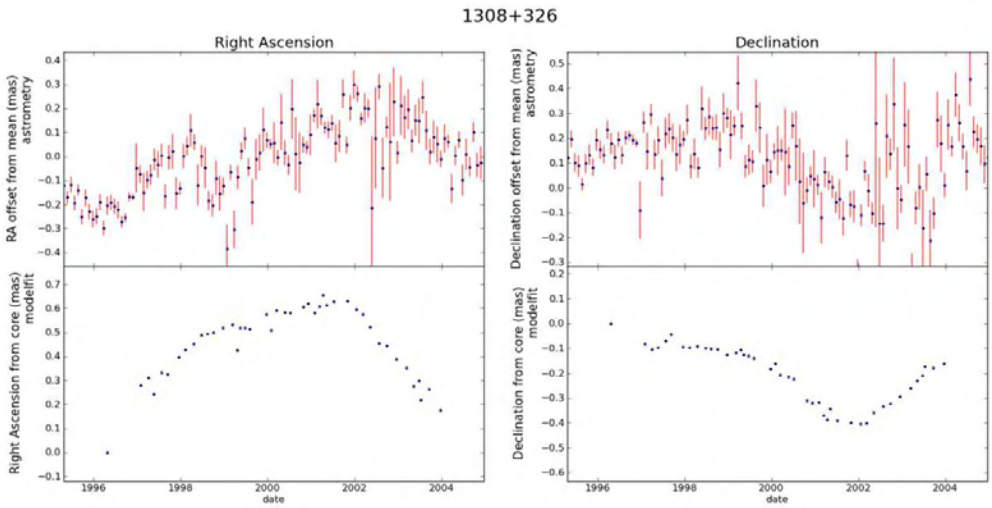

Fig. 1 Comparison of the astrometric position instabilities (upper panels) and brightness centroid motions (lower panels) for the source 1308+326 between 1996 and 2003. The left panels are for right ascension while the right panels are for declination. The vertical scale is in milliarcseconds (mas).

session-based positions over monthly intervals in order to have a sampling similar to that of the imaging data.

Structural variations were taken from the analysis of VLBI jet kinematics reported in Piner et al. (2012). This analysis has made use of 2753 images at 8.4 GHz obtained from 50 Research & Development VLBI sessions organized by the IVS and the Very Long Baseline Array between 1994 and 2003. Six such sessions are carried out every year with a sampling of approximately two months. The network includes 15–20 stations, yielding high-quality VLBI images. 68 sources observed at 20 epochs or more (with a median of 43 epochs per source) are included in the present study.

3 Analysis

For our study, we used a simplified representation of the source structures in the form of a limited number of Gaussian components obtained through model-fitting (as available in Piner et al. (2012)). Such a representation was preferred because it identifies the VLBI core of each source from epoch to epoch and aligns automatically the brightness distributions over time, assuming that the core position is stable. This alignment is crucial since the absolute map position is lost during the imaging process due to self-calibration.

Processing further the source structural information, we calculated the centroid of the brightness distribution (i.e. the centroid of the Gaussian components) at every epoch, allowing us to assess the relative motion of the brightness centroid with time. This calculation was carried out for 68 sources observed at 20 epochs or more for which model-fits are available in Piner et al. (2012). The result is a time series of centroid positions which may be compared with the monthly-averaged VLBI astrometric positions. This comparison assumes that the source motion as seen from the astrometric data is well matched with the motion of the centroid of the brightness distribution detected from VLBI imaging.

4 Results and discussion

An example of the comparisons that we carried out using the scheme explained in the previous section is presented in Fig. 1. The upper panels show the evolution in right ascension and declination of the astrometric position of the source 1308+326 over 1996–2003, while the lower panels show the motion of its brightness centroid over the same period of time. Uncertainties in the astrometric positions were derived as weighted averages (over monthly intervals) of the individual session-based uncertainties. Declination has higher uncertainties due to the predominantly East-West baselines of current VLBI networks. No error bars are given for the centroid positions because model-fitting does not provide a mean to estimate reliable uncertainties for the Gaussian components representing the structure.

Examination of the plots in Fig. 1 indicates similar trends in the evolution of the astrometric and brightness centroid positions. This is also confirmed when

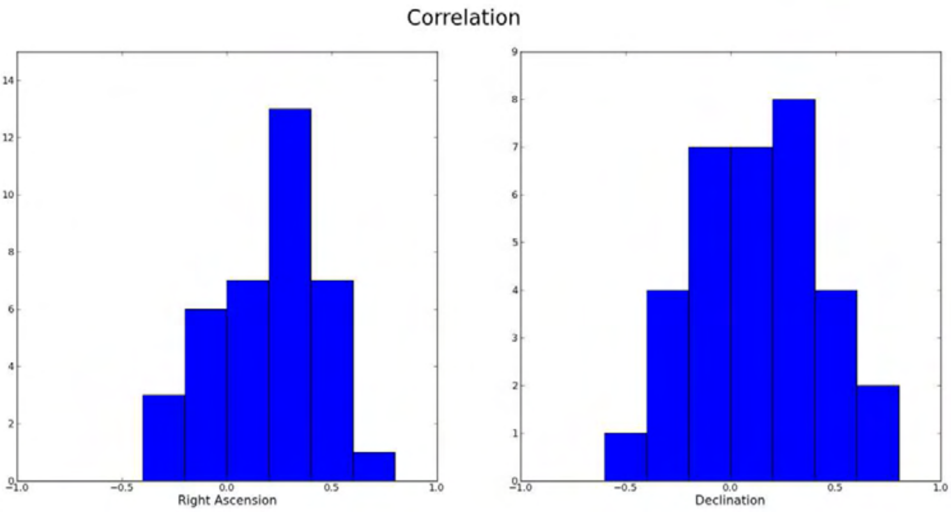

Fig. 2 Distribution of correlation coefficients between astrometric position instabilities and structural variations for all sources with significant astrometric instabilities (reduced $\chi^2 > 4$). Note that the source 0923+392 which shows atypical evolution has been removed from the sample for the purpose of this histogram.

calculating correlation coefficients between the two series, which are 0.30 in right ascension and 0.63 in declination. Applying the same calculation to all sources, an overall positive correlation is found (median value of 0.22 in right ascension and 0.19 in declination) as shown in Fig. 2. This indicates that structural variations and astrometric instabilities are linked at some level.

Looking at Fig. 2, one also notes that a fraction of the sources show a negative correlation. At this stage, it is not understood however whether this negative trend is real or whether it results from the lack of significance of some of the correlation coefficients. For example, the correlation coefficients may be questionable when there is no notable evolution in both the astrometric and brightness centroid positions. Further studies are thus necessary to assess the significance of the correlation coefficients. Ultimately, every source may have to be examined separately to understand any discrepancy that may happen between the two series of positions.

For a full analysis, the S band (2.3 GHz) structures should be considered too since the astrometric positions are derived from a combination of the data at the two frequencies whereas only the X band (8.4 GHz) structures have been considered in the above comparisons. The S band data have a lower weight though and are thus less likely to affect strongly the positions.

5 Conclusion

A comparison between the evolution of astrometric positions and variations of source structure (characterized as the motion of the centroid of the brightness distribution) has been carried out for a sample of 68 sources observed over a period of 10 years between 1994 and 2003. This comparison reveals similar trends in the astrometric and structural time series of positions for some sources showing significant motions like 1308+326. On the other hand, the correlation for sources with smaller motions is more difficult to assess. Overall, a positive correlation is found between the two time series, which favors an explanation of VLBI positions instabilities in terms of structural variations.

In the future, we plan to refine this comparison by examining carefully each individual source in the sample. In some cases, the comparison may not be reliable because position errors are too large and the motions are not significant while in others different trends are seen, which needs to be understood. Possible explanations include misidentification of the core components over the epochs (thereby affecting the alignment of successive images and the brightness centroid relative locations) and effects of the S band data which are implicitly included in the astrometric positions whereas these have not been considered in our structural study (due to their lower weight and a priori smaller impact).

In the longer term, enlarging the source sample and expanding the time span covered by the astrometric and imaging data until to recent years would be desirable.

Acknowledgements The authors gratefully acknowledge support from the CNRS through the "Action Spécifique GRAM" for this project.

References

IERS & IVS Working Group. The Second Realization of the International Celestial Reference Frame by Very Long Baseline Interferometry. *IERS Technical Note* **35**. Eds. A. L. Fey, D. Gordon and C. S. Jacobs. Verlag des Bundesamsts für Kartographie und Geodäsie, Frankfurt am main (2009).

A. L. Fey, P. Charlot. VLBA Observations of Radio Reference Frame Sources. III. Astrometric Suitability of an Additional 225 Sources. *ApJS* **128** (2000) 17-83.

D. Behrend. Data Handling within the International VLBI Service. *Data Science Journal* **12** (2013) WDS81-WDS84.

A.-M. Gontier, S. B. Lambert, & C. Barache. The IVS team at the Paris Observatory: how are we doing? Proceedings of *SF2A-2006: Semaine de l'Astrophysique Francaise*. Eds. D. Barret, F. Casoli, T. Contini, G. Lagache, A. Lecavelier and L. Pagani (2006) 23.

B. G. Piner, A. B. Pushkarev, Y. Y. Kovalev, et al. Relativistic Jets in the Radio Reference Frame Image Database. II. Blazar Jet Accelerations from the First 10 Years of Data (1994-2003). *ApJ* **758** (2012) 84.

A case study of source structure influence on geodetic parameter estimation

N. Zubko, E. Rastorgueva-Foi

Abstract In VLBI analysis, the Earth Orientation parameters and other geodetic parameters can be estimated when the positions of the observed radio sources are fixed to certain values. Normally, the coordinates of the observed sources are taken from the International Celestial Reference Frame Catalog. It is known that the spatial structure in source is time variable that influence VLBI observations and, therefore, it also affects the estimated geodetic parameters. Here, we investigate this influence. Since, the source flux and structure are highly time dependent, it is necessary to evaluate the effect of such variation on calculated geodetic parameters, for example EOP. The principal goal of our study is a critical assessment if it is possible to reveal the influence of certain source on analyzed parameters and estimate how it affects their accuracy.

Keywords VLBI, analysis, source structure, parameter estimation

1 Introduction

The accuracy of GeoVLBI technique depends on various circumstances, one of them is the definition of Celestial Reference Frame (CRF). Extragalactic radio sources, which are observed with GeoVLBI, are used as reference points in space and they define the ICRF. The catalog of ICRF sources extended over time and the current catalog ICRF2 contains 3414 extragalactic radio sources, however, only 295 of them are the so-called defining sources, i.e. they have good consistency with positional stability and source structure performances Fey et al. (2009). Despite the relative stability of ICRF, the spatially extended source structures introduce errors to the GeoVLBI measurements.

Numerous studies on structure and behavior of extragalactic radio sources were carried out with the view of creation of new CRF. Radio-source structure effects were studied by Coates et al. (1975), Charlot (1990), Johnston et al. (1995) among others. As it was shown by Fey and Charlot (1997) and Fey and Charlot (2000) these effects contribute to the time delay, measured with VLBI in the range from picoseconds in the case of the most compact sources up to several nanoseconds for the most extended sources. They can significantly affect the parameter estimation in the GeoVLBI data analysis. It was shown for example in MacMillan et al. (2007), Titov (2007), and Tornatore (2007).

MacMillan et al. (2007) have studied radio source instability in VLBI analysis and showed that the sources with unstable positions are needed to be modeled with taking into account movements of sources. Ignoring the radio source variations leads to significant effect on Earth Orientation Parameters, while TRF coordinates are less sensitive to source variations.

Tornatore (2007) considered the magnitude of radio source structure effects for baselines of the European geodetic VLBI network. It was shown that in the Europe network, with baselines considerably shorter than in intercontinental networks, the sources with slightly extended structure do not affect noticeably the estimated VLBI station locations. However, in case of intercontinental networks, these sources can impair the estimated parameters.

The influence of source structure on geodetic and astrometric solutions was also studied in Titov (2007), where it was shown that the excluding of sources with extended structure can improve the accuracy of the estimated parameters. However, the deficiency of source number in observation also affects the parameter esti-

Nataliya Zubko
Finnish Geodetic institute, Geodeetinrinne 2, FIN-02430, Masala, Finland
Elizaveta Rastorgueva-Foi
Aalto University Metsähovi Radio Observatory, Metsähovintie 114, 02540, Kylmälä, Finland

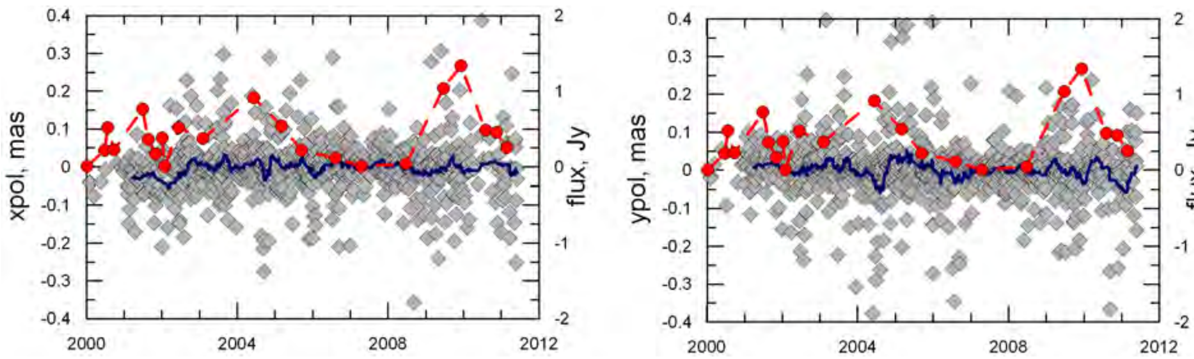

Fig. 1 Difference of xpol (left) and ypol (right)polar motion coordinates (symbols) and their moving averages (solid lines). Flux ratio of inner jet placed at 0.5 mas from the core (dashed lines)

mation; it is especially noticeable in the southern hemisphere, where the number of defining sources is critically small. Thus, the problem of influence of the extended structure sources on GeoVLBI solution cannot be resolved by exclusion of such sources from observations.

To evaluate effect of source flux and structure variations on estimated geodetic parameters, we selected several sources from ICRF2. In this paper we present some results based on study of source 0133+476. This source is included to the list of defining sources ICRF2 and it is regularly observed in Geodetic VLBI sessions. Since the flux and structure of the source 0133+476 is quite variable, we assumed that it is possible to reveal some effects on estimated geodetic parameters caused by this source.

2 Analysis

For our analysis we selected the geodetic VLBI sessions of years 2000-2011, where the observations of source 0133+476 were included to the schedules. The analysis of these data was performed with VieVS software Böhm et al. (2012), where polar motion, nutation and other parameters were estimated. In VieVS software most of the parameters are estimated as continuous piece-wise linier offsets. After the analysis some sessions were rejected due to high standard deviations, thus about 1000 analyzed sessions left at the end. The analysis was done in two steps. First set of estimations was obtained with usual processing of data, named $set1$, and second set was obtained when observations of source 0133+476 were excluded, named $set2$.

3 Results and discussions

To reveal the effect of the exclusion of source 0133+476 from the sessions, the difference of estimated parameters from two sets was calculated. For example, for each session we have estimated a parameter x, one value of the parameter x_1 is taken from $set1$ and another, x_2 from $set2$. It is expected that the difference between these two values $x_2 - x_1$ may clarify an effect of the source on estimated parameter.

Fig.1 shows difference in the estimated parameters of polar motion $xpol_2 - xpol_1$ (left) and $ypol_2 - ypol_1$ (right). In order to smooth the time series and to discriminate possible trend we added a moving average to the plots (solid curve), where smoothing period is 25 data points. As one can see the curves of moving average reveal some features, especially they well seen for the Y polar motion coordinate obtained in 2004.5, 2010 and 2011. To find a possible correlation between these features and source structure changes, the sources jet flux was modeled (see Rastorgueva et al. (2013)). On Fig. 1 flux ratio of inner jet 1 (0.5 mas from the core) to the core is shown (dashed curve). Significant increase of the relative jet flux was observed at 2001, 2004, 2010 and 2011. As one can see in Figure 1 (right), the positions of jet flux peaks coincides with the features reviled for moving average curve. The position correspondence of flux peaks with features of moving average suggests that the estimated parameter ypol1 is influenced by the structure changes of source 0133+476, and the effect can be revealed from analysis of differential value of the parameter $ypol_2 - ypol_1$. Thus, the features observed for estimated y coordinate offset of polar motion represent the effect of changes in source structure on the estimated parameter.

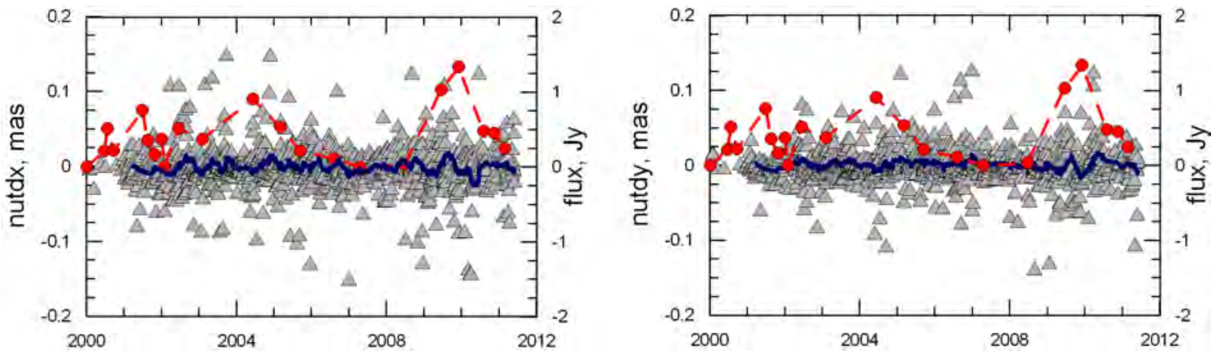

Fig. 2 Difference of dx (left) and dy (right) celestial pole coordinates (symbols) and their moving averages (solid lines). Flux ratio of inner jet placed at 0.5 mas from the core (dashed lines)

It was also checked whether the effect of the source structure changes is observed for other parameters. Figure 2 shows difference of estimated parameters for nutation, $nutdx_2 - nutdx_1$ (left) and $nutdy_2 - nutdy_1$ (right). Here, the moving average trends features in 2010-2011 is also clearly visible for both $nutdx_2 - nutdx_1$ and $nutdy_2 - nutdy_1$ values, when the jet flux is had a significant growth.

4 Conclusions

We found unambiguous effect of variations in spatial structure of radio source on the estimated parameters from GeoVLBI sessions. We are going to apply the same technique for analysis of other defining sources. Further research will be useful for understanding of source structure effect on the geodetic VLBI data and estimated parameters.

Acknowledgement

This work was partly supported by the Academy of Finland project 134952.

References

A. L. Fey, D. Gordon, and C. S. Jacobs (eds.). The Second Realization of the International Celestial Reference Frame by Very Long Baseline Interferometry. *I*ERS Technical Note No. 35, 2009

P. Charlot. Radio-source structure in astrometric and geodetic Very Long Baseline Interferometry. *Astron. J.* , 99 (4), 1309–1326, 1990

A. L. Fey, P. Charlot. VLBA observations of Radio Reference Frame Sources. I. Astrometric suitability based on observed structure. *ApJS* , 111, 95–142, 1997

A. L. Fey, P. Charlot. VLBA observations of Radio Reference Frame Sources. II. Astrometric suitability of an additional 225 sources. *ApJSS* , 128, 17–83, 2000

R. J. Coates, T. A. Clark, C. C. Counselman, I. I. Shapiro, H. F. Hinteregger, A. E. E. Rogers, and A. R. Whitney. *Tectonophysics* 29, 9, 1975

K. J. Johnston, A. L. Fey, N. Zacharias, et al. Radio Reference Frame. *Astron. J.* , 87, 1593–1599, 1995.

D. S. MacMillan and C. Ma. Radio source instability in VLBI analysis. *J. Geodesy*, 81, 443–453, 2007.

O. Titov. Effect of the selection of reference radio sources on geodetic estimates from VLBI observations. *J. Geodesy*, 81, 455-468, 2007.

V. Tornatore and P. Charlot. The impact of radio source structure on European geodetic VLBI measurements. *J. Geodesy*, 81, 469-478, 2007.

J. Böhm, S. Böhm, T. Nilsson, A. Pany, L. Plank, H. Krásná, K. Teke, H. Schuh. The new Vienna VLBI Software VieVS. In: *Proceedings of IAG Scientific Assembly 2009, International Association of Geodesy Symposia Series Vol. 136*, ed. by S. Kenyon, M. C. Pacino, and U. Marti, pp. 1007-1011, 2012. doi: 10.1007/978-3-642-20338-1_126.

E. Rastorgueva-Foi, V. Ramakrishnan, N. Zubko. A Potential use of AGN single-dish monitoring for optimization of GeoVLBI scheduling. *Proceedings of the 21st Meeting of the EVGA*, 2013

A Potential Use of AGN Single-Dish Monitoring for Optimization of Geo-VLBI Scheduling

E. Rastorgueva-Foi, V. Ramakrishnan, N. Zubko

Abstract Source structure is an important characteristic of extragalactic radio sources that are used to keep the celestial reference frame(ICRF2 defining sources). Their structure is variable with time, and its changes are connected to the total flux variations. Observations of total flux variatopns with a single radio telescope is much cheaper time- and laborwise than VLBI imaging. We consider a possibility to use single dish AGN monitoring results as precursor of approaching activity in ICRF2 defining sources that are prone to be unstable in the active state. This information could be used for scheduling of geo-VLBI sessions, when active sources could be temporarily replaced by the currently stable ones.

Keywords source structure, total flux, single-dish, monitoring

1 Introduction

The second realization of the International Celestial Reference Frame (ICRF2) is defined by accurate positions of 295 bright active galactic nuclei (AGN) that are distributed nearly evenly over the sky (Fey et al. , 2009). Extended structure of many ICRF sources introduce additional delays of up to several hundreds ps (Charlot , 1990; Fey & Charlot , 1997, 2000) that limits the accuracy of ICRF axis stability and coordinate determination (e.g., Charlot , 2008). Fey & Charlot (1997) introduced a quantitative measure of the correction needed to compensate for these structure-induces delays: a structure index that runs from 0 (small corrections – compact source) to 4 (large corrections – extended source). One of the selection criteria for the sample of defining sources for ICRF2 was a limit on maximum average continuous structure index of 3.0 (Fey et al. , 2009), that ensured relative compactness of ICRF2 defining sources. This threshold was calculated based on images obtained at S (2 GHz) and X (8 GHz) bands during 1994–2007, with number of observational epochs ranging from 1 to ≈30 (e.g., Charlot , 2008). The resulting noise floor of ICRF2 is 0.04 mas with individual measurements errors up to ≈0.2 mas, and axis stability is 0.01 mas (Fey et al. , 2009).

However, there are two aspects of the AGN physics that should not be neglected: nuclear opacity and connection of the structure changes to the total flux variability. AGN are compact bright cores of massive galaxies, where disc accretion on a central black hole causes a formation of two collimated conical relativistic jets of magnetized plasma, that propagate perpendicularly to the plane of an accretion disc. Jets emit synchrotron radiation in vawebands from radio to far infrared. The compact extragalactic radio sources that are observed at VLBI scale and associated with AGN are in fact optically thick (where synchrotron self-absorption optical depth $\tau = 1$ at a given frequency) unresolved inner regions of the jet at a distance of $r_{core} \approx 10^4 R_g \approx 1pc$ ($R_g = GM_{BH}/c^2$ is gravitational radius of a central black hole) from the center (Blandford & Königl , 1978; **?**). Thus, the observed position of a defining source, measured via VLBI observations, is actually a position of such a VLBI "core" that may change with frequence and time. The location of $\tau = 1$-surface changes with frequency as $r_{core} \propto \nu^{-1/k_r}$, with $k_r = 1$ for a conical jet with the particle and magnetic field energy density equipartition and with domination of synchrotron self-absorption (Blandford & Königl , 1978; Königl , 1981; Lobanov , 1998). Thus, the core shifts upstream at higher frequencies and downstream at lower fre-

Elizaveta Rastorgueva-Foi, Venkatessh Ramakrishnan
Aalto University Metsähovi Radio Observatory, Metsähovintie 114, 02540, Kylmälä, Finland
Nataliya Zubko
Finnish Geodetic Institute, Geodeetinrinne 2, 02430, Masala, Finland

quencies, so that the actual positions of the source at S and X bands may differ at a given time. In addition, random variations in the jet electron density, magnetic field strength and jet inclination to the line of sight (jet bending), as well as regular jet rotation (precession), and their combinations may cause erratic changes of the nuclear opacity and of a τ = 1-surface position with time. A substantial brightening of the VLBI core that is defined at "nuclear flare" causes time variations in the core shift. Kovalev et al. (2008) and Sokolovsky et al. (2011) studied S/X-band core shifts of a number of geodetic sources from ICRF1 catalog, aligning self-calibrated source images comparing relative position of a common optically thin jet component. Unfortunately, this method naturally limits possible targets to the subset of most extended ones. Kovalev et al. (2008), based on imaging of RDV sessions data from 2002 to 2003, found that the median value of core shifts between S and X bands for 29 sources is 0.44 mas with the maximum value as high as 1.4 mas (for 0850+581). A further dedicated VLBA multi-frequency delay study by Sokolovsky et al. (2011) was performed on 20 sources, 15 of which were included also in the sample of Kovalev et al. (2008). It found median value of core shift between S and X bands to be 0.69 mas with the maximum value of 1.34 mas (for 0610+260). These values greatly exceed formal accuracy of the individual source position estimations. Kovalev et al. (2008) estimates a theoretical core shift between X and optical bands to be 0.1 mas that should be taken into account for the alignment between radio and optical ICRFs. They also report that for the sources that have multiple measurements of a core shift, its magnitude was proportional to the X-band VLBI core flux. The magnitude of this effect also suggests that during the nuclear flare physical parameters of the jet plasma change. Another example was reported by Fomalont et al. (2011). They compared relative core positions of four ICRF2 defining sources at 8, 23 and 43 GHz obtained via phase-referenced VLBA and VERA imaging to their nominal ICRF2 positions. The catalog positions are displaced by up to 0.5 mas from the actual core. The direction of the shift was towards the extended structure, and this displacement varied. This effect was attributed to the source structure in three cases, and to the core opacity in one.

Nuclear flare is an indication of a disturbance in the base of the jet. It also leads to the excitation of a shock wave that propagates along the jet away from the core. Propagation of a shock wave manifest itself as an emergence of a bright moving "knot" in the jet that can be traced on series of subsequent VLBI images (e.g., Marscher , 1996). Savolainen et al. (2006) investigated connection between emergence of new jet components in the VLBI images of the blazar jets at 22 and 43 GHz and total flux flares occuring at 22 and 37 GHz (Metsähovi Radio Observatory AGN monitoring). They argue that it is likely that every nuclear flare in a blazar leads to a formation of a shock wave, that is triggered at the moment of an onset of a flare (local minimum before the peak of the total flux light curve). However, in some cases these shock wave has faded out before they reach as far in the jet as to becomes visible at VLBI images. In this case, model-fitting of a source structure and direct inspection of closure phases and their residuals help to reveal the presence of a new component. In other cases, a newly born component becomes resolved approximately at the moment of time when the total flux flare reaches its maximum. Since resolution of geodetic VLBI network at 8 GHz is $\approx$ 0.6 mas, a displacement of the core within this radius may lead to an error of the position estimation since formal errors of coordinates are $\leq$ 0.2 mas. The magnitude of an effect of the resolved source structure on geodetic VLBI performance is comparable to the noise introduced by the imperfection of ionospheric corrections.

During the flare, flux density of a source may increase by the order of magnitude within the time period of several months. Hovatta et al. (2008) reports that for a sample of 55 blazars the duration of flares (from minimum to minimum of a light curve) in radio varies from four month to 13 years, with median value of 2.5 years. Kudryavtseva et al. (2011) determines an activity cycle of AGN as a time period from one nuclear flare to the other. Nuclear flares are characterized, in particular, by frequency-dependent time delays between maxima of the flare at different frequencies. This effect is being attributed to increase in nuclear opacity during the flare. Shabala et al. (2012) argues that such flares cause a substantial degradation of the quality of geodetic data.

Thus, a total-flux flare of an ICRF2 defining source in mm-cm domain is an indicator of intrinsic processes that lead to a substantial reduction of the geodetic data quality. AGN tend to have long recurrent activity cycles (Kudryavtseva et al. , 2011; Hovatta et al. , 2008), thus, at any given moment of time some fraction of the ICRF2 defining sources are flaring, hence, displaying two effects discussed above, nuclear opacity and ejection of a new jet component. Study of 22 and 37 GHz AGN total flux light curves from Metsähovi Radio Telescope shows that behavior of sources differ: some stay most of their time in the quiescent state and some are almost constantly flaring. Such trend is preserved over long time periods. Thus, knowing individual behaviorial patterns of each source, and being supplied with the observational data from other bands, including other radio frequencies, one can make an educated guess about upcoming phenomena in the source, like approaching flare and ejection of a new jet component. We propose to use multifrequency single dish monitoring data and IVS correlated flux at 2 and 8 GHz data in order to make conclusions about starting flares in the ICRF2 defining sources, and reporting them to IVS schedulers. Sources in the active state may be excluded from the schedule for the entire active part of the cycle, and added back later, when the flux decreases and new jet component fades away.

In this paper we describe approach to the analysis of the behavior of individual sources and apply it to the four example sources from ICRF2 defining database: 0133+476, 0552+398, 3C446, 1156+295. We plan to express the found behavior patterns in terms of border conditions for the source flux levels that will be given as parameters to the prototype of the automatic Alert System analysis tool that is currently tested at the Metsähovi AGN monitoring database Rastorgueva-Foi et al. (in prep.).

2 Data and their reduction

In this paper, we consider the following data:

- singe-dish Metsähovi radio telescope AGN monitoring 37 GHz (details of sample selection and data reduction are described in Teräsranta et al. , 2005, and references therein). Metsähovi monitoring list contains 58 out of 295 ICRF2 defining sources, we used time series from 2000 to 2013;
- IVS geo-VLBI correlated flux from cumulative source performance time series (the data is publicly available online[1]), we used time series from 2001 to 2013;
- MOJAVE program (Lister et al. , 2009,b) VLBA monitoring of AGN at 15 GHz (the data is publicly available online[2]). We performed model-fitting of *a-priori* calibrated data for sources 0133+476 and 0552+398 fot the the time period 2000–2013, and for source 1156+295 for the period 2006–2013 in Difmap package using multiple circular components with Gaussian flux density distribution (Taylor , 1997) in addition to the kinematic data from Lister et al. (2009b) for the source 0552+398 for the period of 1997-2006.
- Boston University (BU) 43 GHz VLBI monitoring data for the source 1156+295 (the data is publicly available online[3]).

We used z-transformed Discrete Correlation Function (ZDCF method, Alexander , 1997) to find correlations between light curves at different frequencies and estimate time lags between the flares.

We have to note that the jet structure of 0133+476 was very fine and did not allow to detect clear kinematics for the whole time period (Lister et al. , 2009b), thus, we considered groups of components that characterize brightness of larger portions of the jet instead of individual components. The fluxes in each group were summed. We identified four areas in the jet of the source 0133+476: core, inner jet 1 (0.5 mas from the core), inner jet 2 (1 mas from the core) and “blob”, a stationary feature at the distance of 3 mas from the core (see Fig. 1).

3 Results and discussion

We use MOJAVE 15 GHz VLBA data to trace structural changes of sources 0133+476 and 0552+398. The resolution of these maps is ≈ 0.5 mas, which is close to the resolution of geo-VLBI images (≈ 0.6 mas). However, due to the core opacity, radiation at 15 GHz comes from the deeper layers of the jet than 8 Ghz, so that flux variations seen at 15 GHz may preceding those at 8 GHz. We compared jet structure at 15 and 8 GHz for several epochs, and component positions in both of them coincided within the component size. Whereas resolution of 1156+295 BU 43 GHz VLBA maps is three times better than that of 8 Ghz, and the jet is somewhat shorter due to the optically thin emission mechanism, we compared the jet structure and kinematics between 43 and 15 Ghz, and found that jet components' positions coincide within errors. Optically thin jet emission deterioration played role only at the far end of the jet at the distance of ≥ 3 mas from the core, that is too far away from the core to have significant influence on the phase delay (Charlot , 1990).

3.1 Inner jet VLBI components

Charlot (1990) stated that a bright jet component near the core creates a significant residual phase delay if its flux is $\geq 10\%$ of the peak core flux and its distance from the core is between 0.5 and 1.5 of the maximum

[1] http://lupus.gsfc.nasa.gov/sess/sesshtml/cumulative/source-perf-cumulative.html
[2] http://www.physics.purdue.edu/astro/MOJAVE/
[3] http://www.bu.edu/blazars/VLBAproject.html

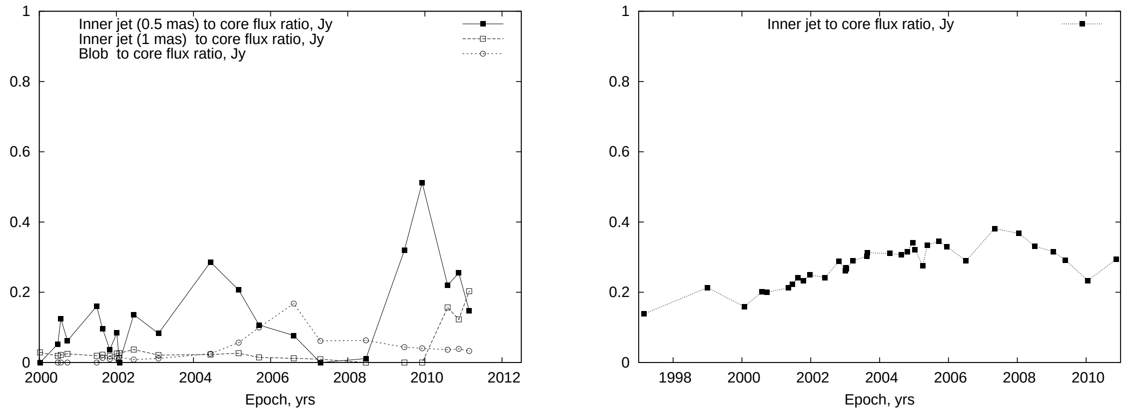

Fig. 1 Jet-to-the-core flux ratios for two ICRF2 defining sources 0133+476 (“bad” geodetic source; left) and 0552+398 (“good” geodetic source; right). 0133+476 has 4 mas long jet with components at 0.5 mas (inner jet 1), 1 mas (inner jet 2) and 3 mas (‘blob”); 0552+398 has one bright jet component at the distance of 0.6 mas from the core

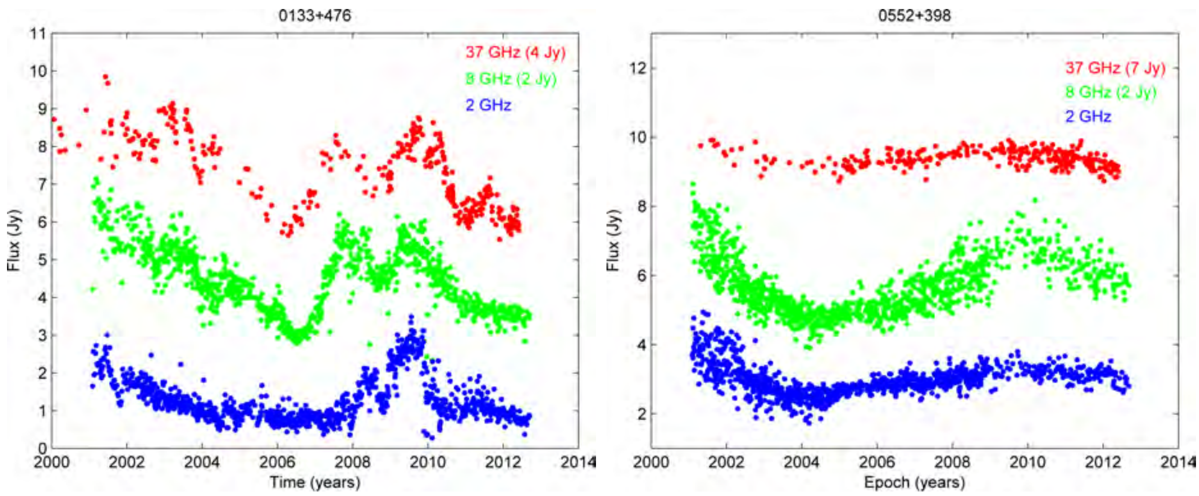

Fig. 2 2 GHz (bottom), 8 GHz (middle) and 37 GHz (top) light curves of two ICRF2 defining sources 0133+476 (“bad” geodetic source; left) and 0552+398 (“good” geodetic source; right). The light curves are offset from each other in the vertical direction: 0133+476 offsets are 2 GHz: no; 8 GHz: +2 Jy, 37 GHz: +4 Jy; 0552+398 offsets are 2 GHz: no; 8 GHz: +2 Jy, 37 GHz: +7 Jy

projected interferometer fringe spacing along the jet axis. Thus, the jet components that affect geo-VLBI observations at 8 GHz are located within first two mas from the core. Time variations of the jet component fluxes relative to the core flux for two ICRF2 defining sources are presented on Fig. 1. For 0133+476, subsequent changes of integrate flux of isolated jet sections (see Sect. 2) reveal a propagation of a bright component along the jet during the active state. However, not every flare corresponds to such an event. Fig. 1 shows also that whereas relative flux of the inner jet of unstable source 0133+476 varies violently and stays most of the time below 20% of the core flux, the relative flux of an inner jet of a stable source 0552+398 stays above 20% most of the time between 2000 and 2012. 0552+398 is essentially a double source: the inner jet component is a stationary feature with a constant flux of ≈0.8 Jy at a constant distance of ≈ 0.6 mas from the core. Variations of the inner jet-core flux ratio were compared to the total flux light curves at 8 and 37 GHz (Fig. 2. The comparison shows that 0133+476 inner jet “peaks” together with the total flux at 8 and 37 GHz (2004.5, 2009.5), whereas in 0552+398 inner jet brightens when the total flux at 8 GHz fades, and there is no connection to the almost featureless 37 GHz light curve. This effect is due to the fact that the bulk of the total flux emission in 0552+398 comes from the VLBI core, and the jet component flux does not vary with time. These two examples show that *each source has different behaviorial pattern, and approach to setting the border conditions for the Alert system must be individualized.*

Source	37 GHz vs 8 GHz Days	Band lags: Ghz
0133+476	6 ± 15	8
0552+398	249 ± 56	8
3C446	281 ± 30	8
1156+295	44 ± 20	8

Table 1 Time lags between light curves at 37 and 8 GHz (X band) for four ICRF2 defining sources, calculated using ZDCF technique for the time period 2000-2012. In all cases X band lags 37 GHz, meaning that flares at 37 GHz tend to start earlier than at the X band.

3.2 Total flux variability

In order to investigate a possibility to use 37 Ghz total flux light curve as a universal indicator of a source's activity, we calculated time lags between 8 and 37 GHz light curves for the time period of 2000-2012. They are summarized in a Table 1. For the source 0133+476 we also applied ZDCF to the inner jet relative flux and the total flux variations, however, the results were insignificant. One of the reasons might be different time sampling. We conclude that the *connection between the inner jet flux and total flux should be considered for each flare individually.* Table 1 show that flares at 37 GHz come generally earlier than those at 8 GHz, thus, *37 GHz total flux variations can be used as an precursor of source activity. It provides a good leeway for the schedulers/observers to react to the approaching activity at X band.*

References

A.L. Fey, D. Gordon, C.S. Jacobs (ed.), IERS Technical Note No. 35 (2009)

P. Charlot, 1990, AJ, 99, 1309

A.L. Fey and P. Charlot, 1997, ApJ SS, 111, 95

A.L. Fey and P. Charlot, 2000. ApJ SS, 128, 17

P. Charlot (2008) Astrophysical stability of Radio Sources and Implication for thr Realzation of the Next ICRF, *Proceedings of the 5th IVS general meeting, Bordeaux, France*

R.D. Blandford & A. Königl 1979, ApJ, 232, 34

A. Königl 1981, ApJ, 243, 700

A.P. Lobanov 1998, A & A, 330, 79

Y.Y. Kovalev, A.P Lobanov, A.B. Pushkarev, and J.A. Zensus 2008, A & A, 483, 759

K.V. Sokolovsky, Y.Y. Kovalev, A.B. Pushkarev, and A.P. Lobanov 2011, A & A, 532, A38

E. Fomalont et al. 2011, AJ, 141, 91

A. Marscher 1996, ASP Conf. Ser. 110, 248

T. Savolainen, K. Wiik1, E. Valtaoja, and M. Tornikoski 2006, A & A, 446, 71

N.A. Kudryavtseva, S. Britzen, M.F. Aller et al. (2008) Activity cycles of blazars and quasars from VLBI observations, *Proceedings of IX EVN Symposium, Bologna, Italy*

S. Shabala et al. (2012), Quasar Structure Effects on the VLBI Reference Frame *Proceedings of 7th IVS General Meeting, Madrid, Spain*

T. Hovatta et al. 2008 A & A, 48, 51

E.A. Rastorgueva-Foi, N. Zubko, S. Scepanovic, V. Ramakrishnan (in prep.)

H. Teräsranta, S. Wiren, P. Koivisto, et al. 2005, A & A, 440, 409

M.L. Lister, H.D. Aller, M.F. Aller et al. 2009, AJ, 137, 3718

M.L. Lister, M.H. Cohen, D.C. Homan et al. 2009, AJ, 138, 1874

G. Taylor 1997, The Difmap Cookbook *Dept. of Radio Astronomy, California Institute of Technology, Pasadena, CA, USA*

T. Alexander, 1997, Astrophys. Space Sci. Library, Vol 218, 163

Searching for an Optimal Strategy to Intensify Observations of the Southern ICRF sources in the framework of the regular IVS observing programs

Z. Malkin, J. Sun, J. Böhm, S. Böhm, H. Krásná

Abstract The quality of the VLBI-derived ICRF in the southern hemisphere is much worse than in the northern hemisphere. The main reason is that only about 3% of the observations have been made of the sources at declinations below –30 deg due to the relatively small number of VLBI stations located in the southern countries. In this paper, we investigated a possibility to increase the number of observations of the existing and prospective southern ICRF radio sources by inclusion of more such sources in the regular IVS sessions like R1 and R4. We tested the influence of adding supplementary southern sources to the IVS R1541 (12JUL09XA) session on EOP and baseline length repeatability with Monte Carlo simulations. We found that adding more observations of southern sources to the standard schedule causes a slight degradation of some geodetic products and a slight improvement of others, depending on the number of added southern sources. Similar results were obtained for the IVS R1591 (13JUN24XA) session. Generally, it has been shown that it is possible to increase the number of observations of southern sources without loss of the overall accuracy of geodetic products. So, the task is to find an optimal trade-off between the maximum increasing of the number of observations of southern sources and the degradation of geodetic results.

Keywords VLBI, IVS, ICRF, scheduling

Zinovy Malkin
Pulkovo Observatory and St. Petersburg State University, Pulkovskoe Sh. 65, St. Petersburg 196140, Russia
Jing Sun, Johannes Böhm, Sigrid Böhm, Hana Krásná
Department of Geodesy and Geoinformation E120/4, Vienna University of Technology, Gußhausstraße 27-29, 1040 Vienna, Austria

1 Introduction

The quality of the ICRF in the southern hemisphere is much worse than in the northern hemisphere. The main reason is that the number of southern VLBI stations participating in the astrometric observing programs is much smaller than that in the northern hemisphere. As a consequence, the number of observations of the southern sources is very small. Only about 3% of the observations have been made of the sources at declinations below -30 deg (see Fig. 1). The situation improves with time, but very slowly despite new southern stations and new CRF-dedicated observing programs (see Fig. 2). The relative number of observations of most southern sources does not improve with time at all.

Deficiency of observations of southern sources leads to the following well recognized consequences:

- the number of the southern ICRF sources is much smaller than the northern;
- the number of the southern ICRF sources with reliable position and stability estimate, herein reliable core/defining sources, is much smaller than the northern;
- the position accuracy of the southern sources is generally worse than the northern.

Special CRF programs for the southern hemisphere are rare, and are often conducted on poor networks of 2-3 stations, which can deteriorate the source position accuracy because of the source structure effect. Two possible ways were proposed by (Malkin et al., 2012) to increase the number of observations of poorly observed and new prospective ICRF sources on the southern sky: inclusion of more such sources in the regular IVS sessions like R1 and R4, and implementing new scheduling strategies not requiring sky coverage for the stations. In this paper, we investigate possible strategies to force an improvement in the ICRF sources observation distribution over the sky by:

- including prospective ICRF sources in the regular IVS observing programs, such as R1 and R4;
- finding a trade-off between a slight degradation of the EOP precision and the long-term ICRF improvement.

We made use of the VieVS scheduling and simulation tools (Böhm et al., 2012) for our study.

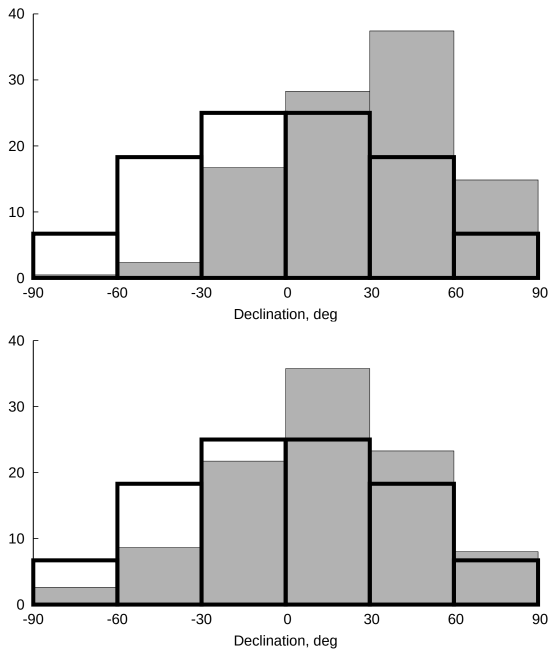

Fig. 1 Percentage of observations by DE bands (top) and percentage of the well observed sources with Nsess $\geq$ 10, Nobs $\geq$ 200 (bottom). Actual numbers of observations are shown by grey boxes, numbers of observations expected for a uniform distribution are shown by thick lines).

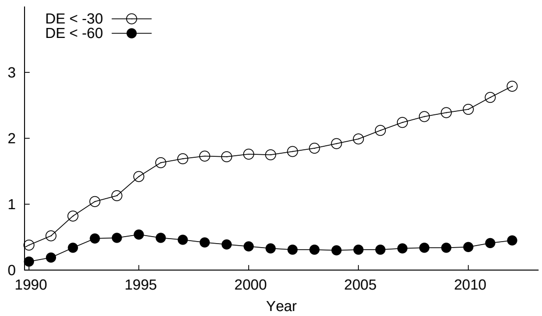

Fig. 2 Percentage of the observations of southern sources (cumulative by date).

2 Monte Carlo Simulation

The IVS R1541 (12JUL09XA) session was used for the Monte Carlo simulations in this paper. The R1541 session network includes 11 stations, 5 of them are located in the southern hemisphere (see Fig. 3). As expected, the Auscope (Australian VLBI Network), station Hartrao, station Tigo, and station Fortleza participated. The southern network size ensures large common view, and the multi-baseline observations are important to mitigate the source structure effects.

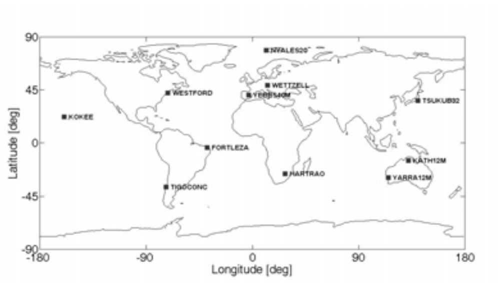

Fig. 3 11 stations network of IVS R1541 session, 5 out of 11 stations are located in the southern hemisphere.

2.1 Scheduling

The original schedule for the R1541 IVS session was generated making use of the SKED software (Gipson, 2010). There are 60 sources observed, 7 southern sources having declination less than -40 degrees. For comparisons, the supplementary southern sources are added to the original source list and experimental schedules are obtained to evaluate the trade-off between the number of southern sources and the accuracy of geodetic products.

Considering all the ICRF2 sources having the declination less than -40 degrees, they are sorted by some generalized criteria involving number of sessions, number of observations, and position uncertainty. “The worst end” of the list shows which sources we should consider first. The strong southern sources have preference in this study.

Schedule ’R1’ is achieved with the original source list. Schedule ’R1+’ includes three more southern sources and schedule ’R1++’ includes six more southern sources as compared with the original R1541 schedule. The three schedules for 24-hour continuous observations are generated with VieVS scheduling package (Sun et al., 2011). The distribution of observed sources is shown in Fig. 4, and detailed information on southern sources is given in Table 1.

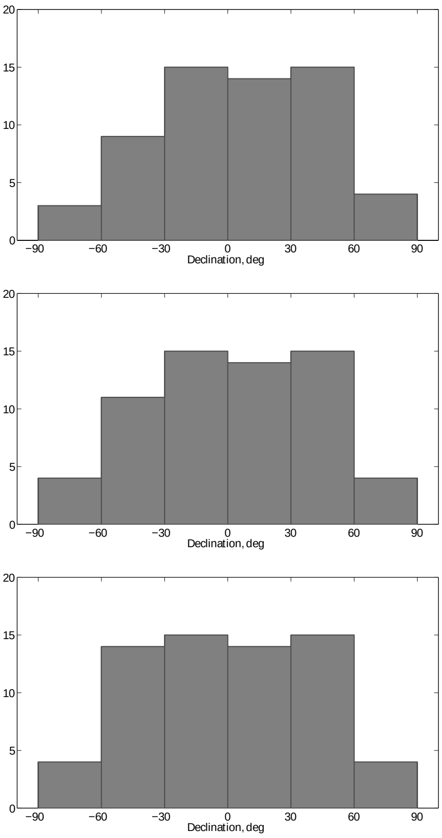

Fig. 4 Distribution of observed sources in the original R1541 schedule (top) and two experimental schedules: R1+ (middle) and R1++ (bottom).

Table 1 Number of scans/observations of southern sources in the IVS R1541 (R1) and two experimental schedules R1+ and R1++.

Source	R1	R1+	R1++
0637-752	39 / 39	42 / 48	37 / 39
0537-441	55 / 88	56 / 91	59 / 102
1104-445	16 / 18	25 / 27	19 / 23
2052-474	42 / 48	49 / 57	46 / 50
2300-683	3 / 3	1 / 1	1 / 1
0048-427	4 / 6	7 / 11	7 / 7
0308-611	4 / 4	6 / 6	2 / 2
2232-488		7 / 7	3 / 3
2204-540		9 / 9	6 / 6
2142-758		7 / 7	3 / 3
0208-512			18 / 18
0332-403			47 / 82
1424-418			42 / 67
Total	178 / 295	209 / 264	290 / 403

Except the different source list, the basic scheduling settings used in VieVS are in correspondence with the original R1541 schedule as summarized below. The optimization of source-based strategy is employed with VieVS for this study.

- frequency setup: R1 frequency setup (X/S band)
- SNR: 20/15 (15/12 for Tigo)
- recording data rate: 256 Mbps
- cut-off elevation angle: 5 degrees
- minimum scan length: 40 seconds
- extra time for settling down, calibration, correlator synchronizing

2.2 Simulating

For the Monte Carlo simulations, 50 sessions were simulated using the same 24-hour schedule but different realizations of noise delays, each time creating new values for wet zenith delay, clocks and white noise to simulate observations as realistic as possible. The random errors in delay measurement were modelled by white noise with given power spectral density (PSD). The clock rate instability was modelled using the Allan standard deviation (ASD). The turbulent troposphere was modelled using the site-dependent structure constant C_n, effective wet height H, and wind velocity V. The simulation parameters are summarized in Tables 2 and 3). See Sun et al., 2011 for details of the stochastic models used during simulation.

Table 2 Simulation parameters.

H [m]	2000
V_n [m/s]	0.00
V_e [m/s]	8.00
wzd_0 [mm]	250
$dhseg$ [h]	2
dh [m]	200
clock ASD	10^{-14}@50 min
WN PSD [ps]	32

Table 3 Site-dependent constant C_n, $m^{-1/3}$.

Sta name	$C_n \cdot 10^7$	Sta name	$C_n \cdot 10^7$
NYALES20	0.65	HARTRAO	1.34
ONSALA60	2.19	KATH12M	1.68
TSUKUB32	3.45	TIGOCONC	2.08
WESTFORD	2.30	WARK12M	1.94
WETTZELL	1.50	YARRA12M	1.76
YEBES40M	1.48	FORTLEZA	2.46
KOKEE	1.39		

3 Results

The simulated NGS data files are entered into the software package VieVS, which computes a classical least squares solution. All the source coordinates were fixed to the ICRF2 positions (Ma et al., 2009). The standard deviation of the 50 EOP estimates and mean formal uncertainties are listed in Table 4.

Table 4 Repeatability and standard deviation of EOP for the IVS R1541 and two experimental schedules R1+ and R1++.

Parameter		R1	R1+	R1++
Number of scans		1258	1351	1375
Number of observations		3905	3813	3997
EOP repeatability	Xp	143.2	125.5	98.2
[μas, μs]	Yp	98.2	79.1	96.8
	UT1	5.6	4.6	5.9
	dX	36.2	42.8	39.1
	dY	45.0	39.5	37.2
Mean EOP uncertainty	Xp	94.8	95.6	93.4
[μas, μs]	Yp	77.2	77.3	74.8
	UT1	4.4	4.6	4.7
	dX	29.8	30.9	29.5
	dY	29.1	29.6	28.1

Fig. 5 shows baseline length repeatability obtained from the simulations. For the baselines shorter than ~5,000 km the R1 schedule shows the best result, and R1+ and R1++ schedules yield worse repeatability, whereas for longer baselines the R1++ schedule is the best, and R1 is the worst. However, in fact, the results obtained with the three schedules are close to each other. The mean baseline length repeatability derived from R1, R1+, and R1++ schedules are 13.5 mm, 12.4 mm, and 11.9 mm, respectively.

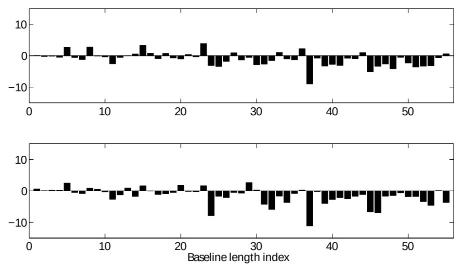

Fig. 5 Differences in baseline length repeatability [mm] between two schedules: R1+ minus R1 (top) and R1++ minus R1 (bottom). The horizontal axis represents the 55 baselines with the shortest one WETTZELL–YEBES40M (1575 km) on the left and the longest one TIGOCONC–TSUKUB32 (12401 km) on the right.

It has been found that further increasing of the number of southern sources (cf. R++ and R+ schedules) leads to a small degradation of baseline length repeatability for short baselines, and small improvement for long baselines. Errors in some EOP become smaller with inclusion of more southern sources, and some EOP show small degradation in the accuracy.

4 Summary

Including more southern sources in the regular IVS sessions may be a practical way to force an improvement of the VLBI-based ICRF in the southern hemisphere. In this paper, we studied a trade-off between the small degradation of the EOP precision and the ICRF improvement using the source-based scheduling algorithm (Sun et al., 2011). We found no degradation of the overall accuracy of main geodetic products, such as EOP and baseline length repeatability after the inclusion of several supplementary southern sources.

Although the number of southern sources added and the number of their observations are not large with respect to the standard scheduling algorithm, regular inclusion of selected sources needed for densification and accuracy improvement of the ICRF in the southern hemisphere will provide a valuable contribution to the next VLBI-based ICRF. Having quarterly observations during two years will give us a good preliminary estimate of both average source position and its stability. Rotating the list of supplementary sources between sessions, e.g., on the quarterly basis, we could substantially increase the number of reliably observed southern sources. The latter is, in particular, very important for selection of new ICRF core (defining) sources.

We tested a new approach to the scheduling using two IVS sessions R1541 (12JUL09XA) and R1591 (13JUN24XA). The results obtained with the first session are described in this paper in detail; the results obtained with the second session are very similar. However, a serious problem for schedule optimization is that southern stations are equipped with relatively small antennas, which makes it difficult to observe the weak sources. However, the much greater recording rate (as compared with the present R1/R4 operations) planned for the VLBI2010 observation mode (Behrend et al., 2008) can mitigate this problem.

The results of our work presented in this paper have shown that it's possible to add more observations of southern sources without degradation of the tested geodetic products, such as EOP and baseline length repeatability. Indeed, more study is needed to find an optimal trade-off between the quality of geodetic and astrometric (CRF) products. More detailed investigations are anticipated for different R1, R4, and other IVS network configurations and an extended list of southern sources. In particular, inclusion of non-ICRF sources shall be considered at the next stage, as well as sources near the southern polar cap. Also, testing with VLI2010 recording parameters would be useful for future scheduling.

References

D. Behrend, J. Böhm, P. Charlot, T. Clark, B. Corey, J. Gipson, R. Haas, Y. Koyama, D. MacMillan, Z. Malkin, A. Niell, T. Nilsson, B. Petrachenko, A. Rogers, G. Tuccari, and J. Wresnik. Recent Progress in the VLBI2010 Development. In: *Observing our Changing Earth*, IAG Symposia, Vol. 133, p. 833–840, 2008. doi: 10.1007/978-3-540-85426-5_96.

J. Böhm, S. Böhm, T. Nilsson, A. Pany, L. Plank, H. Spicakova, K. Teke, and H. Schuh. The new Vienna VLBI Software VieVS. In: S. Kenyon, M. Pacino, and U. Marti (eds.), *Proceedings of the IAG Scientific Assembly 2009*, IAG Symposia, Vol. 136, p. 1007–1011, 2012. doi: 10.1007/978-3-642-20338-1_126.

J. Gipson. An introduction to Sked. In: D. Behrend and K. Baver (eds), *Proceedings of the IVS 2010 General Meeting*, NASA/CP-2010-215864, p. 77–84, 2010.

C. Ma, E.F. Arias, G. Bianco, D.A. Boboltz, S.L. Bolotin, P. Charlot, G. Engelhardt, A.L. Fey, R.A. Gaume, A.-M. Gontier, R. Heinkelmann, C.S. Jacobs, S. Kurdubov, S.B. Lambert, Z.M. Malkin, A. Nothnagel, L. Petrov, E. Skurikhina, J.R. Sokolova, J. Souchay, O.J. Sovers, V. Tesmer, O.A. Titov, G. Wang, V.E. Zharov, C. Barache, S. Boeckmann, A. Collioud, J.M. Gipson, D. Gordon, S.O. Lytvyn, D.S. MacMillan, and R. Ojha. *The Second Realization of the International Celestial Reference Frame by Very Long Baseline Interferometry*. IERS Technical Note No. 35, A.L. Fey, D. Gordon, and C.S. Jacobs (eds.), Verlag des Bundesamts für Kartographie und Geodäsie, Frankfurt am Main, 2009.

Z. Malkin, H. Schuh, C. Ma, and S. Lambert. Interaction between celestial and terrestrial reference frames and some considerations for the next VLBI-based ICRF. In: H. Schuh, S. Böhm, T. Nilsson, and N. Capitaine (eds.), *Proceedings of the Journées 2011 Systèmes de Référence Spatio-temporels*, Vienna, Austria, p. 66–69, 2012.

J. Sun, A. Pany, T. Nilsson, J. Böhm, and H. Schuh. Status and future plans for the VieVS scheduling package. In: W. Alef, S. Bernhart, and A. Nothnagel (eds.), *Proceedings of the 20th EVGA Meeting*, Bonn, Germany, p. 44–48, 2011.

Refining the Uniform Sky Strategy for IVS-INT01 Scheduling

K. Baver, J. Gipson

Abstract The primary purpose of the IVS-INT01 sessions is the estimation of UT1. Improving the accuracy and the precision of the UT1 estimates is an important goal in the scheduling of these sessions. During 2009 and 2010, the GSFC VLBI IVS Analysis Center proposed and tested a new strategy for scheduling the IVS-INT01 sessions. The Uniform Sky Strategy (USS) maximizes sky coverage and the number of scheduled sources. In July 2010, the USNO NEOS IVS Operation Center began to alternate the use of the original and USS strategies in scheduling the operational IVS-INT01 sessions. We compare the results from these two scheduling strategies. In most respects the USS provides superior results to the standard strategy, but there are some circumstances where the results are worse. We discuss some options to improve the USS.

Keywords UT1, IVS-INT01, scheduling

1 Introduction

The primary purpose of the IVS-INT01 sessions is estimating UT1. Therefore improving the accuracy and the precision of the UT1 estimates is an important goal in scheduling these sessions. Better sky coverage has been empirically linked to better UT1 estimate precision and accuracy. But the original, standard scheduling strategy (STN) uses only the strongest sources, and because strong sources are unevenly distributed, IVS-INT01 sessions have limited source availability at some times of the year, resulting in bad sky coverage. The worst source availability occurs in early October, but other times of the year could also use improvement.

Karen Baver and John Gipson
NVI, Inc. 7257D Hanover Parkway, Greenbelt, Maryland, 20770, USA

To address this, in 2009 the GSFC VLBI Analysis Center proposed a new scheduling strategy, the USS (Uniform Sky Strategy), which uses all geodetic sources that are mutually visible at the regular IVS-INT01 stations (Kokee Park and Wettzell). Adding the previously excluded sources should improve sky coverage and therefore improve UT1 precision (i.e., decrease the UT1 formal errors). But the added sources are weaker, and that should increase the formal errors. Also, because it takes longer to observe a weaker source, the number of observations should be reduced, which in turn should increase the formal errors. So the new strategy works both in favor of and against the UT1 formal errors, creating a need to carefully evaluate it.

Since December 2010, the USNO NEOS Operation Center has generated alternating STN and USS operational IVS-INT01 schedules, with, for example, one type of schedule on odd-numbered days of the year and the other type on even-numbered days, in order to develop a basis for evaluating the operational effectiveness of the USS strategy. A 2012 study of the first full year of data (2011) showed that each strategy is superior in some ways. This paper extends the data set through the second year of data (2012), examines factors that affect schedule performance, and explores ways to use the Sked scheduling program to alter these factors in order to improve schedule performance.

This paper uses two non-standard terms as abbreviations. The term UTRMS indicates the RMS about the mean of the UT1-TAI estimates, and the term UTFE indicates the unscaled UT1-TAI formal error or errors. In addition, UT1 indicates UT1-TAI.

2 2011—2012 Sessions

Data results: Analysis of the 2011-2012 data confirms the results from the initial study of the 2011 data

(Baver et al. , 2012). See Fig. 1. Also see http: //lupus.gsfc.nasa.gov/files_presentations/2013mar_evga_baver_uss.pdf for more figures. The USS has better sky coverage, but the average of its UT1 formal errors is higher. The October UT1 formal errors are greatly improved, except for one noisy session, but the UT1 formal errors at some other times of the year could use improvement. Please note that Fig. 1a indirectly shows sky coverage by showing sky emptiness; a smaller value means less emptiness, or more coverage.

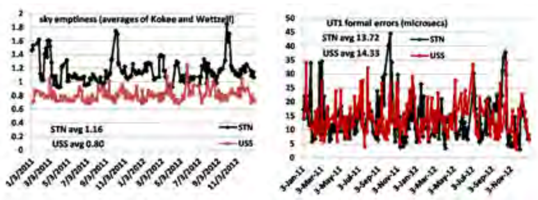

Fig. 1 a) sky emptiness and b) UT1 formal errors.

Robustness: A session is robust if its UT1 estimate does not change much in response to perturbations — e.g., when it fails to observe a scheduled source. We tested the effect of losing a source on STN and USS UT1 estimates. Using the Solve solution configuration used for the 2011—2012 data, we ran a set of solutions for each session in which we suppressed the session's sources, one at a time. We then calculated each session's UTRMS (Fig. 2a). The results are very similar to those from the initial study. Schedules that are less vulnerable to the loss of a source have a lower UTRMS. Fig. 2a shows that throughout the year, the USS UTRMS values are almost always lower than or equal to the STN values. In addition the average of the USS UTRMS values is ~ 2.4 times as good as the STN average. STN schedules typically observe a few sources many times, whereas USS schedules observe many sources a few times. Because of this, the USS provides better protection against source loss.

A session is also robust if its UT1 estimate does not change much with random noise (e.g., atmospheric fluctuations). We ran the Solve solution configuration used for the 2011—2012 data, but we added random noise to simulate atmospheric turbulence and ran the new solution 5000 times per session. We then calculated each session's UTRMS (Fig. 2b). Schedules that are less vulnerable to noise have a lower UTRMS. The results are similar to the initial study, but the STN average has improved and now ties the USS average. But as before, although the USS strategy provides better protection than the STN at some times of the year (especially October), it provides worse protection at other times and could be improved.

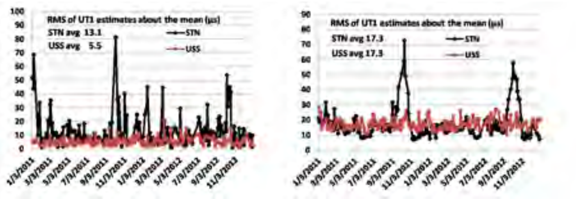

Fig. 2 Results from a) source deletion simulation and b) random turbulent noise simulation.

3 Performance within Hypothetical Schedules

The initial study had empirically indicated that the UTRMS could be improved by achieving better temporal distribution, by reducing the number of low elevation observations, and by achieving better spatial coverage of key areas. We tested these findings.

Temporal Distribution: We used Sked to make an STN-style schedule (three observations each of six sources) and a USS-style schedule (single observations of 15 sources) with equal numbers of mid-left quadrant (L, azimuth ~ 315°), central (C, azimuth ~ 0°), and mid-right quadrant (R, azimuth ~ 45°) hypothetical sources. These schedules ("CYC") cycled through the three areas evenly. We then created two variations of each schedule to a) observe all of the C, then L, then R sources ("CLR") and b) all of the L, then C, then R sources ("LCR"). We ran 5000 solutions per schedule, adding noise to simulate atmospheric turbulence.

More testing is needed, but Tab. 1 indicates that temporal distribution matters. The CLR and LCR cases provide the same spatial coverage as the CYC case, but they leave areas of the sky unobserved for a while and give much higher UTRMS and UTFE values. Balanced temporal distribution gives continuous temporal coverage and, in this test, lower UTRMS and UTFE values.

Observing Order L = left quadrant R = right quadrant C = center (near azimuth 0°)	UTRMS μs STN style	 USS style	UTFE μs STN style	 USS style
(CYC) LRC LRC ... LRC	9.89	13.35	7.45	10.27
(CLR) CCCCC LLLLL RRRRR	38.42	23.64	17.58	16.06
(LCR) LLLLL CCCCC RRRRR	36.41	40.29	18.44	23.51

Table 1 Effect of temporal distribution on the RMS about the mean of the UT1 estimates and the UT1 formal error.

Low Elevation Observations: We used Sked to create 15 baseline cases with maximum elevations of 44, 40, 35, 30, and 25° and minimum elevations of 40, 35, 30, 25, and 20° (i.e., 44-40, 44-35, ..., 44-20, 40-35, ..., 25-20°) at Kokee. For each case, we generated a set of schedules that moved four observations from the minimum elevation to a series of lower elevations selected from 35, 30, 25, 20, 15, 12, 10, and 8°, as appropriate, along azimuths 45° and 330/332° at Kokee (i.e., for baseline case 44-25°, the observations moved to 20, 15, 12, 10, and 8°). Fig. 3 shows an example. We limited azimuth coverage to isolate the effects of elevation and used hypothetical sources at desired positions. We ran 5000 solutions on each schedule, adding noise.

Moving some observations to lower elevations should improve the zenith atmosphere delay estimate and reduce the correlation between the zenith delay and UT1, which in turn should reduce the UTFE. Fig. 3 shows that this is true for both high (44–40°) and moderate (44–20°) starting elevation ranges. In contrast, for the 44–40° case, moving some observations to lower elevations initially reduces the UTRMS but then, starting at ~ 20°, increases it. This is due to two competing effects. On the one hand, lower elevation observations create better geometry for the estimates, reducing the UT1 estimate scatter. But lower elevation observations also introduce extra noise due to atmospheric turbulence, resulting in larger scatter. The improved geometry dominates until ~ 20°, at which point the extra noise dominates. The 44-20° case has good enough initial geometry that only the extra noise matters. USS schedules can start at 8°, so removing their lowest elevation observations should decrease their UTRMS but increase their UTFE, a trade-off that should be considered in actual schedules.

Coverage of Key Areas: The initial study, and later work, had indicated that low UTRMS values might be linked to observing the centers of Kokee and Wettzell's mutually visible quadrants (~ azimuths 45° and 315°) and, to a lesser extent, azimuth 0°, roughly near elevation 30°. We used Sked to create a schedule with hypothetical sources that covered only the key areas. Then we moved observations away from the areas, excluding low elevation observations to eliminate the effects of low elevation, and ran 5000 solutions that added noise.

Fig. 4 and Tab. 2 show four cases. Case 1 fully covers all three areas at a ratio that has been empirically identified as desirable (2-1-2, where 1 represents the coverage of azimuth 0°). In case 2, all areas are covered, but the quadrant centers are only partially covered, because some observations have moved; the UTRMS increases by 14%. In case 3, azimuth 0° is entirely uncovered, and the UTRMS increases over case 1 by 19%. In case 4, all quadrant center observations have moved, leaving the quadrant centers uncovered, and the UTRMS is more than twice that of case 1. The UTFE increases similarly. More testing is needed, but these cases indicate that covering key areas might lower the UTRMS (and the UTFE), with the quadrant centers having more importance than azimuth 0°.

Case	Condition	UTRMS μs	UTFE μs
1	all areas fully covered	11.82	9.90
2	quadrant centers partially uncovered	13.50	10.84
3	azimuth 0° uncovered	14.09	11.96
4	quadrant centers uncovered	26.40	22.75

Table 2 Statistical metrics for coverage of key areas.

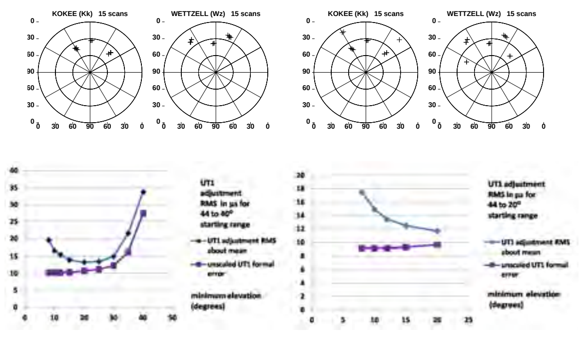

Fig. 3 Low elevation: Top row — AZ/EL plots for 44 to 40° baseline case (left) and its extension to 8° (right). Bottom row – results from the 44 to 40° (left) and the 44 to 20° (right) series.

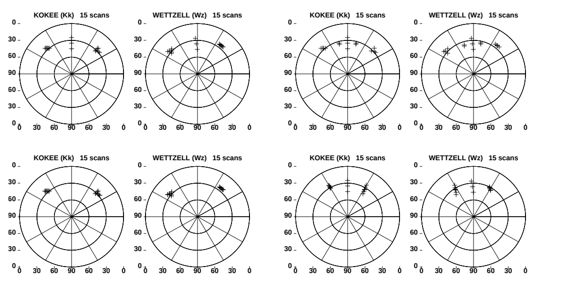

Fig. 4 Key area AZ/EL coverage: Top row, cases 1 (left pair) and 2 (right pair). Bottom row, cases 3 (left pair) and 4 (right pair).

4 Using Sked to Improve Realistic Schedules

Section 3 indicates that the UTRMS can be reduced by 1) improving temporal distribution, 2) improving spatial coverage of key areas, and 3) reducing the number of low elevation observations. We also believe that scheduling stronger sources might reduce the UTRMS. So we started with 26 source sets from actual USS sessions spaced two weeks apart, and we created schedules in which we changed individual or related Sked parameters to try to meet these four goals. We then ran 5000 solutions for each schedule, adding noise. Tab. 3 lists changes that had a signficant effect. It excludes a parameter that had no significant effect (the Endscan weight, which targets stronger sources).

Of the changes that provided significant improvement, the least improvement came from trying to improve temporal coverage with a Minangle value of 30°, which lowered the UTRMS from the value of 18.2 μs (normal Sked parameters) to 16.4 μs (Fig. 5a). One problem is that Minangle only separates successive observations, so the third observation can be close to the first, reducing temporal coverage. Also, we wanted Minangle to force a large azimuth change, but because Minangle is satisfied by an elevation change, it did not fulfill this goal. A Minangle variation that is based on azimuth and/or provides more separation between nonadjacent observations might lower the UTRMS further. Using the Maxscan parameter set to improve source strength worked only slightly better; it only lowered the UTRMS to 16.2 μs (Fig. 5b). One problem might be that in picking stronger sources, this set allows (and can favor) low elevation observations that can raise the UTRMS as shown in Section 3 and in Fig. 5d. We had more success trying to cover key areas by using a horizon mask (with varying minimum elevations) at Kokee (see Tab. 3 for details); a 15° minimum elevation lowered the UTRMS to 15.2 μs (Fig. 5c). The most improvement came from using 18° and especially 15° elevation limits at both stations; raising the USS' 8° elevation limit to 15° lowered the UTRMS from 18.2 to 14.7 μs (Fig. 5d). The 0.5 μs difference between the 15° horizon mask and the 15° elevation limit cases is insignificant, and more work should be done to study and compare the two cases.

Figs. 5c and 5d show that in each case, as the rising elevation limit lowers the UTRMS, it raises the UTFE. This is probably due partly to the UTFE elevation effect noted in Section 3 and partly to changes in sky coverage that occur as the elevation limit removes low elevation observations. So the improvement to the UTRMS

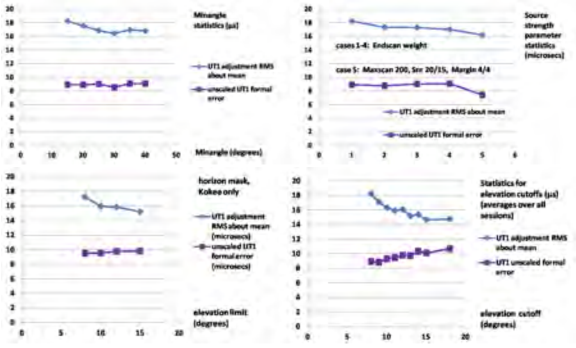

Fig. 5 Effect of Sked parameter changes: Top row, a) Minangle values, b) Maxscan (fifth pair of points). Bottom row, c) Kokee horizon mask with varying minimum elevations, and d) Elevation limits at both Kokee and Wettzell.

comes at the price of raising the UTFE. But the UTFE changes less than the UTRMS (from 8.9 to 10.1 μs, for the 15° elevation limit), so the UTRMS improvement seems worth the larger UTFE.

Fig. 6 compares the 15° elevation limit to the normal Sked parameterization and its 8° limit for the 26 cases. The 15° UTRMS values are better than or comparable to the 8° values in 24 of the 26 sessions, and only the October 2 value is much worse. But another simulation not included here indicates that the UTRMS average could be further improved. October 2 has pathological sky coverage; removal of Wettzell's low elevation sources leaves it with no sources below 32° in one quadrant. Early October might need special handling if an elevation limit is used.

We tried seven combinations of the above parameter changes to try to magnify their effect (Fig. 7). But no combination improved the UTRMS more than the two best individual parameters did. The Endscan weight had little effect on the other parameters, and it can be discarded. We tried four other combinations, but each failed because some of its schedules were truncated to under an hour, because the available source sets could not meet all of the selected conditions.

5 Conclusions and Acknowledgements

The need to refine the USS remains. Target areas are removing low elevation observations and improving temporal distribution, coverage of key areas, and source strength. The best Sked parameter, a 15° elevation limit, improves the average UTRMS from 18.2 to 14.7 μs, but it raises the average UTFE. Also more improvement of the UTRMS is desirable. So new Sked parameters should be identified or created to improve the USS.

Goal	Sked parameter(s)	Purpose	Values that gave improvement
Minimizing low elevation observations	Elevation limit	Minimum elevation allowed for all observations. Applied at both stations.	10,11,12,13,14,15,18°
Coverage of key areas	Horizon mask (station section H line) at Kokee	Specifies a minimum elevation for ranges of azimuths. We set the minimum to 0° at azimuths outside key areas. This forced Sked to only schedule observations within key areas. Then we increased the elevation minimum, starting at 8°, in the key areas.	Minimum elevations of 10,12, and 15° (used for azimuths 300-330, 350-10, and 30-60°; other azimuths had a minimum elevation of 0°)
Stronger sources	1. Maxscan	Maximum allowed scan time. Reducing this excludes weaker sources that cannot achieve an acceptable SNR in the allotted time.	200 seconds (normal Sked value)
	2. Snr	Target minimum SNR.	X-band 20, S-band 15
	3. Margin	Snr minus Margin = absolute minimum SNR.	X-band 4, S-band 4
Better temporal distribution	Minangle	Minimum sky angle between two successive observations. We raised this to try to spread observations (at least successive ones) around.	30°

Table 3 Effect of changing individual (or a set of related) Sked parameters, arranged from most to least effective.

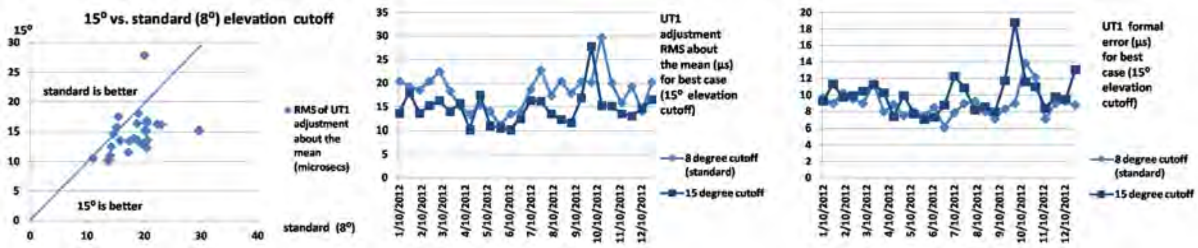

Fig. 6 a) comparison of UTRMS for 15° vs. 8° (normal Sked) elevation limits, b) UTRMS for 15 and 8° limits arranged by date and c) UTFE for 15 and 8° limits by date.

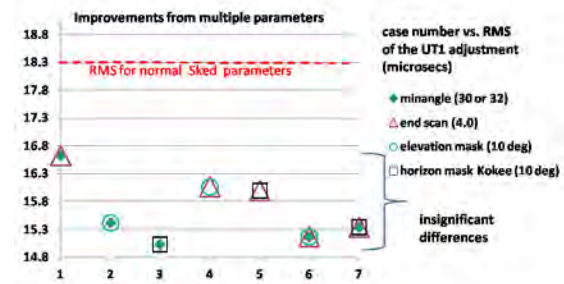

Fig. 7 Combined parameter cases.

We thank Merri Sue Carter (USNO Flagstaff) for generating the alternating STN and USS schedules.

References

K. Baver, J. Gipson, M. S. Carter, and K. Kingham. Assessment of the First Use of the Uniform Sky Strategy in Scheduling the Operational IVS-INT01 Sessions. In D. Behrend and K. Baver, editors, *IVS 2012 General Meeting Proceedings*, pages 251–255. NASA GSFC, NASA/CP-2012-217504.

Assessment of VLBI Intensive Schedules by means of Cluster Analysis

J. Leek, T. Artz, A. Nothnagel

Abstract Intensive VLBI sessions are short duration VLBI experiments of usually one hour duration. They are performed almost daily for a regular determination of UT1 on networks with two or three stations. Due to the small network and the short duration, only a few observations can be performed, i.e., about 30 per single baseline session. Thus, the scheduling is a crucial point for the highest possible quality of the estimated parameters. In this paper, a tool called cluster analysis is examined for its usefulness to compare and classify various schedules. For this purpose, the least-squares adjustment is used to derive similarity values for the different observations. These similarities are subsequently used to group the observations in clusters. For each cluster the impact on a specific parameter, e.g., UT1, can be determined. In this way, groups of important observations are identified. This knowledge yields the opportunity to modify or to create improved schedules.

Keywords Intensives, Scheduling, Cluster Analysis

1 Introduction

The scheduling of VLBI Intensive sessions is a crucial step to obtain reliable results with the best possible accuracy for the Earth's rotation parameter dUT1. Most sensitive for dUT1 determinations are east-west baselines extending to 8000 km and beyond. However, because of the very limited common visibility of the radio telescopes on these baselines and, thus, a small extract of available radio sources, the observations of Intensives have to be selected with great care. Hence, it is desirable to understand and assess the influence of individual observations on the estimated parameters. Applying this knowledge already at the scheduling process will help to create optimized observing plans.

Several studies were done to improve the scheduling of VLBI Intensive sessions (e.g., Baver et al. 2012, or Uunila et al. 2012). In this paper, a new approach for this research area is presented. The main topic of this paper is to get assessment criteria for observing plans via a cluster analysis of the observations. The observations' similarities, which are used for the cluster analysis, are obtained by the least-squares adjustment. More precisely, the similarities are derived from the Jacobian matrix that contain information on the geometry of the design. Thus, it is expected that observations which have been performed under similar geometric conditions would be grouped together. This enables the computation of the influence of groups of observations on the estimated parameters. Furthermore, the influence of these clusters on individual parameters can be detected by the method of parameter reduction.

Judith Leek, Thomas Artz and Axel Nothnagel
Rheinische Friedrich-Wilhelms Universität Bonn, IGG, Nußallee 17, D-53115 Bonn, Germany

2 Cluster Analysis

The basis for the cluster analysis is the data resolution matrix $\mathbf{H}$, which can be computed by the design matrix $\mathbf{A}$ and the covariance matrix $\mathbf{\Sigma_{yy}}$

$$\mathbf{H} = \mathbf{A}\left(\mathbf{A}^T\mathbf{\Sigma}_{\mathbf{yy}}^{-1}\mathbf{A}\right)^{-1}\mathbf{A}^T\mathbf{\Sigma}_{\mathbf{yy}}^{-1} \tag{1}$$

(see e.g. Förstner, 1987).

The following parametrization is used for building the design matrix: the target parameter of Intensive sessions dUT1, three clock parameters for one clock with respect to the reference clock and a zenith wet delay for each station.

The elements of the data resolution matrix have two different meanings. The main diagonal entries h_{ii} are called impact factors because they indicate the in-

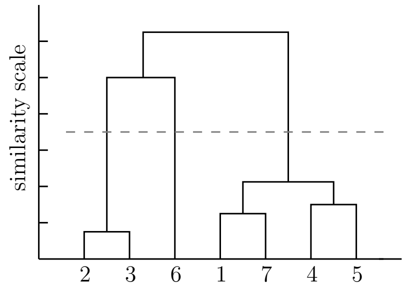

Fig. 1 Dendrogram with a tree cut at a large gap. Beneath the tree cut (dashed line), three clusters with distinct information contents are obtained.

fluence of each observation on the estimated parameters. The off-diagonal elements h_{ij}, named impact co-factors, show the similarities between the observations. Small impact co-factors indicate a significantly distinct information content of the respective observations, whereas large impact co-factors show that the respective observations have been performed under similar geometric conditions. And, thus, the data resolution matrix serves as similarity matrix for the cluster analysis (see, e.g., Gray and Ling 1984, or Hoaglin and Welsch 1978).

The basic cluster analysis algorithm comprises the following simple steps.

1. Compute the similarity matrix (here the data resolution matrix).
2. Merge the closest two clusters into one cluster. [1]
3. Recalculate the similarity matrix to consider the new similarity values between the new cluster and all other clusters. [2]

The steps 2 and 3 have to be repeated until only one cluster remains that contains all observations. In this paper the UPGMA-algorithm (unweighted pair-group method using arithmetic averages, see, e.g., Romesburg 2004) has been used.

The results of the clustering process can be depicted in a map of sorts, called tree or dendrogram. The x-axis of the dendrogram shows the observations and the y-axis shows the similarity scale at which the clusters were merged together. To obtain groups of observations with significantly distinct information contents and not only one big cluster that contains all observations, the subdivision of the dendrogram at a reasonable height is necessary. This so named tree cut defines the number of final clusters and, therefore, the level of detail. A reasonable height for a tree cut is given by a large gap in the dendrogram, which indicates the clustering of two previously significantly distinct clusters, as shown in Fig. 1. Nonetheless, the height of the tree cut is a subjective decision.

[1] Note that each observation is regarded as being in a separate cluster at the very beginning.

[2] By this step, the size of the similarity matrix is reduced by one.

3 Parameter Reduction

The method of parameter reduction enables the estimation of a subset of the original parameters without changing the original functional model (see, e.g., Teunissen, 2000). This method partitions the original linear system (Eq. 2) in a way that the parameter vector $\mathbf{x}$ is divided into two vectors, where the parameters of interest $\mathbf{x}_1$ are separated from the others $\mathbf{x}_2$ (Eq. 3).

$$\mathbf{A}\mathbf{x} = \mathbf{y} \tag{2}$$

$$\begin{bmatrix}\mathbf{A}_1 & \mathbf{A}_2\end{bmatrix}\begin{bmatrix}\mathbf{x}_1 \\ \mathbf{x}_2\end{bmatrix} = \begin{bmatrix}\mathbf{y}_1 \\ \mathbf{y}_2\end{bmatrix} \tag{3}$$

Either a single parameter or a group of parameters can be chosen as parameters of interest. The Eqs. 4 to 6 are used to compute the data resolution matrix and the impact factors for the reduced system.

$$\bar{\mathbf{A}}_1 = \mathbf{A}_1 - \mathbf{A}_2\left(\mathbf{A}_2^T\boldsymbol{\Sigma}_{\mathbf{yy}}^{-1}\mathbf{A}_2\right)^{-1}\mathbf{A}_2^T\boldsymbol{\Sigma}_{\mathbf{yy}}^{-1}\mathbf{A}_1 \tag{4}$$

$$\bar{\mathbf{H}} = \bar{\mathbf{A}}_1\left(\bar{\mathbf{A}}_1^T\boldsymbol{\Sigma}_{\mathbf{yy}}^{-1}\bar{\mathbf{A}}_1\right)^{-1}\bar{\mathbf{A}}_1^T\boldsymbol{\Sigma}_{\mathbf{yy}}^{-1} \tag{5}$$

$$\bar{\mathbf{h}} = diag\left(\bar{\mathbf{H}}\right) \tag{6}$$

In this case the impact factors $\bar{\mathbf{h}}$ indicate the influence of each observation on the parameters of interest only.

This method enables the computation of an average impact factor for each cluster for the parameters of interest. Hence, important groups of observations for individual parameters can be detected.

4 Cluster Analysis of VLBI Intensive Sessions

First, a fictitious Intensive observing plan, at which the result of the clustering can best be seen, has been generated using the scheduling software SEKD (Vandenberg, 1999). For that reason, the uniform sky scheduling method has been used to create an observing plan with the telescopes TSUKUB32 (Japan) and WETTZELL (Germany) using a fictitious source catalog with homogeneously distributed radio sources. The result was an INT2-like session with a uniform cover of the hemisphere above each radio telescope.

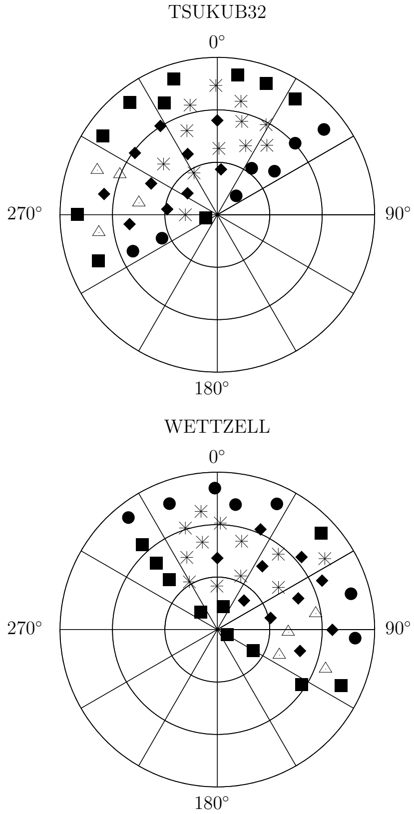

Fig. 2 Sky-plots with clustered observations of the fictitious INT2 session.

	cluster				
	●	△	■	*	◆
dUT1	**0.035**	**0.029**	**0.026**	0.021	0.013
cl_0	0.020	0.007	0.022	0.009	**0.051**
cl_1	0.023	0.004	**0.033**	0.014	**0.032**
cl_2	0.019	0.007	**0.029**	**0.024**	**0.026**
at_A	0.010	0.012	**0.056**	0.013	0.016
at_B	**0.079**	0.004	0.013	0.006	0.023
# obs.	7	4	10	12	10

Table 1 Average impact factors of each cluster for each single parameter. Values that are greater than the average impact factor of one observation on a single parameter (> 0.023) are highlighted. The last row shows the number of observations per cluster.

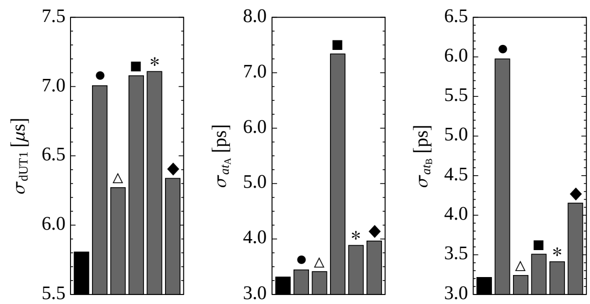

Fig. 3 Formal errors of dUT1 (left), zenith wet delay of station A (center) and zenith wet delay of station B (right). The black bar represents the formal error determined by the original observing plan. The other bars represent the formal error determined without the observations of the labeled cluster.

After applying the cluster analysis to the fictitious session and cutting the dendrogram at a reasonable height five clusters emerged (not shown here). The positioning of the different groups of observations are depicted in the sky-plots of the hemisphere above each telescope (Fig. 2). The observations of the clusters that are denoted by the circle and the square encircle the observations of the other clusters. These are the observations with the lowest elevation values for either telescope.

By the method of parameter reduction, average impact factors of each cluster were computed for each single parameter (Tab. 1). By reference to Tab. 1 can be seen which clusters have a great influence on individual parameters. The important clusters for the target parameter dUT1 are the clusters that are denoted by the circle, the triangle and the square, therefore, observations with low elevations mainly (cf. Fig. 2). The clusters that are denoted by the diamond, the square and the asterisk influence the clock parameters substantially. Observations with low elevations highly influence the atmospheric parameters. Those are arranged in the cluster that is denoted by the square in case of station A (Tsukub32) and the cluster that is denoted by the circle in case of station B (Wettzell).

To validate the identified relations, the formal errors of the parameters were also examined. For this purpose, the changes of the formal errors of the parameters were analyzed if the respective observations of individual clusters were deleted from the observing plan. That is shown for the parameters dUT1, at_A and at_B in Fig. 3. Although the cluster that is denoted by the triangle has a greater average impact factor for dUT1 than the clusters that are denoted by the asterisk and the diamond, the increase of the formal error is bigger when these clusters are removed (Fig. 3 left). This is the result of the greater number of observations in the aforementioned clusters (cf. Tab. 1). The previously identified dominating clusters for the atmospheric parameters were also reflected by the changes of the zenith wet delay's formal errors, i.e., the cluster that is denoted by the square for Tsukub32 and the cluster that is denoted by the circle for Wettzell (Fig. 3 center and right). Since the timing of the observations is crucial for the clock parameters instead of the geometry, the changes of the formal errors of the clock parameters are meaningless. Considering the impact factors for the clock

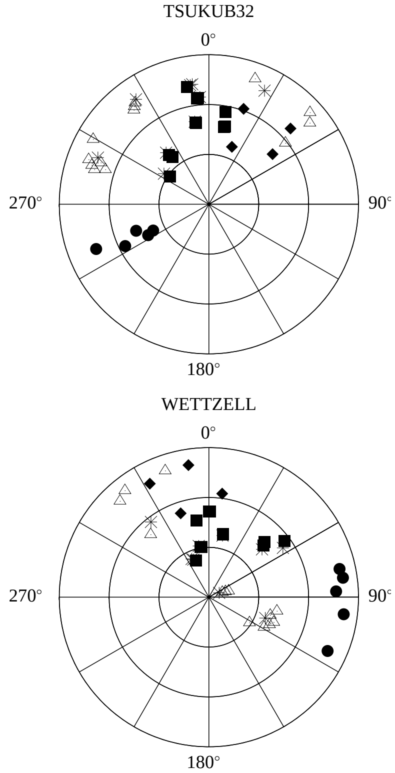

Fig. 4 Sky-plots with clustered observations of the INT2 session k11064.

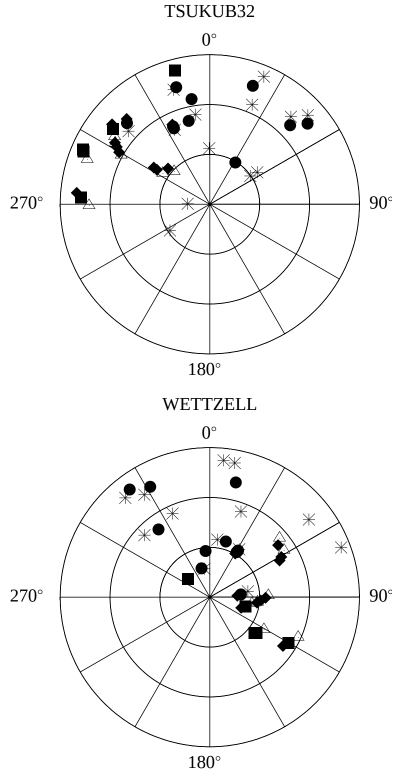

Fig. 5 Sky-plots with clustered observations of the INT2 session k11352.

parameters in chronological order (not shown here), it is visible that the most influential observations are arranged at the beginning, at the middle and at the end of the session. These observations belong to the clusters that are denoted by the diamond, the square and the asterisk mainly.

The analysis of the fictitious session revealed that the cluster analysis is able to detect groups of observations with geometric similarities. Especially observations with low elevations of the respective radio telescopes were separated from other observations. By the reduction of parameters and the examination of the formal errors the influence of different clusters on single parameters was proven.

In the following, results of the cluster analysis of actual Intensive observing plans are examined. For that purpose, two exemplary sessions are shown. Considering the sky-plots of the first session k11064 (Fig. 4), the result of the cluster analysis looks moderately well. In this case the observations of the clusters that are denoted by the circle and the triangle are arranged at the edges mainly and those are the main important clusters for dUT1 and the atmospheric parameters as with the fictitious session (see Tab. 2).

A first look at the second session k11352 assumes that the cluster analysis was not able to group similar observations. The observations of different clusters seem to be distributed almost randomly with no clear geometric distinction. A further investigation revealed a mainly subsequent grouping of the observations. Hence, the conclusion is that the clustering of the observations was also influenced by temporal dependencies between the observations, and thus, that the results of the cluster analysis could not be interpreted purely geometrically.

	cluster				
	●	△	■	*	◆
dUT1	**0.036**	**0.029**	**0.026**	0.013	0.012
at_A	0.009	**0.041**	0.022	0.013	0.017
at_B	**0.060**	**0.033**	0.001	0.018	0.022
# obs.	5	13	11	9	4

Table 2 Average impact factors of each cluster for the parameters dUT1, at_A and at_B of the INT2 session k11064. Values that are greater than the average impact factor of one observation on a single parameter (> 0.023) are highlighted. The last row shows the number of observations per cluster.

	cluster				
	●	△	■	∗	◆
dUT1	**0.033**	**0.032**	**0.028**	0.018	0.008
at_A	0.011	0.011	**0.091**	0.013	0.019
at_B	0.015	0.004	0.002	**0.058**	0.005
# obs.	10	7	5	13	10

Table 3 Average impact factors of each cluster for the parameters dUT1, at_A and at_B of the INT2 session k11352. Values that are greater than the average impact factor of one observation on a single parameter (> 0.022) are highlighted. The last row shows the number of observations per cluster.

5 Conclusions

The data resolution matrix of the least-squares adjustment was used as similarity matrix for the cluster analysis. The influence of different clusters on individual parameters was determined by the method of parameter reduction.

In case of a fictitious Intensive session with homogeneously distributed observations, the cluster analysis detected groups of observations with geometric similarities. Especially observations with low elevations are important for both the target parameter dUT1 and the atmospheric parameters. The cluster analysis of real observing plans revealed an additional influence by temporal dependencies between the observations. Therefore, an important consideration would be to examine the temporal correlations of the observations to strengthen the validity of the cluster analysis, or to find out how they could be considered in the scheduling process. Then the cluster analysis would be a valuable tool to create improved VLBI Intensive observing plans.

Concerning the desire to use the cluster analysis for a classification of observing plans, some probably useful criteria have been found out. These include the number of important clusters for the parameter dUT1, the magnitudes of the average impact factors and the size of the clusters. E.g., since the arithmetic averages of the impact factors of a cluster were used, it is assumable that the more observations in a cluster the less the probability that all of them highly influence the same parameter.

References

K. Baver, J. Gipson, M. S. Carter, and K. Kingham. Assessment of the First Use of the Uniform Sky Strategy in Scheduling the Operational IVS-INT01 Sessions. In D. Behrend and K. Baver, editors, *IVS 2012 General Meeting Proceedings*, pages 251 – 255. NASA/CP, 2012.

W. Förstner. Reliability analysis of parameter estimation in linear models with applications to mensuration problems in computer vision. *Computer Vision, Graphics, and Image Processing*, 40 (3):273 – 310, Dec. 1987.

J. B. Gray and R. F. Ling. K-Clustering as a detection tool for influential subsets in regression. *Technometrics*, 26(4):305 – 318, 1984.

D. C. Hoaglin and R. E. Welsch. The Hat Matrix in Regression and ANOVA. *The American Statistician*, 32(1):pp. 17–22, 1978. ISSN 00031305.

H. Romesburg. *Cluster Analysis For Researchers*. Lulu Press, North Carolina, 2004. ISBN 9781411606173.

P. Teunissen. *Adjustment Theory: An Introduction*. Series on Mathematical Geodesy and Positioning. Delft University of Technology, 2000. ISBN 9789040719745.

M. Uunila, A. Nothnagel, and J. Leek. Inflence of Source Constellations on UT1 Derived from IVS INT1 Sessions. In D. Behrend and K. Baver, editors, *IVS 2012 General Meeting Proceedings*, pages 395 – 399. NASA/CP, 2012.

N. Vandenberg. *Interactive/Automatic Scheduling Program. Program Reference Manual*. NASA/Goddard Space Flight Center, NVI, Inc., 1999.

VLBI Observations of Geostationary Satellites

T. Artz, A. Nothnagel and L. La Porta

Abstract For a consistent realization of a Global Geodetic Observing System (GGOS), a proper tie between the individual global reference systems used in the analysis of space-geodetic observations is a prerequisite. For instance, the link between the terrestrial, the celestial and the dynamic reference system of artificial Earth orbiters may be realized by Very Long O Baseline Interferometry (VLBI) observations of one or several satellites. In the preparation phase for a dedicated satellite mission, one option to realize this is using a geostationary (GEO) satellite emitting a radio signal in X-Band and/or S-Band and, thus, imitating a quasar. In this way, the GEO satellite can be observed by VLBI together with nearby quasars and the GEO orbit can, thus, be determined in a celestial reference frame. If the GEO satellite is, e.g., also equipped with a GNSS-type transmitter, a further tie between GNSS and VLBI may be realized.

In this paper, a concept for the generation of a radio signal is shown. Furthermore, simulation studies for estimating the GEO position are presented with a GEO satellite included in the VLBI schedule. VLBI group delay observations are then simulated for the quasars as well as for the GEO satellite. The analysis of the simulated observations shows that constant orbit changes are adequately absorbed by estimated orbit parameters. Furthermore, the post-fit residuals are comparable to those from real VLBI sessions.

Keywords VLBI, Geostationary Satellites, Signal Characteristics, Scheduling, Simulation

Thomas Artz, Axel Nothnagel and Laura La Porta
Rheinische Friedrich-Wilhelms Universität Bonn, Institut für Geodäsie und Geoinformation, Nußallee 17, D-53115 Bonn, Germany

1 Introduction

Nowadays, two of the fundamental geodetic products are the International Terrestrial Reference Frame (ITRF) and a time series of Earth Orientation Parameters (EOPs). To calculate these products, the geodetic space techniques Doppler Orbitography and Radiopositioning Integrated by Satellite (DORIS), Global Navigation Satellite System (GNSS), Satellite Laser Ranging (SLR), and Very Long Basline Interferometry (VLBI) are used (e.g., Altamimi et al. 2011, Bizouard and Gambis 2011). However, the different techniques have their own observing networks which are only connected by local measurements at so-called fundamental stations. Thus, these local ties provide the backbone of the ITRF and the EOP series. Furthermore, DORIS, GNSS and SLR measurements refer to Earth orbiting satellites which are not connected to each other either.

Concerning the EOPs, another difficulty arises: only VLBI is able to determine the whole set of parameters as these measurements refer to the quasi-inertial frame of radio sources (the International Celestial Reference Frame, ICRF). The other techniques cannot determine Universal time (UT1) and nutation without hypothesis, as these parameters are highly correlated with the ascending nodes of the satellite orbits.

In the last years, several studies have been performed to assess the benefit of Earth orbiting satellites which are equipped with instruments that enable the observation with several geodetic space techniques. These studies have, e.g., been done at the German Research Centre for Geosciences (GFZ) within the MicroGEM (Microsatellites for GNSS Earth Monitoring), NanoGEM or NanoX projects, or at the National Aeronautics and Space Administration (NASA) within the Geodetic Reference Antenna in Space (GRASP) mission proposal. The equipment of a satellite used in such programs might consist of different antennas. These could on the one hand emit signals such as GNSS signals, on the other hand radiation similar to quasar emission, which is then observed by VLBI telescopes on Earth. Furthermore, SLR reflectors or DORIS receiving antennas are possible on board of the satellite. Thus, a tie of the four fundamental techniques would be realized in space. This would significantly improve the Global Geodetic Observing System (GGOS) as the terrestrial, the celestial and the dynamic reference systems of artificial Earth orbiters would be linked together. Furthermore, improvements of the EOPs can be expected as the frame link permits establishing the sensitivity of GNSS and SLR to UT1 as well as to nutation.

To realize this link, VLBI measurements have to be a fundamental part of the observation scenario. These satellite observations with VLBI telescopes are not typical but not new. Especially in the last decade, VLBI was used for orbit determinations in satellite missions (e.g., Pogrebenko et al. 2004, Kikuchi et al. 2009, Ouyang et al. 2010, Tornatore et al. 2011). In contrast to standard VLBI, a different delay model has to be used as a curved wave-front has to be taken into account instead of a plane one (e.g., Klioner 1991, Moyer 2000, Sovers et al. 1998, Sekido and Fukushima 2006).

In this paper, one option for the emission of quasar-like noise on board of a satellite is described. By using a geostationary satellite (GEO), the whole analysis chain is presented. For that purpose, an observing plan for a large observing network is generated where quasar as well as GEO observations are scheduled. In a second step, observations for this session are simulated by taking stochastic components into account. Finally, simple orbit parameters are estimated.

2 Signal Characteristics

To embed GEO observations successfully into geodetic VLBI sessions, any re-configurations of the VLBI equipment should be avoided. Thus, a noise diode which could be placed onboard the satellite to mimic a quasar should produce a signal which meets the prerequisites of the observing antennas.

Currently, it seems feasible to generate full band noise for S/X-band compatibility. This means that 740 MHz in X-band and 160 MHz in S-Band have to be covered. Using the technique of bandwidth synthesis, 16 MHz channels are employed within these bands to represent the sky frequencies of 8210 – 8950 MHz and 2225 – 2385 MHz. This common frequency setup is shown in Fig. 1 a) for X-band. The power requirements for a noise diode on board a GEO satellite that mimics a quasar with a flux density of 0.1 Jy would be

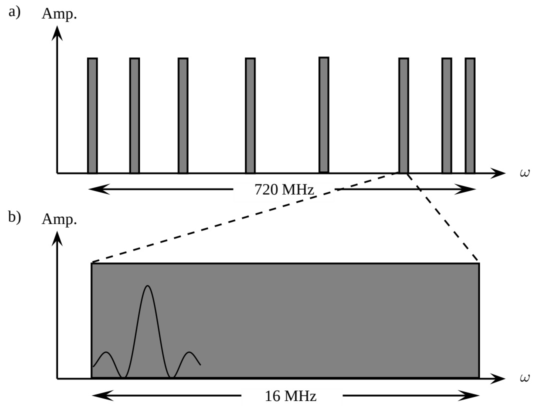

Fig. 1 a) Common frequency setup for VLBI X-band observations; b) narrow band modulation within each 16 MHz subchannel for DOR.

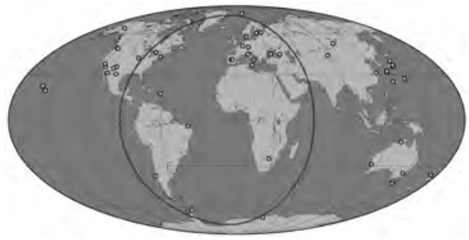

Fig. 2 Footprint of a GEO satellite at longitude 15.5° W for elevations above 15° on Earth together with IVS sites.

about 1.2 mW. Thus, the maintenance of such a VLBI beacon would not be an issue.

As a further thought, a GNSS-like modulation can be applied to each channel (see Fig. 1 b) to enable Differential One-way Ranging (DOR, e.g., James et al. 2009). DOR has not been taken into account in this paper although it provides a higher signal to noise ratio and consequently would permit to determine the observables with better precision.

3 Scheduling

When scheduling VLBI observations of a GEO satellite, one has to take into account that the satellite is always observable with almost identical azimuth and elevation. However, no global network is possible. As the volume of the observing network is crucial for the precision of the EOPs, a GEO longitude of 15.5° W has been chosen. As depicted in Fig. 2, this position allows for observing sites in Europe, the East coast of North America, South America and Antarctica.

If the GEO satellite emits a signal with the characteristics as described in Sec. 2, radio telescopes will be able to observe quasars and GEOs in alternating succession. Thus, the GEO can be added to a scheduling program as a pseudo-quasar. For the scheduling presented here, the program SKED (Gipson, 2012) is used. Although SKED has the build-in option to schedule satellites, some modifications have been made by including the simplified pertubations model (SDP4, Hujsak 1979) on the basis of the Spacetrack #3 report (Hoots and Roehrich, 1980).

The modified version of SKED was used to perform automatic schedules where the GEO has been treated as a quasar and uniform sky-coverage has been used as the optimization criteria. In this way, a session with 11 sites has been derived. The repeat cycle of the GEO is about 40 min. on average. In total, there are 1340 GEO observations in 35 scans compared to 6963 quasar observations.

4 Simulation and Validation

In the next step, a simulation of observations has been performed for the scheduled session. For the simulation process, a deterministic and a stochastic part have been applied.

The deterministic part is calculated using the VTD library (Petrov, 2012) which provides state of the art modeling. Furthermore, VTD generates consistent delay models for far and near zone objects in the Solar System Barycenter Frame. However, the deterministic part is not an issue in the present investigation as the same components are used for simulation as well as for parameter estimation. This part only becomes relevant when the simulated observations are provided to other analysis packages.

For the stochastic part of the VLBI delay, three components have been taken into account as it was also done for the VLBI2010 simulation (e.g., Wresnik et al. 2009). These are clock behavior τ_{cl}, atmospheric variations τ_{at} and baseline dependent white noise τ_ϵ with a standard deviation of 10 ps. The individual stochastic components have been tuned to match a rough estimate of the VLBI error budget (see Tab. 1).

The clock variations have been modeled by a power-law process (Kasdin and Walter, 1992) that has been adjusted to reach an Allan standard deviation (ASD) of $1 \cdot 10^{-14}$@50 min. On different time scales different components are dominating the process. For instance white and flicker phase modulation are dominating on short time scales, while on time scales below one hour, flicker and random walk frequency modulation is dominating. Although atomic clocks are more precise by about one order of magnitude (e.g., Giordano et al. 2011), the chosen ASD is reasonable as the simulations represent variations due to thermal and other physical responses of the cabling between the active hydrogen maser and the receiving system as well.

The atmospheric variations are modeled as equivalent zenith wet delays and mapped to the actual elevation of an observation as presented by Nilsson and Haas (2010). For the simulation a refractive index structure constant of $C_n{}^2 = 1 \cdot 10^{-14} \mathrm{m}^{-\frac{2}{3}}$ and constant wind speeds of 2 m/h in north-south as well as 8 m/h in east-west direction have been used.

An example of the simulated stochastic components is shown in Fig. 3. Obviously, the clock variations dominate the long term variations, while short term fluctuations are primarily forced by the wet atmospheric effects. This result is exactly what could be expected from and was aspired by the simulation setup.

The simulated observations have finally been used in a least squares adjustment with VTD being used to calculate the theoretical delay. Thus, the reduced ob-

Table 1 Rough estimate of the error budged for a VLBI observation at 30° elevation. Ionosphere and hydrostatic atmosphere are considered error free as perfect calibration and modeling can be assumed (RSS = Root Sum Squared).

Individual component c_i		ps
Correlation process	8 ps	8
Ionosphere	0 ps	0
Hydrostatic atmosphere	0 ps	0
Wet atmosphere		
in zenith direction	15 ps	
mapping function	1%	
slant delay	at 30°	30
Clock	17 ps	17
Instrumental delays		
electronics	5 ps	5
paraboloid deformation	6 ps	6
Geophysical model errors	10 ps	10
RSS		38

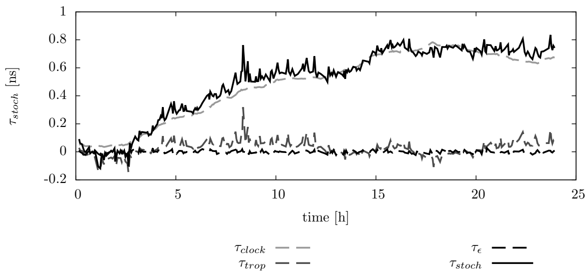

Fig. 3 Simulated stochastic delay variations (black solid line) at Fortaleza (Brazil) for quasar as well as for GEO observations. The individual components are shown by the dashed line: clock variations in light gray, atmospheric variations in dark gray and the white noise process in black.

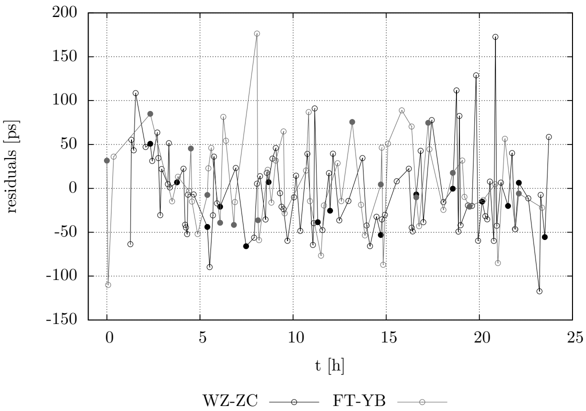

Fig. 4 Post-fit residuals for observations on the baselines Wettzell (Germany) – Zelenchukskaya (Russia) in black and Fortleza (Brazil] – Yebes (Spain) in gray. Solid dots indicate GEO observations and the circles the quasar observations.

servations (observed minus computed) are given only by the stochastic components of the simulated delays. Station positions and EOPs have been estimated as constant correction for the entire session. Furthermore, clock parameters relative to one reference clock have been estimated with second degree polynomials and additional hourly constant piece-wise linear functions (CPWLF). For the atmospheric variations, zenith wet delay has been estimated with hourly CPWLF, and gradients in north-south and east-west direction at the beginning and at the end of the session. Finally, for the GEO orbit, constant corrections in X-, Y- and Z-direction have been estimated for the entire session.

The post-fit residuals on two baselines are depicted in Fig. 4. No difference can be seen between quasar and GEO observations. Furthermore, the weighted root mean squared residual delay for the entire session is 32 ps. This is comparable to real VLBI sessions and also meets the error budged considerations.

When the a priori GEO orbits for the parameter estimation are changed by, e.g., 10 cm w.r.t. the orbits in the simulation run, the results are comparable. The residuals are almost identical and the orbit estimates are offset by the same value as the a priori orbit manipulations. So, these results validate the simulation and prove the suitability of the GEO observations for orbit determination within a standard VLBI session.

5 Conclusions and Outlook

A concept for the realization of a GEO satellite with a VLBI beacon on board has been presented. Together with equipment of other geodetic space techniques, this would provide a link in space and, thus, represent the counterpart to the local ties on Earth. The proposed signal characteristics are full band noise in eight 16 MHz channels for X-band and six channels for S-band which meets todays VLBI receiving systems. Additionally, a modulated narrow band signal in either channel is recommended to enable DOR. Beyond that, investigations concerning broad band noise for VLBI2010 compatibility should be done in the future.

Scheduling of VLBI sessions with a modified version of SKED has been done. In this way, an almost global observing network has been accomplished and realistic observations have been simulated. In a parameter adjustment, typical VLBI as well as orbit parameters have been estimated reliably.

Beside other realizations of the emitted signal, future investigations should be done concerning improved observation scenarios. For instance, quasar – GEO – quasar cycles are imaginable. In addition, the parameterization of the GEO's orbit in the ICRF has to be done in a more sophisticated way, e.g., with Kepler elements and additional stochastic components. However, reasonable progress in this field might only be achieved within a combination of GNSS and VLBI observations.

Acknowledgements This work has been partly performed under ESA contract 4000103328/2011/NL/WE (activity: AO/1-6311/2010/F/WE. "Geodesy and Time Reference in Space (GETRIS)").

References

Z. Altamimi, X. Collilieux, and L. Métivier. ITRF2008: an improved solution of the international terrestrial reference frame. *J Geod*, 85(8):457 – 473, 2011. doi: 10.1007/s00190-011-0444-4.

C. Bizouard and D. Gambis. The combined solution C04 for earth orientation parameters consistent with international terrestrial reference frame 2008. Web document `ftp://hpiers.obspm.fr/iers/eop/eopc04/C04.guide.pdf`, Jan. 2011.

V. Giordano, S. Crop, P. Bourgeois, Y. Kersale, E. Rubiola, M. Mrad, C. Langham, M. Oxborrow, and W. Schäfer. Cryogenic sapphire microwave oscillators for space, metrology and scientific applications. In *General Assembly and Scientific Symposium, 2011 XXXth URSI*, pages 1 – 4, 2011. doi: 10.1109/URSIGASS.2011.6050311.

J. Gipson. GSFC VLBI SKED Software Package. Web document `http://lupus.gsfc.nasa.gov/software_sked.htm`, 2012.

F. R. Hoots and R. L. Roehrich. Spacetrack report no. 3: Models for propagation of NORAD element sets. Technical report, Aerospace Defense Center, Peterson Air Force Base, 1980. (available electronically at `http://www.celestrak.com/NORAD/documentation/spacetrk.pdf`).

R. S. Hujsak. A restricted four body solution for resonating satellite with an oblate earth. In *American Institute of Aeronautics and Astronautics Conference,* 25 – 27 June 1979, Provincetown, Mass., 1979.

N. James, R. Abello, M. Lanucara, M. Mercolino, and R. Madd. Implementation of an ESA delta-dor capability. *Acta Astronaut*, 64(11 – 12):1041 – 1049, 2009. doi: 10.1016/j.actaastro.2009.01.005.

N. Kasdin and T. Walter. Discrete simulation of power law noise. In *Proceedings of the 1992 IEEE Frequency Control Symposium,* 27 – 29 May 1992, Hershey, pp 274 – 283, 1992.

F. Kikuchi, Q. Liu, H. Hanada, N. Kawano, K. Matsumoto, T. Iwata, S. Goossens, K. Asari, Y. Ishihara, S. Tsuruta, T. Ishikawa, H. Noda, N. Namiki, N. Petrova, Y. Harada, J. Ping, and S. Sasaki. Picosecond accuracy VLBI of the two subsatellites of SELENE (KAGUYA) using multifrequency and same beam methods. *Radio Sci*, 44:RS2008, 2009. doi: 10.1029/2008RS003997.

S. A. Klioner. General Relativistic Model of VLBI Observables. In W. E. Carter, editor, *Proceedings of AGU Chapman conference on geodetic VLBI: Monitoring Global Change*, NOAA Technical Report NOS 137 NGS 49, pp 188 – 202. American Geophysical Union, 1991.

T. D. Moyer. Formulation for observed and computed values of deep space 4 network data types for navigation. JPL Monograph JPL Publication 00-7, JPL, 2000.

T. Nilsson and R. Haas. Impact of atmospheric turbulence on geodetic very long baseline interferometry. *JGR*, 115: B03407, 2010. doi: 10.1029/2009JB006579.

Z. Ouyang, C. Li, Y. Zou, H. Zhang, C. L, J. Liu, J. Liu, W. Zuo, Y. Su, W. Wen, W. Bian, B. Zhao, J. Wang, J. Yang, J. Chang, H. Wang, X. Zhang, S. Wang, M. Wang, X. Ren, L. Mu, D. Kong, X. Wang, F. Wang, L. Geng, Z. Zhang, L. Zheng, X. Zhu, Y. Zheng, J. Li, X. Zou, C. Xu, S. Shi, Y. Gao, and G. Gao. Primary scientific results of change-1 lunar mission. *Science China Earth Sciences*, 53(11):1565 – 1581, 2010. doi: 10.1007/s11430-010-4056-2.

L. Petrov. VTD library. Web document `http://vlbi.gsfc.nasa.gov/vtd/`, 2012.

S. V. Pogrebenko, L. I. Gurvits, R. M. Campbell, I. M. Avruch, J.-P. Lebreton, and C. G. M. van't Klooster. VLBI tracking of the Huygens probe in the atmosphere of Titan. In A. Wilson, editor, *Planetary Probe Atmospheric Entry and Descent Trajectory Analysis and Science*, Vol 544 of *ESA Special Publication*, pp 197 – 204, Feb. 2004.

M. Sekido and T. Fukushima. A vlbi delay model for radio sources at a finite distance. *JoG*, 80:137 – 149, 2006. doi: 10.1007/s00190-006-0035-y.

O. J. Sovers, J. L. Fanselow, and C. S. Jacobs. Astrometry and geodesy with radio interferometry: experiments, models, results. *Rev Mod Phys*, 70:1393 – 1454, 1998. doi: 10.1103/RevModPhys.70.1393.

V. Tornatore, R. Haas, D. D. S. Pogrebenko, S. Casey, G. M. Calves, and A. Keimpema. Single baseline GLONASS observations with VLBI: data processing and first results. In W. Alef, S. Bernhart, and A. Nothnagel, editors, *Proceedings of the 20th European VLBI for Geodesy and Astrometry Working Meeting,* 29 – 30 March 2011, Bonn, pages 162 – 165. Schriftenreihe des Instituts für Geodäsie und Geoinformation der Rheinischen-Friedrich-Wilhelms Universität Bonn, No. 22, 2011.

J. Wresnik, J. Boehm, A. Pany, and H. Schuh. VLBI2010 simulations at IGG Vienna. In G. Bourda and P. Charlot and A. Collioud, editor, *Proceedings of the 19th European VLBI for Geodesy and Astrometry Working Meeting,* 24 – 25 March 2009, Bordeaux, pages 147 – 150. Université Bordeaux 1 - CNRS - Laboratoire d'Astrophysique de Bordeaux, Sept. 2009. (available electronically at `http://www.u-bordeaux1.fr/vlbi2009/proceedgs/33_Wresnik.pdf`).

Co-location of space geodetics techniques in Space and on the ground

J. Kodet, Chr. Plötz, K.U. Schreiber, A. Neidhardt, S. Pogrebenko, R. Haas, G. Molera, I. Prochazka

Abstract The most demanding goal of the Global Geodetic Observing System (GGOS) initiative is the definition of station positions to an accuracy of 1 mm and the corresponding velocities to 0.1 mm/year. Fundamental stations are core sites in this respect, because they collocate the geodetic relevant space techniques. However this requires unprecedented control over local ties, intra- and inter-technique biases. To improve the accuracy of the geodetic techniques, new concepts for the monitoring and controlling of local ties and biases have to be implemented. We are developing a symmetric two-way measurement technique to identify unaccounted system delays within and between the instrumentation of the Geodetic Observatory Wettzell. It requires redesign of the VLBI (Very Long Baseline Interferometry) phase calibration generator to be compatible with such an two-way measurement technique and VLBI2010. Another activity is the mapping of Global Navigation Satellite System (GNSS) satellites into the frame of the quasars using VLBI telescope, in geodetic mode. This corresponds to a collocation of geodetic techniques in space. The receiver of the 20 m radio telescope Wettzell (RTW) has been modified to measure the GNSS L1 signal without changing the physical reference point. Preliminary experiments have already been executed.

J. Kodet, K.U. Schreiber and A. Neidhardt
Forschungseinrichtung Satellitengeodäsie, Technische Universität München, Geodätisches Observatorium Wettzell, Sackenrieder Str. 25, D-93444 Bad Kötzting, Germany
Chr. Plötz
Bundesamt für Kartographie und Geodäsie, Geodätisches Observatorium Wettzell, Sackenrieder Str. 25, D-93444 Bad Kötzting, Germany
I. Prochazka
Czech Technical University, Prague, Czech republic
S. Pogrebenko and G. Molera
Joint Institute for VLBI in Europe, Dwingeloo, Netherlands
R. Haas
Onsala Space Observatory, Onsala, Sweden

Keywords GNSS with VLBI, Two-way Measurement, L-band receiver

1 Introduction

All the major measurement techniques of the space geodesy are characterized by a very high measurement sensitivity, which resolves the measured quantities, such as the range to satellites or delays between radio telescopes for signals from quasars sources to about 1 part in 10^9. While all the different observing stations have an impressive precision, the accuracy still carries biases in excess of estimated measurement precision. Within each of the techniques, these errors are minimized by a non linear data fitting process.

Fundamental stations on the other side are important, because they are providing a link from one measurement technique to the other. However this is also the link, where discrepancies between precision and accuracy become evident. The Geodetic Observatory Wettzell is one of these fundamental stations and has repeatedly carried out survey campaigns, which reproduce the geometric relationship between the various geodetic markers on the observatory with 2 mm accuracy. A history of nine such consistent campaigns covering more than 20 years in time has been built up in Wettzell. Summarizing up the results of the local surveys in Wettzell, one can conclude that local ties in Wettzell lies in order of 1-2 mm. It is well below the biases, which one can observe between different observations techniques. Therefore it is important to take a closer look on the intra-technique biases, to undertake every effort for its reduction. In Wettzell we are systematically working on new calibration techniques, which try to capture not measured biases.

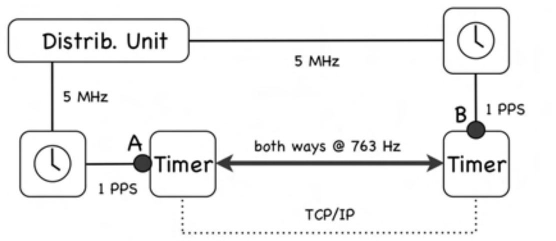

Fig. 1 Block diagram of the TWTT concept for the estimation of the offset and drift of two clocks.

2 Inter-Technique Comparison and Two-Way Measurement Concepts

The Two-Way-Time-Transfer (TWTT) method is a powerful tool for finding offsets and drifts in distributed timing systems (fig. 1). A highly reciprocal system with two highly resolving timers was developed at the Czech Technical University in Prague. The event timers use a measurement method that is based on the fact that a transversal SAW filter, which is excited by a short pulse generates a finite-time signal with highly suppressed spectra outside a narrow frequency band. It results from the sampling theorem, which tells, if the responses to two excitations are sampled at clock ticks, they can be precisely reconstructed from a finite number of samples. Then they can be compared to determine the time interval between the two excitations [Panek (2007)]. A detailed analysis of measurement errors of this method has been given in [Panek (2008-1)] and [Panek (2008-2)].

Using TWTT concepts the differences between the two clocks can be characterized to better than 1ps between two points A and B with a distance of more than 100 m apart. The principal of operation consists of two steps. At first a pulse generator in the timer A generates a pulse, which is timed at both devices, using the interconnecting coaxial cable. Then the process is repeated with a pulse generator in the timer B passing through the cable in the other direction. From this pair of measurements the timescale offset between the two timers can be obtained as

$$\Delta\tau = \frac{1}{2}\left((t_{B1} - t_{A1}) + (t_{B2} - t_{A2})\right). \qquad (1)$$

On the Geodetic Observatory Wettzell we have investigated the stability of the local time offset between the Caesium master standard and the GNSS laboratory. The results are given in fig. 2. Both event timers were connected to a local 100 MHz source at point A (time laboratory) and point B (GNSS room) derived from a common 5 MHz frequency distributor of the observatory. Timing the 1 pps pulses at the master clock and in the GNSS room with the TTWT concept provided a stable offset of around 549.7 ns over almost 20 days.

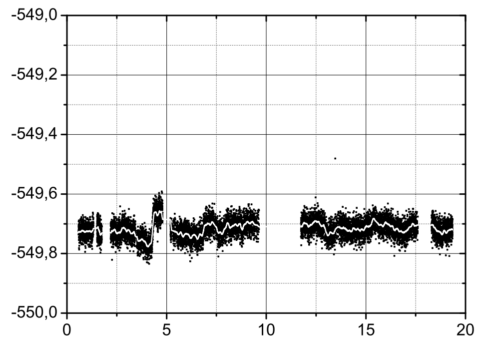

Fig. 2 Time offset comparison between the Master Clock (MC) in the time laboratory and the GNSS room: the time scales in both places are formed by cesium standards and are located in different buildings with a distance of 100 m apart.

3 GNSS satellite observations

Observing the GNSS satellites with telescopes of the VLBI Service for Geodesy and Astrometry (IVS) in near real-time, with high precision and directly in the reference frame, which is defined by the extragalactic radio sources (International Celestial Reference Frame) is challenging, because it can be used for the combining of data from the Satellite Laser Ranging (SLR), the GRACE satellite mission, the DORIS systems, and from the GNSS receivers themselves [Dickey (2010)].

In order to facilitate the inter-technique comparison between GNSS and VLBI, we have added a receiver chain in parallel to the standard S band channel of the 20 m radio telescope Wttzell. The additional receiver allows the detection of L1-band signals of the GNSS satellites with VLBI, keeping the physical reference point of the feed (fig. 3 and 4). The new receiver chain was very helpful in establishing the total power level balance from GNSS satellites. We found that the limiting part of the S-band receiver chain cannot be found in the S-band Low Noise Amplifiers (LNAs), however there is a strong attenuation of the microwave component, which transfers circular to the rectangular waveguide.

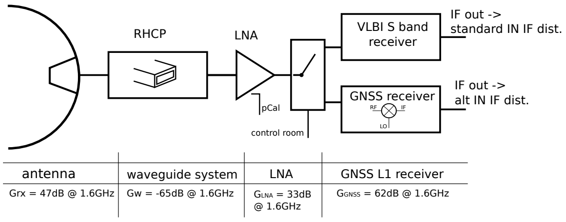

Fig. 3 The block diagram shows, how the L1-band GNSS receiver is connected in parallel with the old S-band receiver.

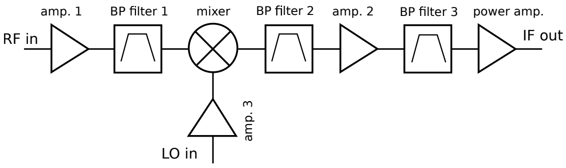

Fig. 4 The principal block diagram of the used components in the new GNSS receiver.

To observe satellite passages with the 20 m radio telescope Wettzell, it was necessary to prepare suitable schedules for the NASA Field System, which is used to control the observation session. To enable this, the prediction software from the Satellite Laser Ranging System, which uses the orbit predictions in form of the Consolidated Prediction Format (CPF), was extended. Now it is able to produce elementary schedule files with pointing information for different time intervals with sampling steps of the passage greater or equal to one second. Another tested possibility was the direct usage of Two-Line Elements, which were converted to track points for the antenna control unit. The preliminary experiments were focused on finding a GNSS signal, which was recorded using the usual Mark5B system. With a preliminary Matlab script we generated Glonass ranging codes and performed a signal acquisition (fig. 5).

We are now working towards a number of common test measurements with the Onsala station. A first common observation with Onsala, Sweden was already possible. The used schedule for this satellite tracking was gently offered by the Joint Institute for VLBI in Europe (JIVE) and used right ascension and declination pointing data with sampling steps of 15 seconds. The first common experiment was already executed successfully. Correlations between the station Onsala and Wettzell were found during the correlation at JIVE. Currently the correlation results are under further analyses.

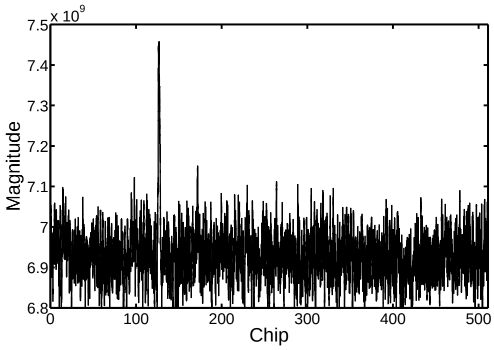

Fig. 5 Results from the correlation between the raging code of Glonass 118, which was generated in a PC, and the recorded VLBI data.

4 Conclusions

The Global Geodetic Observing System (GGOS) requires both, a reduction in measurement errors as well as a considerable reduction of systematic errors within the measurement techniques of space geodesy. At the same time, new demands like highly accurate time transfer emerge. Current geodetic observatories are not yet equipped for these demands. The Geodetic Observatory Wettzell has embarked on the modernization of the time and frequency distribution for all the techniques of space geodesy. It also applies highly resolving two-way time transfer techniques in order to find and eliminate unaccounted systematic errors within VLBI, SLR and GNSS. It must be well assisted by inter- and intra-technique collocations on ground and in space in response to the challenging GGOS demands.

5 Acknowledgement:

This research has been supported by DFG FOR1503. The authors wish to thank the personnel at the VLBI stations of Onsala and at the JIVE correlator for their support of the experiment.

References

Panek, Petr; Prochazka, Ivan: Time interval measurement device based on surface acoustic wave filter excitation, providing 1 ps precision and stability *Review of Scientific Instruments*, volume 79, pages 094701. AIP, 2007. doi: 10.1063/1.2779217.

Panek, Petr: Random Errors in Time Interval Measurement Based on SAW Filter Excitation. *IEEE Transactions on Instrumentation and Measurement*, volume 57, pages 1244-1250., 2008. doi: 10.1109/TIM.2007.915465.

Panek, Petr: Time Interval Measurement Based on SAW Filter Excitation *IEEE Trans. Instr. Meas*, volume 57, pages 2582-2588., 2008. doi: 10.1109/TIM.2008.925014.

Dickey, John: How and Why to do VLBI on GPS *Proceedings of the Sixth General Meeting of the IVS.*, pages 65-69, 2010. *http://ivscc.gsfc.nasa.gov/publications/gm2010/dickey.pdf*.

On the possibility of using VLBI phase referencing to observe GNSS satellites

V. Tornatore, A. Mennella

Abstract The phase referencing technique is an observing method that could contribute to improve accuracy in GNSS satellite positioning and to obtain satellite coordinates directly in ICRF. However, the strong power emitted by the satellites compared to the very low emission of natural radio sources (calibrators) could represent a limiting factor. In fact, the satellite signal can be easily detected through near sidelobes when observing, at the same satellite frequency, the natural calibrator in the main beam. With this work we have run some simulations for some European VLBI antennas using the GRASP (General Reflector antenna Analysis Software Package) v.10 software to assess the relative power contribution of satellites in the near sidelobes when observing in L-band a natural calibrator in the main beam. For each examined station, we have evaluated the minimum angular distance between the satellite and the calibrator to avoid near-sidelobes straylight contamination from the satellite emission when the calibrator is tracked. A discussion of the obtained results is presented and possible observational methods are suggested.

Keywords Phase referencing, GNSS, sky-tie

1 Introduction

Phase referencing is a succesful and increasingly used phase-calibration scheme for VLBI. Two methods have been used extensively for phase-sensitive VLBI: astrometry phase delay fitting and phase-referenced mapping, the lastone for imaging of some faint sources in case it is important to retain phase information (Lane and Muterspaugh (2007)).

In the phase referencing technique a target source is observed almost simultaneously by fast switching antennas, with an adjacent phase reference calibrator, most commonly a quasar. Fringe phase calibration values, of the known quasar, are applied to the fringe phases of the target source in order to compensate for the rapid target fringe phase fluctuations due to the turbolent media of the atmosphere, as well as to remove long-term phase drifts due to geometrical errors and smoothly variable atmospheric delay errors and instrumental errors.

The switching cycle time has to be typically shorter than a few minutes and the calibrator has to be located closely enough to the target (within a few degrees). Various astrometric observations in the VLBI field carried out with the phase referencing technique yielded to relative positions accuracy of the order of 10μas (Asaki et al. (2007)).

Differential observations largely cancel the effects of the errors related to the terms of apriori geometric delay, propagation media (ionosphere and troposphere) and sum of instrumental errors. The difficulty is then to determine the integer number of of phase cycles needed to resolve the phase ambiguity for each interferometer phase delay. In phase delay fitting, this is accomplished iteratively through phase-connection e.g. Shapiro et al. (1979) and Martí-Vidal et al. (2008). When all integers, n, are determined, the phase delays are no longer ambiguous and can be used to estimate, via a weighted least-squares fit, the position of the radio source. In phase-referenced mapping, the integers, n, are not determined directly but rather implicitly, through the coordinates of the fiducial reference point in the map relative to the coordinates of the reference source (Bartel (2003)).

High precision VLBI astrometry since the first phase-referenced VLBI observation (1971) has had

Vincenza Tornatore
Politecnico di Milano, DICA, Sezione Geodesia e Geomatica, Piazza Leonardo da Vinci 32, I-20133 Milano, Italy
Aniello Mennella
Dipartimento di Fisica, Università degli Studi di Milano, via Celoria 16, I-20133 Milano, Italy

an important impact on many areas of astrophysics, physics, geophysics and spacecraft navigation. Here we will focus on space applications, some of the most recent achievements in this field are e.g. Very Long Baseline Array (VLBA) tracking of the Cassini spacecraft at Saturn, Jones et al. (2011) and ESA's spacecraft Venus Express, Duev et al. (2012). For measuring the angular location of a spacecraft with respect to the background natural radio sources a variety of interferometric techniques can be used. Some of them are reviewed in Lanyi et al. (2007).

The general goal of this work concerns geodetic frame ties between the dynamic reference frame and the kinematically defined International Celestial Reference Frame (ICRF). As space probes we intend to use GNSS satellites which highly contribute to the materialisation of the International Terestrial Reference Frame (ITRF).

First step of this work is to analyze if standard astrometric observing schemes, used e.g. for Deep Space navigation, can be used also with GNSS satellites for the determination of the angular distance between the satellite (target) and the natural radio source (calibrator). In Sec. 2 we simulate the antenna patterns of a few European VLBI antennas to get an indication on how secondary lobes decrease with respect to the main beam. In Sec. 3, knowing the satellite signal strenght (we have used in this simulation the GLONASS constellation) we calculate the angular distance from the natural radio source where the satellite should stay to avoid that its signal contaminate the weak signal of the calibrator. Comments on obtained results are given in Sec. 4, where also alternative observing schemes are proposed.

2 Simulation with the software GRASP

The software GRASP allows the investigation of several particular antenna designs offering a wide diversity of possibilities for reflector profiles and feeds. We have used the GRASP to simulate radiation patterns both for reflectors and feeds for the three VLBI antennas: Medicina, Noto, Onsala85(25m). We have calculated the antenna beam pattern for the three stations at 1.6 GHz that is one of the frequencies where GLONASS satellites emit in L-band. The choice of GLONASS constellation depends on the fact that transmitted signals can be caught by all the three antennas, while the GPS frequencies are not covered by the L-band receiver of Medicina.

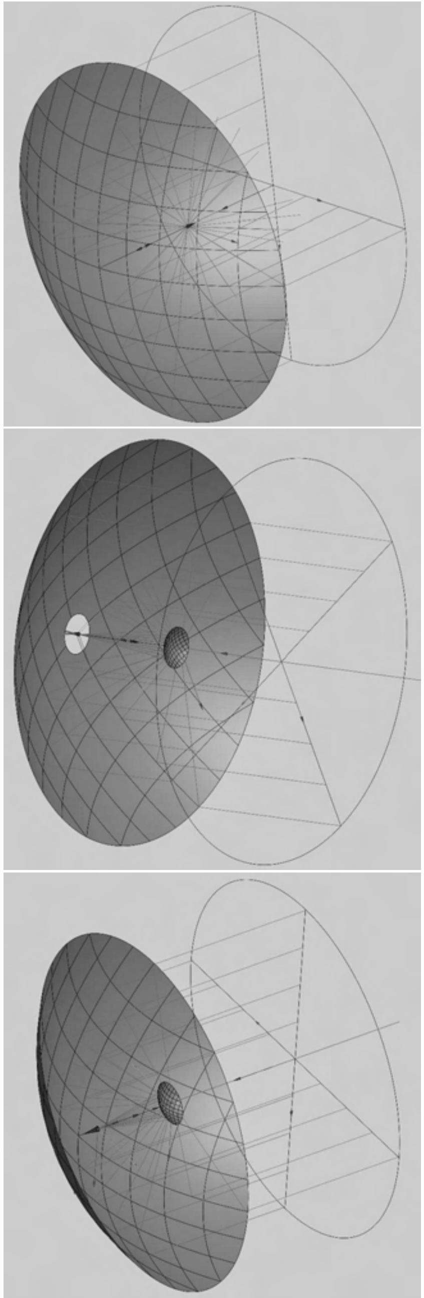

Fig. 1 VLBI radiotelescope optics simulated with GRASP, in the order from top to bottom: Medicina, Noto, Onsala.

All the three antennas have a Cassegrain configuration with a parabolic primary dish and hyperbolic secondary dish. The L-band receiver is mounted in primary focus only at Medicina while for Noto and Onsala85 it is in secondary focus. Secondary focus or subriflector focus has a distance of 22,8 cm from the vertex of the paraboloid, for Medicina (and Noto too) while for Onsala it is 1,595 m.

Fig. 1 shows the GRASP 3D model of the three antennas, while the corresponding beam patterns are

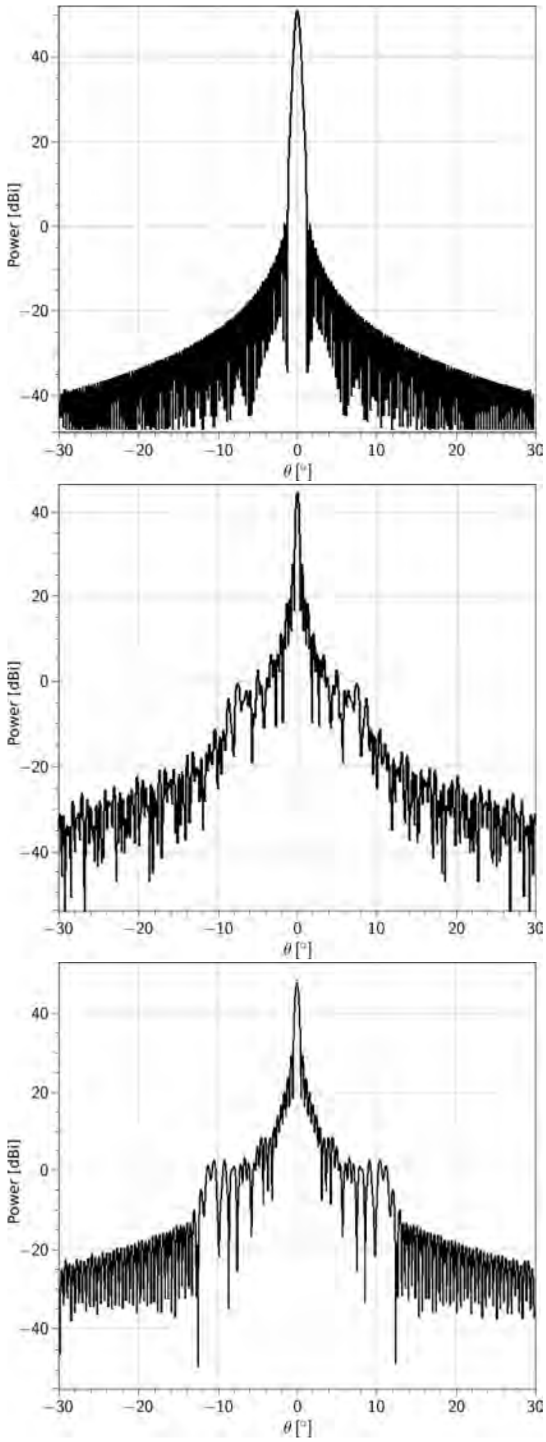

Fig. 2 VLBI radiotelescope optics simulated with GRASP, in the order from top to bottom: Medicina, Noto, Onsala.

shown in Fig. 2. The first sidelobe is between −15 dB and −18 dB from the main beam for Noto and Onsala, while it is around −50 dB for Medicina, meaning that the satellite power signal entering trough first sidelobe will be cut down much more in Medicina rather than in Noto and Onsala.

Antenna	ρ_1	α_1	ρ_2	α_2	ρ_3	α_3
Medicina	$2\cdot10^{10}$	$> 30°$	$2\cdot10^{9}$	$\sim 30°$	$2\cdot10^{7}$	$\sim 7°$
Noto	$2\cdot10^{10}$	$> 30°$	$2\cdot10^{9}$	$> 30°$	$2\cdot10^{7}$	$\sim 30°$
Onsala	$2\cdot10^{10}$	$> 30°$	$2\cdot10^{9}$	$> 30°$	$2\cdot10^{7}$	$\sim 30°$

Table 1 Minimum angular distance between the calibrator and the satellite beyond which the satellite contribution is less than the calibrator.

3 Determination of the minimum angular distance between the satellite and the calibrator

When the calibrator is tracked in the main beam, the received power from the satellite must be not higher than that from the natural radio source, in order to avoid contamination from the satellite emission entering through the sidelobes.
We have defined a coefficient ρ:

$$\rho \approx \frac{S_{sat} \cdot \Delta\nu_{sat}}{S_Q \cdot \Delta\nu_Q}, \tag{1}$$

where S_{sat} and $\Delta\nu_{sat}$ are respectively the flux density of the satellite (in Jy) and the recorded bandwidth of the satellite in MHz. S_Q and $\Delta\nu_Q$ are the correspondent quantities for the quasar (radio source calibrator). The flux density of the satellite ($\approx 4\cdot10^8$ Jy) is that received at a point on the Earth surface, considering that a GLONASS satellite antenna transmits an EIRP (Equivalent Isotropically Radiated Power) in a cone of 38° amplitude equal to 500 watt (or ≈ 27 dBW). The distance of a GLONASS satellite from the Earth surface is of 19.100 km. Concerning the calibrator flux density we have taken a value of 0.2 Jy, that is a good reference number since there are more than 1000 suitable calibrator sources in the sky with this flux (see *http://astrogeo.org/rfc*). The coefficient ρ has been evaluated in three different cases changing the satellite and calibrator bandwidths:
$\rho_1 \approx 2\cdot10^{10}$ ($\Delta\nu_{sat}$ = 10,22 MHz, $\Delta\nu_Q$ = 1 MHz)
$\rho_2 \approx 2\cdot10^{9}$ ($\Delta\nu_{sat}$ = 10,22 MHz, $\Delta\nu_Q$ = 100 MHz)
$\rho_3 \approx 2\cdot10^{7}$ ($\Delta\nu_{sat}$ = 1,022 MHz, $\Delta\nu_Q$ = 100 MHz)
as it is shown in Table 1. We now determine the minimum angular distance of the satellite from the calibrator, $\alpha_{\min}$. We determine this angle by looking, in the beam patterns of the three antennas, the value of the angle at which the sidelobes level reduce the ratio, ρ to a value close to unity. This means that for angles larger than $\alpha_{\min}$ the power received by the satellite will be less than the power received from the calibrator.

In the three cases above, the level of power suppression needed to obtain $\rho \sim 1$ is, respectively, −103 dB, −93 dB, and −73 dB

Looking at the results, we find only one case (for the Medicina antenna) where the angle (satellite-calibrator) has a value at least comparable with values necessary to use the phase referencing technique. It is worth to note that even if Medicina and Noto are twin telescopes, the optics are different when the L-band receiver is used, in fact the receiver is put in primary focus at Medicina and in secondary focus at Noto. This explains why the peak of the first sidelobes of Medicina beam has an attenuation of -50 dB.

4 Conclusions

Considering the GLONASS constellation we have run some simulations with the software GRASP on three European VLBI antennas. To avoid that the satellite signals entering trough the first sidelobes contaminate the calibrator signal (observed in the main beam), we have found, for all examinated the stations that the angular distance between satellite and calibrator should be really large with respect to the values (3-5 deg) recommended to be used for phase referencing. Only in one of the three simulated cases, Medicina presents a values lower than 10 degrees but still rather large. It's good practice that satellite and calibrator are angularly very near if we want to use calibrator information to make corrections of some systematic effects common to the satellites and calibrator. Of course calibrators of high power (1-2 Jy) on a larger recorded bandwidth would allow to decrease the angle between the satellite and calibrator. But the it seems that the key role is played by telescope optical configuration.

To take the advantages of the phase referencing technique, we indicate some possible scenarios in the following.

1) To investigate on a kind of phase referencing technique that makes use of a calibrator frequency different enough with respect to that of the satellite to avoid frequency interferences. At the same time calibrator frequency has to be fairly equal to those of the satellites in order that common systematic effects frequency dependent can be corrected anyhow.

2) To explore how to avoid receiver saturation by the strong signal satellite, (e.g. using automatic attenuation), to observe simultaneously the target and the calibrator, so-called same-beam calibration and take into account phase distortions due to observations carried out within a sidelobe (see Goossens et al. (2011)).

3) To use a MultiView approach e.g. to use multiple high-quality calibrators arranged around the target to reconstruct the ionospheric phase correction required in the direction of that target. The interpolation of the required phases, accounting for linear variations across the field, reduces considerably the need to have the calibrators close to the target (Dodson et al. (2013)).

4) To observe one quasar that is very close to the satellite at station number 1 and in some deg from the satellite at station number 2, then observe another calibrator which is close to station number 2.

Some of these observing schemes have the advantage to have been tested already in some deep space missions and they need only to be tested on Earth orbiting satellites, others have to be tested for the first time with observations and, or simulations.

Acknowledgements The authors wish to thank IRA/INAF, Istituto di Radioastronomia, Italy (Mariotti S., Nicotra G. and Schillirò F.), Onsala85 radio telescope, operated by the Swedish National Facility for Radio Astronomy, Sweden (Lundqvist M. and Pantaleev M.), for having provided antenna dishes geometry and feed characteristics used to make simulation with GRASP.

References

Y. Asaki, H. Sudou, Y. Kono, A. Doi, R. Dotson, N. Pradel, Y. Murata, N. Mochizuki, P.G. Edwards, T. Sasao, E. B. Fomalont. Verification of the Effectiveness of VSOP-2 Phase Referencing with a Newly Developed Simulation Tool, ARIS. Publ. Astron. Soc. Japan, 59, 397, 2007

N. Bartel. VLBI Astrometry. In Astron. Latin America, ADeLA Publ. Ser.Vol 1, 35, 2003; astro-ph/0303342

R. Dodson, M. Rioja, Y. Asaki, H. Imai1, X.Y. Hong, Z. Shen. The application of multiview methods for high-precision astrometric space VLBI at low frequencies. A.J., 145:147 pp. 11, 2013 doi:10.1088/0004-6256/145/6/147

D. Duev, G.M. Calvés, S.V. Pogrebenko, L.I. Gurvits, G. Cimo, B.T. Bocanegra. Spacecraft VLBI and Doppler tracking: algorithms and implementation. A&A, V. 541, A3, pp. 1-9, 2012 doi:10.1051/0004-6361/201218885

S. Goossens, K. Matsumoto, Q. Liu, F. Kikuchi, K. Sato, H. Hanada, Y. Ishihara, H. Noda, N. Kawano, N. Namiki, T. Iwata, F.G. Lemoine, D.D. Rowlands, Y. Harada, M. Chen. Lunar gravity field determination using SELENE same-beam differential VLBI tracking data. J. Geod. 85 pp. 205-228, 2011 doi:10.1007/s00190-010-0430-2

D.L. Jones, E. Fomalont, D. Vivek, R. Jon, W.M. Folkner, G. Lanyi, J. Border, R.A. Jacobson. Very Long Baseline Array Astrometric Observations of the Cassini Spacecraft at Saturn. A.J. 141, pp. 29-38, 2011 doi:10.1088/0004-6256/141/2/29

B. F. Lane and M.W. Muterspaugh. Phase referencing and narrow-angle astrometry in current and future interferometers. In Proceedings of SPIE, V. 5491, N.1, (Ed. W.A. Traub), SPIE Bellingham, WA, 2004, pp. 47-55, 2004 doi:191117/12.549440

G. Lanyi, D.S. Bagri, J.S. Border. Angular Position Determination of Spacecraft by Radio Interferometry. In Vol. 95, No. 11, November 2007, Proceedings of the IEEE, pp. 2193–2201, 2007 doi:10.1109/JPROC.2007.905183

I. Martí-Vidal, J.M. Marcaide, J.C. Guirado, M.A. Pérez-Torres, E. Ros. Absolute kinematics of radio source components in the complete S5 polar cap sample. A&A, V. 478, N 1, pp. 267-275, 2008.

I.I. Shapiro, J.J. Wittels, C.C. Counselman, D.S. Robertson, A.R. Whitney, H.F. Hinteregger, C.A. Knight, A.E.E. Rogers, T.A. Clark, L.K. Hutton, A.E. Niell. Submilliarcsecond astrometry via VLBI. I. Relative position of the radio source 3C345 and NRAO 512. A.J., Vol. 84, N. 10, pp. 1459–1479, 1979.

4-station ultra-rapid EOP experiment with e-VLBI technique and automated correlation/analysis

S. Kurihara, K. Nozawa, R. Haas, J. Lovell, J. McCallum, J. Quick, T. Hobiger

Abstract Since 2007, the Geospatial Information Authority of Japan (GSI) and the Onsala Space Observatory (OSO) have performed the ultra-rapid dUT1 experiments, which can provide us with near real-time dUT1 value. Its technical knowledge has already been adopted for the regular series of the Tsukuba-Wettzell intensive session. Now we tried some 4-station ultra-rapid EOP experiments in association with Hobart and HartRAO so that we can estimate not only dUT1 but also the two polar motion parameters. In this experiment a new analysis software c5++ developed by the National Institute of Information and Communications Technology (NICT) was used. We describe past developments and an overview of the experiment, and conclude with its results in this report.

Keywords ultra-rapid, EOP, UT1-UTC, e-VLBI, c5++

Shinobu Kurihara, Kentaro Nozawa
Geospatial Information Authority of Japan, 1 Kitasato, Tsukuba, Ibaraki 305-0811, Japan
Rüdiger Haas
Chalmers University of Technology, Department of Earth and Space Science, Onsala Space Observatory, SE-43992 Onsala, Sweden
Jim Lovell, Jamie McCallum
University of Tasmania, School of Mathematics and Physics, Private Bag 37, Hobart 7001, Australia
Jonathan Quick
Hartebeesthoek Radio Astronomy Observatory, National Research Foundation, PO Box 443, Krugersdorp 1740, South Africa
Thomas Hobiger
National Institute of Information and Communications Technology, 4-2-1 Nukui-Kitamachi, Koganei, Tokyo 184-8795, Japan

1 Background

In 2007, the Geospatial Information Authority of Japan (GSI), the National Institute of Information and Communications Technology (NICT), the Onsala Space Observatory (OSO), and the Metsähovi Radio Observatory started the Japan-Fennoscandia ultra-rapid dUT1-project by using e-VLBI technique. The purpose of the project is to derive UT1-UTC as soon as possible. In order to realize this, data transfer to correlator should be real-time or near real-time, and some following processes; data format conversion, correlation processing, and analysis, should be automated and made closer to real-time.

So far a few dozens of experiments have been implemented. We succeeded in deriving dUT1 within 4 minutes after the end of the last scan from observed data of Tsukuba-Onsala east-west stretching baseline shown in Fig. 4 (Matsuzaka et al., 2008). Since 2009, the method has been applied to the regular IVS sessions and consecutive dUT1 time series has been obtained (Matsuzaka et al., 2010). In CONT11 campaign performed in 2011, also from Tsukuba-Onsala baseline, a 15-day continuous dUT1 time series was derived. After that, a multi-baseline experiment with Tsukuba-Hobart north-south baseline was also implemented in order to estimate not only dUT1 but also polar motion parameters (Kokado et al., 2012).

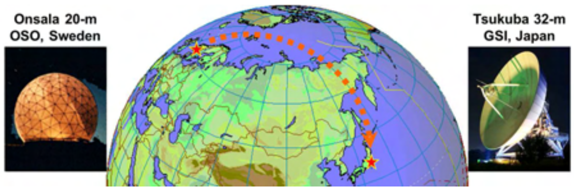

Fig. 1 The data transfer from Onsala to Tsukuba.

2 Data flow and analysis strategy

Fig. 2 shows the data flow of the experiment. The data from Sweden and Australia were transferred to Tsukuba correlator in real-time by Mark5A/PCEVN or in near real-time every scan. Since the system of Tsukuba correlator processes with K5 data format, the format conversion to Mark5 is required. The conversions are processed on eight servers distributedly. After K5 data makes a pair of baseline, a distributed correlation processing starts with 48 processing sockets in 16 servers. Since these servers access their data disk drives in the format conversion and the correlation processing, our system is adopting not NFS but Lustre File System to avoid the bottleneck of the disk accessing. The correlator outputs were reduced and the solutions were derived using fully automated VLBI analysis software c5++ (Hobiger et al., 2010). In order to automate and stabilize the whole sequence of processes, we developed some management programs shown in Table 1. The “rapid” program family is written in Perl, and users can execute the ultra-rapid data processing by issuing easy commands with the experiment code and the name of involved stations. A solution at the middle of the designated time window (ex. 6 hours) was derived from the analysis for the correlator outputs in the window. Once a correlator output comes up, the window slides forward, and the next solution is derived from next dataset in this window. It is so-called “sliding window approach”. By repeating this process, a dataset of the sequential solutions is yielded.

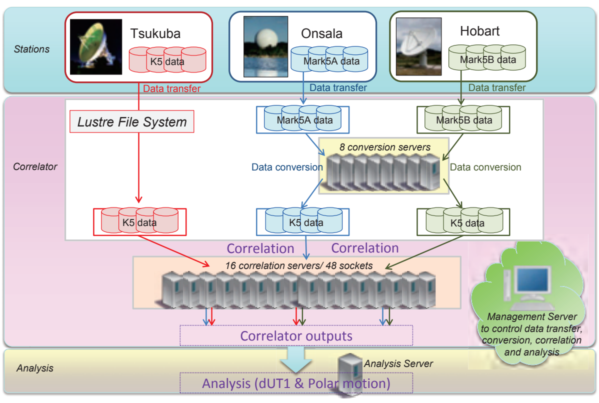

Fig. 2 Data flow of the ultra-rapid e-VLBI experiment.

Table 1 The “rapid_” series of programs to manage the automated data processing.

Name	Summary
rapid_transfer	executes tsunami/tsunamid and transfers data from station to correlator.
rapid_conv	converts the data from Mark5 to K5 if needed.
rapid_cor	runs fringe search and main correlation processing sequentially.
rapid_komb	generates the bandwidth synthesis outputs.

3 4-station/6-baseline experiments

Since 2011, the 4-station/6-baseline experiments adding HartRAO (26-m or 15-m) into Tsukuba-Onsala-Hobart network have been implemented (Fig. 3). The c5++ software has been upgraded to the version of 2012 July in order to estimate not only dUT1 but also polar motions. This version supports a multi baseline network, favorite parameterization, and SINEX output too. In case of dUT1 estimation so far, since the polar motion parameter is dealt with as known parameter, the error of polar motion would be unnecessary offset for the estimated dUT1 with respect to the probable value. It is desirable for avoiding the issue to estimate the whole three EOPs simultaneously.

So far the 11 regular IVS sessions that include at least three stations of four (Tsukuba, Onsala, Hobart, and HartRAO) were implemented as the ultra-rapid EOP experiment. The six sessions of them added Hobart or HartRAO 15-m by so-called “tag-along”, which is a function of SKED to add stations into an original VLBI schedule (Table 2). When the whole processes were carried out smoothly, 90% of the total solutions were derived within 10 minutes (Fig. 4).

As concerns the evaluation of estimated parameters, the poor network geometry of the set of observed baseline data in the sliding window causes some large outliers or uncertainties. It is because the IVS original schedule is not optimized for Hobart and the number of the scans of Hobart is quite a few. Then the ratio of east-west baseline and north-south baseline inclines to either of them. It is improved to some degree by making the dedicated schedule for these four stations. The five experiments with the dedicated schedule were done from November 2012 to February 2013 (Table 3). In the UR1301 in January, which was a 2.5-day long schedule, the EOP was estimated with 2-hour sliding window strategy. Fig. 5 shows the EOP time series of the near real-time c5++ solutions and the 1-hour piece wise liner Calc/Solve solutions, and Fig. 6 shows the network geometry of each solution represented as the rate of the number of observations for east-west baseline, north-south baseline, and the others. Partially, the rate of east-west baseline extremely low, and then the c5++ solution deviates from the prediction. On the other hand, in the periods that include both east-west and north-south baselines with a well-balanced rate, the solutions are consistent with the prediction and Calc/Solve solution. Therefore, in order to estimate whole three EOPs, the 4-station/6-baseline network is a bit poor in geometry, and for more stable sequential EOP solutions, the network like the IVS-R series including globally-distributed at least 8 stations is needed.

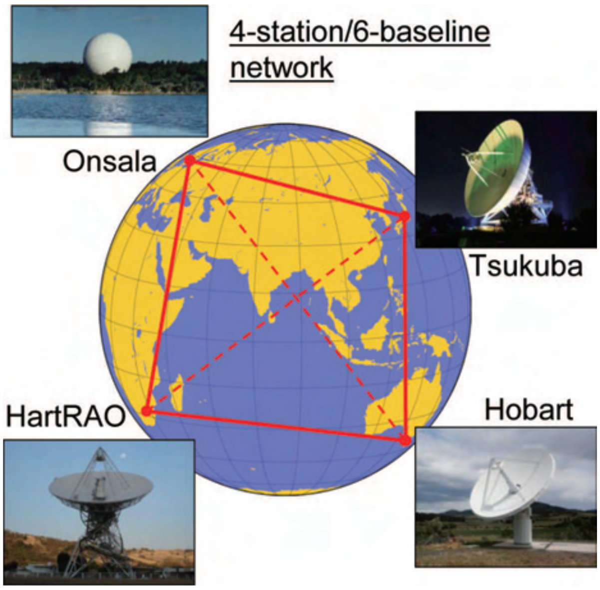

Fig. 3 The 4-station/6-baseline network consists of Tsukuba, Onsala, Hobart, and HartRAO.

Table 2 Recent ultra-rapid EOP experiments behind the IVS regular session.

Session	Date	Time	Stations
IVS-R1554	OCT10	17:00	HhOnTs +Hb
IVS-R1555	OCT15	17:00	HhOnTs +Hb
IVS-R1561	NOV26	17:00	HhOnTs +Hb
IVS-R1563	DEC10	17:00	HhOnTs
IVS-RD1210	DEC11	17:30	HhOnTs
IVS-R1564	DEC18	17:00	HhOnTs
IVS-R1569	JAN22	17:00	HbHhOnTs
IVS-R1570	JAN28	17:00	HhOnTs
IVS-RD1301	JAN29	17:30	HhOnTs +Hb
IVS-R1573	FEB18	17:00	HbOnTs +Ht
IVS-T2088	FEB19	17:30	HhOnTs +Hb

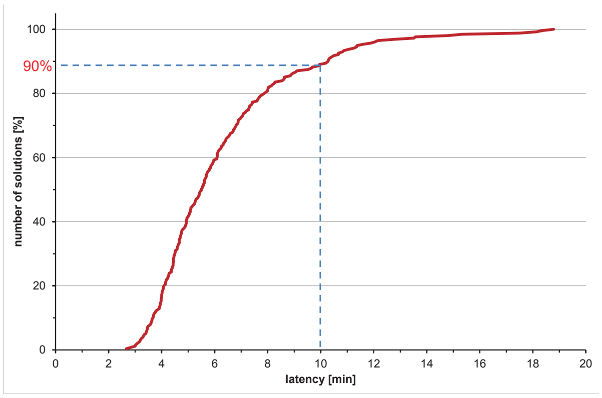

Fig. 4 Latency - Number of solutions in % in the session IVS-R1555 on October 15.

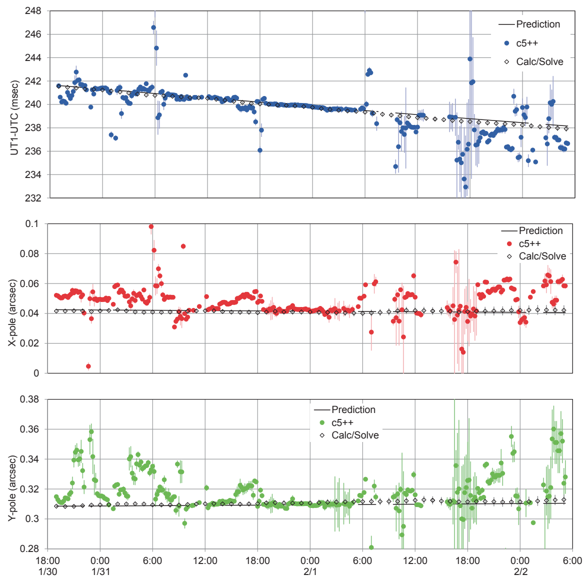

Fig. 5 Estimated EOP with comparison between c5++ and Calc/Solve

Table 3 Recent ultra-rapid EOP experiments with dedicated schedule.

Session	Date	Time	Dur.	Stations	#obs. (cor/skd)
UR1201	NOV29	18:00	24	HbHtTs	382/ 822 (46.5%)
UR1202	DEC06	18:00	24	HbHtTs	363/ 482 (75.3%)
UR1203	DEC17	07:30	35	HbHtOnTs	978/1033 (94.7%)
UR1301	JAN30	18:00	61	HbHtOnTs	1326/1467 (90.4%)
UR1302	FEB05	17:30	48.5	HbHtTs	815/ 943 (86.4%)

4 Summary and future plan

For the purpose of near real-time EOP estimation, some 4-station/6-baseline ultra-rapid EOP experiments with the dedicated schedule were implemented. On

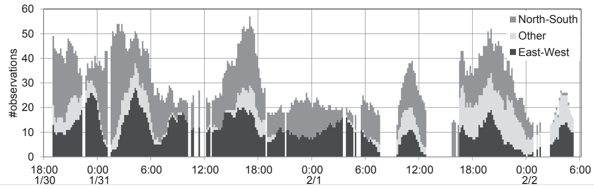

Fig. 6 The network geometry represented as the rate of observations.

the whole, we succeeded in the smooth and near real-time data processing and analysis. Besides, in the periods of poor network geometry in schedule, the solution diverges and it does not seem to estimate EOP correctly. More stations and baselines may resolve this issue, but it is not easy in terms of the capacity of the simultaneous data transfer and the throughput of the Tsukuba correlator, and whether the 5th and 6th stations connected to broad-band network were found or not. After this, some improvements like reconsidering of analysis strategy, upgrade of c5++ for Kalman filter, and real-time transfer of the Mark5B data, are expected.

References

Hobiger, T., T. Otsubo, M. Sekido, T. Gotoh, T. Kubooka, and H. Takiguchi: Fully automated VLBI analysis with c5++ for ultra-rapid determination of UT1, *Earth Planets and Space*, **62(12)**, 933-937, 2010.

Kokado, K., S. Kurihara, R. Kawabata, and K. Nozawa: Recent Activities of Tsukuba Correlator/Analysis Center, In: *"Launching the Next-Generation IVS Network", Proc. IVS 2012 General Meeting*, D. Behrend and K. D. Baver (eds.), 105–114, 2012.

Matsuzaka, S., H. Shigematsu, S. Kurihara, M. Machida, K. Kokado, and D. Tanimoto: Ultra Rapid UT1 Experiment with e-VLBI, In: *"Measuring the Future", Proc. 5th IVS General Meeting*, A. Finkelstein and D. Behrend (eds.), 68–71, 2008.

Matsuzaka, S., S. Kurihara, M. Sekido, T. Hobiger, R. Haas, J. Ritakari, and J. Wagner: Ultra-rapid dUT1 Measurements on Japan–Fennoscandian Baselines - Application to 24-hour Sessions, In: *"VLBI2010: From Vision to Reality", Proc. IVS 2010 General Meeting*, D. Behrend and K. D. Baver (eds.), 143–147, 2010.

The effect of the systematic error in the axis offset value on the coordinates estimated in VLBI data analysis

U. Kallio, N. Zubko

Abstract The axis offset is usually considered as a constant value in the geodetic VLBI analysis. In azimuth-elevation type of telescope the systematic error in the axis offset is mostly projected to the vertical direction, since the influence on the horizontal direction is eliminated by the observation scheme, where the distribution of azimuths of the radio sources is almost uniform. We examined the effect of the axis offset by estimating the coordinates of the Metsähovi radio telescope with various axis offset values. The new value of the axis offset -3.6 mm was estimated from local tie measurements performed during the geo VLBI sessions since 2008. The offset is different from the earlier value +5.1mm estimated using the time delay observations (Petrov, 2007). We investigated the effect of the changing the offset on the coordinates by analyzing the geodetic VLBI campaigns with the old and the new axis offset values. The difference between old and new coordinates shows that the agreement between the vectors from the IGS GPS point METS to the reference point of the VLBI telescope Metsahov calculated from ITRF coordinates and estimated from local tie data could be better when using the new value.

Keywords Axis offset, VLBI, Local tie

1 Introduction

The axis offset is the distances between the reference point and elevation axis. The reference point of the VLBI telescope is in the primary axis at the point where the distance, to the secondary axis is the shortest (Dawson, 2007). The sign of the offset is minus if the direction from reference point to the elevation axis is opposite to the opening direction of the dish. The negative offset value is possible only with azimuth-elevation type of telescopes. In VLBI data processing the influence of the axis offset on the time delay observation is corrected.

The effect of the erroneous axis offset has been studied earlier for example by Ray (Ray, 1993). He generated the time delay observations by adding the contribution of 1 cm increase of the axis offset to the theoretical observations and then estimated the baseline GRAS-FT VLBA using the original offset value. The position offset due to error in axis offset was almost -1 cm in vertical direction at FT VLBA.

The axis offset is a property of the telescope but it can change due to the repair work at the station as reported by Kurdubov (Kurdubov, 2010). He compared the axis offset values derived from time delay observations of the single VLBI sessions, from the global solutions and from local tie at SVETLOE. He also detect the differences between axis offset values derived from local tie and from the VLBI data (Kurdubov, 2010). In our case the installation of the secondary mirror for geodetic VLBI hardly change the axis offset.

The contribution of the axis offset to the signal arrival time is the projection of the axis offset to the direction of the coming wave front devided by the velocity of light and depends on the elevation angle. The influence of the axis offset on the estimated coordinates is visible in vertical direction (Ray, 1993), because the effect in the horizontal direction vanishes when all azimuth positions are included (Fig. 1).

The coordinate difference Metsahov-METS calculated from the ITRF coordinates differs from the local tie vector by 0.025m (ITRF, 2008) in vertical direction. One of the reasons for the discrepancy might be the wrong axis offset value. Another important circumstance, which should be taken into account is that the local tie vector between METS IGS point and the reference point of the Metshovi VLBI telescope was not available during the release of the ITRF2008.

Ulla Kallio and Natalya Zubko
Finnish Geodetic Institute, FGI, Geodeetinrinne 2, Kirkkonummi, Finland

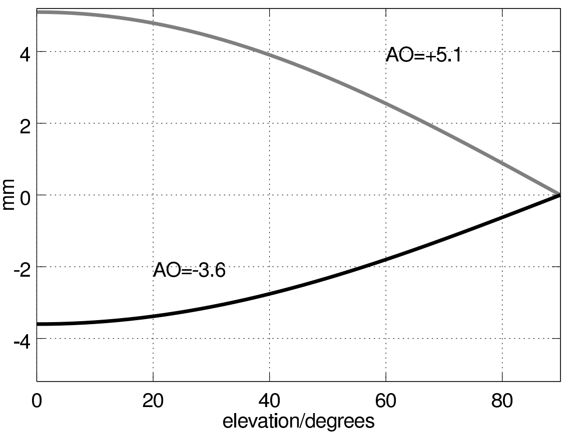

Fig. 1 The contribution of the axis offset to the time delay depends on the elevation angle. Here it is presented in millimeters.

The axis offset values for the Antenna information file used in VLBI data analysis were collected in 2008 and 2009 by Axel Nothnagel (Nothnagel, 2008). The offset value for Metsähovi antenna in Antenna information file is the best value available at the time when the information was collected and it is based on the offset estimated by Leonid Petrov from VLBI time delay observations in 2007 (Petrov, 2007) . At that time we had just started our local tie measurements between the IGS GNSS point METS and the reference point of the VLBI telescope Metsahov and we had only some test results and could not provide the axis offset.

2 Axis offset from local tie measurements

The position vector of a target (or a GPS-antenna attached on a radio telescope) X is the sum of three vectors in cartesian system: the position vector of the reference point X_0, the axis offset vector $(E - X_0)$ rotated by angle α about the azimuth axis a and a vector from the eccentric point E to the antenna point p rotated about the elevation axis e by angle β and about the azimuth axis by angle α. Unknown parameters are X_0, E, a, e, and p. Observations are coordinates X for each antenna point and epoch, and VLBI antenna angle readings α and β for every epoch. The estimated values of E, e and p are those of an antenna initial position which may be zero for both angles. The rotation matrices $R_{\alpha,a}$ and $R_{\beta,e}$ are rotations about the axes.

The basic equation and the rotation matrix of our model are

$$X_0 + R_{\alpha,a}(E - X_0) + R_{\alpha,a}R_{\beta,e}p - X = 0 \qquad (1)$$

Because the rotation axes are unit vectors and the reference point is the intersection of the primary axis with the shortest vector between the primary and secondary axis (Dawson, 2007), four conditions between parameters are necessary:

$$a^T a - 1 = 0, \qquad (2)$$

$$e^T e - 1 = 0, \qquad (3)$$

$$(E - X_0)^T a = 0, \qquad (4)$$

$$(E - X_0)^T e = 0 \qquad (5)$$

The axis offset is the distance between the reference point and the eccentric point:

$$AO = \sqrt{(E - X_0)^T (E - X_0)}. \qquad (6)$$

The standard deviation of axis offset is calculated applying the variance propagation law. We extracted the part of the covariance matrix which includes the reference point coordinates and the coordinates of the point in elevation axis $C_{X_0,E}$ and used the Jacobian matrix J for the standard deviation of the AO.

$$\sigma_{AO} = \sqrt{JC_{X_0,E}J^T} \qquad (7)$$

$$J = \begin{pmatrix} \frac{-(E - X_0)^T}{AO} & \frac{(E - X_0)^T}{AO} \end{pmatrix} \qquad (8)$$

3 Axis offset determinations at Metsähovi radiotelescope

In the table 1 we have compiled axis offset determinations of Metsähovi VLBI telescope. The offset values by Petrov and by Gordon are based on time delay observations (Petrov, 2007), (Petrov, 2013), (MacMillan, 2013) and (Gordon, 2012) and the offsets by Kallio on the local tie data. The offset value (Kallio 2009) is based on terrestrial measurements (Fig. 2). We must point out that it is a single determination with very small number of datapoints, because indirect measurements with tacheometers were possible to perform only in few azimuth positions of the telescope (Fig. 2). The offset value (Kallio 2010) is based on the kinematic GPS trajectory points of four campaigns measured in 2008 and in 2009 and the terrestrial and static GPS local tie campaigns in 2008 and 2009. The offset value (Kallio 2013) is based on kinematic GPS trajectory points of 14 campaigns from 2010 to 2012.

We have determined the local tie between IGS station METS and VLBI antenna reference point with

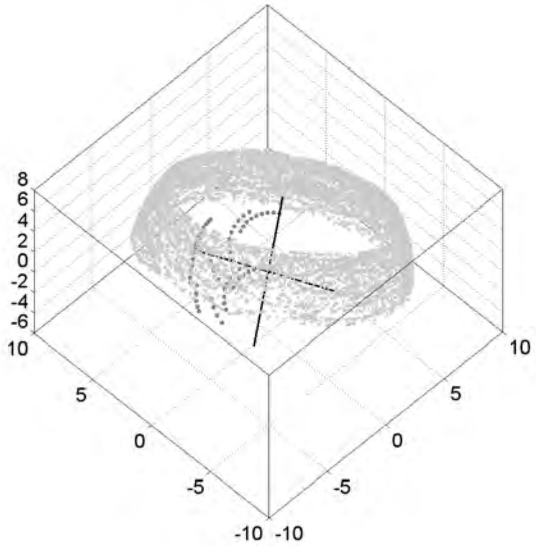

Fig. 2 The datapoints in terrestrial local tie (dark grey) and in combined solution with kinematic GPS trajectory data(light grey).

Reference	offset [mm]	formal precision [mm]
Petrov 2007	+5.1	3.7
Gordon 2012	-2.3	2.4
Petrov 2013	+1.6	2.2
Kallio 2009	+0.3	0.2
Kallio 2010	-2.1	0.3
Kallio 2013	-3.6	0.1

Table 1 Axis offsets from different sources

regurarly kinematic GPS measurements during the geo-VLBI campaigns since December 2008. Because the first experimental campaigns gave promising results, we have continued the measurements during every VLBI campaign. Besides the coordinates of the reference point we estimate also the axis offset and the orientation of the antenna for every campaign. We reported the discrepancy of the offset values of local ties and the offset value in Antenna information file already in 2010 (Kallio, 2012). Now after repeated measurements we can give campaign based estimates for axis offset. Axis offset should be an instrument specific constant. However, our axis offset estimates wich are based on the kinematic trajectory points varies between campaigns from +2mm to -9mm being mostly negative. This variation can be due to systematic behavior of the telescope that we can not yet take into account. Almost all our estimates are negative, but the variation is too high to rely on results of the single campaign. For this reason we estimated the axis offset using the datapoints of 14 succesful 24 hour campaigns (Fig. 2) measured during geo-VLBI campaigns 2010-2012. After rejecting the outliers more than 84000 kinematic GPS positions on the dish edge of the VLBI antenna were used in final reference point and axis offset estimation. Before the estimation the thermal deformation of the antenna were corrected point by point. Datapoints included in adjustment of the reference point were more than 84000.

Petrov estimated the new axis offset of Metsähovi antenna in 2013 by making the global solution, using all the VLBI data from 1980.04.11 through 2013.04.02 and he suggested the zero offset value should be used (Petrov, 2013/2) (Petrov, 2013) . Our estimated value is negative and the latest estimate reported by MacMillan (Gordon, 2012) is also negative.

The formal errors of our estimates for campaign based solutions are from 0.3 to 1.0 mm which are all too optimistic. If we take the standard deviation of mean of the estimates from campaign based local tie offsets we get 1 mm precision. However combining all the datapoints of all campaigns is better choice than the mean value, because the number of datapoints used in the estimations differs in campaigns. The formal error in combined solution is not the total uncertainty but include actually only the geometric precision in one sigma level. The kinematic GPS method has turned out to be good method for reference point estimation but used for estimating the axis offset it is not highly accurate. In order to verify the results we need to complete our terrestrial measurements under the radome. We have determined the reference point and axis offset with terrestrial method (Kallio 2010 in Table 1), but the dataset of space intersections with two precision tachymeters cover only a small part of the antenna positions. The one reason for the variation of campaign based values of the axis offset may be the unstable axis. It seems that the tilt of the axis changes as a function of the azimuth.

4 VLBI data processing and the influence of the axis offset on the estimated coordinates

In order to reveal the influence of the axis offset value on the estimated coordinates, we made a simple test using the offset value of -3.6mm estimated from the local tie measurements instead of the the value +5.1mm estimated from the VLBI time delay observations (Petrov 2007) and calculated the coordinates for Metsahov with the VieVS software. All other settings in VLBI analysis were same. In our study

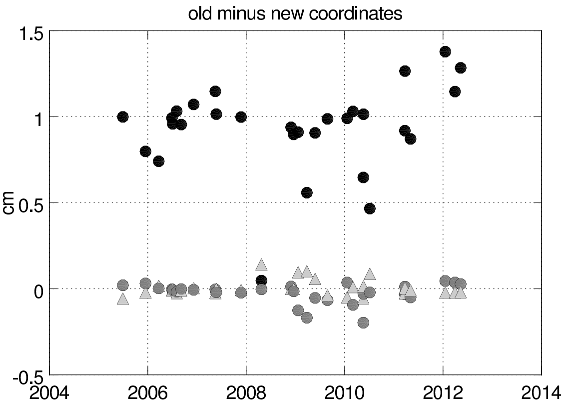

Fig. 3 The influence of the changing the axis offset value on the coordinates, North=grey triangles, East=grey circles and Up= black circles

only geo VLBI sessions which included Metsähovi station were selected. Coordinates were estimated with old and new offset values. The comparison of obtained results shows the difference of 1cm in the up component. In horizontal direction the changes were almost insignificant as was expected. We rejected one campaign because of obvious errors in data or data processing. The elevation of Metsahov is lower when using the new offset value and thus agree better with the local tie solution. The result indicates that one source of the discrepancy may be the axis offset. However, there is still a 1.5 cm difference to explain. It may be due to the fact that METS-Metsahov local tie was not included in the ITRF2008 solution because it was not available. Because the solutions with old and new axis offsets are higly correlated, we can see the influence on the coordinates, although the precisions of the coordinate solutions are not good. When we compare the results of the old and the new solution, we are not able to see any decrease of the absolut values of the residuals in the new solution, because deviation of the observations of Metsahov is too big.

5 Discussion

Our results agree with the results of Ray (Ray, 1993). In our study we didn't touch the observations but use the different offset values in data processing and compared the results. If we assume that we actually has -3.6 mm axis offset but we use the offset value of +5mm in estimation we can expect about +9mm positional offset. Our test show that error in axis offset value can have significant biases in coordinates in vertical direction.

One of the tasks of the IERS WG on site ties and co-locations is to find out the systematic technique specific errors. We calculated the new axis offset and estimated the VLBI coordinates of Metsähovi VLBI reference point with old and new offset value using VieVS software The Analysis of difference between the old and new coordinate solutions indicate that better agreement between GPS based local tie and VLBI coordinates might be achieved with the new offset value.

Which offset value should we use in VLBI analysis? Our latest value -3.6 mm is based on a huge amount of data where the single data point is not accurate. The offset value estimated using only the terrestrial data give zero offset with small amount of accurate datapoints with poor geometry. The offset values based on the time delay observations indicate the zero offset. In our Poster in EVGA meeting we proposed the new value -3.6 mm, because using it the agreement with local tie results is better. Our test shows only the influence on the coordinates but it dosn't prove that some of the values is the least erroneous. In the case of Metsähovi it may be the safest to use zero offset proposed by Petrov (Petrov, 2013/2) althoug the offset value based on more than 84000 datapoints say different. We will continue our study and try to find out the influence of wobbling of the axis on the reference point and on the axis offset. We will also try to omplete our terrestrial measurements.

Acknowledgement

We would like to thank T. Lindfors,A. Mujunen, M. Tornikoski, J. Kallunki, E. Oinaskallio and H. Rönnberg of the Metsäahovi Radio Observatory of the Aalto University for their invaluable help. We also thank all who visited our poster during EVGA meeting for their comments; special thanks to Axel Nothnagel, Dan MacMillan and Leonid Petrov for discussions. This work was partly supported by the Academy of Finland project 134952.

References

J. Dawson, P. Sarti, G.M. Johnston, and L. Vittuari. Indirect approach to invariant point determination for SLR and VLBI systems: an assessment. *J. Geodesy*, **81(6-8)**: 433–441, 2007.

D. Gordon. GSFC2012, Catalog of antenna axis offsets, 2012. Web document `http://gemini.gsfc.nasa.gov/solutions/2012a/2012a.htm`.

ITRF. ITRF2008. Web document. `http://itrf.ensg.ign.fr/ITRF_solutions/2008/`.

D. MacMillan. Personal contact by email 2013.

U. Kallio and M. Poutanen. Can we really promise a mm-accuracy for the local ties on a geo-vlbi antenna. In *S. Kenyon et al. (eds.), Geodesy for Planet Earth*, International Association of Geodesy Symposia 136, doi: 10.1007/978-3-642-20338-1_5, Springer-Verlag Berlin Heidelberg 2012.

S. Kurdubov and E. Skurikhina. Antenna Axis Oset Estimation from VLBI. In *IVS 2010 General Meeting Proceedings*2010

A. Nothnagel. Conventions on thermal expansion modelling of radio telescopes for geodetic and astrometric VLBI. *J. Geodesy*, 2008. doi: 10.1007/s00190-008-0284-z.

A. Nothnagel. Personal contact by email 2013

L. Petrov. VLBI antenna axis offsets. Web document `http://gemini.gsfc.nasa.gov//500/oper/solve_save_files/2007c.axo`.

L. Petrov. Personal contact by email 2013.

L. Petrov. VLBI antenna axis offsets. Web document `http://astrogeo.org/vlbi/solutions/rfc_2013b/rfc_2013b.axof`.

J. Ray, W. Hinwich and C. Knight. Radio Interferometric Survey Between the GRAS and VLBA Antennas, Ft. Davis, TX. *Contribution of Space Geodesy to the Geodynamics: Technology.*, Geodynamics 25 The American Geophysical Union 1993

On the monitoring model of reference point of VLBI antenna

J. Zhang, J. Li

Abstract By parameterizing the rotation of VLBI antenna and modeling in local control network the coordinates of targets fixed on the antenna, it is expected to perform fully automatic monitoring of antenna parameters without any interference to normal operations of the telescope. Some insights and analysis are presented concerning the mathematical monitoring model, the setting of parameters and selection of constraints to the observation equation, which are verified via data simulation analysis to be rational and effective. Some factors which may affect the estimation precision of antenna parameters are analyzed in order to design and develop monitoring procedure, data analysis software and to make necessary preparation to practical application of the new monitoring concept of VLBI antenna.

Keywords VLBI · reference point · axis offset · monitoring model · data simulation

1 Introduction

Since its birth from 1960s the Very Lone Baseline Interferometry (VLBI) has significantly contributed to astrometric and geodetic studies, for instance in the realization of International Celestial Reference Frame (ICRF) as well International Terrestrial Reference Frame (ITRF), and the precisely determination of modern crustal movement, Earth Orientation Parameters (EOP) and so on. VLBI could also contribute to space explorations, for example, in the lunar exploration project of China it is applied to track the orbit of Chang'E satellite.

In the application of VLBI to astrometric and geodetic researches, it is expected that the observed time delay only reflects variations of reference point of an antenna resulted from EOP, crustal motion and so on, rather than those relative to the local control network. That without taking into consideration of local movements of reference point could result in systematic change of the time series of VLBI observations, or such local movements may even be wrongly attributed to other physical reasons and mislead scientific studies and analysis. Therefore the precisely monitoring of reference point in the local control network has been one of the major concerns in the research field of astrometry and geodesy. According to the technical specifications of the next generation of VLBI systems, the VLBI2010[1], the station coordinates and velocities will be determined in the precision of 1mm and 0.1mm/year, and the EOP will be continuously observed. It is therefore of importance to improve the monitoring precision of reference point of VLBI antenna as well as to realize continuously and real-time monitoring.

Zhang Jinwei, Li Jinling
Shanghai Astronomical Observatory, CAS, Nandan Road 80, 200030, Shanghai, China

2 Parameterized model of antenna rotation

2.1 The reference point of VLBI antenna

The reference point is usually within the structure of a VLBI antenna. It is a geometric point rather than a physical one. Its position usually can not be measured directly but indirectly. For an ideal antenna system of azimuth-elevation (Az-El) mount, the primary axis (azimuth) is fixed on the ground, and is perpendicular to and intersects with the secondary axis (elevation). The reference point is defined as the intersection of the two axes[2].

However, the diameter of a practical VLBI antenna is usually larger than 10 m. For example the newly constructed VLBI antenna at Shanghai has an aperture of 65 m in diameter, and some international radio telescopes have apertures as large as 100 m. For large scale antennas the manufacture and installation errors of the plates of reflection surface and mechanical structure, the complicated building and construction procedure as well as deformations due to gravity, temperature and pressure changes related to limitations of material, which are all impact factors lead to that the two axes are not perpendicular to and intersect with each other as well as the change of axis offset with antenna orientation and time, and which further lead to detrimental effects on the delay observations [3,4]. The reference point is thus defined as the intersection of the common perpendicular of axes on the primary axis, and the length of common perpendicular is taken as the axis offset.

2.2 The monitoring model of VLBI antenna

By taking into consideration of the antenna mount style and site condition, and through parametrization of antenna rotation, the coordinates of targets fixed on the antenna structure are mathematically modeled[5−10]. The parameters of the rotation model of antenna are then solved via data processing. The advantage of such monitoring concept is that the normal operation of telescope would not be interrupted, and the antenna monitoring would be realized during astrometric and geodetic VLBI observations. Using this concept, it is expected to perform fully automatic monitoring of VLBI antenna parameters with high precision. The geometric model of antenna based on Az-El style is showed in Fig.1.

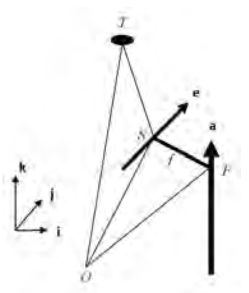

Fig. 1 Geometric demonstration of VLBI antenna monitoring.

The related reference frames and characteristics are as follows:

1. The local reference frame, denoted as O-**ijk**, which represents the local control network surrounding the telescope, whose origin is at point O, and (**i**, **j**, **k**) are the triad vectors, corresponding respectively to east, north and up. Suppose the coordinates of all the network control points are already known through ordinary geodetic measurements, and the transformation of rotation and translation between the local frame and ITRF has been established via for instance GPS observations.
2. The telescope reference frame, whose origin is at the reference point F, the third coordinate axis is along **a** directing approximately to up, the first and second coordinate axis approximately directs to east and north respectively.
3. The dish-fixed frame, which is fixed on the secondary axis of the antenna. The origin is as point S, the intersection of common perpendicular of **a** and **e** on **e**. The first coordinated axis is **e**, the second is **f**, the third is corresponding to but may not be exactly coincided with **a**.

2.3 Analysis of monitoring models

The antenna rotation model is mathematically expressed as:

$$\mathbf{OT} = \mathbf{OF} + R_a(A) f(\mathbf{a} \times \mathbf{e}) + R_a(A) R_e(E) \mathbf{ST} \quad (1)$$

where, **OT** is the position vector of point T in O-**ijk**, obtained via positioning observations. **OF** is the position vector of reference point F in O-**ijk**, constant with the change of antenna orientation. **ST** is the position vector of target T in the dish-fixed frame. f is the axis offset of VLBI antenna. (A,E) are the antenna azimuth and elevation angles. $R_a(A)$ and $R_e(E)$ are rotation transformation matrixes around respectively axis **a** and **e** by angle A and E.

In summary, **OF**, f, **a**, **e** and **ST** are unknowns, among which **e** and **ST** are corresponding to the antenna state as A=0 and E=0. The following constraints are applied to the Eq (1):

$$|\mathbf{a}| = 1, |\mathbf{e}| = 1 \quad (2)$$

$$\mathbf{OS} = f(\mathbf{a} \times \mathbf{e}) + \mathbf{OF} \quad (3)$$

That is the modulus of **a** and **e** are constrained to be unit, and the axis offset is $f = |\mathbf{OS} - \mathbf{OF}|$. The orientation deviation compared with the design could be deduced from the solutions to **a** and **e**, and the intersection angle between the two axes at A=0 and E=0 is $\cos^{-1}(\mathbf{a}\cdot\mathbf{e})$.

3 Simulation examination and analysis

Preset the antenna parameters in local reference frame and the positions of targets in dish-fixed frame, taken as true values of unknowns and denoted as *True*, which are substituted into monitoring models Eq (1) to calculate the coordinates of targets in the local control network, which after added with some noises and then are taken as the positioning observations of targets, denoted as O. Take the deviated *True* values as adopted initials of estimated parameters, then substituted into monitoring models to calculate the theoretical observations, denoted as C. Via linearization of observation equation to iteratively solve for the corrections to adopted values of parameters by least squares adjustment of *(O-C)*, and finally get the estimated values of parameters, denoted as *Est*.

Except for specific instructions, the simulation conditions are set as that there are four targets uniformly distributed along the edge of antenna dish and with 60 antenna orientations. The elevation is within 10 to 82 degrees with a step as 8 degrees, that for azimuth is from 0 to 360 degrees and with a step determined by the number of orientations. The antenna orientation (A,E) is given by the driving system and is taken as precisely known. The axis $\mathbf{e}$ is approximately to the east when the antenna is at rest. The standard deviation of coordinate component of target positioning observation is $\sigma_0 = 5mm$. The relative deviation of the adopted initials of parameters is 5%, that is *Est*=(1-5%)*True*. The iteration procedure will be terminated when the absolute of corrections to parameters are less than 1×10^{-6} or the number of iterations is over 50.

Due to the added noise to observations there are fluctuations among the results of independent simulations even with same setting of initial conditions. Though the general characteristics of solved parameters are not confused by the fluctuations, the following simulation results are all the average of multiple independent simulations in order to suppress the detrimental effect of added noises.

The monitoring model adopted in data simulation is showed by Eq (1). We concerned the effect on estimation precision of antenna parameters by the factors including 1) the number of observations, 2) the positioning precision of targets, 3) the detection and deletion of outlier observations, 4) the distribution of targets along the edge of antenna dish, 5) the dynamical range of adopted initials of parameters and so on.

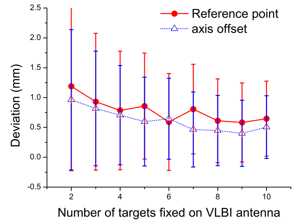

Fig. 2 Deviation of the estimated reference point position and axis offset versus the number of targets fixed on VLBI antenna.

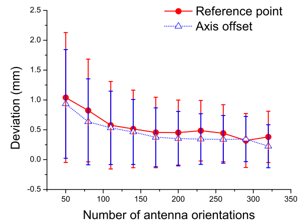

Fig. 3 Deviation of the estimated reference point position and axis offset versus the number of VLBI antenna orientations.

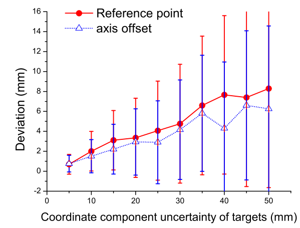

Fig. 4 Deviation of the estimated reference point position and axis offset versus the uncertainty of target positioning observations.

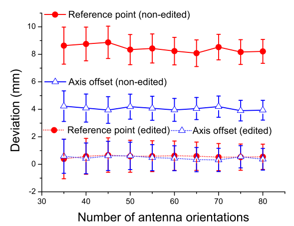

Fig. 5 Deviation of the estimated reference point position and axis offset after the observation edition.

According to Fig. 2 and Fig. 3, it is clear that, the increase in targets or in antenna orientations are all corresponding to the increase in target positioning data points, and so the increase in the number of observation equations, which is therefore understandable to improve the estimation precision of parameters in the sense of least squares adjustment. With the same number of observations, the determination precision of parameters is mainly dependent on the observation uncertainties, proved by Fig. 4. And as showed in Fig. 5, the deletion of outliers will significantly benefit the precision of estimated parameters. In such condition, the effect of distribution manner of targets (Fig. 6) or the deviation of adopted initials of parameters relative to the true values (Fig. 7) on the estimated precision of parameters is not significant.

4 Conclusions

Simulation results show that it is practicable to monitoring antenna parameters by some targets fixed on the antenna without any restrictions to the antenna rotation mode, and which could achieve precisely, automatically and realtime monitoring of antenna parameters during the astrometric and geodetic VLBI observations, and therefore it is of positive importance to the realization of continuous observations of station coordinates with high precision with the VLBI2010 technical specifications.

Results from simulation show that the analysis and investigation in this paper concerning the monitoring model of VLBI antenna, the setting of parameters, the selection of constraints and so on are rational, and that the significant factors which determine the monitoring precision of antenna parameters include the number of targets fixed on the VLBI antenna, antenna orientations, and the precision of target positioning observations. It is also shown the necessity to detect and delete outliers from target positioning observations.

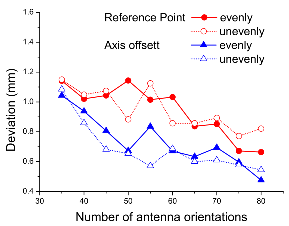

Fig. 6 Deviation of the estimated reference point position and axis offset versus the distribution of targets on the edge of the dish.

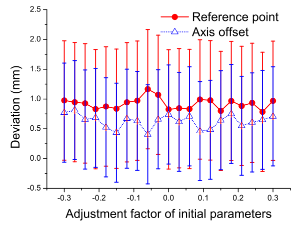

Fig. 7 Deviation of the estimated reference point position and axis offset versus the adopted initials of parameters.

In practical implementation it is difficult to completely avoid the occurrence of blocking of observations, failure in instrumentation and data collection. During the procedure the VLBI antenna changes radio sources the position of a target fixed on the antenna is relatively quickly changing with time, and so the positioning precision should be very limited. There are random and systematic errors in the orientations given by antenna driving system, which should leave detrimental effects on the estimation of antenna parameters. It is worth to consider issues related to the practical way of target positioning observation, the development of automatic software of data processing and so on. In summary, further analysis, examination and practical tests are still necessary concerning the automatic monitoring of antenna parameters with high precision.

References

Petrachenko B, Niell A, Behrend D, et al. Design aspects of the VLBI2010 system. *IVS Annual Report 2008*, NASA/TP-2009-214183,2009: 13-67

Johnston G, Dawson J. The 2003 Yarragadee (Moblas 5) local tie survey. *Geoscience Australia, Record 2004/19*, 27pp, 2004, 1-33

Sarti P, Sillard P, Vittuari L. Surveying co-located space geodetic instruments for ITRF computation. *J Geodesy*, 2004, 78(3): 210-222

Sarti P, Abbondanza C, Petrov L, et al. Height bias and scale effect induced by antenna gravitational deformations in geodetic VLBI data analysis. *J Geodesy*, 2011, 85(1):1-8

Lösler M. Reference point determination with a new mathematical model at the 20 m VLBI radio telescope in Wettzell. *Journal of Surveying Engineering*, 2008, 2: 233-238

Lösler M. New mathematical model for reference point determination of an azimuth-elevation type radio telescope. *Journal of Surveying Engineering*, 2009, 135(4): 131-135

Neidhardt A, Lösler M, Eschelbach C, et al. Permanent Monitoring of the Reference Point of the 20m Radio Telescope Wettzell. *IVS 2010 General Meeting Proceedings*, NASA/CP-2010-215864: 133-137

Schmeing B, Behrend D, Gipson J, et al. Proof-of-Concept Studies for a Local Tie Monitoring System. *IVS 2010 General Meeting Proceedings*, NASA/CP-2010-215864: 138-142

Kallio U, Poutanen M. Simulation of local tie accuracy on VLBI antennas. *IVS 2010 General Meeting Proceedings*, NASA/CP-2010-215864, 2010: 360-364

Lösler M, Hennes M. An innovative mathematical solution for a time-efficient IVS reference point determination. *Proceedings of the FIG2008 - Measuring the changes*,2008

Automated IVS Reference Point Monitoring - First Experience from the Onsala Space Observatory

C. Eschelbach, R. Haas, M. Lösler

Abstract The realization of the International Terrestrial Reference Frame (ITRF) builds upon a combination of results derived from several geodetic space techniques, such as Very Long Baseline Interferometry (VLBI), Satellite and Lunar Laser Ranging (SLR and LLR) or Global Navigation Satellite Systems (GNSS). To combine the different techniques and their results in a meaningful way, co-location sites are important where equipment for several techniques is located reasonably close to each other. The relative geometries (local tie vectors) between the geometric reference points of the different techniques can be derived by terrestrial survey at these co-location sites. Within the Global Geodetic Observing System (GGOS) the requirements in terms of e.g. accuracy and frequency of local survey campaigns have been increased to guarantee that the local tie vectors reach an utmost level of global accuracy. In response to this request we developed a concept to achieve automated and continuous monitoring of radio telescope reference points. This concept was realized and tested in 2012 at the Onsala Space Observatory where an automated monitoring system was installed for a continual determination of the reference point of the 20 m radio telescope. The results confirm that uncertainties on the sub-mm level can be achieved with this approach. Furthermore, a recursive estimation method is suggested for continual determinations of the reference point position that form the basis of time series of local tie vectors.

Cornelia Eschelbach
cornelia.eschelbach@fb1.fh-frankfurt.de
University of Applied Sciences Frankfurt, Nibelungenplatz 1, DE-60318 Frankfurt am Main, Germany

Rüdiger Haas
rudiger.haas@chalmers.se
Chalmers University of Technology, Onsala Space Observatory SE-439 92 Onsala, Sweden

Michael Lösler
michael.loesler@bkg.bund.de
Bundesamt für Kartographie und Geodäsie Frankfurt, Richard-Strauss-Allee 11, DE-60598 Frankfurt am Main, Germany

Keywords VLBI, Radio Telescope, Reference Point Determination, Monitoring, Error Budget

1 Motivation

Frequent and accurate surveys of the reference points of space geodetic equipment at geodetic co-location stations is a challenging task for metrology-engineers. It is the basis for local tie vectors of an utmost level of accuracy that are necessary to guarantee meaningful multi-technique combinations within GGOS. Automated and continuous monitoring are desired to reduce time-consuming field work. The monitoring system HEIMDALL was developed and tested for an automated and continuous determination of the IVS reference point of the 20 m radio telescope at the Onsala Space Observatory in 2012.

2 Concept of Automated Reference Point Determination

In standard monitoring the motions or deformations of the observed object are directly related to the observed points that are fixed on the object. A radio telescope reference point that is located somewhere in the telescope structure cannot be observed directly but needs to be derived in an indirect way based on observations to points fixed on the moving parts of the telescope. In contrast to a standard monitoring, an automated reference point determination is an ambitious metrological challenge, because the observed points change their positions as a function of the azimuth α and elevation angles ϵ of the radio telescope. Thus, a JAVA-based monitoring software was developed that considers the specific conditions of an automated reference point determination. Basically, the concept can be divided into four sub-tasks: the determination of a-priori positions, the network adjustment, the reference point determination, and the analysis of time series (cf. Lösler et al. (2013a)).

2.1 Determination of a-priori positions

From an operational point of view an automated monitoring should be carried out ideally during a regular VLBI session. The predicted positions of the mounted targets $\mathbf{P}^i_{\text{Obs}}(\alpha,\epsilon)$ have to be derived from the VLBI schedule and from a-priori information concerning the local site network. Furthermore, a verification of the measurability of the predicted positions $\mathbf{P}^i_{\text{Obs}}(\alpha,\epsilon)$ is necessary to reduce unneeded total station activities. The predicted position is expressed by

$$\mathbf{P}^i_{\text{Obs}}(\alpha,\epsilon) = \mathbf{P}^0_{\text{RP}} + \mathbf{R}_{\alpha,\epsilon}(\mathbf{P}^i_{\text{Obs}} - \mathbf{P}^0_{\text{RP}}) \tag{1}$$

where $\mathbf{R}$ denotes a rotation matrix, $\mathbf{P}^i_{\text{Obs}}$ is the initial position of the mounted target observed at $\alpha = \epsilon = 0$, and $\mathbf{P}^0_{\text{RP}}$ is an approximate position of the reference point. In addition to the initial position $\mathbf{P}^i_{\text{Obs}}$, the normal direction vector $\mathbf{n}^i_{\text{Obs}}$ of the prism has to observed to be able to determine the angle of incidence δ at the i^{th} target with respect to the survey point $\mathbf{P}_{\text{TS}}$

$$\cos\tau^i = \frac{[\mathbf{P}_{\text{TS}} - \mathbf{P}^i_{\text{Obs}}(\alpha,\epsilon)]^T \mathbf{R}_{\alpha,\epsilon}\mathbf{n}^i_{\text{Obs}}}{|\mathbf{P}_{\text{TS}} - \mathbf{P}^i_{\text{Obs}}(\alpha,\epsilon)||\mathbf{n}^i_{\text{Obs}}|} \tag{2}$$

This angle of incidence has to be smaller than the specified opening angle of the used prism type to verify the accessibility.

2.2 Network Adjustment

The first analysis step is a common spatial network adjustment based on a Gauß-Markov model (e.g. Koch (2007)). For this purpose, the network adjustment combines the measured data and delivers the coordinates of the points at the telescope structure $\mathbf{P}^i_{\text{Obs}}(\alpha,\epsilon)$ and their variance-covariance-matrix. If some of the $\mathbf{P}^i_{\text{Obs}}(\alpha,\epsilon)$ are observed redundantly, outlier detection is possible within the network adjustment, and variance-component-estimation can be used to derive the uncertainties. In any other case, mismeasurements must be detected within the reference point determination in the next step. Furthermore, the estimated variance factor has only a limited validity and the derived variance-covariance-matrix is strongly depended on the a-priori stochastic model used in the network adjustment.

2.3 Reference Point Determination

We restrict the discussion on azimuth-elevation type radio telescopes, because most of the radio telescopes that are used for geodetic VLBI in the framework of the International VLBI Service for Geodesy and Astrometry (IVS) are of this type. The reference point of these radio telescopes is defined as the projection of the elevation axis on the fixed azimuth axis. Typically, the reference point is determined by indirect methods because it is not materialized. An often used method to estimate the reference point is based on circle fitting (Eschelbach and Haas (2003)) and was adopted by several groups (e.g. Dawson et al. (2007), Leinen et al. (2007)). Spatial circles result from a predefined observation configuration, fixing one axis while turning the other. Thus, the method is not suitable for a monitoring during normal operations of the radio telescope. For normal operations, Lösler's transformation model is an applicable alternative (Lösler (2009)):

$$\mathbf{P}_{\text{Obs}} = \mathbf{P}_{\text{RP}} + \mathbf{R}^{\mathbf{x}}_{\theta}\mathbf{R}^{\mathbf{y}}_{\phi}\mathbf{R}^{\mathbf{z}}_{\alpha-\mathbf{O}_\alpha}\mathbf{R}^{\mathbf{y}}_{\psi}(\mathbf{E_{cc}} + \mathbf{R}^{\mathbf{x}}_{\epsilon-\mathbf{O}_\epsilon}\mathbf{P}_{\text{Tel}}) \tag{3}$$

where $\mathbf{P}_{\text{Tel}} = [b\,a\,0]^T$ is a point in the telescope system, $\mathbf{E_{cc}}$ denotes the axis-offset, and the angle ψ describes the non-orthogonality between the azimuth- and elevation-axes. The vertical misalignment of the azimuth-axis is parameterized by θ and ϕ, and O_α and O_ϵ are additional orientation angles. This model has been adapted by Kallio and Poutanen (2012) by reformulating the rotation matrices in a commutative way (c.f. Nitschke and Knickmeyer (2000)). Nevertheless, both notations are equivalent and fulfill the requirements for an automated reference point monitoring. The positions $\mathbf{P}^i_{\text{Obs}}(\alpha,\epsilon)$ and their related azimuth angles α and elevation angles ϵ are fitted to the described model that delivers the reference point and additional parameters like the axis-offset in an orthogonal distance fit (e.g. Eschelbach and Lösler (2012)). Outliers can be identified during the adjustment process of the reference point determination using multiple statistical tests (Lösler (2009)).

2.4 Time Series Analysis

In general, the results of a single survey epoch will be treated as invariant until a new measurement is carried out. In most cases the repeat-rate for a reference point determination is on the order of one or two years (cf. Klügel et al. (2011), Sarti et al. (2013)). Therefore, seasonal variations or abrupt changes can hardly be detected. More frequent reference point determinations result from an automated monitoring and advanced analyses are possible. The results of m reference point determinations $\mathbf{x_j}$ and their corresponding variance-covariance-matrices $\mathbf{Q_{x_jx_j}}$ can be combined by introducing recursive parameter estimation (cf. Koch (2007), Lösler et al. (2013a)).

$$\hat{\mathbf{x}}_j = \hat{\mathbf{x}}_{j-1} + \mathbf{K}_{j-1,j}(\mathbf{x}_j - \hat{\mathbf{x}}_{j-1}) \tag{4}$$

with the gain matrix

$$\mathbf{K}_{j-1,j} = \mathbf{Q}_{\hat{\mathbf{x}}_{j-1}\hat{\mathbf{x}}_{j-1}}(\mathbf{Q}_{\mathbf{x}_j\mathbf{x}_j} + \mathbf{Q}_{\hat{\mathbf{x}}_{j-1}\hat{\mathbf{x}}_{j-1}})^{-1} \tag{5}$$

The variance-covariance-matrix $\mathbf{Q}_{\hat{\mathbf{x}}_j\hat{\mathbf{x}}_j}$ follows with (e.g. Koch (2007))

$$\mathbf{Q}_{\hat{\mathbf{x}}_j\hat{\mathbf{x}}_j} = \mathbf{Q}_{\hat{\mathbf{x}}_{j-1}\hat{\mathbf{x}}_{j-1}} - \mathbf{K}_{j-1,j}\mathbf{Q}_{\hat{\mathbf{x}}_{j-1}\hat{\mathbf{x}}_{j-1}} \tag{6}$$

It is assumed, that a single determination is not invariant with time, thus an additional variance matrix of the process noise $\mathbf{C}_{\mathrm{nn}} = \mathrm{diag}(\dot{\sigma}^2_{x_{\mathbf{P}_{\mathrm{RP}}}} \dot{\sigma}^2_{y_{\mathbf{P}_{\mathrm{RP}}}} \dot{\sigma}^2_{z_{\mathbf{P}_{\mathrm{RP}}}})$ is introduced and delivers

$$\mathbf{Q}^{\Delta t}_{\mathbf{x}_j\mathbf{x}_j} = \mathbf{Q}_{\mathbf{x}_j\mathbf{x}_j} + \mathbf{B}\mathbf{C}_{\mathrm{nn}}\mathbf{B}^{\mathrm{T}} \tag{7}$$

The recursive parameter estimation enables the ongoing integration of the results of a current measurement epoch into a time series to achieve immediately reliable results.

2.5 Error Budget

Whereas random errors are handled by the stochastic model, systematic errors distort the results and have to be taken into account. In general, grouping the errors based on their sources is useful and can be depicted easily in an Ishikawa diagram (cf. Figure 1).

The telescope-dependent systematic errors are primarily the gravitational and thermal deformations. External sensors and specific observation strategies are needed to compensate for these deviations (e.g. Clark and Thomsen (1988), Haas et al. (1999), Sarti et al. (2011), Lösler et al. (2013b)). Systematic errors concerning the total station are mainly instrumental errors, e.g. encoder errors, trunnion axis error or horizontal collimation error (cf. Eschelbach and Lösler (2012)). Most of these errors are compensated by carrying out so-called two-face measurements as well as by applying reliable calibration values. In addition meteorology errors influence the scale parameter of the EDM-unit of the total station. Clock errors and time drifts have to be taken into account if time depending observations of different sensors are combined with each other. The stability and the configuration of the network affect the reliability of the measurement (cf. Abbondanza and Sarti (2012)).

Furthermore, the angle of incidence δ of a target beam from the total station's survey station point to the mounted glass-body prisms at the telescope varies as a function of α and ϵ. This causes a systematic displacement of the prism centre depending on the orientation of the prism relative to the total station. The radial derivation $\varepsilon_{\mathrm{radial}}$ and the lateral deviation $\varepsilon_{\mathrm{lateral}}$ are given by Pauli (1969)

$$\varepsilon_{\mathrm{radial}} = d\Big(n - \sqrt{n^2 - \sin^2\delta}\Big) - e(1 - \cos\delta) \tag{8}$$

and Rüeger (1990)

$$\varepsilon_{\mathrm{lateral}} = (d - e)\sin\delta - d\sec\delta_G\sin(\delta - \delta_G) \tag{9}$$

where $\delta_G = \arcsin\frac{\sin\delta}{n}$, e and d are the distance between the front surface of the prism and the apex and the corner point of the triple prism, respectively, and n denotes the refractive index ratio of glass and air.

Figure 2 depicts observed $\varepsilon_{\mathrm{radial}}$ and $\varepsilon_{\mathrm{lateral}}$ of a GPR121-type prism in a test setup (square and triangle markers), and for comparison the predicted values using Eq. (8) and Eq. (9), respectively. A misalignment of e.g. $\delta = 35°$ leads to deviations of $\varepsilon_{\mathrm{lateral}} = 1.2$ mm and $\varepsilon_{\mathrm{radial}} = 0.2$ mm. This means, if this is ignored it becomes a large contribution for the error budget of the point position. Unfortunately, this effect has never been taken into account in reference point determinations so far. The distance measurement can be corrected by

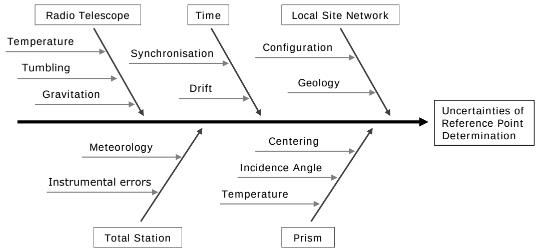

Fig. 1 Ishikawa-diagram for the error budget

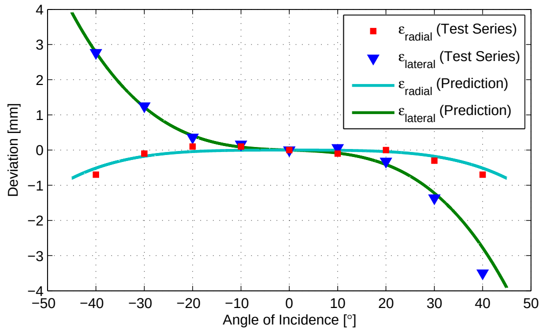

Fig. 2 Lateral and radial deviation for GPR121. The squares and triangles show measured radial and lateral deviations while the solid lines show the deviations according to equations 8 and 9.

adding $\varepsilon_{\text{radial}}$, but the lateral derivation $\varepsilon_{\text{lateral}}$ needs to be split-up into a horizontal and a vertical component. These components can be derived by a projection along the direction of the true position.

$$\mathbf{P}^*_{\text{Obs}} = \mathbf{P}^i_{\text{Obs}} - \frac{|\varepsilon_{\text{lateral}}|}{|\mathbf{q}^i_{\text{Obs}}|}\mathbf{q}^i_{\text{Obs}} \tag{10}$$

Here, the projection of the normal vector $\mathbf{n}_{\text{Obs}}$ into the observation plane is given by

$$\mathbf{q}^i_{\text{Obs}} = \mathbf{R}_{\alpha,\epsilon}\mathbf{n}^i_{\text{Obs}} - \left(\frac{[\mathbf{P}^i_{\text{Obs}} - \mathbf{P}_{\text{TS}}]^T \mathbf{R}_{\alpha,\epsilon}\mathbf{n}^i_{\text{Obs}}}{[\mathbf{P}^i_{\text{Obs}} - \mathbf{P}_{\text{TS}}]^T [\mathbf{P}^i_{\text{Obs}} - \mathbf{P}_{\text{TS}}]}\right)[\mathbf{P}^i_{\text{Obs}} - \mathbf{P}_{\text{TS}}] \tag{11}$$

If v and t are the estimated vertical and direction angles w.r.t. the observed point $\mathbf{P}_{\text{Obs}}$ and v^* and t^* are the estimated vertical and direction angles w.r.t. the projected position $\mathbf{P}^*_{\text{Obs}}$, respectively, the angle deviations are $\varepsilon_{\text{t}} = t^* - t$ and $\varepsilon_{\text{v}} = v^* - v$. This calculation can directly follow the measurements of the initial position and the normal direction vector of the prisms. The correction values are calculated in advance along with the observation plan so that the observations can be corrected already during the monitoring, just-in-time before being saved to the data base.

3 Monitoring Campaign at the Onsala Space Observatory

At the Onsala Space Observatory, four monitoring approaches (DMR, DMO, VMO and VSO) were carried out at the 20 m radio telescope using a high precision total station of type Leica TS30 and ten prisms of type GPR121 and GMP104.

The DMO-experiment was carried out twice, because it is assumed that a homogenous point cloud provides reliable results (cf. Table 1). Table 2 summarizes the smoothed results and their uncertainties derived from the analysis using eq. (4) – (7).

Table 1 Configurations of Survey Epochs.

Approaches/Experiment	I	II	III	IV	V
Dedicated survey/Real **V**LBI schedule	D	D	V	D	V
Single/**M**ultiple survey stand point(s)	M	M	M	M	S
Target was observed **O**nce/**R**edundantly	R	O	O	O	O

Table 2 'Smoothed' results from combining successive measurement campaigns.

Experiment	I+II	I+II+III	I+...+IV	I+...+V
$x_{\mathbf{P}_{\text{RP}}}$ [m]	90.1236	90.1236	90.1236	90.1236
	± 0.0002	± 0.0001	± 0.0001	± 0.0001
$y_{\mathbf{P}_{\text{RP}}}$ [m]	35.9493	35.9492	35.9492	35.9492
	± 0.0002	± 0.0002	± 0.0001	± 0.0001
$z_{\mathbf{P}_{\text{RP}}}$ [m]	22.7592	22.7592	22.7593	22.7592
	± 0.0002	± 0.0002	± 0.0002	± 0.0002
E_{cc} [mm]	−6.1	−6.1	−6.1	−6.0
	± 0.2	± 0.2	± 0.1	± 0.1

The smoothed results are presented in Figure 3 as green line with a 3σ error band, and the individual determinations based on the five experiments are shown as blue dots with 3σ error bars.

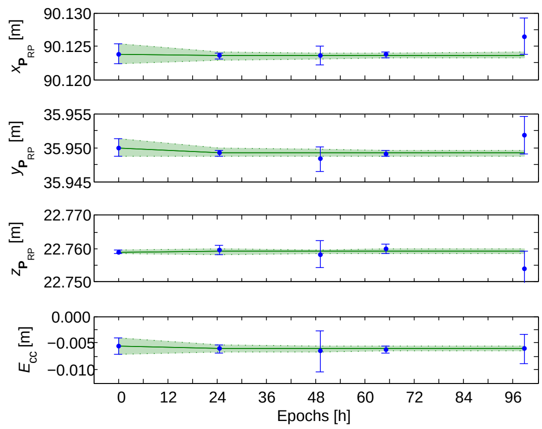

Fig. 3 Time series of the reference point coordinates and the telescope axis offset.

4 Conclusion

In 2012 the monitoring system HEIMDALL was installed for continuous observations of the IVS reference point of the 20 m radio telescope at the Onsala

Space Observatory. Five campaigns with different approaches were evaluated and combined by introducing a recursive parameter estimation. Furthermore, the use of glass-body prisms provides systematic errors up to the mm-level, which were for the first time considered by the authors for a reference point determination.

References

C. Abbondanza and P. Sarti. Impact of network geometry, observation schemes and telescope structure deformations on local ties: simulations applied to Sardinia Radio Telescope. *Journal of Geodesy*, **86**, 181–192, 2012.

T.A. Clark, P. Thomsen Deformations in VLBI antennas. Tech. rep., 100696, NASA, Greenbelt, MD, 1988.

J. Dawson, P. Sarti, G. Johnston, L. Vittuari. Indirect approach to invariant point determination for SLR and VLBI systems: an assessment. *Journal of Geodesy*, **81**, 433–441, 2007.

C. Eschelbach and R. Haas. The IVS-Reference Point at Onsala – High End Solution for a real 3D-Determination. In: *Proceedings of the 16th Meeting of the European VLBI Group for Geodesy and Astronomy*, 109–118, 2003.

C. Eschelbach and M. Lösler. Alternative ways for appropriate data analysis in industrial metrology. In: *Proceedings of the LowCost3D*, Deutsches Zentrum für Luft- und Raumfahrt, Berlin, 2012.

R. Haas, A. Nothnagel, H. Schuh, O. Titov. Explanatory supplement to the section 'Antenna Deformation' of the IERS Conventions (1996). In: *DGFI report nr. 71*, Deutsches Geodätisches Forschungsinstitut (DGFI), Munich (Germany), 26–29, 1999.

U. Kallio and M. Poutanen. Can We Really Promise a mm-Accuracy for the Local Ties on a Geo-VLBI Antenna. In: *Geodesy for Planet Earth*, International Association of Geodesy Symposia, 136, Springer-Verlag Berlin Heidelberg, 35–42, 2012.

K.R. Koch *Introduction to Bayesian Statistics*, Springer, Heidelberg/Berlin, 2nd edn., 2007.

T. Klügel, S. Mähler, C. Schade. Ground Survey and Local Ties at the Geodetic Observatory Wettzell. In: *17th Workshop on Laser Ranging*, Bad Kötzting, 2011.

S. Leinen, M. Becker, J. Dow, J. Feltens, K. Sauermann. Geodetic Determination of Radio Telescope Antenna Reference Point and Rotation Axis Parameters. *Journal of Surveying Engineering*, **133**, 41–51, 2007.

M. Lösler. New Mathematical Model for Reference Point Determination of an Azimuth-Elevation Type Radio Telescope. *Journal of Surveying Engineering*, **135**, 131–135, 2009.

M. Lösler, R. Haas, C. Eschelbach. Automated and Continual Determination of Radio Telescope Reference Points With Sub-mm Accuracy – Results from a campaign at the Onsala Space Observatory. *Journal of Geodesy* (Accepted for Publication), 2013a.

M. Lösler, A. Neidhardt, S. Mähler. Impact of Different Observation Strategies on Reference Point Determination – Evaluations from a Campaign at the Geodetic Observatory Wettzell. In: *Proceedings of the 21th Meeting of the European VLBI Group for Geodesy and Astronomy*, 2013b, this issue.

M. Nitschke, E.H. Knickmeyer. Rotation Parameters - A survey of Techniques. *Journal of Surveying Engineering*, **126**, 83–105, 2000.

W. Pauli. Vorteile eines kippbaren Reflektors bei der elektrooptischen Streckenmessung. *Vermessungstechnik*, 412–415, 1969.

J.M. Rüeger. *Electronic Distance Measurement - An Introduction*, Springer, Heidelberg/Berlin, 3rd edn., 1990.

S. Sarti, C. Abbondanza, L. Petrov, M. Negusini. Height bias and scale effect induced by antenna gravitational deformations in geodetic VLBI data analysis. *Journal of Geodesy*, **85**, 1–8, 2011.

S. Sarti, C. Abbondanza, J. Legrand, C. Bruyninx, L. Vittuari, J. Ray. Intrasite motions and monument instabilities at Medicina ITRF co-location site. *Geophys. J. Int.*, **192**, 1–10, 2013.

Impact of Different Observation Strategies on Reference Point Determination – Evaluations from a Campaign at the Geodetic Observatory Wettzell

M. Lösler, A. Neidhardt, S. Mähler

Abstract The strategy document VLBI2010 and the Global Geodetic Observing System (GGOS) claim continuous local survey of the reference points of different geodetic space techniques, such as Very Long Baseline Interferometry (VLBI). Therefore, alternative observation and analysis strategies have to be evaluated, to reach an utmost level of accuracy. Different simulation studies reveal a significant influence of the terrestrial observation schemes on the uncertainty of the reference points. At the Geodetic Observatory Wettzell a measurement campaign was carried out to investigate different terrestrial observation schemes and the additional benefit of the use of a second total station. Modifying the collected data allows different analysis strategies such as the evaluation of simultaneous dual polar observations, redundant forward intersections or, by neglecting the observations of one total station, single polar observations. Furthermore, the influence on variations of the telescope height caused by thermal expansion was analysed within the reference point determination.

Keywords VLBI, Radio Telescope, Reference Point Determination, Observation Scheme, Thermal Deformation

Michael Lösler and Swetlana Mähler
`michael.loesler@bkg.bund.de`, `swetlana.maehler@bkg.bund.de`
Bundesamt für Kartographie und Geodäsie Frankfurt, BKG, Richard-Strauss-Allee 11, DE-60598 Frankfurt am Main, Germany

Alexander Neidhardt
`neidhardt@fs.wettzell.de`
Technische Universität München, Forschungseinrichtung Satellitengeodäsie, FESG, Sackenrieder Str. 25, DE-93444 Bad Kötzting, Germany

1 Motivation

The Geodetic Observatory Wettzell (GOW) is operated by the Federal Agency for Cartography and Geodesy (BKG) together with the Research Facility for Satellite Geodesy (FESG) of the Technische Universität München (Technical University Munich) (Hugentobler et al., 2011). The observatory is a so-called co-location station and hosts equipment for several geodetic space techniques such as Very Long Baseline Interferometry (VLBI), Satellite and Lunar Laser Ranging (SLR and LLR) or Global Navigation Satellite Systems (GNSS). With the knowledge of the relative geometries (local ties) between these techniques on co-location stations, a combination of geodetic space techniques is permitted in the context of the International Terrestrial Reference Frame (ITRF). Two VLBI2010 compliant radio telescopes (TWIN), which are identical in construction, will be operable soon. These new radio telescopes fulfil the increased requirements of the VLBI2010 agenda and the Global Geodetic Observing System (GGOS) (Niell et al., 2006; Plag and Pearlman, 2009). In addition to the requirements of the VLBI2010 telescopes the specifications on local ground survey, the reference points of the geodetic space techniques and therefore the local tie vectors are increased in terms of e.g. uncertainties and frequency of surveying campaigns. To reach an utmost level of accuracy of the IVS reference point, different simulations studies were carried out.

Schmeing et al. (2010) simulate the impact of the number of survey standpoints on the uncertainties of the reference point and conclude that a single survey standpoint meets the sub-mm goal already. Kallio and Poutanen (2010) and Li et al. (2013) analysed the influence on the reference point due to the position and the number of targets, which are mounted on the alidade of the radio telescope. There is shown, that only a few targets are needed to reach the sub-mm level. Furthermore, the best position of the targets is near the elevation axis. This configuration was used by e.g. Eschelbach and Haas (2003); Lösler (2008); Eschelbach et al. (2013). Santamaría-Gómez et al. (2012) assume that this position is less prone to gravitational deformations. Moreover, they assess the benefit of more than one observation instrument and assert that the uncertainty of the reference point is bisected using a second instrument. Another extensive simulation study has been carried out by Abbondanza and Sarti (2012). They investigate the reference point variations caused by different terrestrial observation schemes, network configurations, gravitational and thermal deformations. Moreover, the terrestrial observation schemes and radio telescope deformations influence the position of the reference point significantly.

2 Feasibility Study

In spring 2012, a measurement campaign was performed with one of the TWIN Radio Telescope Wettzell (TTW2), Germany, to test different terrestrial surveying schemes and the additional benefit of the usage of a second total station. For the survey, four prisms of the type RFI-0.5" (Leica) were mounted per telescope side near the elevation axis (cf. Figure 1), 12 more precision surveying monitoring prisms of type Leica GPH1P were used for the connection to the local ground network.

To get a homogeneous point cloud, an increment of 10° and 40° for the elevation and azimuth angle, respectively, was chosen. To keep the observation process as automated as possible, two high precision total stations were used namely a Leica TCA2003 and its successor TS30 (Lienhart et al. (2009)). Both instruments were endued with automatic target recognition (ATR). Therefore, the telescope targets were measured by simultaneous dual polar observations (DPO). Modifying the collected data allows further analysis strategies such as redundant forward intersections (RFI) excluding distance measurements and, by neglecting the observations of one total station, single polar observations (SPO). The topographical conditions made us use the measurement distances to the telescope between 15-25 m.

Due to the short measurement distance and the limited angle of incidence of the prisms, which are also affected by the telescope rotation, a small base between the total stations had to be chosen (cf. Figure 2). Thus, glancing intersections could be anticipated, which increase the uncertainties of the RFI method. The best intersection is given by an angle of 100 gon (cf. Fig-

Fig. 1 VLBI2010 Radio Teleskop TTW2 (top). Mounted Targets at TWIN-Telescope (bottom).

Table 1 Results of the Network Adjustment

Configuration	DPO	RFI	SPO-TS30	SPO-TCA
Mean Target Error	0.7 mm	4.9 mm	0.8 mm	0.5 mm
Degree of Freedom	2257	1095	261	187

ure 3). Whereas the redundant DPO and RFI configuration allows a reliable uncertainty budgeting based on variance component estimation, the uncertainties of the SPO method result only from the a-priori stochastic model.

Table 1 summarizes the result of the free network adjustment derived from JAG3D[1] and points out the mean error of the measured targets on the telescope

[1] `http://derletztekick.com/software/netzausgleichung`

Fig. 2 Simultaneous Observations with TS30 and TCA2003.

(excluding network measurements) and the degree of freedom. In comparison to the other configurations the uncertainty of the RFI method is enlarged. Note that the poorer results of RFI arise from the glancing intersections and cannot be generalized to this method. Favourable results are expected by increasing the intersecting angle (e.g. Eschelbach and Haas (2003)). Figure 4 depicts the observed connections between the survey points (red circles) of the local survey network (blue triangles) and the telescope points (red dots) in the local coordinate system.

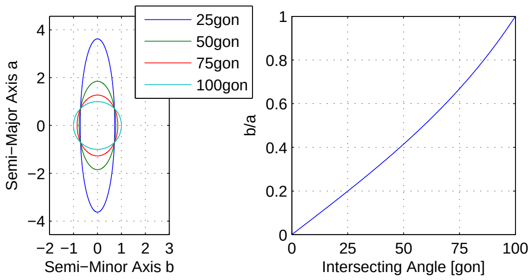

Fig. 3 Ratio between Major and Minor Semi-Axis of the Confidence Ellipse as a Function of Intersecting Angle.

In contrast to the 20 m Radio Telescope Wettzell (RTW), where an invar wire is installed to monitor the height variations, the TTW2 has no opportunity to observe the expansion caused by temperature directly. Therefore, a temperature sensor of type MSR145 was placed inside the telescope cabin to register the internal temperature. Combined with the thermal expansion coefficients γ_S and γ_F for the antenna and for the foundation, respectively, the height h_S of the reference point with respect to the foundation, and the height h_F of the foundation, the variations $z_{\mathbf{P}_{\mathrm{RP}}}(\Delta T_i)$ can be compensated (cf. Nothnagel (2009)).

$$z_{\mathbf{P}_{\mathrm{RP}}}(\Delta T_i) = z_{\mathbf{P}_{\mathrm{RP}}} + (\gamma_S h_S + \gamma_F h_F)\Delta T_i \qquad (1)$$

where ΔT_i is the difference between the reference temperature and the temperature of the telescope structure.

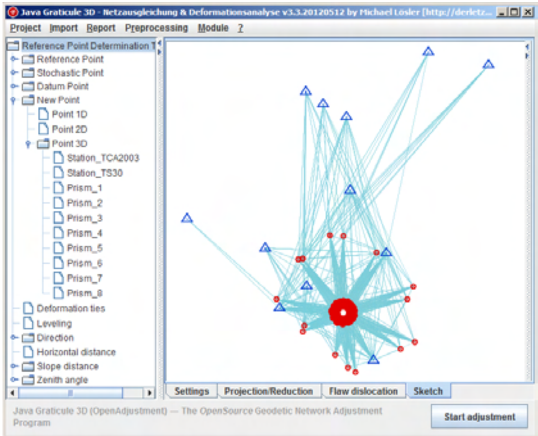

Fig. 4 Sketch of the Local Ground Control Network.

3 Reference Point Determination

Using the four data sets (DPO, RFI, SPO-TS30 and SPO-TCA) and their full variance-covariance-matrices the reference point of the TTW2 was derived by Lösler's transformation model (Lösler, 2009). Since contaminated data could not be detected during the network adjustment for SPO configuration, multiple tests have been introduced for trusted outlier detection within the reference point determination (Lösler, 2008). The observation with a maximum exceeding of a defined threshold was excluded. This procedure was repeated until no more outliers were detected. Table 2 summarises the estimated reference point coordinates and the axis offset with associated uncertainties derived by each analysed data set. To avoid an overestimation of the derived uncertainties, the estimated uncertainties were adapted with respect to the mean point-error of the observed target positions (cf. Ghilani and Wolf (2006), Lösler et al. (2013)).

Obviously, the symmetrical configuration of the point cloud compensated the poorer accuracy of the estimated points of the RFI method. The terrestrial observation schemes had a minor influence on the reference point determination, because all methods provided almost the same results and comparable uncertainties.

Considering the height variations caused by temperature, a simplification of eq. (1) was used. With

$\gamma = \gamma_S = \gamma_F$ eq. (1) becomes

$$z_{\mathbf{P}_{\mathrm{RP}}}(\Delta T_i) = z_{\mathbf{P}_{\mathrm{RP}}} + \mu(h_S + h_F)\gamma\Delta T_i \qquad (2)$$

where the damping parameter μ is introduced as an additional weighting parameter to find an optimal compensation within the reference point determination. As shown by Abbondanza and Sarti (2012) the uncertainties of the reference point were insensitive to telescope deformations. Nevertheless, the sum of the squared residuals Ω of the reference point determination could be used to evaluate the model compatibility of eq. (2), if each observed target position is corrected by their *individual* thermal expansion value.

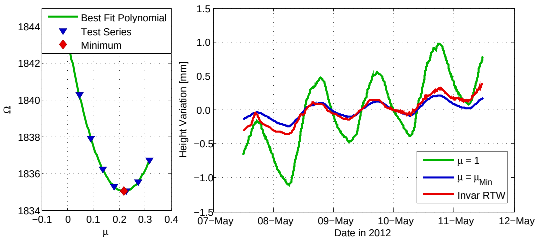

Fig. 5 Damping Parameter μ vs. Objective Function Ω (left), Height Variation (right).

Figure 5 (left) shows Ω as a function of μ. Using the first derivation of the fitted polynomial, a minimum could be derived for $\mu_{Min} = 0.22$. The estimated height variations, calculated by eq. (2), are plotted for $\mu = \mu_{Min}$ (blue) and $\mu = 1$ (green). The RTW and the TTW2 have similar monument heights. Thus, the recorded data of the RTW invar wire (red) are also shown for comparison and confirm the derived damping parameter (cf. Figure 5 (right)). The overcompensation for $\mu = 1$ is abundantly clear. If each observed target position is corrected by their individual thermal expansion value, the influence of the thermal deformation can be estimated and compensated within the reference point determination. However, more than one temperature sensor should be integrated to observe the representative monument temperature of the radio telescope.

4 Conclusion

VLBI2010 and GGOS define new goals for the reference points and local ties. Many simulation studies were analysed by different research groups to answer the question, how the new specification can be reached. At the GOW a measurement campaign was carried out to investigate different terrestrial surveying schemes and the additional benefit of the use of a second total station during the reference point determination. The benefit of a second total station and the resulting opportunities during the network adjustment on the reference point are slightly. However, a second total station allows a reliable uncertainty budgeting for targets at the turnable telescope part in the course of the network adjustment. Observing a homogeneous point cloud seems to compensate the lower uncertainty of a measurement method or an unfavourable configuration. Furthermore, the influence on variations of the telescope height, caused by thermal expansion, was analysed and an optimal compensation was derived. The comparison to the recorded invar data confirms this procedure.

Table 2 Estimated Reference Point and Axis-Offset with Uncertainties

	DPO	RFI	SPO-TS30	SPO-TCA
X [m]	99.9422	99.9422	99.9423	99.9423
	±0.0004	±0.0004	±0.0004	±0.0005
Y [m]	172.5700	172.5700	172.5701	172.5700
	±0.0003	±0.0004	±0.0003	±0.0004
Z [m]	38.3420	38.3422	38.3420	38.3422
	±0.0005	±0.0010	±0.0005	±0.0006
Ecc [m]	−0.0003	−0.0002	−0.0004	−0.0003
	±0.0004	±0.0004	±0.0004	±0.0004

References

C. Abbondanza and P. Sarti. Impact of network geometry, observation schemes and telescope structure deformations on local ties: simulations applied to Sardinia Radio Telescope. *Journal of Geodesy*, **86**, 181–192, 2012.

C. Eschelbach and R. Haas. The IVS-Reference Point at Onsala – High End Solution for a real 3D-Determination. In: *Proceedings of the 16th Working Meeting on European VLBI for Geodesy and Astronomy*, edited by W. Schwegmann and V. Thorandt, 109–118, 2003.

C. Eschelbach, R. Haas and M. Lösler. Automated IVS Reference Point Monitoring – First Experience from the Onsala Space Observatory. In: *Proceedings of the 21th Working Meeting on European VLBI for Geodesy and Astronomy*, 2013, this issue.

C.D. Ghilani and P.R. Wolf. Adjustment Computations – Spatial Data Analysis, Wiley and Sons, Hoboken, New Jersey, 4nd edn., 2006.

U. Hugentobler, A. Neidhardt, P. Lauber, M. Ettl, K.U. Schreiber, R. Dassing, T. Klügel, S. Riepl, G. Herold, G. Kronschnabl, C. Plötz, U. Hessels. The Geodetic Observatory Wettzell – a fundamental reference point. In: *Proceedings of Fragile Earth International Conference, GSA Field Guides*, Geological Society of America (GSA), edited by S. Carena, A.M. Friedrich and B. Lammerer, **22**, 1–6, 2011.

U. Kallio and M. Poutanen. Simulation of Local Tie Accuracy on VLBI Antennas. In: *VLBI2010: From Vision to Reality, IVS 2010 General Meeting Proceedings, NASA/CP-2010-215864*, edited by D. Behrend and K. D. Baver, 360–364, 2010.

J. Li, J. Zhang and L. Guo. On the monitoring model of reference point of VLBI antenna In: *Proceedings of the 21th Working Meeting on European VLBI for Geodesy and Astronomy*, 2013, this issue.

W. Lienhart, H.-M. Zogg, D. Nindl. Innovative Lösungen zur Erreichung höhster Genauigkeit und Geschwindigkeit am Beispiel der TS30 Totalstation von Leica Geosystems. *Allgemeine Vermessungs-Nachrichten* (AVN), **11-12**, 374–381, 2009.

M. Lösler. Reference point determination with a new mathematical model at the 20 m VLBI radio telescope in Wettzell. *Journal of Applied Geodesy*, **2**, 233–238, 2008.

M. Lösler. New Mathematical Model for Reference Point Determination of an Azimuth-Elevation Type Radio Telescope. *Journal of Surveying Engineering*, **135**, 131–135, 2009.

M. Lösler, R. Haas, C. Eschelbach. Automated and Continual Determination of Radio Telescope Reference Points With Sub-mm Accuracy – Results from a campaign at the Onsala Space Observatory. *Journal of Geodesy* (Accepted for Publication), 2013.

A. Niell, A. Whitney, B. Petrachenko, W. Schlüter, N. Vandenberg, H. Hase, Y. Koyama, C. Ma, H. Schuh and G. Tuccari. VLBI2010: Current and Future Requirements for Geodetic VLBI Systems. In: *IVS Annual Report 2005, NASA/TP-2006-214136*, edited by D. Behrend and K. D. Baver, 13–40, 2006.

A. Nothnagel. Conventions on thermal expansion modelling of radio telescopes for geodetic and astrometric VLBI. *Journal of Geodesy*, **83**, 787–792, 2009.

H.P. Plag and M. Pearlman (Eds.) *The Global Geodetic Observering System. Meeting the Requirements of a Global Society on an Changing Planet in 2020*, Springer, Heidelberg/Berlin, 2009.

A. Santamaría-Gómez, S. García-Espada, R. Haas and J. López-Ramasco. Estimation of the invariant reference point: First steps at Yebes. In: *Proceedings of the 7th IVS General Meeting - Launching the Next-Generation IVS Network, March 4-9, Madrid (Spain)*, edited by D. Behrend and K. D. Baver, 147–151, 2012.

S. Schmeing, D. Behrend, J. Gipson and A. Nothnagel. Proof-of-Concept Studies for a Local Tie Monitoring System. In: *VLBI2010: From Vision to Reality, IVS 2010 General Meeting Proceedings, NASA/CP-2010-215864*, edited by D. Behrend and K. D. Baver, 360–364, 2010.

Index of authors

SUOMEN GEODEETTISEN LAITOKSEN TIEDONANTOJA
REPORTS OF THE FINNISH GEODETIC INSTITUTE

73:1 JUSSI KÄÄRIÄINEN: Über die 50-m lange Rohrlibelle zur Untersuchung der Neigung der Erdkruste. 21 pages.
73:2 TEUVO PARM: Observing procedure and meteorological factors for electronic distance measurements. 6 pages. (distributed at Lagos Seminar 1973).
73:3 TEUVO PARM: A determination of the velocity of light using laser geodimeter. 12 pages.
73:4 Geodeettisen laitoksen vuosikertomus 1972. 25 sivua. (in Finnish).
74:1 JUHANI KAKKURI: Base triangulation for unsurveyed areas. 6 pages. (distributed at Khartoum Symposium 1974).
74:2 KALEVI KALLIOMÄKI and JUHANI KAKKURI: Time keeping methods applied in Finland. 40 pages.
74:3 Geodeettisen laitoksen vuosikertomus 1973. 25 sivua. (in Finnish).
74:4 JUHANI KAKKURI: Results of tracking of the GEOS-2 satellite at Helsinki Astronomical Observatory (COSPAR No 9435). 9 pages.
74:5 MIKKO TAKALO: The laser rod comparator. 14 pages.
75:1 JORMA KORHONEN: Program for the adjustment of the Finnish First Order Triangulation. 11 pages.
75:2 Geodeettisen laitoksen vuosikertomus 1974. 24 sivua. (in Finnish).
75:3 OSSI OJANEN: On the determination of elliptic orbits from the time micrometer observations. 15 pages.
75:4 AIMO KIVINIEMI: Measurements of wave motion in the ice surface. 12 pages.
75:5 ERKKI KÄÄRIÄINEN: Land uplift in Finland on the basis of sea level recordings. 14 pages.
75:6 TAUNO HONKASALO: Finnish observations and research on earth tides in 1971-1974. 6 pages. (distributed at the XVI General Assembly of the IUGG in Grenoble 1975).
75:7 TEUVO PARM: High precision traverse for scale determination of satellite and stellar triangulation and for controlling the first order triangulation. 16 pages. (distributed at the XVI General Assembly of the IUGG in Grenoble 1975).
75:8 SEPPO HALME, JUHANI KAKKURI and MATTI PAUNONEN: The Finnish - Swedish satellite laser system. 8 pages. (distributed at the XVI General Assembly of the IUGG in Grenoble 1975).
75:9 T.J. KUKKAMÄKI: Utilization of the 890 km long laser geodimeter traverse in space geodesy. 5 pages. (distributed at the Symposium on New Methods of the Space Geodesy in Leningrad 1975).
75:10 A.B. SHARMA: An integrating, centroid timing, receiver for satellite ranging. 25 pages.
75:11 MATTI V. PAUNONEN: A high power Q-switched ruby laser for satellite ranging. 8 pages.
76:1 OSSI OJANEN: Tietokoneohjelma satelliittilaserin teleskoopin suuntausta varten. 31 sivua. (in Finnish).
76:2 Geodeettisen laitoksen vuosikertomus 1975. 27 sivua. (in Finnish).
76:3 A.B. SHARMA: A theoretical analysis of optical receivers used in satellite ranging. 27 pages.
76:4 JUHANI KAKKURI and KARI KALLIOMÄKI: An automatically operated weather station. 19 pages.
76:5 RAIMO KONTTINEN: Stellar triangulation points Niinisalo, Tuorla and Naulakallio. 12 pages.
76:6 LIISI OTERMA: Lunette de Galilee pour controle faisceau laser. 3 pages.
77:1 A.B. SHARMA: Experimental performance of the Metsähovi laser radar receiver. 24 pages.
77:2 ERKKI HYTÖNEN: The National Report of Finland for the Commission for the New Adjustment of the European Triangulation. 10 pages. (distributed at the Symposium on the Readjustment of the European Trigonometric Network in Bruxelles 1977).
77:3 Geodeettisen laitoksen vuosikertomus 1976. 25 sivua. (in Finnish).
77:4 SEPPO J. HALME and JUHANI KAKKURI: Description and operation of a satellite laser system. 63 pages.
77:5 MATTI PAUNONEN: A fast subnanosecond rise time electro-optical shutter for the shortening of a Q-switched ruby laser pulse. 12 pages.
77:6 KARI KALLIOMÄKI: Guiding and data processing system of the Finnish satellite laser range finder. 32 pages.
78:1 TEUVO PARM: On the determination of the scale of the Finnish stellar triangulation net. 24 pages.
78:2 Geodeettisen laitoksen vuosikertomus 1977. 33 sivua. (in Finnish).
78:3 MIKKO TAKALO: Measuring method for the third levelling of Finland. 41 pages.
78:4 Contributions of the Finnish Geodetic Institute to the 8th Meeting of the Nordic Geodetic Commission. 52 pages.
78:5 MARKKU HEIKKINEN: CALC - an interactive computer language with unlimited numerical precision. 96 pages.
78:6 S. MIKKOLA: Computing astronomical refraction by means of continued fractions. 13 pages.
78:7 JUHANI HAKKARAINEN: Image evaluation of aerial cameras in Finland. 34 pages.

78:8 JUHANI KAKKURI, OSSI OJANEN and MATTI PAUNONEN: Ranging precision of the Finnish satellite laser range finder. 11 pages.
79:1 OSSI OJANEN: On the analysis of the return pulse of the satellite laser. 38 pages.
79:2 Geodeettisen laitoksen vuosikertomus 1978. 33 sivua (in Finnish).
79:3 S. MIKKOLA: Employing aerological measurements data for refraction evaluation. 3 pages.
79:4 MARKKU HEIKKINEN: Space-time representation of the gravity field. 22 pages.
80:1 TEUVO PARM (ed): Proceedings of the IAG-Symposium High Precision Geodetic Length Measurements, June 19-22, 1978. 364 pages.
80:2 Geodeettisen laitoksen vuosikertomus 1979. 32 sivua (in Finnish).
80:3 JUHA JAAKKOLA: Radial calibration of a grid for the goniometer. 19 pages.
81:1 MARTIN VERMEER: QIKAIM, a fast semi-numerical algorithm for the generation of minute-of-arc accuracy satellite predictions. 28 pages.
81:2 MARKKU HEIKKINEN: Solving the shape of the earth by using digital density models. 69 pages.
81:3 Geodeettisen laitoksen vuosikertomus 1980. 30 sivua (in Finnish).
81:4 VELI-MATTI TAAVITSAINEN: Vertical temperature gradient prediction by second degree response surface analysis. 14 pages.
81:5 JUHANI HAKKARAINEN: Effect of some flight factors on image quality. 26 pages.
82:1 Geodeettisen laitoksen vuosikertomus 1981. 32 sivua (in Finnish).
82:2 MATTI PAUNONEN: Studies on the Metsähovi satellite laser ranging system. 47 pages.
82:3 PEKKA LEHMUSKOSKI: Systematic error resulting from asymmetric handling of a Zeiss Ni 002 automatic levelling instrument. 12 pages.
82:4 AIMO NIEMI: A technical report of the photographic astrolabe of Turku Observatory. 57 pages.
82:5 JUHA JAAKKOLA: Photogrammetric height determination of gravity points. 19 pages.
83:1 OLLI SUUTARINEN: Recomputation of land uplift values in Finland. 17 pages.
83:2 MARTIN VERMEER: Chronometric levelling. 7 pages.
83:3 JUHANI HAKKARAINEN: Radial and tangential distortion of aerial cameras. 47 pages.
83:4 MARTIN VERMEER: A new SEASAT altimetric geoid for the Baltic. 10 pages.
84:1 T.J. KUKKAMÄKI and PEKKA LEHMUSKOSKI: Influence of the earth magnetic field on Zeiss Ni 002 levels. 11 pages.
84:2 HORST MONTAG, REINHARD DIETRICH, TEUVO PARM and MATTI OLLIKAINEN: The interstation distance Metsähovi - Potsdam based on satellite measurements. 8 pages.
84:3 MARTIN VERMEER: Geoid studies on Finland and the Baltic. 30 pages.
85:1 JUHANI KAKKURI and MARTIN VERMEER: The study of land uplift using the third precise levelling of Finland. 11 pages.
85:2 MIKKO TAKALO: Horizontal - vertical laser rod comparator. 14 pages.
85:3 CL. ELSTNER, R. FALK and AIMO KIVINIEMI: Determination of the local gravity field by calculations and measurements. 8 pages.
85:4 JAAKKO MÄKINEN, MARTIN EKMAN, ÅGE MIDTSUNDSTAD and OLE REMMER: The Fennoscandian land uplift gravity lines 1966-1984. 238 pages.
87:1 A. CZOBOR, J. ADAM, SZ. MIHALY, T. PARM and M. OLLIKAINEN: Results of the Finnish-Hungarian Doppler Observation Campaign (FHDOC). 21 pages.
87:2 E.W. GRAFAREND, H. KREMERS, J. KAKKURI and M. VERMEER: Modelling vertical refraction in the SW Finland Triangular Network TAGNET 3-D adjustment. 15 pages.
87:3 GÜNTER W. HEIN, HERBERT LANDAU, JUHANI KAKKURI and MARTIN VERMEER: Integrated 3D-adjustment of the SW Finland Test Net with the FAF Munich OPERA 2.3 software. 35 pages.
87:4 MATTI OLLIKAINEN: Astro-geodetic deflections of the vertical at first-order triangulation stations. 15 pages.
88:1 RAIMO KONTTINEN: Baseline multiplication using the Kern Mekometer ME 3000. 10 pages.
88:2 W. JAKS, P. FRACZYK, K. ZELLER, M. OLLIKAINEN and T. PARM: Results of the Finnish -Polish Doppler Observation Campaign (FINPOLDOC). 11 pages.
88:3 RUIZHI CHEN: Plate tectonics at the joint of Pamirs and Tien-Shan in Central Asia. 14 pages.
88:4 V. PISARENKO, N. RECHITSKAYA and J. KAKKURI: The dependence of gradients of modern movements of the Earth crust on space scale in Finland. 7 pages.
88:5 JUKKA RÄTY and JUHANI HAKKARAINEN: Quality testing of system cameras. 16 pages.
89:1 R. KONTTINEN, M. MARTIKAINEN and M. TAKALO: The Jämijärvi Calibration Baseline. 20 pages.

89:2 JUHA JAAKKOLA, OLLI JAAKKOLA, KIRSI MAKKONEN ja TAPANI SARJAKOSKI: Satelliittikuvista karttatuotteeksi - esitutkimus kartoituksen asiantuntijajärjestelmän kehittämiseksi. 146 sivua. (in Finnish).
89:3 MARTIN VERMEER: FGI studies on satellite gravity gradiometry. 1. Experiments with a 5-degree buried masses grid representation. 26 pages.
90:1 MARTIN VERMEER: FGI studies on satellite gravity gradiometry. 2. Geopotential recovery at 0.5-degree resolution from global satellite gradiometry data sets. 26 pages.
90:2 C.C. TSCHERNING, R. FORSBERG and M. VERMEER: Methods for regional gravity field modelling from SST and SGG data. 17 pages.
90:3 ANTON HØGHOLEN and JUHA JAAKKOLA: The influence of temperature variations on the photo coordinates in an analytical plotter. 38 pages.
91:1 RUIZHI CHEN: On the horizontal crustal deformations in Finland. 98 pages.
91:2 ABD. MAJID A. KADIR: Gravity field mapping over the Southeast Asian region using spaceborne gravimetry techniques. 75 pages.
91:3 MARJAANA LAUREMA, OLLI JAAKKOLA, TAPANI SARJAKOSKI and LARS SCHYLBERG: Formalization of cartographic knowledge using an expert system shell. 49 pages.
91:4 JUHANI HAKKARAINEN: The use of MTF as a criterion of image quality. 18 pages.
92:1 MARTIN VERMEER: FGI studies on satellite gravity gradiometry. 3. Regional high resolution geopotential recovery in geographical coordinates using a Taylor expansion FFT technique. 30 pages.
92:2 A. KIVINIEMI, R. KONTTINEN, A. KUIVAMÄKI, M. TAKALO and P. VUORELA: Geodetic observations on the Pasmajärvi postglacial fault. 18 pages.
92:3 RUIZHI CHEN: Processing of the 1991 GPS campaigns in central Finland for crustal deformation studies. 16 pages.
93:1 YU XIAOWEI and RISTO KUITTINEN: The radiometric errors of preprocessed Landsat TM images and their effect on the accuracy of numerical interpretation. 47 pages.
93:2 JÜRI RANDJÄRV: Vertical movements of the Earth's crust in the Baltic region. 33 pages.
93:3 KASPARS KUKUMS: Latvian geoid determination with mass point frequency domain inversion. 16 pages.
93:4 RISTO KUITTINEN and JUHANI LAAKSONEN: The effect of the spatial resolution of the satellite image on the object interpretation accuracy. 40 pages.
93:5 ANTON HØGHOLEN: Kinematic GPS in aerotriangulation in Finland. 13 pages.
93:6 JORMA JOKELA, MATTI OLLIKAINEN, PAAVO ROUHIAINEN and HEIKKI VIRTANEN: The gravity and GPS survey in Western Queen Maud Land, Antarctica, 1989-1992. 46 pages.
93:7 PEKKA LEHMUSKOSKI and PAAVO ROUHIAINEN: The behaviour of the Wild N3 levelling instrument under varying temperature conditions. 24 pages.
94:1 MARTIN VERMEER: A fast delivery GPS-gravimetric geoid for Estonia. 7 pages + 1 map.
94:2 JUHANI KAKKURI (Ed.): Final results of the Baltic Sea Level 1990 GPS campaign. Research works of the SSG 5.147 of the International Association of Geodesy. 57 pages.
94:3 JORMA JOKELA, MARKKU POUTANEN and RAIMO KONTTINEN: The program for the 1993 adjustment of the Finnish First-Order Terrestrial Triangulation. 23 pages.
94:4 OLLI JAAKKOLA: Finnish CORINE land cover - A feasibility study of automatic generalization and data quality assessment. 42 pages.
94:5 V.I. BOGDANOV, M.Yu. MEDVEDEV and K.A. TAYBATOROV: On the persistence of the oceanic background of apparent sea level changes in the Baltic Sea. 21 pages.
95:1 HEIKKI VIRTANEN and JUSSI KÄÄRIÄINEN: The installation of and first results from the superconducting gravimeter GWR20 at the Metsähovi station, Finland. 15 pages.
95:2 JUHANI KAKKURI (Ed.): Final results of the Baltic Sea Level 1993 GPS Campaign. Research works of the SSG 5.147 of the International Association of Geodesy. 123 pages.
95:3 HANNA KEMPPAINEN: On the formalization of the semantics of spatial objects. 99 pages.
95:4 MARTIN VERMEER (Ed.): Coordinate systems, GPS, and the geoid. Proceedings, NorFA Urgency Seminar held at Hanasaari, Espoo, Finland, June 27-29, 1994. 144 pages.
95:5 MARTIN VERMEER: Two new geoids determined at the FGI. 24 pages.
95:6 MARKKU POUTANEN and MATTI OLLIKAINEN: GPS measurements at the Nuottavaara post glacial fault. 24 pages.
95:7 MARTIN VERMEER (Ed.): Latest Developments in the Computation of Regional Geoids. Proceedings, Session G4, European Geophysical Society XX General Assembly, Hamburg, Germany, 3-7 April, 1995. 73 pages.
96:1 DIMITRI ARABELOS and MARTIN VERMEER: Gravity Field Mapping from a Combination of Satellite Altimetry and Sea Gravimetry in the Mediterranean Sea. 22 pages.

96:2 ILIAS N. TZIAVOS and MARTIN VERMEER (Eds.): Techniques for Local Geoid Determination. Proceedings, Session G7, European Geophysical Society XXI General Assembly. The Hague, The Netherlands, 6-10 May, 1996. 183 pages.

96:4 RISTO KUITTINEN (Ed.): Remote Sensing in Agriculture. Proceedings NJF Seminar, Finnish Agricultural Research Centre, Jokioinen, 21-23 Oct., 1996. 103 pages.

96:5 PEKKA LEHMUSKOSKI: Active fault line search in Southern and Central Finland with precise levellings. 16 pages.

97:1 LEENA MATIKAINEN, YU XIAOWEI, RISTO KUITTINEN AND EERO AHOKAS: Updating topographic maps by using multisource data and knowledge-based interpretation. 60 pages.

97:2 RISTO KUITTINEN (Ed.): Proceedings of the Finnish - Russian seminar on remote sensing in Helsinki, 29. Aug. - 1. Sep., 1994. 140 pages.

97:3 MIKKO TAKALO: Automated calibration of precise levelling rods in Finland. 14 pages.

97:4 HEIKKI VIRTANEN and JUSSI KÄÄRIÄINEN: The GWR T020 superconducting gravimeter 1994 - 1996 at the Metsähovi station, Finland. 26 pages.

97:5 MARTIN VERMEER, JIANCHENG LI and CHUNXI GUO: Geoid Determination by FFT Techniques and MGM in the Western China Test Area. 15 pages.

98:1 LEENA MATIKAINEN, MIKA KARJALAINEN and RISTO KUITTINEN: SAR images and ancillary data in crop species interpretation. 47 pages.

98:2 RISTO KUITTINEN... (et al.): An early crop yield estimation method for Finnish conditions: the crop growth monitoring system of the joint research centre with and without remotely sensed and other additional input data. 114 pages.

98:3 HELDUR SILDVEE: Gravity measurements of Estonia. 8 pages.

98:4 MARTIN VERMEER and JÓZSEF ÁDÁM (Eds.): Second Continental Workshop on the Geoid in Europe. Proceedings. Hungary, Budapest, March 10-14, 1998. 288 pages.

98:5 HEIKKI VIRTANEN: On superconducting gravimeter observations above 8 mHz at the Metsähovi station, Finland. 19 pages.

99:1 EIJA HONKAVAARA, HARRI KAARTINEN, RISTO KUITTINEN, ASKO HUTTUNEN and JUHA JAAKKOLA: Quality of FLPIS orthophotos. 33 pages.

99:2 HARRI KAARTINEN, ASKO HUTTUNEN, RISTO KUITTINEN, EIJA HONKAVAARA and JUHA JAAKKOLA: Quality of FLPIS Land Parcel Digitization. 26 pages.

99:3 JORMA JOKELA, PETRAS PETROŠKEVICIUS and VYTAUTAS TULEVICIUS: Kyviškes Calibration Baseline. 15 pages.

99:4 MARKKU POUTANEN and KAKKURI, JUHANI (Eds.): Final results of the Baltic Sea Level 1997 GPS campaign. Research works of the SSC 8.1 of the International Association of Geodesy. 182 pages.

99:5 EIJA HONKAVAARA, MIRJAM BILKER, XIAOWEI YU, JUHA JAAKKOLA, HARRI KAARTINEN, JANNE YLÖNEN: Orientation of Optical Airborne and Spaceborne Images for Small and Medium Scale Mapping Purposes. 57 pages.

99:6 TIINA KILPELÄINEN (Ed.): Map Generalisation in the Nordic Countries. 58 pages.

99:7 MIKKO TAKALO: Verification of Automated Calibration of Precise Levelling Rods in Finland. 36 pages.

99:8 LEENA MATIKAINEN, JOCHEN GRANDELL, RISTO KUITTINEN, JENNI VEPSÄLÄINEN: Snowmelt Monitoring Using Multisource Satellite Image and Ground Measurement Data. 46 pages.

2000:1 V.I.BOGDANOV, M. YU. MEDVEDEV, V.A. SOLODOV, YU. A. TRAPEZNIKOV, G.A. TROSHKOV, A.A. TRUBITSINA: Mean Monthly Series of Sea Level Observations (1777-1993) at the Kronstadt Gauge. 34 pages.

2000:2 JUHA OKSANEN and OLLI JAAKKOLA: Interpolation and Accuracy of Contour-based Raster DEMs. 32 pages.

2001:1 MIRJAM BILKER and HARRI KAARTINEN: The Quality of Real-Time Kinematic (RTK) GPS Positioning. 25 pages.

2004:1 MIKKO TAKALO, PAAVO ROUHIAINEN, JORMA JOKELA, HANNU RUOTSALAINEN and JOEL AHOLA: Geodetic measurements at the Pasmajärvi and Nuottavaara faults. 49 pages.

2006:1 MIKKO TAKALO, YURI KUZNETSOV, PEKKA LEHMUSKOSKI, VLADIMIR KAFTAN, JAAKKO MÄKINEN, ELENA BIKOVA, GLEB DEMIANOV, VLADIMIR HABAROV, MARKKU POUTANEN, ALEKSANDER YUSKEVICH and VIKTOR ZABNEV: Connection of the Russian and Finnish Levelling Networks. 40 pages.

2011:1 SIMO MARILA ja EIJA HONKAVAARA: Peltolohkorekisterin tarkkuustutkimus, EU-laadunvalvonta ja peltolohkorekisterin tarkkuuteen vaikuttavista tekijöistä. 36 sivua (in Finnish).

2013:1 NATALIYA ZUBKO and MARKKU POUTANEN (Eds.). Proceedings of the 21st Meeting of the European VLBI Group for Geodesy and Astronomy, Finland, Espoo, March 5-8, 2013. 268 pages.